



Nanoparticles Functionalized Paper for Biodiagnostic Applications

**Thesis in the fulfilment of the requirement for the degree of
Doctor of Philosophy in Chemical Engineering**

by

Ying Hui Ngo

B. Engg. (Chem.)

Department of Chemical Engineering

Faculty of Engineering

MONASH UNIVERSITY

December 2012

This page is intentionally blank

Copyright Notice

Under the Copyright Act 1968, this thesis must be used only under the normal conditions of scholarly fair dealing. In particular no results or conclusions should be extracted from it, nor should it be copied or closely paraphrased in whole or in part without the written consent of the author. Proper written acknowledgement should be made for any assistance obtained from this thesis.

I certify that I have made all reasonable efforts to secure copyright permissions for third party content included in this thesis and have not knowingly added copyright content to my work without the owner's permission.



.....
Ying Hui Ngo

This page is intentionally blank

TABLE OF CONTENTS

	Page
Title Page	i
Copyright Notice	iii
General Declaration	vii
Dedication	viii
Acknowledgements	ix
Abstract	xi
List of Publications	xiii
List of Figures	xv
List of Tables	xx
List of Abbreviations	xxi
List of Nomenclature	xxiii
Chapter 1 Introduction and Literature Review	25
Chapter 2 Gold Nanoparticle-Paper as a Three-Dimensional Surface Enhanced Raman Scattering Substrate	79
Chapter 3 Effect of Cationic Polyacrylamides on the Aggregation and SERS Performance of Gold Nanoparticles-treated Paper	111
Chapter 4 Effect of Cationic Polyacrylamide Dissolution on the Adsorption State of Gold Nanoparticles on Paper and Their Surface Enhanced Raman Scattering Properties	145
Chapter 5 Formation of Polyelectrolyte-Gold Nanoparticles Chaplets on Paper	169
Chapter 6 Gold Nanoparticles Paper as a SERS bio-diagnostic Platform	191
Chapter 7 Conclusion	215
Appendix	
Appendix I Papers Included in Each Chapter in Their Published Format	I-1
I(A) Paper Surfaces Functionalized by Nanoparticles	I-3
I(B) Gold Nanoparticle-Paper as a Three-Dimensional Surface Enhanced Raman Scattering Substrate	I-18
I(C) Effect of Cationic Polyacrylamides on the Aggregation and SERS Performance of Gold Nanoparticles-treated Paper	I-27
I(D) Effect of Cationic Polyacrylamide Dissolution	I-37

on the Adsorption State of Gold Nanoparticles
on Paper and Their Surface Enhanced Raman
Scattering Properties

Appendix II	Related Co-Authored Manuscript Not Included in the Main Body of This Thesis	II-1
	Gold Nanoparticle-Functionalized Thread as a Substrate for Surface Enhanced Raman Scattering (SERS)	
Appendix III	Patent Generated from This Thesis in the Main Body of This Thesis	III-1
	Metallic Nanoparticle Treated Cellulosic Substrate as a SERS Bidiagnostic Platform	
Appendix IV	Book Chapter Generated from This Thesis	IV-1
	Paper, Printing and the Apple Pie	

Monash University
Monash Research Graduate School

Declaration for thesis based or partially based on conjointly published or unpublished work

General Declaration

In accordance with Monash University Doctorate Regulation 17 Doctor of Philosophy and Research Master's regulations the following declarations are made:

I hereby declare that this thesis contains no material which has been accepted for the award of any other degree or diploma at any university or equivalent institution and that, to the best of my knowledge and belief, this thesis contains no material previously published or written by another person, except where due reference is made in the text of the thesis.

This thesis includes four original papers published in peer reviewed journals, and two manuscripts in preparation and to be submitted to peer reviewed journals. The core theme of the thesis is to investigate the fundamental science and engineering mechanisms to develop and optimize nanoparticles functionalized paper as a bio-diagnostics platform. The ideas, development and writing up of all the papers in the thesis were the principal responsibility of myself, the candidate, working within the Department of Chemical Engineering under the supervision of Prof. Gil Garnier, Prof. George Simon and Prof. Dan Li.

The inclusion of co-authors reflects the fact that the work came from active collaboration between researchers and acknowledges input into team-based research.

In the case of all the chapters listed below, my contribution to the work involved the following:

Thesis chapter	Publication title	Publication status*	Nature and extent of candidate's contribution
1	Paper Surfaces Functionalized by Nanoparticles	Published	Initiation, key ideas, experimental works, analysis works, development and writing up.
2	Gold Nanoparticle-Paper as a Three-Dimensional Surface Enhanced Raman Scattering Substrate	Published	
3	Effect of Cationic Polyacrylamides on the Aggregation and SERS Performance of Gold Nanoparticles-treated Paper	Published	
4	Effect of Cationic Polyacrylamide Dissolution on the Adsorption State of Gold Nanoparticles on Paper and Their Surface Enhanced Raman Scattering Properties	Published	
5	Formation of Polyelectrolyte-Gold Nanoparticles Chaplets on Paper	Manuscript in Preparation	
6	Gold Nanoparticles Paper as a SERS bio-diagnostic Platform	Manuscript in Preparation	

Signed:

.....

Date:

Dedicated to my family and husband

ACKNOWLEDGEMENTS

First of all, I would like to thank God, my savior for blessing me with the opportunity to come and study in Australia, constantly reminding me that nothing is impossible with God and giving me the strength and determination during the course of this work.

I would like to express my sincere gratitude and thanks to my supervisors Prof. Gil Garnier, Prof. George Simon, Prof. Dan Li and Prof. Wei Shen for their encouragement, patience and support throughout my candidature. I am most deeply grateful to my main supervisor, Prof. Gil Garnier, for his constant guidance and support. He made me realize that I can do better than what I would expect from myself; trained me to think critically and manage my time wisely between experiments and writing; taught me to improve my writing skills for publication in top level journals and be a better speaker. He also motivated me to always aim higher and never afraid of failure. When I am in stress and in doubt, he is always there to help me and guide me through. I really appreciate his supervision and enjoy working with him.

I would like to acknowledge my co-supervisor, Prof. George Simon. He is one of the most passionate researchers I have ever worked with. He always provides me with a lot of creative ideas for my research and is always there when I need his guidance and advice in my experiments and paper writing. I would also like to thank my other co-supervisor, Prof. Dan Li, for his motivation to help me think critically and work independently. I also acknowledge the guidance of Prof. Wei Shen and feel privileged to have the opportunity to work with him, the most creative scientist that I have ever met.

I gratefully acknowledge ARC Linkage Grant and Monash University for providing me the living allowance and tuition fee scholarship which have made my PhD work possible.

I would like to thank all the academic staff members at APPI and Department of Chemical Engineering at Monash University. I would like to acknowledge Dr. Warren Batchelor from APPI for his help with my scholarship application before I came to Australia. Special thanks to Finlay Shanks from Department of Chemistry, Dr. Tim Williams and Dr. Peter Miller from Monash University Centre for Electron Microscopy (MCEM) for their technical training and kind suggestions. I also acknowledge the support of the administrative staff and the technical staff at APPI and Department of Chemical

Engineering, particularly Janette Anthony, Lilyanne Price, Jill Crisfield, Kim Phu, Ron Graham, Gamini Ganegoda, for their assistance throughout my candidature.

I would like to thank Whui Lyn Then, David Ballerini, and Ling Qiu for their support and help during the experimental work as well as in paper writing. I would also like to thank Xu Li, Miaosi Li, Hui Hui Chiam, Sigappi Narayanan, Rosiana Lestiani, Matthew O'Connor, Tina Arbatan, Liyuan Zhang, Sharmiza Adnan, Galuh Yuliani, Scot Sharman, Henri Kröling, Dr. Ping Peng, Purim Jarujamrus, Jielong Su, Dr. Wade Mosse, Lizi Li and V Varanasi Swambabu at APPI for their friendship throughout my PhD study.

Last but most importantly, I would like to thank my parents, my sisters, brother and my parents in law for their lifetime support and encouragement. I would like to express my deepest gratitude to my husband Samson Sim, for his love, support, understanding and patience throughout my entire PhD study.

ABSTRACT

The research reported in this thesis focuses on the fundamental science and engineering required for the fabrication and optimization of nanoparticles functionalized paper as Surface Enhanced Raman Scattering (SERS) bio-diagnostics platform. It addresses the current Sensitivity, Selectivity, Simplicity and Strength (4S) limitations of bioactive paper. The research vision is to develop a nanoparticles treated paper as a generic diagnostic platform to identify and quantify low concentrations of a specific (bio)analyte in aqueous solutions. The product concept is a “dipstick sensor” based on functionalized gold nanoparticle treated paper (AuNP paper) for SERS detection. Such AuNP paper test would allow the direct, rapid and easy detection of (bio)analyte molecules at very low concentrations (below the nanomolar range), making it suitable for biomedical analysis, such as in cancer detection. It also eliminates the tedious preparation of multiple reactants and washing steps involved in current technology such as the Enzyme-Linked Immunosorbent Assay (ELISA) based bioactive paper.

Three parallel research length scales are investigated: **nano**, **micro** and **macro**. This involves quantifying the distribution and adsorption state of nanoparticles on paper (**nanoscale**). The effects of gold nanoparticles (AuNPs) concentration and 3-dimensional (3D) distribution profile on their adsorption and aggregation states on paper were explored. The surface coverage of AuNPs on paper scaled linearly with their concentration profile in solutions. The SERS performances of the AuNPs-treated papers were evaluated with a model Raman molecule, 4-aminothiophenol (4-ATP), and their SERS intensities increased linearly with the density of AuNPs on paper. The role of z-distribution of AuNPs within the bulk of paper was highlighted; their three-dimensional (3D) architecture was able to quench the background noise through interlayer plasmon coupling, thus amplifying the SERS signal.

The retention and aggregation state of nanoparticles on paper was controlled to drastically optimize the SERS performance (**microscale**). Paper substrates were pre-treated with a series of cationic polyacrylamide (CPAM) solutions to control the AuNPs adsorption and aggregation state on paper. The CPAM pre-treated paper produced a more uniform distribution of AuNPs compared to untreated paper. CPAM chains which adsorbed on paper in a high loops and tails conformation promotes efficient bridging of AuNPs to achieve higher surface coverage and aggregation of AuNPs on paper. This configuration is favored by CPAM solutions of higher concentration, charge density and molecular weight.

A simple approach to form and visualize polyelectrolyte-nanoparticles chaplet like structures on paper was developed by using negatively-charged gold nanoparticles (AuNPs) to decorate polymer chain of CPAM. AuNP chaplets were adsorbed in an opposite direction to the cellulose fibers and along the length of the CPAM molecules which were draped over the fibers. The effects of CPAM polymer concentration, charge density and molecular weight on the dimension of AuNP chaplets were quantified. Assembling nanometer-scale components (AuNPs) into micrometer-scale arrays (chaplets) on a porous paper substrate can be a promising strategy for low-cost nanoelectronics applications

The SERS properties of nanoparticles functionalized paper were quantified and optimized (**macroscale**). The effect of CPAM concentration, charge density and molecular weight on the aggregation and surface coverage of AuNPs on paper and ultimately the SERS signal of 4-ATP was quantified. The optimized AuNPs-CPAM paper showed a higher sensitivity and Raman enhancement factor (EF), which was almost an order of magnitude higher than the untreated AuNPs paper. The effect of CPAM dissolution kinetic on the SERS reproducibility was also quantified. SERS reproducibility of AuNPs on CPAM pre-treated paper both increase with dissolution time of CPAM, as the heterogeneity of AuNP distribution and aggregate size decreases; increasing CPAM charge density accentuated this tendency.

After the SERS efficiency towards the detection of model Raman molecule (4-ATP) was proven, AuNPs paper was upgraded by functionalizing the AuNPs with biotin/streptavidin assemblies for the detection of antibody-antigen binding. The modification of antibody local structure due to the interaction with antigen was detected. Evidence of antigen binding was elucidated from the SERS spectra, confirming the presence of antigen. Reproducible spectra features were observed for the functionalized AuNP papers which were exposed to different concentration of antigen; their intensity increased as a function of antigen concentration.

By conducting these studies and merging these three length scales of research, a novel strategy to engineer AuNPs functionalized paper as a low-cost and generic SERS platform for bio-diagnostic applications was developed.

LIST OF PUBLICATIONS

Peer-Reviewed Journal Papers

The following published papers are included in this thesis as individual chapters. The sections of these published papers have been renumbered in order to generate a consistent presentation within the thesis. Papers in their published format are included in this thesis as Appendix I.

1. Ngo, Y.H., D. Li, G.P. Simon, and G. Garnier, Paper surfaces functionalized by nanoparticles, *Advances in Colloid and Interface Science*, 2011. **163**(1): p. 23-38.
2. Ngo, Y.H., D. Li, G.P. Simon, and G. Garnier, Gold Nanoparticle–Paper as a Three-Dimensional Surface Enhanced Raman Scattering Substrate, *Langmuir*, 2012. **28**(23): p. 8782-8790.
3. Ngo, Y.H., D. Li, G.P. Simon, and G. Garnier, Effect of cationic polyacrylamides on the aggregation and SERS performance of gold nanoparticles-treated paper. *Journal of Colloid and Interface Science*, 2013. 392(0): p. 237-246.
4. Ngo, Y.H., D. Li, G.P. Simon, and G. Garnier, Effect of cationic polyacrylamide dissolution on the adsorption state of gold nanoparticles on paper and their Surface Enhanced Raman Scattering properties. *Colloids and Surfaces A: Physicochemical and Engineering Aspects*, 2013. 420(0): p. 46-52.

Manuscripts in Preparation

The following manuscripts in preparation are included in this thesis as individual chapters.

1. Ngo, Y.H., D. Li, G.P. Simon, and G. Garnier, Formation of Polyelectrolyte-Gold Nanoparticles Chaplets on Paper, *Manuscript in preparation and to be submitted to Journal of Colloid and Interface Science*.
2. Ngo, Y.H., W.L. Then, W. Shen, and G. Garnier, Gold Nanoparticles Paper as a SERS bio-diagnostic Platform, *Manuscript in preparation and to be submitted to Biomacromolecule*.

The following co-authored manuscript in preparation is generated during this doctoral study. They are related to the main body of this thesis, and therefore are included in this thesis as Appendix II.

1. Ngo, Y.H., D. Li, G.P. Simon, and G. Garnier, Formation of Polyelectrolyte-Gold Nanoparticles Chaplets on Paper, *Manuscript in preparation and to be submitted to Langmuir*.

Book Chapter

1. Garnier, G., Khan, M. S., Ngo, Y.H., and Mosse, W. (2012). "Paper, Printing and Apple Pie.", *Fundamental and Applied Pulp & Paper Modelling Symposium 2011*, Ed. Gaudreault, R., Robert, S., and Whitehead, M.A., Cascades Inc., Kingsey Falls, Quebec, In Press.

Patent

1. Ngo, Y.H., W.L. Then, D. Li, G.P. Simon, and G. Garnier. "Metallic Nanoparticle Treated Cellulosic Substrate as a SERS Biodiagnostic Platform", Australia Provisionaal Patent, AU2012902470, 28 June, 2012.

Conference Papers

The following conference papers have been presented by the author in international and national conferences during this doctoral study, but not included in this thesis.

1. Ngo, Y.H., D. Li, G.P. Simon, and G. Garnier, Gold Nanoparticles-SERS for Paper Biodiagnostics Applications, 244th ACS National Meeting & Exposition, Philadelphia, Pennsylvania, 2012.
2. Ngo, Y.H., D. Li, G.P. Simon, and G. Garnier, Gold Nanoparticles-SERS for Paper Biodiagnostics Applications, Australian Colloid and Surface Science Student Conference, Newcastle, Australia, 2012.
3. Ngo, Y.H., D. Li, G.P. Simon, and G. Garnier, Gold Nanoparticles-SERS for Paper Biodiagnostics Applications, Chemeca, Sydney, Australia, 2012.
4. Ngo, Y.H., D. Li, G.P. Simon, and G. Garnier, Functionalized Nanotechnology on Paper, Chemeca, Adelaide, Australia, 2011.
5. Ngo, Y.H., D. Li, G.P. Simon, and G. Garnier, Paper Surface Functionalized by Nanoparticles, 64th Appita Annual Conference and Exhibition, Melbourne, Australia, 2010.

LIST OF FIGURES

Chapter 1

- Figure 1:** Photo-induced redox reaction of TiO_2 . (redrawn from [16]).
- Figure 2:** Photo-induced hydrophilic and hydrophobic conversion of TiO_2 . (redrawn from [16]).
- Figure 3:** Colorimetric detection of biological targets by AuNPs. (redrawn from [21]).
- Figure 4:** Photodecomposition of acetaldehyde vapours by TiO_2 powder (crosses), TiO_2 paper (open diamonds) and pulp/ TiO_2 mixture (closed squares). Reprinted from [29], Copyright (2007), with permission from Elsevier.
- Figure 5:** Layer-by-layer coating method. (redrawn from [37]).
- Figure 6:** Purification of polluted soil using solar energy and photocatalytic TiO_2 paper. (redrawn from [47]).
- Figure 7:** Organic destruction by photocatalytic paper. (redrawn from [51]).
- Figure 8:** Aptamer (nucleic acid that specifically binds a target compound or moiety)/nanoparticle-based lateral flow device. (a) Blue color of AuNP aggregates is broken into red colored AuNP dispersion upon the addition of adenosine. (b) DNA sequences and linkages in AuNP aggregates. Lateral flow devices loaded with the aggregates (on the conjugation pad) and streptavidin (on the membrane in cyan color) (c) before use and in (d) negative or (e) positive test. Reprinted with permission from [60]. Copyright 2010 WILEY-VCH.
- Figure 9:** DNase I-sensing bioactive paper. (A) Color shift from blue to red when redispersion of DNA crosslinked AuNP aggregates is triggered by the addition of DNase I. (B) The sequences of DNA oligonucleotides. (C) Reaction of DNase I assay on PVA-coated hydrophilic paper [7], Copyright (2008), with permission from American Chemical Society.
- Figure 10:** Adenosine-sensing bioactive paper. (A) Color shift from blue to red when redispersion of DNA crosslinked AuNP aggregates is triggered by the addition of Adenosine. (B) The sequences of the DNA molecules used. (C) and (D) Reaction of Adenosine assays on hydrophobic and hydrophilic paper. Reprinted from [7], Copyright (2008), with permission from American Chemical Society.
- Figure 11:** Self-erasing films for rewritable paper. (a) Upon UV irradiation, trans-MUA coated AuNPs isomerize to cis-MUA. (b) During UV irradiation, photoactive AuNPs (red) form metastable aggregates (blue) (c) Writing into AuNPs film using a light pen ($I_{\text{UV}}=10 \text{ mWcm}^{-2}$) at 3 mms^{-1} . Reprinted with permission from [62]. Copyright 2009 WILEY-VCH.
- Figure 12:** (a) Raman spectrum of SWCNTs and (b) SERS of SWCNTs on gold coated filter paper. Reprinted from [46], Copyright (2006), with permission from Elsevier.

- Figure 13:** (A) Growth of bacterial colonies around grafted filter paper (B) zone of inhibition around the AgNPs loaded grafted filter paper. Reprinted from [4], Copyright (2009), with permission from Elsevier.
- Figure 14:** (a) Raman spectrum of SWCNTs and (b) SERS of SWCNTs on silver coated filter paper. Reprinted from [46], Copyright (2006), with permission from Elsevier.
- Figure 15:** (a) Raman spectrum of solid PHBA (b) FT-SERS spectra of PHBA in AgNPs solution and (c) on AgNPs-coated filter paper. Reprinted from [6], Copyright (2003), with permission from Elsevier.
- Figure 16:** Fluorescence emission spectra of Rose Bengal on paper and Ag colloid deposited paper (left) and fluorescence emission spectra of PtOEP on paper and Ag colloid-deposited paper (right). Reprinted from [5], Copyright (2008), with permission from Elsevier.
- Figure 17:** Different length scales of the constituents of paper.
- Figure 18:** Schematic cross section illustration of light interaction with (a) nanoparticles on a glass substrate, (b) nanoparticles on a paper substrate, (c) Thickness, z of nanoparticles paper, (d) Ideal control of aggregation state of nanoparticles on paper substrates.
- Figure 19:** SEM with image analysis (analysed via Image J) for analyzing the distribution and adsorption state of TiO_2 on filter paper substrate. Unpublished results from [75].

Chapter 2

- Figure 1:** Colour intensity of filter papers treated with AuNP solutions of different concentration.
- Figure 2:** FESEM images and histograms of particle size distribution of filter papers dipped into (a) 0.02 mg/mL, (b) 0.05 mg/mL, (c) 0.10 mg/mL, (d) 0.15 mg/mL and (e) 0.20 mg/mL of AuNP solutions.
- Figure 3:** Effect of the concentration of AuNP solutions on the amount of AuNPs retained on the paper surface and bulk after dipping (estimated from UV-Vis and FESEM analysis based on the FESEM images in Figure 2).
- Figure 4:** (Left) Raman spectrum of 1 mM of 4-ATP adsorb on (a) plain filter paper and SERS spectra of 4-ATP on filter paper dipped in AuNP solutions of (b) 0.02 mg/mL, (c) 0.05 mg/mL, (d) 0.10 mg/mL, (e) 0.15 mg/mL and (f) 0.20 mg/mL. (Right) SERS intensity of 4-ATP at 1077 cm^{-1} band from paper dipped in different concentration of AuNP solutions.
- Figure 5:** (a) SERS spectra of different concentration of 4-ATP from AuNPs treated paper (0.20 mg/mL AuNP solutions). (b) SERS intensity of different concentration of 4-ATP from the AuNPs treated paper at 1077 cm^{-1} band.

- Figure 6:** (a) SERS spectra of different concentration of 4-ATP from AuNPs treated silicon (0.20 mg/mL of AuNP solutions). (b) SERS intensity of different concentration of 4-ATP from the AuNPs treated silicon at 1077 cm^{-1} band.
- Figure 7:** Relationship between the amount of AuNPs and the EF of 4-ATP measured at the 1077 cm^{-1} band for filter paper and silicon. The contributions of the AuNPs adsorbed at (a) the surface of paper and also in (b) the bulk of paper were analyzed.
- Figure 8:** (a) Low and (b) high magnification FESEM images of (1) filter paper (2) silicon wafer and (3) hydrophobized paper substrates treated with 1 μL droplet of AuNPs (0.20 mg/mL). (c) SERS spectra of 4-ATP absorbed on the droplets respectively (taken at four different spots: two from the centre and two from the edge of the droplet as indicated with numbers in the FESEM images).

Chapter 3

- Figure 1:** Colour intensity of filter paper dipped in 0.20 mg/mL of AuNP solutions without CPAM pre-treatment and with CPAM pre-treatment of 0.01 mg/mL, 0.05 mg/mL and 0.10 mg/mL polymer concentration.
- Figure 2:** FESEM images and histograms of AuNPs' particle size distribution of filter paper dipped in 0.20 mg/mL of AuNP solutions (a) without CPAM pre-treatment and with CPAM pre-treatment of (b) 0.01 mg/mL (c) 0.05 mg/mL and (d) 0.10 mg/mL polymer concentration.
- Figure 3:** (Left) Raman spectrum of 4-ATP adsorbed on (a) plain filter paper, SERS spectra of 4-ATP on AuNPs paper (b) without CPAM pre-treatment and with CPAM pre-treatment of (c) 0.01 mg/ml (d) 0.05 mg/ml and (e) 0.10 mg/ml polymer's concentration. (Right) Relationship between the (a) average size and (b) surface coverage of AuNP aggregates and the EF of 4-ATP measured at the 1077 cm^{-1} band (error bars show standard deviation of 5 measurements from different spots on the substrate).
- Figure 4:** FESEM images and histograms of particle size distribution of AuNPs-CPAM papers treated with polymer solution charge density of (a) 5 wt%, (b) 10 wt% and (c) 40wt%.
- Figure 5:** (Left) SERS spectra of 4-ATP on AuNPs-CPAM papers with polymer's charge density of (a) 5 wt%, (b) 10 wt% and (c) 40wt%. (Right) Relationship between the (a) average size and (b) surface coverage of AuNP aggregates and the EF of 4-ATP measured at the 1077 cm^{-1} band (error bars show standard deviation of 5 measurements from different spots on the substrate).
- Figure 6:** FESEM images and histograms of particle size distribution of AuNPs-CPAM papers with polymer's molecular weight of (a) 6 MDa and (b) 13 MDa.
- Figure 7:** (Left) SERS spectra of 4-ATP on AuNPs-CPAM papers with polymer's molecular weight of (a) 6 MDa and (b) 13 MDa. (Right) Relationship between the (a) average size and (b) surface coverage of AuNP aggregates

and the EF of 4-ATP measured at the 1077 cm^{-1} band (error bars show standard deviation of 5 measurements from different spots on the substrate).

- Figure 8:** SERS spectra of different concentration of 4-ATP from untreated AuNPs paper.
- Figure 9:** SERS spectra of different concentration of 4-ATP from AuNPs-CPAM paper.
- Figure 10:** SERS intensity of different concentration of 4-ATP from (a) AuNPs paper and (b) AuNPs-CPAM paper at 1077 cm^{-1} band.
- Figure 11:** (a) Polymer attains a flat conformation with many trains at the interface. (b) Polymer attains a conformation with many loops and tails tangling out of the surface.

Chapter 4

- Figure 1:** Effect of dissolution time and CPAM charge density on the viscosity of polymer solutions. CPAM (13MDa) 0.10 mg/mL at room temperature in water.
- Figure 2.** Effect of dissolution time and CPAM charge density on the average hydrodynamic diameter. CPAM (13MDa) 0.10 mg/mL at room temperature in water. Error bars indicate the standard deviations from five measurements. Error bars indicate the standard deviations from five measurements.
- Figure 3:** FESEM of AuNPs on paper substrate pre-treated by CPAM of 5 wt%, 10 wt% and 40 wt% charge density at different dissolution time.
- Figure 4:** Average size of AuNP aggregates on paper substrate pre-treated by CPAM of different charge density vs. dissolution time of CPAM.
- Figure 5:** Surface coverage of AuNP aggregates on paper substrate pre-treated by CPAM of different charge density vs. dissolution time of CPAM.
- Figure 6:** Average SERS spectra of 4-ATP on AuNPs-CPAM papers with CPAM of (a) 5 wt%, (b) 10 wt% and (c) 40 wt% charge density prepared at different dissolution times.
- Figure 7:** Raman enhancement factor (EF) of 4-ATP at 1077 cm^{-1} on AuNPs-CPAM papers treated with CPAM of different charge density as a function of CPAM dissolution time. Error bars are standard deviations from five measurements at different point on the substrates.
- Figure 8:** Schematic representation of the dissolution kinetic of CPAM; the red circles represent the gel aggregates

Chapter 5

- Figure 1:** The formation process of CPAM-AuNPs chaplets by vacuum filtration.
- Figure 2:** FESEM images of AuNPs on paper (A) without CPAM and AuNPs chaplet on paper pre-treated with CPAM (40 wt% charge density, 13 MDa) of different concentration: (B) 0.01 mg/mL, (C) 0.05 mg/mL and (D) 0.10 mg/mL under (1) low and (2) high magnification power.
- Figure 3:** FESEM images of AuNPs chaplets on paper pre-treated with CPAM (0.10 mg/mL concentration, 13 MDa) of different charge density: (A) 0.05 wt%, (B) 0.10 wt% and (C) 0.40 wt% under (1) low and (2) high magnification power.
- Figure 4:** FESEM images of AuNPs chaplets on paper pre-treated with CPAM (0.10 mg/mL concentration, 40 wt% charge density) of different molecular weight: (A) 6 MDa and (B) 13 MDa under (1) low and (2) high magnification power.
- Figure 5:** FESEM images of (a) CPAM followed by AuNPs vacuum filtered paper, (b) CPAM followed by AuNPs dip-coated paper, (c) CPAM dip-coated, dried followed by AuNPs vacuum filtered paper, (d) CPAM dip coated, dried, re-wetted followed by AuNPs vacuum filtered paper, (e) CPAM followed by AuNPs filtered paper without vacuum, (f) CPAM followed by AuNPs vacuum filtered silicon.
- Figure 6:** Proposed mechanism involved in the formation of AuNP chaplets.

Chapter 6

- Figure 1:** Functionalization procedure of SERS platform on AuNPs paper.
- Figure 2:** FESEM images and histograms of AuNPs particle size distribution on paper.
- Figure 3:** SERS spectra of (a) AuNPs paper and (b) BAT/TEG functionalized AuNPs paper.
- Figure 4:** SERS spectra of (a) Strep on AuNPs paper and (b) Strep-BAT/TEG functionalized AuNPs paper.
- Figure 5:** SERS spectra of (a) biotinylated antibody on AuNPs paper and (b) biotinylated antibody-Strep-BAT/TEG functionalized AuNPs paper.
- Figure 6:** SERS spectra of (a) antigen on AuNPs paper and (b) antigen-biotinylated antibody-Strep-BAT/TEG functionalized AuNPs paper.
- Figure 7:** (a) SERS spectra of antigen-biotinylated antibody-Strep-BAT/TEG functionalized AuNPs paper exposed to different concentration of antigen. (b) SERS intensity of different concentration of antigen on functionalized AuNPs paper at 1590 cm^{-1} band.

LIST OF TABLES

Chapter 1

Table I: Roadmap of nanoparticles.

Chapter 2

Table I: Effect of concentration on Zeta potential of AuNPs.

Chapter 3

Table I: Zeta potential of CPAM solutions with different concentration, charge density and molecular weight.

Chapter 5

Table I: Estimated dimension of AuNP chaplets formed on paper pre-treated by CPAM of different concentration.

Table II: Estimated dimension of AuNP chaplets formed on paper pre-treated by CPAM of different charge density.

Table III: Estimated dimension of AuNP chaplets formed on paper pre-treated by CPAM of different molecular weight.

Chapter 6

Table I: Size or molecular weight of each component.

LIST OF ABBREVIATIONS

3D	Three dimensional
4-ATP	4-aminothiophenol
Ag	Silver
AgNPs	Silver nanoparticles
AKD	Alkyl Ketene Dimer
APPI	Australian Pulp and Paper Institute
ASA	Alkenyl Succinic Anhydride
Au	Gold
AuNPs	Gold nanoparticles
BAT	Biotinylated thiol
CD	Cross-machine direction
CMC	Carboxymethyl cellulose
CPAM	Cationic polyacrylamide
CPAM	Cationic Polyacrylamide
Cu	Copper
DLS	Dynamic Light Scattering
DNA	Deoxyribonucleic acid
E. Coli	Escherichia coli
EF	Enhancement Factor
ELISA	Enzyme-Linked Immunosorbent Assay
ELISA	Enzyme-Linked Immunosorbent Assay
EM	Electromagnetic
FEG	Field Emission Gun
FESEM	Field Emission Scanning Electron Microscopy
Igg	Immunoglobulin G
LBL	Layer by layer
MB	Methylene Blue
MCEM	Monash Centre for Electron Microscopy
MD	Machine direction
MEF	Metal-enhanced fluorescence
MNA	M-nitroaniline
MUA	(11-mercaptoundecanoxy)azobenzene
OH	Hydroxyl
ONA	O-nitroaniline
PAE	Polyamide-epichlorohydrin

PAM	Polyacrylamide
PEG	Polyethylene glycol
PEI	Polyethyleimine
PEO	Polyethylene Oxide
PHBA	P-hydroxybenzoic acid
PNA	P-nitroaniline
Poly(DADMAC)	Poly(diallyldimethylammonium chloride)
PSS	Poly(styrenesulfonate)
PtOEP	Pt(II) octaethylporphine
RB	Rose Bengal
ROS	Reactive oxygen species
SERS	Surface Enhanced Raman Scattering
SPB	Surface Plasmon Band
SPR	Surface Plasmon Resonance
SS	Supra-spherical
SWCNTs	Single-walled carbon nanotubes
TAPPI	Technical Association of the Pulp and Paper
Industry	
TEG	Triethylene glycol mono-11-mercaptoundecyl ether
TiO ₂	Titanium Dioxide
UV	Ultraviolet
VOCs	Volatile Organic Compunds

LIST OF NOMENCLATURE

°C	degree Celsius
μL	microlitre
cm	centimetre
cSt	centistokes
kV	kilovolt
mg	milligram
mL	millilitre
mM	millimolar
mW	milli watt
nm	nanometer
pA	pikoampere
t	time
η	viscosity
ρ	density

This page is intentionally blank

Chapter 1

Introduction and Literature Review

This page is intentionally blank

Monash University

Declaration for Thesis Chapter 1

Declaration by candidate

In the case of Chapter 1, the nature and extent of my contribution to the work was the following:

Nature of contribution	Extent of contribution (%)
Initiation, key ideas, review of updated literature, development and writing up of paper	80

The following co-authors contributed to the work. Co-authors who are students at Monash University must also indicate the extent of their contribution in percentage terms:

Name	Nature of contribution	Extent of contribution (%) for student co-authors only
Gil Garnier	Initiation, key ideas, reviewing and editing of the paper.	Supervisor
George Simon	Initiation, key ideas, reviewing and editing of the paper.	Co-supervisor
Dan Li	Initiation, key ideas, reviewing and editing of the paper.	Co-supervisor

Candidate's Signature

Date 13.03.2013

Declaration by co-authors

The undersigned hereby certify that:

- (1) the above declaration correctly reflects the nature and extent of the candidate's contribution to this work, and the nature of the contribution of each of the co-authors.
- (2) they meet the criteria for authorship in that they have participated in the conception, execution, or interpretation, of at least that part of the publication in their field of expertise;
- (3) they take public responsibility for their part of the publication, except for the responsible author who accepts overall responsibility for the publication;
- (4) there are no other authors of the publication according to these criteria;
- (5) potential conflicts of interest have been disclosed to (a) granting bodies, (b) the editor or publisher of journals or other publications, and (c) the head of the responsible academic unit; and
- (6) the original data are stored at the following location(s) and will be held for at least five years from the date indicated below:

Location(s)

ulp and Paper Institute (APPI), Department of Chemical
Monash University, Clayton, VIC 3800, Australia.

Signature 1

Date 11/12/2012

Signature 2

Date 12/12/12

Signature 3

Date 11/12/2012

This page is intentionally blank

Content

1.1	Introduction	31
1.2	Literature Review	34
1.2.1	Abstract	34
1.2.2	Introduction	35
1.2.3	Properties of Nanoparticles	36
1.2.3.1	Photocatalytic	36
1.2.3.2	Surface Plasmon Resonance (SPR)	38
1.2.3.3	Surface Enhanced Raman Scattering (SERS)	39
1.2.3.4	Antimicrobial	40
1.2.4	Attachment Methods of Nanoparticles to Paper	42
1.2.4.1	Wet-end Addition	42
1.2.4.2	Surface Treatments	43
1.2.4.2.1	Size-press Treatment.....	44
1.2.4.2.2	Layer-by-layer Deposition (LbL).....	44
1.2.4.2.3	Sol-gel Method	46
1.2.4.2.4	Direct Assembly.....	46
1.2.4.2.5	In situ Assembly.....	47
1.2.5	Applications of Nanoparticles-functionalized Paper	49
1.2.5.1	Titania Paper	49
1.2.5.1.1	Self-cleaning	49
1.2.5.1.2	Organic Destruction	49
1.2.5.1.3	Disinfection.....	51
1.2.5.2	Gold Nanoparticle Paper	51
1.2.5.2.1	Colorimetric Sensor	51
1.2.5.2.2	Rewritable Paper	54
1.2.5.2.3	SERS	55
1.2.5.3	Silver Nanoparticle Paper	57
1.2.5.3.1	Antimicrobial	57
1.2.5.3.2	SERS	58
1.2.5.3.3	Anti-counterfeiting.....	59
1.2.6	Challenges and Opportunities	60
1.2.6.1	Paper Chemical and Physical Heterogeneities	61
1.2.6.2	Optical Properties	63

Chapter 1

1.2.6.2.1	SERS and SPR.....	64
1.2.6.3	Photocatalytic Properties	65
1.2.6.4	Analytical Techniques	66
1.2.7	Conclusion	67
1.2.8	Acknowledgement	69
1.3	Research Objectives and Aims	70
1.4	Thesis Outline	71
1.5	References	74

1.1 Introduction

Bioactive paper has recently been the focus of a renewed research interests as a diagnostic platform for health and environmental applications as it offers great promise of inexpensive, sensitive and selective diagnostic devices [1-4]. The combination of printing technology and Enzyme-Linked Immunosorbent Assay (ELISA) colorimetric technique has been employed to regulate and detect analytes on paper [3, 5]. Blood typing paper strips have been fabricated to detect blood group antigens by monitoring blood agglutination which is triggered by specific antibody-antigen interactions [6]. However, bioactive paper is generally challenged by 4 major limitations: 1) Sensitivity, 2) Selectivity, 3) Simplicity and 4) Strength- the 4S. While ELISA is a standard solution-based technique, its application to paper, while possible, requires multiple reactants and tedious washing steps, which at the limit, goes against the philosophy of simplicity and instantaneous reporting expected from paper diagnostics [7-8]. However, most bioactive papers rely on colorimetric techniques to communicate the result of the analysis. Although direct and convenient, this technique suffers from complications when identifying antibodies at lower concentrations (less than 10^{-6} M) and smaller dimensions (such as for immunoglobulin G). For applications that required high sensitivity and selectivity, such as cancer detection, this accuracy might not be sufficient and detection ranging from 10^{-9} to 10^{-12} M is desired. The challenge is how to increase the sensitivity by 3 to 6 orders of magnitude without compromising the cost or ease of use of paper diagnostics.

Nanotechnology, which involves the control or arrangement of individual nanoparticles or their aggregates into desired configurations to produce materials with unique properties [9], shows promising potential in addressing the 4S issues of bioactive paper. The synthesis and attachment of nanoparticles, both within and onto, cellulosic materials have gained great research interest for their potential to manufacture low cost and functional substrates [10]. Paper, a non-woven cellulosic material with natural porous morphology and high oxygen density, is able to provide a strong capillary force to absorb nanoparticles over a higher surface area compared to other flat substrates such as glass, silicon or polymer. In addition, paper is low cost, biodegradable, biocompatible and renewable. Furthermore, only an infinitesimal volume of nanoparticles deposited on paper is capable of producing a wide range of devices with excellent and new properties [11-

16]. Metallic nanoparticles such as gold (AuNPs), silver (AgNPs), and titania nanoparticles (TiO_2) have been synthesized within or attached to paper for optical [11], antibacterial [12-13] and anti-counterfeiting [14], Surface Enhanced Raman Scattering (SERS) [15] and biosensor [16] applications. Amongst all of these unique properties, SERS, which allows direct contact of analytes on nanoparticles treated paper for single molecular detection, shows a great potential in addressing the current limitations of bioactive paper.

Most research to date has focused on the adsorption and assembly of nanoparticles on flat substrates, such as glass and silicon. Studies on nanoparticles treated paper have mostly relied on paper as a low-grade inert support and mainly focused on demonstrating the applications. There is a lack of understanding on the underlying mechanisms involved in the adsorption of nanoparticles on the imperfect, rough and fibrous substrate that is paper. The effect of the paper heterogeneous morphology and its surface characteristics (such as through post-treatment) on the adsorption state of nanoparticles are neither understood nor quantified. This knowledge is technologically important due to a strong expected correlation between nanoparticle/paper morphology at the various length scales and the resulting optical, electrical and catalytic properties. The realization of nanotechnology on paper also depends particularly on the control of the dispersion and aggregation state of the nanoparticles on paper. For instance, a plasmon absorbance region is displayed at the close contact points of metallic nanoparticles (aggregation), and the coupling of these plasmon absorbances result in an enhanced electromagnetic (EM) field, which governs SERS applications. Thus, formation of nanoparticles into aggregates is able to generate a greater SERS signal enhancement, compared to their individual isolated nanoparticles [17]. However, very few studies, if any, have attempted to understand, quantify and control the various nanoparticle/paper structures at different length scales for optimal property enhancement.

In an effort to address the current research gaps, this thesis is focused on three parallel research length scales: **nano**, **micro** and **macro**. It has three global objectives. The first, is quantifying the distribution and adsorption state of nanoparticles on paper (**nanoscale**). The second is controlling the adsorption and aggregation state of nanoparticles on the microporous paper surface (**microscale**). The third is optimizing the SERS properties of nanoparticles functionalized paper to develop a generic SERS bio-diagnostic platform

(macroscale). By conducting these studies and reconciling the three structural length scales, we have attempted to engineer AuNPs functionalized paper as a low-cost and generic SERS platform for bio-diagnostic applications.

The objective of Chapter 1 is to critically review the development of nanoparticles-functionalized paper and assess the potential of nanotechnology on paper in addressing the current limitations of bioactive paper. This chapter consists of three main sections (Section 1.2, 1.3 and 1.4). The first is a literature review paper published in *Advances in Colloid and Interface Science* (the original publication are provided in Appendix I). This literature review presents an overview of three main metallic nanoparticles: gold, silver and titania nanoparticles, which are majorly used to functionalized paper. Different preparation methods of the nanoparticles-functionalized paper are reviewed, focusing on their ability to control the morphology and structure of paper as well as the spatial location and adsorption state of nanoparticles which are critical in achieving their optimum applications. The main applications of the nanoparticles-functionalized papers are also highlighted and their critical challenges are discussed, followed by a perspective on the future direction in this research. The second section presents how this doctoral study aims to fulfil the current research gaps to engineer nanoparticles treated paper as an optimum SERS bio-diagnostic platform. The last section presents the organization of the thesis.

1.2 Literature Review

Paper surfaces functionalized by nanoparticles

Ying Hui Ngo¹, Dan Li², George P. Simon² and *Gil Garnier¹

¹ *BioPRIA, Australian Pulp and Paper Institute (APPI), Department of Chemical Engineering Monash University, Clayton, VIC 3800, Australia.*

² *Department of Material Engineering Monash University, Clayton, VIC 3800, Australia*

*Corresponding author. Email: [REDACTED]; Tel: [REDACTED]; Fax: [REDACTED]

1.2.1 Abstract

Nanomaterials with unique electronic, optical and catalytic properties have recently been at the forefront of research due to their tremendous range of applications. Taking gold, silver and titania nanoparticles as examples, we have reviewed the current research works on paper functionalized by these nanoparticles. The functionalization of paper with only a very small concentration of nanoparticles is able to produce devices with excellent photocatalytic, antibacterial, anti-counterfeiting, Surface Enhanced Raman Scattering (SERS) and Surface Plasmon Resonance (SPR) performances. This review presents a brief overview of the properties of gold, silver and titania nanoparticles which contribute to the major applications of nanoparticles-functionalized paper. Different preparation methods of the nanoparticles-functionalized paper are reviewed, focusing on their ability to control the morphology and structure of paper as well as the spatial location and adsorption state of nanoparticles which are critical in achieving their optimum applications. In addition, main applications of the nanoparticles-functionalized papers are highlighted and their critical challenges are discussed, followed by perspectives on the future direction in this research field. Whilst a few studies to date have characterized the distribution of nanoparticles on paper substrates, none have yet optimized paper as a nanoparticles' substrate. There remains a strong need to improve understanding on the optimum adsorption state of nanoparticles on paper and the heterogeneity effects of paper on the properties of these nanoparticles.

Keywords: Nanoparticles, gold, silver, titania, paper, photocatalytic, SERS, SPR, heterogeneity.

1.2.2 Introduction

The area of nanotechnology reviewed in this article involves controlled deposition of individual nanoparticles or their aggregates into desired configurations on paper, to produce materials with unique properties and functions [9]. Nanoparticles with distinctive electronic, optical and catalytic properties have been at the forefront of research due to their tremendous applications. A wide range of techniques have been used to synthesize nanoparticles in different solid mediums, such as glass [18], metallic [19] and polymeric films [20] to realize new applications. However, development of simpler and more direct methods is still needed to readily generate the desired size, shape, and adsorption of nanoparticles on appropriate and strategic substrates. Taking gold (AuNPs), silver (AgNPs) and titania nanoparticles (TiO_2) as examples, the state of paper functionalized by these nanoparticles is analyzed in this review.

The porous structure and hydrophilic fiber surface allow paper to absorb suspensions of nanoparticles by capillary forces, yielding a high loading of nanoparticles upon drying. Furthermore, paper is a low cost substrate and only a very small volume of TiO_2 , AuNPs and AgNPs deposited on paper can produce devices which show excellent optical [11], antibacterial [12-13], anti-counterfeiting [14], Surface Enhanced Raman Scattering (SERS) [15] and Surface Plasmon Resonance (SPR) [16] performances. In addition, paper has the advantage of being biodegradable, biocompatible and renewable whilst its structural morphology as well as surface chemistry can be readily engineered.

The objectives of this article are to critically review the development of nanoparticles-functionalized paper and assess missing knowledge and opportunities. A brief overview of the properties of TiO_2 , AuNPs and AgNPs is presented first, to provide a background for further discussion of the nanoparticles-functionalized paper. These nanoparticles have been selected due to their wide usage and unique applications. This review then focuses on the deposition/assembly and applications of the nanoparticles-functionalized paper. Finally, the future challenges and opportunities of this field are presented.

1.2.3 Properties of Nanoparticles

Before analyzing the preparation methods and applications of nanoparticles-functionalized paper, the properties of TiO_2 , AuNPs and AgNPs are presented in this section. Due to extensive range of properties displayed by these three nanoparticles, we only intend to provide a brief overview of their photocatalytic, Surface Plasmon Resonance (SPR), Surface Enhanced Raman Scattering (SERS) and antibacterial properties which are related to the end-use of the respective nanoparticles-functionalized paper.

1.2.3.1 Photocatalytic

After photocatalytic properties of TiO_2 were discovered by Fujishima and Honda [21], Matsubara et al. [22] demonstrated the photocatalytic properties of TiO_2 -containing paper in 1995. Since then, TiO_2 has been widely used to produce photocatalytic paper. This review focuses on the photocatalytic properties and applications of TiO_2 -paper, instead of their traditional usage as whitening fillers.

Basically, TiO_2 is a broad band gap semiconductor material which is able to convert energy from light into chemical redox energy (Figure 1). The two most important and easily synthesized polymorphs of TiO_2 are rutile, with a band gap of 3.05 eV (equivalent to light of wavelength of 407 nm), and anatase, with a band gap of 3.26 eV (= 381 nm) [23]; anatase is more active in photocatalysis although the physical causes are not completely understood so far. Upon irradiation of UV light, two types of photochemical reactions occur on the TiO_2 surface – photo-induced redox reaction of the adsorbed substances, and photo-induced hydrophilic conversion of TiO_2 itself [24]. In the first reaction, photoelectrons (e^-) are generated in the conduction band and holes (h^+) are produced in the valence band. These occur whenever TiO_2 absorbs UV light of wavelength less than 380nm, an energy which is greater than its band gap energy (3.26 eV). [24]. The photoelectrons then react with molecular oxygen (O_2) to produce superoxide radical anions ($\bullet\text{O}^{2-}$), and the holes react with water to produce hydroxyl ($\bullet\text{OH}$) radicals. Finally, these two types of radicals work together to photodecompose organic compounds [25].

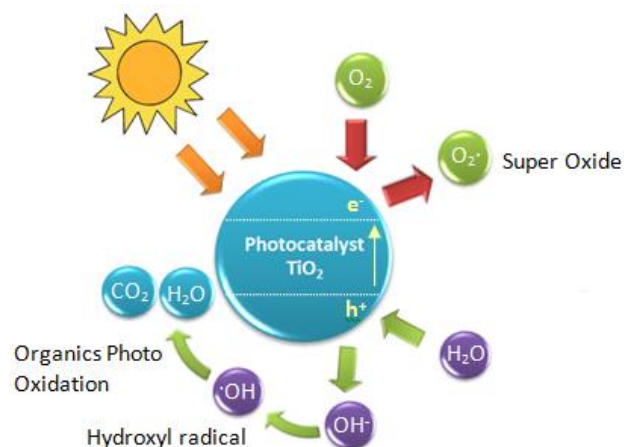


Figure 1: Photo-induced redox reaction of TiO_2 . (redrawn from [23]).

Conversely, in the second reaction, the electrons and holes are also photogenerated upon UV irradiation but they react differently. The photoelectrons tend to reduce the Ti(IV) cations to the Ti(III) state, whilst the holes oxidize the O^{2-} anions. In this process, O_2 molecules are ejected, creating oxygen vacancies (Figure 2), which are then occupied by water molecules, producing adsorbed OH groups that make the surface hydrophilic. The surface is transformed into an energetically-metastable state after the OH groups' adsorption. When the films are removed from the light, the adsorbed OH groups are slowly substituted by atmospheric oxygen, and the surface reverts back to its original state.

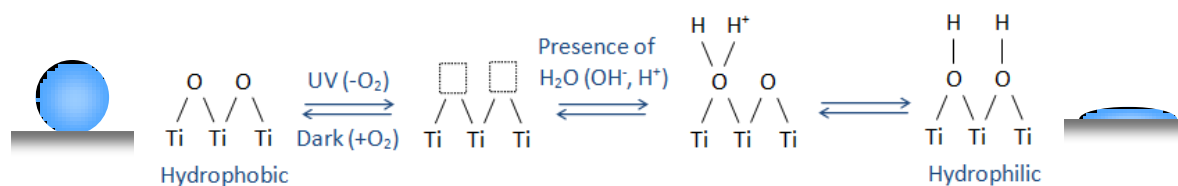


Figure 2: Photo-induced hydrophilic and hydrophobic conversion of TiO_2 . (redrawn from [23]).

Due to high photocatalytic properties of TiO_2 , its oxidizing activity tends to decompose paper substrate, limiting immobilization of TiO_2 on the substrate and reducing paper strength. In order to produce an efficient photocatalytic paper, TiO_2 must be strongly fixed to paper whilst avoiding deterioration of the paper. Distribution of TiO_2 nanoparticles over the thickness of paper sheet (z-plane) and their distribution profile within a layer (x-y plane) are also believed to be critical in achieving high photocatalytic

efficiency. To achieve maximum photo activity, a homogenous distribution of TiO_2 over the paper's volume is preferred instead of aggregation, in order to increase accessibility of target molecules and light to the TiO_2 surfaces. In addition, thickness and porosity of paper are also important parameters in determining photocatalytic efficiency of the TiO_2 -functionalized paper. Target molecules must be very close to TiO_2 on the paper surface, preferably in direct contact. Furthermore, decomposed compound must be transported/diffused away from the catalytic sites on paper to avoid blockage for future targets.

1.2.3.2 Surface Plasmon Resonance (SPR)

According to Mie's theory, SPR of nanoparticles is mainly related to their size, shape, volume concentration (aggregated or isolated assembly), interparticle distance as well as dielectric constant or refractive index of their surrounding mediums. Detection of analyte molecules is possible, as their presence changes interparticle distance or refractive index of the nanoparticles, which causes a shift in the Surface Plasmon adsorption band.

AgNPs demonstrate the highest efficiency of plasmon excitation among all the three metals (Ag, Au and Cu) which exhibit plasmon resonances within the visible spectrum [26]. According to Chin [27], AgNPs display a sharper resonance peak than AuNPs and thus AgNPs can provide a higher sensitivity and better shift detection. The optical excitation of their plasmon resonances has a more efficient light interaction mechanism. Since their absorption or scattering cross sections are higher compared to their geometric cross section, AgNPs are able to capture more light than its physical size would permit [26]. However, AgNPs are predisposed to oxidation, leading to problems with long term storage.

Compared to AgNPs, AuNPs are more stable and are commonly used to produce sensitive colorimetric sensors. Small and well-dispersed AuNPs (diameter of 10-50nm) show an intense red color with extinction coefficients which are much higher than those of common dyes, due to their localized SPR. The surface of AuNPs can be tailored by ligand-functionalization to selectively bind biomarkers. The most general approaches are chemical functionalization and thiol-linking of DNA of AuNPs to detect specific binding of proteins or antibodies. Upon the addition of analyte, functionalized and well-dispersed

AuNPs are induced into aggregates which show a significant color shift from red to blue (Figure 3). This is due to interparticle plasmon coupling which occurs as the surface plasmon of the individual AuNPs combine when their interparticle distance is smaller than their diameter.

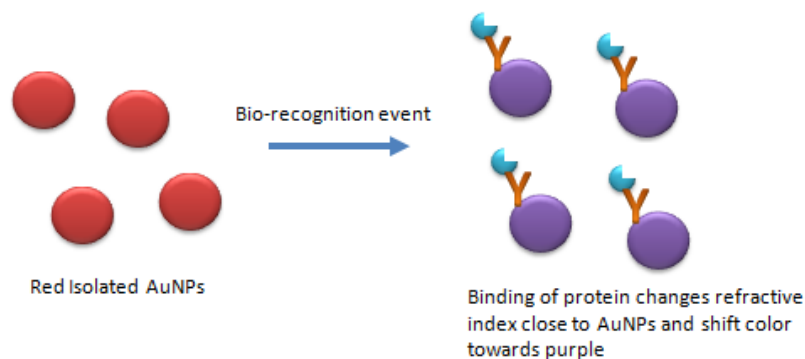


Figure 3: Colorimetric detection of biological targets by AuNPs. (redrawn from [28]).

In order to achieve an efficient SPR performance on paper, higher coverage of AgNPs and AuNPs must be obtained on the paper surface to enhance sensitivity of the nanoparticles-functionalized paper. It is important for paper structure to maintain the adsorption state of nanoparticles (e.g. dispersed or aggregated) upon drying. To carry out ideal colorimetric detection, the activity of nanoparticles must be preserved during storage and remain functional upon rehydration for use. Furthermore, careful control of nanoparticles' size and porosity of paper is required, so that the nanoparticles will not be entrapped inside the pores within the paper structure, which would restrict the aggregation or dispersion of the nanoparticles and accessibility of target analyte.

1.2.3.3 Surface Enhanced Raman Scattering (SERS)

Raman scattering is a light scattering technique in which Raman photons are scattered by vibrational and rotational transitions in a molecule. However, its sensitivity is limited because the Raman signal is very weak. The development of Surface Enhanced Raman Scattering (SERS) has increased dramatically since Fleischmann et al. [29] published their discovery on enhanced Raman signals from pyridine on a rough silver electrode. This discovery of SERS has transformed Raman spectroscopy from a structural analytical tool to a sensitive single-molecule detection and nanoscale probe [30]. As reported by Brus and co-workers [17], intense SERS enhancement is often present at the point of

contact between two or more metal nanoparticles. As the metal nanoparticles are contacted to form aggregates, their transition dipoles couple to each other and the enhanced fields of each nanoparticle coherently interfere at their contact point. When molecules are adsorbed in this contact point ('hot spot'), their Raman signals can be significantly enhanced (10^{14} – 10^{15}) [31]. Aggregates of nanoparticles have more efficient SERS properties than individual nanoparticles because larger enhancements can be achieved at particle junctions of the aggregates.

Since the aggregation of nanoparticles plays an important role in enhancing the SERS signal, their adsorption and aggregation state must be maintained within the paper structure. Stability of nanoparticles on the paper substrates must also be preserved so that they can be stored for long periods between measurements. Reproducibility of their aggregation state is another important factor to achieve accurate SERS results. Since the spot size of Raman's laser beam is approximately $1\mu\text{m}$, an ideal SERS active substrate needs to have uniform distribution of nanoparticles on a submicrometer scale in order to achieve high degree of reproducibility. This is a critical issue that must be addressed when paper is used as a SERS substrate, since it is a challenge to achieve uniform distribution of nanoparticles on paper due to its high roughness and porosity. In addition, due to high sensitivity of SERS, the paper substrates must be free of additives or fillers to avoid any background or fluorescence interference during the analysis.

1.2.3.4 Antimicrobial

AgNPs have been widely used in a range of bactericidal applications due to their broad-spectrum antimicrobial activities and high toxicity to different type of micro-organisms [32]. The antimicrobial properties of AgNPs are dependent on their concentration and rate of Ag ions released to the micro-organisms. AgNPs are inert in their metallic state, but become ionized upon contact and reaction with moisture of skin or wound [33]. The strong reactivity of ionized Ag causes cell destruction and death, as the bacterial cell wall undergoes structural changes once it binds to tissue proteins.

The antimicrobial properties of AgNPs are believed to be size-dependent, where smaller AgNPs, with larger surface areas accessible for interaction provide more antimicrobial effect than larger AgNPs [34]. In this case, aggregation of AgNPs on the paper structure

must be avoided to produce an efficient antimicrobial paper. This is because the aggregation will drastically decrease the accessibility of nanoparticles' surface, resulting in insufficient functionality. Therefore, homogenous distribution of AgNPs over the paper surface is preferred for better contact and reaction with the micro-organisms. The potential toxicity of AgNPs to human is still a matter of considerable debate. Hence, strong binding forces between AgNPs and paper substrate are desirable to reduce possible exposure.

Table 1: Roadmap of nanoparticles.

Nanoparticles	Titania (TiO ₂)	Gold (AuNPs)	Silver (AgNPs)
Structures and Properties	<ul style="list-style-type: none"> Three major crystalline forms: anatase, rutile, brookite. Rutile is predicted to be the most stable phase. Anatase is the most photoactive form. TiO₂ surface exhibit coordination vacancies and occupied by hydroxyl groups through water chemisorption. Raman scattering peaks of TiO₂ nanoparticles become broader as their size decreases. Photocatalyst: wide band gap semiconductor capable of converting light energy into chemical redox energy. Reversible/switchable superhydrophilic and superhydrophobic properties. 	<ul style="list-style-type: none"> Size and shape dependent optical properties. Surface plasmon band (SPB) tuned by nanoparticle size, shape and surface functionalities. Oscillation frequency influenced by dielectric constant of surrounding materials and types of solvent used. Electromagnetic properties influenced by degree of dispersion and proximity. Colors highly dependent on interparticle distance where a color shift from red to blue results when individual spherical AuNPs aggregates and comes into proximity. (interparticle plasmon coupling). 	<ul style="list-style-type: none"> Properties dependent on size, shape, synthesis method and differences in dielectric environment. Good conductivity. Chemical stability. Antibacterial and antimicrobial. Highest efficiency of plasmon excitation among all three metals (Ag, Au and Cu) - plasmon resonances within visible spectrum. Highest SERS signal enhancement among other metal nanoparticles.
Common Methods of Synthesis	<ul style="list-style-type: none"> Solution routes: <ul style="list-style-type: none"> - Precipitation. - Sol-gel: non-alkoxide and alkoxide. - Combustion. - Electrochemical. Gas phase method: <ul style="list-style-type: none"> - Chemical Vapor Deposition. - Physical Vapor Deposition. - Spray Pyrolysis Deposition. 	<ul style="list-style-type: none"> Bottom up (chemical): <ul style="list-style-type: none"> - Nanosphere lithography. - Citrate reduction method. - Seeding technique. - Two-phase reaction. Top down (Physical): <ul style="list-style-type: none"> - Photolithography. - Electron beam lithography. 	<ul style="list-style-type: none"> Bottom up (chemical): <ul style="list-style-type: none"> - Lee-Meisel method. - Borohydride, citrate, ascorbate, and elemental hydrogen reduction. Top down (Physical): <ul style="list-style-type: none"> - Microwave irradiation. - Photo-reduction. - Microemulsion. Biological: <ul style="list-style-type: none"> - Enzymatic reduction. - Non-enzymatic reduction.

General Applications	<ul style="list-style-type: none"> • Photocatalysis. • Stain-proofing and self-cleaning. • Gas and humidity sensors. • Photovoltaics. • Photocleavage of water. • Photodegradation of organic pollutants. 	<ul style="list-style-type: none"> • Homogenous and heterogeneous catalysis. • Biosensors. • Drug and protein delivery. • SERS. • Anti-counterfeiting. 	<ul style="list-style-type: none"> • Excellent catalyst. • Antimicrobial products. • Colorimetric sensor. • Enhanced Infrared absorption spectroscopy. • SERS. • Anti-counterfeiting.
-----------------------------	---	---	---

1.2.4 Attachment Methods of Nanoparticles to Paper

There are many publications and patents describing methods of attachment/binding of nanoparticles onto paper, particularly for TiO₂-functionalized paper. A brief review of the major strategies is presented in this section. Basically, there are two approaches for attaching nanoparticles onto paper, “wet-end addition”, where nanoparticles are adhered onto individual fibers before paper sheet formation, and “surface treatment”, where dry paper sheet is impregnated with nanoparticles by passing through a bath of chemicals which impregnates the paper surface or by coating [35].

1.2.4.1 Wet-end Addition

Wet-end addition is more commonly used to prepare TiO₂ photocatalytic paper. Fukahori *et al.* [36] and Iguchi *et al.* [37] produced photocatalytic papers, which are made of TiO₂ supported by ceramic fibers, using the wet-end addition process. A TiO₂-containing paper of high stability was fabricated by preferential immobilization of photoactive TiO₂ nanoparticles onto the inorganic fibers, followed by incorporation into the layered pulp fiber network. This TiO₂ paper was made from beaten pulps and ceramic fibers according to Technical Association of the Pulp and Paper Industry (TAPPI) Test Methods T205. As shown in Figure 4, the TiO₂ paper displayed a remarkably higher photocatalytic performance than TiO₂ powder and pulp mixture. This synergy is due to the paper’s macrovoid structure, and the paper strength is maintained by presence of the ceramic and TiO₂ fiber matrix. However, the retention of TiO₂ on the paper surface may be insufficient due to drainage force occurring during the filtration process.

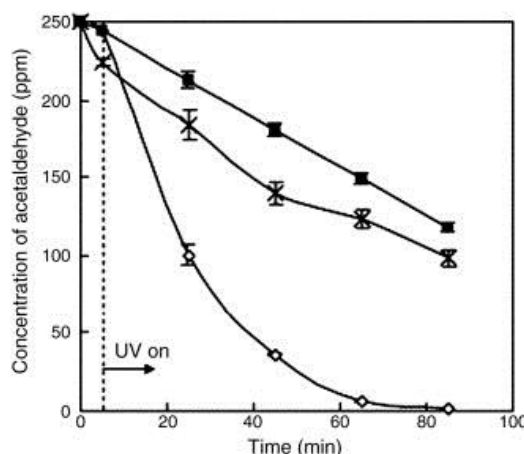


Figure 4: Photodecomposition of acetaldehyde vapours by TiO₂ powder (crosses), TiO₂ paper (open diamonds) and pulp/TiO₂ mixture (closed squares). Reprinted from [36], Copyright (2007), with permission from Elsevier.

A patent by Nishibori [38] explained preparation of molded photocatalytic pulp from waste paper (preferably from newspaper) and TiO₂ using a thermoplastic resin in a dry forming process. The process involved stirring a photocatalytic pulp mixture comprise of pulp, TiO₂ and thermoplastic resin (which acts as a binder). The heat and impact force generated by shearing were used to dry the mixture and drive the TiO₂ nanoparticles to the fiber's surface. Next, a foaming agent was added into the photocatalytic pulp, followed by molding, drying and laminating to produce a laminated photocatalytic paper. The foamed and molded photocatalytic paper has high air and water permeability which serves as an excellent photodecomposition filter.

1.2.4.2 Surface Treatments

Surface treatments are more promising than the wet-end addition, since nanoparticles can be concentrated near the paper surfaces. The extent of penetration of the nanoparticles into paper is controllable by the paper's hydrophobicity (sizing) and porosity (paper structure). There are different types of surface treatments, but we only intend to review the major existing methods to coat or impregnate nanoparticles onto paper, which are size press, layer-by-layer deposition (LbL), sol-gel method, direct assembly and *in situ* assembly.

1.2.4.2.1 Size-press Treatment

Dry paper sheets are generally coated with a mixture of TiO_2 and different types of binder, to produce photocatalytic paper by using a size press in the papermaking process. [35]. There are several patents which incorporate different binders to coat TiO_2 onto paper substrates. For instance, colloidal silica used by Ahlstrom [39], resin binders used by Eln Kohsan Co. [38] and silicone binders used by Nippon Soda [40]. These binders play an important role in immobilizing TiO_2 onto paper and protecting the paper from photodegradation by TiO_2 at the same time. Aguedach *et al.* [41] and Railard *et al.* [42] also coated paper with a mixture of TiO_2 and colloidal silica using a size press. These studies highlighted the role of silica binder in increasing adsorption capacity of TiO_2 to produce an efficient photocatalyst which is able to decompose textile dye in wastewater. Compared to TiO_2 powder, the textile dye removal by the photocatalyst paper, which consists of silica supported TiO_2 , is more economical and effective since it avoids the tedious and costly filtration step of TiO_2 from the water. However, characterization of the TiO_2 coating, such as thickness and distribution, was not studied; this knowledge is crucial in determining the optimum efficiency of photocatalysis.

1.2.4.2.2 Layer-by-layer Deposition (LbL)

LbL deposition is a technique based on adsorption of oppositely charged polyelectrolytes on a solid substrate (Figure 5). Lu *et al.* [43] coated lignocellulose fibers with well-organized multilayers of linear polyelectrolyte and TiO_2 . Positively-charged TiO_2 nanoparticles were alternately attached onto the surface of the wood fibers with negatively-charged Poly(styrenesulfonate) (PSS), using the standard LbL assembly process. During the adsorption of TiO_2 , some hydrogen bonding between lignocellulose fibers and TiO_2 were replaced by electrostatic attraction of the positive and negative polyelectrolyte fiber coatings. This electrostatic bonding between fibers and fillers was able to increase the paper's dry strength drastically. Thicker layers of polyelectrolyte increased the fiber interactions in paper, producing structures of higher dry strength and porosities. However, wet strength of the resultant paper, which is important for photocatalytic usage in water, was not discussed in their work. Although increasing the thickness of polyelectrolyte layer increases the paper's strength, it also causes TiO_2 nanoparticles to pile up and shield themselves from light and pollutants, reducing their photocatalytic activity. Therefore, an optimum TiO_2 and polyelectrolyte layer thickness

must be obtained to achieve high photocatalytic efficiency without compromising the paper strength.

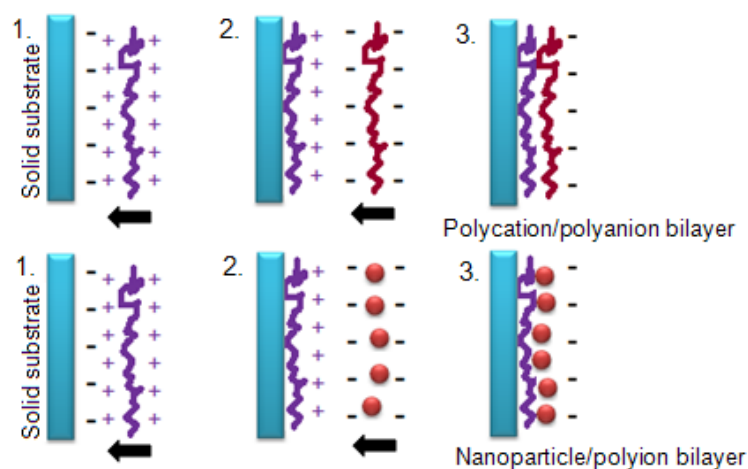


Figure 5: Layer-by-layer coating method. (redrawn from [44]).

Pinto *et al.* [45] also synthesized and deposited silica-coated AuNPs onto cellulosic fibers. This was the first time that cellulose was used as substrate for LbL assembly of AuNPs. The cellulose fibers were previously treated with polyelectrolytes to provide cationic charge by alternate dipping in poly(diallyldimethylammonium chloride) (polyDADMAC), poly(sodium 4-styrenesulfonate (PSS), and again in the polyDADMAC solutions (the basis of the layer-by-layer method). These treated cellulose fibres were then immersed in the Au colloids. The silica shells ensured that the individual Au cores were well separated, and prevented variation of plasmon oscillation frequency in the final assemblies. The adjustable optical properties, which can be obtained by modifying the surface of nanoparticles with silica shells, made these nanocomposites very attractive, particularly in the manufacture of security paper [45]. Since it is important to prevent aggregation of AgNPs which will reduce their antimicrobial efficiency, this method could also be applied for AgNPs to develop antimicrobial paper, since the silica shells are able to maintain a good distribution of nanoparticles on the cellulose surface. However, diffusion of nanoparticles into the polyelectrolyte macromolecule should be further studied because this would reduce their contact with light and pollutants, thus decreasing their performance.

1.2.4.2.3 Sol-gel Method

Sol-gel method for deposition of TiO_2 onto cellulose fibers is developed from the processing of sol-gel TiO_2 composites. It introduces negatively-charged functional groups which anchor TiO_2 on cellulose surfaces [46]. Uddin *et al.* [46] developed an easy and reproducible procedure for anchoring TiO_2 to cellulose by sol-gel technique, to produce self-cleaning, antibacterial and photochromic surfaces. Continuous and homogeneous distribution of TiO_2 films was formed on the surface of fibers, thus enhancing photodegradation of pollutant molecules. The TiO_2 film did not promote a simultaneous degradation of cellulose fibers, even though it was highly efficient in pollutant degradation. They suggested that this is due to the homogeneous characteristics of the TiO_2 film which completely adheres and protects the fibres from attack by O^{2-} and OH^\bullet species generated during the exposure to light.

1.2.4.2.4 Direct Assembly

In direct assembly, AuNPs and AgNPs are usually synthesized by citrate reduction of aqueous Au and Ag salt solutions and then assembled onto paper. The citrate groups serve the dual role of reducing agent and stabilizer [47]. They impart negative surface charges to nanoparticles from weakly bound citrate ions, which prevent agglomeration in solution and immobilize them on the substrates through electrostatic self-assembly [48].

Dong and Hinestroza [47] made cationic cellulose from cotton via grafting of positively charged ammonium ions for electrostatic deposition of AuNPs. The AuNPs are directly assembled onto cellulose by immersing cationic cellulose into a citrate-reduced Au colloidal solution. Increasing concentration of the citrate enhanced negative surface potential of AuNPs and led to higher packing density of AuNPs on the substrate. Their procedure shows promise to allow deposition of other negatively charged metal nanoparticles onto cationically-modified cellulose substrates. Yet, the adsorption state of nanoparticles must be controlled to achieve a reproducible distribution, since it affects optical properties of the nanoparticles.

Wu *et al.* [15] and Ma *et al.* [49] performed direct synthesis of gold and silver colloids by chemical oxidation-reduction reactions, using potassium tetrachloroaurate (KAuCl_4) and silver nitrate (AgNO_3). The resulting colloids were added drop wise onto filter papers for

SERS application. These studies illustrate the high potential of nanoparticles coated paper as a highly SERS active substrate. However, the spotting method described is not able to provide a reproducible and uniform distribution of nanoparticles on paper substrates as more aggregation will be formed at the edge of the droplets during the drying process (coffee stain phenomenon). Position of laser beam on the nanoparticles' droplets during the SERS experiment was not specified in these studies (either on the edge or the center of the nanoparticles' droplet). This is critical because the aggregation state of nanoparticles is the main contributing factor to the SERS performance.

In another interesting approach, Zhao *et al.* [16] synthesized DNA crosslinked AuNPs to produce a thermally-stable bioactive paper. Thiol-modified DNA was added to a citrate-reduced AuNP solution for DNA coupling. The blue colored DNA-cross-linked AuNP aggregates were then deposited on paper substrates. When endonuclease and adenosine were present, the bioactive paper degraded the crosslinked AuNP aggregates producing a deep red color. DNA crosslinked AuNPs were spotted on different types of paper substrates. Hydrophobic and (poly(vinyl alcohol)-coated) hydrophilic paper were found to be the best biosensor substrates, whereas untreated hydrophilic paper caused "bleeding" and precipitation resulting from surface drying [16]. This work demonstrates the feasibility of functionalizing paper substrates with AuNPs to produce an effective, renewable and disposable bioactive paper. Nanoparticles can be dried on paper, heated and stored whilst still maintaining their aggregation/dispersion, as well as their activity upon subsequent exposure to target analytes.

1.2.4.2.5 *In situ* Assembly

In situ assembly is initiated by attaching metal complex ions onto cationically-modified cellulose surfaces. Dong and Hinestroza [47] performed this method by a first immersion of cationic cellulose substrate into a sodium tetrachloroaurate dihydrate ($\text{NaAuCl}_4 \cdot 2\text{H}_2\text{O}$) solution, followed by immersion in a sodium borohydride (NaBH_4) solution to reduce the metal ions to zero-valence metal. Compared to the direct assembly method, *in situ* assembly does not require protective citrate ions. The absence of citrate ions can be helpful in applications such as catalysis, since their surface coverage may reduce the reactivity of the nanoparticles [47]. However, no comparison between surface coverage or

adsorption state of AuNPs on the paper substrates produced by both direct and *in situ* methods has been presented.

Cai *et al.* [50] performed another *in situ* formation of AuNPs in cellulose gel by physical reduction method. Transparent cellulose hydrogel films were immersed in a HAuCl_4 solution, followed by heating at 80°C for 24 h to achieve hydrothermal reduction. Highly dispersed and thermally-stable AuNPs were formed in the cellulose gels [50]. The high porosity, near transparency and high mechanical strength of these AuNPs impregnated cellulose gels offer an attractive substrate for nanoparticle synthesis/support medium. This composite material is interesting for use in molecular detection via transmission UV-Vis spectroscopy.

The presence of molecules will change the dielectric constant of the AuNPs and produce a shift in their absorbance peak. However, distribution reproducibility of AuNPs within the cellulose gels needs to be addressed.

He *et al.* [51] performed *in situ* synthesis of AgNPs in the porous cellulose fibers from lint-free cellulose paper and filter paper. The size distributions of the nanoparticles were controlled by adjusting synthesis conditions such as the concentration of metal ion, resulting in monodispersed metal nanoparticles. The ether oxygen and hydroxyl groups of cellulose bind the metal ions tightly onto the fibers through ion-dipole interactions and stabilize AgNPs by strong bonding with their surface metal atoms.

Fernández *et al.* [52] found that nanoparticle size is important for high antimicrobial activity; samples, with large, aggregated AgNPs being almost ineffective. They performed *in situ* synthesis of AgNPs in fluff pulp and nanostructured Lyocell fibers by immersion in AgNO_3 , and subsequent transformation of the attached silver ions into AgNPs by physical (thermal/UV) and chemical (NaBH_4) reduction. The AgNPs formed by physical methods were uniform in shape and well distributed, whilst chemical reduction produced aggregation of AgNPs [53]. This finding is important because both methods can be used for different applications; e.g. physical methods can be applied to produce antimicrobial paper (where well distribution of AgNPs is preferred), whilst chemical methods can be used to produce a SERS-active substrate (where aggregation of AgNPs is preferred).

1.2.5 Applications of Nanoparticles-functionalized Paper

1.2.5.1 Titania Paper

1.2.5.1.1 Self-cleaning

The unique combination of photocatalytic and hydrophilic properties of TiO_2 has markedly increased their application range, especially as a coating on cellulosic materials such as paper [54]. The ability of water to soak between stain and highly hydrophilic TiO_2 surface results in easy and efficient stain removal. Hence, TiO_2 -coated surfaces have been widely used in outdoors. An example is a Japanese paper window blind with excellent self-cleaning properties, wherein stain is decomposed by photocatalysis and washed off by rainfall.

In a related area, Uddin *et al.* [55] developed cotton fibers covered by a thin Au/TiO_2 film which are also photocatalytically-active under solar light. The Au/TiO_2 -covered cotton fibers show high efficiency in Methylene Blue (MB) photodegradation, suggesting highly photocatalytic properties under solar light. The sol-gel synthetic method covers the cotton fibers with TiO_2 and Au/TiO_2 films, which ensured a great stability for repeatable washing cycles and prolonged photodegradation. These composite cotton fibers show high potential and commercial significance for self cleaning under visible light [55].

1.2.5.1.2 Organic Destruction

Organic destruction is a common mechanism where organic targets, such as organic dye and volatile organic compounds (VOCs), are adsorbed onto TiO_2 surface via attachment by reactive oxygen species (ROS), or direct oxidation by donating electrons to trapped holes on the TiO_2 surface [35]. Matsubara [22] and Iguchi *et al.* [37] described the preparation of TiO_2 handsheets and their use to decompose acetaldehyde vapors; and since then many studies have improved the photocatalytic properties of TiO_2 paper in terms of organic destruction. Commercial TiO_2 paper-based products have been extensively used as air filter papers, wallpapers, calendars, writing papers and magazines [37].

Hashimoto *et al.* [24] designed photocatalytic sheets to sanitize VOCs-polluted soil by using natural sunlight. As shown in Figure 6, the photocatalytic sheet is made of corrugated paper consisting of TiO_2 attached on activated carbon powders. Polluted soil

can be purified by covering it with the sheet, followed by heating via mixing with calcium oxide. This procedure volatilizes the pollutant gases, which then adsorb on the activated carbon of the sheet. TiO_2 subsequently decomposes the pollutants by photocatalytic mechanism.

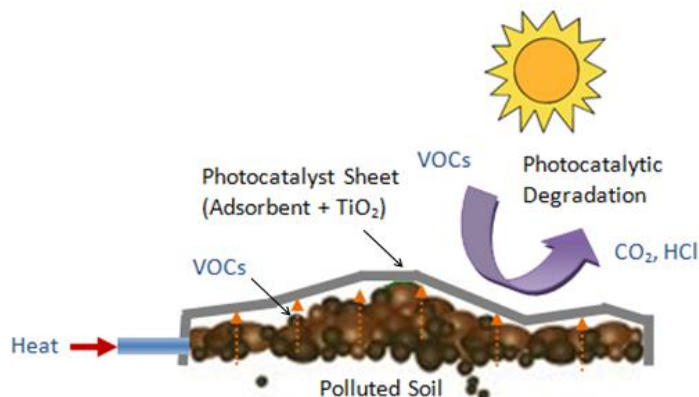


Figure 6: Purification of polluted soil using solar energy and photocatalytic TiO_2 paper. (redrawn from [54]).

According to Pelton's review [35], there are a few commercial applications of photocatalytic TiO_2 paper. Ahlstrom has made photocatalytic nonwoven products since 1996 [56]. Nippon Paper (Tokyo, Japan) has developed "Light Catalytic Newsprint" with Yomiuri, one of Japan's largest newspaper publishers [57]. The newsprint contained TiO_2 which cleaned the surrounding air photocatalytically when irradiated by UV and visible light (Figure 7). Nippon Paper [57] has also produced air-deodorizing tissue box which can purify air for babies, rooms with pets and the interior of vehicles.

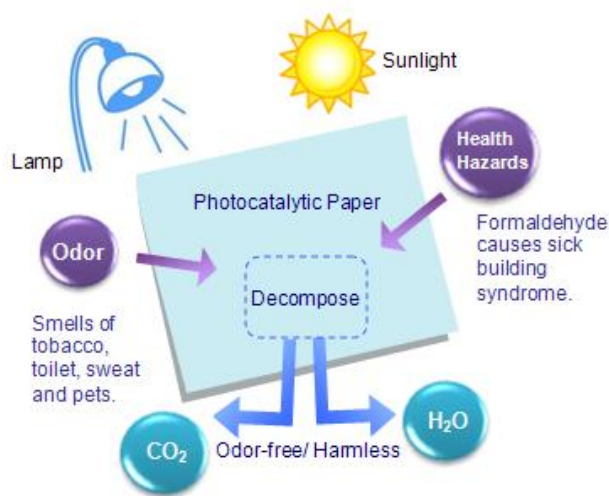


Figure 7: Organic destruction by photocatalytic paper. (redrawn from [58]).

1.2.5.1.3 Disinfection

TiO₂ paper can detect pathogenic organisms and disinfect, by destroying their cellular structure. Most common disinfection technologies are insufficient to kill microorganisms since some generate exotoxins (heat sensitive proteins) and endotoxins (lipopolysaccharides) that remain after the bacteria is eliminated [35]. However, it was shown that TiO₂ can destroy the endotoxins which are associated with *Escherichia coli* (*E. coli*) photocatalytically. Matsubara *et al.* [22] reported that *E. coli* on TiO₂-containing paper was almost completely disinfected by 90 minutes upon UV light irradiation. Geng *et al.* [12] studied the feasibility of producing paper with antibacterial properties based on the photocatalytic activity of TiO₂; 80% of the bacteria deposited onto the photocatalytic paper were killed by 30 minutes exposure to 25 W/m² UVA [12]. It was discovered that the water content of the paper must be at least 40%, and that the TiO₂ must be well positioned on the exposed surface to attain this good performance.

The market for antibacterial paper containing TiO₂ is significant. Domtar [59] launched North America's first antimicrobial office paper for protection against bacteria growth, surrounding odours, fungus, mould and mildew in order to reduce the propagation of bacteria in offices. Japan [60] developed the technology to adhere small amounts of anatase TiO₂ to pulp. They produced an antibacterial wall paper which utilized paper's natural porous surface to absorb bacteria or hazardous substances floating within a hospital room, and paper's filtering function to fully decompose them.

1.2.5.2 Gold Nanoparticle Paper

1.2.5.2.1 Colorimetric Sensor

Innovative developments in bioactive papers and paper microfluidic system can be found with applications in blood testing [6], biomolecular stability [61-63] and functional printing [64-65]. Martinez *et al.* [66] demonstrated the prospect of paper as a platform for bioassays where dye molecules were responsible for color changes that were altered by enzymatic reactions. Since then, the potential of AuNPs (which possess a higher extinction coefficient than dye molecules on paper) as a biosensor has been explored. Liu and Lu demonstrated a AuNPs' dipstick assay in their publication [67] and patent [68]. This dipstick assay detects target analytes by immersing a lateral flow device into a testing solution. Blue-colored aggregates of AuNPs were immobilized on the lateral flow

device. They were broken into red-colored dispersed AuNPs upon addition of target analytes in the flow buffer (Figure 8). However, these devices involve rather complicated components such as wicking pads, conjugate pads, polymer membranes, absorbent pads and plastic adhesive backing, which may limit their practical use.

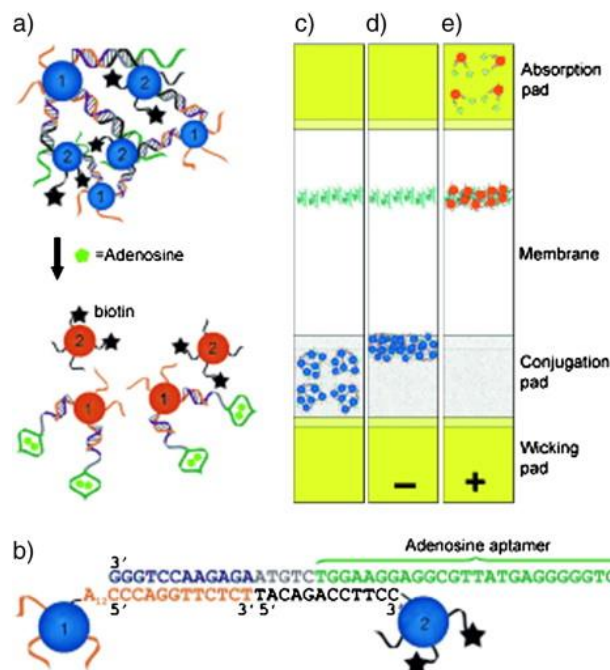


Figure 8: Aptamer (nucleic acid that specifically binds a target compound or moiety)/nanoparticle-based lateral flow device. (a) Blue color of AuNP aggregates is broken into red colored AuNP dispersion upon the addition of adenosine. (b) DNA sequences and linkages in AuNP aggregates. Lateral flow devices loaded with the aggregates (on the conjugation pad) and streptavidin (on the membrane in cyan color) (c) before use and in (d) negative or (e) positive test. Reprinted with permission from [67]. Copyright 2010 WILEY-VCH.

Zhao *et al.* [16] prepared a paper-supported AuNPs biosensor (gold bioactive paper) which is capable of detecting the presence of DNase I, an endonuclease (Figure 9), as well as adenosine, a small biomolecule (Figure 10). This sensitive biosensor can be dried on paper, heated and stored while still maintaining its activity during the detection of target solution. Basically, it functions based on the unique SPR of AuNPs: well-dispersed AuNPs show a red color; whereas aggregated AuNPs have a blue or purple color. These significant color changes can be detected whenever the aggregation and redispersion of AuNPs are triggered by a target analyte or a biological process. Since the interparticle

plasmon coupling results in a huge absorption band shift (up to 300 nm), the color shift can be observed instantly by naked eye without analytical instrumentation [16].

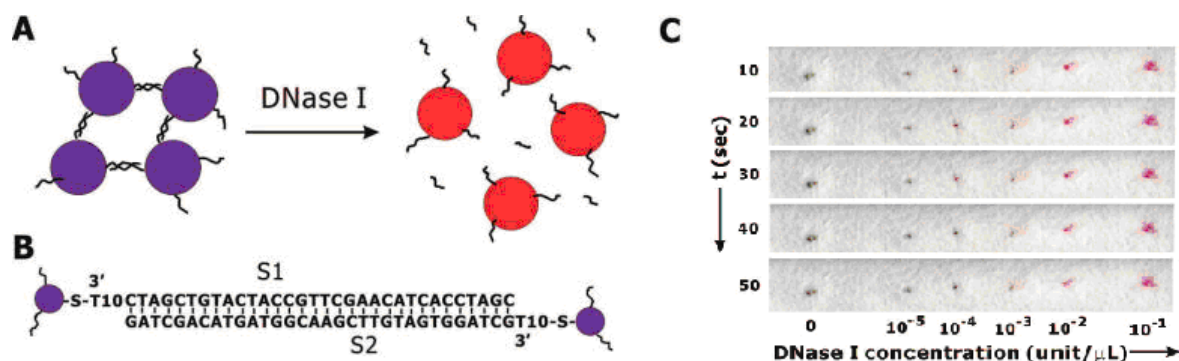


Figure 9: DNase I-sensing bioactive paper. (A) Color shift from blue to red when redispersion of DNA crosslinked AuNP aggregates is triggered by the addition of DNase I. (B) The sequences of DNA oligonucleotides. (C) Reaction of DNase I assay on PVA-coated hydrophilic paper [16], Copyright (2008), with permission from American Chemical Society.

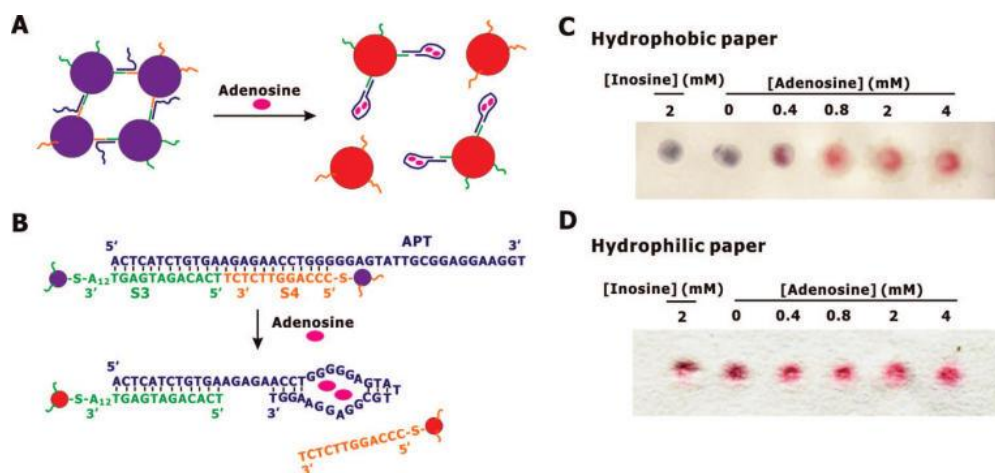


Figure 10: Adenosine-sensing bioactive paper. (A) Color shift from blue to red when redispersion of DNA crosslinked AuNP aggregates is triggered by the addition of Adenosine. (B) The sequences of the DNA molecules used. (C) and (D) Reaction of Adenosine assays on hydrophobic and hydrophilic paper. Reprinted from [16], Copyright (2008), with permission from American Chemical Society.

By controlling the interparticle distance of the AuNPs, their corresponding aggregation and dispersion can give visual detection for a wide range of biological entities. This makes AuNPs a perfect transmitter for paper-based assays. Furthermore, the AuNPs

sensor is cost effective, as only small volumes (1 μL in the Zhao's work [16]) of both DNA-AuNPs aggregate probes and target samples are required due to the exceptionally high extinction coefficient of AuNPs.

1.2.5.2.2 Rewritable Paper

Klajn *et al.* [69] developed a novel self-erasing material which consists of AuNPs and AgNPs embedded in thin, flexible organogel films. Both “writing” and self-erasure of color images are controlled by dynamic non-equilibrium aggregation of the NPs (Figure 11). Upon exposure to UV light, the trans-4-(11-mercaptoundecanoxy)azobenzene (trans-MUA) groups, which coat the NPs, isomerize to cis-azobenzene (cis-MUA), having a large dipole moment [69]. The NPs then aggregate into supra-spherical (SS) assemblies, whose apparent color depends on the duration of UV irradiation.

Since the SS are metastable and fall apart spontaneously in the absence of UV irradiation, the two-color or multicolor images written onto the films gradually self-erase. Erasure times can be controlled by the number of dipoles induced on the NPs, and can also be accelerated upon exposure to visible light or heat [69]. Multiple images can be written into the same film, either concurrently or sequentially after erasure.

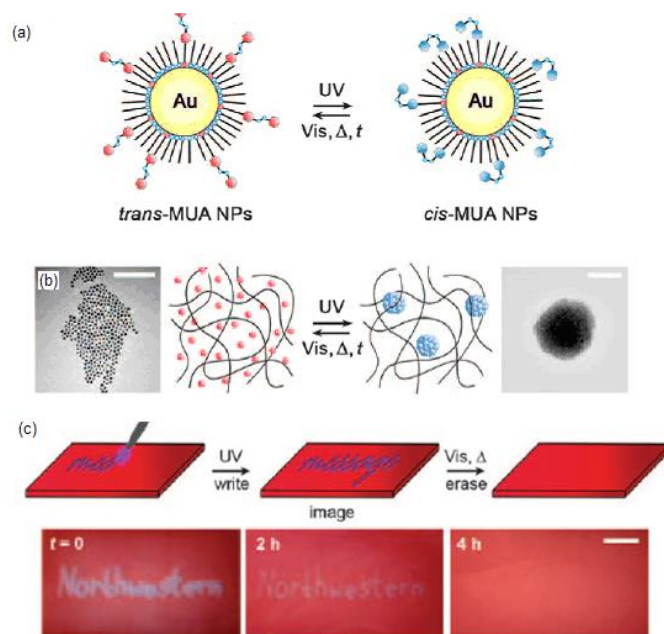


Figure 11: Self-erasing films for rewritable paper. (a) Upon UV irradiation, trans-MUA coated AuNPs isomerize to cis-MUA. **(b)** During UV irradiation, photoactive

AuNPs (red) form metastable aggregates (blue) (c) Writing into AuNPs film using a light pen ($I_{UV}=10 \text{ mWcm}^{-2}$) at 3 mms^{-1} . Reprinted with permission from [69]. Copyright 2009 WILEY-VCH.

These materials are practical for storing temporary information such as self-expiring tickets. However, the organogels used are not environmentally-friendly, hence alternative substrates, such as paper, and technologies, such as coating and printing, should be explored.

1.2.5.2.3 SERS

Surface-enhanced Raman scattering (SERS) using AuNPs is an exceptional technique for quantifying the adsorption of target molecules on substrates, and allowing different orientations and interactions of the molecules with the substrates to be determined [15]. Single molecule detection is achievable via SERS and this concept has been used to design protein and nucleic acid biosensors [70].

A highly SERS-active substrate is the most important factor in producing efficient SERS applications. Previously, aqueous metal colloids were employed in most SERS techniques, but this limits the application of SERS since the specimen analyzed must be water-soluble. To overcome this restriction and enhance the SERS techniques, solid and rough SERS-active surfaces such as nanorod arrays on glass [71], metal island films formed through thermal evaporation [70, 72] and laser ablated metal plates [73] were explored. However, these methods involve complex preparations of substrates, which limit the applications of SERS. Filter paper coated with AuNPs offers a much simpler method and the compounds examined do not have to be water-soluble.

Luo *et al.* [74] and Ma *et al.* [49] demonstrated the use of AuNPs-coated filter paper in a variety of SERS measurements. They studied the SERS of C60/C70 adsorbed on filter paper coated with highly SERS active AuNPs. This AuNPs paper had a greater enhancement factor than AuNPs solution, since it was not influenced by solvents in a C60/C70 solution or water in gold hydrosols [74]. They discovered that the distribution and aggregation of AuNPs strongly influenced the SERS intensity of C60/C70 and that the Raman intensity saturated as the thickness of AuNPs coating was increased. However,

the ideal aggregation state of nanoparticles and paper structure were not identified nor explored.

Niu *et al.* [53] also reported SERS spectra of single-walled carbon nanotubes (SWCNTs) on AuNPs-coated filter paper. Enhancement of common Raman spectrum of SWCNTs, as well as several new bands, were obtained (Figure 12) [53]. These produced an excellent sensor for analyzing fine molecular structures. Furthermore, this method is promising and highly sensitive for examining feature of SWCNTs, compared to the existing methods.

SERS spectra of p-, m-, and o-nitroaniline (PNA, MNA, and ONA) adsorbed on AuNPs were also studied by Ma *et al.* [49] on dried AuNPs-coated filter paper. They found that the coverage density of AuNPs affected the SERS spectra of the PNA molecules, but did not affect MNA and ONA. The adsorption performance of molecules is dependent on the substrate's surface and the surface configurations of adsorbate. This demonstrates the potential of AuNPs-coated filter paper as a powerful tool for studying the surface configuration of molecules in SERS applications. However, little information on the AuNPs–paper interaction or their heterogeneity has been provided.

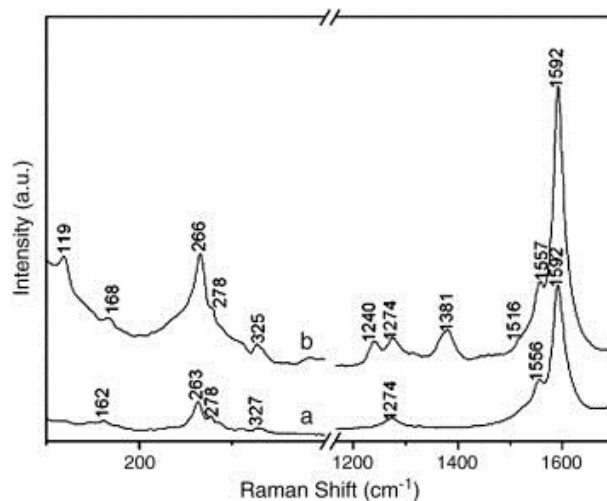


Figure 12: (a) Raman spectrum of SWCNTs and (b) SERS of SWCNTs on gold coated filter paper. Reprinted from [53], Copyright (2006), with permission from Elsevier.

1.2.5.3 Silver Nanoparticle Paper

1.2.5.3.1 Antimicrobial

With increasing awareness of disease and infection transmissions from microorganisms, the number of antimicrobial products such as protective clothing for medical and chemical works, antibacterial packaging materials and tissue papers has recently increased. AgNPs are well known for their broad spectrum antimicrobial activity. They deactivate bacteria by interacting with thiol groups of bacterial proteins and enzymes [32].

Fernández *et al.* [52] studied cellulose substrates as holders of AgNPs to form a cellulose-AgNPs hybrid material in order to preserve aseptic conditions in an absorbent pad. Relationships between both Ag ion release and antimicrobial efficiency against *E. coli* and *Staphylococcus aureus* bacteria were confirmed. Furthermore, the highest concentrations tested were able to decrease microbial content in poultry exudates. Therefore, AgNPs shows high potential to be used in the food industry. In a separate study, Tankhiwale and Bajpai [13] developed AgNP-loaded filter papers with excellent antimicrobial properties against *E. coli* (Figure 13). The degradable nature of paper makes it an attractive alternative for antibacterial food-packaging material, as a replacement for synthetic polymeric films [13]. However, the effects of distribution and bonding strength of AgNPs on the paper structure were not reported.

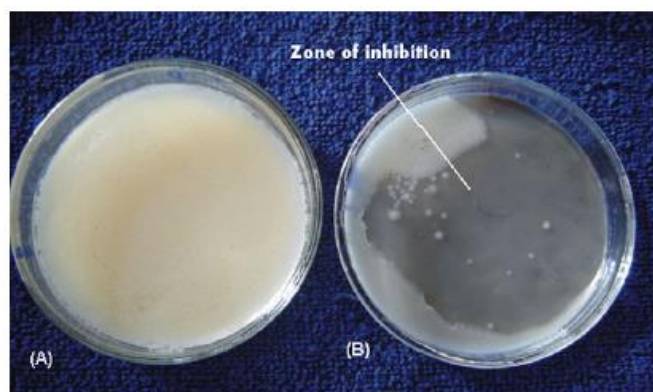


Figure 13: (A) Growth of bacterial colonies around grafted filter paper (B) zone of inhibition around the AgNPs loaded grafted filter paper. Reprinted from [13], Copyright (2009), with permission from Elsevier.

1.2.5.3.2 SERS

Similar to AuNPs, AgNPs can also be coated on paper to produce a highly SERS-active substrate. Niu *et al.* [53] obtained a SERS spectrum of Single Wall Carbon Nanotubes (SWCNTs) on AgNPs-coated filter paper which can be used as a highly sensitive probe for analyzing the synthesis quality of SWCNTs (Figure 14). The AgNPs SERS substrates have a higher Raman signal enhancement than AuNPs. However, since the Ag metal surface tends to oxidize in air, it has a limited durability as a SERS substrate compared to AuNPs [75].

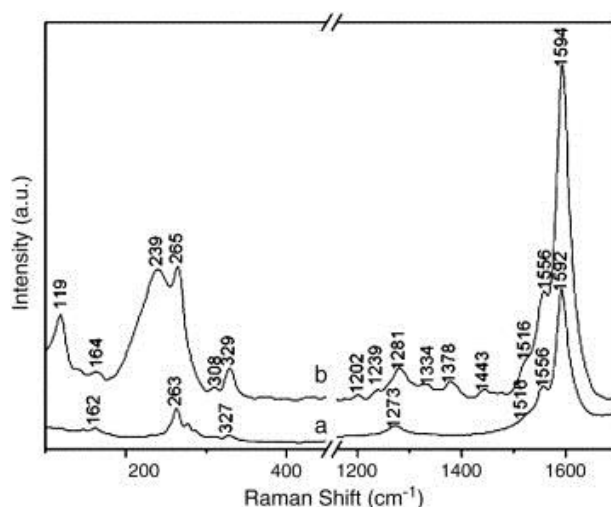


Figure 14: (a) Raman spectrum of SWCNTs and (b) SERS of SWCNTs on silver coated filter paper. Reprinted from [53], Copyright (2006), with permission from Elsevier.

Wu *et al.* [15] also obtained excellent SERS signals of p-hydroxybenzoic acid (PHBA) on AgNPs-coated filter paper. The adsorption state of PHBA molecules on AgNPs-coated filter paper was unlike the adsorption in the AgNPs colloid. The molecules were located in an upright position on the surfaces of the AgNPs colloids through the carboxyl moiety, but were tilted between the benzene ring and the surfaces of AgNPs on the filter paper [15]. As shown in Figure 15, AgNPs-coated filter paper provided higher SERS signal of PHBA than AgNPs colloid.

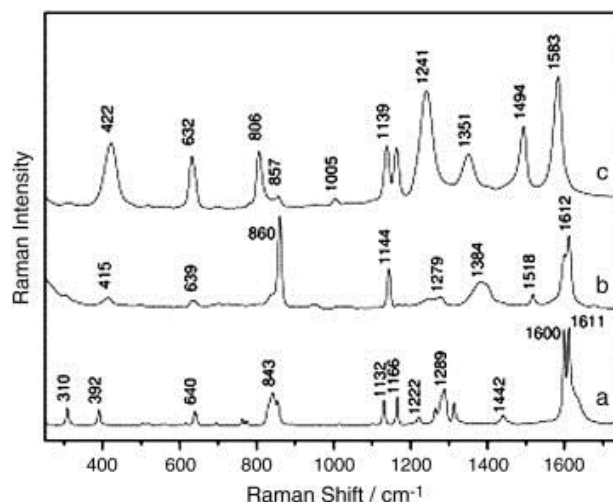


Figure 15: (a) Raman spectrum of solid PHBA (b) FT-SERS spectra of PHBA in AgNPs solution and (c) on AgNPs-coated filter paper. Reprinted from [15], Copyright (2003), with permission from Elsevier.

Laserna *et al.* [76] [77] [70] reported the assembly, morphology and optical properties of AgNPs-coated filter paper as a promising substrate for SERS. High and reproducible spectra of a range of ionic and molecular adsorbates including p-aminobenzoic acid, acridine, 9-aminoacridine, 2-aminoanthracene, 6-nitroquinoline and 5-aminoquinoline were achieved [78]. These filter-paper substrates could be used when a random dispersion of particle sizes and shapes is required, but were inadequate for theoretical studies requiring monodispersed systems. However, the main advantages of AgNPs-coated filter papers are their ease of use, low production cost and detection speed.

1.2.5.3.3 Anti-counterfeiting

Counterfeiting has increased around the world where almost all kinds of documents including banknotes, passports, certificates, bus and train tickets have been virtually forged [14]. More advanced security printing methods are continuously being designed to protect such documents, including security inks and security paper. Fluorescence plays a key function in many of these anti-counterfeiting technologies by identifying source subject from detected optical signal through irradiation [14]. However, fluorophores typically have low quantum yield and poor photostability, which lead to their photophysical limitation. AgNPs can augment the fluorescence emission intensity of up to 3000-fold upon close contact with the fluorophores and increase their detection limits [14]. Numerous studies have reported fluorescence emission from different AgNP

surfaces, such as AgNP colloids, nano-triangles and nano-rods, as well as fractal-like AgNP surfaces.

Zhang *et al.* [14] first reported metal-enhanced fluorescence (MEF) from AgNPs-coated filter paper. The luminescence intensities of Rose Bengal (RB) and Pt(II) octaethylporphine (PtOEP) were increased by 5- and 9-fold, respectively, on AgNPs-deposited paper substrates (Figure 16). The background luminescence emission from standard filter paper is rather large, but could be reduced subsequently by MEF. This work shows the great potential of AgNPs-functionalized paper to be used in security paper and anti-counterfeiting applications.

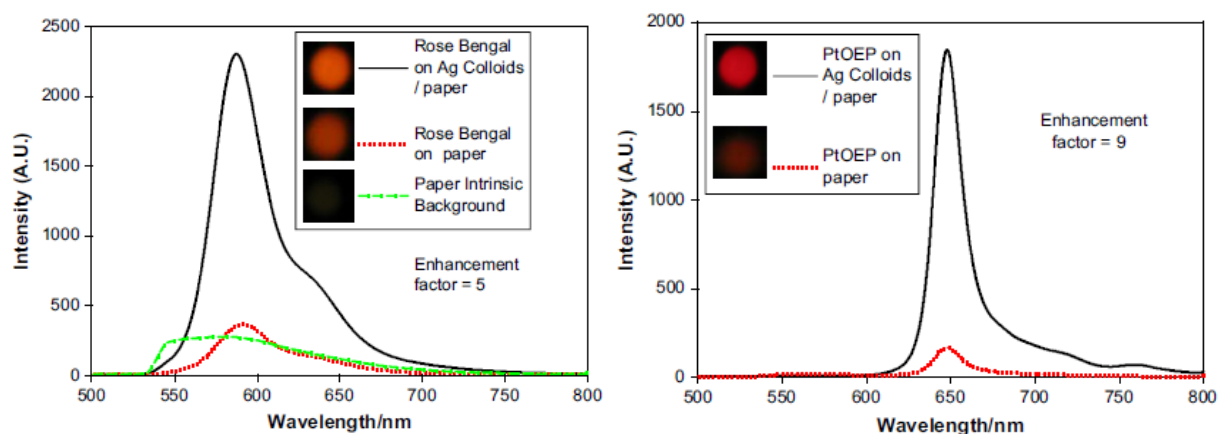


Figure 16: Fluorescence emission spectra of Rose Bengal on paper and Ag colloid deposited paper (left) and fluorescence emission spectra of PtOEP on paper and Ag colloid-deposited paper (right). Reprinted from [14], Copyright (2008), with permission from Elsevier.

1.2.6 Challenges and Opportunities

Most studies have relied on paper as an inert support for nanoparticles and very few, if any, have considered the distribution of nanoparticles in the three dimensions (3D) of paper, or the concept of heterogeneity and the effect of manipulating different length scales possible. Furthermore, little attention has been devoted to engineer the properties of nanoparticles-paper composite. In some instances of photocatalysis, SPR and SERS, nanoparticles on paper have provided better properties than unsupported nanoparticles (in air or in solution). Hence, there clearly remains some substrate-nanoparticles effect that can be optimized. Various nanoparticles-functionalized papers, which are reviewed in this

article, differ mostly in terms of type, size, shape, aggregation and content of nanoparticles, as well as their distribution within the 3D paper structure. The vast majority of studies used filter paper which is entirely made of cellulose fibers (cotton, softwood), without any additives such as fillers or dye. The structure, chemical composition and heterogeneity length scale of paper can now be well engineered and controlled with current technology. It is therefore of interest to investigate the optimal structure and chemical composition of paper for each application, whether it relies on SPR, SERS, colorimetric or photocatalytic principles. This section analyses the effect of heterogeneity, interaction between light with nanoparticles-functionalized paper (optical and photocatalytic properties) as well as their analytical techniques.

1.2.6.1 Paper Chemical and Physical Heterogeneities

Paper is a heterogeneous substrate involving many length scales of physical and chemical periodicity. Paper can be considered as a non-woven material made of short discontinuous fibers with additives. From a chemical point of view, paper is made of lignocellulosic fibers and functional additives. Commonly used additives are inorganic filler (calcium carbonate, titanium dioxide, kaolin), dyes (UV brightner, colour, anti-yellowing), sizing agents (Alkyl Ketene Dimer (AKD), Alkenyl Succinic Anhydride (ASA), rosin/alum), retention aids (polyelectrolytes: Polyacrylamide (PAM), Polyethyleimine (PEI); neutral polymers: Polyethylene Oxide (PEO), starch; and microparticles: bentonite, silica), coating (latex, starch, calcium carbonate, styrene maleic anhydride) and strength agents (Polyamide-epichlorohydrin (PAE), Carboxymethyl cellulose (CMC), Poly(diallyldimethylammonium chloride) (polyDADMAC)). As additives are normally added at 0.5 to 5 kg/Ton fibers and with processes to maximize the dispersion, they form distinct chemical domains on the fibers at a surface coverage typically ranging from 5 to 50%. The length scales of the chemical domains are in the order of 0.1 nm for the dyes, 10-50 nm for the polymer coils and polymer domains, 100-2000 nm for the fillers.

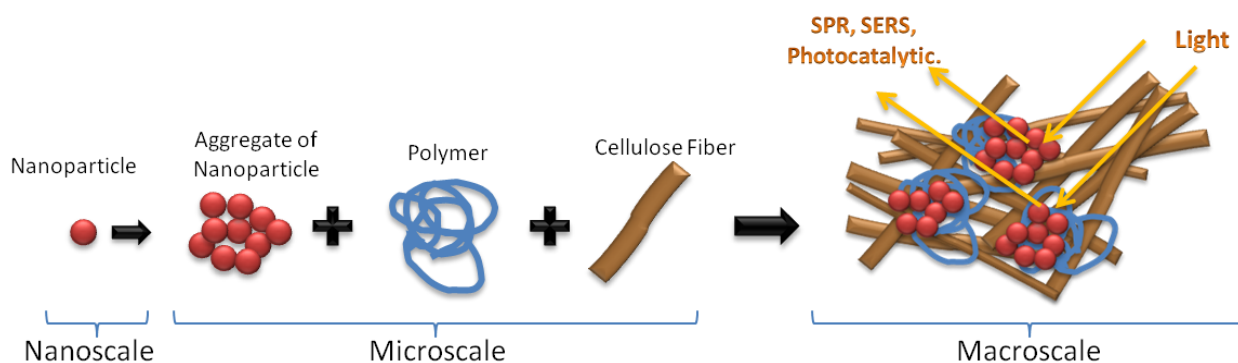


Figure 17: Different length scales of the constituents of paper.

Paper is mostly made of softwood fibers (length (L) = 2-3 mm, diameter (d) = 20-30 μm) or hardwood fibers (L = 1-2 mm, d = 10-20 μm) and fines/small fiber fragments (L = 50 μm , d = 1 μm). Figure 17 presents the comparative length scale of the paper constituents. From a physical aspect, paper has complementary length scales ranging over 7 decades, from the nanometer (nanoparticles) to the centimeter (fiber floc). Important physical heterogeneity is found in the 3D structure of paper. In the X-Y plane, there is a distinct fiber floc size distribution (often referred to as formation) and a preferential fiber orientation. Small fibers in a suspension have a tendency to flocculate as they lose some of their rotational and translation freedom due to a crowding effect amplified by the fiber concentration, rigidity and length. Since the fiber flocs are not completely destroyed during the dewatering process on the drainage wire, the paper web is made of periodic zones of high fiber density having diameters ranging from 2 to 12 mm. These flocculated zones have slightly different optical, strength and absorption properties than the bulk of paper.

Paper is made by impinging a suspension of cellulosic fibers onto a continuous wire moving (1000 to 2500 m/min) over a series of drainage elements. Any speed differential between the wire and the furnish solution therefore causes a preferential fiber alignment. In “*rushing*”, fibers are impinged at a velocity typically 5 to 50 m/min slower than the wire, therefore causing preferential fiber alignment in the machine direction (MD); in “*dragging*”, the fiber furnish is deposited at a faster speed than the moving wire, causing preferential alignment in the cross-machine direction (CD).

All these processes result in paper having a networked, heterogeneous and highly porous structure. Paper pore diameter ranges over five orders of magnitude, corresponding to interfiber gap (100 μm), cellulose fiber cell wall's pore (bordered pit with torus 1-10 μm) and fibrils' thickness and gap (nm). Hence, there are many capillarities in the pores in which nanoparticles can be attached.

1.2.6.2 Optical Properties

Amongst all of the unique properties of nanoparticles, their optical properties on novel substrate supports have gained the most research interests in chemical and biosensing. This is due to large electromagnetic fields generated in the vicinity of their surface when excited near plasmon frequency. High localization of this electromagnetic energy renders their optical properties as excellent SPR and SERS probes. Since the optical properties of nanoparticles are responsive to electric permittivity of their surrounding medium, they will also be affected by the presence of their substrates. Effects of substrates on the optical properties of nanoparticles are well addressed by a full numerical solution of Maxwell's equations [79] and other numerical techniques such as finite-difference time-domain [80] and discrete dipole approximation [81]. However, these methods do not account for substrate-nanoparticles interactions for heterogeneous substrates (e.g. paper) in which nanoparticles are absorbed within the cellulose fiber matrix. Consequently, there is still no clear understanding on how paper substrates can influence the optical properties of nanoparticles.

In this review, we proposed three important factors which affect the optical properties and light interactions between nanoparticles and paper substrates: (1) spatial location of nanoparticles, (2) refractive index of paper substrates and (3) aggregation state of nanoparticles within the cellulose fibers of paper substrates. As shown in Figure 18, the spatial location of nanoparticles after absorption on paper substrate (Figure 18b) is different compared to their location on flat substrates such as glass (Figure 18a). The penetration of nanoparticles through the rough and porous structure of paper will produce a different light interaction compared to a flat and nonporous substrate. To our knowledge, no study has analyzed the effect of refractive index and thickness of nanoparticles-impregnated paper (Figure 18c) on the optical properties of nanoparticles. We propose that the intertwined structure of cellulose fibers is able to retain the aggregate

state of nanoparticles upon drying (Figure 18d), which is important to control their SPR and SERS properties. However, the reproducibility of the aggregation and adsorption state of nanoparticles are restricted by the roughness and random fibrous morphology of paper substrates. Therefore, more in-depth studies are required to understand the optical properties of nanoparticles paper as functions of location of nanoparticles, refractive index, and aggregation state of nanoparticles within the paper substrates.

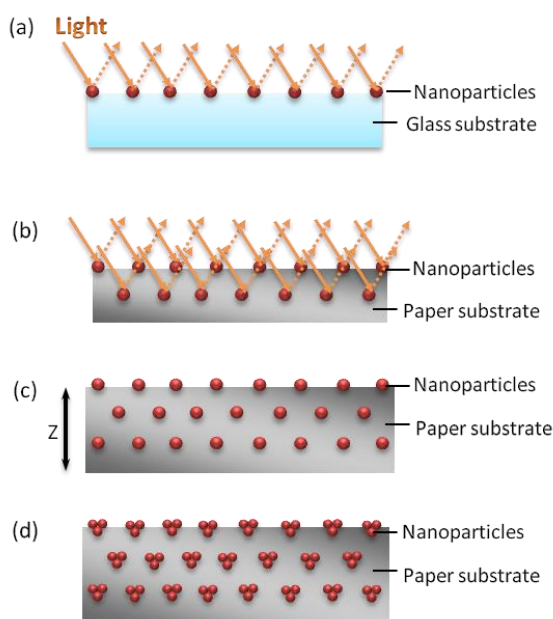


Figure 18: Schematic cross section illustration of light interaction with (a) nanoparticles on a glass substrate, (b) nanoparticles on a paper substrate, (c) Thickness, z of nanoparticles paper, (d) Ideal control of aggregation state of nanoparticles on paper substrates.

1.2.6.2.1 SERS and SPR

SERS is optimal when contact points of multiple metal nanoparticles (Au, Ag) enhance the intensity of Raman scattering. This means that aggregates made of very small NPs would provide best use of the noble metals. However, at some point as the aggregate size increases, light will not be able to reach the inner most nanoparticles within the paper substrate, and clearly an optimum in the size of nanoparticles' aggregate is expected. Little is known on the effect of aggregate polydispersity, size or distribution within 3D porous media have on SERS performance. Furthermore, there has been no effort to optimize the structure of paper for SERS applications. So far, filter paper has been used as an inert substrate. Preliminary results in our laboratory have shown that SERS intensity

of analyte adsorbed on AuNPs can be higher on paper than in aqueous solution. This suggests that there exists a preferential 3D structure for nanoparticles and that the interaction between nanoparticles and paper can be beneficial. The effect of substrate refractive index (air, water, cellulose) and heterogeneity on SERS is therefore of interest.

SPR is controlled by the nanoparticles' diameter, shape, volume fraction and aggregate state, dielectric constant, refractive index and interparticle distance. The challenge for SPR applications of nanoparticles-functionalized paper is to report the event in a simple and convenient way. In most analytical SPR techniques (such as for the BIAcore), adsorbed target molecules are detected by measuring a shift in plasmon angle which indicates a change in refractive index caused by change of mass at the interphase (around 50 nm above of AuNPs). Specificity is assured by immobilizing probe specific molecules such as antigens and enzymes that only bind with the analyte of interest (such as antibody, substrate). For paper tests, this practice is not convenient due to the diffused reflectance characteristic of the paper surface. Direct use of color change upon the shift of surface plasmon would be preferred. However, porosity of paper as well as size of nanoparticles and their aggregates should be optimized to allow easy dispersion and aggregation of nanoparticles within the cellulose structure of paper upon detection of target molecules.

1.2.6.3 Photocatalytic Properties

TiO₂-functionalized papers suffer a major drawback, low degradation rate. Currently, the time frame of degradation of organic compounds by TiO₂ photocatalytic reaction (hours-days) is often orders of magnitudes longer than the typical period of product use (seconds-minutes). Strategies involving the capture and retention of the component or pathogen are then used to compensate this mismatch. What is the maximum photocatalytic reaction rate of TiO₂? And how can paper best be engineered to operate TiO₂ under its optimum conditions? These are two critical questions. The photocatalytic degradation of a component/pathogen involves two steps: (1) light irradiation of TiO₂ and its substrate, (2) UV emission from TiO₂; alternative steps include: (3) the retention of contaminant/pathogen within the porous structure and (4) the liberation of degradation products. These last two steps are diffusion-controlled phenomena which are slow. A

priori, TiO_2 nanoparticles are best dispersed at the external surface, forming a TiO_2 monolayer on paper. This configuration would maximize steps 1 and 2.

Is there an opportunity to amplify incident light of the emitted UV through design of the paper structure on reflecting additives? Should entrapment of microorganisms and organic compounds within paper be useful? Would semi-permeable external layers of TiO_2 over a porous paper structure maximize photocatalysis and pathogen capture/retention within paper? Development is needed to identify these questions and maximize the critical optical properties of the TiO_2 functionalized paper and cellulosic fibers.

1.2.6.4 Analytical Techniques

There is a vast literature on understanding the colloid and surface science related to adsorption of nanoparticles from their colloidal suspensions onto a solid substrate and control of their arrangements. However, most research has focused on the adsorption assembly of nanoparticles onto flat substrates, such as glass and silicon. There is a lack of understanding on the underlying mechanisms involved in the self-assembled architectures of nanoparticles on the imperfect, rough and fibrous paper surface. The analytical techniques for nanoparticles-functionalized papers need to be focused on three length scales: nano, micro and macro. This involves quantifying the dispersion and aggregation state of nanoparticles (nanoscale), analyzing the adsorption state and coverage of nanoparticles on the microporous paper surface (microscale) as well as exploring the optical properties of nanoparticles-functionalized paper (macroscale). By merging these three lines of analytical techniques, a novel methodology to enhance the properties of nanoparticles-functionalized paper can be achieved.

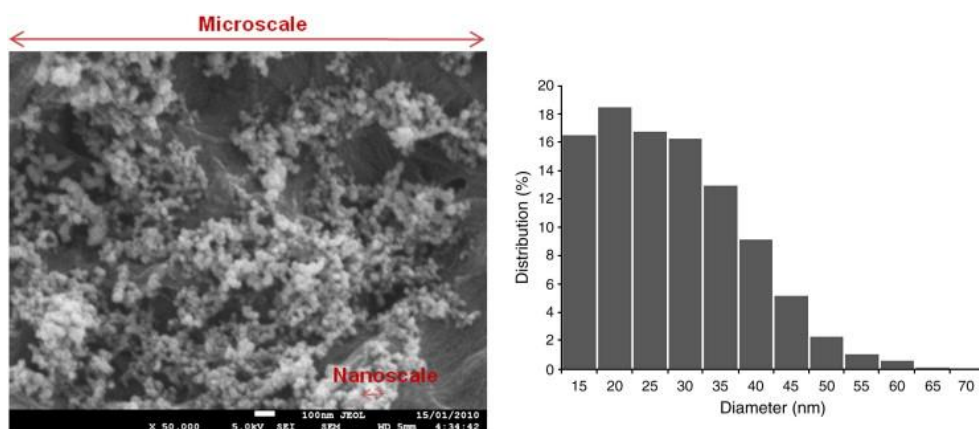


Figure 19: SEM with image analysis (analysed via Image J) for analyzing the distribution and adsorption state of TiO_2 on filter paper substrate. Unpublished results from [82].

Nanoparticles-functionalized paper has promising applications due to their unique photocatalytic, SPR, SERS and antimicrobial properties. Controlling these properties depends particularly on a fundamental understanding of the dispersion and aggregation state of nanoparticles on paper. Quantification techniques such as zeta potential sizing, electronic microscopy analysis (SEM, TEM) coupled with image analysis (Figure 19) are able to characterize the interaction between paper substrates and nanoparticles as well as the dispersion/aggregation state of the nanoparticles on paper. Characterization techniques such as UV-Vis spectroscopy and Raman analysis can also be employed to quantify the properties of the nanoparticles-functionalized paper. Since nanoparticles-functionalized paper has great potential as photocatalytic, SPR and SERS active substrates, it is critical to develop comprehensive analytical techniques to achieve reproducible nanoparticles-functionalized paper substrates.

1.2.7 Conclusion

A critical review of the properties, attachment methods and applications of nanoparticles-functionalized paper has been presented. Three types of nanoparticles were reviewed: titania, AuNPs and AgNPs. Paper is a low cost, cellulosic non-woven and only a very small volume fraction of these nanoparticles is needed to significantly alter its properties, especially the photocatalytic and optical properties. The emerging applications of nanoparticles-functionalized paper mostly involve interaction of light with the nanoparticles. These applications can be divided into three categories: (1) low-cost diagnostics for health and environment, (2) photocatalytic, disinfections and antimicrobial non-woven products, and (3) anti-counterfeiting and security papers.

Most previous research has focused on demonstrating some novel application of nanoparticles-functionalized paper. Filter paper has been universally used as an inert support due to simplicity, and there remains a lack of understanding of paper as a composite. Very few studies have characterized the distribution of nanoparticles within paper, and none has optimized paper as a nanoparticles' substrate. The application of

nanoparticles-functionalized paper for SERS and SPR is a new technology in which some synergetic effects of nanoparticles-paper have been observed but not explained. Different adsorption state of nanoparticles would produce different coupling of electromagnetic fields surrounding the nanoparticles. These regions of high electromagnetic field intensity are responsible for large enhancement effects of their optical signals. Therefore, controlling the absorption state of nanoparticles on the paper surface (i.e. singlet, doublet or triplet) is critical in achieving the desired magnitude of the SERS and SPR effects.

There is a need to better understand interaction of light-nanoparticles and how it is affected by the distribution of nanoparticles within the heterogeneous structure of paper substrate. More specifically, for each application, whether it is SPR, SERS or photocatalysis, the question remains as to the best spatial distribution of nanoparticles within the 3D structure of paper. What is their critical aggregation state? How can it best be achieved? A few of the related challenges include the ability to: (1) control the state of particle aggregation or size of nanoparticles on paper, and (2) control the average distance between nanoparticles and the spatial location of nanoparticles within the 3D heterogeneous paper structure. Better and simpler analytical techniques are also desired for quantifying the distribution of nanoparticles, to produce the best conditions for SERS, SPR, photocatalytic and other specific applications.

The properties of paper also need to be optimized. Paper is a heterogeneous, porous composite. Effects of different length scales of its physical and chemical heterogeneity can be reconciled with the distribution of nanoparticles and the properties of the composites. For example, the optical properties of paper (refractive index, opacity) can be engineered using dyes, treating fibers and functionalized micro-particles. Papermaking also offers opportunities to engineer the chemical composition, 3D structure and heterogeneity length scale of paper. Furthermore, coating nanoparticles on paper by printing is an attractive process to enhance nanoparticles-functionalized paper in terms of reproducibility. Nanoparticles-functionalized paper can become a disruptive technology for diagnostics and catalysis, should the critical challenges be overcome, whilst retaining the low cost and product/process flexibility associated with papermaking, surface treatment and printing.

1.2.8 Acknowledgement

Many thanks to Dr. Peter Miller and Dr. Tim Williams from Monash Centre for Electron Microscopy (MCEM) for discussions and SEM technical suggestions. The financial supports of the ARC Linkage - Project grant (LP0989823), the Australian Pulp and Paper Institute and Monash University are acknowledged.

1.3 Research Objectives and Aims

The objective of this research is twofold. First, to understand the major mechanisms involved in metallic nanoparticle enhanced paper for analytical purposes in terms of fundamental phenomena; second, to develop nanoparticles treated paper as an optimum SERS platform which allows rapid molecular signal detection for low cost bio-diagnostics applications. From the literature review, the critical steps of this study have been identified and generally classified into research in three parallel but complementary length scales:

1. Nanoscale: Quantifying the distribution and adsorption state of nanoparticles.
2. Microscale: Controlling the adsorption and aggregation state of nanoparticles on the cellulose fibers of paper.
3. Macroscale: Optimizing the SERS properties of nanoparticles functionalized paper to develop a generic SERS bio-diagnostic platform.

To address these issues, the specific aims of this study are:

1. To quantify the effects of the concentration of the nanoparticles suspension on their adsorption states and 3-dimensional (3D) distribution profile in paper.
2. To elucidate the effects of substrate on the SERS properties of nanoparticles in terms of signal enhancement and reproducibility.
3. To control the retention and aggregation of nanoparticles by quantifying the effect of the cationic polyelectrolyte adsorption on paper.
4. To quantify the effect of aggregation state and surface coverage of nanoparticles on paper on the SERS enhancement factor and sensitivity.
5. To quantify the dissolution kinetics of cationic polyelectrolyte on its adsorption conformation and the aggregation state of nanoparticles to optimize the SERS reproducibility of AuNPs treated paper.
6. To quantify the effects of cationic polyelectrolyte concentration, charge density and molecular weight on the assembly of nanoparticles.
7. To optimize and assess the feasibility of nanoparticles paper substrates as a low-cost and generic SERS platform for bio-diagnostic applications.

1.4 Thesis Outline

This thesis is presented in the format of “Thesis by Publication” based on the Monash University Handbook for Doctoral and MPhil Degrees 2011 [83] and the Thesis by Published and Unpublished papers (Monash Research Graduate School) [84]. It consists of six publications: three published, one accepted and two manuscripts in preparation; each one presented as a chapter. All published papers are reformatted to generate a consistent presentation within the thesis, whilst the content remains unchanged. The original publications are provided in Appendix I. The objective and contribution of each chapter are as followed:

- **Chapter 1: Paper Surfaces Functionalized by Nanoparticles**

(Paper 1: Ngo, Y.H., D. Li, G.P. Simon, and G. Garnier, Paper surfaces functionalized by nanoparticles, Advances in Colloid and Interface Science, 2011. 163(1): p. 23-38.)

This chapter reviews the properties of metallic nanoparticles which contribute to the major applications of nanoparticles functionalized paper. Different preparation methods and applications of nanoparticles-functionalized paper are highlighted. The critical challenges are discussed, followed by perspectives on the future direction in this research field.

- **Chapter 2: Gold Nanoparticle-Paper as a Three-Dimensional Surface Enhanced Raman Scattering Substrate**

(Paper 2: Ngo, Y.H., D. Li, G.P. Simon, and G. Garnier, Gold Nanoparticle–Paper as a Three-Dimensional Surface Enhanced Raman Scattering Substrate, Langmuir, 2012. 28(23): p. 8782-8790.)

This chapter investigates the heterogeneity of paper as a SERS substrate by depositing gold nanoparticles (AuNPs) on paper using a dipping method. The surface coverage of AuNPs on paper was found to scale linearly to their concentration profile in solution. SERS performances of the AuNPs-treated papers were evaluated with 4-ATP as the Raman molecule, and their SERS intensities increased linearly with the AuNPs’ concentration. To better understand the effect of the substrates, AuNPs were also adsorbed onto silicon wafer and hydrophobized paper and their SERS spectra were analyzed in terms of signal enhancement and reproducibility. The role of the z-distribution of AuNPs within

the bulk of the paper was highlighted; it produced a 3-dimensional (3D) multilayer structure that allows inter- and intralayer plasmon coupling, and amplify the SERS signal.

- **Chapter 3: Effect of Cationic Polyacrylamides on the Aggregation and SERS Performance of Gold Nanoparticles-treated Paper**

(Paper 3: Ngo, Y.H., D. Li, G.P. Simon, and G. Garnier, Effect of cationic polyacrylamides on the aggregation and SERS performance of gold nanoparticles-treated paper, Journal of Colloid and Interface Science, 2013. 392(0): p. 237-246.)

This chapter examines and quantifies the effect of cationic polyelectrolyte adsorption on paper on the aggregation and retention of AuNPs to optimize their SERS enhancement factor and sensitivity. The Raman enhancement factor of AuNPs-CPAM paper was almost an order of magnitude greater than for the untreated AuNPs paper. The high loading and uniform distribution of AuNPs aggregates on CPAM pre-treated paper contributed towards the excellent SERS reproducibility, sensitivity and high enhancement factor. This configuration of AuNP on paper was favoured by treating the substrate with CPAM solutions of higher concentrations, higher charge density and greater molecular weight.

- **Chapter 4: Effect of Cationic Polyacrylamide Dissolution on the Adsorption State of Gold Nanoparticles on Paper and Their Surface Enhanced Raman Scattering Properties**

(Paper 4: Ngo, Y.H., D. Li, G.P. Simon, and G. Garnier, Effect of cationic polyacrylamide dissolution on the adsorption state of gold nanoparticles on paper and their Surface Enhanced Raman Scattering properties, Colloids and Surfaces A: Physicochemical and Engineering Aspects, 2013. 420(0): p. 46-52.)

This chapter studies and quantifies the effect of CPAM dissolution kinetics and charge density on the adsorption and aggregation state of AuNPs on paper and the resulting SERS performance. The degree of dissolution of CPAM greatly affected the surface coverage and aggregation of AuNPs on the CPAM pre-adsorbed paper substrate and their SERS reproducibility. CPAM of higher charge density dissolves faster and produced a more uniform aggregation and higher surface coverage of AuNPs on paper for a higher and more reproducible Raman EF.

Understanding the CPAM dissolution process enables the optimization of SERS performance of the AuNPs-paper as a bio-diagnostic platform.

- **Chapter 5: Formation of Polyelectrolyte-Gold Nanoparticles Chaplets on Paper**

(Manuscript 1, Ngo, Y.H., D. Li, G.P. Simon, and G. Garnier, Formation of Polyelectrolyte-Gold Nanoparticles Chaplets on Paper, Manuscript in preparation and to be submitted to Langmuir.)

This chapter demonstrated a novel and simple method to form and visualize polyelectrolyte-nanoparticle chaplet like structures on paper, which could be applied to other porous surfaces. One-dimensional chaplets of negatively charged AuNPs have been electrostatically assembled along the polymer chain of cationic CPAM on paper substrates. Individual AuNPs were lined up with nearly contacting edges along the cationic CPAM template. The effects of CPAM polymer concentration, charge density and molecular weight on the assembly of AuNPs were studied. This technique enables the visualization of individual polyelectrolyte molecules and the formation of very organized and reproducible polyelectrolyte-nanoparticle chaplets on a porous substrate.

- **Chapter 6: Gold Nanoparticles Paper as a SERS bio-diagnostic Platform**

(Manuscript 2, Ngo, Y.H., W.L. Then, W. Shen, and G. Garnier, Gold Nanoparticles Paper as a SERS bio-diagnostic Platform, Manuscript in preparation and to be submitted to Biomacromolecule.)

This chapter demonstrated a standard SERS platform for antibody-antigen binding based on the functionalization of AuNP aggregates on paper by taking advantage of the high affinity association between the Streptomyces avidinii-derived protein, streptavidin, and biotin. First, the streptavidin was bound to the AuNPs treated paper using biotinylated-thiol. Subsequently, the desired biotinylated-antibody was bound to streptavidin, thus creating a monolayer of antibody on the surface of AuNPs. SERS spectra of each functionalization or binding step were obtained to ensure the specific adsorption of the biomolecules. The binding interaction of the antibody with its specific antigen was detected using SERS. The feasibility of AuNPs paper substrates as a low-cost and generic SERS platform for bio-diagnostic application was demonstrated.

1.5 References

1. Martinez, A.W., S.T. Phillips, M.J. Butte, and G.M. Whitesides, *Patterned Paper as a Platform for Inexpensive, Low-Volume, Portable Bioassays*. Angewandte Chemie International Edition, 2007. **46**(8): p. 1318-1320.
2. Martinez, A.W., S.T. Phillips, E. Carrilho, S.W. Thomas, H. Sindi, and G.M. Whitesides, *Simple Telemedicine for Developing Regions: Camera Phones and Paper-Based Microfluidic Devices for Real-Time, Off-Site Diagnosis*. Analytical Chemistry, 2008. **80**(10): p. 3699-3707.
3. Li, X., J. Tian, and W. Shen, *Quantitative biomarker assay with microfluidic paper-based analytical devices*. Analytical and Bioanalytical Chemistry, 2010. **396**(1): p. 495-501.
4. Pelton, R., *Bioactive paper provides a low-cost platform for diagnostics*. TrAC Trends in Analytical Chemistry, 2009. **28**(8): p. 925-942.
5. Li, X., J. Tian, T. Nguyen, and W. Shen, *Paper-Based Microfluidic Devices by Plasma Treatment*. Analytical Chemistry, 2008. **80**(23): p. 9131-9134.
6. Khan, M.S., G. Thouas, W. Shen, G. Whyte, and G. Garnier, *Paper Diagnostic for Instantaneous Blood Typing*. Analytical Chemistry, 2010. **82**(10): p. 4158-4164.
7. Tian, J., X. Li, and W. Shen, *Printed two-dimensional micro-zone plates for chemical analysis and ELISA*. Lab on a Chip, 2011. **11**(17): p. 2869-2875.
8. Cheng, C.-M., A.W. Martinez, J. Gong, C.R. Mace, S.T. Phillips, E. Carrilho, K.A. Mirica, and G.M. Whitesides, *Paper-Based ELISA*. Angewandte Chemie International Edition, 2010. **49**(28): p. 4771-4774.
9. Farhang, B., *Nanotechnology and lipids*. Lipid Technology, 2007. **19**(6): p. 132-135.
10. Ngo, Y.H., D. Li, G.P. Simon, and G. Garnier, *Paper surfaces functionalized by nanoparticles*. Advances in Colloid and Interface Science, 2011. **163**(1): p. 23-38.
11. Klajn, R., Paul J. Wesson, Kyle J.M. Bishop, and Bartosz A. Grzybowski, *Writing Self-Erasing Images using Metastable Nanoparticle Inks*. Angewandte Chemie International Edition, 2009. **48**(38): p. 7035-7039.
12. Geng, X., C. Filipe, and R. Pelton, *Antibacterial paper from photocatalytic TiO₂*. APPITA Journal, 2008. **61**(6): p. 456-460.
13. Tankhiwale, R. and S.K. Bajpai, *Graft copolymerization onto cellulose-based filter paper and its further development as silver nanoparticles loaded antibacterial food-packaging material*. Colloids and Surfaces B: Biointerfaces, 2009. **69**(2): p. 164-168.
14. Zhang, Y., K. Aslan, M.J.R. Previte, and C.D. Geddes, *Metal-enhanced fluorescence from paper substrates: Modified spectral properties of dyes for potential high-throughput surface analysis and assays and as an anti-counterfeiting technology*. Dyes and Pigments, 2008. **77**(3): p. 545-549.
15. Wu, D. and Y. Fang, *The adsorption behavior of p-hydroxybenzoic acid on a silver-coated filter paper by surface enhanced Raman scattering*. Journal of Colloid and Interface Science, 2003. **265**(2): p. 234-238.
16. Zhao, W., M.M. Ali, S.D. Aguirre, M.A. Brook, and Y. Li, *Paper-Based Bioassays Using Gold Nanoparticle Colorimetric Probes*. Analytical Chemistry, 2008. **80**(22): p. 8431-8437.
17. Michaels, A.M., Jiang, and L. Brus, *Ag Nanocrystal Junctions as the Site for Surface-Enhanced Raman Scattering of Single Rhodamine 6G Molecules*. The Journal of Physical Chemistry B, 2000. **104**(50): p. 11965-11971.
18. Xu, X., M. Stevens, and M.B. Cortie, *In Situ Precipitation of Gold Nanoparticles onto Glass for Potential Architectural Applications*. Chemistry of Materials, 2004. **16**(11): p. 2259-2266.
19. Hutter, E., S. Cha, J.F. Liu, J. Park, J. Yi, J.H. Fendler, and D. Roy, *Role of Substrate Metal in Gold Nanoparticle Enhanced Surface Plasmon Resonance Imaging*. The Journal of Physical Chemistry B, 2000. **105**(1): p. 8-12.

20. Wang, Y., Q. Yang, G. Shan, C. Wang, J. Du, S. Wang, Y. Li, X. Chen, X. Jing, and Y. Wei, *Preparation of silver nanoparticles dispersed in polyacrylonitrile nanofiber film spun by electrospinning*. Materials Letters, 2005. **59**(24-25): p. 3046-3049.
21. Fujishima, A. and K. Honda, *Electrochemical Photolysis of Water at a Semiconductor Electrode*. Nature, 1972. **238**: p. 37-38.
22. Matsubara, H., M. Takada, S. Koyama, K. Hashimoto, and A. Fujishima, *Photoactive TiO₂ Containing Paper: Preparation and Its Photocatalytic Activity under Weak UV Light Illumination*. Chemistry Letters, 1995. **24**(9): p. 767-768.
23. Carp, O., C.L. Huisman, and A. Reller, *Photoinduced reactivity of titanium dioxide*. Progress in Solid State Chemistry, 2004. **32**(1-2): p. 33-177.
24. Hashimoto, K., K. Wasada, M. Osaki, E. Shono, K. Adachi, N. Toukai, H. Kominami, and Y. Kera, *Photocatalytic oxidation of nitrogen oxide over titania-zeolite composite catalyst to remove nitrogen oxides in the atmosphere*. Applied Catalysis B: Environmental, 2001. **30**(3-4): p. 429-436.
25. Fujishima, A., T.N. Rao, and D.A. Tryk, *Titanium dioxide photocatalysis*. Journal of Photochemistry and Photobiology C: Photochemistry Reviews, 2000. **1**(1): p. 1-21.
26. Jr., D.D.E. and G. Chumanov, *Synthesis and Optical Properties of Silver Nanoparticles and Arrays*. ChemPhysChem, 2005. **6**(7): p. 1221-1231.
27. Chin, C., *Fabrication of metallic nanoparticle arrays*. Process and Characterization, 2006.
28. Nath, N. *Gold Nanoparticles: Worth their Weight in Gold!* 2009 [cited 2010 20 March].
29. Fleischmann, M., P.J. Hendra, and A.J. McQuillan, *Raman spectra of pyridine adsorbed at a silver electrode*. Chemical Physics Letters, 1974. **26**(2): p. 163-166.
30. Freeman, R., K. Grabar, K. Allison, R. Bright, J. Davis, A. Guthrie, M. Hommer, M. Jackson, P. Smith, D. Walter, and M. Natan, *Self-assembled metal colloid monolayers: an approach to SERS substrates*. Science, 1994. **267**(5204): p. 1629-1632.
31. Toderas, F., M. Baia, L. Baia, and S. Astilean, *Controlling gold nanoparticle assemblies for efficient surface-enhanced Raman scattering and localized surface plasmon resonance sensors*. Nanotechnology, 2007. **18**.
32. Morones, J.R., J.L. Elechiguerra, A. Camacho, K. Holt, J.B. Kouri, J.T. Ramirez, and M.J. Yacaman, *The bactericidal effect of silver nanoparticles*. Nanotechnology, 2005. **16**(10): p. 2346-2353.
33. Rai, M., A. Yadav, and A. Gade, *Silver nanoparticles as a new generation of antimicrobials*. Biotechnology Advances, 2008. **27**(1): p. 76-83.
34. Sharma, V.K., R.A. Yngard, and Y. Lin, *Silver nanoparticles: Green synthesis and their antimicrobial activities*. Advances in Colloid and Interface Science, 2009. **145**(1-2): p. 83-96.
35. Pelton, R., X. Geng, and M. Brook, *Photocatalytic paper from colloidal TiO₂--fact or fantasy*. Advances in Colloid and Interface Science, 2006. **127**(1): p. 43-53.
36. Fukahori, S., Y. Iguchi, H. Ichiura, T. Kitaoka, H. Tanaka, and H. Wariishi, *Effect of void structure of photocatalyst paper on VOC decomposition*. Chemosphere, 2007. **66**(11): p. 2136-2141.
37. Iguchi, Y., H. Ichiura, T. Kitaoka, and H. Tanaka, *Preparation and characteristics of high performance paper containing titanium dioxide photocatalyst supported on inorganic fiber matrix*. Chemosphere, 2003. **53**(10): p. 1193-1199.
38. Nishibori, S., *Process For Producing A Photocatalytic Pulp Composition and Molded Photocatalytic Pulp*, in United States Patent. 2006, Ein Kohsan Co., Ltd.: Japan.
39. Escaffre, P., P. Girard, J. Dussaud, and L. Bouvier, *Photocatalytic Composition*, in United States Patent. 2005, Ahlstrom Research and Services.
40. Kimura, N., S. Abe, T. Yoshimoto, and S. Fukayama, *Photocatalyst-carrying Structure and Photocatalyst Coating Material*, in United States Patent. 2001, Nippon Soda Co., Ltd.

41. Aguedach, A., S. Brosillon, J. Morvan, and E.K. Lhadi, *Photocatalytic degradation of azo-dyes reactive black 5 and reactive yellow 145 in water over a newly deposited titanium dioxide*. Applied Catalysis B: Environmental, 2005. **57**(1): p. 55-62.
42. Raillard, C., V. Héquet, P. Le Cloirec, and J. Legrand, *Kinetic study of ketones photocatalytic oxidation in gas phase using TiO₂-containing paper: effect of water vapor*. Journal of Photochemistry and Photobiology A: Chemistry, 2004. **163**(3): p. 425-431.
43. Lu, Z., S. Eadula, Z. Zheng, K. Xu, G. Grozdits, and Y. Lvov, *Layer-by-layer nanoparticle coatings on lignocellulose wood microfibers*. Colloids and Surfaces A: Physicochemical and Engineering Aspects, 2007. **292**(1): p. 56-62.
44. Varahramyan, K. and Y. Lvov, *Nanomanufacturing by layer-by-layer assembly*. Nanoengineering and nanosystems, 2006. **220**: p. 29-37.
45. Pinto, R.J.B., P.A.A.P. Marques, M.A. Martins, C.P. Neto, and T. Trindade, *Electrostatic assembly and growth of gold nanoparticles in cellulosic fibres*. Journal of Colloid and Interface Science, 2007. **312**(2): p. 506-512.
46. Uddin, M.J., F. Cesano, F. Bonino, S. Bordiga, G. Spoto, D. Scarano, and A. Zecchina, *Photoactive TiO₂ films on cellulose fibres: synthesis and characterization*. Journal of Photochemistry and Photobiology A: Chemistry, 2007. **189**(2-3): p. 286-294.
47. Dong, H. and J.P. Hinestroza, *Metal nanoparticles on natural cellulose fibers: electrostatic assembly and in situ synthesis*. ACS Applied Materials & Interfaces, 2009. **1**(4): p. 797-803.
48. Henglein, A. and M. Giersig, *Formation of Colloidal Silver Nanoparticles: Capping Action of Citrate*. Journal of Physical Chemistry B, 1999. **103**(44): p. 9533-9539.
49. Ma, W. and Y. Fang, *Experimental (SERS) and theoretical (DFT) studies on the adsorption of p-, m-, and o-nitroaniline on gold nanoparticles*. Journal of Colloid and Interface Science, 2006. **303**(1): p. 1-8.
50. Cai, J., S. Kimura, M. Wada, and S. Kuga, *Nanoporous cellulose as metal nanoparticles support*. Biomacromolecules, 2009. **10**(1): p. 87-94.
51. He, J., T. Kunitake, and A. Nakao, *Facile in situ synthesis of noble metal nanoparticles in porous cellulose fibers*. Chemistry of Materials 2003. **15**(23): p. 4401-4406.
52. Fernández, A., E. Soriano, G. López-Carballo, P. Picouet, E. Lloret, R. Gavara, and P. Hernández-Muñoz, *Preservation of aseptic conditions in absorbent pads by using silver nanotechnology*. Food Research International, 2009. **42**(8): p. 1105-1112.
53. Niu, Z. and Y. Fang, *Surface-enhanced Raman scattering of single-walled carbon nanotubes on silver-coated and gold-coated filter paper*. Journal of Colloid and Interface Science, 2006. **303**(1): p. 224-228.
54. Hashimoto, K., H. Irie, and A. Fujishima, *TiO₂ photocatalysis: a historical overview and future prospects*. Japanese Journal of Applied Physics, 2005. **44**(12): p. 8269-8285.
55. Uddin, M.J., F. Cesano, D. Scarano, F. Bonino, G. Agostini, G. Spoto, S. Bordiga, and A. Zecchina, *Cotton textile fibres coated by Au/TiO₂ films: Synthesis, characterization and self cleaning properties*. Journal of Photochemistry and Photobiology A: Chemistry, 2008. **199**(1): p. 64-72.
56. Ahlstrom. 2006 [cited 2009 September 23]; Available from: <http://www.ahlstrom.com>.
57. Nippon paper industries develops photocatalytic newsprint with air purification effect. 2006, Nippon Paper Group.
58. Japan, W. *Air-purifying paper*. 2008 [cited 2010 March 20].
59. *New antibacterial office paper*. 2006 [cited 2009 September 3]; Available from: www.domtar.com.
60. *Antibacterial pulp*. 2006 [cited 2009 October 15]; Available from: www.ein.co.jp/en/paper/explain.html.

61. Peng, P. and G. Garnier, *Effect of Cationic Polyacrylamide Adsorption Kinetics and Ionic Strength on Precipitated Calcium Carbonate Flocculation*. Langmuir, 2010: p. 16949–16957.
62. Khan, M.S., S.B.M. Haniffa, A. Slater, and G. Garnier, *Effect of polymers on the retention and aging of enzyme on bioactive papers*. Colloids and Surfaces B: Biointerfaces, 2010. **79**(1): p. 88-96.
63. Khan, M.S., X. Li, W. Shen, and G. Garnier, *Thermal stability of bioactive enzymatic papers*. Colloids and Surfaces B: Biointerfaces, 2010. **75**(1): p. 239-246.
64. Khan, M.S., D. Fon, X. Li, J. Tian, J. Forsythe, G. Garnier, and W. Shen, *Biosurface engineering through ink jet printing*. Colloids and Surfaces B: Biointerfaces, 2010. **75**(2): p. 441-447.
65. Li, X., J. Tian, G. Garnier, and W. Shen, *Fabrication of paper-based microfluidic sensors by printing*. Colloids and Surfaces B: Biointerfaces, 2010. **76**(2): p. 564-570.
66. Martinez, Andres W., Scott T. Phillips, Manish J. Butte, and George M. Whitesides, *Patterned Paper as a Platform for Inexpensive, Low-Volume, Portable Bioassays*. Angewandte Chemie International Edition, 2007. **46**(8): p. 1318-1320.
67. Liu, J. and Y. Lu, *A Simple and Sensitive "Dipstick" Test in Serum Based on Lateral Flow Separation of Aptamer-Linked Nanostructures*. Angew Chem, 2006. **118**: p. 8123-8127.
68. Debapriya, M., L. Juewen, and L. Yi, *Lateral Flow Devices*, in *United States Patent*. 2007: United States.
69. Klajn, R., Paul J. Wesson, Kyle J.M. Bishop, and Bartosz A. Grzybowski, *Writing Self-Erasing Images using Metastable Nanoparticle 'Ink'*. Angewandte Chemie International Edition, 2009. **48**(38): p. 7035-7039.
70. Bizzarri, M.S.P.A.R. and M.S.P.S. Cannistraro, *SERS detection of thrombin by protein recognition using functionalized gold nanoparticles*. Nanomedicine: Nanotechnology, Biology and Medicine, 2007. **3**(4): p. 306-310.
71. Kincade, K., *RAMAN SPECTROSCOPY: SERS and silver nanorods quickly reveal viral structures*. 2007, Laser Focus World.
72. Hesse, E. and J.A. Creighton, *Investigation of cyanide ions adsorbed on platinum and palladium coated silver island films by surface-enhanced Raman spectroscopy*. Chemical Physics Letters, 1999. **303**(1-2): p. 101-106.
73. Chen, Y.-H. and C.-S. Yeh, *Laser ablation method: use of surfactants to form the dispersed Ag nanoparticles*. Colloids and Surfaces A: Physicochemical and Engineering Aspects, 2002. **197**(1-3): p. 133-139.
74. Luo, Z. and Y. Fang, *SERS of C60/C70 on gold-coated filter paper or filter film influenced by the gold thickness*. Journal of Colloid and Interface Science, 2005. **283**(2): p. 459-463.
75. Coluccio, M.L., G. Das, F. Mecarini, F. Gentile, A. Pujia, L. Bava, R. Talerico, P. Candeloro, C. Liberale, F. De Angelis, and E. Di Fabrizio, *Silver-based surface enhanced Raman scattering (SERS) substrate fabrication using nanolithography and site selective electroless deposition*. Microelectronic Engineering, 2008. **86**(4-6): p. 1085-1088.
76. Berthod, A., J.J. Laserna, and J.D. Winefordner, *Analysis by surface enhanced Raman spectroscopy on silver hydrosols and silver coated filter papers*. Journal of Pharmaceutical and Biomedical Analysis, 1988. **6**(6-8): p. 599-608.
77. Cabalín, L.M. and J.J. Laserna, *Fast spatially resolved surface-enhanced Raman spectrometry on a silver coated filter paper using charge-coupled device detection*. Analytica Chimica Acta, 1995. **310**(2): p. 337-345.
78. Laserna, J.J., A.D. Campiglia, and J.D. Winefordner, *Surface-enhanced Raman spectrometry on a silver-coated filter paper substrate*. Analytica Chimica Acta, 1988. **208**: p. 21-30.
79. Garnett, J.C.M., *Colours in Metal Glasses and in Metallic Films*. Philosophical Transactions of The Royal Society A, 1904. **203**: p. 385-420.

80. Jason, M.M. and et al., *Theory and modeling of light interactions with metallic nanostructures*. Journal of Physics: Condensed Matter, 2008. **20**(32): p. 323201.
81. Noguez, C., *Optical properties of isolated and supported metal nanoparticles*. Optical Materials, 2005. **27**(7): p. 1204-1211.
82. Ngo, Y., D. Li, G.P. Simon, and G. Garnier. *Paper Surface Functionalized by Nanoparticles*. in *APPITA Conference*. 2010. Melbourne.
83. *Handbook for Doctoral and MPhil Degrees*. Available from: http://www.mrgs.monash.edu.au/research/doctoral/archive/handbook_cd_2011/handbook/index.html.
84. *Thesis by Published and Unpublished Papers*. Available from: <http://www.mrgs.monash.edu.au/research/examination/thesis-bypublication/index.html>.

Chapter 2

Gold Nanoparticle-Paper as a Three-Dimensional Surface Enhanced Raman Scattering Substrate

This page is intentionally blank

Monash University

Declaration for Thesis Chapter 2

Declaration by candidate

In the case of Chapter 2, the nature and extent of my contribution to the work was the following:

Nature of contribution	Extent of contribution (%)
Initiation, key ideas, experimental and analysis works, development and writing up of paper	80

The following co-authors contributed to the work. Co-authors who are students at Monash University must also indicate the extent of their contribution in percentage terms:

Name	Nature of contribution	Extent of contribution (%) for student co-authors only
Gil Garnier	Initiation, key ideas, reviewing and editing of the paper.	Supervisor
George Simon	Initiation, key ideas, reviewing and editing of the paper.	Co-supervisor
Dan Li	Initiation, key ideas, reviewing and editing of the paper.	Co-supervisor

Candidate's Signature

Date 13.03.2013

Declaration by co-authors

The undersigned hereby certify that:

- (1) the above declaration correctly reflects the nature and extent of the candidate's contribution to this work, and the nature of the contribution of each of the co-authors.
- (2) they meet the criteria for authorship in that they have participated in the conception, execution, or interpretation, of at least that part of the publication in their field of expertise;
- (3) they take public responsibility for their part of the publication, except for the responsible author who accepts overall responsibility for the publication;
- (4) there are no other authors of the publication according to these criteria;
- (5) potential conflicts of interest have been disclosed to (a) granting bodies, (b) the editor or publisher of journals or other publications, and (c) the head of the responsible academic unit; and
- (6) the original data are stored at the following location(s) and will be held for at least five years from the date indicated below:

Location(s) Australian Pulp and Paper Institute (APPI), Department of Chemical Engineering, Monash University, Clayton, VIC 3800, Australia.

Signature 1

Date 11/12/12

Signature 2

Date 12/12/12

Signature 3

Date 11/12/2012

This page is intentionally blank

Gold Nanoparticle-Paper as a Three-Dimensional Surface Enhanced Raman Scattering Substrate

Ying Hui Ngo¹, Dan Li², George P. Simon² and *Gil Garnier¹

¹ BioPRIA, Australian Pulp and Paper Institute (APPI), Department of Chemical Engineering Monash University, Clayton, VIC 3800, Australia.

² Department of Material Engineering Monash University, Clayton, VIC 3800, Australia

*Corresponding author. Email: [REDACTED]; Tel: [REDACTED]; Fax: [REDACTED]

Content

2.1	Abstract	83
2.2	Introduction	84
2.3	Experimental Section	86
2.3.1	Materials	86
2.3.2	Synthesis and Deposition of Nanoparticles on Paper	87
2.3.3	Preparation of Raman Active Substrates	87
2.3.4	Instrumentation	87
2.4	Results and Discussion	88
2.4.1	Deposition of AuNPs on Paper	88
2.4.2	Deposition of AuNPs on Silicon	95
2.4.3	AuNPs Droplet Test	97
2.5	Conclusion	99
2.6	Acknowledgement	100
2.7	References	101
2.8	Supporting Information	104

2.1 Abstract

This work investigates the effect of gold nanoparticles' (AuNPs) addition to paper substrate and examines the ability of these composite materials to amplify the Surface Enhanced Raman Scattering (SERS) signal of a dye adsorbed. Paper has a three dimensional (3D), porous and heterogeneous morphology. The manner in which paper adsorbs the nanoparticles is crucial to its SERS properties, particularly with regards to

aggregation. In this work, we sought to maintain the same degree of aggregation, whilst changing the concentration of nanoparticles deposited on paper. We achieved this by dipping paper into AuNP solutions of different, known concentration and found that the initial packing density of AuNPs in solutions was retained on paper with the same degree of aggregation. The surface coverage of AuNPs on paper was found to scale linearly to their concentration profile in solutions. The SERS performances of the AuNPs-treated papers were evaluated with 4-aminothiophenol (4-ATP) as the Raman molecule, and their SERS intensities increased linearly with the AuNPs' concentration. Compared to AuNPs-treated silicon, the Raman enhancement factor (EF) from paper was relatively higher due to a more uniform and greater degree of adsorption of AuNPs. The effect of the spatial distribution of AuNPs in their substrates on SERS activity was also investigated. In this experiment, the number of AuNPs was kept constant (a 1 μ L droplet of AuNPs was deposited on all substrates), and the distribution profile of AuNPs was controlled by the nature of the substrate; paper, silicon and hydrophobized paper. The AuNP droplet on paper showed the most reproducible and sensitive SERS signal. This highlighted the role of the z-distribution (through film) of AuNPs within the bulk of the paper, producing a 3-dimensional (3D) multilayer structure to allow inter- and intralayer plasmon coupling, and hence amplifying the SERS signal. The SERS performance of nanoparticles-functionalized paper can thus be optimized by controlling the 3D distribution of the metallic nanoparticles, and such control is critical if these systems are to be implemented as a low-cost and highly sensitive bioassay platform.

Keywords: SERS, gold nanoparticles (AuNPs), paper, heterogeneity, 3-dimensional, amplification, sensitivity, bioassay.

2.2 Introduction

Paper has recently been rediscovered as substrate for low cost analytical tests in health and environmental applications [1-3]. Flexible micro-fluidic systems, reactors and valves have already been printed on paper to regulate, measure and control the flow of analytes and reagents [3-4]. In paper blood typing assays, blood group antigens can be displayed directly by the red blood cells that elude or absorb on paper depending on whether they react with a specific or a non-specific antibody which was previously adsorbed [5]. However, the identification of antibodies can be complicated because of their typical low

concentration and small dimensions, such as for immunoglobulin G (IgG). While Enzyme-Linked Immunosorbent Assay (ELISA) is a standard solution-based technique, its application to paper, while possible, requires multiple reactants and washing steps [6-7]. A direct approach involving a simple contact between paper substrate and analytes, followed by signal amplification using some instrumentation techniques would be ideal. Surface Enhanced Raman Scattering (SERS) presents an attractive technique where analytes such as antibodies can be selectively adsorbed onto antigens capped metallic nanoparticles on treated paper substrate and detected at very low concentrations.

SERS is a technique that enhances the Raman scattering which measures the small energy changes of the light scattered from a molecule absorbed on a metallic surface, typically a metallic nanoparticle. The enhancement factor can be as much as 10^{14} – 10^{15} [8], which enables SERS as a single-molecule detection technique to identify analytes at trace levels. The critical requirements of a substrate for SERS application in routine analytical procedures include low cost, sensitivity, robustness, reproducibility and stability to allow for long term storage between measurements. The immobilization of metallic nanoparticles onto solid substrates provides an attractive alternative to metal aqueous colloid as SERS substrates because of its higher flexibility and easy application to non water-soluble compounds. In particular, there has been significant progress in surface sciences and nanofabrication technology that have allowed the control of size, shape and aggregation of nanoparticles deposited on conventional SERS substrates such as silicon and glass by electron beam lithography [9], focused ion beam patterning [10] and thermal evaporation [11]. However, these techniques are time consuming, costly, require sophisticated equipment, and the substrates are often fragile and suffer from poor storage stability.

With excellent features such as low cost, flexibility, robustness, long term stability (1 month-1 year) and ease of use, paper offers a promising platform as a SERS substrate for bioassays. The soft texture of paper substrates allows conformal contact with the surface of analytes by swabbing [12]. This provides an efficient and practical method to collect traces of analytes from the body and many surfaces, compared to silicon and glass which are rigid, brittle and confined to laboratory experiments. Paper is an efficient substrate for routine SERS analysis as highlighted in many articles [12-20]. However, most of these

studies have used paper simply as an inert support and have not explored how the rough, composite and heterogeneous nature of paper can affect the distribution of nanoparticles and the SERS signal generated.

In this study, the heterogeneity of paper as a SERS substrate was explored by depositing gold nanoparticles (AuNPs) on paper using a dipping method. Our objective was to quantify the effect of AuNPs' concentration and 3-dimensional (3D) distribution profile on paper to their SERS performance. Standard filter paper (Whatman #1), which consists of 98% α -cellulose, was selected as it is a convenient model paper of well defined structure and to ensure minimal interference from process components (polymers or coatings). The filter papers were dipped into AuNP solutions of different concentration. This simple dipping method was selected to ensure that the size of AuNPs retained on papers is constant, and to minimize aggregation. The distribution profile and particle size of AuNPs adsorbed on papers were characterized by FESEM/image analysis. A model Raman dye, 4-aminothiophenol (4-ATP), was adsorbed on the AuNPs-paper substrates and their SERS spectra were measured. To better understand the effect of substrates, AuNPs were also adsorbed onto silicon wafer and hydrophobized paper and their SERS spectra were analyzed in terms of signal enhancement and reproducibility. It is the goal of this study to optimize the SERS efficiency of AuNPs coated paper as a platform for emerging bioassay applications.

2.3 Experimental Section

2.3.1 Materials

Hydrogen tetrachloroaurate trihydrate ($\text{HAuCl}_4 \cdot 3\text{H}_2\text{O}$), sodium citrate tribasic dihydrate ($\text{Na}_3\text{C}_6\text{H}_5\text{O}_7 \cdot 2\text{H}_2\text{O}$), 4-aminothiophenol (4-ATP) and alkyl ketene dimer (AKD) were purchased from Sigma-Aldrich and used as received. Whatman filter paper #1 and pre-cut silicon wafers purchased from ProSciTech were selected as substrates. Hydrophobized paper was prepared by treating the Whatman filter paper #1 with AKD. Ultrapure water purified with a Millipore system (18 M Ω .cm) was used in all aqueous solutions and rinsing procedures.

2.3.2 Synthesis and Deposition of Nanoparticles on Paper

AuNPs were synthesized by using 1 mM $\text{HAuCl}_4 \cdot 3\text{H}_2\text{O}$ and 1% aqueous $\text{Na}_3\text{C}_6\text{H}_5\text{O}_7 \cdot 2\text{H}_2\text{O}$ according to the Turkevich method [21]. Filter papers were used as received and dipped into Petri dishes which contained 10 mL solution of AuNPs for 24 hours. After dipping, the paper substrates were rinsed thoroughly with distilled water to remove loosely bound AuNPs, and the papers were dried and equilibrated at 50% relative humidity and 23°C before further analysis.

2.3.3 Preparation of Raman Active Substrates

Solutions of 1 mM of 4-ATP were prepared in ethanol. Since 4-ATP is well known for its strong affinity to the surface of AuNPs (its S-H bond is easily cleaved to form an Au-S bond upon adsorption), the dried AuNPs-deposited substrates were dipped into 2 mL of the 4-ATP ethanol solution for a shorter period of time of 5 minutes to create a 4-ATP monolayer on the substrates. After thorough rinsing with ethanol and drying, the treated papers were subjected to Raman characterization. The Raman enhancement factors (EF) of 1 mM of 4-ATP on a substrate was calculated according to [22-23]:

$$\text{EF} = \frac{[I_{\text{SERS}}]}{[I_{\text{bulk}}]} \times \frac{[N_{\text{bulk}}]}{[N_{\text{ads}}]} \quad (1)$$

where I_{SERS} is the intensity of a specific band in the SERS spectrum of 4-ATP and I_{bulk} is the intensity of the same band in the Raman spectrum from the bulk solution sample. For all spectra, the intensity of the band at 1077 cm^{-1} was used to calculate EF values. N_{bulk} is the number of molecules of the bulk 4-ATP in the laser illumination volume while N_{ads} is the number of molecules adsorbed and sampled on the SERS active substrate within the laser spot.

2.3.4 Instrumentation

Field Emission Scanning Electron Microscopy (FESEM), which produces higher resolution, less sample charging and less damaged images than conventional FESEM, was performed using a JEOL 7001 Field Emission Gun (FEG) system operating at 5 kV and 180 pA. The Zeta potential and Dynamic Light Scattering (DLS) measurements were performed with a Zetasizer Nano ZS (Malvern Instruments) in a Folded Capillary cell (DTS1060) at 25 °C. UV-Vis absorbance was measured using a Varian Cary 300Bio

spectrophotometer. All Raman and SERS spectra were obtained in air using a Renishaw Invia Raman microscope equipped with a 300 mW 633 nm laser. The laser beam was positioned through a Leica imaging microscope objective lens (50×), whilst the instrument's wavenumber was calibrated with a silicon standard centered at 520.5 cm^{-1} shift. Due to the smaller spot size of the laser compared with the large surface area of the samples, the spectra were obtained at different points of the surface. The position of the spectra bands remained the same, but differed only in intensity. The average Raman intensity of 5 measurements was presented after baseline subtraction from the control sample.

2.4 Results and Discussion

2.4.1 Deposition of AuNPs on Paper

AuNPs are nanoparticles of choice for analysing the SERS potential of paper, since they are more stable and less susceptible to oxidation than most other SERS-active nanoparticles, such as silver nanoparticles (AgNPs) [24]. A stock solution of 0.20 mg/mL of AuNPs was synthesized using the Turkevich method [21] (method of calculation in Supporting Information, S1). The resulting red wine- coloured AuNPs suspension showed the typical UV-Vis absorbance spectra centered at around 530 nm, which was assigned to their Surface Plasmon Resonance (SPR). Particle size measurement by Dynamic Light Scattering (DLS) revealed a highly monodispersed AuNPs suspension with an average diameter of 23.2 nm (Supporting Information, S2). During the synthesis of AuNPs, the citrate groups served the dual role of reducing agent and stabilizer [25]. The weakly bound citrate ions imparted a negative surface charge onto the AuNPs, which prevented their agglomeration in solution [26]. Zeta potential analysis revealed a strong negative charge of AuNPs higher than 30 mV, and providing colloidal stability [27]. AuNPs of different concentrations (0.15 mg/mL, 0.10 mg/mL, 0.05 mg/mL, 0.02 mg/mL) were prepared by diluting the stock solution (0.20 mg/mL). The negative charge of AuNPs decreased upon dilution; this might be due to the decrease in the quantity of citrate-capped AuNPs (Table 1). However, the AuNPs still maintains their stability, even when diluted up to 0.02 mg/mL.

Table 1: Effect of concentration on Zeta potential of AuNPs.

	Concentration of AuNPs (mg/mL)				
	0.02	0.05	0.10	0.15	0.20
Zeta Potential (mV)	-36.2	-37.4	-40.9	-43.2	-44.6

Filter paper samples were dipped into the AuNP solutions for 24 hours. This procedure was aimed at keeping the size of AuNPs retained on paper constant. The colour intensity of the dried AuNPs treated papers was analyzed with ImageJ software (Figure 1). AuNPs treated paper turned from white to red purple and the colour became more intense as the concentration of AuNP solutions was increased.

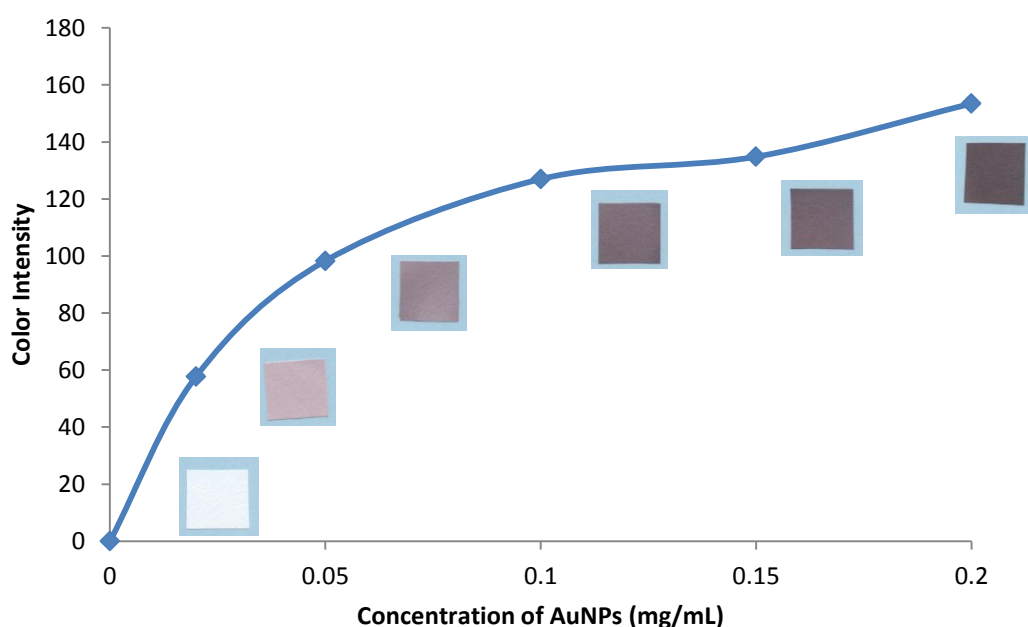


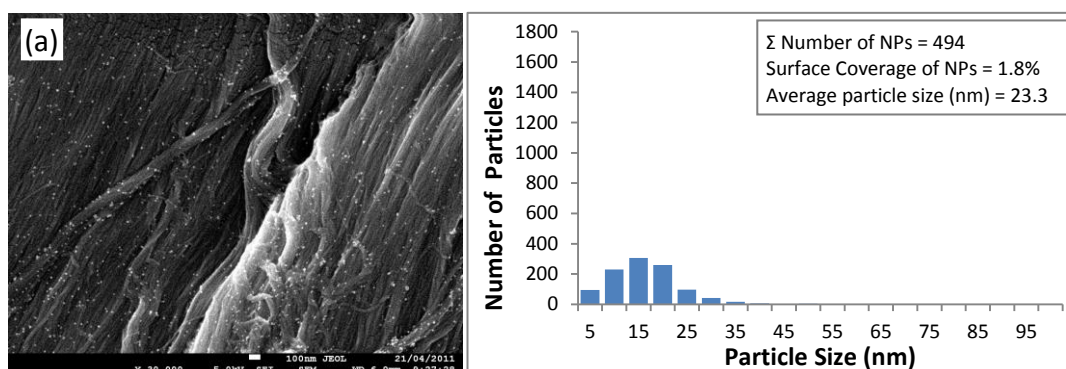
Figure 1: Colour intensity of filter papers treated with AuNP solutions of different concentration.

FESEM images (Figure 2) were analyzed by using ImageJ software to measure the quantity and size distribution of AuNPs adsorbed on paper. The size distribution of AuNP remained constant for all experiments with an average size of 25 ± 3 nm; this means that most AuNPs are retained on paper as individual particles. The total number of AuNPs was estimated by dividing the total area of AuNPs on paper (in each FESEM images) by the area of an individual AuNP ($d=23.2$ nm). The concentration of AuNPs on paper increased monotonically with the solution concentration in which the papers were dipped in; the particle distribution was denser and more uniform on paper when treated with

AuNP solutions of higher concentration. The average distances between the AuNPs on paper decreased from 100-200 nm to 10-50 nm (Figure 2). At high concentrations, AuNPs were electrostatically stabilized and closely packed in solution. This high packing density and uniform configuration of AuNPs was retained on the paper. This required the AuNPs to diffuse from solution into the porous structure of paper, adsorb onto a cellulose surface and resist the capillary forces of drying.

Paper has a weak negative charge caused by the carboxyl groups from the hemicelluloses of cellulose fibers [28]. The AuNPs were well dispersed and adsorbed on paper, even though both materials were negatively charged. According to the DLVO theory, negative particles (AuNPs) can adsorb on a negative surface (cellulose fibers) if the total interaction force is negative (attraction); this means that the van der Waals forces (attraction) are higher than the repulsive forces (electrostatic). Such high adsorption of AuNPs was easily achieved on paper without any retention aid. This contrasts earlier works [12, 28] where cationically-modified AuNPs/Au nanorods were produced and deemed necessary to achieve effective adsorption on the cellulose fibers.

FESEM cross sectional analysis of 0.20 mg/mL AuNPs treated paper was performed to analyze the distribution of AuNPs through the thickness of the paper substrate (Supporting Information, S3). The AuNPs were relatively well dispersed across the thickness of paper, suggesting intense electrostatic repulsion among the NPs. AuNPs were present both on the surfaces and within the bulk of paper.



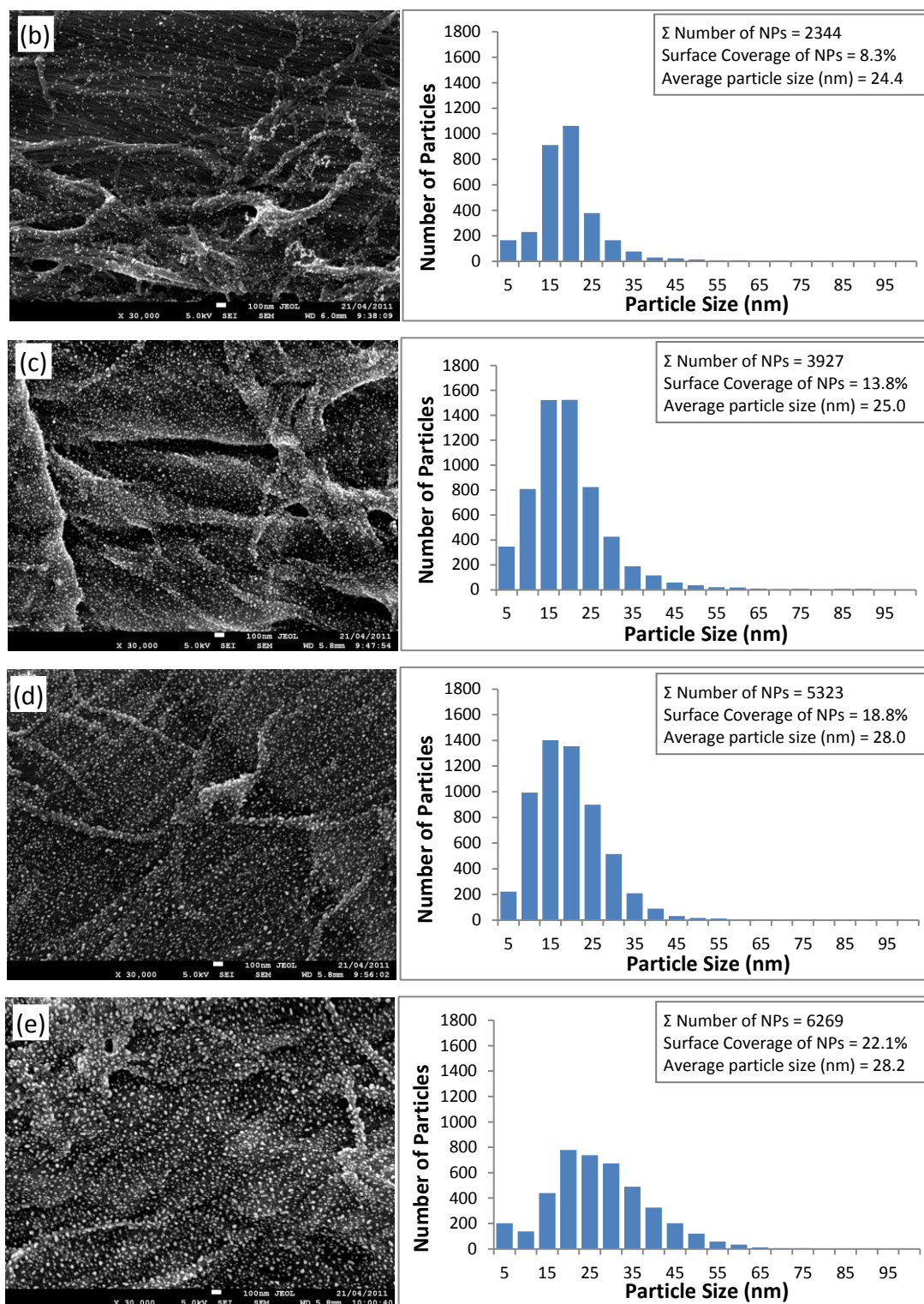


Figure 2: FESEM images and histograms of particle size distribution of filter papers dipped into (a) 0.02 mg/mL, (b) 0.05 mg/mL, (c) 0.10 mg/mL, (d) 0.15 mg/mL and (e) 0.20 mg/mL of AuNP solutions.

UV-Vis analysis was performed on the AuNP solutions before and after paper dipping to quantify the total amount of AuNPs retained on paper from the differences in the intensities of absorbance peaks (Supporting Information, S4). The number of AuNPs adsorbed on paper increased relatively linearly with the concentration of AuNP solutions into which the paper was immersed (Figure 3). A dynamic equilibrium between adsorption and desorption of AuNPs was expected. This quantity of adsorbed AuNPs on paper was approximately an order of magnitude higher than that measured from FESEM image analysis. Since the FESEM image analysis (Figure 2) only quantified the number of AuNPs on the paper surface, this suggests that most of the AuNPs were retained within the bulk of paper, as confirmed by the cross-sectional FESEM analysis (Supporting Information, S3). The density of AuNPs in the bulk of paper was estimated by subtracting their density on the paper surface (FESEM) from their total density (UV-Vis). There was only 40% of AuNPs adsorbed on both surfaces of paper, while the remaining fraction (60%) appeared to have diffused and adsorbed within the bulk of paper (Figure 3). The attachment of AuNPs on paper is controlled by the 3-dimensional (3D) network of paper which consists of a large volume fraction of pores providing strong capillary forces for the distribution of AuNPs from solution.

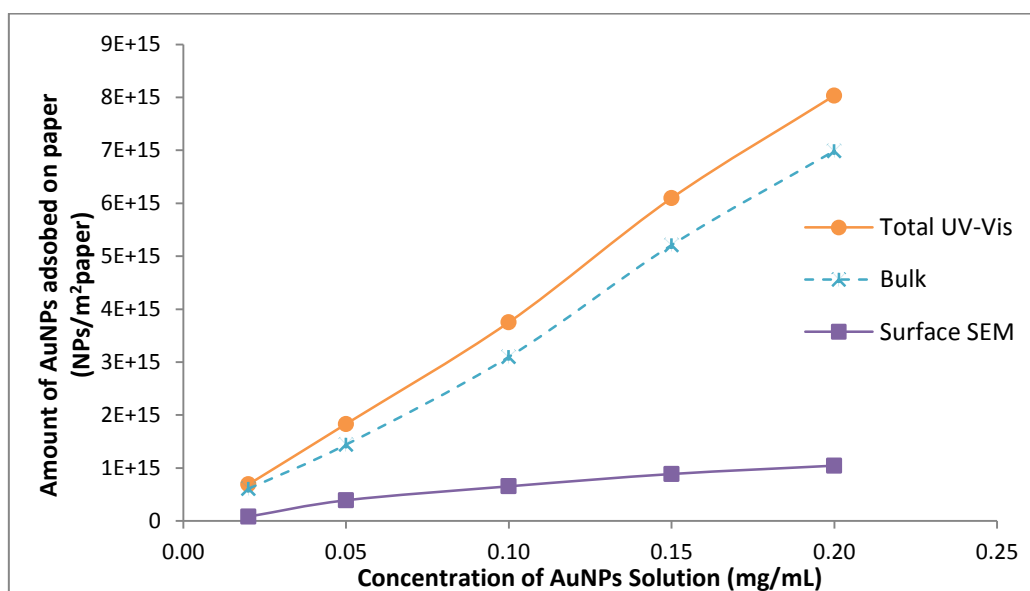


Figure 3: Effect of the concentration of AuNP solutions on the amount of AuNPs retained on the paper surface and bulk after dipping (estimated from UV-Vis and FESEM analysis based on the FESEM images in Figure 2).

4-Aminothiophenol (4-ATP) was selected as the probe molecule in the Raman analysis because of its distinct Raman features, strong affinity for metal surfaces via thiol bonding and formation of self-assembled monolayers [29]. Control paper and AuNP treated papers were dipped into 1 mM of 4-ATP for 5 minutes, washed, dried and analyzed by Raman spectroscopy. The concentration effect of AuNP solutions on the SERS signal from paper substrates was quantified (Figure 4). All spectra exhibited similar peak positions and relative height; only the intensity of the spectra varied. The spectra were dominated by three strong bands: $\delta(\text{C-S})$ at 387 cm^{-1} , $\nu(\text{C-S})$ at 1077 cm^{-1} and $\nu(\text{C-C})$ at 1584 cm^{-1} , which were the a_1 vibrational modes (in-plane, in-phase modes) of the 4-ATP molecules [30]. The significant enhancement of a_1 modes was related to the enhancement of the electromagnetic field between the AuNPs, which was produced by the strong inter-nanoparticles coupling among the close contacted AuNPs. Notably, the b_2 bending modes (in-plane, out-of-phase modes) were $\delta(\text{C-H})$ at 1137 cm^{-1} , $\delta(\text{C-H}) + \nu(\text{C-C})$ at 1386 cm^{-1} and $\delta(\text{C-H}) + \nu(\text{C-C})$ at 1433 cm^{-1} [30]. The significant enhancement of b_2 modes may be attributed to the charge transfer of AuNPs to the absorbed 4-ATP molecules which was largely dependent on the energy of the excitation laser.

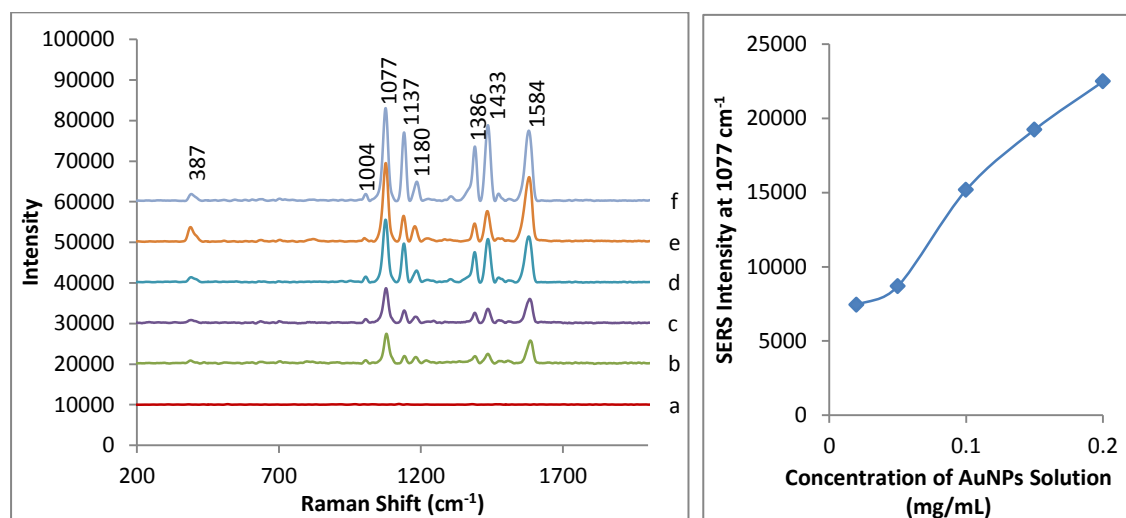


Figure 4: (Left) Raman spectrum of 1 mM of 4-ATP adsorb on (a) plain filter paper and SERS spectra of 4-ATP on filter paper dipped in AuNP solutions of (b) 0.02 mg/mL, (c) 0.05 mg/mL, (d) 0.10 mg/mL, (e) 0.15 mg/mL and (f) 0.20 mg/mL. (Right) SERS intensity of 4-ATP at 1077 cm^{-1} band from paper dipped in different concentration of AuNP solutions.

The SERS potential of AuNP treated papers was demonstrated by the drastic increase in intensities. Treating paper with 0.02 mg/mL of AuNPs significantly enhanced the Raman signal of 4-ATP (Figure 4a and 4b). The SERS intensity of AuNPs-treated paper was found to increase linearly with the concentration of AuNP solutions applied to paper (Figure 4). As the concentration increased, AuNPs were more closely packed together in the solution; they adsorbed onto paper substrate and maintain their packing density. As the average distance between the AuNPs decreased from approximately 100-200 nm to 10-50 nm, it is believed that effective ‘hot spots’ appeared and their interparticle plasmon coupling gave rise to the enhancement of electromagnetic field which intensified the SERS signals of the 4-ATP [31]. This significant SERS signal enhancement was particularly observed when paper was treated with 1.0 mg/mL of AuNPs (Figure 4) as the interparticle distance of the AuNPs became closer to their diameter (25 ± 3 nm). Overall, the SERS enhancement was increased by approximately a factor of four as the concentration of AuNP solution was increased from 0.02 mg/mL to 1.0 mg/mL (Figure 4). It is not as much as expected. However, the peak definition and the spectra clarity have drastically increased with increased AuNP concentration on paper. A possible explanation for the lack of enhancement with AuNP concentration is that all AuNP were adsorbed as single particle; the concentration of doublet and n-let is constant, and therefore the concentration of hotspots is relatively independent upon concentration of AuNP on paper. That is until the average distance between two AuNPs is equal or shorter than the distance of SERS enhancement; however, this distance might be smaller than the average distance resulting from electrostatic repulsion of AuNP. Relating experimental findings with theoretical efficiency on SERS clearly needs further understanding.

The SERS sensitivity of AuNPs paper was quantified. Paper treated with a 0.20 mg/mL of AuNP solutions was exposed to different concentrations of 4-ATP and their Raman spectra was measured (Figure 5a). The concentration of 4-ATP investigated ranged over 6 orders of magnitude, from 1 mM to 1 nM. The detection limit of AuNPs paper substrates for 4-ATP is lower than 1 nM, because even the spectrum of the 1 nM sample had good signal-to-noise ratio and the main peaks at 1077 cm^{-1} and 1584 cm^{-1} were still observable. A sigmoidal relationship between the SERS intensity and concentration of 4-ATP was observed. The SERS intensities were mostly linear when the concentration of 4-ATP was low. At high concentration, a nonlinear response emerged and saturation of SERS signal

occurred, indicating that the adsorption of 4-ATP onto the AuNPs became saturated beyond this level [32-33].

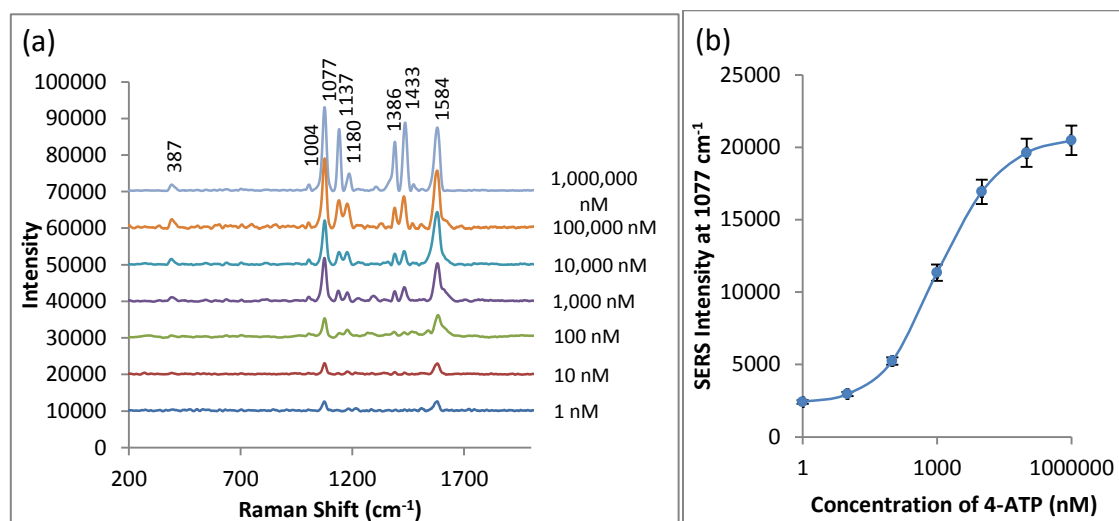


Figure 5: (a) SERS spectra of different concentration of 4-ATP from AuNPs treated paper (0.20 mg/mL AuNP solutions). (b) SERS intensity of different concentration of 4-ATP from the AuNPs treated paper at 1077 cm⁻¹ band.

2.4.2 Deposition of AuNPs on Silicon

To investigate the effect of the substrate on the distribution of AuNPs and their SERS properties, a silicon wafer was dipped into AuNPs suspension of 0.20 mg/mL; the spatial distribution of AuNPs was measured and compared with paper. Silicon is a flat and smooth substrate, whilst paper is heterogeneous, with a rough, porous and fibrillar morphology. Silicon has a point of zero charge between pH 2 to 3 [34] with a negative charge at pH greater than 3. Thus, the silicon surface was negatively charged when dipped in the AuNP solutions (pH 6). The attachment of the negatively charged AuNPs on silicon wafer was also driven by the van der Waals force. The adsorption of AuNPs from solution onto the silicon substrate (Supporting Information, S5) was much lower than on paper (Figure 2e) due to the absence of porous and hydrophilic surface, as found in paper, which readily absorbed and retained AuNPs upon dipping or drying. The particle size of AuNPs adsorbed on silicon was constant with an average diameter of 25±3 nm.

The SERS sensitivity of AuNPs treated silicon wafer (0.20 mg/mL of AuNP solutions) to a concentration range of 4-ATP was evaluated (Figure 6). Compared to paper (Figure 5), the SERS intensity of most Raman peaks from silicon was relatively low. At low concentrations of 4-ATP, the spectra became poorly resolved. Unlike the SERS signal from paper, the main peaks of 4-ATP at 1077 cm^{-1} and 1584 cm^{-1} were hardly detectable below 100 nM 4-ATP.

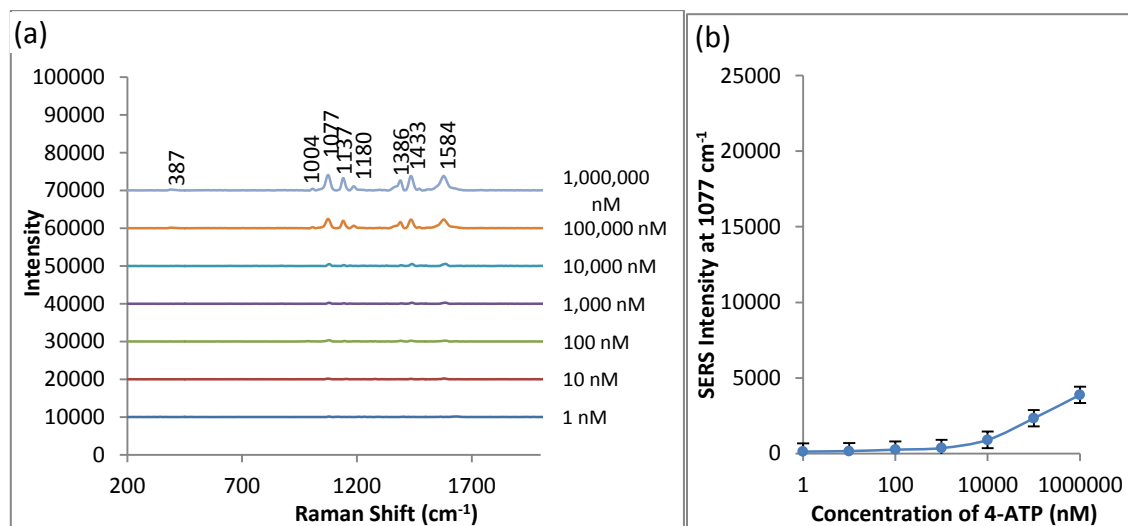


Figure 6: (a) SERS spectra of different concentration of 4-ATP from AuNPs treated silicon (0.20 mg/mL of AuNP solutions). (b) SERS intensity of different concentration of 4-ATP from the AuNPs treated silicon at 1077 cm^{-1} band.

The enhancement factors (EF) calculated for 4-ATP on paper and silicon substrates were calculated for the corresponding density of AuNPs and are shown in Figure 7. Relatively linear relationships relate the EF of 4-ATP to the density of AuNPs on the substrates (Figure 7); the aggregation state of AuNPs for all materials being constant. The EF of AuNPs treated silicon (0.20 mg/mL of AuNP solutions) was lower by more than an order of magnitude compared to paper even though its surface concentration of AuNPs was only half that of paper. AuNPs can only be retained on the surface of silicon wafer whilst paper has additional AuNPs adsorbed through its cellulose layers. Taking into account the amount of AuNPs within the bulk of paper, the SERS intensity curve of paper in Figure 7 is shifted to the right. This suggests that the significant difference of SERS intensity between paper and silicon wafer can be due to: (1) different amount of AuNPs retained by

the substrates and (2) difference in the spatial location of AuNPs (surface/bulk for paper, and surface only for silicon).

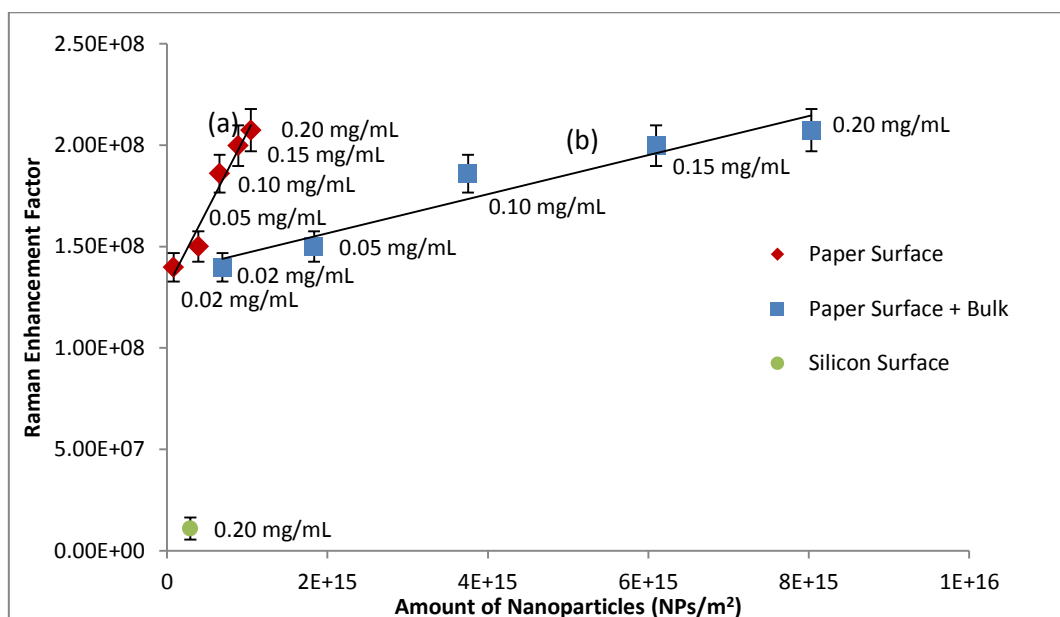


Figure 7: Relationship between the amount of AuNPs and the EF of 4-ATP measured at the 1077 cm^{-1} band for filter paper and silicon. The contributions of the AuNPs adsorbed at (a) the surface of paper and also in (b) the bulk of paper were analyzed.

2.4.3 AuNPs Droplet Test

To better understand the role of the substrate and the x-y-z distribution of AuNPs on the SERS efficiency, a $1\text{ }\mu\text{L}$ droplet from 0.20 mg/mL of AuNP solutions was deposited on paper and silicon to provide an identical amount of AuNPs on the different substrates. The AuNPs droplet on paper diffused and dried instantly, whilst the droplet on silicon took longer time to dry. The intertwined structure of cellulose fibers was able to ‘freeze’ the adsorption state of nanoparticles by rapidly drawing away the water upon drying, resulting in a more uniform distribution of AuNPs on paper (Figure 8a1 and 8a2). However, the non-porous and smooth surface of silicon wafer caused the AuNPs droplet to form aggregates around its edge which led to uneven distribution (Figure 8b1 and 8b2). This was due to the slower evaporation of water in the vicinity of the NPs which promoted the AuNPs suspension to concentrate around the edge of the droplet, forming a ‘coffee ring’ during drying [35]. The SERS spectra of 4-ATP was measured at 4 different

locations (2 at the centre and 2 at the edge of the AuNPs droplet) on paper (Figure 8a3) and silicon wafer (Figure 8b3). The peak spectra of 4-ATP were constant for both substrates, but the peaks' intensity from paper was higher compared to silicon. For silicon, the SERS signal was not reproducible: the signal from the edge of the droplet had a higher intensity than at its centre due to the presence of AuNPs aggregates, which led to higher contact point between the NPs for electromagnetic field enhancement. This means that SERS intensity and reproducibility of a same amount of AuNPs is much higher on paper than on silicon wafer.

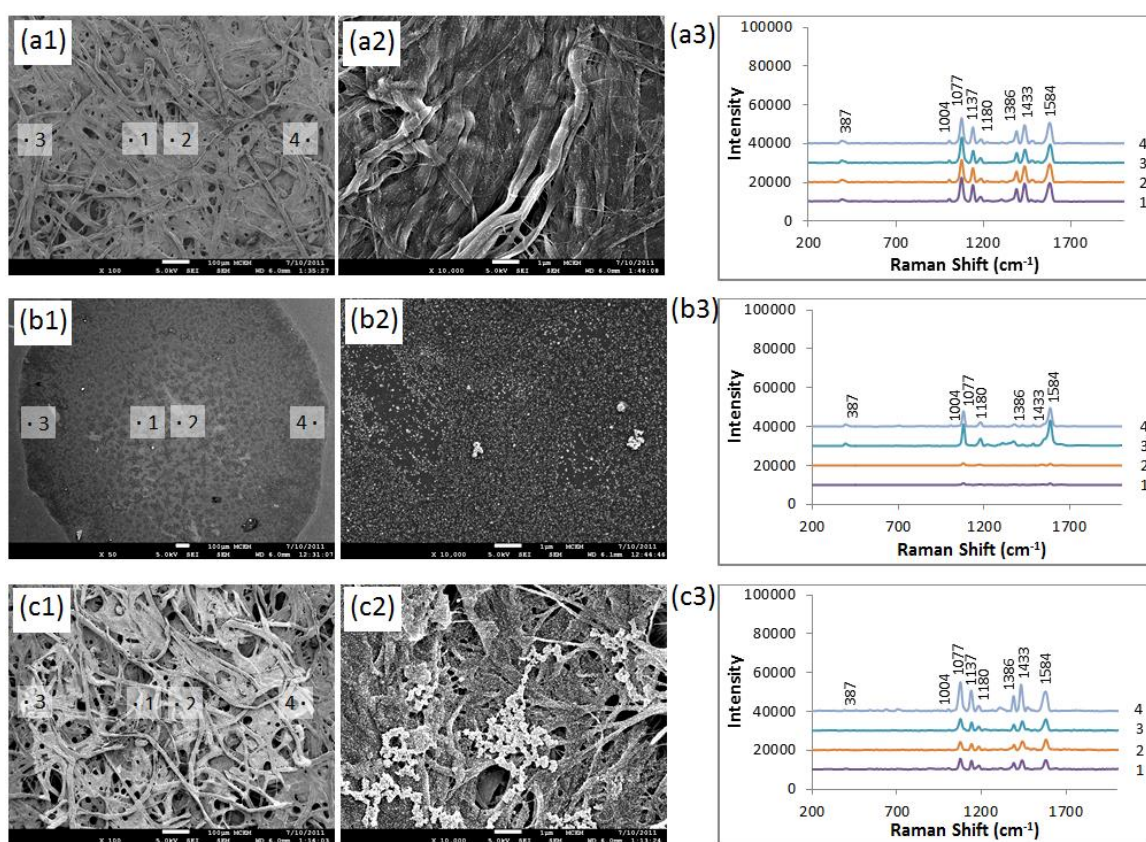


Figure 8: (a) Low and (b) high magnification FESEM images of (1) filter paper (2) silicon wafer and (3) hydrophobized paper substrates treated with 1 μ L droplet of AuNPs (0.20 mg/mL). (c) SERS spectra of 4-ATP absorbed on the droplets respectively (taken at four different spots: two from the centre and two from the edge of the droplet as indicated with numbers in the FESEM images).

A difference between the SERS performance of silicon and paper substrates might be due to the presence of AuNPs within the bulk of paper which increases the concentration of

“hotspots”. To explore the effect of the 3-dimensional spatial distribution of AuNPs, a 1 μ L droplet from 0.20 mg/mL of AuNP solution was deposited onto a hydrophobized paper. Similar to silicon, the AuNPs droplet on the hydrophobized paper took a longer time to dry and formed a ring (smaller). FESEM analysis revealed that adsorption and aggregation of AuNPs on the hydrophobized paper was higher compared to the normal paper (Figure 8a2 and Figure 8c2). FESEM cross sectional analysis showed that the AuNPs were only retained on the surface of cellulose fibers and were absent from the bulk of paper (Supporting Information, S6). The SERS spectra of 4-ATP on hydrophobic paper had a higher intensity at the edge compared to the centre of the AuNPs droplet (Figure 8c3). However, the overall SERS signal showed a lower signal-to-noise ratio than the normal paper (Figure 8a3). The AuNPs absorbed through the bulk of paper played an important role in quenching the background noise, thus producing a more sensitive SERS signal.

The silicon and hydrophobized paper treated with a single droplet of AuNP solutions did not have a significantly higher SERS intensity than that of the normal paper, even though their AuNPs had higher aggregation. The AuNPs on silicon and hydrophobized paper were only adsorbed on the surface but not distributed within the interface/bulk of the substrates. Hence, the interparticle plasmon coupling only occurred in a monolayer on the 2-dimensional (2D) surface. In contrast, the adsorption of AuNPs on the surface and into the bulk of paper presented a 3D multilayer architecture for intralayer and interlayer plasmon coupling. The z-distribution of AuNPs throughout the multilayer of cellulose fibers is believed to be responsible for amplifying the SERS signal via interlayer enhancement.

2.5 Conclusion

The effect of AuNPs' concentration and 3D distribution profile within paper on the SERS performance of paper was quantified. The objective was to drastically increase the sensitivity and selectivity of low-cost SERS paper substrate as bio-diagnostic platform. AuNPs were adsorbed from solutions onto paper and silicon wafer by physisorption using a dipping method, and the particle distribution (size, surface coverage) was quantified by FESEM/image analysis. A surface coverage of AuNPs ranging from 1.8 to 22.1% was achieved on paper; however, the particles on the surfaces represented only 40% of the

AuNPs' loading, with the majority uniformly adsorbed within the bulk of paper. The AuNPs were mostly adsorbed as singlets, and as very small aggregates. In the absence of any retention aid, the adsorption of AuNPs on paper substrate was still relatively high, even higher by an order of magnitude than on silicon when both substrates were treated similarly. Enhancement factor of a model dye (4-ATP) adsorbed onto AuNPs treated paper was higher by more than one order of magnitude than AuNP treated silicon. The high loading and uniform distribution of AuNPs on paper contributed towards the excellent SERS reproducibility and high enhancement factor.

The role of AuNPs within the bulk of paper was explored by depositing a 1 μ L droplet of AuNP solutions on paper, silicon wafer and hydrophobized paper. The paper treated with an AuNPs droplet had a higher SERS efficiency than the silicon and hydrophobized paper similarly treated, regardless of its lower surface aggregation. This highlights the importance of the z-distribution of AuNPs within the bulk of paper in quenching the background noise through interlayer plasmon coupling, thus enhancing the SERS signal of the analyte.

The paper substrate effectively 'transferred' the high packing density and uniform distribution from the AuNPs in solutions onto the cellulose fibers, and 'freezed' their adsorption state during the drying process. The SERS intensity scaled linearly with the density of AuNPs on paper. This highlights the great potential of paper as an inert and robust substrate to maintain a controlled adsorption state of AuNPs for carrying out molecular sensing with high sensitivity.

Paper is a cheap, flexible, stable, easy to use and dispose SERS substrate. It emerges as a viable substitute to commercial silicon substrate (Klarite) for routine bio-diagnostic applications. All that is needed is to optimize the distribution of NPs on the heterogeneous structure of paper to enhance SERS performance.

2.6 Acknowledgement

Thanks to Dr. T. Williams, Monash Centre for Electron Microscopy (MCEM), for FESEM technical expertise, F. Shanks from Monash Molecular Spectroscopy and Centre for Biospectroscopy for Raman technical advice, S. Narayanan and Dr. X. Li for technical

expertise. The financial supports from the ARC Linkage LP0989823 and Visy, Amcor, SCA, Norske Skog, Australian Paper, the Australian Pulp and Paper Institute and Monash University are acknowledged.

2.7 References

1. Martinez, A.W., S.T. Phillips, M.J. Butte, and G.M. Whitesides, *Patterned Paper as a Platform for Inexpensive, Low-Volume, Portable Bioassays*. *Angewandte Chemie International Edition*, 2007. **46**(8): p. 1318-1320.
2. Martinez, A.W., S.T. Phillips, E. Carrilho, S.W. Thomas, H. Sindi, and G.M. Whitesides, *Simple Telemedicine for Developing Regions: Camera Phones and Paper-Based Microfluidic Devices for Real-Time, Off-Site Diagnosis*. *Analytical Chemistry*, 2008. **80**(10): p. 3699-3707.
3. Li, X., J. Tian, and W. Shen, *Quantitative biomarker assay with microfluidic paper-based analytical devices*. *Analytical and Bioanalytical Chemistry*, 2010. **396**(1): p. 495-501.
4. Li, X., J. Tian, T. Nguyen, and W. Shen, *Paper-Based Microfluidic Devices by Plasma Treatment*. *Analytical Chemistry*, 2008. **80**(23): p. 9131-9134.
5. Khan, M.S., G. Thouas, W. Shen, G. Whyte, and G. Garnier, *Paper Diagnostic for Instantaneous Blood Typing*. *Analytical Chemistry*, 2010. **82**(10): p. 4158-4164.
6. Tian, J., X. Li, and W. Shen, *Printed two-dimensional micro-zone plates for chemical analysis and ELISA*. *Lab on a Chip*, 2011. **11**(17): p. 2869-2875.
7. Cheng, C.-M., A.W. Martinez, J. Gong, C.R. Mace, S.T. Phillips, E. Carrilho, K.A. Mirica, and G.M. Whitesides, *Paper-Based ELISA*. *Angewandte Chemie International Edition*, 2010. **49**(28): p. 4771-4774.
8. Toderas, F., M. Baia, L. Baia, and S. Astilean, *Controlling gold nanoparticle assemblies for efficient surface-enhanced Raman scattering and localized surface plasmon resonance sensors*. *Nanotechnology*, 2007. **18**.
9. Lee, S.W., Y.-B. Shin, K.S. Jeon, S.M. Jin, Y.D. Suh, S. Kim, J.J. Lee, and M.-G. Kim, *Electron beam lithography-assisted fabrication of Au nano-dot array as a substrate of a correlated AFM and confocal Raman spectroscopy*. *Ultramicroscopy*, 2008. **108**(10): p. 1302-1306.
10. Min, Q., M.J.L. Santos, E.M. Girotto, A.G. Brolo, and R. Gordon, *Localized Raman Enhancement from a Double-Hole Nanostructure in a Metal Film*. *Journal of Physical Chemistry C*, 2008. **112**(39): p. 15098-15101.
11. Stokes, D.L., Z. Chi, and T. Vo-Dinh, *Surface-Enhanced-Raman-Scattering-Inducing Nanoprobe for Spectrochemical Analysis* *Applied Spectroscopy*, 2004. **58**(3): p. 257-354.
12. Lee, C.H., L. Tian, and S. Singamaneni, *Paper-Based SERS Swab for Rapid Trace Detection on Real-World Surfaces*. *ACS Applied Materials & Interfaces*, 2010. **2**(12): p. 3429-3435.
13. Luo, Z. and Y. Fang, *SERS of C60/C70 on gold-coated filter paper or filter film influenced by the gold thickness*. *Journal of Colloid and Interface Science*, 2005. **283**(2): p. 459-463.
14. Berthod, A., J.J. Laserna, and J.D. Winefordner, *Analysis by surface enhanced Raman spectroscopy on silver hydrosols and silver coated filter papers*. *Journal of Pharmaceutical and Biomedical Analysis*, 1988. **6**(6-8): p. 599-608.
15. Cabalín, L.M. and J.J. Laserna, *Fast spatially resolved surface-enhanced Raman spectrometry on a silver coated filter paper using charge-coupled device detection*. *Analytica Chimica Acta*, 1995. **310**(2): p. 337-345.

16. Ma, W. and Y. Fang, *Experimental (SERS) and theoretical (DFT) studies on the adsorption of p-, m-, and o-nitroaniline on gold nanoparticles*. Journal of Colloid and Interface Science, 2006. **303**(1): p. 1-8.
17. Niu, Z. and Y. Fang, *Surface-enhanced Raman scattering of single-walled carbon nanotubes on silver-coated and gold-coated filter paper*. Journal of Colloid and Interface Science, 2006. **303**(1): p. 224-228.
18. Wu, D. and Y. Fang, *The adsorption behavior of p-hydroxybenzoic acid on a silver-coated filter paper by surface enhanced Raman scattering*. Journal of Colloid and Interface Science, 2003. **265**(2): p. 234-238.
19. Lee, C.H., M.E. Hankus, L. Tian, P.M. Pellegrino, and S. Singamaneni, *Highly Sensitive Surface Enhanced Raman Scattering Substrates Based on Filter Paper Loaded with Plasmonic Nanostructures*. Analytical Chemistry, 2011. **83**(23): p. 8953-8958.
20. Cheng, M.-L., B.-C. Tsai, and J. Yang, *Silver nanoparticle-treated filter paper as a highly sensitive surface-enhanced Raman scattering (SERS) substrate for detection of tyrosine in aqueous solution*. Analytica Chimica Acta, 2011. **708**(1-2): p. 89-96.
21. Turkevich, J., P.C. Stevenson, and J. Hillier, *A study of the nucleation and growth processes in the synthesis of colloidal gold*. Discussions of the Faraday Society 1951. **11**: p. 55-75.
22. Camargo, P.H.C., L. Au, M. Rycenga, W. Li, and Y. Xia, *Measuring the SERS enhancement factors of dimers with different structures constructed from silver nanocubes*. Chemical Physics Letters, 2010. **484**(4-6): p. 304-308.
23. Hu, X., T. Wang, L. Wang, and S. Dong, *Surface-Enhanced Raman Scattering of 4-Aminothiophenol Self-Assembled Monolayers in Sandwich Structure with Nanoparticle Shape Dependence: Off-Surface Plasmon Resonance Condition*. Journal of Physical Chemistry C, 2007. **111**(19): p. 6962-6969.
24. Schwartzberg, A.M., C.D. Grant, A. Wolcott, C.E. Talley, T.R. Huser, R. Bogomolni, and J.Z. Zhang, *Unique Gold Nanoparticle Aggregates as a Highly Active Surface-Enhanced Raman Scattering Substrate*. Journal of Physical Chemistry B, 2004. **108**(50): p. 19191-19197.
25. Dong, H. and J.P. Hinestroza, *Metal nanoparticles on natural cellulose fibers: electrostatic assembly and in situ synthesis*. ACS Applied Materials & Interfaces, 2009. **1**(4): p. 797-803.
26. Henglein, A. and M. Giersig, *Formation of Colloidal Silver Nanoparticles: Capping Action of Citrate*. Journal of Physical Chemistry B, 1999. **103**(44): p. 9533-9539.
27. Kim, T., K. Lee, M.-s. Gong, and S.-W. Joo, *Control of Gold Nanoparticle Aggregates by Manipulation of Interparticle Interaction*. Langmuir, 2005. **21**(21): p. 9524-9528.
28. Pinto, R.J.B., P.A.A.P. Marques, A.M. Barros-Timmons, T. Trindade, and C.P. Neto, *Novel SiO₂/cellulose nanocomposites obtained by in situ synthesis and via polyelectrolytes assembly*. Composites Science and Technology, 2008. **68**(3-4): p. 1088-1093.
29. Peacock, A.C., A. Amezcua-Correa, J. Yang, P.J.A. Sazio, and S.M. Howdle, *Highly efficient surface enhanced Raman scattering using microstructured optical fibers with enhanced plasmonic interactions*. Applied Physics Letters, 2008. **92**(14).
30. Hu, X., T. Wang, L. Wang, and S. Dong, *Surface-Enhanced Raman Scattering of 4-Aminothiophenol Self-Assembled Monolayers in Sandwich Structure with Nanoparticle Shape Dependence: Off-Surface Plasmon Resonance Condition*. Journal of Physical Chemistry C, 2007. **111**(19): p. 6962-6969.
31. Oh, M.K., S. Yun, S.K. Kim, and S. Park, *Effect of layer structures of gold nanoparticle films on surface enhanced Raman scattering*. Analytica Chimica Acta, 2009. **649**(1): p. 111-116.

32. Qiu, C., L. Zhang, H. Wang, and C. Jiang, *Surface-Enhanced Raman Scattering on Hierarchical Porous Cuprous Oxide Nanostructures in Nanoshell and Thin-Film Geometries*. Journal of Physical Chemistry, 2012. **3**(5): p. 651-657.
33. Wang, H.H., C.Y. Liu, S.B. Wu, N.W. Liu, C.Y. Peng, T.H. Chan, C.F. Hsu, J.K. Wang, and Y.L. Wang, *Highly Raman-Enhancing Substrates Based on Silver Nanoparticle Arrays with Tunable Sub-10 nm Gaps*. Advanced Materials, 2006. **18**(4): p. 491-495.
34. Wang, Y. and M. Ferrari, *Surface modification of micromachined silicon filters*. Journal of Materials Science, 2000. **35**(19): p. 4923-4930.
35. Bankar, A., B. Joshi, A. Ravi Kumar, and S. Zinjarde, *Banana peel extract mediated synthesis of gold nanoparticles*. Colloids and Surfaces B: Biointerfaces, 2010. **80**(1): p. 45-50.
36. Lewis, D.J., T.M. Day, J.V. MacPherson, and Z. Pikramenou, *Luminescent nanobeads: attachment of surface reactive Eu(iii) complexes to gold nanoparticles*. Chemical Communications, 2006(13): p. 1433-1435.
37. Liu, X., M. Atwater, J. Wang, and Q. Huo, *Extinction coefficient of gold nanoparticles with different sizes and different capping ligands*. Colloids and Surfaces B: Biointerfaces, 2007. **58**(1): p. 3-7.
38. BarathManiKanth, S., K. Kalishwaralal, M. Sriram, S. Pandian, H.-s. Youn, S. Eom, and S. Gurunathan, *Anti-oxidant effect of gold nanoparticles restrains hyperglycemic conditions in diabetic mice*. Journal of Nanobiotechnology, 2010. **8**(1): p. 16.

2.8 Supporting Information

S1: Calculation of AuNPs' concentration ^[36-38]

Assuming AuNPs are metal clusters which consist of a number of Au atoms.

$$V_{\text{cluster}} = NV_{\text{atom}} \quad (1)$$

$$\frac{4}{3}\pi(R_{\text{cluster}})^3 = N\frac{4}{3}\pi(R_{\text{atom}})^3 \quad (2)$$

Where V is the cluster volume or atomic volume, R is the cluster or atomic volume and N is the total number of atoms per cluster of NPs.

Rearranging (2):

$$R_{\text{cluster}} = N^{\frac{1}{3}}R_{\text{atom}} \quad (3)$$

Knowing the cluster radius, the surface area (S) of a NP can be calculated:

$$\text{Surface area of AuNPs cluster, } S_{\text{cluster}} = 4\pi(R_{\text{cluster}})^2 \quad (4)$$

From DLS analysis, $R_{\text{cluster}} = 23.2\text{nm}/2 = 11.6\text{nm}$

Ionic radius of gold atom, $R_{\text{atom}} = 0.137\text{nm}$

Substituting into equation (3):

$$N = (R_{\text{cluster}}/R_{\text{atom}})^3 = 6.07 \times 10^5 \text{ Au atoms per AuNP}$$

$$\begin{aligned} \text{Molecular weight of a single NP, } M_w &= M_{\text{Au}} \times N = 196.97 \times 6.07 \times 10^5 \\ &= 1.20 \times 10^8 \text{ g/mol} \end{aligned}$$

During the synthesis of AuNPs, 20 mL of 1 mM HAuCl₄ was reduced by citrate. Assuming the reduction from gold(III) to gold atoms was 100% complete:

$$\text{Moles of Au}^{3+} = 20 \times 10^{-3} \times 1 \times 10^{-3} = 2 \times 10^{-5} \text{ mol}$$

$$\text{Moles of AuNPs formed} = 2 \times 10^{-5} / N = 3.29 \times 10^{-11} \text{ mol}$$

$$\text{Mass of AuNPs formed} = 3.29 \times 10^{-11} \times M_w = 3.95 \text{ mg}$$

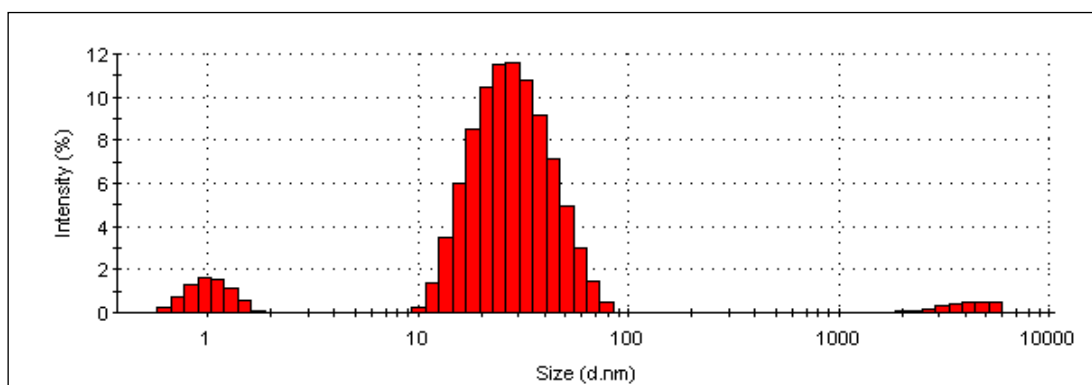
$$\text{Concentration of AuNPs} = 3.95 / 20 = 0.20 \text{ mg/mL}$$

Range of concentration of AuNPs used in the experiment after diluting 0.20 mg/mL of stock solution by a factor of 1/4 to lower concentration: 0.20 mg/mL, 0.15 mg/mL, 0.10 mg/mL, 0.05 mg/mL, 0.02 mg/mL.

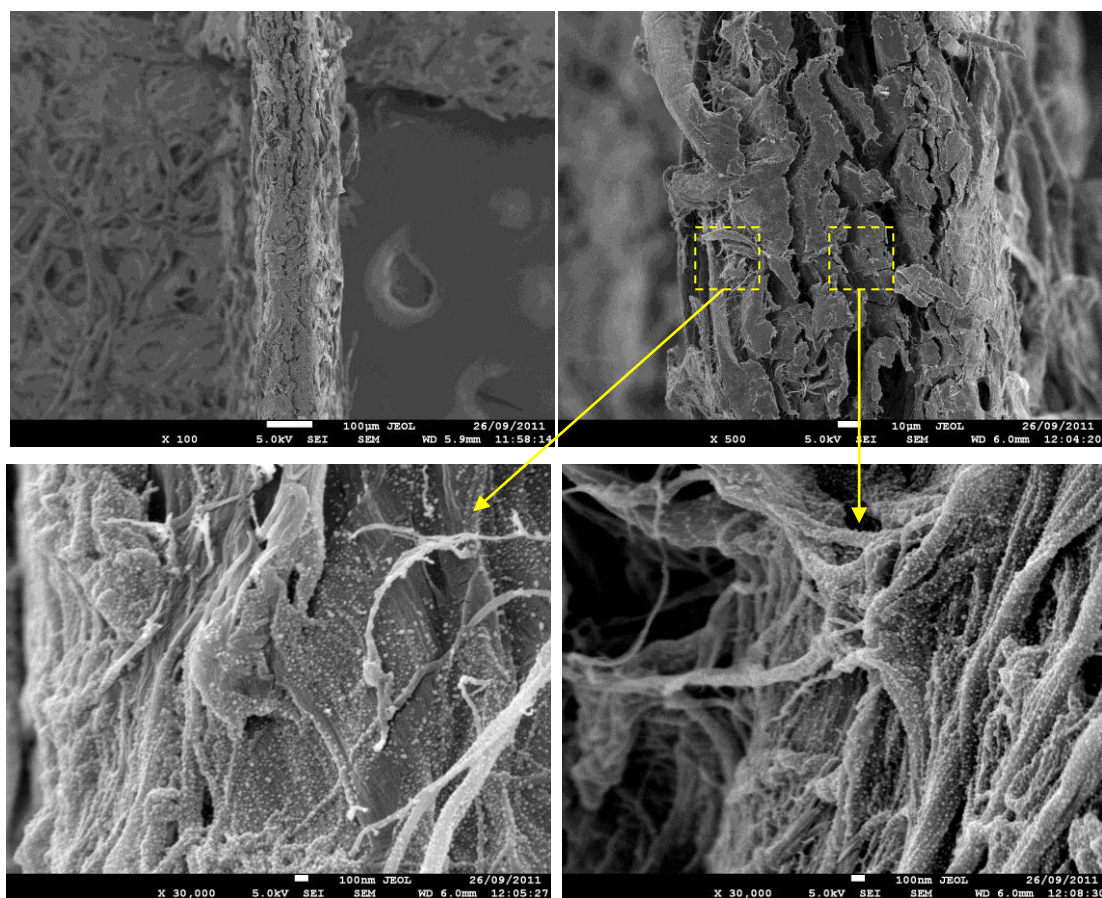
References

- (1) Lewis, D. J.; Day, T. M.; MacPherson, J. V.; Pikramenou, Z., Luminescent nanobeads: attachment of surface reactive Eu(iii) complexes to gold nanoparticles. *Chem. Commun.* **2006**, (13), 1433-1435.
- (2) Liu, X.; Atwater, M.; Wang, J.; Huo, Q., Extinction coefficient of gold nanoparticles with different sizes and different capping ligands. *Colloids Surf., B* **2007**, 58 (1), 3-7.
- (3) BarathManiKanth, S.; Kalishwaralal, K.; Sriram, M.; Pandian, S.; Youn, H.-s.; Eom, S.; Gurunathan, S., Anti-oxidant effect of gold nanoparticles restrains hyperglycemic conditions in diabetic mice. *J. Nanobiotechnol.* **2010**, 8 (1), 16.

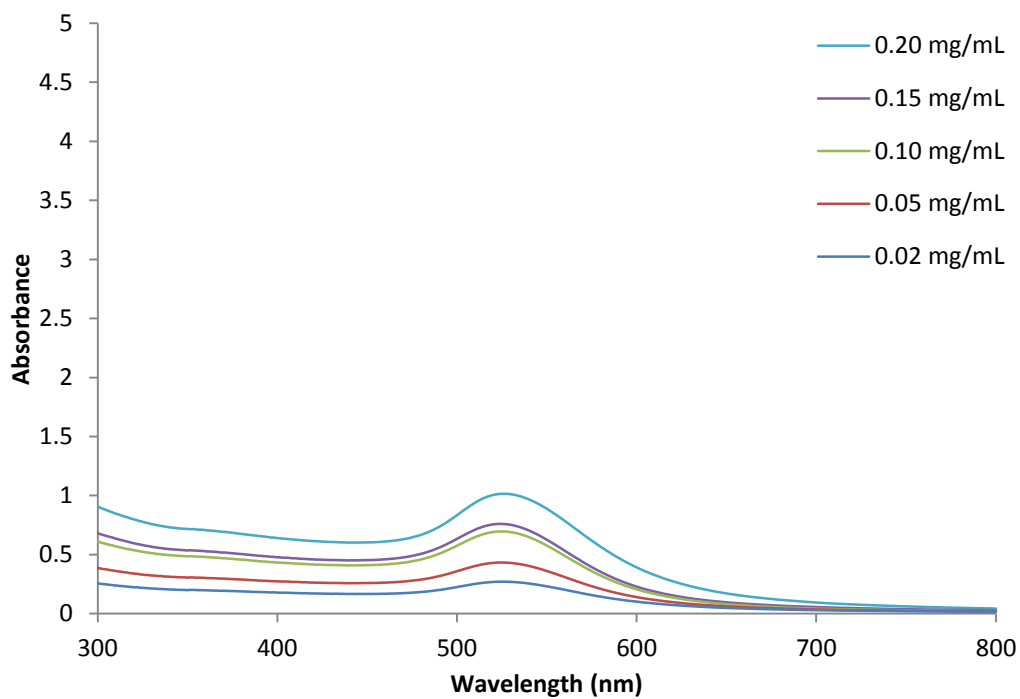
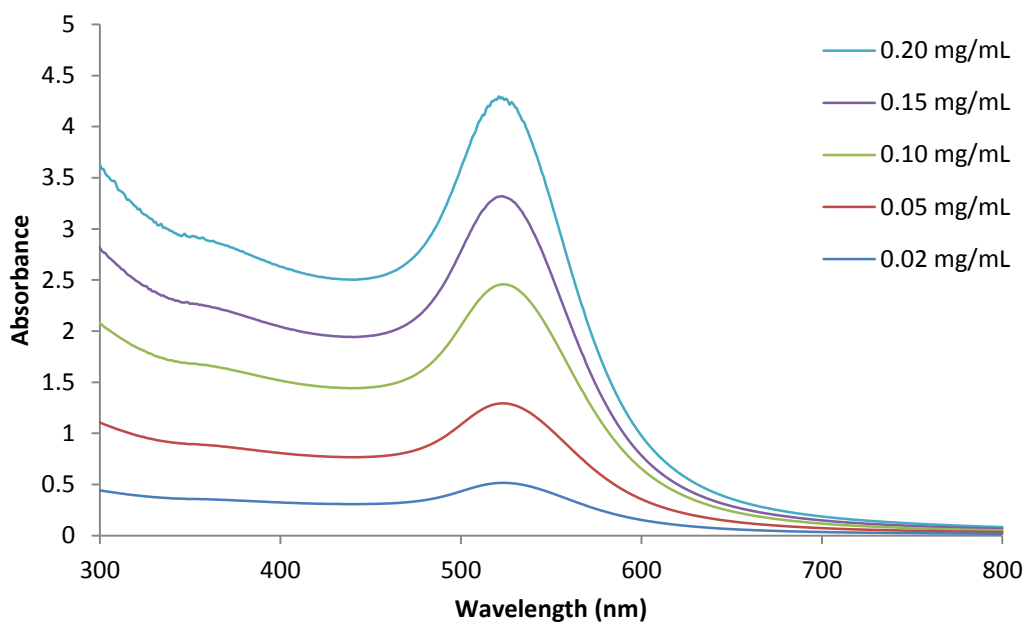
S2: Particle size distribution of 0.20 mg/mL of AuNPs in aqueous solution measured by DLS.



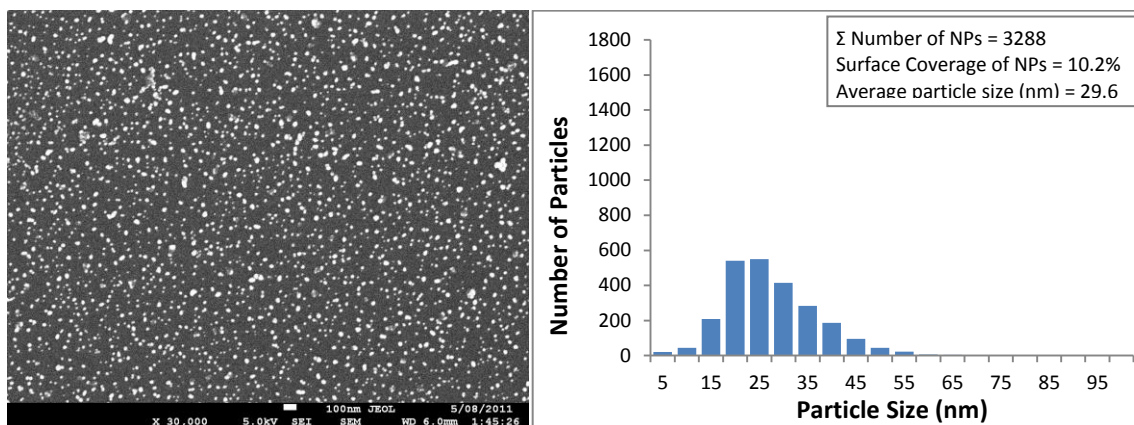
S3: FESEM cross sectional view of 0.20 mg/mL of AuNPs treated paper.



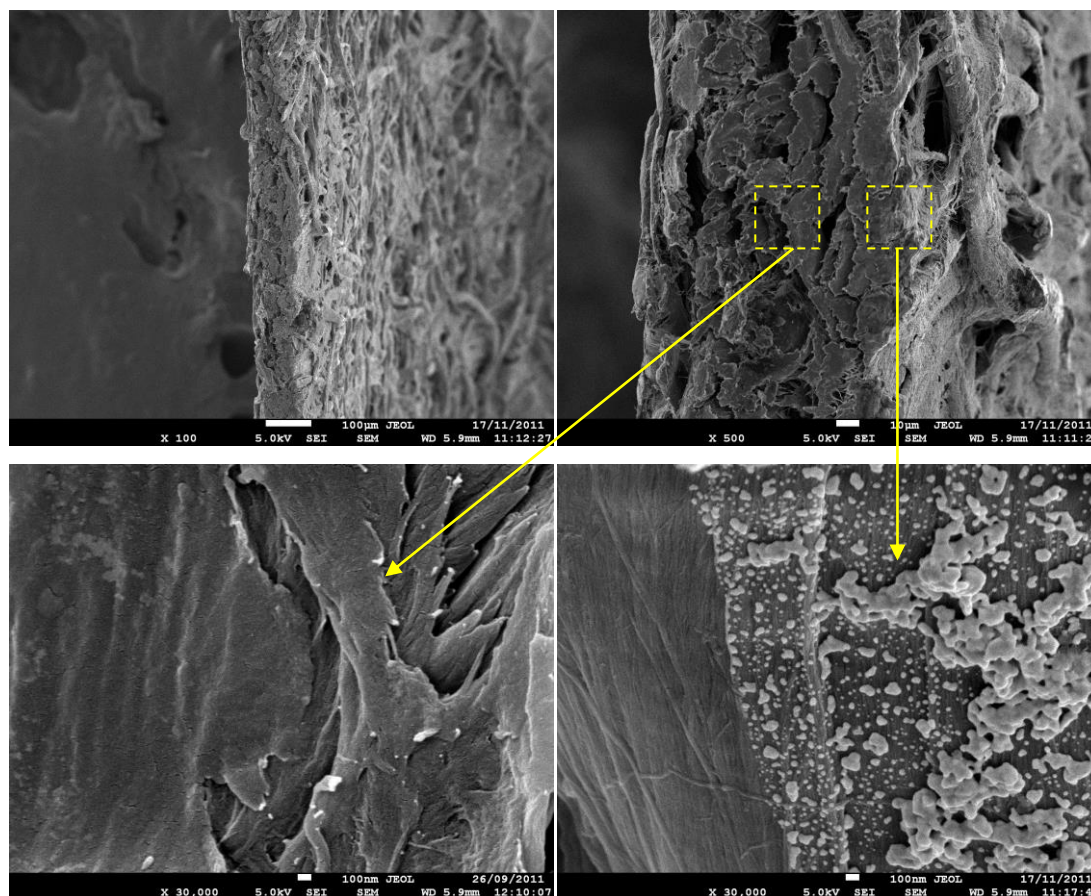
S4: UV-Vis absorbance spectra of AuNPs solutions before (upper) and after (bottom) dipping of filter papers.



S5: FESEM image and particle size distribution of silicon wafer dipped in 0.20 mg/mL AuNP solution.



S6: SEM cross sectional view of 1 μL of 0.20 mg/mL AuNPs droplet on hydrophobic paper.



This page is intentionally blank

Chapter 3

Effect of Cationic Polyacrylamides on the Aggregation and SERS Performance of Gold Nanoparticles-treated Paper

This page is intentionally blank

Monash University

Declaration for Thesis Chapter 3

Declaration by candidate

In the case of Chapter 3, the nature and extent of my contribution to the work was the following:

Nature of contribution	Extent of contribution (%)
Initiation, key ideas, experimental and analysis works, development and writing up of paper	80

The following co-authors contributed to the work. Co-authors who are students at Monash University must also indicate the extent of their contribution in percentage terms:

Name	Nature of contribution	Extent of contribution (%) for student co-authors only
Gil Garnier	Initiation, key ideas, reviewing and editing of the paper.	Supervisor
George Simon	Initiation, key ideas, reviewing and editing of the paper.	Co-supervisor
Dan Li	Initiation, key ideas, reviewing and editing of the paper.	Co-supervisor

Candidate's Signature

Date 13.03.2013

Declaration by co-authors

The undersigned hereby certify that:

- (1) the above declaration correctly reflects the nature and extent of the candidate's contribution to this work, and the nature of the contribution of each of the co-authors.
- (2) they meet the criteria for authorship in that they have participated in the conception, execution, or interpretation, of at least that part of the publication in their field of expertise;
- (3) they take public responsibility for their part of the publication, except for the responsible author who accepts overall responsibility for the publication;
- (4) there are no other authors of the publication according to these criteria;
- (5) potential conflicts of interest have been disclosed to (a) granting bodies, (b) the editor or publisher of journals or other publications, and (c) the head of the responsible academic unit; and
- (6) the original data are stored at the following location(s) and will be held for at least five years from the date indicated below:

Location(s)

At [redacted] Institute (APPI), Department of Chemical
Engineering, Monash University, Clayton, VIC 3800, Australia.

Signature 1

Date 11/12/12

Signature 2

Date 12/12/12

Signature 3

Date 11/12/2012

This page is intentionally blank

Effect of Cationic Polyacrylamides on the Aggregation and SERS Performance of Gold Nanoparticles-treated Paper

Ying Hui Ngo¹, Dan Li², George P. Simon² and *Gil Garnier¹

¹ BioPRIA, Australian Pulp and Paper Institute (APPI), Department of Chemical Engineering Monash University, Clayton, VIC 3800, Australia.

² Department of Material Engineering Monash University, Clayton, VIC 3800, Australia

*Corresponding author. Email: [REDACTED]; Tel: [REDACTED]; Fax: [REDACTED]

Content

3.1	Abstract	116
3.2	Introduction	116
3.3	Experimental Section	118
3.3.1	Materials	118
3.3.2	Synthesis and Deposition of Nanoparticles on Paper Substrates	119
3.3.3	Preparation of Raman Active Substrates	119
3.3.4	Instrumentation	120
3.4	Results	121
3.4.1	Effect of CPAM Concentration	121
3.4.2	Effect of CPAM Charge Density	125
3.4.3	Effect of CPAM Molecular Weight	127
3.4.4	Sensitivity of AuNPs-CPAM paper	129
3.4.5	Stability of AuNPs-CPAM paper	130
3.5	Discussion	130
3.5.1	SERS Optimization	130
3.5.2	Mechanism	132
3.6	Conclusion	135
3.7	Acknowledgement	136
3.8	References	137
3.9	Supporting Information	140

3.1 Abstract

This study examines and quantifies the effect of cationic polyelectrolyte adsorption on paper on the aggregation and retention of gold nanoparticles (AuNPs) to optimize their Surface Enhanced Raman Scattering (SERS) enhancement factor and sensitivity. Aggregation of metallic nanoparticles is known as a key factor for intense SERS enhancement. Paper substrates were treated with aqueous solutions of cationic polyacrylamide (CPAM) varying in concentration, charge density and molecular weight to control the AuNPs' aggregate size distribution and surface coverage on paper. The Raman enhancement factor of AuNPs-CPAM paper was almost an order of magnitude greater than for the untreated AuNPs paper. The high loading and uniform distribution of AuNPs aggregates on CPAM pre-treated paper contributed towards the excellent SERS reproducibility, sensitivity and high enhancement factor. This configuration of AuNP on paper was favoured by treating the substrate with CPAM solutions of higher concentrations, higher charge density and greater molecular weight.

Keywords: SERS, gold nanoparticles (AuNPs), aggregates, paper, cationic polyacrylamide (CPAM), concentration, charge density, molecular weight.

3.2 Introduction

Paper is gaining wide interest as a low-cost diagnostic platform for health and environmental applications. Paper is cheap and easy to engineer, biodegradable, biocompatible and allows full use of functional printing technology [1-2]. Flexible micro-fluidic systems, reactors and valves have been printed on paper to regulate, measure and control the flow of analytes and reagents [3-7]. Paper also allows the use of Enzyme-Linked Immunosorbent Assay (ELISA) for the quantification of antibody concentration [2-3]. However, ELISA methods often require the preparation of multiple reactants and tedious washing procedures. A straight-forward and attractive alternative involves direct contact between paper substrate and analytes, followed by rapid molecular signal detection using Surface Enhanced Raman Scattering (SERS) spectroscopy.

SERS involves enhancement of Raman signal to detect small energy changes occurring when light is scattered from a molecule which is absorbed on a metallic surface, typically

a metallic nanoparticle. The enhancement factor can be as much as 10^{14} – 10^{15} [8], which makes SERS a sensitive, single-molecule detection technique to identify analytes in trace levels. In the recent years, Raman spectroscopy has been developed from conventional laboratory system to portable handheld device for rapid on-site detection. The emerging applications of SERS include prompt detection of chemical warfare, biological agents, explosives and drug compounds.

With all the advantages offered by SERS, many studies have been directed towards fabricating an ideal SERS substrate which is low-cost, sensitive, selective, reproducible, flexible and stable for long term storage between measurements. Metal aqueous colloids are one of the first commonly used substrate; but unfortunately, their application has been challenged by low reproducibility and stability. This has led to the development of different techniques to immobilize metallic nanoparticles on solid substrates, in particular electron beam lithography [9], focused ion beam patterning [10] and thermal evaporation [11] have all been used to deposit nanoparticles of controlled size, shape and aggregation on inorganic substrates such as glass and silicon. However, these techniques are time consuming, costly, require sophisticated equipment, and the substrates are often fragile and suffer from poor storage stability.

Whilst many issues are still associated with other SERS substrates, paper has emerged as an efficient substrate for routine SERS analysis in a few studies due to its robustness [12–17]. However, very few studies have controlled the distribution of particles within paper [18–21], and none has optimized the aggregation of nanoparticles on paper as a SERS substrate. In a previous study [22], we reported the fabrication of SERS paper substrates by dipping filter paper into suspensions of gold nanoparticles (AuNPs) of constant particle size with different nanoparticle concentrations. The AuNPs were mostly adsorbed as singlets, and as very small aggregates on the paper. We found that different surface coverage and spatial distribution of the AuNPs produced different electromagnetic coupling and thus degree of SERS enhancement. Here, we report a method based on pre-treatment of paper with polyelectrolytes to induce and control the aggregation state of AuNPs in order to optimise the magnitude of their SERS effects.

Aggregation of metallic nanoparticles is known as a key factor for intense SERS enhancement since it was first reported by Brus et al. [23]. As the metal nanoparticles are contacted to form aggregates, their transition dipoles couple to each other, and the enhanced fields of each nanoparticle start to coherently interfere at their contact points. When analyte molecules are adsorbed in this contact point ('hot spot'), their Raman signals can be significantly enhanced (10^{14} – 10^{15}) [8]. Hence, aggregates of nanoparticles have more efficient SERS properties than individual nanoparticles, because larger enhancements can be achieved at the particle junctions of aggregates.

This study has two objectives. The first is to quantify the effect of cationic polyelectrolyte's adsorption on paper on the aggregation and retention of AuNPs. The second objective is to relate the aggregation and surface coverage of AuNPs on paper to the optimum SERS enhancement factor and sensitivity. Paper was treated with aqueous solutions of cationic polyacrylamide (CPAM) varying in concentration, charge density and molecular weight. The aggregate size distribution and surface coverage of AuNPs on paper were quantified and related to their SERS performance. The longer term aim of this study is thus to develop AuNPs treated paper as a multifunctional platform for low cost bio-diagnostics.

3.3 Experimental Section

3.3.1 Materials

Hydrogen tetrachloroaurate trihydrate ($\text{HAuCl}_4 \cdot 3\text{H}_2\text{O}$), sodium citrate tribasic dihydrate ($\text{Na}_3\text{C}_6\text{H}_5\text{O}_7 \cdot 2\text{H}_2\text{O}$) and 4-aminothiophenol (4-ATP) were purchased from Sigma-Aldrich and used as received. The cationic trimethylamino-ethyl-methacrylate polyacrylamide (CPAM) polymers were supplied by AQUA+TECH Switzerland from their SnowFlake Cationics product range, and used as received (chemical structure shown in Supporting Information). They were identified as: I1 (5 wt% charge density, molecular weight 13 MDa), H1 (10 wt% charge density, molecular weight 13 MDa), F1 (40 wt% charge density, molecular weight 13 MDa) and F3 (40 wt % charge density, molecular weight 6 MDa). The unit of wt % represents the percentage of polymer chains with charge within the polymer and the values were obtained from the manufacturer's specification. The actual charge density of the polymers was also measured by titration with an anionic

polymer (sodium polyethylene sulphonate). Details and results are presented in Supporting Information (S4). Whatman qualitative filter paper #1, which consists of 98% α -cellulose, was selected as the paper substrate as it is a convenient model paper of well defined structure and to ensure minimal SERS interference from process components (polymers or coatings). Ultrapure water purified with a Millipore system (18 M Ω .cm) was used in all aqueous solutions and rinsing procedures.

3.3.2 Synthesis and Deposition of Nanoparticles on Paper Substrates

AuNPs were synthesized by using 1 mM H₂AuCl₄·3H₂O and 1% aqueous Na₃C₆H₅O₇·2H₂O according to the Turkevich method [24]. A stock solution of CPAM was prepared on the day of the experiment by diluting dry powder to 0.1 mg/mL with Millipore water, and gently mixing the dispersions for 8 hours at 23°C to facilitate the dissolution process. Filter papers (55 mm diameter) were used as received, or were pretreated with the cationic polymer. For treatment, the filter papers were dipped into 10 mL polymer solutions for 1 hour, rendering the paper cationic. The treated papers were rinsed with distilled water to remove any unbounded polymer. Wet pieces of untreated and polymer-treated paper substrates were then dipped immediately into Petri dishes containing 10 mL solution of AuNPs for 24 hours. After dipping, the paper substrates were rinsed thoroughly with distilled water to remove any loosely bound AuNPs, and the papers were air-dried and stored at 50% relative humidity and 23°C until further analysis.

3.3.3 Preparation of Raman Active Substrates

Solutions of 1 mM of 4-ATP were prepared in ethanol. 4-ATP is known for its strong affinity to the surface of AuNPs (its S-H bond is easily cleaved to form Au-S bond upon adsorption). The dried AuNPs-treated substrates were dipped into 2 mL of the 4-ATP ethanol solution 5 minutes to obtain a monolayer of 4-ATP on the substrates. After thorough rinsing with ethanol and drying, they were subjected to Raman characterization. The Raman enhancement factor (EF) of 1 mM of 4-ATP on a substrate was calculated according to [25-26]:

$$EF = \frac{[I_{SERS}]}{[I_{bulk}]} \times \frac{[N_{bulk}]}{[N_{ads}]} \quad (1)$$

where I_{SERS} is the intensity of a specific band in the SERS spectrum of 4-ATP and I_{bulk} is the intensity of the same band in the Raman spectrum from the bulk solution sample. For all spectra, the intensity of the band at 1077 cm^{-1} was used to calculate EF values. N_{bulk} is the number of molecules of the bulk 4-ATP in the laser illumination volume while N_{ads} is the number of molecules adsorbed and sampled on the SERS active substrate within the laser spot.

3.3.4 Instrumentation

Field Emission Scanning Electron Microscopy (FESEM), which produces higher resolution, less sample charging and less damaged images than conventional SEM, was performed using a JEOL 7001 Field Emission Gun (FEG) system operating at 5 kV and 180 pA. ImageJ analysis software was used to determine the coverage of AuNPs on the cellulose fibers in the FESEM images and estimate particle size distribution. The total number of AuNPs was calculated by dividing the total area of AuNPs on paper (in each FESEM images) by the area of an individual AuNP measured by Dynamic Light Scattering (DLS) method ($d=23.2\text{ nm}$). The Zeta potential and DLS measurements were performed with a Zetasizer Nano ZS (Malvern Instruments) in a Folded Capillary cell (DTS1060) at $25\text{ }^{\circ}\text{C}$. For the zeta-potential measurement, laser Doppler electrophoresis measures the net velocity of the nanoparticles in the liquid that results when an electric field is applied. The fundamental quantity measured is the net electrophoretic mobility (μ) of the particles, which is then converted to the zeta-potential using Henry's approximation. UV-Vis absorbance was measured using a Varian Cary 300Bio spectrophotometer. All Raman and SERS spectra were obtained in air using a Renishaw Invia Raman microscope equipped with a 300 mW 633 nm laser. The laser beam was positioned through a Leica imaging microscope objective lens ($50\times$), whilst the instrument's wavenumber was calibrated with a silicon standard centered at 520.5 cm^{-1} shift. Due to the smaller spot size of the laser compared with the large surface area of the samples, the spectra were obtained at 5 different points of the surface. The position of the spectra band from different points on the surface were the same, but differed only in intensity. The average Raman intensity (of 5 measurements) was presented as the final result after baseline subtraction from the control samples.

3.4 Results

3.4.1 Effect of CPAM Concentration

Aggregates of nanoparticles are expected to have a higher SERS efficiency than individual nanoparticles because of the greater SERS enhancement at their points of contact [23]. To investigate this hypothesis, filter paper samples were pre-treated with CPAM solutions of different concentrations. A high molecular weight and highly charged CPAM was selected. This was to induce a positive charge on paper (which is originally negatively charged) and to create a polymer layer able to adsorb, retain and aggregate the negatively charged AuNPs. The CPAM used here had a molecular weight of 13 MDa and 40 wt% of charge density. The positive charge of the CPAM solutions increased with their polymer concentration, as measured by their zeta potential (Table I). After CPAM pre-treatment, the filter papers were rinsed and directly dipped into a 0.20 mg/mL AuNPs solution for 24 hours. The AuNPs had a zeta potential of -44.6 mV, and an average diameter of 23.2 nm, as judged by Field Emission Scanning Electron Microscopy (FESEM).

Table 1: Zeta potential of CPAM solutions with different concentration, charge density and molecular weight.

	Concentration of CPAM (40 wt% Charge Density, 13 MDa Molecular Weight) (mg/mL)			Charge Density of CPAM (0.10 mg/mL concentration, 13 MDa Molecular Weight) (wt %)			Molecular Weight of CPAM (0.10 mg/mL concentration, 40 wt% Charge Density) (MDa)	
	0.01	0.05	0.10	5	10	40	6	13
Zeta Potential (mV)	12.2	27.2	32.6	18.7	25.3	32.6	5.08	32.6

The colour intensity of the dried AuNPs and AuNPs-CPAM treated papers was analyzed with ImageJ software (Figure 1). The colour of the paper turned from reddish-purple (AuNPs on untreated paper) to dark purple when the paper was pre-treated with CPAM, followed by AuNPs and the colour became darker as the concentration of CPAM was increased.

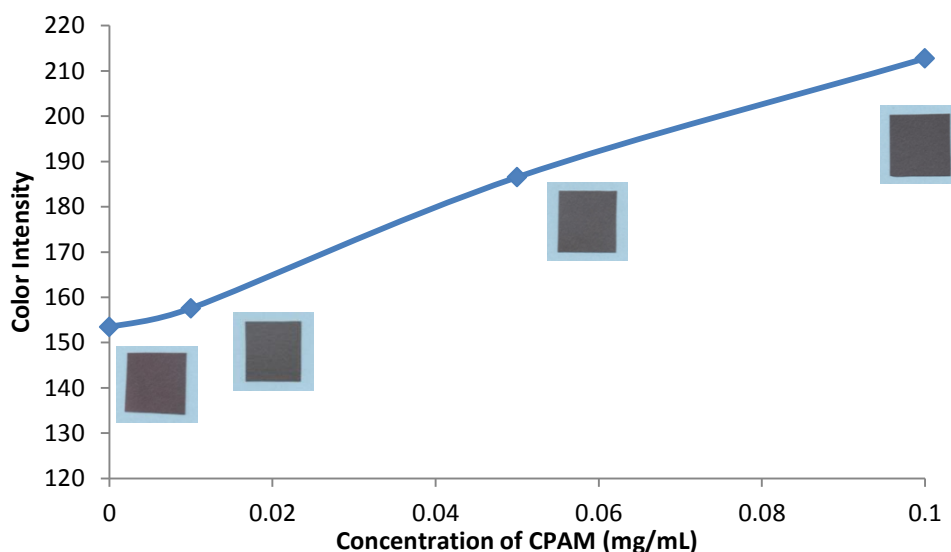
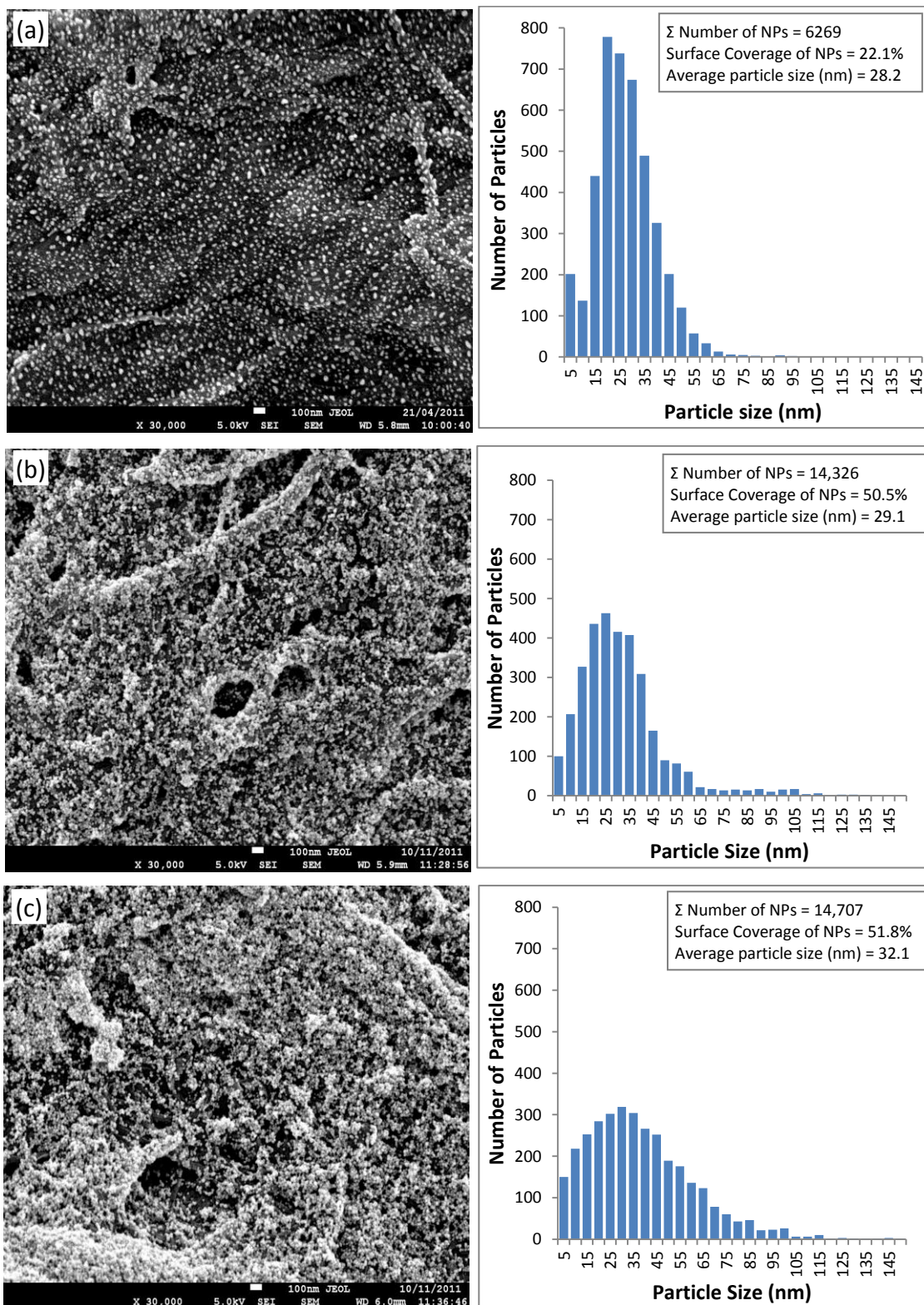


Figure 1: Colour intensity of filter paper dipped in 0.20 mg/mL of AuNP solutions without CPAM pre-treatment and with CPAM pre-treatment of 0.01 mg/mL, 0.05 mg/mL and 0.10 mg/mL polymer concentration.

FESEM analysis was performed to examine the adsorption of AuNPs on the untreated and CPAM pre-treated papers. Pre-treating paper with the dilute 0.01 mg/mL CPAM did not increase AuNP aggregate size but more than doubled the AuNP paper surface coverage (Figures 2a and 2b). A significant increase was observed in the AuNPs' surface coverage on CPAM pre-treated papers compared to untreated paper. As the concentration of CPAM solution was increased, the assemblies of AuNPs were drawn together, forming a random distribution of two- and three-dimensional clusters within the paper microstructure (Figure 2). The surface coverage and size of AuNPs aggregates also increased dramatically to 84.6% and 59.6 nm, respectively, for paper pre-treated with the concentrated CPAM solution (0.10 mg/mL) (Figure 2e).



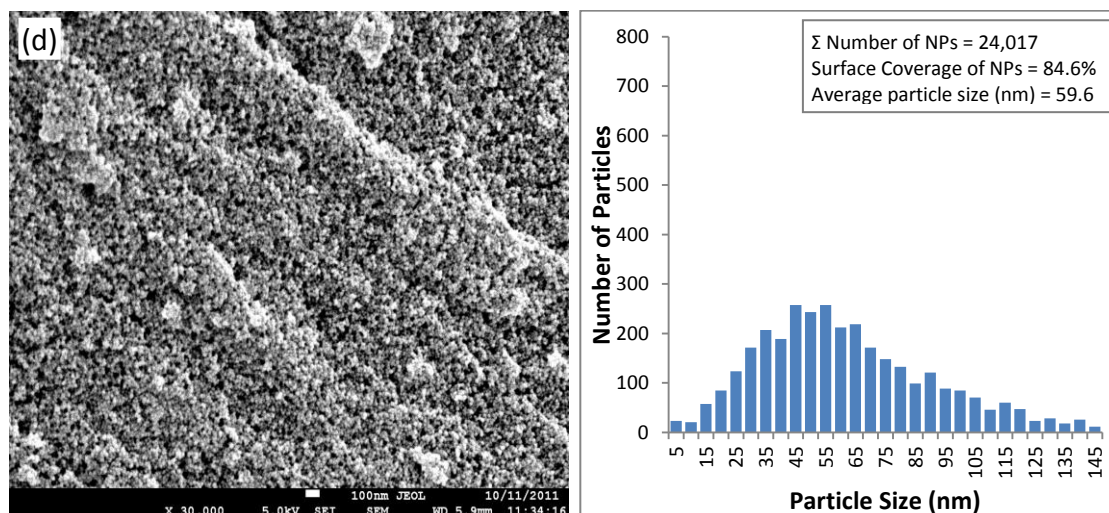


Figure 2: FESEM images and histograms of AuNPs' particle size distribution of filter paper dipped in 0.20 mg/mL of AuNP solutions (a) without CPAM pre-treatment and with CPAM pre-treatment of (b) 0.01 mg/mL (c) 0.05 mg/mL and (d) 0.10 mg/mL polymer concentration.

4-Aminothiophenol (4-ATP) was selected as the probe molecule in the Raman analysis for its distinct Raman features, strong affinity for Au surfaces via thiol bonding and formation of self-assembled monolayers [27]. The concentration effect of CPAM solutions on the SERS signal of 4-ATP from paper substrates was quantified (Figure 3). The SERS spectra were dominated by three strong characteristic bands: $\delta(\text{C-S})$ at 387 cm^{-1} , $\nu(\text{C-S})$ at 1077 cm^{-1} and $\nu(\text{C-C})$ at 1584 cm^{-1} , which represent the a_1 vibrational modes (in-plane, in-phase modes) of the 4-ATP molecules [28]. The significant enhancement of a_1 modes was related to the enhancement of the electromagnetic field between the AuNPs, which was produced by the strong inter-nanoparticles coupling among the close contacted AuNPs. Notably, the b_2 bending modes (in-plane, out-of-phase modes) were $\delta(\text{C-H})$ at 1137 cm^{-1} , $\delta(\text{C-H}) + \nu(\text{C-C})$ at 1386 cm^{-1} and $\delta(\text{C-H}) + \nu(\text{C-C})$ at 1433 cm^{-1} [28]. The significant enhancement of b_2 modes may be attributed to the charge transfer of AuNPs to the absorbed 4-ATP molecules, which was largely dependent on the energy of the excitation laser. Figure 3 also shows the Raman Enhancement Factor (EF) of 4-ATP doubled when paper was pre-treated with 0.01 mg/mL of CPAM. The Raman Enhancement Factor (EF) increased pseudo-linearly with the concentration of CPAM used for paper pre-treatment.

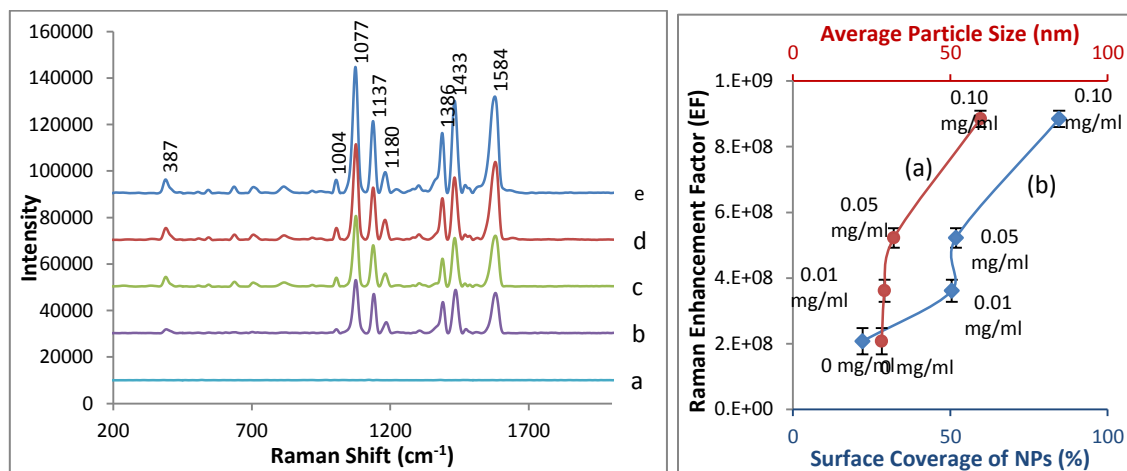


Figure 3: (Left) Raman spectrum of 4-ATP adsorbed on (a) plain filter paper, SERS spectra of 4-ATP on AuNPs paper (b) without CPAM pre-treatment and with CPAM pre-treatment of (c) 0.01 mg/ml (d) 0.05 mg/ml and (e) 0.10 mg/ml polymer's concentration. (Right) Relationship between the (a) average size and (b) surface coverage of AuNP aggregates and the EF of 4-ATP measured at the 1077 cm⁻¹ band (error bars show standard deviation of 5 measurements from different spots on the substrate).

3.4.2 Effect of CPAM Charge Density

The paper substrates were pre-treated with 0.10 mg/mL CPAM solutions of constant molecular weight (13MDa) but different charge density, after which they were dipped in 0.20 mg/mL of AuNP solution. CPAM with a charge density of 5 wt%, 10 wt% and 40 wt% were tested. The charge density of the polymer quantifies the mass fraction of charged monomers forming the polymer. Titration experiments with an anionic polymer were performed to measure the actual charge density of polymer. Results are provided in Supporting Information (S4). The zeta potential of the CPAM solutions is shown in Table I; the zeta potential increasing with the charge density of polymer. The surface coverage and average aggregate diameters of AuNPs increased from 62.2% to 84.6% and from 34.8 nm to 59.6 nm, respectively, as a function of the CPAM's charge density (Figure 4). The cluster size distribution also became wider.

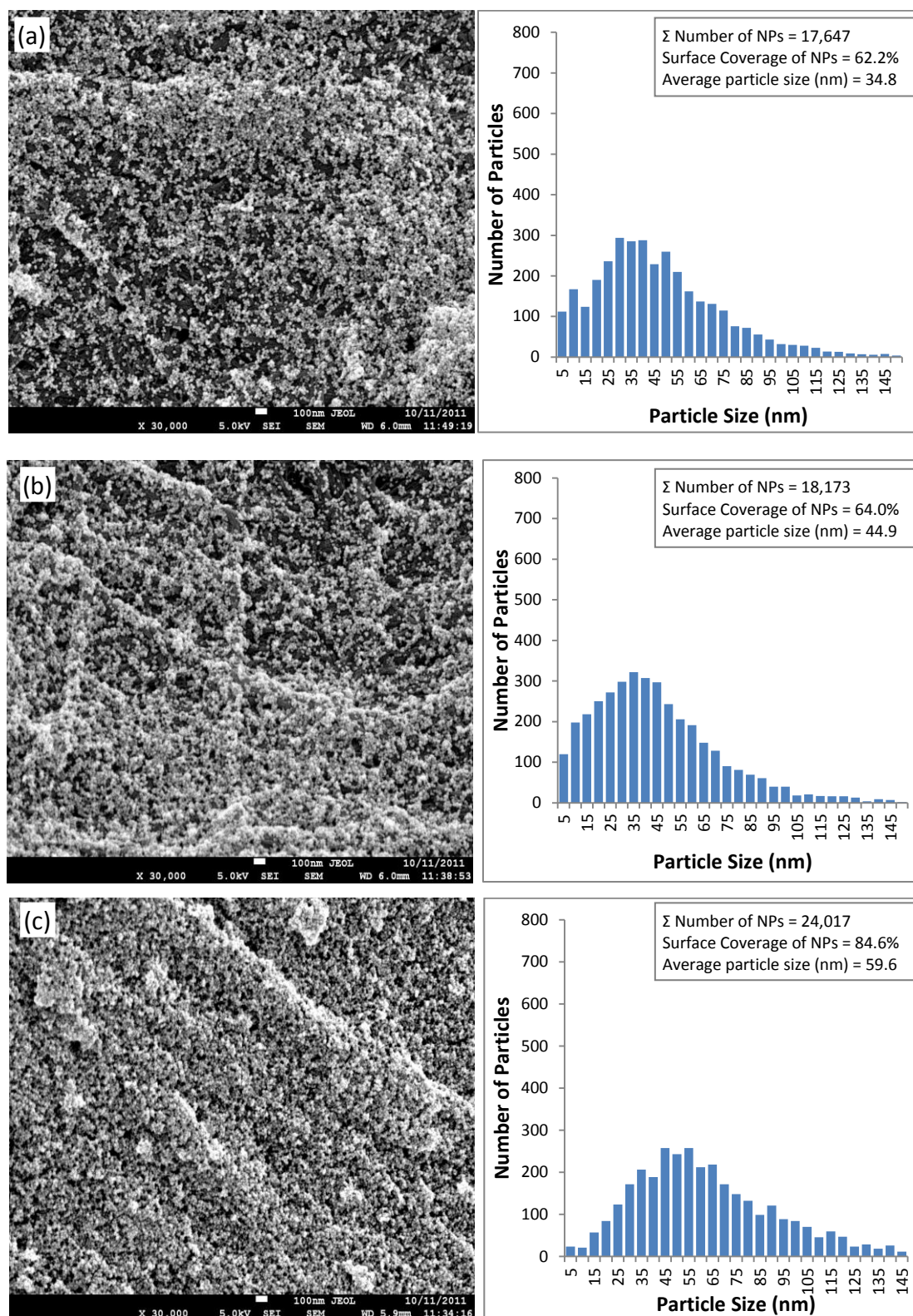


Figure 4: FESEM images and histograms of particle size distribution of AuNPs-CPAM papers treated with polymer solution charge density of (a) 5 wt%, (b) 10 wt% and (c) 40wt%.

The charge density of the CPAM solution strongly affected the SERS enhancement of the AuNPs-CPAM paper (Figure 5). From an initial Raman EF of 2.1×10^8 , the EF increased by a factor of 4 to 8.9×10^8 .

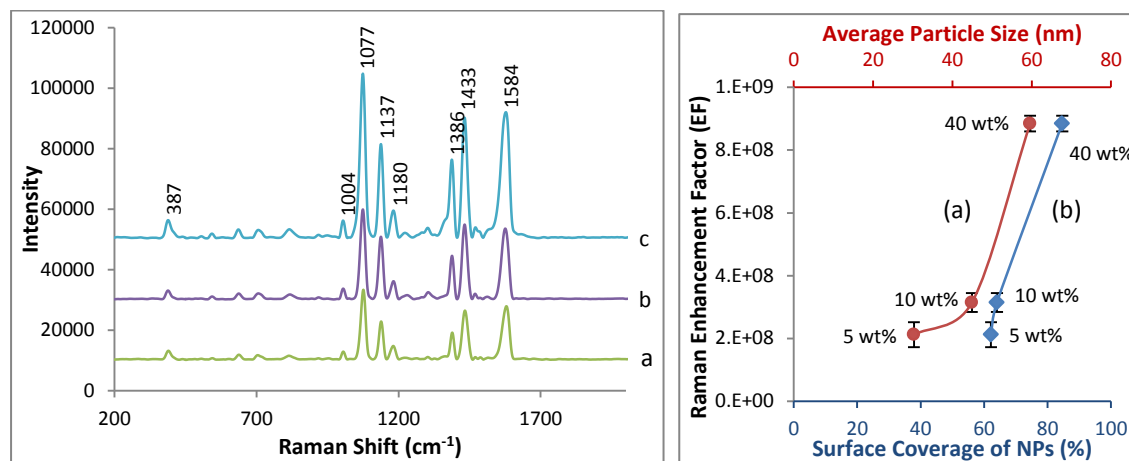


Figure 5: (Left) SERS spectra of 4-ATP on AuNPs-CPAM papers with polymer's charge density of (a) 5 wt%, (b) 10 wt% and (c) 40wt%. (Right) Relationship between the (a) average size and (b) surface coverage of AuNP aggregates and the EF of 4-ATP measured at the 1077 cm⁻¹ band (error bars show standard deviation of 5 measurements from different spots on the substrate).

3.4.3 Effect of CPAM Molecular Weight

The effect of CPAM's molecular weight on the aggregation and adsorption of AuNPs on paper was investigated. Paper was pre-treated with a lower molecular weight CPAM of 6 MDa (40 wt% charge density and 0.10 mg/mL concentration). CPAM of 6 MDa has a relatively lower zeta potential compared to CPAM of 13 MDa (Table I).

The molecular weight of the CPAM strongly influenced the surface coverage and aggregation state of AuNPs. By doubling CPAM's molecular weight, the surface coverage and average diameter of AuNP aggregates increased, from 49% to 85% and 35nm to 60 nm, respectively (Figure 6). The Raman EF of AuNPs-CPAM paper was increased almost by a factor 3, from 3.1×10^8 to 8.9×10^8 , when paper was pre-treated with CPAM of higher molecular weight (Figure 7).

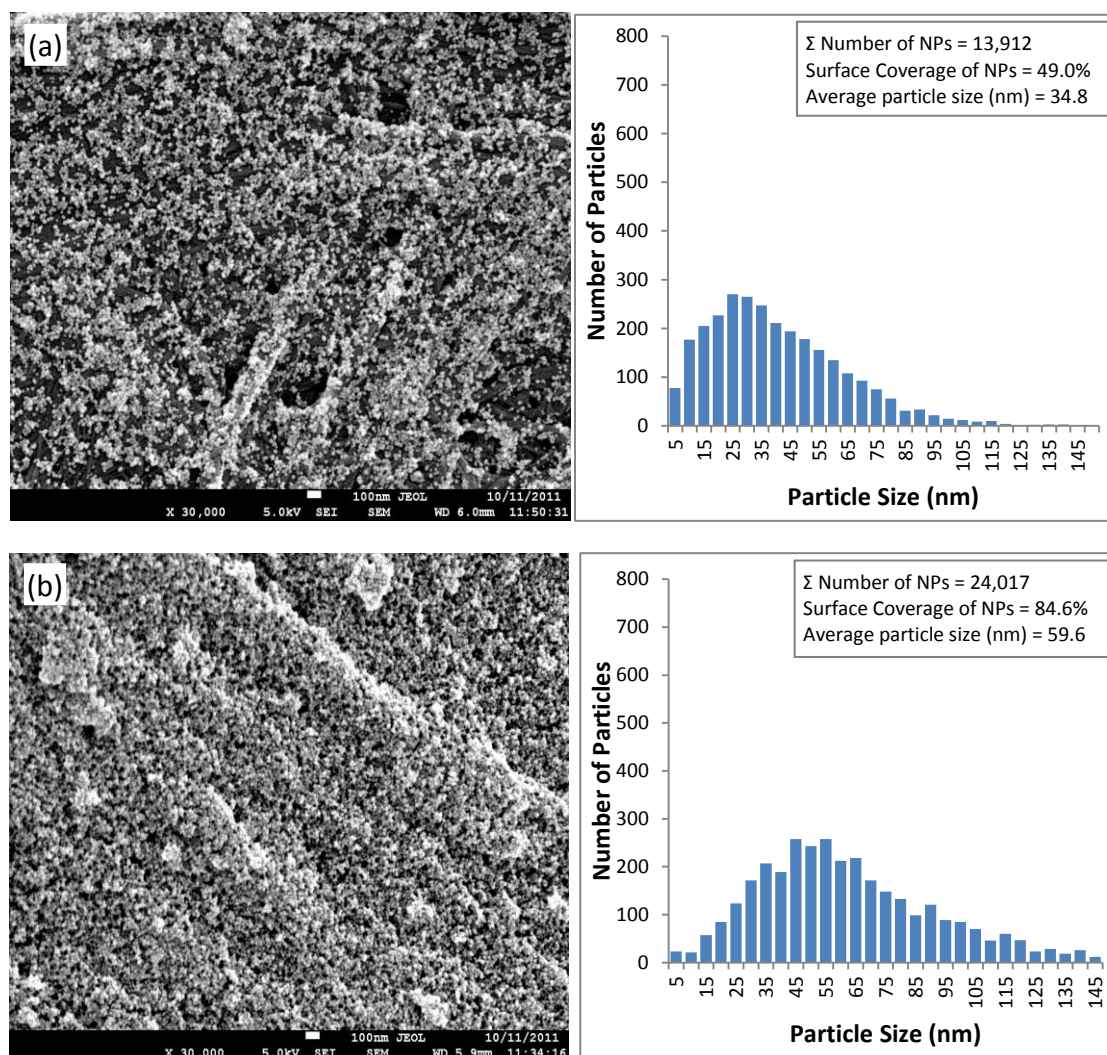


Figure 6: FESEM images and histograms of particle size distribution of AuNPs-CPAM papers with polymer's molecular weight of (a) 6 MDa and (b) 13 MDa.

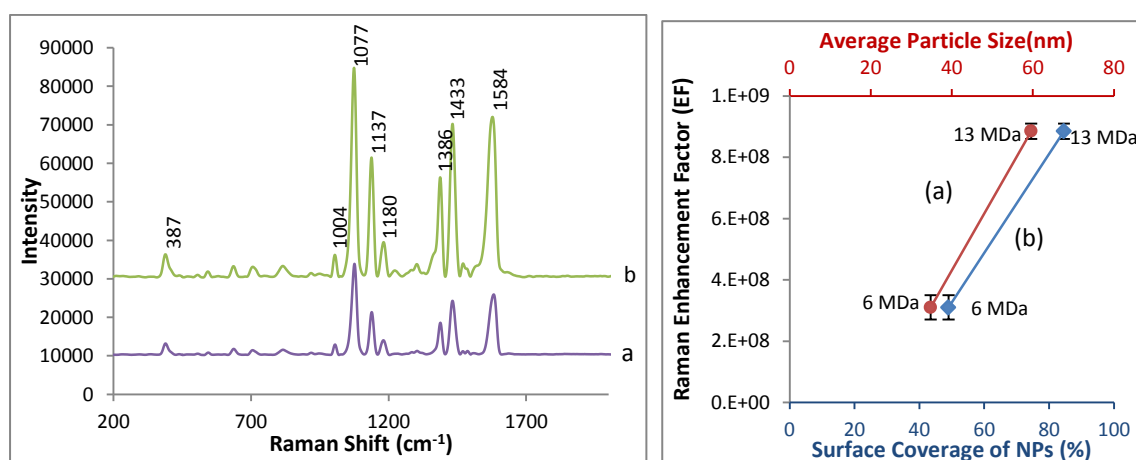


Figure 7: (Left) SERS spectra of 4-ATP on AuNPs-CPAM papers with polymer's molecular weight of (a) 6 MDa and (b) 13 MDa. (Right) Relationship between the (a)

average size and (b) surface coverage of AuNP aggregates and the EF of 4-ATP measured at the 1077 cm^{-1} band (error bars show standard deviation of 5 measurements from different spots on the substrate).

3.4.4 Sensitivity of AuNPs-CPAM paper

The SERS sensitivity of AuNPs-CPAM paper was quantified and compared with untreated AuNPs paper. Both untreated paper and paper pre-treated with CPAM (0.10 mg/mL, 13 MDa and 40 wt% charge density) were dipped into 0.20 mg/mL AuNP solutions, exposed to different concentrations of 4-ATP and their Raman spectra were measured (Figure 8 and Figure 9). The concentration of 4-ATP investigated ranged over 6 orders of magnitude, from 1 mM to 1 nM. Whilst the SERS spectra of 4-ATP for both papers were very similar, the SERS peaks were better defined on CPAM pre-treated paper. The detection limit of AuNPs-CPAM paper substrates was lower than for AuNPs on untreated paper as the spectrum of 1 nM of 4-ATP had good signal-to-noise ratio and the main peaks at 1077 cm^{-1} and 1584 cm^{-1} were more distinct (Figure 9). The Raman intensity from AuNPs-CPAM-treated paper was doubled than that of the AuNPs on the untreated paper over the entire range of 4-ATP concentration.

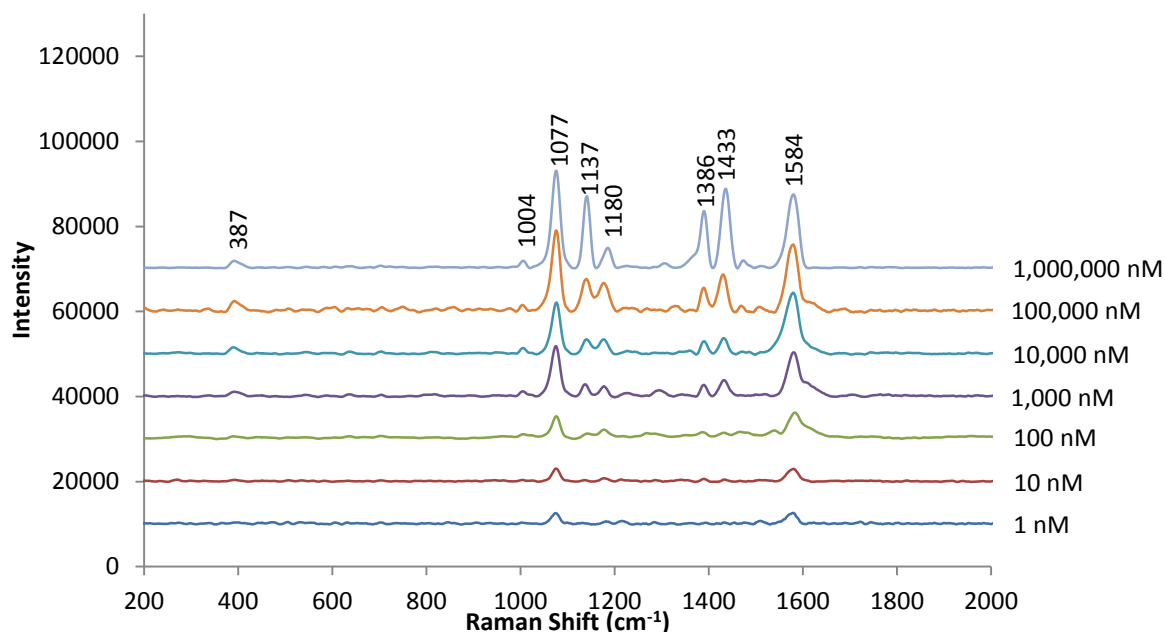


Figure 8: SERS spectra of different concentration of 4-ATP from untreated AuNPs paper.

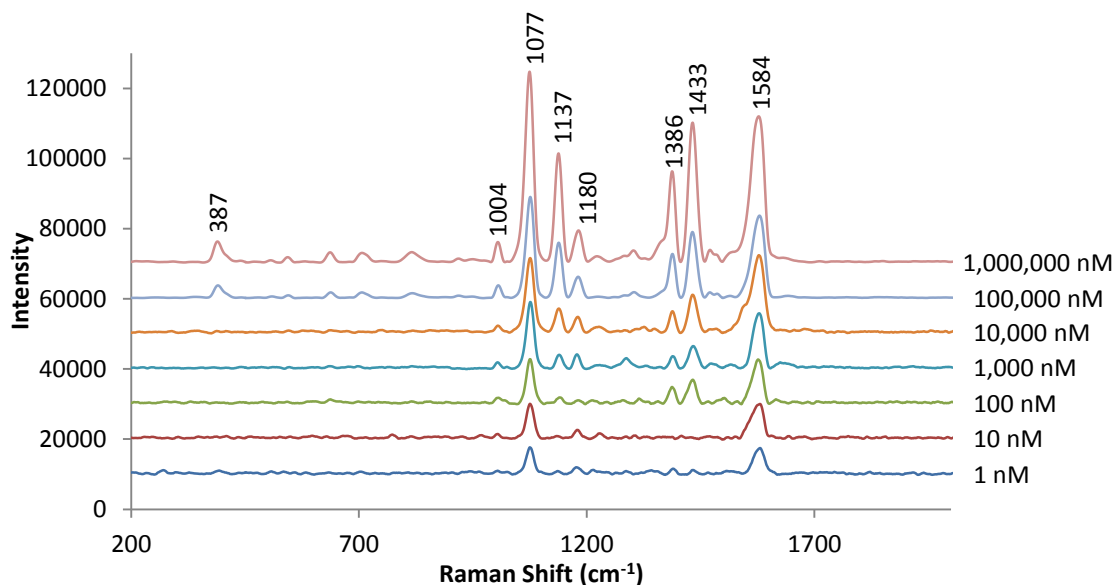


Figure 9: SERS spectra of different concentration of 4-ATP from AuNPs-CPAM paper.

3.4.5 Stability of AuNPs-CPAM paper

The FESEM images of AuNPs-CPAM paper (CPAM of 0.10 mg/mL, 13 MDa and 40 wt% charge density) before and after dipping in the 4-ATP ethanolic solution were analysed to investigate the possibility of AuNPs desorption (Supporting Information, S1). It was found that 99.7% of the AuNPs were retained on paper after 4-ATP deposition, and the cluster size of the NPs remained constant. This confirms that immersion in 4-ATP ethanolic solution did not affect the AuNPs paper.

The Raman spectra of plain paper and AuNPs-CPAM paper (CPAM of 0.10 mg/mL, 13 MDa and 40 wt% charge density) were measured to ensure that the CPAM pre-treatment of paper did not alter the analyte's Raman spectra (Supporting Information, S2). Both spectra exhibited Raman bands of very weak intensity and no significant variation of their spectral features was observed.

3.5 Discussion

3.5.1 SERS Optimization

Filter paper pre-treated by CPAM of high concentration, high charge density and high molecular weight was found to lead to a more uniform and denser distribution of AuNP aggregates. The increased proportion of aggregated AuNPs and smaller interparticle

spacing in CPAM-treated AuNP-deposited paper increased the coupling of Localized Surface Plasmon Resonances (LSPRs), which arise from the collective oscillation of electrons within metallic NPs [29]. This resulted in the formation of enhanced electromagnetic fields (hot spots), particularly at curved surfaces or gaps in between the AuNPs, thereby improving amplification of SERS signal. Increasing the SERS enhancement factor by decreasing the spacing between the nanostructures has previously been studied; nanostructures with gaps smaller than 10 nm can achieve higher Raman enhancement factor (EF) [30-34]. Pre-treating paper with CPAM maximized the spatial density of AuNPs aggregates, forming hot spots with less than 10 nm of interparticle spacing (Figure 2, 4 and 6). The three-dimensional and porous structure of paper is able to provide a greater surface area to localize the adsorption of analyte molecules in the vicinity of the hot spots, particularly at ultra-low concentrations. Figure 3 shows that the Raman EF of 1 mM of 4-ATP from the AuNPs-CPAM paper (8.9×10^8) was almost an order of magnitude greater than that of untreated AuNPs paper (2.1×10^8). This Raman EF exceeds 10^7 , which is a typical enhancement factor for many micro/nanofabricated nanoclusters SERS substrates under excitation of Raman red laser [35-37]. Such EF (within the range of 10^7 to 10^8) is sufficient for single molecule SERS detection [38-39]. Besides the magnitude of EF, reproducibility of a SERS substrate is critical since most of the SERS-based sensing is relying on the intensity of particular spectral bands to determine the analyte concentration. The AuNPs-CPAM paper showed a lower signal deviation ($\pm 12\%$) than the untreated AuNPs paper ($\pm 29\%$) (Figure 3), therefore improving reproducibility. The AuNPs-CPAM paper also scattered the surface enhanced Raman signal at different points with minimum variation in intensity.

An ideal SERS active substrate needs uniform distribution of nanoparticles at the sub-micrometer scale to achieve high degree of reproducibility [40]. This is a critical issue to develop paper as a SERS substrate, since it is a challenge to achieve uniform distribution of nanoparticles on paper due to heterogeneity at the micron level (fiber and surface roughness), meso level (porosity fibers dimensions) and macro level (fiber flocculation). This issue was overcome with CPAM pre-treated paper which produced a coating of well-dispersed AuNPs aggregates compared to the plain paper substrate (Figure 2); this contributed to a more reproducible SERS signal (Figure 3). Important considerations in the fabrication of AuNPs-CPAM paper substrates are the stability of substrate during

application of analyte and SERS signal interference of CPAM to the SERS signal of analyte. It was found that AuNPs were well retained on paper by CPAM and their desorption was negligible during the analyte detection process (Supporting Information, S1). Furthermore, CPAM adsorbed on paper has very weak SERS spectral features (Supporting Information S2), and does not interfere with the SERS signal of analyte.

In terms of SERS sensitivity, AuNPs-CPAM paper showed a higher SERS intensity at all concentrations of 4-ATP and lower detection limit than for AuNPs on untreated paper (Figure 8 and Figure 9). A sigmoidal relationship between the SERS intensity and concentration of 4-ATP was observed for both paper substrates (Figure 10). At low analyte concentration, the response was linear, while SERS intensity became saturated when the concentration of 4-ATP was high. The intensity plateau for AuNPs-CPAM paper is three times higher than that of the AuNPs paper, probably because of the higher surface coverage and concentration of AuNPs. Overall, the aggregation and higher density of AuNPs induced by CPAM at least doubled the SERS sensitivity of the substrate over the complete 4-ATP concentration range.

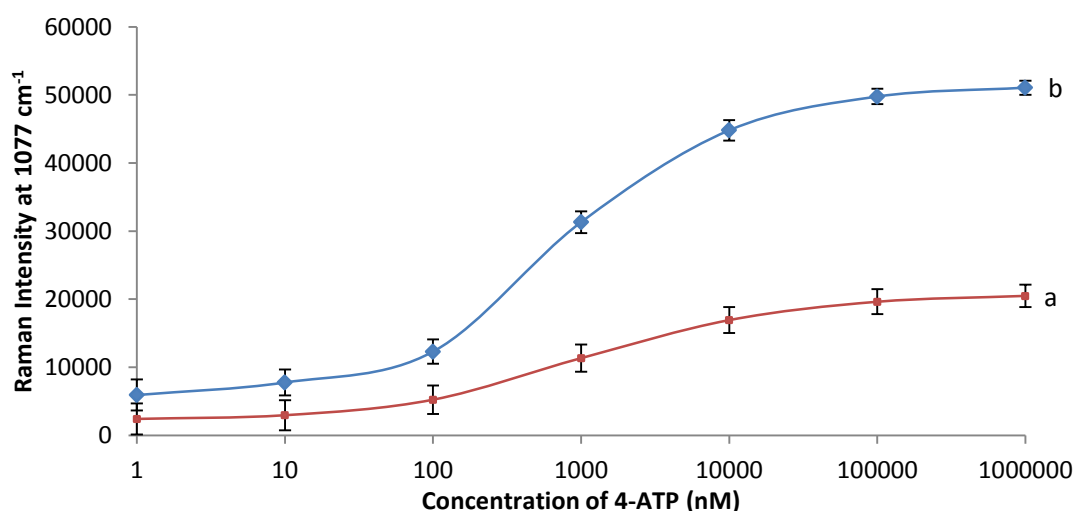


Figure 10: SERS intensity of different concentration of 4-ATP from (a) AuNPs paper and (b) AuNPs-CPAM paper at 1077 cm⁻¹ band.

3.5.2 Mechanism

AuNPs were previously adsorbed and retained as individual particles on paper upon dipping in an AuNPs suspension [22]; their surface coverage on paper scaled linearly with the concentration of AuNP solutions, and the Raman Enhancement Factor (EF)

increased proportionally with the surface coverage of AuNPs. In this study, paper was pre-treated with cationic polyacrylamides (CPAM) of different concentration, charge densities and molecular weight to drastically increase the surface coverage of AuNPs on paper, as well as to control and increase their aggregate size. CPAM polymers are generally used as retention aids in the papermaking process, but they have not been investigated for their ability to retain or flocculate NPs onto paper. An objective of this study was to exploit this mechanism to significantly amplify the SERS signal by increasing the concentration of hot spots.

CPAM affected both the AuNPs inter-particle interaction and their adsorption on cellulose fibers. The adsorption of CPAM contributed to an electrostatic attraction (AuNP-AuNP and AuNPs-fiber) and introduced bridging and steric components. The extended and adsorbed conformation of a polyelectrolyte in solution or adsorbed on a surface is affected by pH, ionic strength, concentration, charge density and molecular weight of the polymer. In this study, ionic strength and pH were kept constant.

The main driving forces for the adsorption of CPAM on cellulose fibers are van der Waals and electrostatic forces [41-42]. The cationic polyelectrolyte adsorbed onto the negatively-charged cellulose fibers forming train, loop, and tail. The tails and loops extended into the solution phase, driven by strong intramolecular electrostatic repulsion and affinity for water, while the train sections adhered to the surface due to electrostatic affinity [43-46]. During the dipping of CPAM pre-treated papers into AuNPs solution, aggregation and retention of AuNPs could be induced by a combination of bridging, charge neutralization or patch interaction mechanisms [47]. This triple role of CPAM produced a much higher surface coverage and higher aggregation of AuNPs compared to the untreated paper (Figure 2a and Figure 2b).

The concentration of the CPAM solution with which paper was pre-treated played a dominant role in the adsorption and aggregation of AuNPs on paper (Figure 2). Charged patch mechanisms would be most likely for papers pre-treated with CPAM at lower concentration [46]. At such low CPAM concentrations, a flat polymer chain conformation (Figure 11a) is expected due to a low density of chains on the surface and their tendency to relax into a flatter configuration [47]. Increasing the polymer concentration in solution

leads to increased extended polymer tails and loops having a superior bridging ability [47], and results in a higher adsorption and aggregation of AuNPs (Figure 11b). Charge neutralization can also occur, where the average negative charge of cellulose fibers is reduced, neutralized and reverted to a positive charge upon adsorption of CPAM. The increased positive charge on paper with increased concentration of CPAM produced a greater electrostatic interaction between paper surface and negatively-charged AuNPs.

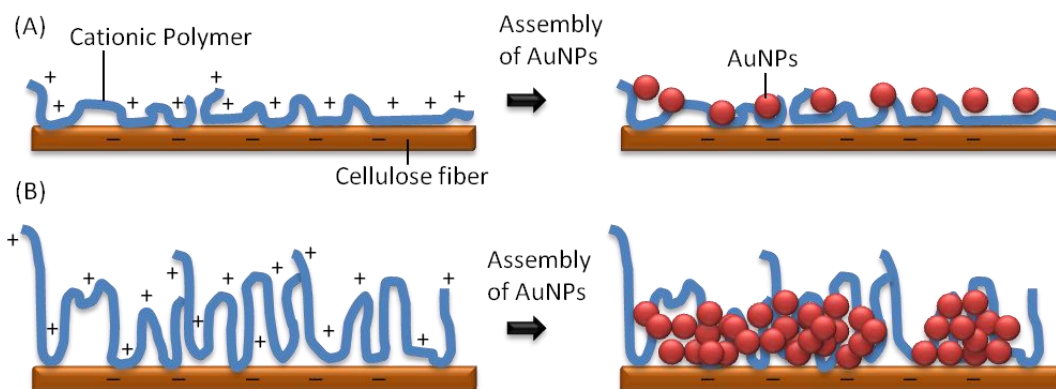


Figure 11: (a) Polymer attains a flat conformation with many trains at the interface. (b) Polymer attains a conformation with many loops and tails tangling out of the surface.

The magnitude of the Raman EF of the AuNPs-CPAM paper substrate can be tuned by controlling the concentration of CPAM (Figure 3). Higher surface coverage and aggregation of AuNPs resulted in the formation of rough metallic surfaces ('hot spots') as paper was pre-treated with higher concentration of CPAM. This gave rise to stronger electromagnetic coupling to enhance the Raman signal of 4-ATP (EF of almost an order of magnitude higher than the untreated AuNPs paper).

Coulombic interactions between polymer segments and surface, as well as between charges in the polymer chains affect polymer adsorption. Flocculation of AuNPs by lower charged CPAM was expected to occur through bridging since polymer with lower charge density tends to form loops and tails upon adsorption [42, 44]. Higher surface coverage and aggregation of AuNPs were observed when paper was pre-treated by CPAM of higher charge density (Figure 4). The high charged CPAM probably adsorbed on cellulose fibers via charge neutralization. This is because polymer with a higher charge

density tends to have a flat conformation on the surface, driven by electrostatic attraction [48-49]. However, bridging could also be involved. Since the highly charged CPAM has a higher charge density than paper, there is a possibility that the excess charge of the polymer could provide an electrostatic force that might repel some polymer segments from those adsorbed on paper, resulting in more loops and tails [50]. We believe that in a combination of charge neutralization and bridging mechanisms, CPAM of higher charge density produced a higher surface coverage and greater aggregation of AuNPs for a higher Raman EF (Figure 5).

Higher levels of adsorption and greater aggregation of AuNPs were achieved with paper pre-treated with CPAM of higher molecular weight (Figure 6). This agrees well with several studies [51-53] reporting that the bridging effectiveness of cationic polymer increases with their molecular weight. The increase of the estimated radius of gyration for CPAM with molecular weight of 6 MDa and 13 MDa from 26 nm to 38 nm supported this observation (Supporting Information, S3). CPAM of higher molecular weight had a greater bridging effect due to the greater extension of loops and tails, increasing its ability to adsorb more AuNPs (Figure 11b) which enhanced the SERS performance (Figure 7).

3.6 Conclusion

Paper treated with gold nanoparticles (AuNPs) was engineered as substrate for SERS application to develop a robust and low-cost biodiagnostic platform. The objective of this study was to drastically increase the SERS enhancement factor (EF) of AuNPs paper by controlling the aggregation size and surface coverage of AuNPs on paper. This was achieved by pre-treating paper with a cationic polyelectrolyte to control the extent of AuNPs coagulation on paper. A series of cationic polyacrylamides (CPAM) was studied. The effect of CPAM solution concentration, polymer charge density and molecular weight on AuNPs' adsorption/aggregation behaviour and SERS properties was measured. Paper was first dipped into the CPAM solution before a second dipping in the AuNP suspension, and 4-aminothiophenol (4-ATP) was selected as the SERS probe. The aggregate size distribution and surface coverage of AuNPs on paper were quantified by FESEM image analysis.

The Raman enhancement factor (EF) increased pseudo-linearly with the surface coverage and the aggregation size of AuNPs on paper. The surface coverage, average particle size and particle size distribution all increased with the concentration, charge density and molecular weight of CPAM solution with which paper was pre-treated.

The CPAM pre-treated paper produced a more uniform coating of AuNPs compared to bare paper substrate. A surface coverage of AuNPs on paper up to 80% with average AuNP aggregates up to 60 nm were achieved. The AuNPs were adsorbed as well dispersed aggregates on paper despite the inherent heterogeneity of the substrate morphology. These AuNP aggregates formed a rough metallic surface, with increased particles junction for a stronger electromagnetic coupling that tremendously amplified the Raman signal of 4-ATP. The Raman EF of AuNPs-CPAM paper was almost an order of magnitude higher and more reproducible than the untreated AuNPs paper at constant concentration of AuNPs suspension.

We believe the CPAM chains adsorbed on paper in a high loops and tails conformation which promote efficient bridging of AuNPs to adsorb at higher surface coverage on paper and form larger aggregates. This configuration was favoured by CPAM solutions of higher concentration, charge density and molecular weight.

AuNPs paper is an excellent substrate for SERS applications, especially when the aggregation state and surface coverage of AuNPs are engineered by pre-treating paper with CPAM. This approach offers a robust bio-diagnostics platform to yield molecular structural information for qualitative analysis.

3.7 Acknowledgement

Thanks to Dr. T. Williams, Monash Centre for Electron Microscopy (MCEM), for FESEM technical expertise and F. Shanks from Monash Molecular Spectroscopy and Centre for Biospectroscopy for Raman technical advice. The financial supports from the ARC Linkage LP0989823 and Visy, Amcor, SCA, Norske Skog, Australian Paper, the Australian Pulp and Paper Institute and Monash University are all acknowledged.

3.8 References

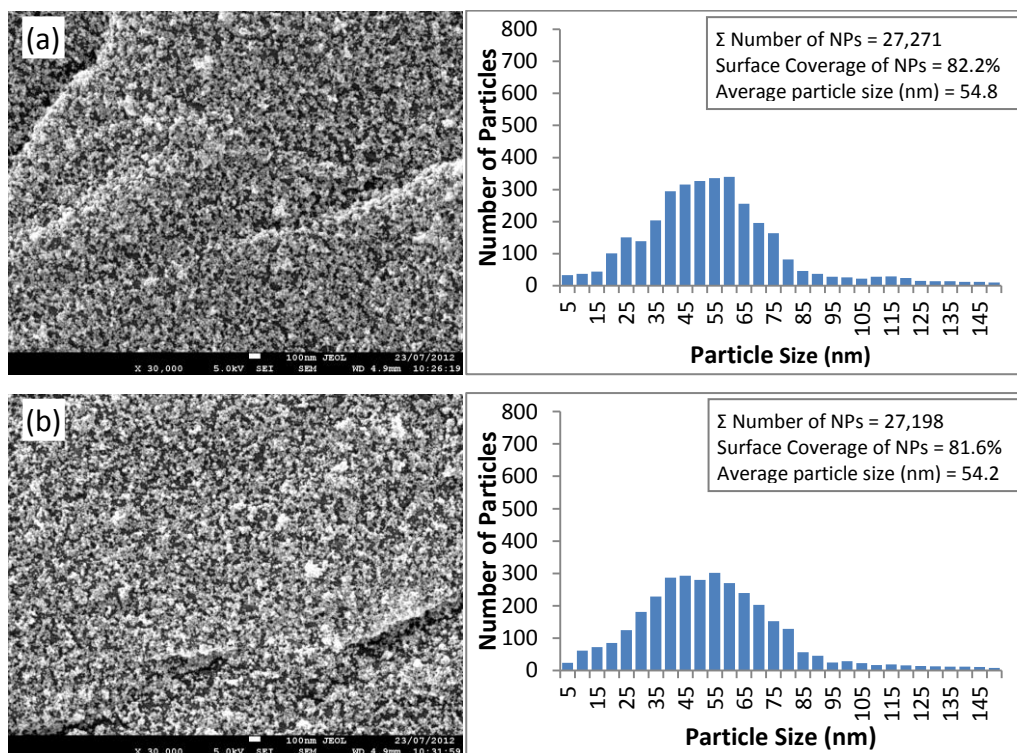
1. Al-Tamimi, M., W. Shen, R. Zeineddine, H. Tran, and G. Garnier, *Validation of Paper-Based Assay for Rapid Blood Typing*. Analytical Chemistry, 2011. **84**(3): p. 1661-1668.
2. Khan, M.S., G. Thouas, W. Shen, G. Whyte, and G. Garnier, *Paper Diagnostic for Instantaneous Blood Typing*. Analytical Chemistry, 2010. **82**(10): p. 4158-4164.
3. Li, X., J. Tian, and W. Shen, *Quantitative biomarker assay with microfluidic paper-based analytical devices*. Analytical and Bioanalytical Chemistry, 2010. **396**(1): p. 495-501.
4. Li, X., J. Tian, T. Nguyen, and W. Shen, *Paper-Based Microfluidic Devices by Plasma Treatment*. Analytical Chemistry, 2008. **80**(23): p. 9131-9134.
5. Khan, M.S., D. Fon, X. Li, J. Tian, J. Forsythe, G. Garnier, and W. Shen, *Biosurface engineering through ink jet printing*. Colloids and Surfaces B: Biointerfaces, 2010. **75**(2): p. 441-447.
6. Li, X., J. Tian, G. Garnier, and W. Shen, *Fabrication of paper-based microfluidic sensors by printing*. Colloids and Surfaces B: Biointerfaces, 2010. **76**(2): p. 564-570.
7. Khan, M.S., J. Tian, L. Xu, W. Shen, and G. Garnier, eds. *Bioactive Enzymatic Papers*. Advances in Pulp and Paper Research. Vol. 2. 2009, St. Anne's College: Oxford.
8. Toderas, F., M. Baia, L. Baia, and S. Astilean, *Controlling gold nanoparticle assemblies for efficient surface-enhanced Raman scattering and localized surface plasmon resonance sensors*. Nanotechnology, 2007. **18**.
9. Lee, S.W., Y.-B. Shin, K.S. Jeon, S.M. Jin, Y.D. Suh, S. Kim, J.J. Lee, and M.-G. Kim, *Electron beam lithography-assisted fabrication of Au nano-dot array as a substrate of a correlated AFM and confocal Raman spectroscopy*. Ultramicroscopy, 2008. **108**(10): p. 1302-1306.
10. Min, Q., M.J.L. Santos, E.M. Girotto, A.G. Brolo, and R. Gordon, *Localized Raman Enhancement from a Double-Hole Nanostructure in a Metal Film*. Journal of Physical Chemistry C, 2008. **112**(39): p. 15098-15101.
11. Stokes, D.L., Z. Chi, and T. Vo-Dinh, *Surface-Enhanced-Raman-Scattering-Inducing Nanoprobe for Spectrochemical Analysis* Applied Spectroscopy, 2004. **58**(3): p. 257-354.
12. Luo, Z. and Y. Fang, *SERS of C60/C70 on gold-coated filter paper or filter film influenced by the gold thickness*. Journal of Colloid and Interface Science, 2005. **283**(2): p. 459-463.
13. Berthod, A., J.J. Laserna, and J.D. Winefordner, *Analysis by surface enhanced Raman spectroscopy on silver hydrosols and silver coated filter papers*. Journal of Pharmaceutical and Biomedical Analysis, 1988. **6**(6-8): p. 599-608.
14. Cabalín, L.M. and J.J. Laserna, *Fast spatially resolved surface-enhanced Raman spectrometry on a silver coated filter paper using charge-coupled device detection*. Analytica Chimica Acta, 1995. **310**(2): p. 337-345.
15. Ma, W. and Y. Fang, *Experimental (SERS) and theoretical (DFT) studies on the adsorption of p-, m-, and o-nitroaniline on gold nanoparticles*. Journal of Colloid and Interface Science, 2006. **303**(1): p. 1-8.
16. Niu, Z. and Y. Fang, *Surface-enhanced Raman scattering of single-walled carbon nanotubes on silver-coated and gold-coated filter paper*. Journal of Colloid and Interface Science, 2006. **303**(1): p. 224-228.
17. Wu, D. and Y. Fang, *The adsorption behavior of p-hydroxybenzoic acid on a silver-coated filter paper by surface enhanced Raman scattering*. Journal of Colloid and Interface Science, 2003. **265**(2): p. 234-238.
18. Alince, B., F. Bednar, and T.G.M. van de Ven, *Deposition of calcium carbonate particles on fiber surfaces induced by cationic polyelectrolyte and bentonite*. Colloids and Surfaces A: Physicochemical and Engineering Aspects, 2001. **190**(1-2): p. 71-80.

19. Vanerek, A., B. Alince, and T.G.M. Van De Ven, *Colloidal behaviour of ground and precipitated calcium carbonate fillers: Effects of cationic polyelectrolytes and water quality*. Journal of Pulp and Paper Science, 2000. **26**(4): p. 135-139.
20. Antunes, E., F.A.P. Garcia, P. Ferreira, and M.G. Rasteiro, *Flocculation of PCC filler in papermaking: Influence of the particle characteristics*. Chemical Engineering Research and Design, 2008. **86**(10): p. 1155-1160.
21. Cechova, M., B. Alince, and T.G.M. van de Ven, *Stability of ground and precipitated CaCO₃ suspensions in the presence of polyethylene oxide and kraft lignin*. Colloids and Surfaces A: Physicochemical and Engineering Aspects, 1998. **141**(1): p. 153-160.
22. Ngo, Y.H., D. Li, G.P. Simon, and G. Garnier, *Gold Nanoparticle–Paper as a Three-Dimensional Surface Enhanced Raman Scattering Substrate*. Langmuir, 2012. **28**(23): p. 8782-8790.
23. Michaels, A.M., Jiang, and L. Brus, *Ag Nanocrystal Junctions as the Site for Surface-Enhanced Raman Scattering of Single Rhodamine 6G Molecules*. The Journal of Physical Chemistry B, 2000. **104**(50): p. 11965-11971.
24. Turkevich, J., P.C. Stevenson, and J. Hillier, *A study of the nucleation and growth processes in the synthesis of colloidal gold*. Discussions of the Faraday Society 1951. **11**: p. 55-75.
25. Camargo, P.H.C., L. Au, M. Rycenga, W. Li, and Y. Xia, *Measuring the SERS enhancement factors of dimers with different structures constructed from silver nanocubes*. Chemical Physics Letters, 2010. **484**(4–6): p. 304-308.
26. Hu, X., T. Wang, L. Wang, and S. Dong, *Surface-Enhanced Raman Scattering of 4-Aminothiophenol Self-Assembled Monolayers in Sandwich Structure with Nanoparticle Shape Dependence: Off-Surface Plasmon Resonance Condition*. Journal of Physical Chemistry C, 2007. **111**(19): p. 6962-6969.
27. Peacock, A.C., A. Amezcua-Correa, J. Yang, P.J.A. Sazio, and S.M. Howdle, *Highly efficient surface enhanced Raman scattering using microstructured optical fibers with enhanced plasmonic interactions*. Applied Physics Letters, 2008. **92**(14).
28. Hu, X., T. Wang, L. Wang, and S. Dong, *Surface-Enhanced Raman Scattering of 4-Aminothiophenol Self-Assembled Monolayers in Sandwich Structure with Nanoparticle Shape Dependence: Off-Surface Plasmon Resonance Condition*. Journal of Physical Chemistry C, 2007. **111**(19): p. 6962-6969.
29. He, J., P. Zhang, J. Gong, and Z. Nie, *Facile synthesis of functional Au nanopatches and nanocups*. Chemical Communications, 2012. **48**(59): p. 7344-7346.
30. Dhawan, A., Y. Zhang, F. Yan, M. Gerhold, and T. Vo-Dinh. *Nano-engineered surface-enhanced Raman scattering (SERS) substrates with patterned structures on the distal end of optical fibers*. 2008. San Jose, CA, USA: SPIE.
31. Chen, A., A.E. DePrince, A. Demortière, A. Joshi-Imre, E.V. Shevchenko, S.K. Gray, U. Welp, and V.K. Vlasko-Vlasov, *Self-Assembled Large Au Nanoparticle Arrays with Regular Hot Spots for SERS*. Small, 2011. **7**(16): p. 2365-2371.
32. Cuifeng, T., L. Zhen, J. Jiehong, L. Sergei, H. Cheng, Y. Hongjun, L. Rui, W. Liqun, S. Xiaoping, D. Bingjun, W. Stefan, S. Thomas, and F. Jixiang, *Gold mesoflower arrays with sub-10 nm intraparticle gaps for highly sensitive and repeatable surface enhanced Raman spectroscopy*. Nanotechnology, 2012. **23**(16): p. 165604.
33. Chu, H., J. Wang, L. Ding, D. Yuan, Y. Zhang, J. Liu, and Y. Li, *Decoration of Gold Nanoparticles on Surface-Grown Single-Walled Carbon Nanotubes for Detection of Every Nanotube by Surface-Enhanced Raman Spectroscopy*. Journal of the American Chemical Society, 2009. **131**(40): p. 14310-14316.
34. Cho, W.J., Y. Kim, and J.K. Kim, *Ultrahigh-Density Array of Silver Nanoclusters for SERS Substrate with High Sensitivity and Excellent Reproducibility*. ACS Nano, 2011. **6**(1): p. 249-255.

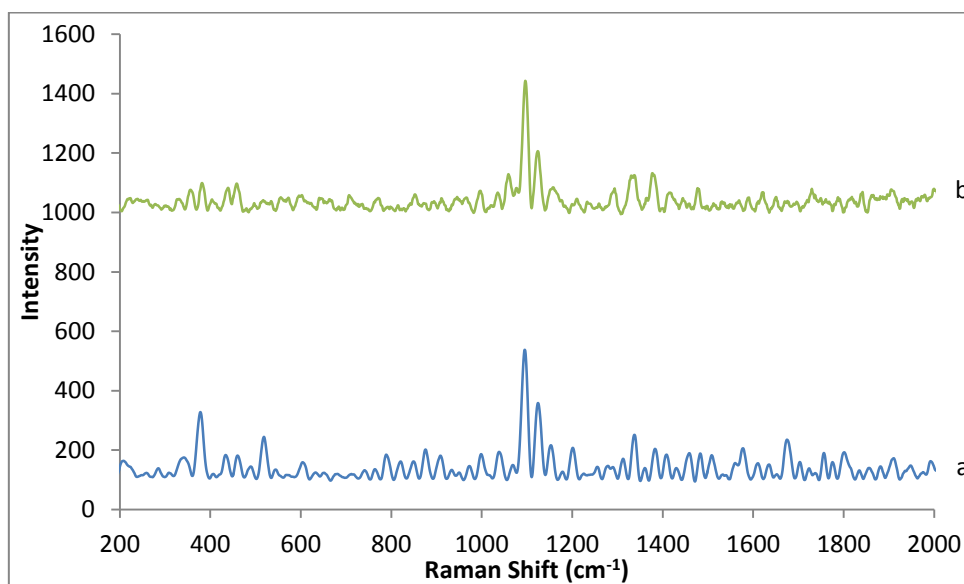
35. Yu, W.W. and I.M. White, *Inkjet Printed Surface Enhanced Raman Spectroscopy Array on Cellulose Paper*. Analytical Chemistry, 2010. **82**(23): p. 9626-9630.
36. Cheng, M.-L., B.-C. Tsai, and J. Yang, *Silver nanoparticle-treated filter paper as a highly sensitive surface-enhanced Raman scattering (SERS) substrate for detection of tyrosine in aqueous solution*. Analytica Chimica Acta, 2011. **708**(1–2): p. 89-96.
37. Lee, C.H., M.E. Hankus, L. Tian, P.M. Pellegrino, and S. Singamaneni, *Highly Sensitive Surface Enhanced Raman Scattering Substrates Based on Filter Paper Loaded with Plasmonic Nanostructures*. Analytical Chemistry, 2011. **83**(23): p. 8953-8958.
38. Etchegoin, P.G. and E.C. Le Ru, *A perspective on single molecule SERS: current status and future challenges*. Physical Chemistry Chemical Physics, 2008. **10**(40): p. 6079-6089.
39. Le Ru, E.C., E. Blackie, M. Meyer, and P.G. Etchegoin, *Surface Enhanced Raman Scattering Enhancement Factors: A Comprehensive Study*. The Journal of Physical Chemistry C, 2007. **111**(37): p. 13794-13803.
40. Ngo, Y., D. Li, G.P. Simon, and G. Garnier. *Paper Surface Functionalized by Nanoparticles*. in APPITA Conference. 2010. Melbourne.
41. Borkovec, M. and G. Papastavrou, *Interactions between solid surfaces with adsorbed polyelectrolytes of opposite charge*. Current Opinion in Colloid & Interface Science, 2008. **13**(6): p. 429-437.
42. Hubbe, M.A., H. Nanko, and M.R. McNeal, *Retention aid polymer interactions with cellulosic surfaces and suspensions: A Review*. Bioresources, 2009. **4**(2): p. 850-906.
43. Abu-Sharkh, B., *Structure and Mechanism of the Deposition of Multilayers of Polyelectrolytes and Nanoparticles*. Langmuir, 2006. **22**(7): p. 3028-3034.
44. Fleer, G.J., M.A.C. Stuart, J.M.H.M. Scheutjens, T. Cosgrove, and B. Vincent, *Polymers at Interfaces*. 1998, London: Chapman & Hall.
45. Wågberg, L., *Polyelectrolyte adsorption on cellulose fibres - a review*. Nordic Pulp & Paper Research Journal, 2000. **15**(5): p. 586-597.
46. Mosse, W.K.J., D.V. Boger, G.P. Simon, and G. Garnier, *Effect of Cationic Polyacrylamides on the Interactions between Cellulose Fibers*. Langmuir, 2012. **28**(7): p. 3641-3649.
47. Sennerfors, T., *Polymer-Nanoparticle Complexes: Fundamentals and Applications of Interfacial Behavior*. Encyclopedia of Surface and Colloid Science: Second Edition, 2006: p. 4874 - 4884.
48. Polverari, M. and T.G.M. van de Ven, *Dilute Aqueous Poly(ethylene oxide) Solutions: Clusters and Single Molecules in Thermodynamic Equilibrium*. The Journal of Physical Chemistry, 1996. **100**(32): p. 13687-13695.
49. Lindstrom, T., C. Soremark, C. Heinegard, and S. Martin-Lof, *The importance of electrokinetic properties of wood fiber for papermaking*. Tappi Journal, 1974. **57**(12): p. 94-96.
50. Claesson, P.M., M.A.G. Dahlgren, and L. Eriksson, *Forces between polyelectrolyte-coated surfaces: relations between surface interaction and floc properties*. Colloids and Surfaces A: Physicochemical and Engineering Aspects, 1994. **93**: p. 293-303.
51. Lindström, T. and C. Söremark, *Adsorption of cationic polyacrylamides on cellulose*. Journal of Colloid and Interface Science, 1976. **55**(2): p. 305-312.
52. Zhang, H., F. Chen, and H. Hu, *Preparations and application of high molecular weight cationic polyacrylamides*. China Pulp Paper, 2003. **22**(4): p. 15-18.
53. Gill, R.I.S. and T.M. Herrington, *The effect of surface charge on the flocculation of Kaolin suspensions with cationic polyacrylamides of varying molar mass but similar cationic character*. Colloids and Surfaces, 1987. **25**(2–4): p. 297-310.

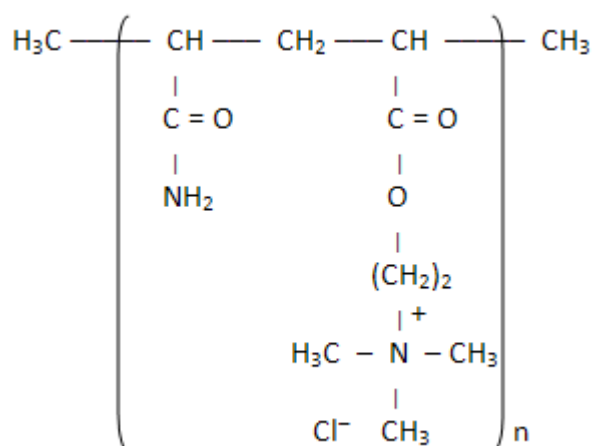
3.9 Supporting Information

S1: FESEM images and histograms of particle size distribution of AuNPs-CPAM papers (a) before and (b) after dipping in 4-ATP ethanolic solution.



S2: Raman spectra of (a) plain filter paper (b) filter paper pre-treated with CPAM and dipped in AuNP solution.



S3: Theoretical estimation of the size of CPAM

Cationic trimethylamino-ethyl-methacrylate polyacrylamide
 Molecular weight = 13MDa

$$r_g = b \sqrt{\frac{N}{6}}$$

r_g = radius of gyration, b = monomer length, N = number of monomers

Radius of Gyration of CPAM (nm)	Molecular Weight (MDa)	
	6	13
	26	38

S4: Titration experiment of CPAM

The titration experiment was performed by using a Mütek Particle Charge Detector PCD02. 10 mL of CPAM solution was titrated by using an anionic Sodium Polyethelyene Suphonate solution at a rate of 0.6 mL/min. The charge of CPAM solution was calculated by using the following equation:

$$\text{Charge quantity (eq/g)} = \frac{\text{Volume of Titrant use (L)} \times \text{Concentration of Titrant (eq/L)}}{\text{Weight of solids of the sample (g)}}$$

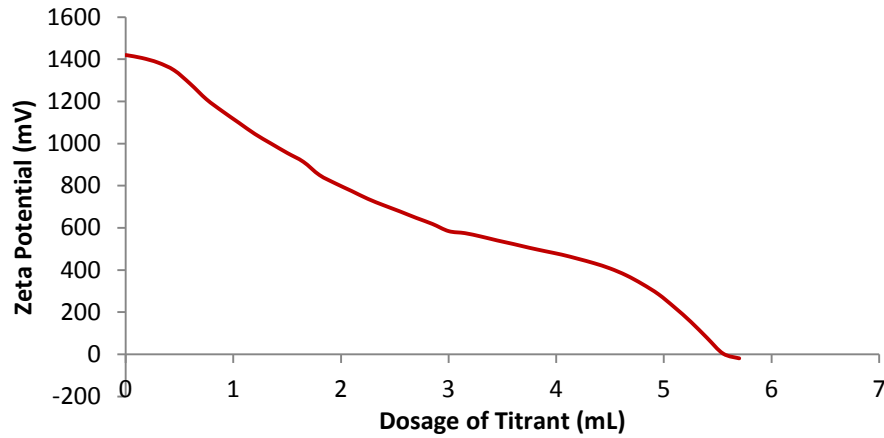


Figure 1: Titration of CPAM F1 (40 wt% charge density) by anionic PES-Na (2.5×10^{-4} eq/L).

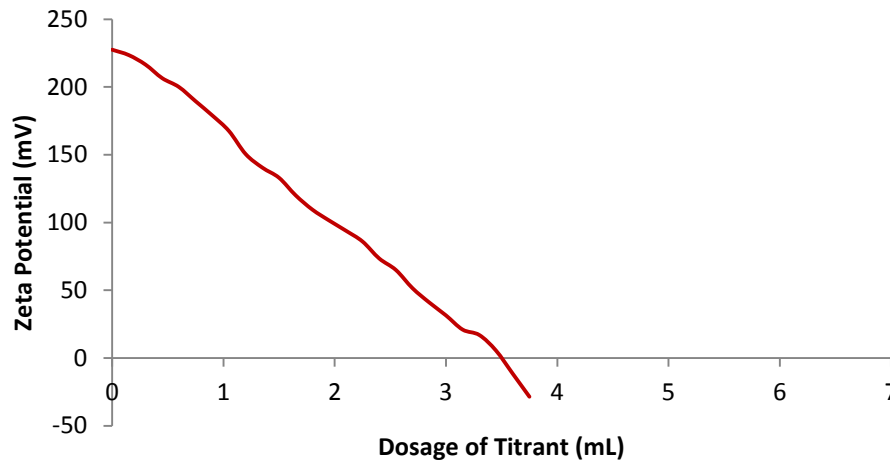


Figure 2: Titration of CPAM H1 (10 wt% charge density) by anionic PES-Na (6.25×10^{-5} eq/L).

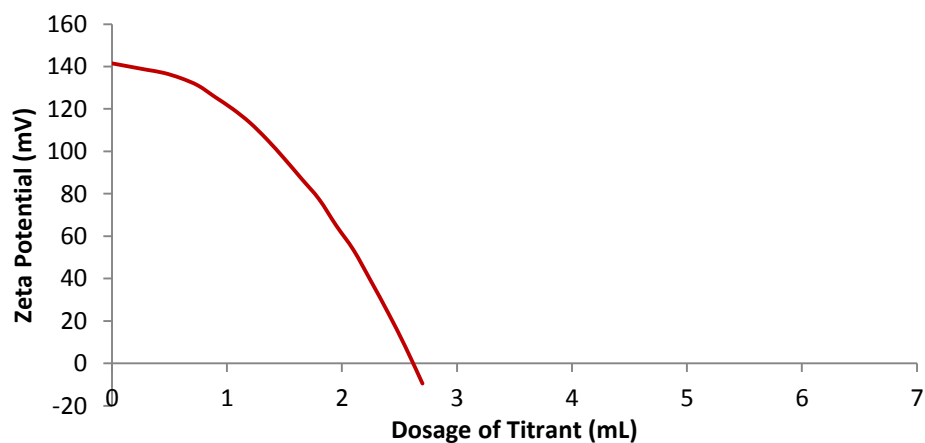


Figure 3: Titration of CPAM I1 (5 wt% charge density) by anionic PES-Na (6.25×10^{-5} eq/L).

Table 1: Calculated Charge density of CPAM from Titration Experiment.

Charge Density ($\mu\text{eq/g}$)	CPAM (0.10 mg/mL concentration, 13 MDa Molecular Weight)		
	F1 (40 wt%)	H1 (10 wt%)	I1 (5 wt%)
	14	2.2	1.6

Chapter 4

Effect of Cationic Polyacrylamide Dissolution on
the Adsorption State of Gold Nanoparticles on
Paper and Their Surface Enhanced Raman
Scattering Properties

This page is intentionally blank

Monash University

Declaration for Thesis Chapter 4

Declaration by candidate

In the case of Chapter 4, the nature and extent of my contribution to the work was the following:

Nature of contribution	Extent of contribution (%)
Initiation, key ideas, experimental and analysis works, development and writing up of paper	80

The following co-authors contributed to the work. Co-authors who are students at Monash University must also indicate the extent of their contribution in percentage terms:

Name	Nature of contribution	Extent of contribution (%) for student co-authors only
Gil Garnier	Initiation, key ideas, reviewing and editing of the paper.	Supervisor
George Simon	Initiation, key ideas, reviewing and editing of the paper.	Co-supervisor
Dan Li	Initiation, key ideas, reviewing and editing of the paper.	Co-supervisor

Candidate's Signature

Date 13.03.2013

Declaration by co-authors

The undersigned hereby certify that:

- (1) the above declaration correctly reflects the nature and extent of the candidate's contribution to this work, and the nature of the contribution of each of the co-authors.
- (2) they meet the criteria for authorship in that they have participated in the conception, execution, or interpretation, of at least that part of the publication in their field of expertise;
- (3) they take public responsibility for their part of the publication, except for the responsible author who accepts overall responsibility for the publication;
- (4) there are no other authors of the publication according to these criteria;
- (5) potential conflicts of interest have been disclosed to (a) granting bodies, (b) the editor or publisher of journals or other publications, and (c) the head of the responsible academic unit; and
- (6) the original data are stored at the following location(s) and will be held for at least five years from the date indicated below:

Location(s)

At the And Paper Institute (APPI), Department of Chemical Engineering, Monash University, Clayton, VIC 3800, Australia.

Signature 1

Date 12/12/12

Signature 2

Date 12/12/12

Signature 3

Date 11/12/2012

This page is intentionally blank

Effect of Cationic Polyacrylamide Dissolution on the Adsorption State of Gold Nanoparticles on Paper and Their Surface Enhanced Raman Scattering Properties

Ying Hui Ngo¹, Dan Li², George P. Simon² and *Gil Garnier¹

¹ BioPRIA, Australian Pulp and Paper Institute (APPI), Department of Chemical Engineering Monash University, Clayton, VIC 3800, Australia.

² Department of Material Engineering Monash University, Clayton, VIC 3800, Australia

*Corresponding author. Email: [REDACTED]; Tel: [REDACTED] Fax: [REDACTED]

Content

4.1	Abstract	150
4.2	Introduction	150
4.3	Materials and Methods	152
4.3.1	Material	152
4.3.2	Dissolution rate of CPAM	152
4.3.3	Synthesis and Deposition of Nanoparticles on Paper Substrates	153
4.3.4	Preparation of Raman Active Substrates	153
4.3.5	Instrumentation	154
4.4	Results	154
4.4.1	Dissolution of CPAM	154
4.4.2	Properties of AuNPs-CPAM paper	156
4.5	Discussion	160
4.5.1	Mechanism of CPAM Dissolution	160
4.5.2	Properties of AuNPs-CPAM paper	163
4.6	Conclusion	164
4.7	Acknowledgement	165
4.8	References	166
4.9	Supporting Information	168

4.1 Abstract

This study examines and quantifies the effect of cationic polyacrylamide (CPAM) dissolution kinetics and charge density on the adsorption and aggregation state of gold nanoparticles (AuNPs) on paper and the resulting Surface Enhanced Raman Scattering (SERS) performance. Dissolution kinetics of CPAM of different charge density was studied by monitoring their viscosity and hydrodynamic diameter over regular intervals of time. It was found that the degree of dissolution of CPAM greatly affected the surface coverage and aggregation of AuNPs on the CPAM pre-adsorbed paper substrate and their SERS reproducibility. CPAM of higher charge density dissolves faster and produced a more uniform aggregation and higher surface coverage of AuNPs on paper for a higher and more reproducible Raman EF. Understanding the CPAM dissolution process enables the optimization of SERS performance of the AuNPs-paper as a bio-diagnostic platform.

Keywords: cationic polyacrylamide (CPAM), dissolution, SERS, gold nanoparticles (AuNPs), aggregates, paper, charge density, reproducibility.

4.2 Introduction

Paper has emerged as a substrate of choice in the fabrication of low-cost diagnostic platforms for medical and environmental applications [1-2]. One of these developing applications is bioactive paper diagnostic for blood typing, wherein blood agglutination is triggered by specific antibody-antigen interactions and indicated by chromatographic separation on paper [1-3]. However, bioactive papers often suffer from four major issues: Specificity, Selectivity, Sensitivity and Simplicity (4S). Among these issues, sensitivity can be a major limiting factor, with a detection range of 10^{-6} M for many colorimetric techniques. For certain applications, such as cancer detection, this can be inadequate and a detection range up to 10^{-9} or 10^{-12} M might be desirable. To address this issue, paper can be treated with metallic nanoparticles to produce a Surface Enhanced Raman Scattering (SERS) active substrate to identify analytes at trace levels [4-10].

SERS involves the enhancement of Raman signal to detect small energy changes occurring when light is scattered from a molecule which is absorbed on a metallic substrate, typically metallic nanoparticles [11]. The SERS enhancement factor is

generally increased with the density of “hotspots” created by close contact points between metallic nanoparticles. In a previous study, filter paper was pre-treated with high molecular weight cationic polyacrylamide (CPAM) to retain gold nanoparticles (AuNPs) on paper and to increase the “hot spot” concentration by controlling the aggregation of AuNPs [12]. The aggregate size, surface coverage of AuNPs on paper and SERS enhancement factor all increased with the concentration, charge density and molecular weight of CPAM adsorbed on paper. Importantly, the preparation of CPAM solution was found to have a strong influence on the aggregation state of AuNPs on paper and the SERS reproducibility. The optimum preparation method was also found to vary depending on the CPAM charge density and molecular weight. CPAM was selected as polyelectrolyte for its wide industrial use as retention aid and flocculant; very high molecular CPAM were chosen for their enhanced ability to coagulate nano-colloids and also to serve as spacer for biomolecules.

Reproducibility of SERS substrate is critical, since SERS-based sensing typically rely on the intensity of particular spectral bands to determine analyte concentration. The reproducibility of SERS intensity from nanoparticles treated paper depends on the packing density and arrangement of the nanoparticles. The formation of uniform surface coverage, aggregation state and distribution of the AuNPs on paper at the nano- and micron-scale is especially important and challenging due to the high heterogeneity inherent of paper. The porosity, surface roughness, fiber size and distribution within a floc all affect paper heterogeneity over three orders of magnitude, from the micrometer (μm) to the centimetre (cm) length scale. It is therefore important to understand and optimize how polymer can retain the AuNPs in a constant and reproducible distribution on paper.

In this study, we first quantify the effect of CPAM dissolution kinetics and charge density on the adsorption and aggregation state of AuNPs on paper. We then link the AuNPs distribution on paper to the resulting SERS performance. We investigate the hypothesis that the preparation of the CPAM solution is a critical variable affecting the final conformation and uniformity of CPAM adsorbed on paper, which then controls the subsequent AuNPs adsorption state on paper and the reproducibility of the SERS signal. It is the objective of this study to quantify and control the effect of polymer dissolution

kinetics on its adsorption conformation and the aggregation state of nanoparticle to optimize the SERS efficiency of AuNPs treated paper used as a bio-diagnostic platform.

4.3 Materials and Methods

4.3.1 Material

Hydrogen tetrachloroaurate trihydrate ($\text{HAuCl}_4 \cdot 3\text{H}_2\text{O}$), sodium citrate tribasic dihydrate ($\text{Na}_3\text{C}_6\text{H}_5\text{O}_7 \cdot 2\text{H}_2\text{O}$) and 4-aminothiophenol (4-ATP) were purchased from Sigma-Aldrich and used as received. The cationic polyacrylamide (CPAM) polymers were kindly supplied by AQUA+TECH Switzerland from their SnowFlake Cationics product range, and used as received. These were copolymers of uncharged acrylamide with cationic dimethylaminoethylacrylate methyl chloride and identified as: I1 (5 wt% charge density, molecular weight 13 MDa), H1 (10 wt% charge density, molecular weight 13 MDa) and F1 (40 wt% charge density, molecular weight 13 MDa). The granulometry (particle size distribution) of all the CPAMs was similar and ranges from 0.125 μm to 1.120 μm , as specified by the supplier. Whatman qualitative filter paper #1, which consists of 98% α -cellulose, was selected as the paper substrate; it is a convenient model paper of well defined structure and to ensure minimal SERS interference from process components (polymers or coatings). Ultrapure water purified with a Millipore system (18 $\text{M}\Omega \cdot \text{cm}$) was used in all aqueous solutions and rinsing procedures.

4.3.2 Dissolution rate of CPAM

The dissolution rate of CPAM in solution was studied by dissolving dry powder of CPAM to 0.1 mg/mL with Millipore water in 10 beakers, and gently shaking the dispersions in a shaking incubator (23°C, 150 r.p.m.). Each beaker of CPAM solution was taken out from the incubator every 1-2 hours to test its viscosity. The viscosity was determined with a BS/U-tube capillary viscometer of size A (viscosity range from 0.9 to 3 cSt) to measure the time needed for the solution to pass through a certain length of the capillary. The viscosity of CPAM was estimated using the following equation:

$$\eta_2 = \frac{\eta_1 \rho_2 t_2}{\rho_1 t_1} \quad (1)$$

where η_1 , ρ_1 and t_1 are the viscosity, density and average time for water (control) and η_2 , ρ_2 and t_2 are the viscosity, density and average time for CPAM. For this experiment, $\eta_1 = 1$ cSt, $\rho_1 = 1.00$ g/cm³ and $\rho_2 = 0.97$ g/cm³.

4.3.3 Synthesis and Deposition of Nanoparticles on Paper Substrates

AuNPs were synthesized by using 1 mM HAuCl₄·3H₂O and 1% aqueous Na₃C₆H₅O₇·2H₂O according to the Turkevich method [13]. Filter papers (55 mm diameter) were used as received, or were pre-treated with the cationic polymer. For polymer treatment, the filter papers were dipped into 10 mL polymer solutions for 1 hour, rendering the paper cationic. The treated papers were then rinsed with distilled water. Without drying, pieces of untreated and polymer-treated paper substrates were subsequently dipped directly into Petri dishes which contained 10 mL solution of AuNPs for 24 hours. After dipping, the paper substrates were rinsed thoroughly with distilled water to remove any loosely bound AuNPs, and the papers were air-dried and stored at 50% relative humidity and 23°C until further analysis.

4.3.4 Preparation of Raman Active Substrates

Solutions of 1 mM of 4-ATP were prepared in ethanol. 4-ATP is known for its strong affinity for the gold surface of AuNPs; its S-H bond is easily cleaved to form Au-S bond upon adsorption. The dried AuNPs-deposited substrates were dipped into 2 mL of the 4-ATP ethanol solution for a shorter period of time of 5 minutes to obtain a monolayer of 4-ATP on the substrates. After thorough rinsing with ethanol and drying, they were subjected to Raman characterization. The Raman enhancement factor (EF) of 1 mM of 4-ATP on a substrate was calculated according to [14-15]:

$$EF = \frac{[I_{SERS}]}{[I_{bulk}]} \times \frac{[N_{bulk}]}{[N_{ads}]} \quad (2)$$

where I_{SERS} is the intensity of a specific band in the SERS spectrum of 4-ATP and I_{bulk} is the intensity of the same band in the Raman spectrum from the bulk solution sample. For all spectra, the intensity of the band at 1077 cm⁻¹ was used to calculate EF values. N_{bulk} is the number of molecules of the bulk 4-ATP in the laser illumination volume while N_{ads} is number of molecules adsorbed and sampled on the SERS active substrate within the laser spot.

4.3.5 Instrumentation

Field Emission Scanning Electron Microscopy (FESEM), which produces higher resolution, less sample charging and less damaged images than conventional SEM, was performed using a JEOL 7001 Field Emission Gun (FEG) system operating at 5 kV and 180 pA. The Dynamic Light Scattering (DLS) measurements were performed with a Zetasizer Nano ZS (Malvern Instruments) in a Folded Capillary cell (DTS1060) at 25 °C. All Raman and SERS spectra were obtained in air using a Renishaw Invia Raman microscope equipped with 300 mW 633 nm laser (integration time of 1s). The laser beam was positioned through a Leica imaging microscope objective lens (50×), whilst the instrument's wavenumber was calibrated with a silicon standard centered at 520.5 cm⁻¹. Due to the smaller spot size of the laser compared with the large surface area of the samples, the spectra were obtained at 5 different points of the surface. The position of the spectra band from different points on the surface were the same, but differed only in intensity. The averaged Raman intensity (of 5 measurements) was presented as the final result, after baseline subtraction from the control samples.

4.4 Results

4.4.1 Dissolution of CPAM

The different CPAM polymer powders were dissolved in water under constant shear, temperature and concentration, and the viscosity of the polymer solution was measured as a function of time. The viscosity of all CPAM solutions initially increased with mixing time and levelled-off (Figure 1). The viscosity of the CPAM solutions increased with the polymer charge density at a constant molecular weight. The viscosity of CPAM of 40 wt% charge density increased to reach a plateau after 8 hours. For CPAM of 10 wt% and 5 wt% charge density, the solution viscosity became constant only after 12 hours of mixing.

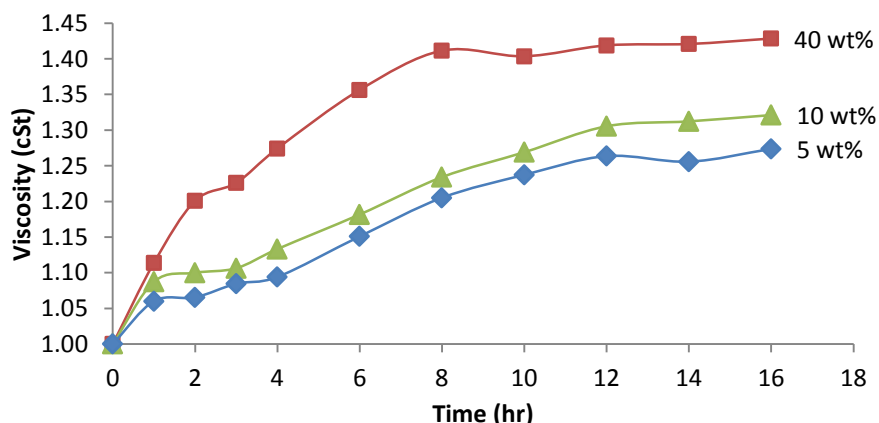


Figure 1: Effect of dissolution time and CPAM charge density on the viscosity of polymer solutions. CPAM (13MDa) 0.10 mg/mL at room temperature in water.

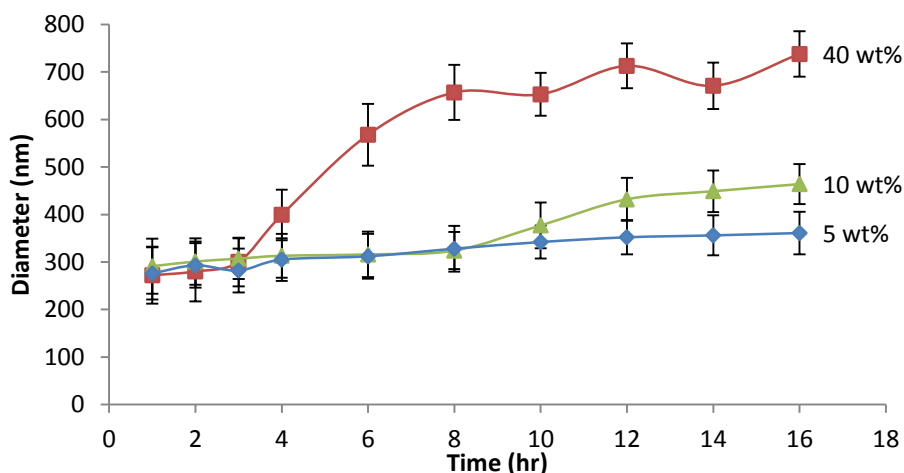


Figure 2. Effect of dissolution time and CPAM charge density on the average hydrodynamic diameter. CPAM (13MDa) 0.10 mg/mL at room temperature in water. Error bars indicate the standard deviations from five measurements.

The viscosity of a polymer solution is an indication of the concentration, structure, organization and size of the dissolving polymer molecules. Dynamic light scattering (DLS) measurements of the CPAM solutions were performed at the same regular intervals. The relationship between the hydrodynamic diameter of CPAM and their dissolution time (Figure 2) was similar to the relationship between their viscosity and mixing time (Figure 1). For polymer solutions made with CPAM 5 wt% charge density, viscosity increased in a similar fashion as with the other CPAMs (although with less intensity), but hydrodynamic diameter remained fairly constant over the dissolution time.

The absolute value of the hydrodynamic diameters of CPAM aggregate/coil must be interpreted with care, as the measured values were often outside the usual range of polydispersity ($P \geq 1$), indicated by the instrument software. The hydrodynamic diameter of dissolved CPAM molecules increased with mixing time to reach a plateau after 8 hours and 12 hours of mixing for CPAM of 40 wt%, 10 wt% and 5 wt% (less gradual increase) charge density, respectively. The increase in the size of CPAM with time could be due to their polydispersity which caused the low molecular weight fraction to dissolve first, and leave the high molecular weight fraction to preferentially remain in the grains and dissolve later.

4.4.2 Properties of AuNPs-CPAM paper

Filter papers were pre-treated with a series of CPAM solutions, which were prepared for different mixing time periods; and followed by dipping in a 0.20 mg/mL of AuNP solution. Particle size measurement of the AuNP solution by DLS revealed highly monodispersed AuNPs with an average diameter of 23.2 nm. FESEM analysis was performed to examine the adsorption of AuNPs on the CPAM pre-treated paper substrates (Figure 3). The average aggregate diameter and surface coverage of AuNPs were quantified by applying a threshold so that the AuNPs in the FESEM images were changed to black colour and the cellulose fibers to white using ImageJ software from the National Institute of Health (NIH).

The surface coverage of AuNPs was the proportional percentage of black coloured area to the total area of the images. The average diameter (Figure 4) and surface coverage (Figure 5) of AuNPs on paper increased and levelled off as a function of the CPAM's charge density. The levelling effect of AuNPs surface coverage (Figure 5) was not attributed to the depletion of the NPs concentration as the amount of AuNPs in suspension was in large excess (Supporting Information). The AuNPs were adsorbed as aggregates of random size and lower surface coverage when papers were pre-treated with CPAM dissolved in a shorter period of time. As the CPAM solution was mixed longer, the distribution of AuNP aggregates on paper was more uniform and denser. (Figure 3)

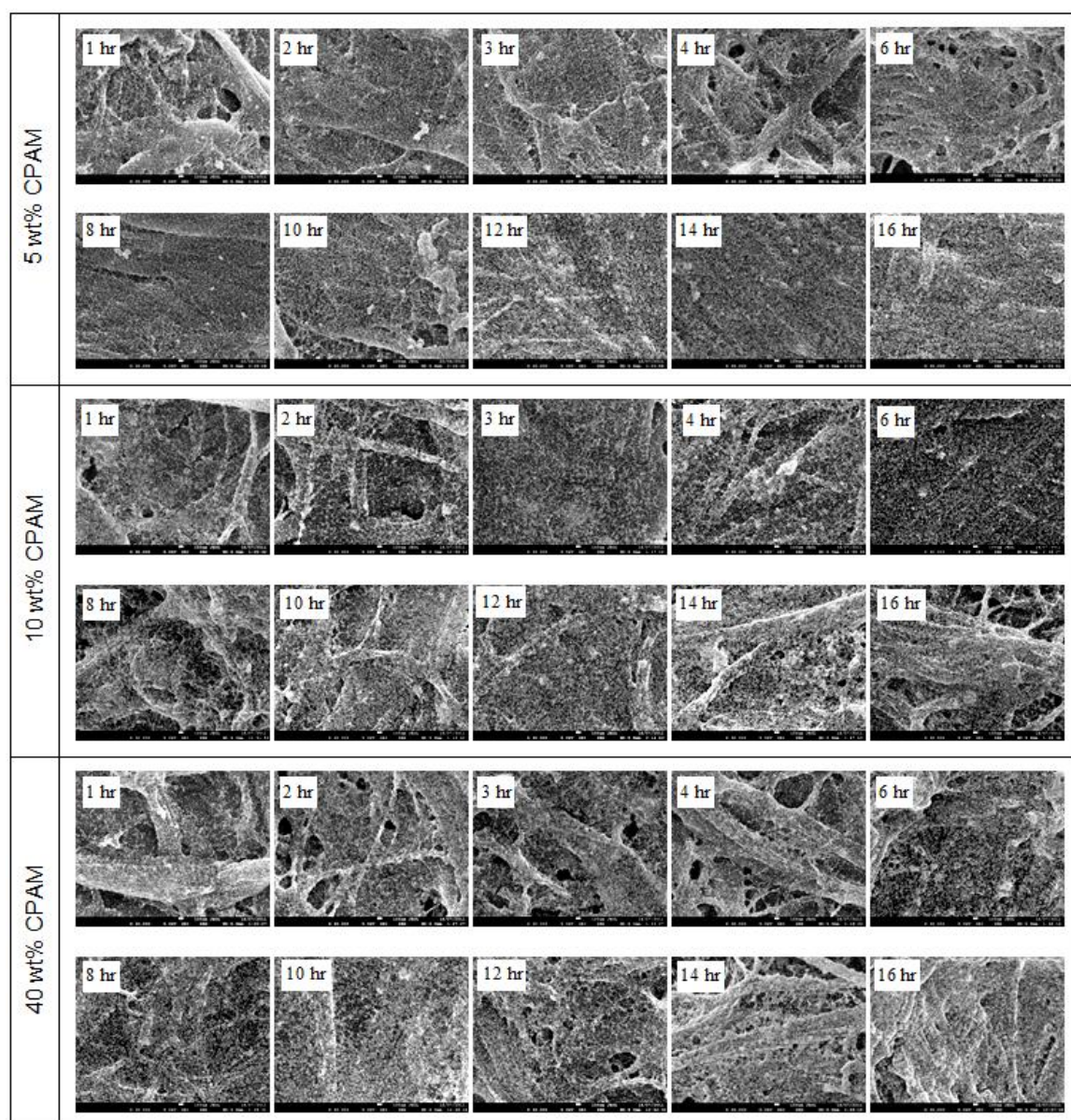


Figure 3: FESEM of AuNPs on paper substrate pre-treated by CPAM of 5 wt%, 10 wt% and 40 wt% charge density at different dissolution time.

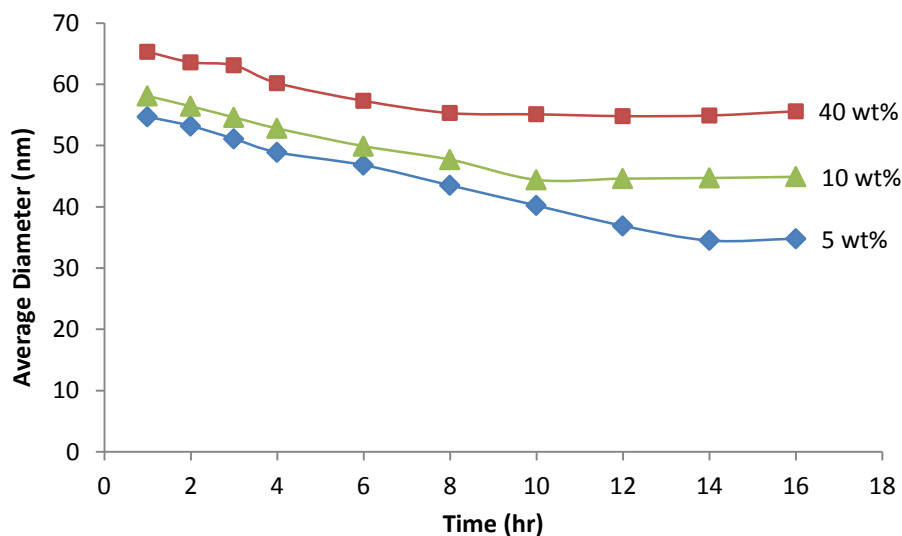


Figure 4: Average size of AuNP aggregates on paper substrate pre-treated by CPAM of different charge density vs. dissolution time of CPAM.

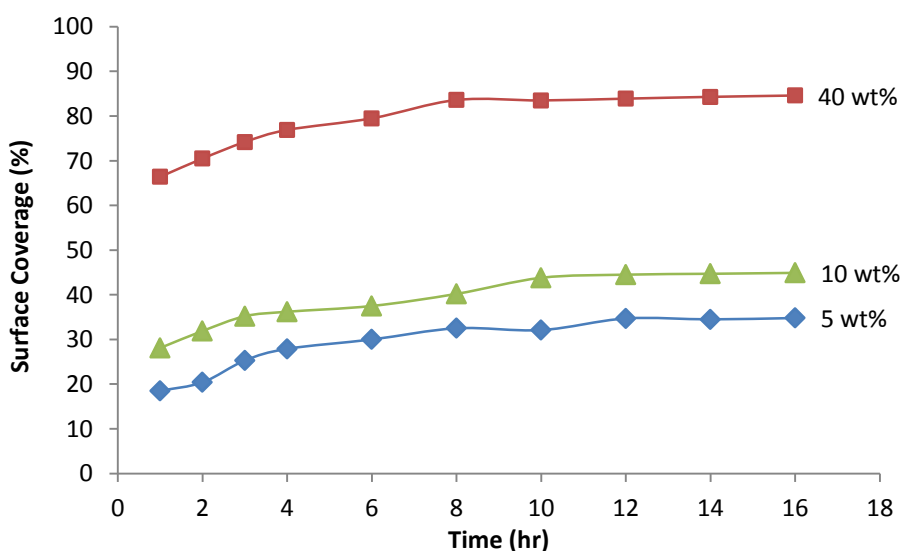
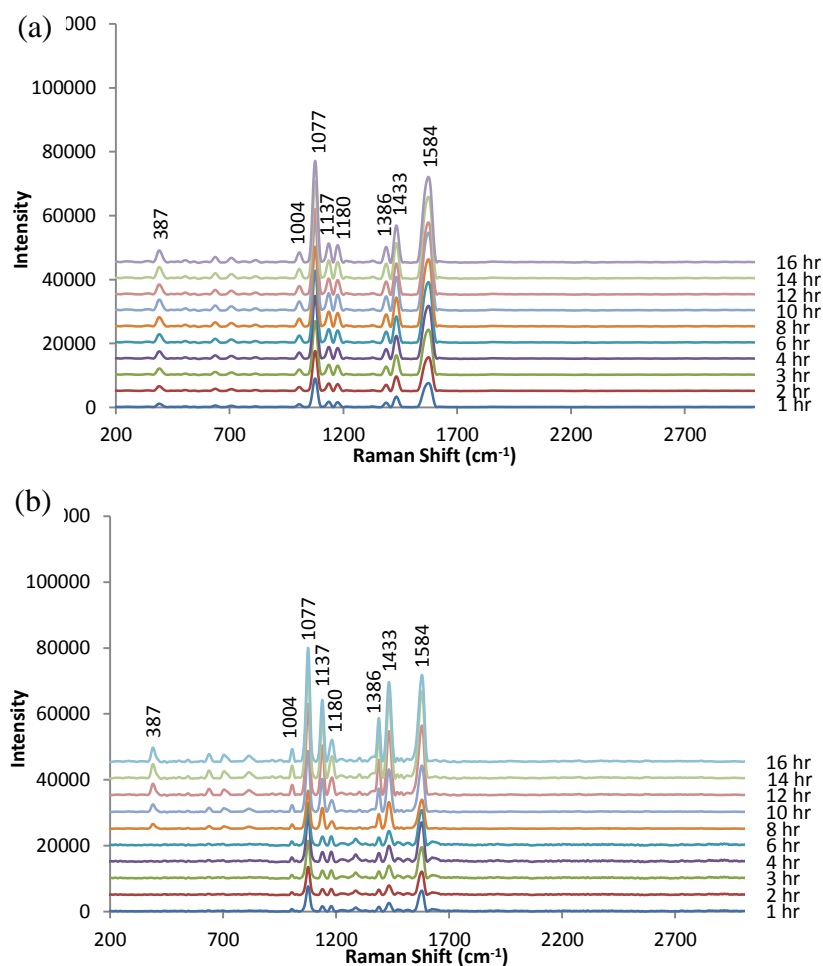


Figure 5: Surface coverage of AuNP aggregates on paper substrate pre-treated by CPAM of different charge density vs. dissolution time of CPAM.

4-Aminothiophenol (4-ATP) was selected as the probe molecule for the Raman analysis, as in our previous studies [12]. The SERS spectra of 4-ATP were dominated by three strong characteristic peaks: $\delta(\text{C-S})$ at 387 cm^{-1} , $\nu(\text{C-S})$ at 1077 cm^{-1} and $\nu(\text{C-C})$ at 1584 cm^{-1} , which were the a_1 vibrational modes (in-plane, in-phase modes) of the 4-ATP molecules (Figure 6). The significant enhancement of a_1 modes was related to the enhancement of the electromagnetic field between the AuNPs, which was produced by strong inter-nanoparticle coupling among the AuNPs in close contact. The SERS spectra

showed a higher signal to noise ratio as the dissolution period of CPAM was increased; the characteristic peaks were better defined. The SERS intensity was increased as the charge density of CPAM was increased from 5 wt% to 40 wt% (Figure 6). Figure 7 shows the Raman EF of 4-ATP measured at 1077 cm^{-1} band when paper was pre-treated with CPAM solutions of different charge density which were prepared at different dissolution times. As the charge density of the CPAM solution was increased, the EF of the AuNPs-CPAM paper increased by almost an order of magnitude. The standard deviations of EF were smaller for paper pre-treated with CPAM solutions that were allowed to mix and dissolve for a longer period.



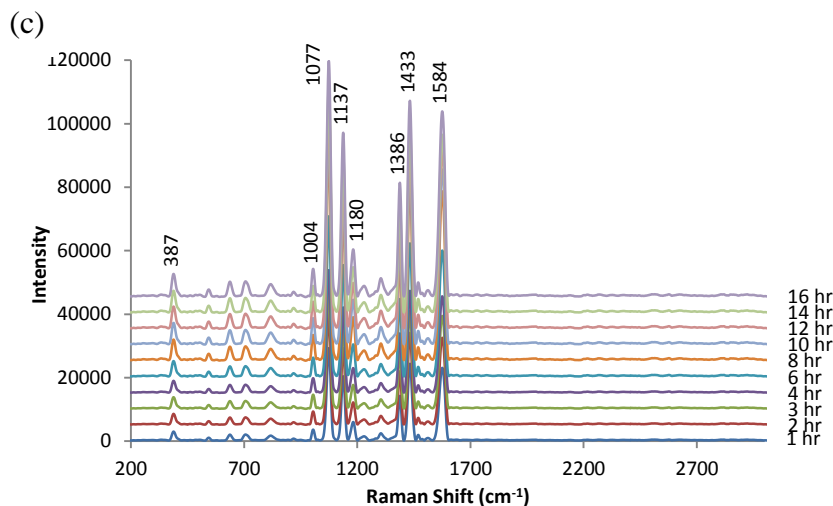


Figure 6: Average SERS spectra of 4-ATP on AuNPs-CPAM papers with CPAM of (a) 5 wt%, (b) 10 wt% and (c) 40 wt% charge density prepared at different dissolution times.

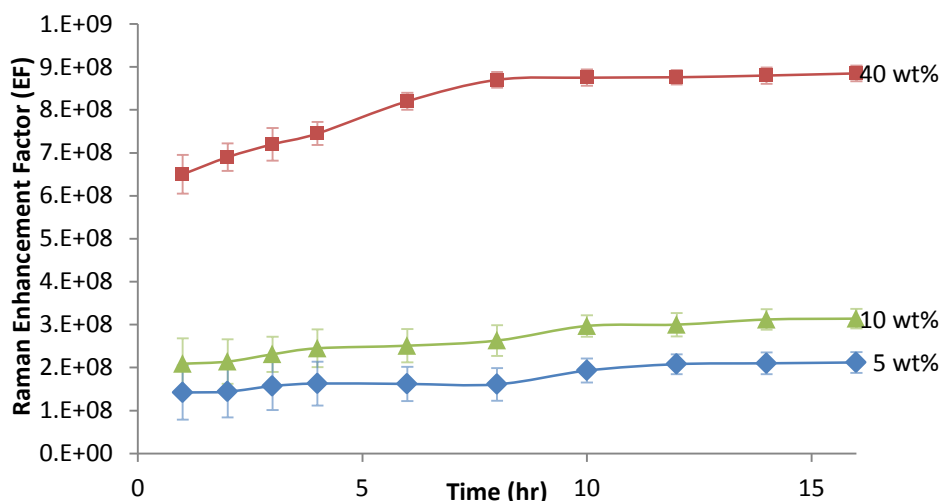


Figure 7: Raman enhancement factor (EF) of 4-ATP at 1077 cm^{-1} on AuNPs-CPAM papers treated with CPAM of different charge density as a function of CPAM dissolution time. Error bars are standard deviations from five measurements at different point on the substrates.

4.5 Discussion

4.5.1 Mechanism of CPAM Dissolution

The degree of dissolution of CPAMs, which were pre-adsorbed on paper, greatly affected the adsorption state of AuNPs on paper substrates and their SERS reproducibility. The CPAMs studied have a very high molecular weight (13 MDa). Their dissolution process

from a powder to a solution at equilibrium is long and complex as many different configurations are achievable by the polymer, giving rise to high entropy. The long polymer chains are made of numerous flexible segments which tend to entangle with each other. According to the Stokes-Einstein equation, viscosity scales inversely with diffusion coefficient [16]. The rate of a diffusion-controlled dissolution decreases as the viscosity increases, whilst the viscosity of a polymer solution depends on the size of the critical unit of the dissolved polymer's [17-18]. The dissolution rate of CPAM in solution was monitored by measuring macroscopic viscosity and hydrodynamic diameter.

The viscosity and hydrodynamic diameter of the polymer solution show a similar trend when the CPAM powder was added to water and mixed up to 16 hours (Figures 1 and 2). DLS measurements of the CPAM solutions had very high polydispersity indexes, indicating preferential size measurement of the larger polymer aggregates instead of reflecting the average hydrodynamic diameter of the polymer units. The critical polymer dimension measured by DLS (250 nm) is almost an order of magnitude larger than the radius of gyration calculated for the polymer random coil (38 nm). This can be expected due to the extended configuration of CPAM as a high molecular weight polyelectrolyte. Since the trend of the DLS measurement (Figure 2) is consistent with the viscosity results (Figure 1), it can be interpreted in a relative sense. Both the viscosity and average diameter of CPAM increased and reached a plateau after a critical time. A two stages process is proposed: an induction period followed by the dissolution step [18-19]. During the induction period, water diffuses into the polymer powder (Figure 8a to 8b) and a swollen surface layer results (Figure 8c). Attraction and repulsion forces start acting between the segments of the dissolved polymer as they gain mobility. The polymer-solvent and charge-charge interactions overcome the polymer-polymer attraction forces, causing the chain segment to absorb solvent molecules, increasing the volume of the polymer matrix, and the dimensions of its coils (Figure 8d). At this stage, the polymer segments are considered as "solvated". The "solvation-unfolding-swelling" process continues until all segments are solvated [19]. The viscosity and critical unit size of CPAM solution slowly increases during the induction period at 1 to 3 hour of mixing (Figures 1 and 2). Figure 8 schematically illustrates the process. It was expected that the polymer size of CPAM at the earlier stages of dissolution (Figure 8a and 8b) to be larger than those at the subsequent stages (Figure 8d and 8e). However, the hydrodynamic

diameter measured by DLS (Figure 2) shows the opposite. This could be due to limitation of the DLS equipment, which can only detect size ranging from 0.6 nm to 6 μm ; the particle size of the original CPAM polymer particles is between 0.125 mm to 1.120 mm. The CPAM powder could also settle down at the bottom of the capillary cell during DLS measurement.

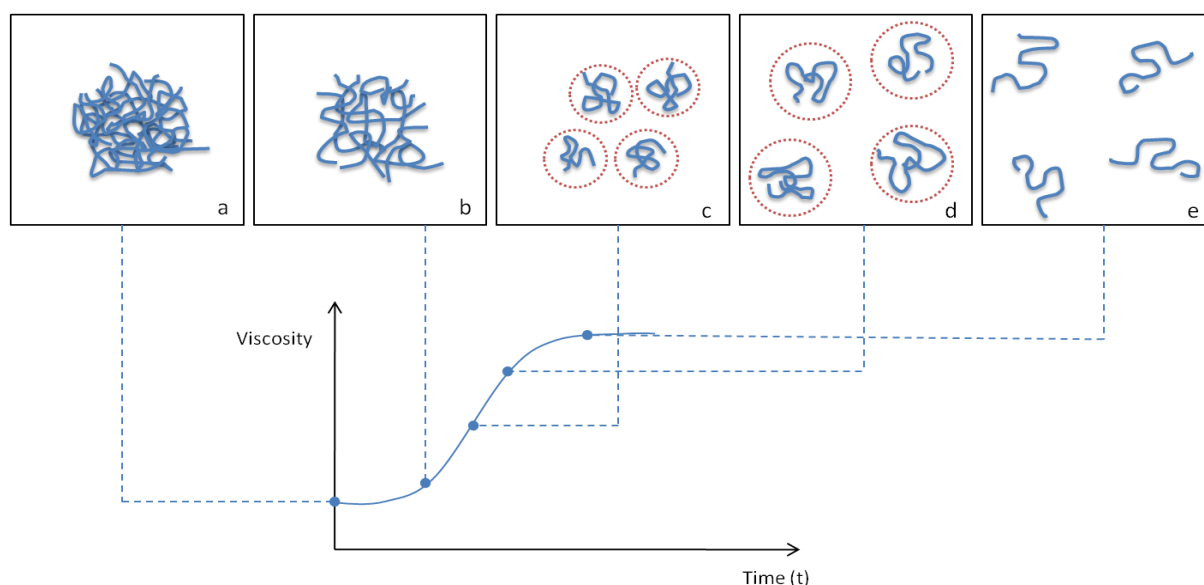


Figure 8: Schematic representation of the dissolution kinetic of CPAM; the red circles represent the gel aggregates

The viscosity and critical unit size of CPAM increased dramatically after 4 hours of mixing (Figures 1 and 2); this is particularly evident for CPAM of 40 wt% charge density. The dissolution mechanism dominates this stage as the loosened coil can diffuse from the swollen polymer and become intimately mixed with solvent. The plateaux of Figures 1 and 2 correspond to the full dissolution and solvation of CPAM. The hydrated polymer coils are expected to adopt a spherical or ellipsoidal shape (Figure 8e).

The interactions between charged groups on a CPAM molecule have a strong influence on the conformation of the polymer coil in solution. The viscosity and DLS measurements show that the dimensions of the polymer critical unit vary linearly with the charge density of CPAM (Figures 1 and 2). A highly charged polymer has a more extended conformation in solution due to stronger inter- and intra-molecular repulsion

between charged segments [20]. Therefore, CPAM with the highest charge density can dissolve and reach its plateau the fastest (Figures 1 and 2).

4.5.2 Properties of AuNPs-CPAM paper

The adsorption and aggregation state of AuNPs were strongly influenced by the extent of CPAM dissolution upon paper dip-coating (Figure 3). Polymer molecules are known to adsorb on fibrous paper substrates in a conformation where some of its segments maintain contact with the fibre surface (trains), some segments between two adjacent trains extend into solution (loops) and some free ends are dangling into solution (tails) [21]. In this study, the adsorption and aggregation of AuNPs induced by CPAM which was pre-adsorbed onto paper were analysed in terms of the CPAM dissolution behaviour.

AuNPs were adsorbed onto the cellulose fibers of paper as well dispersed individual nanoparticles when plain paper was directly dipped into the AuNP solution without CPAM pre-treatment [10]. When the paper pre-treated with CPAM solutions, which were dissolved only for 1 to 4 hours (prior to the viscosity and coil diameter reaching a plateau), was dipped into the AuNP solution, partial coverage resulted with AuNPs aggregates (Figure 3). CPAM dissolution is incomplete at this stage and the polymer exists in a mixture of swollen gel aggregates and polymer coils (Figure 8b-8c). The cationic polymer adsorbs onto the negatively-charged cellulose fibers mostly in an entangled conformation [22]. A charged polymer patch mechanism is expected to be predominant; the partial surface coverage of one or more molecules of CPAM created a positively charged “patch” which interacts with a negatively charged “patch” of AuNPs through electrostatic interaction [23]. These patches of AuNP aggregates produced low SERS enhancement and reproducibility (Figure 7). This is probably due to the absence of uniformly and the densely distributed AuNP aggregates at the sub-micrometer scale. The length scale of AuNP heterogeneity is higher than the critical dimension of the Raman detection; the diameter of the Raman’s laser beam is approximately 1 μm .

As the dissolution period increases, the CPAM polymer chains loosen and uncoil, adsorbing on cellulose fibers in a more extended train-loop-tail conformation. The tails and loops extend into the solution phase driven by strong intramolecular electrostatic repulsion and affinity for water, while the train sections adhere to the negatively charged

cellulose by electrostatic affinity. This state of extended polymer tails and loops produced uniformly distributed AuNP aggregates through polymer bridging and charge neutralization [24] (Figure 4). At uniform CPAM coverage, the negative charge of cellulose fibers was reduced, neutralized and even reversed. This created an electrostatic interaction between paper and AuNPs (negatively-charged), leading to a higher AuNPs surface coverage (Figure 5). This higher surface coverage and uniformly distributed AuNP aggregates contributed to SERS spectra having a higher signal to ratio and well defined characteristic peaks (Figure 6). Raman EF and reproducibility were increased as the lateral dimension of AuNP distribution heterogeneity became smaller than the critical dimension of Raman measurement (1 μm).

The charge density of CPAM polymer chain has a drastic effect on their conformations, which affects the adsorption and aggregation state of NPs (Figure 4 and Figure 5). At lower charge density, polymer molecules tends to form more loops and tails upon adsorption [21, 25]. The flocculation of AuNPs is expected to occur mostly through bridging [21]. When paper was pre-treated with CPAM of higher charge density, higher surface coverage and more uniform distribution of AuNP aggregates resulted. Polymers of higher charge density tend to reorganize in a flatter conformation upon adsorption [26]. Flocculation of AuNPs is probably driven by a charge neutralization mechanism. Bridging could also be involved. As the highly charged CPAM had a higher charge density than paper, intra-molecular repulsive forces induced by the excess polymer charge could generate an adsorbed polymer configuration with more loops and tails [27]. CPAM with higher charge density produced a uniform aggregation (Figure 4) and higher surface coverage (Figure 5) of AuNPs, leading to the formation of rough metallic surfaces ('hot spots') which gave rise to stronger electromagnetic coupling to enhance the Raman signal of 4-ATP (Figure 6 and Figure 7).

4.6 Conclusion

The dissolution kinetics of a polyelectrolyte, from a powder to an equilibrium solution, can affect the adsorption and coagulation behaviour of colloids. An example is in the retention and coagulation of gold nanoparticles (AuNPs), which are used as Surface Enhanced Raman Scattering (SERS) signal enhancer in the fabrication of paper bio-diagnostics platform, with cationic polyacrylamide (CPAM) serving as retention aid. This

study aimed at improving the sensitivity and reproducibility of AuNPs treated paper used as routine substrate for SERS analysis.

A series of high molecular weight (13MDa) CPAM powders varying in charge density was dissolved in water. The viscosity and the critical aggregate size of the CPAM solutions were measured as a function of their dissolution time. Filter papers were dipped into a polymer solution, rinsed and dipped again into a standard AuNP solution. The ability of CPAM to adsorb and coagulate AuNPs on paper was quantified. The surface coverage and aggregate size of AuNPs on paper were both measured by FESEM/image analysis. A model dye (4-ATP) was adsorbed onto the AuNP paper substrates, its Raman spectra were measured and the SERS performance was analysed.

The viscosity and critical aggregate/coil size of a high molecular weight, low charge density CPAM solution both slowly increase to reach a plateau after 12 hours. Increasing the charge density of the polymer shortened the time required to reach steady state (8 hours). The surface coverage of AuNPs on paper increased and their average aggregate size decreased as paper was pre-treated with a CPAM solution which had been mixed for a longer period; increasing CPAM charge density accentuated this tendency. SERS intensity and reproducibility of AuNPs paper both increase with dissolution time of CPAM, as the heterogeneity of AuNP distribution and aggregate size decreases below 1 μm , the critical SERS dimension corresponding to the diameter of the Raman laser beam.

Controlling the dissolution time of a high molecular weight polyelectrolyte from a powder to a solution affects the conformation of its critical unit in water (aggregates to coil), influences its subsequent adsorption on a surface, and determines its ability to coagulate nanoparticles. The heterogeneity of AuNPs distribution on paper is related to variability in the bridging and aggregation of nanoparticles caused by the dissolution kinetic of CPAM. This understanding of polymer dissolution kinetic is critical to optimize the SERS performance of AuNPs paper.

4.7 Acknowledgement

Thanks to Dr. T. Williams and F. Shanks, Monash University for technical expertise and AQUA+TECH for supplying the CPAM polymers (SnowFlake Cationics). The financial

support from the ARC Linkage LP0989823 and Visy, Amcor, SCA, Norske Skog, Australian Paper, the Australian Pulp and Paper Institute and Monash University are acknowledged.

4.8 References

1. Al-Tamimi, M., W. Shen, R. Zeineddine, H. Tran, and G. Garnier, *Validation of Paper-Based Assay for Rapid Blood Typing*. Analytical Chemistry, 2011. **84**(3): p. 1661-1668.
2. Khan, M.S., G. Thouas, W. Shen, G. Whyte, and G. Garnier, *Paper Diagnostic for Instantaneous Blood Typing*. Analytical Chemistry, 2010. **82**(10): p. 4158-4164.
3. Li, M., J. Tian, M. Al-Tamimi, and W. Shen, *Paper-Based Blood Typing Device That Reports Patient's Blood Type "in Writing"*. Angewandte Chemie International Edition, 2012. **51**(22): p. 5497-5501.
4. Luo, Z. and Y. Fang, *SERS of C60/C70 on gold-coated filter paper or filter film influenced by the gold thickness*. Journal of Colloid and Interface Science, 2005. **283**(2): p. 459-463.
5. Berthod, A., J.J. Laserna, and J.D. Winefordner, *Analysis by surface enhanced Raman spectroscopy on silver hydrosols and silver coated filter papers*. Journal of Pharmaceutical and Biomedical Analysis, 1988. **6**(6-8): p. 599-608.
6. Cabalín, L.M. and J.J. Laserna, *Fast spatially resolved surface-enhanced Raman spectrometry on a silver coated filter paper using charge-coupled device detection*. Analytica Chimica Acta, 1995. **310**(2): p. 337-345.
7. Ma, W. and Y. Fang, *Experimental (SERS) and theoretical (DFT) studies on the adsorption of p-, m-, and o-nitroaniline on gold nanoparticles*. Journal of Colloid and Interface Science, 2006. **303**(1): p. 1-8.
8. Niu, Z. and Y. Fang, *Surface-enhanced Raman scattering of single-walled carbon nanotubes on silver-coated and gold-coated filter paper*. Journal of Colloid and Interface Science, 2006. **303**(1): p. 224-228.
9. Wu, D. and Y. Fang, *The adsorption behavior of p-hydroxybenzoic acid on a silver-coated filter paper by surface enhanced Raman scattering*. Journal of Colloid and Interface Science, 2003. **265**(2): p. 234-238.
10. Ngo, Y.H., D. Li, G.P. Simon, and G. Garnier, *Gold Nanoparticle-Paper as a Three-Dimensional Surface Enhanced Raman Scattering Substrate*. Langmuir, 2012. **28**(23): p. 8782-8790.
11. Toderas, F., M. Baia, L. Baia, and S. Astilean, *Controlling gold nanoparticle assemblies for efficient surface-enhanced Raman scattering and localized surface plasmon resonance sensors*. Nanotechnology, 2007. **18**.
12. Ngo, Y.H., G. Garnier, D. Li, and G. Simon, *Effect of Cationic Polyacrylamides on the Aggregation and SERS Performance of Gold Nanoparticles-treated Paper*. Journal of Colloid and Interface Science, 2012. **In press**.
13. Turkevich, J., P.C. Stevenson, and J. Hillier, *A study of the nucleation and growth processes in the synthesis of colloidal gold*. Discussions of the Faraday Society 1951. **11**: p. 55-75.
14. Camargo, P.H.C., L. Au, M. Rycenga, W. Li, and Y. Xia, *Measuring the SERS enhancement factors of dimers with different structures constructed from silver nanocubes*. Chemical Physics Letters, 2010. **484**(4-6): p. 304-308.
15. Hu, X., T. Wang, L. Wang, and S. Dong, *Surface-Enhanced Raman Scattering of 4-Aminothiophenol Self-Assembled Monolayers in Sandwich Structure with Nanoparticle*

- Shape Dependence: Off-Surface Plasmon Resonance Condition*. Journal of Physical Chemistry C, 2007. **111**(19): p. 6962-6969.
16. Sarisuta, N. and E.L. Parrott, *Relationship of dissolution rate to viscosity of polymeric solutions*. Journal of Pharmaceutical Sciences, 1982. **71**(12): p. 1375-1380.
17. Ebewele, R.O., *Solution Properties of Polymers*, in *Polymer Science and Technology*. 2000, CRC Press.
18. Miller-Chou, B.A. and J.L. Koenig, *A review of polymer dissolution*. Progress in Polymer Science, 2003. **28**(8): p. 1223-1270.
19. Billmeyer, F.W., *Textbook of Polymer Science*. 1984: Wiley.
20. Dobrynin, A.V. and M. Rubinstein, *Theory of polyelectrolytes in solutions and at surfaces*. Progress in Polymer Science, 2005. **30**(11): p. 1049-1118.
21. Fleer, G.J., M.A.C. Stuart, J.M.H.M. Scheutjens, T. Cosgrove, and B. Vincent, *Polymers at Interfaces*. 1998, London: Chapman & Hall.
22. Wågberg, L., *Polyelectrolyte adsorption on cellulose fibres - a review*. Nordic Pulp & Paper Research Journal, 2000. **15**(5): p. 586-597.
23. Mosse, W.K.J., D.V. Boger, G.P. Simon, and G. Garnier, *Effect of Cationic Polyacrylamides on the Interactions between Cellulose Fibers*. Langmuir, 2012. **28**(7): p. 3641-3649.
24. Sennerfors, T., *Polymer-Nanoparticle Complexes: Fundamentals and Applications of Interfacial Behavior*. Encyclopedia of Surface and Colloid Science: Second Edition, 2006: p. 4874 - 4884.
25. Hubbe, M.A., H. Nanko, and M.R. McNeal, *Retention aid polymer interactions with cellulosic surfaces and suspensions: A Review*. Bioresources, 2009. **4**(2): p. 850-906.
26. Shin, Y., J.E. Roberts, and M.M. Santore, *The Relationship between Polymer/Substrate Charge Density and Charge Overcompensation by Adsorbed Polyelectrolyte Layers*. Journal of Colloid and Interface Science, 2002. **247**(1): p. 220-230.
27. Claesson, P.M., M.A.G. Dahlgren, and L. Eriksson, *Forces between polyelectrolyte-coated surfaces: relations between surface interaction and floc properties*. Colloids and Surfaces A: Physicochemical and Engineering Aspects, 1994. **93**: p. 293-303.
28. Lewis, D.J., T.M. Day, J.V. MacPherson, and Z. Pikramenou, *Luminescent nanobeads: attachment of surface reactive Eu(iii) complexes to gold nanoparticles*. Chemical Communications, 2006(13): p. 1433-1435.
29. Liu, X., M. Atwater, J. Wang, and Q. Huo, *Extinction coefficient of gold nanoparticles with different sizes and different capping ligands*. Colloids and Surfaces B: Biointerfaces, 2007. **58**(1): p. 3-7.
30. BarathManiKanth, S., K. Kalishwaralal, M. Sriram, S. Pandian, H.-s. Youn, S. Eom, and S. Gurunathan, *Anti-oxidant effect of gold nanoparticles restrains hyperglycemic conditions in diabetic mice*. Journal of Nanobiotechnology, 2010. **8**(1): p. 16.

4.9 Supporting Information

Calculation of AuNPs' concentration [28-30]

Assuming AuNPs are metal clusters which consist of a number of Au atoms.

$$V_{\text{cluster}} = NV_{\text{atom}} \quad (1)$$

$$\frac{4}{3}\pi(R_{\text{cluster}})^3 = N\frac{4}{3}\pi(R_{\text{atom}})^3 \quad (2)$$

Where V is the cluster volume or atomic volume, R is the cluster or atomic volume and N is the total number of atoms per cluster of NPs.

Rearranging (2):

$$R_{\text{cluster}} = N^{\frac{1}{3}}R_{\text{atom}} \quad (3)$$

Knowing the cluster radius, the surface area (S) of a NP can be calculated:

$$\text{Surface area of AuNPs cluster, } S_{\text{cluster}} = 4\pi(R_{\text{cluster}})^2 \quad (4)$$

From DLS analysis, the average diameter of AuNP is 23.2 nm, $R_{\text{cluster}} = 23.2\text{nm}/2 = 11.6\text{nm}$

Ionic radius of gold atom, $R_{\text{atom}} = 0.137\text{nm}$

Substituting into equation (3):

$$N = (R_{\text{cluster}}/R_{\text{atom}})^3 = 6.07 \times 10^5 \text{ Au atoms per AuNP}$$

During the synthesis of AuNPs, 20 mL of 1 mM HAuCl₄ was reduced by citrate. Assuming the reduction from gold(III) to gold atoms was 100% complete:

$$\text{Moles of Au}^{3+} = 20 \times 10^{-3} \times 1 \times 10^{-3} = 2 \times 10^{-5} \text{ mol}$$

$$\text{Number of Au atoms} = 2 \times 10^{-5} \times N_A = 2 \times 10^{-5} \times 6.022 \times 10^{23} = 1.20 \times 10^{19}$$

$$\text{Number of AuNPs formed} = 1.20 \times 10^{19} / N = 1.98 \times 10^{13} \text{ NPs}$$

$$\text{Area of filter paper used (55 mm diameter)} = 2.40 \times 10^{-3} \text{ m}^2$$

$$\text{Number of AuNPs/area of paper} = 8.25 \times 10^{15} \text{ NPs/m}^2$$

$$\text{Area of filter paper in the FESEM images} = 1.2 \times 10^{-11} \text{ m}^2$$

Theoretical maximum adsorption of AuNPs on paper in the FESEM images = 99,000 NPs

According to Figure 5, the highest surface coverage of AuNPs on paper = 84.6%

$$\text{Hence, the area of AuNPs occupied on paper in the FESEM images} = 1.02 \times 10^{-11} \text{ m}^2$$

$$\text{The area of an AuNP of 23.2 nm diameter} = 4.22 \times 10^{-16} \text{ m}^2$$

Hence, the number AuNPs on paper in the FESEM images = 24,129 NPs (24% of the theoretical maximum number)

Chapter 5

Formation of Polyelectrolyte-Gold Nanoparticles Chaplets on Paper

This page is intentionally blank

Monash University

Declaration for Thesis Chapter 5

Declaration by candidate


In the case of Chapter 5, the nature and extent of my contribution to the work was the following:

Nature of contribution	Extent of contribution (%)
Initiation, key ideas, experimental and analysis works, development and writing up of paper	80

The following co-authors contributed to the work. Co-authors who are students at Monash University must also indicate the extent of their contribution in percentage terms:

Name	Nature of contribution	Extent of contribution (%) for student co-authors only
Gil Garnier	Initiation, key ideas, reviewing and editing of the paper.	Supervisor
George Simon	Initiation, key ideas, reviewing and editing of the paper.	Co-supervisor
Dan Li	Initiation, key ideas, reviewing and editing of the paper.	Co-supervisor

Candidate's Signature

	Date 13.03.2013
---	-----------------

Declaration by co-authors


The undersigned hereby certify that:

- (1) the above declaration correctly reflects the nature and extent of the candidate's contribution to this work, and the nature of the contribution of each of the co-authors.
- (2) they meet the criteria for authorship in that they have participated in the conception, execution, or interpretation, of at least that part of the publication in their field of expertise;
- (3) they take public responsibility for their part of the publication, except for the responsible author who accepts overall responsibility for the publication;
- (4) there are no other authors of the publication according to these criteria;
- (5) potential conflicts of interest have been disclosed to (a) granting bodies, (b) the editor or publisher of journals or other publications, and (c) the head of the responsible academic unit; and
- (6) the original data are stored at the following location(s) and will be held for at least five years from the date indicated below:

Location(s)

Australian Pulp and Paper Institute (APPI), Department of Chemical Engineering, Monash University, Clayton, VIC 3800, Australia.


Signature 1

	Date 11/12/12
---	---------------

Signature 2

	Date 12/12/12
---	---------------

Signature 3

	Date 11/12/2012
---	-----------------

This page is intentionally blank

Formation of Polyelectrolyte-Gold Nanoparticles

Chaplets on Paper

Ying Hui Ngo¹, Dan Li², George P. Simon² and *Gil Garnier¹

¹ BioPRIA, Australian Pulp and Paper Institute (APPI), Department of Chemical Engineering Monash University, Clayton, VIC 3800, Australia.

² Department of Material Engineering Monash University, Clayton, VIC 3800, Australia

*Corresponding author. Email: [REDACTED]; Tel: [REDACTED]; Fax: [REDACTED]

Content

5.1	Abstract	173
5.2	Introduction	174
5.3	Experimental Section	175
5.3.1	Materials	175
5.3.2	Synthesis and Fabrication of Polyelectrolyte-Nanoparticles	
	Chaplet on Paper	176
5.3.3	Instrumentation	176
5.4	Results and Discussion	177
5.4.1	Effect of CPAM Concentration	177
5.4.2	Effect of CPAM Charge Density	179
5.4.3	Effect of CPAM Molecular Weight	181
5.4.4	Mechanisms	182
5.5	Conclusion	185
5.6	Acknowledgement	186
5.7	References	186
5.8	Supporting Information	188

5.1 Abstract

We have developed a simple method to form and visualize individual polyelectrolyte-nanoparticle chaplet like structures on paper. This method can be applied to other porous surfaces. In this work, one-dimensional chaplets of negatively charged gold nanoparticles (AuNPs) have been electrostatically assembled along the backbone of a cationic polyacrylamide (CPAM) chain adsorbed on paper. The process involves rapidly passing a

dilute CPAM solution through filter paper, adsorbing the polyelectrolyte on the surface, followed by the immediate filtration of an AuNP suspension through the same filter paper. The nanoparticles used were negatively charged, citrate ion capped AuNPs with average diameter of 20 nm. Scanning electron microscopy images of the dried paper sample showed that the AuNP chaplets were adsorbed in an opposite direction to the cellulose fibers and along the length of the CPAM molecules which were draped over the fibers. The effects of CPAM polymer concentration, charge density and molecular weight on such assembly of AuNPs were studied. This technique enables the visualization of individual polyelectrolyte molecules and the formation of very well organized and reproducible polyelectrolyte-nanoparticle chaplets on a porous substrate.

Keywords: Gold nanoparticles (AuNPs), paper, cationic polyacrylamide (CPAM), chaplets, nanoparticle-polymer complex.

5.2 Introduction

There is a renewed interest in functionalizing paper with nanoparticles to produce a range of low-cost photocatalytic [1-2], anti-microbial [3-4], anti-counterfeiting [5] and Surface Enhanced Raman Scattering (SERS) substrates [6-8]. Polymers, and particularly charged polymers (polyelectrolytes), are often used to retain and control the state of adsorption or aggregation of nanoparticles on or within the porous and heterogeneous paper structure [9-10]. To facilitate and optimize the assembly of nanoparticles and the integration of these nanocomposites into devices such as a SERS bio-diagnostic sensor requires control of the adsorbed polymer chain morphology. However, understanding how the process variables affect the polymer/nanoparticle complex morphology and how this influences the end-use of paper properties is still limited. For example, how can a three-dimensional (3D) polymer chain in solution dramatically change its conformation to form nicely aligned two-dimensional (2D) chains upon adsorption on paper.

Chaplet like structures between nanoparticles and polymers were originally observed by Nanko et al. [11] and Lee et al. [12]. However, the structures formed were not quantified nor was the mechanisms elucidated. Recently, chaplets formed by decorating DNA (which is classified as a polymer from nucleic acid monomers) with metallic

nanoparticles have also been reported [13-16]. To the best of our knowledge, the formation of no such complexes has been reported and controlled using common polyelectrolytes such as cationic polyacrylamide (CPAM).

In this study, we report a simple method to form and visualize polyelectrolyte-nanoparticles chaplet like structures on paper, using negatively charged gold nanoparticles (AuNPs) to decorate positively charged polyelectrolyte. This concept consists of forming a dilute cationic polyacrylamide (CPAM) solution where the polymer chains are well dissolved and relaxed, rapidly filtering the polyelectrolyte solution through a filter paper via vacuum filtration and immediately filtering through the suspension of AuNPs (negatively-charged). Field Emission Scanning electron microscopy (FESEM) images of the dried paper sample showed individual AuNPs lined up with nearly contacting edges along the CPAM polymer chain which are orientated in an opposite direction to the axis of the cellulose fibers.

In this study, the effects of CPAM polymer concentration, charge density and molecular weight on the formation of the chaplet structures are quantified. The physical mechanisms involved are analyzed and a mechanism is proposed. This technique enables the visualization of individual single charged polymer chains and the formation of well organized polyelectrolyte-nanoparticles chaplets. It also allows the polymer to act as a scaffold in promoting the self-assembly of nanoparticles into regular 2D arrays on paper, which is promising for nanoelectronics and bio-diagnostic applications.

5.3 Experimental Section

5.3.1 Materials

Hydrogen tetrachloroaurate trihydrate ($\text{HAuCl}_4 \cdot 3\text{H}_2\text{O}$) and sodium citrate tribasic dihydrate ($\text{Na}_3\text{C}_6\text{H}_5\text{O}_7 \cdot 2\text{H}_2\text{O}$) were purchased from Sigma-Aldrich and used as received. The cationic trimethylamino-ethyl-methacrylate polyacrylamide (CPAM) polymers were graciously supplied by AQUA+TECH Switzerland from their SnowFlake Cationics product range, and used as received (chemical structure shown in Supporting Information). They were identified as: I1 (5 wt% charge density, molecular weight 13 MDa), H1 (10 wt% charge density, molecular weight 13 MDa), F1 (40 wt% charge

density, molecular weight 13 MDa) and F3 (40 wt % charge density, molecular weight 6 MDa). Whatman qualitative filter paper #1 (55 mm diameter), which consists of 98% α -cellulose, was selected as the paper substrate as it is a convenient model paper of well defined structure without process components (polymers or coatings); basis weight was 88 g/m². Ultrapure water purified with a Millipore system (18 M Ω .cm) was used in all aqueous solutions and rinsing procedures.

5.3.2 Synthesis and Fabrication of Polyelectrolyte-Nanoparticles Chaplet on Paper

Negatively charged citrate-capped AuNPs were synthesized by using 1 mM HAuCl₄·3H₂O and 1% aqueous Na₃C₆H₅O₇·2H₂O according to the Turkevich method [17]. A stock solution of CPAM was prepared on the day of the experiment by diluting dry powder to 0.1 mg/mL with Millipore water, and gently mixing the dispersions for 8 hours at 23°C to facilitate the dissolution process. 10 mL of CPAM solution was filtered through the filter paper using vacuum filtration (Figure 1). The time for filtering the polymer solution was of 10 s. After that, 10 mL of AuNP solution (0.20 mg/mL) was immediately filtered through the CPAM pre-treated paper (Figure 1). The paper were then air-dried and stored at 50% relative humidity and 23°C until further analysis.

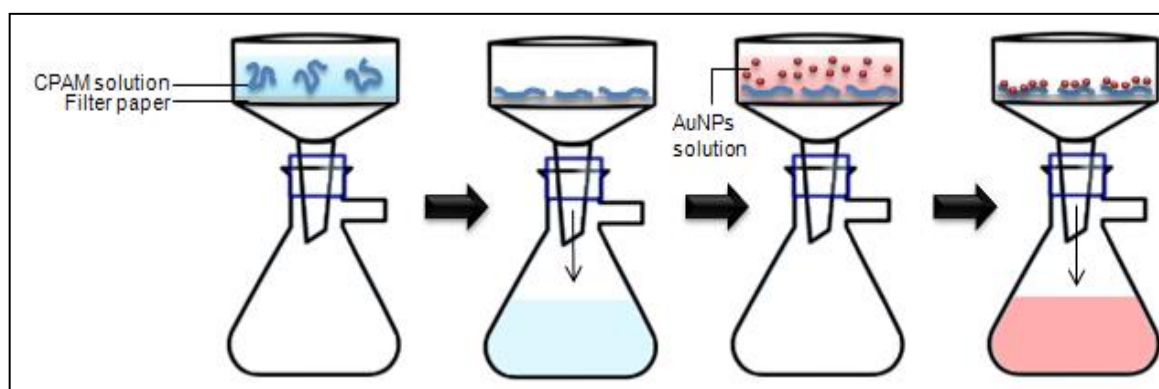


Figure 1: The formation process of CPAM-AuNPs chaplets by vacuum filtration.

5.3.3 Instrumentation

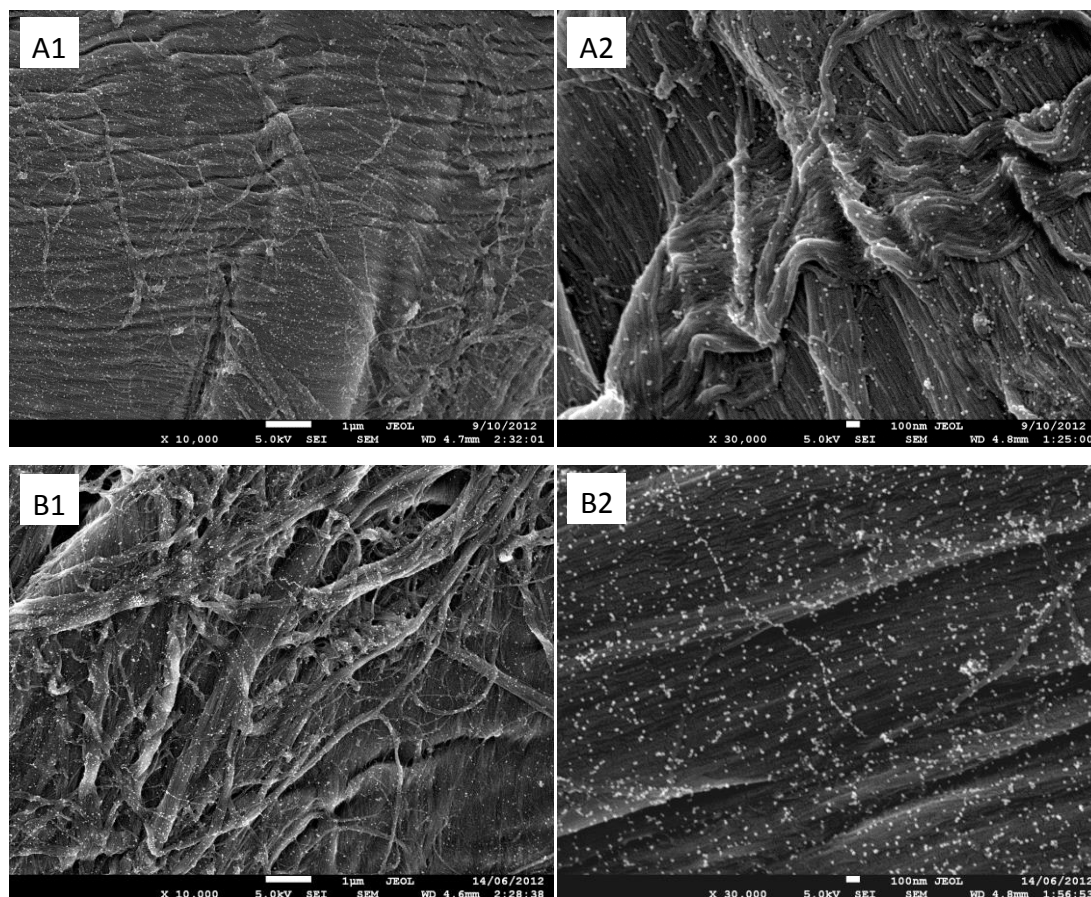
Field Emission Scanning Electron Microscopy (FESEM), which produces higher resolution, less sample charging and less damaged images than conventional SEM, was performed using a JEOL 7001 Field Emission Gun (FEG) system operating at 5 kV and

180 pA. ImageJ analysis software developed by National Institute of Health (NIH) was used to quantify the dimension of AuNPs decorated polymer.

5.4 Results and Discussion

5.4.1 Effect of CPAM Concentration

Filter papers were pre-treated with 10 mL of CPAM solutions of different concentration followed by 10 mL of AuNP solution (0.20 mg/mL) via vacuum filtration. The concentration of CPAM was varied by diluting the stock solution (0.10 mg/mL). FESEM analysis was performed to examine the adsorption state of AuNPs on paper (Figure 2). Vacuum filtration of AuNPs on paper without CPAM produced AuNPs which were well dispersed on the cellulose fibers (Figure 2-A2). When CPAM solution was vacuum filtered through paper followed by AuNP solution, the AuNPs were adsorbed as a chaplet-like structure across the cellulose fibers alongside with some other individual AuNPs (Figure 2-B2 to 2-D2). ImageJ software was used to quantify the structure of the AuNP chaplets (Supporting Information) and the results were summarized in Table I.



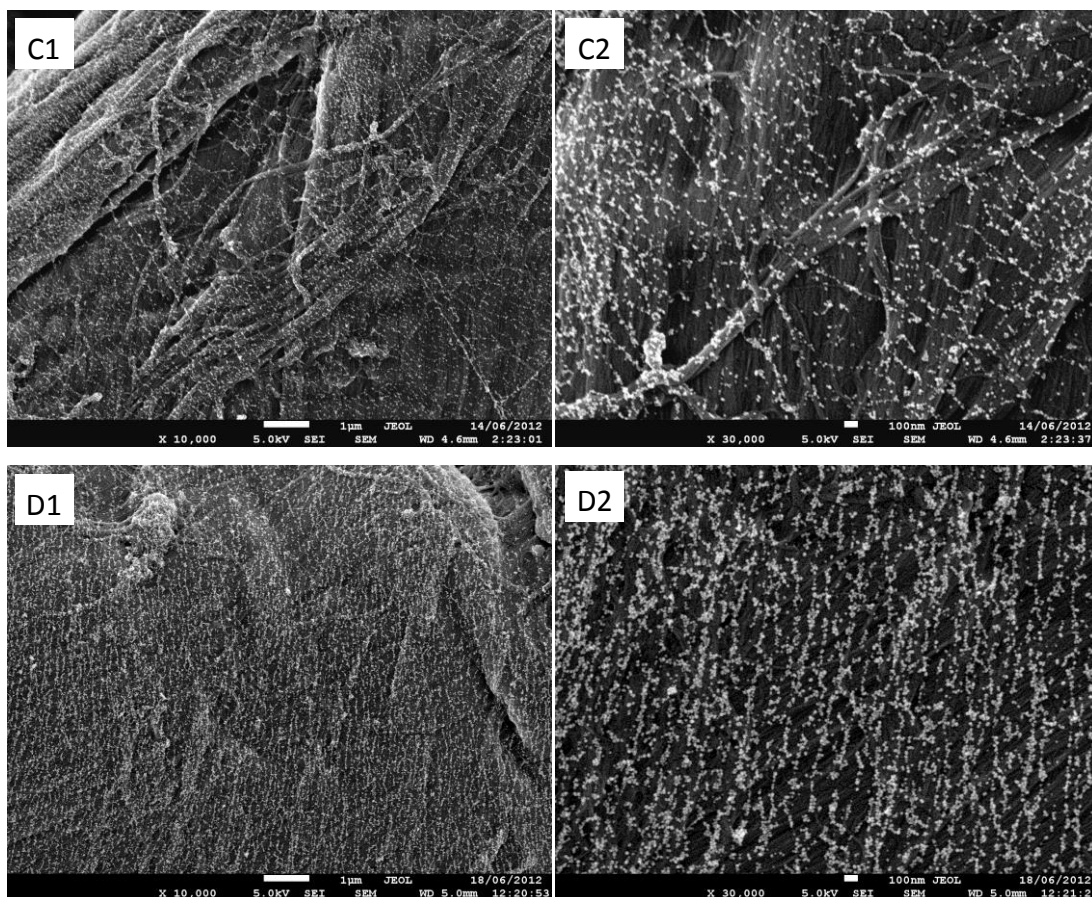


Figure 2: FESEM images of AuNPs on paper (A) without CPAM and AuNPs chaplet on paper pre-treated with CPAM (40 wt% charge density, 13 MDa) of different concentration: (B) 0.01 mg/mL, (C) 0.05 mg/mL and (D) 0.10 mg/mL under (1) low and (2) high magnification power.

Table 1: Estimated dimension of AuNP chaplets formed on paper pre-treated by CPAM of different concentration.

CPAM Concentration (mg/mL)	Number of Chaplets, N	Length of Chaplets, L (nm)	Distance between Chaplets, D (nm)	Thickness of Chaplets, t (nm)	Distance between AuNPs in a chaplet, d (nm)
0.01	7	742	511	23	37
0.05	38	747	256	40	27
0.10	71	818	141	53	23

The length of chaplets increased slightly as the concentration of CPAM was increased. The theoretical estimation of the radius of gyration for CPAM is 38 nm and the end-to-end distance is 22,744 nm (Supporting Information). This indicated that the CPAM

polymer chains were stretched out during the filtration process. As the length of the chaplets quantified from FESEM image analysis (Table I) was less than the estimated end-to-end distance of CPAM by two order of magnitude, we believe that the some segments of the polymer chain could be adsorbed into the bulk of paper. As the concentration of CPAM was increased, the number of chaplets was also increased and the distance between the chaplet strings was reduced drastically due to the higher amount of CPAM adsorbed on paper (Table I). This shows that the formation of chaplet-like structures was due to the adsorption of AuNPs along the CPAM polymer chain previously adsorbed and was not caused by physical adsorption along the cellulose microfibrils (negatively charged). Notably, there is an increase in the chaplet thickness and the average distance between two adjacent AuNPs within the chaplets at higher CPAM concentration (Table I). The average length of the chaplet increased from 742 to 818 nm as increased polymer concentration. At low polymer concentration, the width of the chaplet corresponds to the diameter of the AuNP; at high concentration, it is over twice the AuNP diameter. The average distance between two adjacent AuNPs decreases from 37 to 23 nm (the diameter of an AuNP) upon increase in polymer concentration. This is as expected; increasing the concentration of CPAM solution leads to more extended polymer tails and loops which have a superior bridging ability [18], and results in a higher adsorption of AuNPs on the polymer chains (Figure 2-C2).

5.4.2 Effect of CPAM Charge Density

To study the effect of polyelectrolyte charge density, CPAMs solutions of different charge density but constant concentration and molecular weight were adsorbed on paper followed by the AuNP solution (Figure 3). Columbic interactions between polymer segments and surface, as well as between charges in the polymer chains affect the polymer adsorption (Figure 3). The metrics of chaplet structures in terms of chaplet length, thickness, distance between two adjacent AuNPs is shown as a function of CPAM charge density in Table II. As CPAM charge density increases, the number of chaplet, their length and thickness all increase, while the distance between two adjacent AuNPs decreases. This could be due to higher electrostatic interaction between CPAM and the negatively charged cellulose fibers, leading to higher density of polymer chains adsorbed on fibers. The AuNP chaplets were shorter and slightly coiled at lower charge density and became longer and stretched out as the charge density of CPAM was increased (Figure 3).

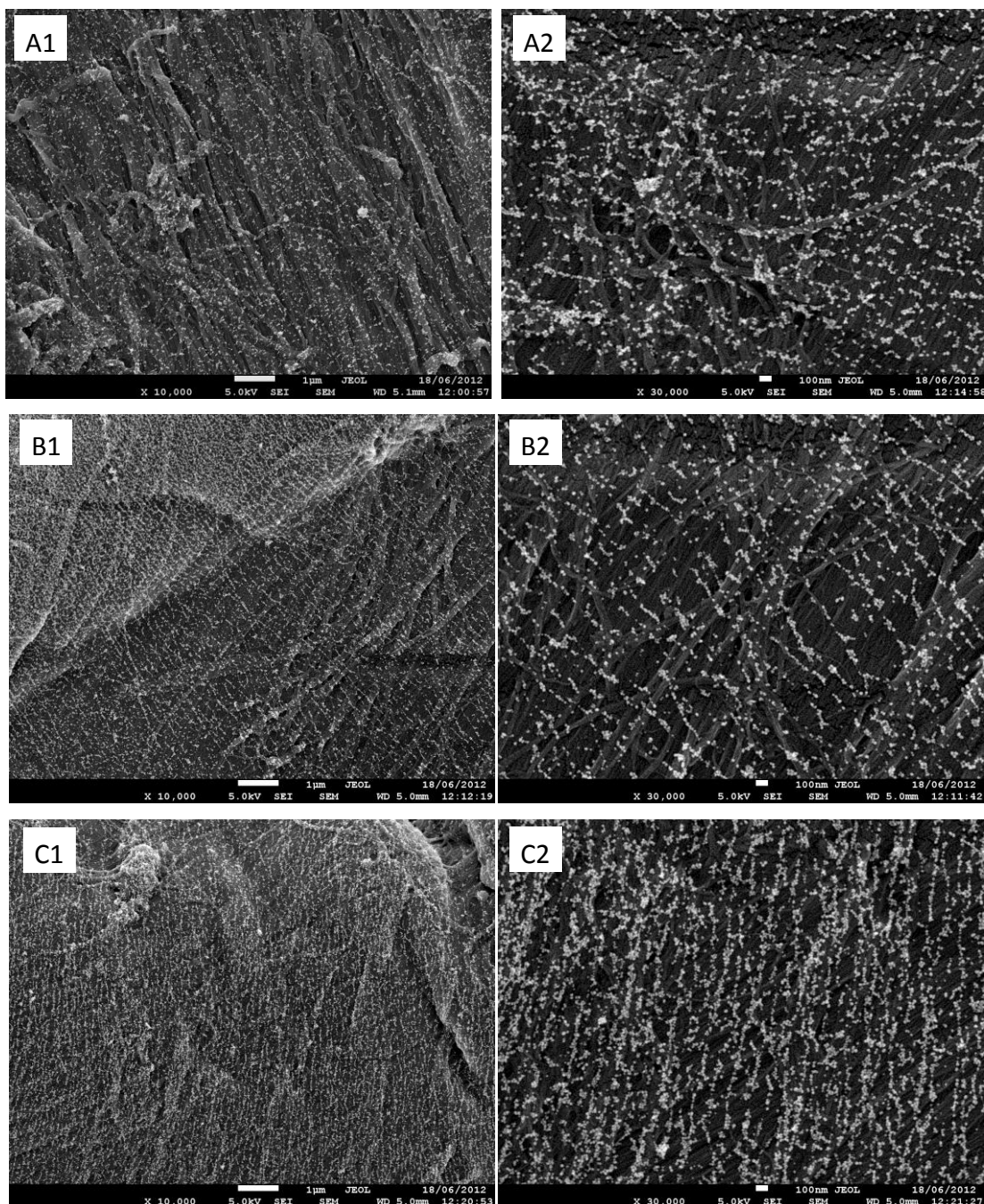


Figure 3: FESEM images of AuNPs chaplets on paper pre-treated with CPAM (0.10 mg/mL concentration, 13 MDa) of different charge density: (A) 0.05 wt%, (B) 0.10 wt% and (C) 0.40 wt% under (1) low and (2) high magnification power.

The estimated thickness and length of chaplet was increased significantly with CPAM charge density (Table II). This could be due to the tendency of lower charged polymers to form loops and tails upon adsorption [19-20] while higher charged polymers tend to have a flat and more extended conformation on the surface [21]. The average distance between two adjacent AuNPs within a chaplet was shorter when a higher charged CPAM was used

(Table II). This is caused by the increased positive charge between the polymer chain segments, leading to a higher number of negatively charged AuNPs adsorbed on each chain/chaplet. The distance between two adjacent ions on the polyelectrolyte chain is around three orders of magnitude smaller than the AuNP diameter.

Table 2: Estimated dimension of AuNP chaplets formed on paper pre-treated by CPAM of different charge density.

CPAM Charge Density (wt %)	Number of Chaplet, N	Length of Chaplet, L (nm)	Distance between Chaplet, D (nm)	Thickness of Chaplet, t (nm)	Distance between AuNPs in a chaplet, d (nm)
5	27	398	600	32	35
10	50	578	214	40	30
40	71	818	141	53	23

5.4.3 Effect of CPAM Molecular Weight

The effect of CPAM molecular weight on the structure of the AuNP chaplets formed on paper was investigated. At lower molecular weight, the chaplets are in a coiled and shorter conformation; their length increased with the molecular weight of CPAM (Figure 4). This follows the end-to-end distance estimated for CPAMs of molecular weight of 6 MDa and 13 MDa (Supporting Information). Table III shows that the number of chaplets, distance between the chaplets and distance between the AuNPs in each chaplet were unaffected by the molecular weight. However, there is a significant increase in the length and thickness of the chaplets. This is due to the increased polymer chain length and a greater extension of the polymer tail and loops [22-24] with higher molecular weight CPAMs.

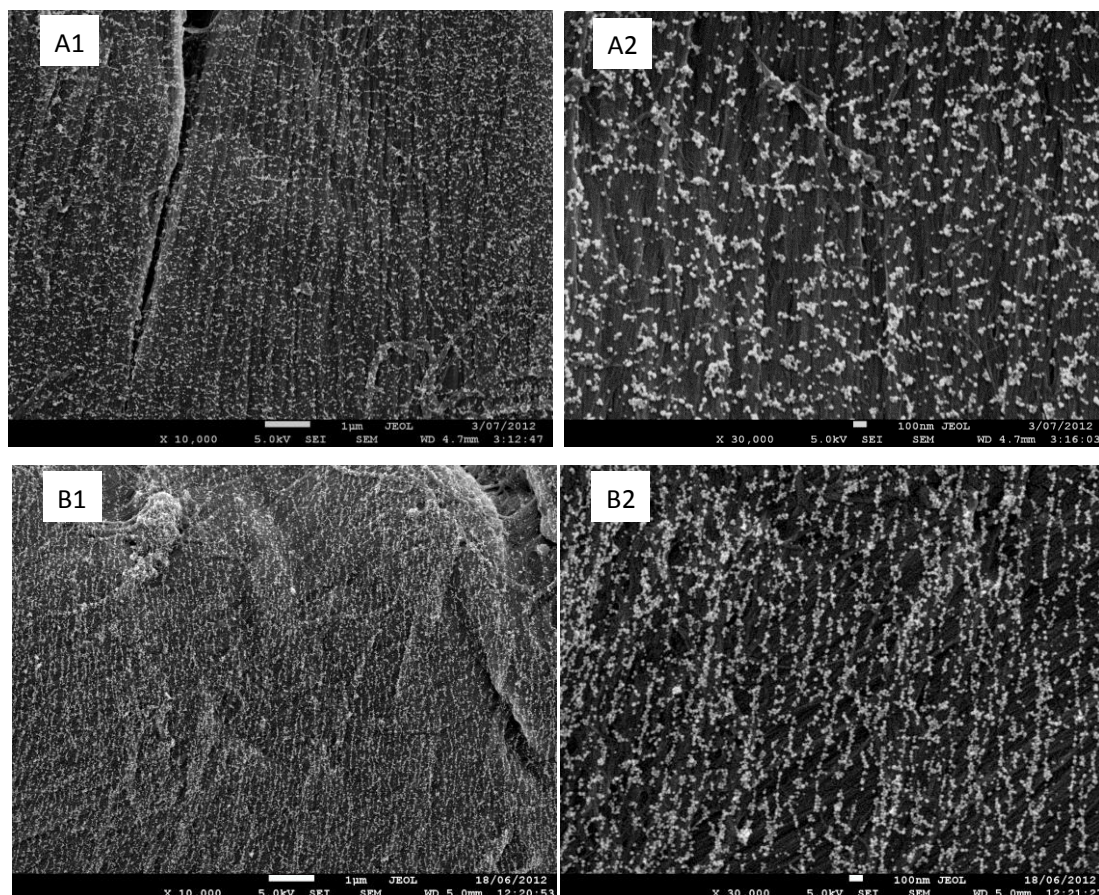


Figure 4: FESEM images of AuNPs chaplets on paper pre-treated with CPAM (0.10 mg/mL concentration, 40 wt% charge density) of different molecular weight: (A) 6 MDa and (B) 13 MDa under (1) low and (2) high magnification power.

Table 3: Estimated dimension of AuNP chaplets formed on paper pre-treated by CPAM of different molecular weight.

CPAM Molecular Weight (MDa)	Number of Chaplet, N	Length of Chaplet, L (nm)	Distance between Chaplet, D (nm)	Thickness of Chaplet, t (nm)	Distance between AuNPs in a chaplet, d (nm)
6	68	439	148	47	28
13	71	818	141	53	23

5.4.4 Mechanisms

We showed that the dimension of AuNP chaplets can be controlled by adjusting the concentration, charge density and molecular weight of CPAM. To better understand the physical mechanism involved in the formation of these chaplets, a series of experiments

was performed by using CPAM under optimum conditions (0.10 mg/mL, 40 wt% charge density and 13 MDa).

Figure 5b shows a significantly different assembly of AuNPs when the same AuNPs and CPAM solutions were adsorbed on paper using the dip-coating method. Clusters of AuNPs were formed on paper (Figure 5b) instead of the chaplet-like structure formed by the vacuum filtration method (Figure 5a). It is hypothesized that vacuum filtration of CPAM through paper produced a physical force able to stretch the CPAM chains and immobilize them on the surface of a cellulose fiber (Figure 6a to 6b). The immediate filtration of the AuNPs suspension assembled the negatively charged NPs along the stretched cationic polymer chains (Figure 6c). We believe three main criteria are required for the formation of AuNP chaplets. The first is a short time frame of contact between polymer and porous media freezing the CPAM chain in a stretched conformation; the second is rough and hydrophilic surface locking the stretched polymer chains conformation; the third is a wet and swollen polymer chain.

To test these hypotheses, a filter paper was dipped into a CPAM solution, dried and then an AuNP suspension was vacuum filtered through it. The AuNPs were well dispersed on the cellulose fiber but without the chaplet formation (Figure 5c). This could be due to the absence of wet and flowing condition able to stretch the polymer chain. To support this claim, another filter paper was dipped in CPAM solution and dried. It was then dipped into water for 24 hours to wet/relax the CPAM polymer. Water was vacuum filtered through it three times to recreate the flowing environment able to stretch out the polymer chains. Figure 5d shows that the nice AuNP chaplets features were achieved on the cellulose fibers. When the CPAM and AuNP solutions are filtered through filter paper but without vacuum, the extent of chaplet formation is lesser (Figure 5e). There is however a higher number of AuNPs adsorbed on the paper due to the longer contact time between paper with solutions. This series of experiments supports the hypothesis that a wet and flowing condition is necessary to produce a stretched polymer chain for self assembly of AuNP into chaplet structures.

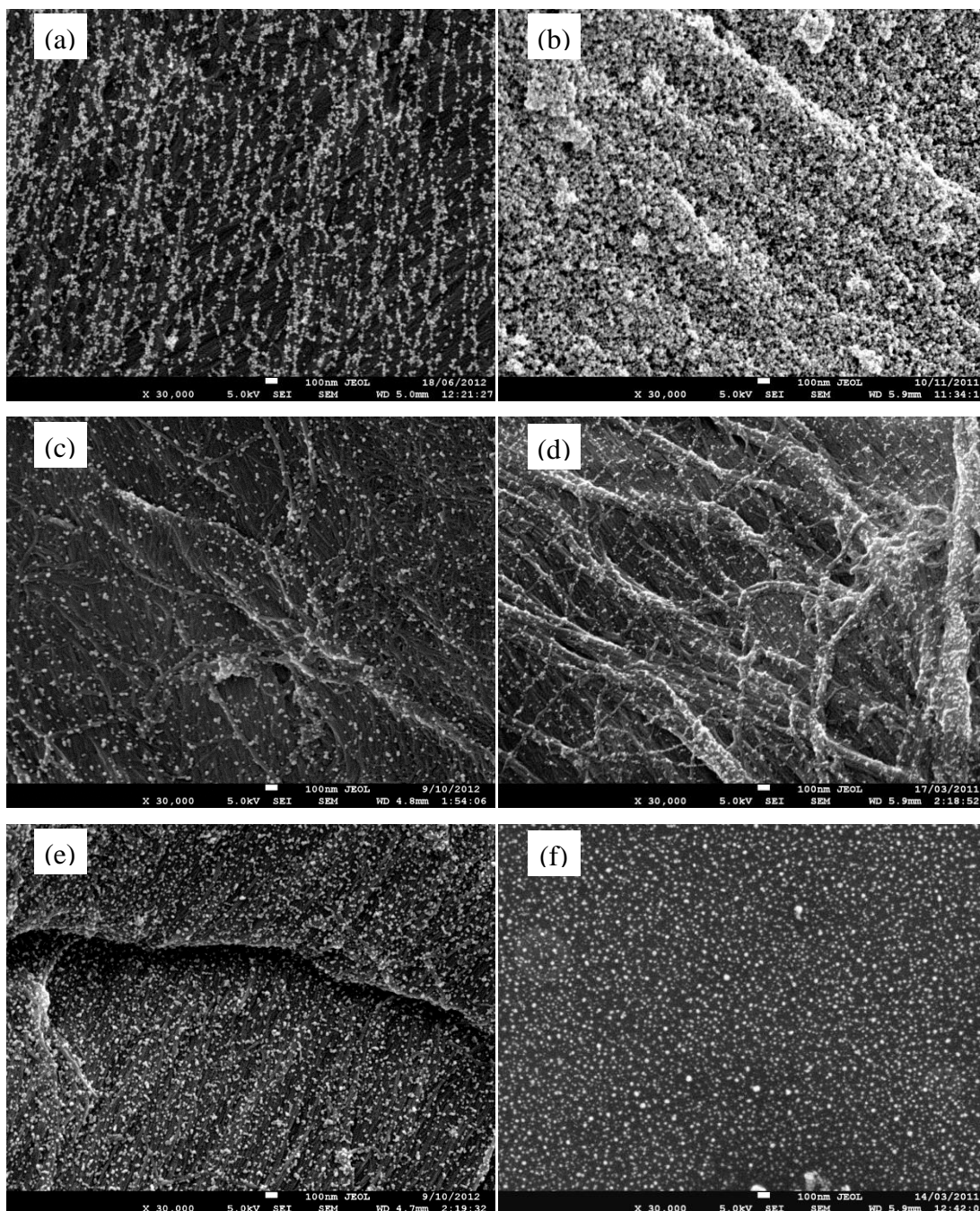


Figure 5: FESEM images of (a) CPAM followed by AuNPs vacuum filtered paper, (b) CPAM followed by AuNPs dip-coated paper, (c) CPAM dip-coated, dried followed by AuNPs vacuum filtered paper, (d) CPAM dip coated, dried, re-wetted followed by AuNPs vacuum filtered paper, (e) CPAM followed by AuNPs filtered paper without vacuum, (f) CPAM followed by AuNPs vacuum filtered silicon.

To study the effect of the substrate, filter paper was replaced by a smooth silicon wafer in the same vacuum filtration experiment. The silicon substrate is nonporous - unlike paper; it is noted that the water was not filtered through silicon, but a similar flowing condition

was present during the process. AuNP chaplets features were observed on silicon (Figure 5f), but less defined compared to filter paper (Figure 5a). Hence, a rough and hydrophilic surface (Figure 6) is preferred to immobilize stretched polymer chains into long and extended AuNP chaplets assemblies.

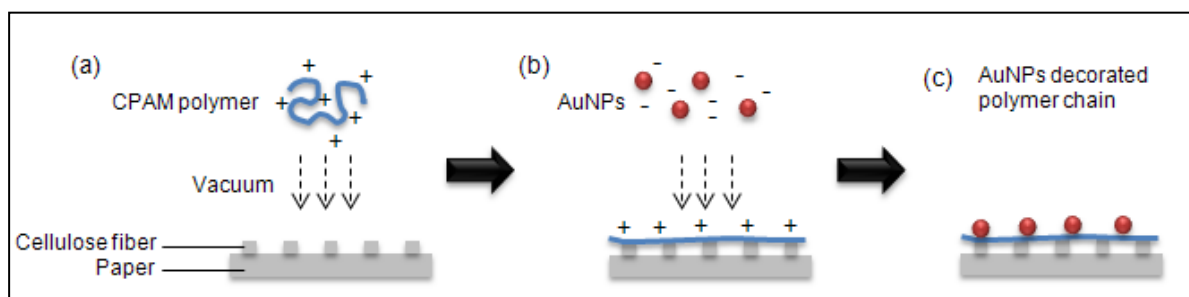


Figure 6: Proposed mechanism involved in the formation of AuNP chaplets.

5.5 Conclusion

A simple method was demonstrated to form and visualize polyelectrolyte-nanoparticles chaplet structures on paper, using negatively charged gold nanoparticles (AuNPs) to decorate polymer chain of cationic polyacrylamide (CPAM). This concept consists of forming a dilute CPAM solution where the polymer chains are well dissolved and relaxed, rapidly filtering it through a filter paper via vacuum filtration and immediately filtering through a suspension of AuNPs. The dimension of the AuNP chaplets assemblies can be tuned by adjusting the concentration, charge density and molecular weight of the CPAM in solution. The density and thickness of the AuNP chaplets are increased at higher CPAM concentrations. Longer chaplets with more AuNPs per unit length are achieved by increasing the charge density of CPAM. The length and thickness of AuNP chaplets can also be increased with higher molecular weight CPAM.

Three requirements were identified to reproducibly form chaplets structures. First, a short contact time between a well relaxed dilute CPAM solution flowing through paper-achieved by filtration; second, a hydrophilic, porous and rough surface - paper; third, a wet and swollen adsorbed polymer chain.

Assembling nanometer-scale components (AuNPs) into micrometer-scale arrays (chaplets) on a porous paper substrate can be a promising strategy for low-cost

nanoelectronics applications. It also offers a simple method to visualize individual polyelectrolyte chains.

5.6 Acknowledgement

Thanks to Dr. T. Williams, Monash University for FESEM technical advice. The financial support from the ARC Linkage LP0989823 and Visy, Amcor, SCA, Norske Skog, Australian Paper, the Australian Pulp and Paper Institute and Monash University are acknowledged. Many thanks to AQUA+TECH for providing polymer and technical expertise.

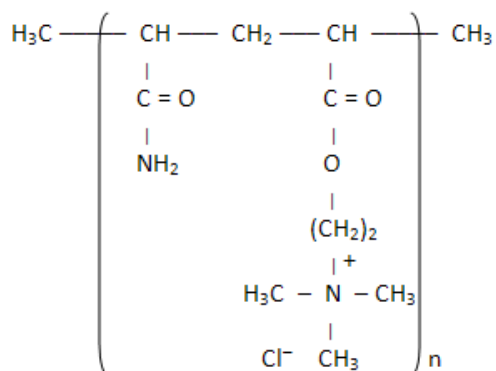
5.7 References

1. Matsubara, H., M. Takada, S. Koyama, K. Hashimoto, and A. Fujishima, *Photoactive TiO₂ Containing Paper: Preparation and Its Photocatalytic Activity under Weak UV Light Illumination*. Chemistry Letters, 1995. **24**(9): p. 767-768.
2. Iguchi, Y., H. Ichiura, T. Kitaoka, and H. Tanaka, *Preparation and characteristics of high performance paper containing titanium dioxide photocatalyst supported on inorganic fiber matrix*. Chemosphere, 2003. **53**(10): p. 1193-1199.
3. Fernández, A., E. Soriano, G. López-Carballo, P. Picouet, E. Lloret, R. Gavara, and P. Hernández-Muñoz, *Preservation of aseptic conditions in absorbent pads by using silver nanotechnology*. Food Research International, 2009. **42**(8): p. 1105-1112.
4. Tankhiwale, R. and S.K. Bajpai, *Graft copolymerization onto cellulose-based filter paper and its further development as silver nanoparticles loaded antibacterial food-packaging material*. Colloids and Surfaces B: Biointerfaces, 2009. **69**(2): p. 164-168.
5. Zhang, Y., K. Aslan, M.J.R. Previte, and C.D. Geddes, *Metal-enhanced fluorescence from paper substrates: Modified spectral properties of dyes for potential high-throughput surface analysis and assays and as an anti-counterfeiting technology*. Dyes and Pigments, 2008. **77**(3): p. 545-549.
6. Ngo, Y.H., D. Li, G.P. Simon, and G. Garnier, *Paper surfaces functionalized by nanoparticles*. Advances in Colloid and Interface Science, 2011. **163**(1): p. 23-38.
7. Ngo, Y.H., D. Li, G.P. Simon, and G. Garnier, *Gold Nanoparticle–Paper as a Three-Dimensional Surface Enhanced Raman Scattering Substrate*. Langmuir, 2012. **28**(23): p. 8782-8790.
8. Lee, C.H., L. Tian, and S. Singamaneni, *Paper-Based SERS Swab for Rapid Trace Detection on Real-World Surfaces*. ACS Applied Materials & Interfaces, 2010. **2**(12): p. 3429-3435.
9. Ngo, Y.H., G. Garnier, D. Li, and G. Simon, *Effect of Cationic Polyacrylamides on the Aggregation and SERS Performance of Gold Nanoparticles-treated Paper*. Journal of Colloid and Interface Science, 2012. **In press**.
10. Peng, P. and G. Garnier, *Effect of Cationic Polyacrylamide Adsorption Kinetics and Ionic Strength on Precipitated Calcium Carbonate Flocculation*. Langmuir, 2010: p. 16949–16957.
11. Nanko, H., M. McNeal, and S. Pan. *Understanding wet-end polymer performance through visualization of macromolecular events by transmission electron microscopy*. in

- Pan Pacific Conference*. 2006. Seoul, Korea: Advances in Pulp & Paper Sciences and Technologies.
12. Lee, K.E., B.T. Poh, N. Morad, and T.T. Teng, *Synthesis and Characterization of Hydrophobically Modified Cationic Polyacrylamide with Low Concentration of Cationic Monomer*. Journal of Macromolecular Science, Part A, 2009. **46**(3): p. 240-249.
 13. Alivisatos, A.P., K.P. Johnsson, X. Peng, T.E. Wilson, C.J. Loweth, M.P. Bruchez, and P.G. Schultz, *Organization of 'nanocrystal molecules' using DNA*. Nature, 1996. **382**(6592): p. 609-611.
 14. Le, J.D., Y. Pinto, N.C. Seeman, K. Musier-Forsyth, T.A. Taton, and R.A. Kiehl, *DNA-Templated Self-Assembly of Metallic Nanocomponent Arrays on a Surface*. Nano Letters, 2004. **4**(12): p. 2343-2347.
 15. Braun, G., K. Inagaki, R.A. Estabrook, D.K. Wood, E. Levy, A.N. Cleland, G.F. Strouse, and N.O. Reich, *Gold Nanoparticle Decoration of DNA on Silicon*. Langmuir, 2005. **21**(23): p. 10699-10701.
 16. Ma, Y., J. Zhang, G. Zhang, and H. He, *Polyaniline Nanowires on Si Surfaces Fabricated with DNA Templates*. Journal of the American Chemical Society, 2004. **126**(22): p. 7097-7101.
 17. Turkevich, J., P.C. Stevenson, and J. Hillier, *A study of the nucleation and growth processes in the synthesis of colloidal gold*. Discussions of the Faraday Society 1951. **11**: p. 55-75.
 18. Sennerfors, T., *Polymer-Nanoparticle Complexes: Fundamentals and Applications of Interfacial Behavior*. Encyclopedia of Surface and Colloid Science: Second Edition, 2006: p. 4874 - 4884.
 19. Fleer, G.J., M.A.C. Stuart, J.M.H.M. Scheutjens, T. Cosgrove, and B. Vincent, *Polymers at Interfaces*. 1998, London: Chapman & Hall.
 20. Hubbe, M.A., H. Nanko, and M.R. McNeal, *Retention aid polymer interactions with cellulosic surfaces and suspensions: A Review*. Bioresources, 2009. **4**(2): p. 850-906.
 21. Shin, Y., J.E. Roberts, and M.M. Santore, *The Relationship between Polymer/Substrate Charge Density and Charge Overcompensation by Adsorbed Polyelectrolyte Layers*. Journal of Colloid and Interface Science, 2002. **247**(1): p. 220-230.
 22. Lindström, T. and C. Söremark, *Adsorption of cationic polyacrylamides on cellulose*. Journal of Colloid and Interface Science, 1976. **55**(2): p. 305-312.
 23. Zhang, H., F. Chen, and H. Hu, *Preparations and application of high molecular weight cationic polyacrylamides*. China Pulp Paper, 2003. **22**(4): p. 15-18.
 24. Gill, R.I.S. and T.M. Herrington, *The effect of surface charge on the flocculation of Kaolin suspensions with cationic polyacrylamides of varying molar mass but similar cationic character*. Colloids and Surfaces, 1987. **25**(2-4): p. 297-310.

5.8 Supporting Information

S1: Theoretical estimation of the size of CPAM



Generic structure of random co-polymer Cationic trimethylamino-ethyl-methacrylate polyacrylamide

Molecular weight = 13MDa

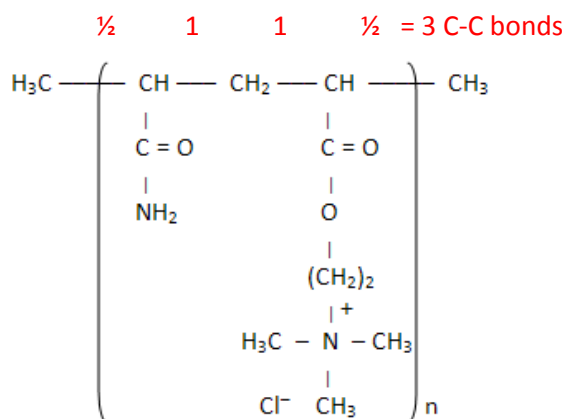
$$r_g = b \sqrt{\frac{N}{6}}$$

r_g = radius of gyration, b = monomer length, N = number of monomers

Molecular weight of monomers:

	Number of atoms	Mw	Total Mw
C	10	12	120
H	19	1	19
O	3	16	48
N	2	14	28
			215 g/mol

$$\text{Number of monomers, } N = \frac{\text{Total Mw of polymer}}{\text{Total Mw of monomers}} = \frac{13 \times 10^6}{215} = 60.47 \times 10^3$$



Monomer length, $b = 3 \times \sin \frac{109^\circ}{2} \times 1.54 \times 10^{-10} = 3.76 \times 10^{-10} \text{ m}$
 (C-C bond) (bond angle) (C-C bond length)

$$r_g = b \sqrt{\frac{N}{6}} \times 2.68 \times 10^{-10} \times \sqrt{\frac{60.47 \times 10^3}{6}} = 38 \text{ nm}$$

Estimation of end-to-end distance when the polymer is stretch out = $b \times N = 22.74 \mu\text{m} = 22,744 \text{ nm}$

	Molecular Weight (MDa)	
	6	13
Radius of Gyration of CPAM (nm)	26	38
End-to-end distance (nm)	10,493	22,744

S2: Theoretical estimation of the surface coverage of CPAM

Area of filter paper used (55 mm diameter) = $2.38 \times 10^{-3} \text{ m}^2$

Grammage of filter paper used = 88 g/ m^2

Weight of filter paper used = $88 \times 2.38 \times 10^{-3} = 0.21 \text{ g}$

Weight of CPAM used (0.10 mg/mL) = 1 mg

For most linear, water-soluble polymers, a saturated adsorbed layer of polymer corresponds to approximately 1mg/m^2 cellulose fibers.

Assuming the area of cellulose fiber = $1 \text{ m}^2/\text{g}$ paper,

Theoretical weight of CPAM for full coverage on cellulose fibers

= $1 \text{ m}^2/\text{g} \times 0.21 \text{ g} \times 1 \text{ mg/m}^2 = 0.21 \text{ mg}$

Hence, the CPAM polymer is in excess to form a monolayer of full coverage on cellulose fibers of paper.

Chapter 6

Gold Nanoparticles Paper as a SERS bio- diagnostic Platform

This page is intentionally blank

Monash University

Declaration for Thesis Chapter 6

Declaration by candidate

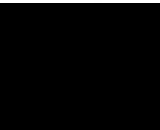
In the case of Chapter 6, the nature and extent of my contribution to the work was the following:

Nature of contribution	Extent of contribution (%)
Initiation, key ideas, experimental and analysis works, development and writing up of paper	45

The following co-authors contributed to the work. Co-authors who are students at Monash University must also indicate the extent of their contribution in percentage terms:

Name	Nature of contribution	Extent of contribution (%) for student co-authors only
Whui Lyn Then	Initiation, key ideas, experimental and analysis works, development and writing up of paper	45%
Gil Garnier	Initiation, key ideas, reviewing and editing of the paper.	Supervisor
Wei Shen	Initiation, key ideas, reviewing and editing of the paper.	Co-supervisor

Candidate's Signature

		Date 13.03.2013
--	---	-----------------

Declaration by co-authors

The undersigned hereby certify that:

- (1) the above declaration correctly reflects the nature and extent of the candidate's contribution to this work, and the nature of the contribution of each of the co-authors.
- (2) they meet the criteria for authorship in that they have participated in the conception, execution, or interpretation, of at least that part of the publication in their field of expertise;
- (3) they take public responsibility for their part of the publication, except for the responsible author who accepts overall responsibility for the publication;
- (4) there are no other authors of the publication according to these criteria;
- (5) potential conflicts of interest have been disclosed to (a) granting bodies, (b) the editor or publisher of journals or other publications, and (c) the head of the responsible academic unit; and
- (6) the original data are stored at the following location(s) and will be held for at least five years from the date indicated below:

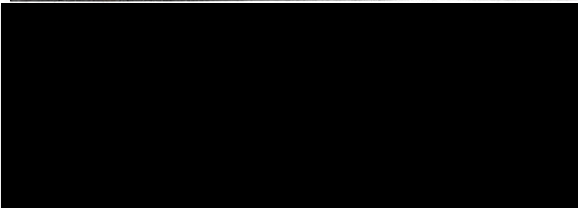
Location(s)

Australian Pulp and Paper Institute (APPI), Department of Chemical Engineering, Monash University, Clayton, VIC 3800, Australia.

Signature 1

Signature 2

Signature 3

		Date 11/12/12
		Date 11/12/12
		Date 13/12/12

This page is intentionally blank

Gold Nanoparticles Paper as a SERS bio-diagnostic Platform

Ying Hui Ngo, Whui Lyn Then and Gil Garnier*

BioPRIA, Australian Pulp and Paper Institute (APPI), Department of Chemical Engineering Monash University, Clayton, VIC 3800, Australia.

*Corresponding author. Email: [REDACTED]; Tel: [REDACTED] Fax: [REDACTED]

Content

6.1	Abstract	195
6.2	Introduction	196
6.3	Experimental Section	198
6.3.1	Materials	198
6.3.2	Fabrication of AuNPs treated Paper	198
6.3.3	Functionalization of AuNPs	198
6.3.4	Instrumentation	200
6.4	Results	200
6.5	Discussion	204
6.6	Conclusion	207
6.7	Acknowledgement	208
6.8	References	208
6.9	Supporting Information	210

6.1 Abstract

Bioactive papers are usually challenged by four major limitations: sensitivity, selectivity, simplicity and strength (4S). In this study, AuNPs on paper substrate are functionalized by a series of biomolecules to develop a generic SERS platform for selective antibody-antigen detection. The functionalization steps were performed by taking advantage of the high affinity association between the *Streptomyces avidini*-derived protein, streptavidin, and biotin. Firstly, the streptavidin was bound to the AuNPs treated paper using biotinylated-thiol. Subsequently, the desired biotinylated-antibody was bound to streptavidin, thus creating a monolayer of antibody on the surface of the AuNPs. SERS

spectra of each functionalization or binding step were obtained to ensure the specific adsorption of the biomolecules. The modification of antibody local structure due to the interaction with antigen was detected. Evidence of antigen binding was elucidated from the SERS spectra, confirming the presence of antigen. Reproducible spectra features were observed for papers subjected to different concentration of antigen; their intensity increased as a function of antigen concentration. The feasibility of AuNPs paper substrates as a low-cost and generic SERS platform for bio-diagnostic application was demonstrated.

Keywords: Gold nanoparticles (AuNPs), paper, Surface Enhanced Raman Scattering (SERS), antibody, antigen, biotin, streptavidin.

6.2 Introduction

Bioactive paper has been recognized as a low cost diagnostic platform for health and environmental applications [1-3]. The combination of printing technology and Enzyme-Linked Immunosorbent Assay (ELISA) colorimetric technique has been developed to regulate and detect analytes on paper [3-4]. Blood typing paper strips have been fabricated to detect blood group antigens by monitoring blood agglutination which is triggered by specific antibody-antigen interactions [5]. However, bioactive paper is generally challenged by 4 major limitations: 1) Sensitivity, 2) Selectivity, 3) Simplicity and 4) Strength- the 4S. Besides involving multiple reactants and tedious washing steps for techniques such as for ELISA, bioactive paper often suffers from limitations in sensitivity when relying on colorimetric techniques to quantify the concentration of analyte. Reproducibility can also be a major issue when identifying antibodies at lower concentrations (less than 10^{-6} M) and smaller dimensions, such as for the immunoglobulin G (IgG).

Surface Enhanced Raman Scattering (SERS), a vibrational molecular spectroscopy which derives from an inelastic light scattering process, presents an attractive alternative to address the 4S issues [6-7]. During the Raman scattering process, a laser photon is scattered by a sample molecule and energy changes of the irradiating photon is characteristic for a particular bond in the molecule. Therefore, the implementation of SERS with paper is able to produce a powerful bio-diagnostic platform capable of

generating a precise molecular spectral fingerprint to identify biomolecule at trace levels. Biomolecules such as antigens can theoretically be detected by antibody capped metallic nanoparticles treated paper at very low concentrations (10^{-9} – 10^{-12} M) if the biomolecule is SERS sensitive.

In our previous studies, gold nanoparticles (AuNPs) treated paper has been demonstrated as a robust three dimensional (3D) SERS active substrate [8]. The SERS enhancement factor of a model Raman molecule (4-Aminothiophenol- 4 ATP) adsorbed onto AuNPs paper exceeded 10^7 , which has the potential for single molecule SERS detection [8-10]. In this study, AuNPs on paper substrate are functionalized by a series of biomolecules to develop a generic SERS platform for antibody-antigen detection. The efficiency of biomolecules detection depends on the success of surface functionalization, the nature of the biomolecule and its immobilization [11]. The sequence of functionalization involves three standard steps: (i) surface functionalization, for instance, chemically, (ii) binding a linker or spacer onto the functionalized surface, and finally, (iii) covalently attaching a bioactive compound onto the functionalized surface [11]. Selective detection of the desired antigen is reliant on the immobilization of a specific antibody [12]. However this cannot be achieved without the important first two steps. In this study, we functionalize AuNPs on paper using streptavidin/biotin assemblies for their well known stability of molecular assembly ($K_d \approx 10^{-15}$) and the high affinity between the biotin derivatives and the tetrameric active sites in streptavidin [13-14].

SERS paper substrate was fabricated by first dip-coating filter paper into a suspension of AuNPs. The AuNPs on paper were then functionalized by biotinylated thiol followed by streptavidin and biotinylated anti-rabbit IgG (antibody). SERS spectra of each functionalization or binding step were recorded and analysed for specific adsorption of the biomolecules. The functionalized AuNPs papers were also subjected to different concentrations of rabbit IgG (antigen) to quantify their SERS sensitivity. To the best of our knowledge, no previous study has explored the functionalization steps of nanoparticles on paper and its potential for antibody-antigen analysis. Detection of antibody-antigen interactions is the primary step in immunoassays and bio-diagnostic for health and environmental applications [15-16]. It is the goal of this study to develop a novel and generic SERS platform on AuNPs paper for emerging bioassay applications.

6.3 Experimental Section

6.3.1 Materials

Hydrogen tetrachloroaurate trihydrate ($\text{HAuCl}_4 \cdot 3\text{H}_2\text{O}$), sodium citrate tribasic dihydrate ($\text{Na}_3\text{C}_6\text{H}_5\text{O}_7 \cdot 2\text{H}_2\text{O}$) were purchased from Sigma-Aldrich and used as received. Whatman qualitative filter paper #1, which consists of 98% α -cellulose, was selected as the paper substrate as it is a convenient model paper of well-defined structure and to ensure minimal SERS interference from process components (polymers or coatings). Ultrapure water purified with a Millipore system (18 M Ω .cm) was used in all aqueous solutions and rinsing procedures. Biotinylated polyethylene glycol (PEG) thiol was purchased from Nanocs, Wisconsin, USA. Triethylene glycol mono-11-mercaptopundecyl ether (TEG) and recombinant streptavidin lyophilized powder was purchased from Sigma-Aldrich. Anti-rabbit IgG-biotin and rabbit IgG were purchased from Protein Mods, New York, USA.

6.3.2 Fabrication of AuNPs treated Paper

AuNPs were synthesized by using 1 mM $\text{HAuCl}_4 \cdot 3\text{H}_2\text{O}$ and 1% aqueous $\text{Na}_3\text{C}_6\text{H}_5\text{O}_7 \cdot 2\text{H}_2\text{O}$ according to the Turkevich method [17]. Filter papers (55 mm diameter) were dipped into Petri dishes containing 10 mL solution of AuNPs for 24 hours. After dipping, the paper substrates were rinsed thoroughly with distilled water to remove any loosely bound AuNPs, and the papers were air-dried and stored at 50% relative humidity and 23°C until further analysis.

6.3.3 Functionalization of AuNPs

The dried AuNPs papers were immersed in an ethanol solution for 30 min. They were then immersed into a 5×10^{-4} M TEG (blocking thiol) and 5×10^{-4} M BAT (biotinylated thiol) solution (9:1 volume ratio) for 6 hours (Figure 1b). After drying, the samples were immersed into a 5×10^{-7} M Streptavidin solution in PBS for 2 hours (Figure 1c). After rinsing with a PBS solution, the samples were dipped in a 0.1 M antibody solution for 30 min (Figure 1d). The functionalization step was completed by dipping the dried samples in a 0.1 M antigen solution for 60 min (Figure 1e). All solution treatments were at room temperature (22 °C).

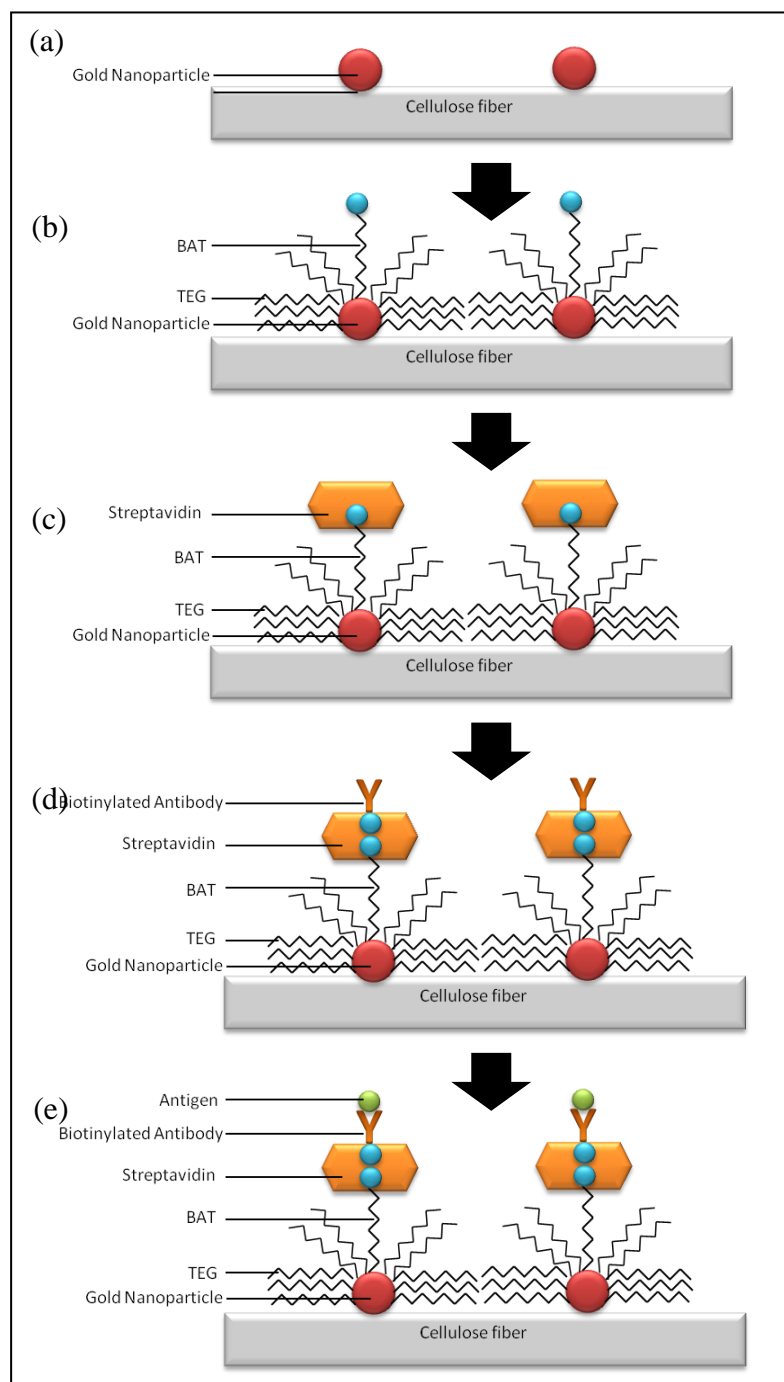


Figure 1: Functionalization procedure of SERS platform on AuNPs paper.

Table I: Size or molecular weight of each component.

Component	Size/ molecular weight
AuNPs	23.2 nm
TEG	376.53 Da
BAT	5 kDa
Strep	75 kDa
Biotinylated Antibody	150 kDa
Antigen	8-10 kDa

6.3.4 Instrumentation

Field Emission Scanning Electron Microscopy (FESEM), which produces higher resolution, less sample charging and less damaged images than conventional SEM, was performed using a JEOL 7001 Field Emission Gun (FEG) system operating at 5 kV and 180 pA. ImageJ analysis software was used to determine the coverage of AuNPs on the cellulose fibers in the FESEM images and estimate the particle size distribution. All Raman and SERS spectra were obtained in air using a Renishaw Invia Raman microscope equipped with a 300 mW 633 nm laser. The laser beam was positioned through a Leica imaging microscope objective lens (50 \times), whilst the instrument's wavenumber was calibrated with a silicon standard centered at 520.5 cm^{-1} shift. Due to the smaller spot size of the laser compared with the large surface area of the samples, the spectra were obtained at 5 different points of the surface. The average Raman intensity (of 5 measurements) was presented as the final result after baseline subtraction from the control samples.

6.4 Results

Gold nanoparticles (AuNPs) treated paper was characterized by FESEM. The distribution of nanoparticles was dense and uniform over the cellulose fibers of paper (Figure 2).

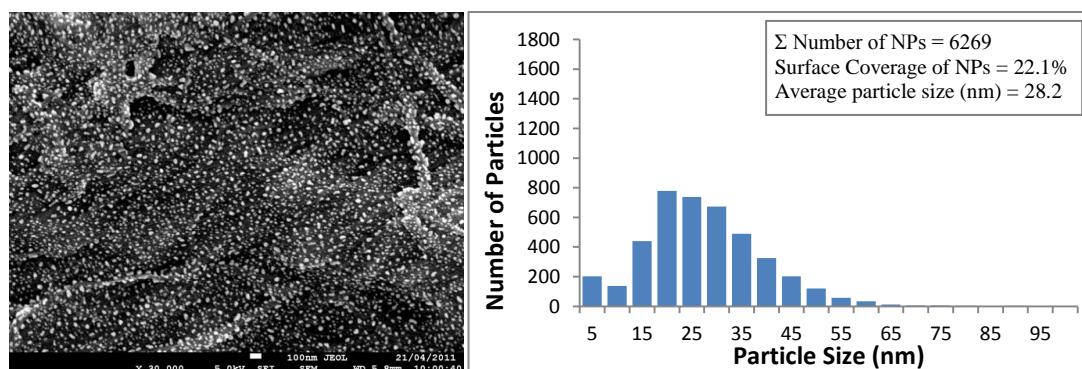


Figure 2: FESEM images and histograms of AuNPs particle size distribution on paper.

The fabrication of AuNPs-paper SERS immunoassay platform was performed through a series of step-wise processes as illustrated in Figure 1. To functionalize the AuNPs adsorbed on paper, a mixture of biotinylated alkane thiol (BAT) and alkane thiol (TEG) was first adsorbed on the AuNPs via the strong affinity Au-S bonding. Figure 3 shows the

corresponding SERS spectra before and after the AuNPs paper was treated with the thiol mixture. It was dominated by four strong characteristic bands: $\omega(\text{CH}_2)$ at 1349 cm^{-1} , Bio/ $\nu(\text{CH}_2)$ ring at 1424 cm^{-1} and 1499 cm^{-1} and $\nu(\text{C-N})$ at 1581 cm^{-1} [13].

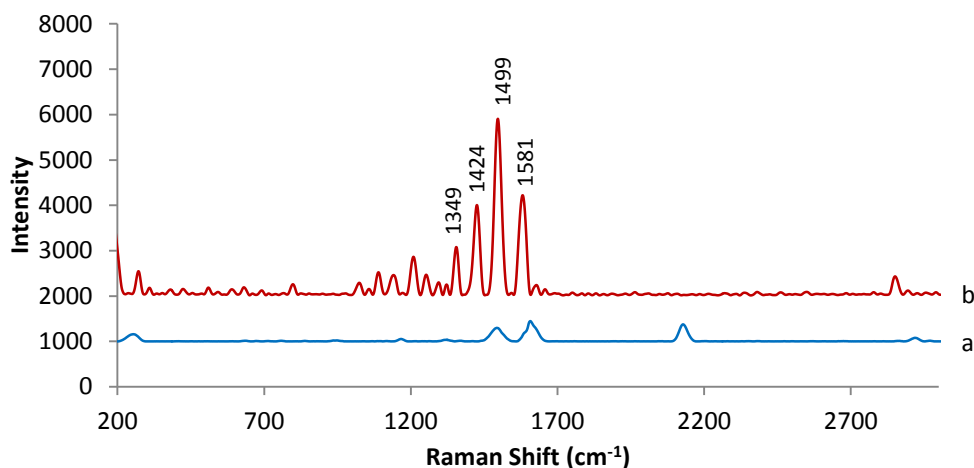


Figure 3: SERS spectra of (a) AuNPs paper and (b) BAT/TEG functionalized AuNPs paper.

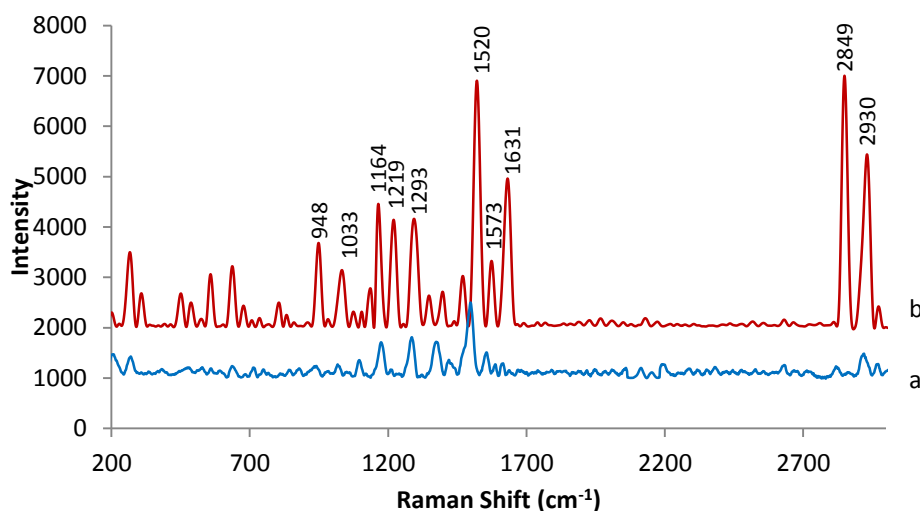


Figure 4: SERS spectra of (a) Strep on AuNPs paper and (b) Strep-BAT/TEG functionalized AuNPs paper.

Streptavidin was then bound onto the biotinylated thiol. A significantly different SERS spectrum (Figure 4) resulted, confirming the successful binding of streptavidin. Please note that all SERS spectra have the same scales for easy comparison (Figures 3-6). The resulting spectrum was dominated by Trp16 observed at 948 cm^{-1} , Phe, Ser at 1033 cm^{-1} ,

$\nu(\text{C-N})$, Trp13 at 1164 cm^{-1} , amide III (β sheet) at 1219 cm^{-1} , $\omega(\text{CH}_2)$ at 1293 cm^{-1} , Trp3 at 1520 cm^{-1} , Trp2 at 1573 cm^{-1} , amide I (β sheet) at 1631 cm^{-1} and $\nu(\text{C-H})$ at 2849 cm^{-1} to 2930 cm^{-1} [13].

The characteristic SERS bands of the antibody rabbit IgG were observed following adsorption of the biotinylated antibody onto streptavidin (Figure 5) [11, 18-19]. The predominant β -sheet structure in IgG was identified by the characteristic amide III band around 1243 cm^{-1} and a higher intensity band at 1625 cm^{-1} in the amide I region. α -helix structure was represented by the amide III band at 1293 cm^{-1} . The other vibration bands generally associated with protein structures are assigned as follows: $\nu(\text{C-H})$ around 2856 cm^{-1} to 2974 cm^{-1} , $\rho(\text{CH}_2)$ band was observed around 1461 cm^{-1} . The bands related to tyrosine were observed around 817 cm^{-1} and 643 cm^{-1} . Trp residue bands were observed around 1573 cm^{-1} and 1406 cm^{-1} [11, 18]. The bands in the region 923 cm^{-1} could be assigned to $\rho(\text{CH}_2)$ and the ones around 986 cm^{-1} to $\rho(\text{CH}_3)$ vibrations. Backbone skeletal $\nu(\text{C-C})$ vibration bands were also observed in region of 1135 cm^{-1} to 1037 cm^{-1} .

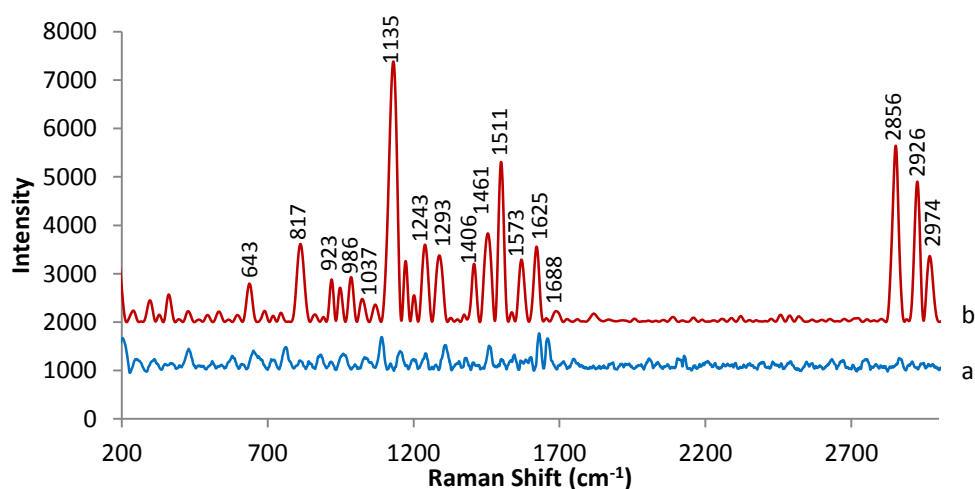


Figure 5: SERS spectra of (a) biotinylated antibody on AuNPs paper and (b) biotinylated antibody-Strep-BAT/TEG functionalized AuNPs paper.

After antigen was bound onto the capturing antibody, conformational changes of the antibody were observed (Figure 6). Comparing Figure 5 and Figure 6, the amide III region (1243 cm^{-1} and 1625 cm^{-1}) corresponding to β -sheet structure reduced in intensity with a small shift. Moreover, the Amide III band at 1293 cm^{-1} associated with α -helix slightly shifted to the left to 1280 cm^{-1} . An important observation from the antibody-

antigen interaction spectra is the predominant presence of Trp residue bands around 1590 cm^{-1} and 1406 cm^{-1} . A few new bands at 741 cm^{-1} , 780 cm^{-1} and 831 cm^{-1} associated with tyrosine residue were also observed [18].

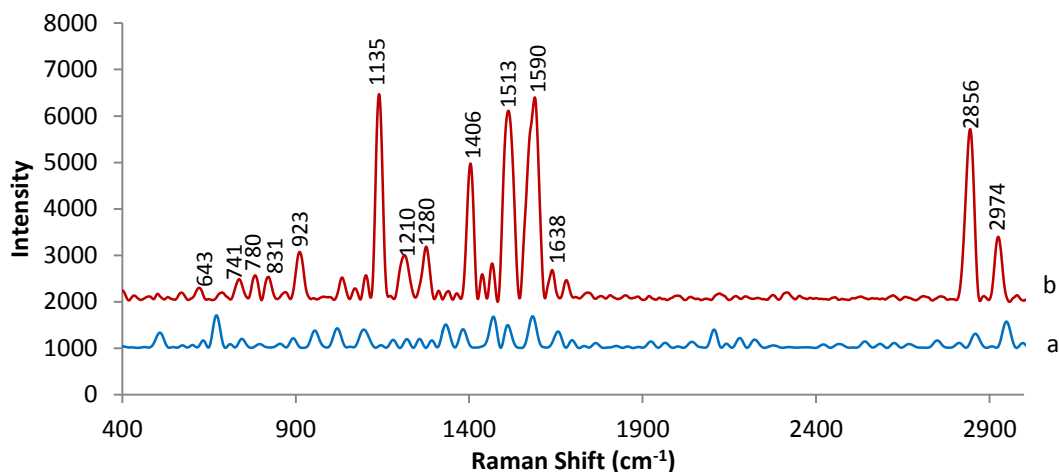


Figure 6: SERS spectra of (a) antigen on AuNPs paper and (b) antigen-biotinylated antibody-Strep-BAT/TEG functionalized AuNPs paper.

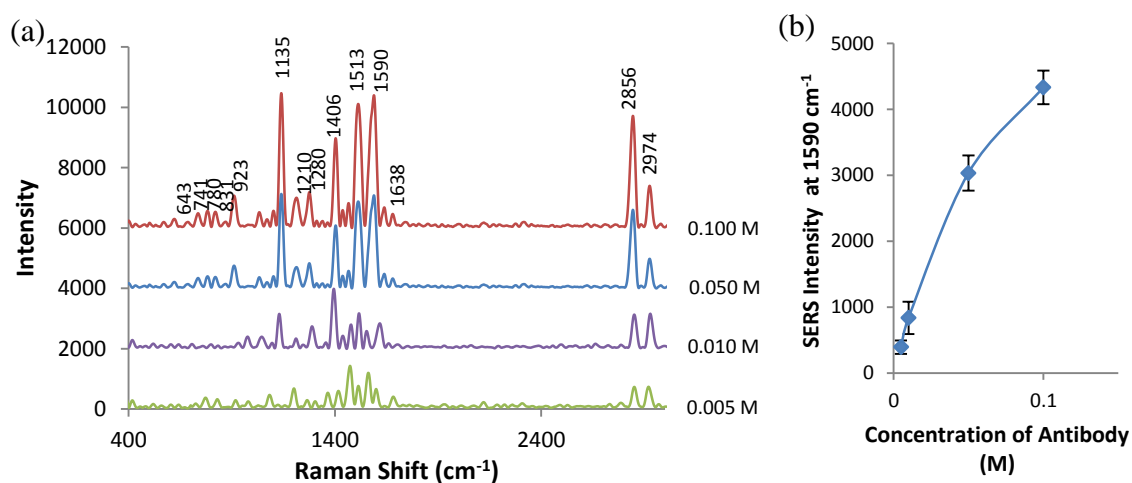


Figure 7: (a) SERS spectra of antigen-biotinylated antibody-Strep-BAT/TEG functionalized AuNPs paper exposed to different concentration of antigen. (b) SERS intensity of different concentration of antigen on functionalized AuNPs paper at 1590 cm^{-1} band.

The SERS sensitivity of the AuNPs paper was quantified. The AuNPs papers functionalized step by step with BAT/TEG, strep and antibody were exposed to different concentrations of antigen solutions and their SERS spectra were measured (Figure 7). The SERS intensity was increased as the function of the concentration.

6.5 Discussion

The AuNPs treated paper was previously shown to be SERS active in detecting a standard Raman molecule, 4-aminothiophenol (4-ATP) [8, 20]. In this study, the ability of AuNP paper to detect antibody-antigen interaction was explored and quantified. Similar to the model Raman molecule, the electromagnetic enhancement of the biomolecules was expected to be localized closer to the contact point of AuNPs on paper (Figure 2).

Streptavidin/biotin assemblies were chosen in this study to functionalize the AuNPs for antibody-antigen detection since they are a well-known model system for molecular recognition and biorecognition and their stable bio-structure. The strong affinity of both molecules is based on the intra- and intermolecular interactions between tryptophan (Trp) residues and the non-polar side chain of streptavidin with the non-polar moieties of biotin [13]. A mixture of 5×10^{-4} M blocking thiol (TEG) and 5×10^{-4} M biotinylated thiol (BAT) solution (9:1 ratio) was bound onto the AuNPs for subsequent binding of streptavidin (strep). Due to the large structure of Streptavidin, it is necessary to use the blocking thiol, TEG, to block unbound sites of AuNPs in spaces between the BAT molecules. This prevents the nonspecific binding of other molecular compounds to the surface of AuNPs. The SERS spectrum in Figure 3b shows a strong characteristic SERS band of BAT and TEG on AuNPs paper compared to the untreated AuNPs paper, confirming the successful binding of the thiol mixture. The presence of adsorbed streptavidin on biotinylated thiol functionalized AuNPs paper was then detected based on a significantly different SERS spectral feature in Figure 4b. This SERS spectrum (Figure 4b) is a complex spectrum where both contributions of streptavidin and thiol mixture are present with some overlap in the SERS band. However, by referring to the SERS spectrum of streptavidin alone on AuNPs paper (Figure 4a), specific SERS bands on the spectrum that correspond only to streptavidin binding were detected. All the spectra of BAT/TEG and Streptavidin-BAT/TEG functionalized AuNPs paper were obtained from the average of five Raman measurements of different spots (Supporting Information S1). The laser power was maintain at 10% and the exposure time was kept at 1 sec to prevent the biomolecule to denature. The position of all the characteristic bands was reproducible with little variation in intensity (± 10 -20%) (Supporting Information, S1). Meanwhile, the presence and shifting of additional bands were observed. These irreproducible bands could be attributed to the signal noise or little structural changes caused by denaturation of the

biomolecule when exposed to laser heat. Overall, the first two steps of the functionalization of AuNPs paper show a reasonably good SERS reproducibility.

Biotinylated anti-rabbit IgG, which predominantly consist of β -sheet (47%), 7% of α -helices, and remaining percentage of turns and coils [21], was then adsorbed onto the streptavidin-BAT/TEG functionalized AuNPs paper. SERS spectrum of the antibody was averaged based on five Raman measurements and its characteristic SERS bands were observed, confirming the binding of this biotinylated antibody onto the streptavidin (Figure 5). The characteristic bands of the antibody show a good reproducibility with small variation in their Raman shift (± 10 -20 cm^{-1}) and intensity (± 20 -30%).

After validating the reliability and reproducibility of the SERS spectrum of the antibody, the rabbit IgG antigen was adsorbed onto the antibody-streptavidin-BAT/TEG functionalized AuNPs paper. The combination of an antibody with its relative antigen is generally considered as a reversible bimolecular reaction with negligible changes in free energy. The antibody typically binds the antigen with very weak bonds as for example van der Waals forces, Coulombic interactions between groups of opposite charges and hydrogen bonds [22]. Since all these interactions are very weak, the immunocomplex stability should depend on the simultaneous formation of many very weak bonds. Due to the weakness of the interaction, the mean secondary structure of antigen and antibody does not change significantly [22]. However, some interesting and new spectral features assumed to be produced by antibody-antigen interaction can still be observed. Some shifts in the main SERS bands associated with the β -sheet structure and α -helix were observed by comparing Figure 5 and Figure 6; this could be attributed to the modification of the local structure of each entity due to the interaction. SERS bands of tryptophan and tyrosine were clearly observed (Figure 6). They are all reproducible from measurement to measurement (Supporting Information, S1), providing a reliable means of detecting the presence of antigen. These observations are spectroscopic evidences for the antigen-antibody interaction as tryptophan and tyrosine residues are known to be involved in antibody-antigen binding [15, 23].

To investigate the optimum SERS performance of this functionalized AuNPs paper, three key questions were raised. The first concerns the role of the blocking thiol (TEG); is it

necessary to block BAT unbound site of AuNPs to prevent non-specific binding? To explore this issue, Raman measurements were performed on antigen-antibody-Streptavidin-BAT functionalized AuNPs paper without TEG (Supporting Information, S2). The resulting SERS intensity and signal to noise ratio was decreased without TEG, compared to Figure 6b. Some additional peaks also appeared (e.g. 2074 cm^{-1} and 2122 cm^{-1}), interfering the SERS detection of antigen. So, we believed that TEG had aided in preventing the background interferences of undesired molecules and thus contributed in amplifying the SERS spectra of the specific biomolecules; this is supported by the literature [13, 24].

Second, will the SERS signal be affected by biomolecules adsorbed on the area of paper which are not covered by AuNPs? Each of the biomolecules investigated was also deposited onto paper which was not treated by AuNPs as a control (supporting information, S3). It was found that the Raman signals of the biomolecules were not detectable on the plain paper; the main spectra features originate from the paper itself. This means that non-specific adsorption of biomolecule should not cause a problem in affecting the resulting SERS signal (intensity and peak position).

Third question: Does the distance between the biomolecules of interest and the surface of the AuNPs on paper influence the intensity of the resulting SERS signal? The theory of electromagnetic mechanism predicts that SERS does not require the adsorbed molecules to be in direct contact with the surface of metallic nanoparticles but within a certain sensing volume [25]. Therefore, the extension of the SERS effect above the surface of AuNPs would be limited to a few nanometers and the intensities of antigen, antibody and streptavidin would presumably be less intense than those of BAT/TEG. However, in this study, the corresponding SERS intensity was increased after each component of biomolecules (BAT/TEG, streptavidin, followed by antibody) was adsorbed onto the AuNPs on paper (Figure 3 to Figure 5). We believe that other factors such as the size and chemical structure of the biomolecule could be responsible in amplifying the SERS signal. The SERS intensity decreased by 17% as antigen, a smaller biomolecule, was absorbed onto the antibody-streptavidin-BAT/TEG functionalized AuNPs paper (Figure 6). Further improvement in SERS intensity should be possible by decreasing the distance between the antigen and AuNPs surface with smaller receptor molecules or a shorter

functionalization step. However, the functionalized AuNPs paper still shows good sensitivity in detecting different concentration of antigen (Figure 7). The SERS intensity shows an almost linear relationship with the concentration of antigen. This suggests that this SERS bio-diagnostic platform can be used for both qualitative and quantitative analysis.

6.6 Conclusion

This study demonstrated a novel approach to functionalize gold nanoparticles (AuNPs) on paper by a step by step approach which produced good quality SERS spectra characteristic of the antibody-antigen interaction. SERS paper substrate was fabricated by dip-coating filter paper into a suspension of AuNPs. The AuNPs on paper were then functionalized by biotinylated thiol followed by streptavidin and biotinylated anti-rabbit IgG (antibody). SERS spectra of each functionalization or binding step were analysed for specific adsorption of the biomolecules. The shifts of Raman band associated with α -helix and β -sheet structure indicated the modification of the local structure of antibody due to the interaction with antigen. Predominant tryptophan and tyrosine residue bands were detected upon antigen binding, confirming the presence of antigen. Reproducible spectra features were quantified as AuNP papers were subjected to antigen solutions of different concentration; the intensity of the spectra increased as the function of the antigen concentration.

The role of blocking thiol (TEG) in the functionalization steps was elucidated; it prevents background interference from undesired molecules which amplifies the SERS signal of the biomolecules of interest. Non-specific adsorption of biomolecules on non-covered areas of paper by AuNPs was shown to be Raman inactive and not to interfere with the resulting SERS signal. Further improvement in SERS intensity was proposed by decreasing the distance between the antigen and AuNPs surface with smaller receptor molecules or a shorter functionalization step.

Functionalized AuNPs paper substrate has the potential to become a generic SERS platform to identify and quantify low concentrations of antigens in complex environments. Simple dipping of an AuNP paper dipstick into a biomolecule solution is

promising for rapid SERS detection. This method is also cost-effective, robust and convenient as fluorescent labeling is not required for detection. It has the potential to provide a simple, fast, label-free, selective, and economical substrate for detecting a wide range of adsorbed biomolecules. The detection of low concentration biomolecules in clinical, forensic, industrial, and environmental laboratories are prospective applications of the technology.

6.7 Acknowledgement

Thanks to Dr. T. Williams, Monash Centre for Electron Microscopy (MCEM), for FESEM technical expertise and F. Shanks from Monash Molecular Spectroscopy and Centre for Biospectroscopy for Raman technical advice. The financial supports from the ARC Linkage LP0989823 and Visy, Amcor, SCA, Norske Skog, Australian Paper, the Australian Pulp and Paper Institute and Monash University are all acknowledged.

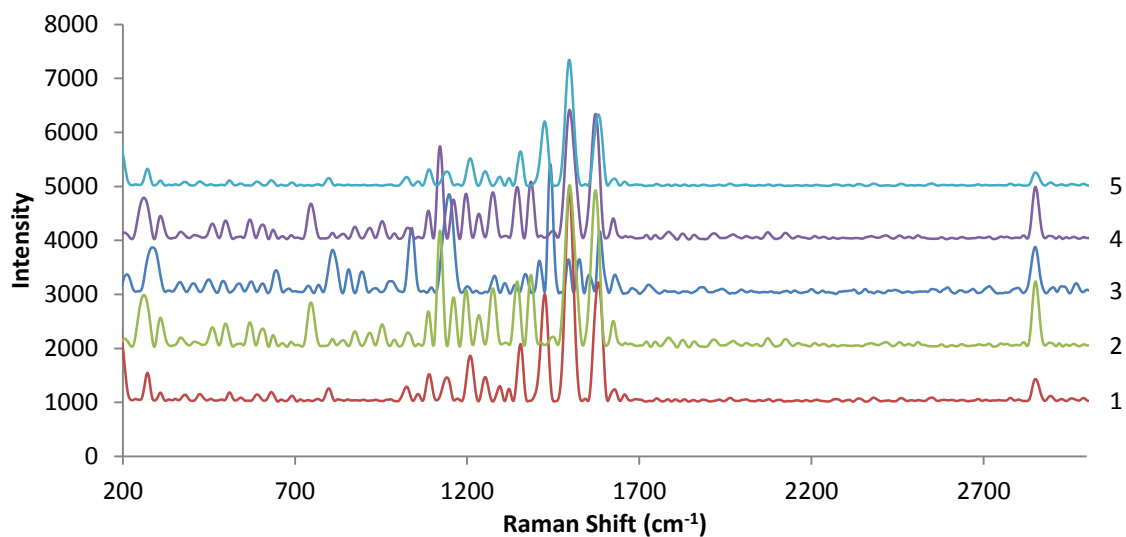
6.8 References

1. Martinez, A.W., S.T. Phillips, M.J. Butte, and G.M. Whitesides, *Patterned Paper as a Platform for Inexpensive, Low-Volume, Portable Bioassays*. Angewandte Chemie International Edition, 2007. **46**(8): p. 1318-1320.
2. Martinez, A.W., S.T. Phillips, E. Carrilho, S.W. Thomas, H. Sindi, and G.M. Whitesides, *Simple Telemedicine for Developing Regions: Camera Phones and Paper-Based Microfluidic Devices for Real-Time, Off-Site Diagnosis*. Analytical Chemistry, 2008. **80**(10): p. 3699-3707.
3. Li, X., J. Tian, and W. Shen, *Quantitative biomarker assay with microfluidic paper-based analytical devices*. Analytical and Bioanalytical Chemistry, 2010. **396**(1): p. 495-501.
4. Li, X., J. Tian, T. Nguyen, and W. Shen, *Paper-Based Microfluidic Devices by Plasma Treatment*. Analytical Chemistry, 2008. **80**(23): p. 9131-9134.
5. Khan, M.S., G. Thouas, W. Shen, G. Whyte, and G. Garnier, *Paper Diagnostic for Instantaneous Blood Typing*. Analytical Chemistry, 2010. **82**(10): p. 4158-4164.
6. Ngo, Y.H., D. Li, G.P. Simon, and G. Garnier, *Paper surfaces functionalized by nanoparticles*. Advances in Colloid and Interface Science, 2011. **163**(1): p. 23-38.
7. Campion, A. and P. Kambhampati, *Surface-enhanced Raman scattering*. Chemical Society Reviews, 1998. **27**(4): p. 241-250.
8. Ngo, Y.H., D. Li, G.P. Simon, and G. Garnier, *Gold Nanoparticle–Paper as a Three-Dimensional Surface Enhanced Raman Scattering Substrate*. Langmuir, 2012. **28**(23): p. 8782-8790.
9. Etchegoin, P.G. and E.C. Le Ru, *A perspective on single molecule SERS: current status and future challenges*. Physical Chemistry Chemical Physics, 2008. **10**(40): p. 6079-6089.
10. Le Ru, E.C., E. Blackie, M. Meyer, and P.G. Etchegoin, *Surface Enhanced Raman Scattering Enhancement Factors: A Comprehensive Study*. The Journal of Physical Chemistry C, 2007. **111**(37): p. 13794-13803.

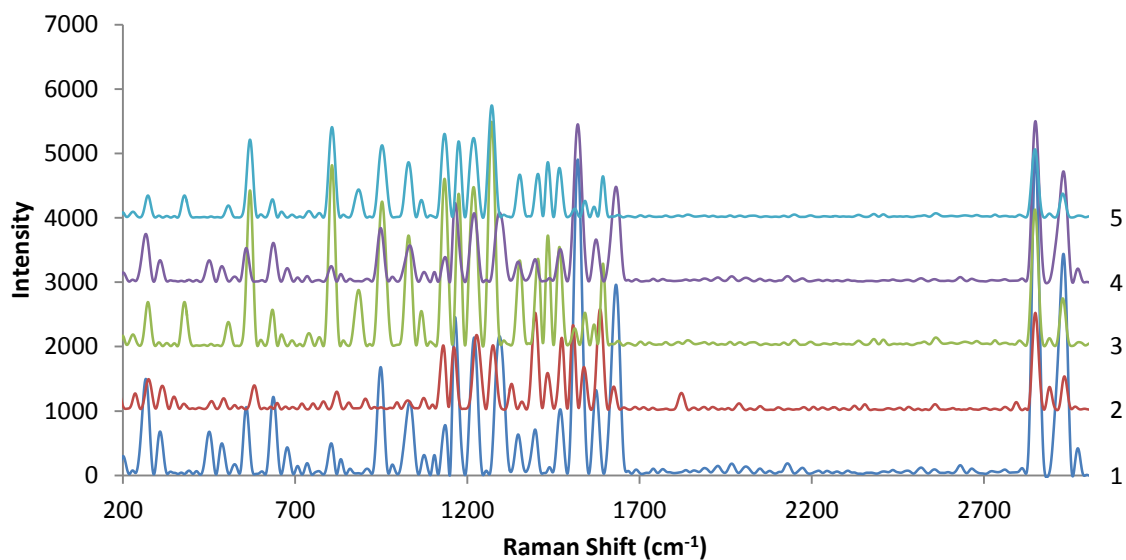
11. Kengne-Momo, R.P., P. Daniel, F. Lagarde, Y.L. Jeyachandran, J.F. Pilard, M.J. Durand-Thouand, and G. Thouand, *Protein Interactions Investigated by the Raman Spectroscopy for Biosensor Applications*. International Journal of Spectroscopy, 2012. **2012**: p. 7.
12. Arruebo, M., M. Valladares, #243, nica, Gonz, #225, lez-Fern, ndez, #193, and frica, *Antibody-Conjugated Nanoparticles for Biomedical Applications*. Journal of Nanomaterials, 2009. **2009**.
13. Galarreta, B.C., P.R. Norton, and F.o. Lagugné-Labarthet, *SERS Detection of Streptavidin/Biotin Monolayer Assemblies†*. Langmuir, 2011. **27**(4): p. 1494-1498.
14. Fagnano, C., A. Torreggiani, and G. Fini, *Raman spectroscopic studies of the anhydrous complexes of avidin and streptavidin with biotin*. Biospectroscopy, 1996. **2**(4): p. 225-232.
15. Davies, D.R. and G.H. Cohen, *Interactions of protein antigens with antibodies*. Proceedings of the National Academy of Sciences, 1996. **93**(1): p. 7-12.
16. Ng, A.C., U. Uddayasankar, and A. Wheeler, *Immunoassays in microfluidic systems*. Analytical and Bioanalytical Chemistry, 2010. **397**(3): p. 991-1007.
17. Turkevich, J., P.C. Stevenson, and J. Hillier, *A study of the nucleation and growth processes in the synthesis of colloidal gold*. Discussions of the Faraday Society 1951. **11**: p. 55-75.
18. Naumann, D., *FT-INFRARED AND FT-RAMAN SPECTROSCOPY IN BIOMEDICAL RESEARCH*. Applied Spectroscopy Reviews, 2001. **36**(2-3): p. 239-298.
19. Chou, I.H., M. Benford, H.T. Beier, G.L. Coté, M. Wang, N. Jing, J. Kameoka, and T.A. Good, *Nanofluidic biosensing for beta-amyloid detection using surface enhanced Raman spectroscopy*. Nano Letters, 2008. **8**(6): p. 1729-1735.
20. Ngo, Y.H., G. Garnier, D. Li, and G. Simon, *Effect of Cationic Polyacrylamides on the Aggregation and SERS Performance of Gold Nanoparticles-treated Paper*. Journal of Colloid and Interface Science, 2012. **In press**.
21. Sjöholm, I., *Protein A from Staphylococcus aureus*. European Journal of Biochemistry, 1975. **51**(1): p. 55-61.
22. Matharu, Z., A.J. Bandodkar, V. Gupta, and B.D. Malhotra, *Fundamentals and application of ordered molecular assemblies to affinity biosensing*. Chemical Society Reviews, 2012. **41**(3): p. 1363-1402.
23. Ohno, S., N. Mori, and T. Matsunaga, *Antigen-Binding Specificities of Antibodies are Primarily Determined by Seven Residues of VH*. Proceedings of the National Academy of Sciences of the United States of America, 1985. **82**(9): p. 2945-2949.
24. Zeiri, L., B.V. Bronk, Y. Shabtai, J. Eichler, and S. Efrima, *Surface-Enhanced Raman Spectroscopy as a Tool for Probing Specific Biochemical Components in Bacteria*. Applied Spectroscopy, 2004. **58**(1): p. 33-40.
25. Stiles, P.L., J.A. Dieringer, N.C. Shah, and R.P. Van Duyne, *Surface-Enhanced Raman Spectroscopy*. Annual Review of Analytical Chemistry, 2008. **1**(1): p. 601-626.

6.9 Supporting Information

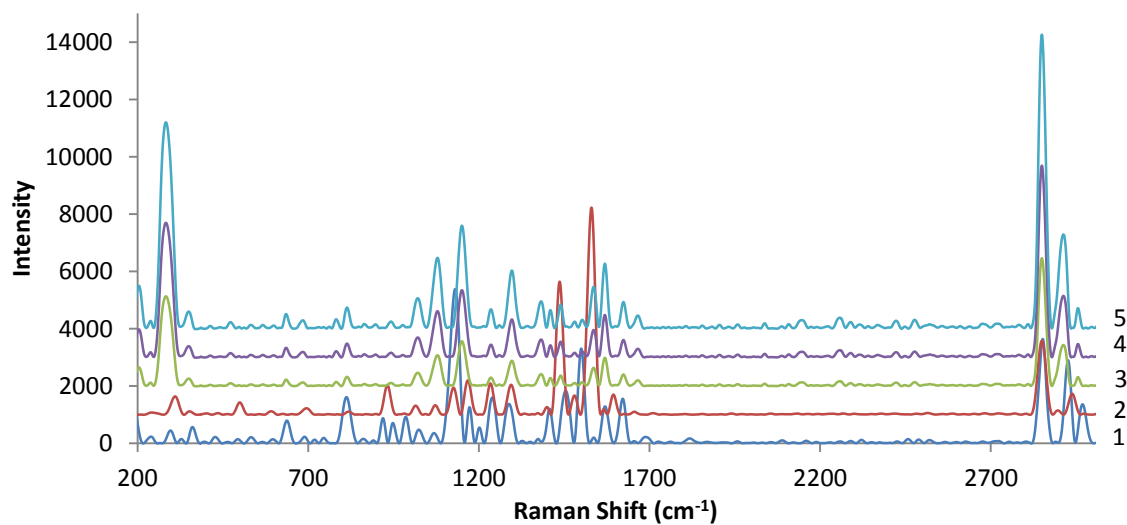
S1: SERS spectra of each component in the functionalization steps from five measurement of at different spots on the AuNPs paper substrate.



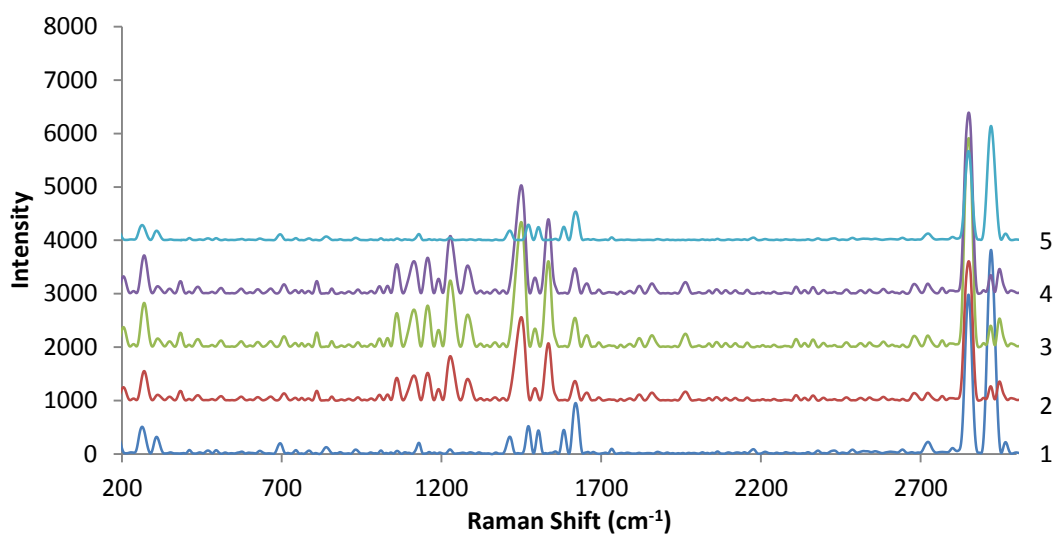
BAT/TEG functionalized AuNPs paper.



Streptavidin-BAT/TEG functionalized AuNPs paper.

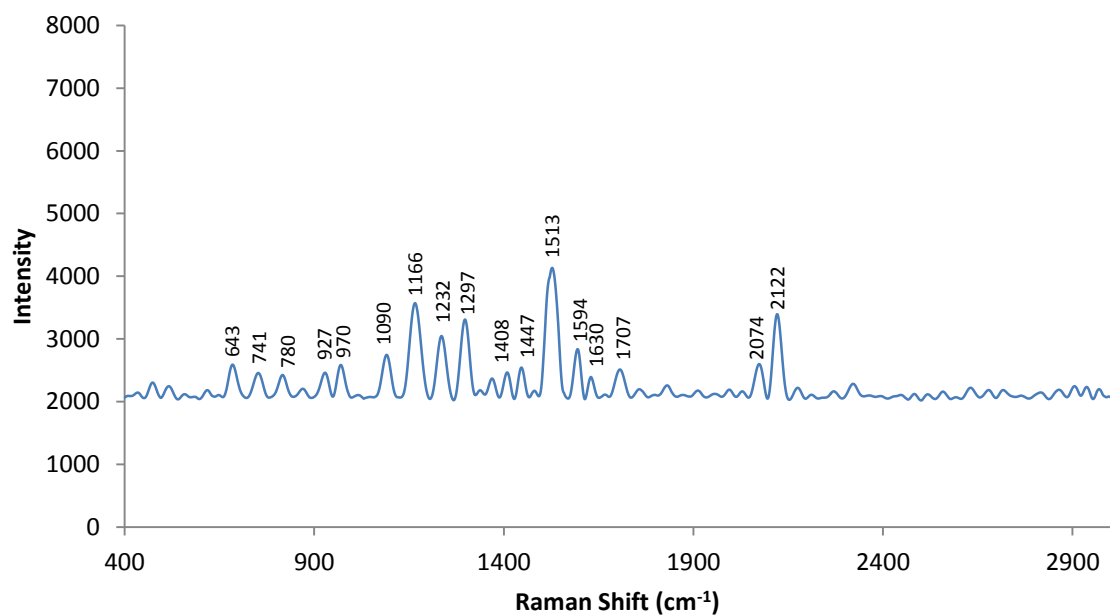


Antibody-Streptavidin-BAT/TEG functionalized AuNPs paper.

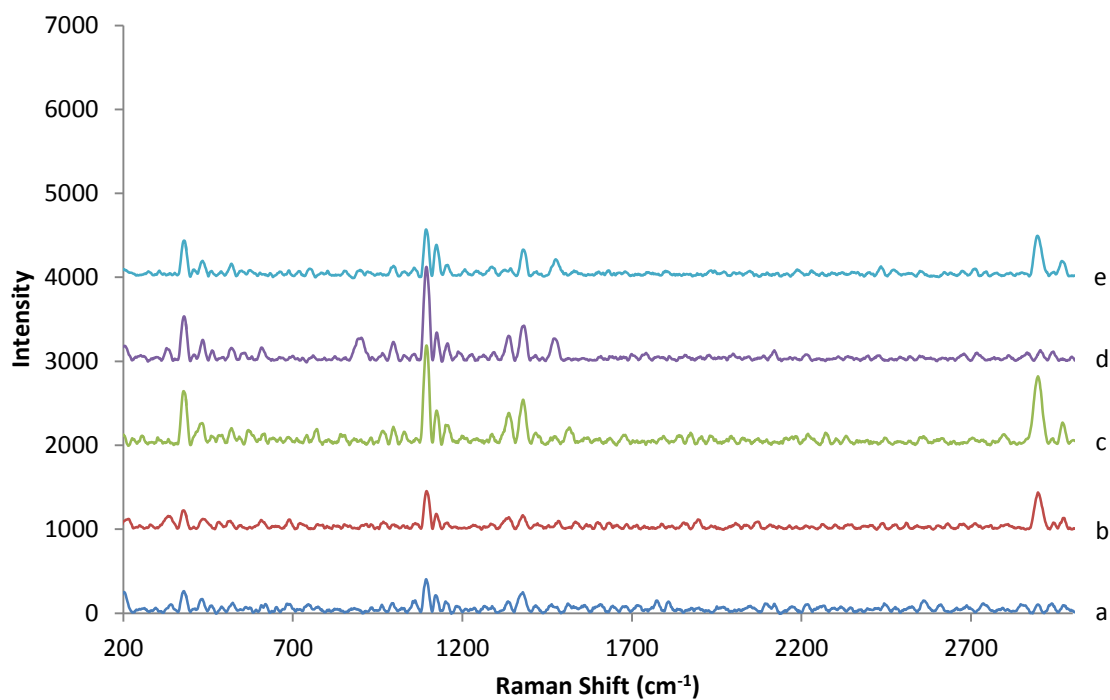


Antigen-antibody-Streptavidin-BAT/TEG functionalized AuNPs paper.

S2: SERS measurement of antigen-antibody-Streptavidin-BAT functionalized AuNPs paper without blocking thiol (TEG).



Antigen-antibody-Streptavidin-BAT functionalized AuNPs paper without blocking thiol (TEG).

S3: Raman measurement of each component on untreated plain paper.

Raman spectra of (a) paper, (b) BAT/TEG on paper, (c) Streptavidin-BAT/TEG on paper, (d) antibody-Streptavidin-BAT/TEG on paper and (e) antigen-antibody-Streptavidin-BAT/TEG on paper.

This page is intentionally blank

Chapter 7

Conclusion

This page is intentionally blank

This doctoral thesis optimized the surface enhanced Raman scattering (SERS) performance of gold nanoparticles (AuNP) functionalized paper and investigated the critical mechanisms involved. It aims at engineering sensitive and reproducible SERS active paper substrate for routine bio-diagnostic applications. Most previous studies have simply used paper as an inert support, and have not considered nor explored how the rough, composite and heterogeneous structure inherent of paper can affect the distribution of nanoparticles as well as the resulting properties. None have attempted to quantify and control the adsorption state of nanoparticles within the heterogeneous paper structure to optimize the potential applications. The objective of this thesis was to address these gaps in research by investigating three parallel research length scales (**nano, micro and macro**), which are critical for the development of sensitive, selective and low cost bio-diagnostics.

The effect of the AuNP concentration and distribution profile within paper on the SERS performance of paper was quantified (**nanoscale**). A surface coverage of AuNPs ranging from 1.8 to 22.1% was achieved on paper; however, the particles on the surfaces represented only 40% of the AuNPs loading, with the majority uniformly adsorbed within the bulk of paper. The SERS intensity scaled linearly with the density of AuNPs on paper. In the absence of retention aids, the adsorption of AuNPs on paper substrate was still relatively higher than on silicon when both substrates were treated similarly. SERS enhancement factor (EF) of a model dye (4-aminothiophenol, 4-ATP) adsorbed onto AuNPs treated paper was higher by more than one order of magnitude than AuNPs treated silicon. This was due to the AuNPs adsorbed on the surface and within the bulk of paper acting as a three-dimensional (3D) multilayer architecture for intralayer and interlayer plasmon coupling.

In order to maximize the spatial density of SERS hotspots for amplified SERS signals, the aggregation size and surface coverage of AuNPs on paper was controlled by pre-treating paper with a series of cationic polyacrylamide (CPAM) solutions (**microscale**). The effect of CPAM solution concentration, polymer charge density and molecular weight on AuNPs adsorption/aggregation behavior and SERS properties was quantified. CPAM of higher concentration, charge density and molecular weight were identified as the optimized conditions to achieve higher surface coverage and aggregation on paper. A

more uniform coating of AuNPs was formed compared to the bare paper substrate. A surface coverage of AuNPs up to 80% with average AuNP aggregates up to 60 nm on paper was achieved. These AuNP aggregates formed a rough metallic surface with increased particles junction for a stronger electromagnetic coupling that tremendously amplified the Raman signal of 4-ATP. The resulting Raman EF from AuNPs-CPAM paper was almost an order of magnitude higher and more reproducible than the untreated AuNPs paper at constant concentration of AuNPs suspension.

To further improve the sensitivity and reproducibility of AuNPs-CPAM paper as an efficient routine SERS substrate, the dissolution kinetics of CPAM, from a powder to an equilibrium solution was studied (**macroscale**). The heterogeneity of AuNPs distribution on paper was related to variability in the bridging and aggregation of nanoparticles caused by the dissolution kinetic of CPAM. Both viscosity and critical aggregate/coil size of a high molecular weight, low charge density CPAM solution slowly increased to reach a plateau after 12 hours of dissolution time. Increasing the charge density of the polymer shortened the time required to reach steady state (8 hours). The surface coverage of AuNPs on paper increased, and their average aggregate size was more uniform as paper was pre-treated with a CPAM solution which had been mixed for a longer period; increasing CPAM charge density accentuated this tendency. SERS intensity and reproducibility of AuNPs paper both increase with dissolution time of CPAM, as the heterogeneity of AuNP distribution and aggregate size decrease below 1 μm , the critical SERS dimension corresponding to the diameter of the Raman laser beam.

A simple method was developed to form and visualize polyelectrolyte-nanoparticles chaplet like structures on paper, using negatively charged gold nanoparticles (AuNPs) to decorate polymer chain of cationic polyacrylamide (CPAM). FESEM images of the dried paper sample showed that individual AuNPs were lined up with nearly contacting edges along the CPAM polymer chain and in an opposite direction against the cellulose fibers. The dimension of the resulting AuNP chaplets can be tuned by adjusting the concentration, charge density and molecular weight of CPAM. The density and thickness of AuNP chaplets can be increased predominantly by using higher concentration CPAM. On the other hand, longer chaplets with more AuNPs per length can be achieved by increasing the charge density of CPAM. The length and thickness of AuNP chaplets was

able to be increased with higher molecular weight CPAM. Wet and flowing condition during the vacuum filtration process is believed to contribute towards the stretching of the CPAM polymer chains. The rough and hydrophilic nature of cellulose fibers is responsible for immobilizing the stretched polymer chains on the paper substrate for subsequent self assembly of negatively charged AuNPs, forming AuNPs decorated polymer chains. This approach of assembling nanometer-scale components (AuNPs) into micrometer-scale arrays (chaplets) on a porous paper substrate suggests a promising strategy for integrating paper with nanoelectronics applications.

A novel approach was demonstrated to optimize AuNPs treated paper as a SERS bio-diagnostic platform for quantitative and qualitative detection of antibody-antigen interaction. AuNPs on paper was functionalized step by step by using streptavidin/biotin assemblies to produce SERS spectra of antibody-antigen interaction. The shifts of Raman band associated with α -helix and β -sheet structure indicated the modification of the local structure of antibody due to the interaction with antigen. Predominant tryptophan and tyrosine residue bands were detected upon antigen binding, confirming the presence of antigen. Reproducible spectral features with varying intensity were also observed as papers were subjected to different concentrations of antigen solutions. This functionalized AuNPs paper substrate can be further developed as a generic SERS platform capable of specifically detecting trace amounts of antigens in complex environments. The generic functionalization approach established will facilitate the development of low cost paper based immuno-sensors for detecting many types of antigens or antibodies with little variation in procedure.

By reconciling the above studies on the nanoscale, microscale and macroscale of AuNPs functionalized paper, a generic SERS platform offering high sensitivity and selectivity to low cost bio-diagnostics applications has been developed.

This page is intentionally blank

Appendix

This page is intentionally blank

Appendix I: Papers Included in Each Chapter in Their Published Format

This page is intentionally blank



Paper surfaces functionalized by nanoparticles

Ying Hui Ngo^a, Dan Li^b, George P. Simon^b, Gil Garnier^{a,*}

^a BioPRIA, Australian Pulp and Paper Institute (APPI), Department of Chemical Engineering, Monash University, Clayton, VIC 3800, Australia

^b Department of Material Engineering, Monash University, Clayton, VIC 3800, Australia

article info

Available online 22 January 2011

Keywords:

Nanoparticles

Gold

Silver

Titania

Paper

Photocatalytic

SERS

SPR

Heterogeneity

abstract

Nanomaterials with unique electronic, optical and catalytic properties have recently been at the forefront of research due to their tremendous range of applications. Taking gold, silver and titania nanoparticles as examples, we have reviewed the current research works on paper functionalized by these nanoparticles. The functionalization of paper with only a very small concentration of nanoparticles is able to produce devices with excellent photocatalytic, antibacterial, anti-counterfeiting, Surface Enhanced Raman Scattering (SERS) and Surface Plasmon Resonance (SPR) performances. This review presents a brief overview of the properties of gold, silver and titania nanoparticles which contribute to the major applications of nanoparticles-functionalized paper. Different preparation methods of the nanoparticles-functionalized paper are reviewed, focusing on their ability to control the morphology and structure of paper as well as the spatial location and adsorption state of nanoparticles which are critical in achieving their optimum applications. In addition, main applications of the nanoparticles-functionalized papers are highlighted and their critical challenges are discussed, followed by perspectives on the future direction in this research field. Whilst a few studies to date have characterized the distribution of nanoparticles on paper substrates, none have yet optimized paper as a nanoparticles' substrate. There remains a strong need to improve understanding on the optimum adsorption state of nanoparticles on paper and the heterogeneity effects of paper on the properties of these nanoparticles.

Crown Copyright © 2011 Published by Elsevier B.V. All rights reserved.

Contents

1. Introduction	24
2. Properties of nanoparticles	24
2.1. Photocatalytic	24
2.2. Surface Plasmon Resonance (SPR)	25
2.3. Surface Enhanced Raman Scattering (SERS)	25
2.4. Antimicrobial	25
3. Attachment methods of nanoparticles to paper	26
3.1. Wet-end addition	26
3.2. Surface treatments	26
3.2.1. Size-press treatment	27
3.2.2. Layer-by-layer deposition (LbL)	27
3.2.3. Sol–gel method	27
3.2.4. Direct assembly	28
3.2.5. In situ assembly	28
4. Applications of nanoparticles-functionalized paper	29
4.1. Titania paper	29
4.1.1. Self-cleaning	29
4.1.2. Organic destruction	29
4.1.3. Disinfection	29
4.2. Gold nanoparticle paper	30
4.2.1. Colorimetric sensor	30
4.2.2. Rewritable paper	31
4.2.3. SERS	31

* Corresponding author. Tel.: +61 3 9905 9180; fax: +61 3 9905 3413.

E-mail address: Gil.Garnier@monash.edu (G. Garnier).001-8686/\$ – see front matter. Crown Copyright © 2011 Published by Elsevier B.V. All rights reserved.
doi:10.1016/j.cis.2011.01.004

4.3.	Silver nanoparticle paper	33
4.3.1.	Antimicrobial	33
4.3.2.	SERS	33
4.3.3.	Anti-counterfeiting	33
5.	Challenges and opportunities	34
5.1.	Paper chemical and physical heterogeneities	34
5.2.	Optical properties	35
5.2.1.	SERS and SPR	35
5.3.	Photocatalytic properties	36
5.4.	Analytical techniques	36
6.	Conclusion	37
	Acknowledgements	37
	References	37

1. Introduction

The area of nanotechnology reviewed in this article involves controlled deposition of individual nanoparticles or their aggregates into desired configurations on paper, to produce materials with unique properties and functions [1]. Nanoparticles with distinctive electronic, optical and catalytic properties have been at the forefront of research due to their tremendous applications. A wide range of techniques have been used to synthesize nanoparticles in different solid mediums, such as glass [2], metallic [3] and polymeric films [4] to realize new applications. However, development of simpler and more direct methods is still needed to readily generate the desired size, shape, and adsorption of nanoparticles on appropriate and strategic substrates. Taking gold (AuNPs), silver (AgNPs) and titania nanoparticles (TiO_2) (Table 1) as examples, the state of paper functionalized by these nanoparticles is analyzed in this review.

The porous structure and hydrophilic fiber surface allow paper to absorb suspensions of nanoparticles by capillary forces, yielding a high loading of nanoparticles upon drying. Furthermore, paper is a low cost substrate and only a very small volume of TiO_2 , AuNPs and AgNPs deposited on paper can produce devices which show excellent optical [5], antibacterial [6,7], anti-counterfeiting [8], Surface Enhanced Raman Scattering (SERS) [9] and Surface Plasmon Resonance (SPR) [10] performances. In addition, paper has the advantage of being biodegradable, biocompatible and renewable whilst its structural morphology as well as surface chemistry can be readily engineered.

The objectives of this article are to critically review the development of nanoparticles-functionalized paper and assess missing knowledge and opportunities. A brief overview of the properties of TiO_2 , AuNPs and AgNPs is presented first, to provide a background for further discussion of the nanoparticles-functionalized paper. These nanoparticles have been selected due to their wide usage and unique applications. This review then focuses on the deposition/assembly and applications of the nanoparticles-functionalized paper. Finally, the future challenges and opportunities of this field are presented.

2. Properties of nanoparticles

Before analyzing the preparation methods and applications of nanoparticles-functionalized paper, the properties of TiO_2 , AuNPs and AgNPs (Table 1) are presented in this section. Due to extensive range of properties displayed by these three nanoparticles, we only intend to provide a brief overview of their photocatalytic, Surface Plasmon Resonance (SPR), Surface Enhanced Raman Scattering (SERS) and antibacterial properties which are related to the end-use of the respective nanoparticles-functionalized paper.

2.1. Photocatalytic

After photocatalytic properties of TiO_2 were discovered by Fujishima and Honda [11], Matsubara et al. [12] demonstrated the

photocatalytic properties of TiO_2 -containing paper in 1995. Since then, TiO_2 has been widely used to produce photocatalytic paper. This review focuses on the photocatalytic properties and applications of TiO_2 -paper, instead of their traditional usage as whitening fillers.

Basically, TiO_2 is a broad band gap semiconductor material which is able to convert energy from light into chemical redox energy (Fig. 1). The two most important and easily synthesized polymorphs of TiO_2 are rutile, with a band gap of 3.05 eV (equivalent to light of wavelength of 407 nm), and anatase, with a band gap of 3.26 eV (= 381 nm) [13]; anatase is more active in photocatalysis although the physical causes are not completely understood so far. Upon irradiation of UV light, two types of photochemical reactions occur on the TiO_2 surface—photo-induced redox reaction of the adsorbed substances, and photo-induced hydrophilic conversion of TiO_2 itself [14]. In the first reaction, photoelectrons (e^-) are generated in the conduction band and holes (h^+) are produced in the valence band. These occur whenever TiO_2 absorbs UV light of wavelength less than 380 nm, an energy which is greater than its band gap energy (3.26 eV). [14]. The photoelectrons then react with molecular oxygen (O_2) to produce superoxide radical anions ($\text{O}_2^{\cdot-}$), and the holes react with water to produce hydroxyl (OH^\cdot) radicals. Finally, these two types of radicals work together to photodecompose organic compounds [15].

Conversely, in the second reaction, the electrons and holes are also photogenerated upon UV irradiation but they react differently. The photoelectrons tend to reduce the Ti(IV) cations to the Ti(III) state, whilst the holes oxidize the O^{2-} anions. In this process, O_2 molecules are ejected, creating oxygen vacancies (Fig. 2), which are then occupied by water molecules, producing adsorbed OH groups that make the surface hydrophilic. The surface is transformed into an energetically-metastable state after the OH groups' adsorption. When

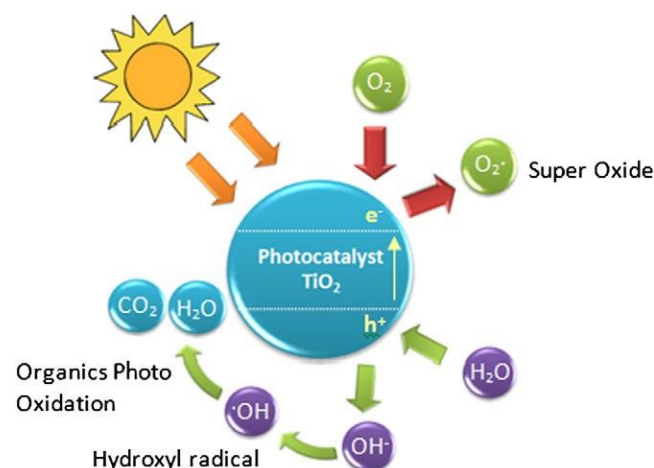


Fig. 1. Photo-induced redox reaction of TiO_2 . (redrawn from [13]).

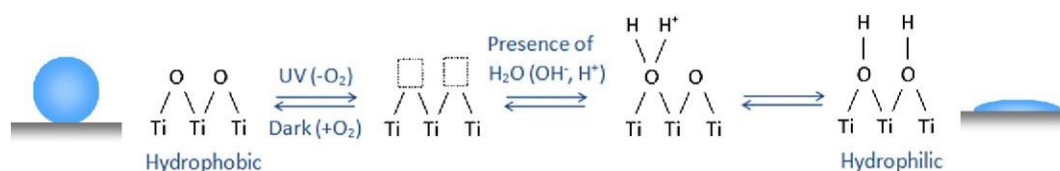


Fig. 2. Photo-induced hydrophilic and hydrophobic conversion of TiO_2 . (redrawn from [13]).

the films are removed from the light, the adsorbed OH groups are slowly substituted by atmospheric oxygen, and the surface reverts back to its original state.

Due to high photocatalytic properties of TiO_2 , its oxidizing activity tends to decompose paper substrate, limiting immobilization of TiO_2 on the substrate and reducing paper strength. In order to produce an efficient photocatalytic paper, TiO_2 must be strongly fixed to paper whilst avoiding deterioration of the paper. Distribution of TiO_2 nanoparticles over the thickness of paper sheet (z-plane) and their distribution profile within a layer (x–y plane) are also believed to be critical in achieving high photocatalytic efficiency. To achieve maximum photo activity, a homogenous distribution of TiO_2 over the paper's volume is preferred instead of aggregation, in order to increase accessibility of target molecules and light to the TiO_2 surfaces. In addition, thickness and porosity of paper are also important parameters in determining photocatalytic efficiency of the TiO_2 -functionalized paper. Target molecules must be very close to TiO_2 on the paper surface, preferably in direct contact. Furthermore, decomposed compound must be transported/diffused away from the catalytic sites on paper to avoid blockage for future targets.

2.2. Surface Plasmon Resonance (SPR)

According to Mie's theory, SPR of nanoparticles is mainly related to their size, shape, volume concentration (aggregated or isolated assembly), interparticle distance as well as dielectric constant or refractive index of their surrounding mediums. Detection of analyte molecules is possible, as their presence changes interparticle distance or refractive index of the nanoparticles, which causes a shift in the surface plasmon adsorption band.

AgNPs demonstrate the highest efficiency of plasmon excitation among all the three metals (Ag, Au and Cu) which exhibit plasmon resonances within the visible spectrum [16]. According to Chin [17], AgNPs display a sharper resonance peak than AuNPs and thus AgNPs can provide a higher sensitivity and better shift detection. The optical excitation of their plasmon resonances has a more efficient light interaction mechanism. Since their absorption or scattering cross sections are higher compared to their geometric cross section, AgNPs are able to capture more light than its physical size would permit [16]. However, AgNPs are predisposed to oxidation, leading to problems with long term storage.

Compared to AgNPs, AuNPs are more stable and are commonly used to produce sensitive colorimetric sensors. Small and well-dispersed AuNPs (diameter of 10–50 nm) show an intense red color with extinction coefficients which are much higher than those of common dyes, due to their localized SPR. The surface of AuNPs can be tailored by ligand-functionalization to selectively bind biomarkers. The most general approaches are chemical functionalization and thiol-linking of DNA of AuNPs to detect specific binding of proteins or antibodies. Upon the addition of analyte, functionalized and well-dispersed AuNPs are induced into aggregates which show a significant color shift from red to blue (Fig. 3). This is due to interparticle plasmon coupling which occurs as the surface plasmon of the individual AuNPs combine when their interparticle distance is smaller than their diameter.

In order to achieve an efficient SPR performance on paper, higher coverage of AgNPs and AuNPs must be obtained on the paper surface

to enhance sensitivity of the nanoparticles-functionalized paper. It is important for paper structure to maintain the adsorption state of nanoparticles (e.g. dispersed or aggregated) upon drying. To carry out ideal colorimetric detection, the activity of nanoparticles must be preserved during storage and remain functional upon rehydration for use. Furthermore, careful control of nanoparticles' size and porosity of paper is required, so that the nanoparticles will not be entrapped inside the pores within the paper structure, which would restrict the aggregation or dispersion of the nanoparticles and accessibility of target analyte.

2.3. Surface Enhanced Raman Scattering (SERS)

Raman scattering is a light scattering technique in which Raman photons are scattered by vibrational and rotational transitions in a molecule. However, its sensitivity is limited because the Raman signal is very weak. The development of Surface Enhanced Raman Scattering (SERS) has increased dramatically since Fleischmann et al. [19] published their discovery on enhanced Raman signals from pyridine on a rough silver electrode. This discovery of SERS has transformed Raman spectroscopy from a structural analytical tool to a sensitive single-molecule detection and nanoscale probe [20]. As reported by Brus and co-workers [21], intense SERS enhancement is often present at the point of contact between two or more metal nanoparticles. As the metal nanoparticles are contacted to form aggregates, their transition dipoles couple to each other and the enhanced fields of each nanoparticle coherently interfere at their contact point. When molecules are adsorbed in this contact point ('hot spot'), their Raman signals can be significantly enhanced (10^{14} – 10^{15}) [22]. Aggregates of nanoparticles have more efficient SERS properties than individual nanoparticles because larger enhancements can be achieved at particle junctions of the aggregates.

Since the aggregation of nanoparticles plays an important role in enhancing the SERS signal, their adsorption and aggregation state must be maintained within the paper structure. Stability of nanoparticles on the paper substrates must also be preserved so that they can be stored for long periods between measurements. Reproducibility of their aggregation state is another important factor to achieve accurate SERS results. Since the spot size of Raman's laser beam is approximately 1 μm , an ideal SERS active substrate needs to have uniform distribution of nanoparticles on a submicrometer scale in order to achieve high degree of reproducibility. This is a critical issue that must be addressed when paper is used as a SERS substrate, since it is a challenge to achieve uniform distribution of nanoparticles on paper due to its high roughness and porosity. In addition, due to high sensitivity of SERS, the paper substrates must be free of additives or fillers to avoid any background or fluorescence interference during the analysis.

2.4. Antimicrobial

AgNPs have been widely used in a range of bactericidal applications due to their broad-spectrum antimicrobial activities and high toxicity to different type of micro-organisms [23]. The antimicrobial properties of AgNPs are dependent on their concentration and rate of Ag ions released to the micro-organisms. AgNPs are inert in their metallic state, but become ionized upon contact and reaction with

Table 1
Roadmap of nanoparticles.

Nanoparticles	Titania (TiO ₂)	Gold (AuNPs)	Silver (AgNPs)
Structures and properties anatase, rutile, brookite.	<ul style="list-style-type: none"> • Three major crystalline forms: • Rutile is predicted to be the most stable phase. • Anatase is the most photoactive form. • TiO₂ surface exhibit coordination vacancies and occupied by hydroxyl groups through water chemisorption. • Raman scattering peaks of TiO₂ nanoparticles become broader as their size decreases. • Photocatalyst: wide band gap semiconductor capable of converting light energy into chemical redox energy. • Reversible/switchable superhydrophilic and superhydrophobic properties. 	<ul style="list-style-type: none"> • Size and shape dependent optical properties. • Surface plasmon band (SPB) tuned by nanoparticle size, shape and surface functionalities. • Oscillation frequency influenced by dielectric constant of surrounding materials and types of solvent used. • Electromagnetic properties influenced by degree of dispersion and proximity. • Colors highly dependent on interparticle distance where a color shift from red to blue results when individual spherical AuNPs aggregates and comes into proximity. (interparticle plasmon coupling). 	<ul style="list-style-type: none"> • Properties dependent on size, shape, synthesis method and differences in dielectric environment. • Good conductivity. • Chemical stability. • Antibacterial and antimicrobial. • Highest efficiency of plasmon excitation among all three metals (Ag, Au and Cu) – plasmon resonances within visible spectrum. • Highest SERS signal enhancement among other metal nanoparticles.
Common methods of synthesis	<ul style="list-style-type: none"> • Solution routes – Precipitation – Sol–gel: non-alkoxide and alkoxide – Combustion – Electrochemical • Gas phase method – Chemical vapor deposition – Physical vapor deposition – Spray pyrolysis deposition 	<ul style="list-style-type: none"> • Bottom up (chemical) – Nanosphere lithography – Citrate reduction method – Seeding technique – Two-phase reaction • Top down (physical) – Photolithography – Electron beam lithography 	<ul style="list-style-type: none"> • Bottom up (chemical) – Lee–Meisel method – Borohydride, citrate, ascorbate, and elemental hydrogen reduction • Top down (physical) – Microwave irradiation – Photo-reduction – Microemulsion • Biological – Enzymatic reduction – Non-enzymatic reduction
General applications	<ul style="list-style-type: none"> • Photocatalysis • Stain-proofing and self-cleaning • Gas and humidity sensors • Photovoltaics • Photocleavage of water • Photodegradation of organic pollutants 	<ul style="list-style-type: none"> • Homogenous and heterogeneous catalysis • Biosensors • Drug and protein delivery • SERS • Anti-counterfeiting 	<ul style="list-style-type: none"> • Excellent catalyst • Antimicrobial products • Colorimetric sensor • Enhanced Infrared absorption spectroscopy • SERS • Anti-counterfeiting

moisture of skin or wound [24]. The strong reactivity of ionized Ag causes cell destruction and death, as the bacterial cell wall undergoes structural changes once it binds to tissue proteins.

The antimicrobial properties of AgNPs are believed to be size-dependent, where smaller AgNPs, with larger surface areas accessible for interaction provide more antimicrobial effect than larger AgNPs [25]. In this case, aggregation of AgNPs on the paper structure must be avoided to produce an efficient antimicrobial paper. This is because the aggregation will drastically decrease the accessibility of nanoparticles' surface, resulting in insufficient functionality. Therefore, homogenous distribution of AgNPs over the paper surface is preferred for better contact and reaction with the micro-organisms. The potential toxicity of AgNPs to human is still a matter of considerable debate. Hence, strong binding forces between AgNPs and paper substrate are desirable to reduce possible exposure.

3. Attachment methods of nanoparticles to paper

There are many publications and patents describing methods of attachment/binding of nanoparticles onto paper, particularly for TiO₂-functionalized paper. A brief review of the major strategies is presented in this section. Basically, there are two approaches for attaching nanoparticles onto paper, “wet-end addition”, where nanoparticles are adhered onto individual fibers before paper sheet formation, and “surface treatment”, where dry paper sheet is impregnated with nanoparticles by passing through a bath of chemicals which impregnates the paper surface or by coating [26].

3.1. Wet-end addition

Wet-end addition is more commonly used to prepare TiO₂ photocatalytic paper. Fukahori et al. [27] and Iguchi et al. [28] produced

photocatalytic papers, which are made of TiO₂ supported by ceramic fibers, using the wet-end addition process. A TiO₂-containing paper of high stability was fabricated by preferential immobilization of photoactive TiO₂ nanoparticles onto the inorganic fibers, followed by incorporation into the layered pulp fiber network. This TiO₂ paper was made from beaten pulps and ceramic fibers according to Technical Association of the Pulp and Paper Industry (TAPPI) Test Methods T205. As shown in Fig. 4, the TiO₂ paper displayed a remarkably higher photocatalytic performance than TiO₂ powder and pulp mixture. This synergy is due to the paper's macrovoid structure, and the paper strength is maintained by presence of the ceramic and TiO₂ fiber matrix. However, the retention of TiO₂ on the paper surface may be insufficient due to drainage force occurring during the filtration process.

A patent by Nishibori [29] explained preparation of molded photocatalytic pulp from waste paper (preferably from newspaper) and TiO₂ using a thermoplastic resin in a dry forming process. The process involved stirring a photocatalytic pulp mixture comprise of pulp, TiO₂ and thermoplastic resin (which acts as a binder). The heat and impact force generated by shearing were used to dry the mixture and drive the TiO₂ nanoparticles to the fiber's surface. Next, a foaming agent was added into the photocatalytic pulp, followed by molding, drying and laminating to produce a laminated photocatalytic paper. The foamed and molded photocatalytic paper has high air and water permeability which serves as an excellent photodecomposition filter.

3.2. Surface treatments

Surface treatments are more promising than the wet-end addition, since nanoparticles can be concentrated near the paper surfaces. The extent of penetration of the nanoparticles into paper is controllable by the paper's hydrophobicity (sizing) and porosity (paper structure). There are different types of surface treatments, but we only intend to review the

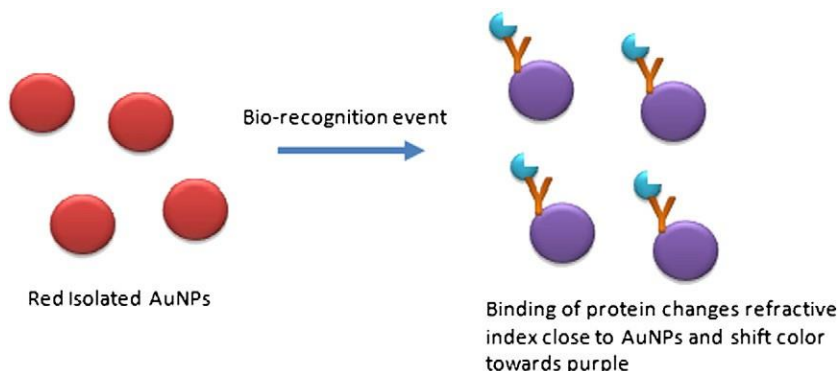


Fig. 3. Colorimetric detection of biological targets by AuNPs. (redrawn from [18]).

major existing methods to coat or impregnate nanoparticles onto paper, which are size press, layer-by-layer deposition (LbL), sol–gel method, direct assembly and in situ assembly.

3.2.1. Size-press treatment

Dry paper sheets are generally coated with a mixture of TiO_2 and different types of binder, to produce photocatalytic paper by using a size press in the papermaking process. [26]. There are several patents which incorporate different binders to coat TiO_2 onto paper substrates. For instance, colloidal silica used by Ahlstrom [30], resin binders used by Eln Kohsan Co. [29] and silicone binders used by Nippon Soda [31]. These binders play an important role in immobilizing TiO_2 onto paper and protecting the paper from photodegradation by TiO_2 at the same time. Aguedach et al. [32] and Railard et al. [33] also coated paper with a mixture of TiO_2 and colloidal silica using a size press. These studies highlighted the role of silica binder in increasing adsorption capacity of TiO_2 to produce an efficient photocatalyst which is able to decompose textile dye in wastewater. Compared to TiO_2 powder, the textile dye removal by the photocatalyst paper, which consists of silica supported TiO_2 , is more economical and effective since it avoids the tedious and costly filtration step of TiO_2 from the water. However, characterization of the TiO_2 coating, such as thickness and distribution, was not studied; this knowledge is crucial in determining the optimum efficiency of photocatalysis.

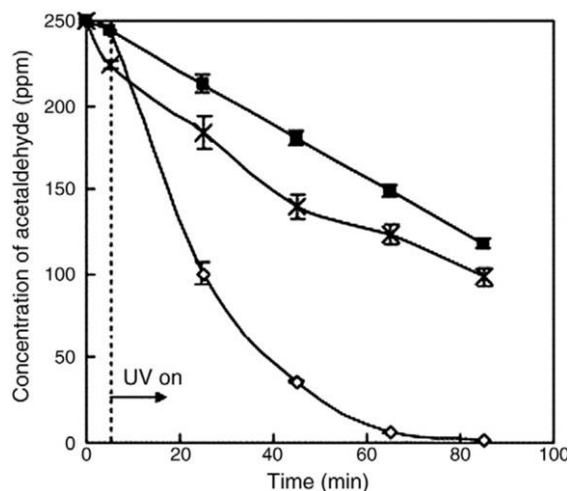


Fig. 4. Photodecomposition of acetaldehyde vapours by TiO_2 powder (crosses), TiO_2 paper (open diamonds) and pulp/ TiO_2 mixture (closed squares). Reprinted from [27], Copyright (2007), with permission from Elsevier.

3.2.2. Layer-by-layer deposition (LbL)

LbL deposition is a technique based on adsorption of oppositely charged polyelectrolytes on a solid substrate (Fig. 5). Lu et al. [34] coated lignocellulose fibers with well-organized multilayers of linear polyelectrolyte and TiO_2 . Positively-charged TiO_2 nanoparticles were alternately attached onto the surface of the wood fibers with negatively-charged Poly(styrenesulfonate) (PSS), using the standard LbL assembly process. During the adsorption of TiO_2 , some hydrogen bonding between lignocellulose fibers and TiO_2 were replaced by electrostatic attraction of the positive and negative polyelectrolyte fiber coatings. This electrostatic bonding between fibers and fillers was able to increase the paper's dry strength drastically. Thicker layers of polyelectrolyte increased the fiber interactions in paper, producing structures of higher dry strength and porosities. However, wet strength of the resultant paper, which is important for photocatalytic usage in water, was not discussed in their work. Although increasing the thickness of polyelectrolyte layer increases the paper's strength, it also causes TiO_2 nanoparticles to pile up and shield themselves from light and pollutants, reducing their photocatalytic activity. Therefore, an optimum TiO_2 and polyelectrolyte layer thickness must be obtained to achieve high photocatalytic efficiency without compromising the paper strength.

Pinto et al. [36] also synthesized and deposited silica-coated AuNPs onto cellulosic fibers. This was the first time that cellulose was used as substrate for LbL assembly of AuNPs. The cellulose fibers were previously treated with polyelectrolytes to provide cationic charge by alternate dipping in poly(diallyldimethylammonium chloride) (polyDADMAC), poly(sodium 4-styrenesulfonate) (PSS), and again in the polyDADMAC solutions (the basis of the layer-by-layer method). These treated cellulose fibers were then immersed in the Au colloids. The silica shells ensured that the individual Au cores were well separated, and prevented variation of plasmon oscillation frequency in the final assemblies. The adjustable optical properties, which can be obtained by modifying the surface of nanoparticles with silica shells, made these nanocomposites very attractive, particularly in the manufacture of security paper [36]. Since it is important to prevent aggregation of AgNPs which will reduce their antimicrobial efficiency, this method could also be applied for AgNPs to develop antimicrobial paper, since the silica shells are able to maintain a good distribution of nanoparticles on the cellulose surface. However, diffusion of nanoparticles into the polyelectrolyte macromolecule should be further studied because this would reduce their contact with light and pollutants, thus decreasing their performance.

3.2.3. Sol–gel method

Sol–gel method for deposition of TiO_2 onto cellulose fibers is developed from the processing of sol–gel TiO_2 composites. It introduces negatively-charged functional groups which anchor TiO_2 on cellulose surfaces [37]. Uddin et al. [37] developed an easy and reproducible procedure for anchoring TiO_2 to cellulose by sol–gel technique, to produce self-cleaning, antibacterial and photochromic

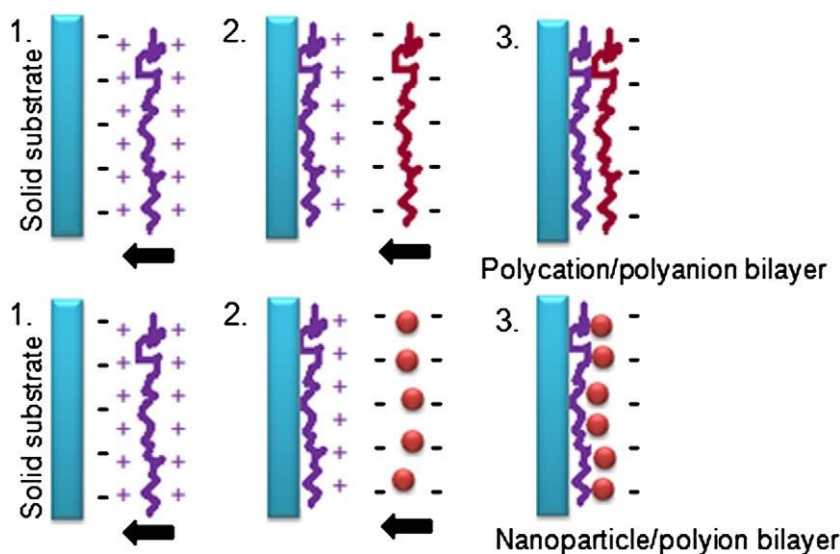


Fig. 5. Layer-by-layer coating method. (redrawn from [35]).

surfaces. Continuous and homogeneous distribution of TiO_2 films was formed on the surface of fibers, thus enhancing photodegradation of pollutant molecules. The TiO_2 film did not promote a simultaneous degradation of cellulose fibers, even though it was highly efficient in pollutant degradation. They suggested that this is due to the homogeneous characteristics of the TiO_2 film which completely adheres and protects the fibers from attack by O^{2-} and OH^\bullet species generated during the exposure to light.

3.2.4. Direct assembly

In direct assembly, AuNPs and AgNPs are usually synthesized by citrate reduction of aqueous Au and Ag salt solutions and then assembled onto paper. The citrate groups serve the dual role of reducing agent and stabilizer [38]. They impart negative surface charges to nanoparticles from weakly bound citrate ions, which prevent agglomeration in solution and immobilize them on the substrates through electrostatic self-assembly [39].

Dong and Hinestroza [38] made cationic cellulose from cotton via grafting of positively charged ammonium ions for electrostatic deposition of AuNPs. The AuNPs are directly assembled onto cellulose by immersing cationic cellulose into a citrate-reduced Au colloidal solution. Increasing concentration of the citrate enhanced negative surface potential of AuNPs and led to higher packing density of AuNPs on the substrate. Their procedure shows promise to allow deposition of other negatively charged metal nanoparticles onto cationically-modified cellulose substrates. Yet, the adsorption state of nanoparticles must be controlled to achieve a reproducible distribution, since it affects optical properties of the nanoparticles.

Wu et al. [9] and Ma et al. [40] performed direct synthesis of gold and silver colloids by chemical oxidation–reduction reactions, using potassium tetrachloroaurate (KAuCl_4) and silver nitrate (AgNO_3). The resulting colloids were added drop wise onto filter papers for SERS application. These studies illustrate the high potential of nanoparticles coated paper as a highly SERS active substrate. However, the spotting method described is not able to provide a reproducible and uniform distribution of nanoparticles on paper substrates as more aggregation will be formed at the edge of the droplets during the drying process (coffee stain phenomenon). Position of laser beam on the nanoparticles' droplets during the SERS experiment was not specified in these studies (either on the edge or the center of the nanoparticles' droplet). This is critical because the aggregation state of nanoparticles is the main contributing factor to the SERS performance.

In another interesting approach, Zhao et al. [10] synthesized DNA crosslinked AuNPs to produce a thermally-stable bioactive paper. Thiol-modified DNA was added to a citrate-reduced AuNP solution for DNA coupling. The blue colored DNA-cross-linked AuNP aggregates were then deposited on paper substrates. When endonuclease and adenosine were present, the bioactive paper degraded the crosslinked AuNP aggregates producing a deep red color. DNA crosslinked AuNPs were spotted on different types of paper substrates. Hydrophobic and (poly(vinyl alcohol)-coated) hydrophilic paper were found to be the best biosensor substrates, whereas untreated hydrophilic paper caused “bleeding” and precipitation resulting from surface drying [10]. This work demonstrates the feasibility of functionalizing paper substrates with AuNPs to produce an effective, renewable and disposable bioactive paper. Nanoparticles can be dried on paper, heated and stored whilst still maintaining their aggregation/dispersion, as well as their activity upon subsequent exposure to target analytes.

3.2.5. In situ assembly

In situ assembly is initiated by attaching metal complex ions onto cationically-modified cellulose surfaces. Dong and Hinestroza [38] performed this method by a first immersion of cationic cellulose substrate into a sodium tetrachloroaurate dihydrate ($\text{NaAuCl}_4 \cdot 2\text{H}_2\text{O}$) solution, followed by immersion in a sodium borohydride (NaBH_4) solution to reduce the metal ions to zero-valence metal. Compared to the direct assembly method, in situ assembly does not require protective citrate ions. The absence of citrate ions can be helpful in applications such as catalysis, since their surface coverage may reduce the reactivity of the nanoparticles [38]. However, no comparison between surface coverage or adsorption state of AuNPs on the paper substrates produced by both direct and in situ methods has been presented.

Cai et al. [41] performed another in situ formation of AuNPs in cellulose gel by physical reduction method. Transparent cellulose hydrogel films were immersed in a HAuCl_4 solution, followed by heating at 80°C for 24 h to achieve hydrothermal reduction. Highly dispersed and thermally-stable AuNPs were formed in the cellulose gels [41]. The high porosity, near transparency and high mechanical strength of these AuNPs impregnated cellulose gels offer an attractive substrate for nanoparticle synthesis/support medium. This composite material is interesting for use in molecular detection via transmission UV–Vis spectroscopy. The presence of molecules will change the dielectric constant of the AuNPs and produce a shift in their

absorbance peak. However, distribution reproducibility of AuNPs within the cellulose gels needs to be addressed.

He et al. [42] performed in situ synthesis of AgNPs in the porous cellulose fibers from lint-free cellulose paper and filter paper. The size distributions of the nanoparticles were controlled by adjusting synthesis conditions such as the concentration of metal ion, resulting in monodispersed metal nanoparticles. The ether oxygen and hydroxyl groups of cellulose bind the metal ions tightly onto the fibers through ion–dipole interactions and stabilize AgNPs by strong bonding with their surface metal atoms.

Fernández et al. [43] found that nanoparticle size is important for high antimicrobial activity; samples, with large, aggregated AgNPs being almost ineffective. They performed in situ synthesis of AgNPs in fluff pulp and nanostructured Lyocell fibers by immersion in AgNO_3 , and subsequent transformation of the attached silver ions into AgNPs by physical (thermal/UV) and chemical (NaBH_4) reduction. The AgNPs formed by physical methods were uniform in shape and well distributed, whilst chemical reduction produced aggregation of AgNPs [44]. This finding is important because both methods can be used for different applications; e.g. physical methods can be applied to produce antimicrobial paper (where well distribution of AgNPs is preferred), whilst chemical methods can be used to produce a SERS-active substrate (where aggregation of AgNPs is preferred).

4. Applications of nanoparticles-functionalized paper

4.1. Titania paper

4.1.1. Self-cleaning

The unique combination of photocatalytic and hydrophilic properties of TiO_2 has markedly increased their application range, especially as a coating on cellulosic materials such as paper [45]. The ability of water to soak between stain and highly hydrophilic TiO_2 surface results in easy and efficient stain removal. Hence, TiO_2 -coated surfaces have been widely used in outdoors. An example is a Japanese paper window blind with excellent self-cleaning properties, wherein stain is decomposed by photocatalysis and washed off by rainfall.

In a related area, Uddin et al. [46] developed cotton fibers covered by a thin Au/TiO_2 film which are also photocatalytically-active under solar light. The Au/TiO_2 -covered cotton fibers show high efficiency in Methylene Blue (MB) photodegradation, suggesting highly photocatalytic properties under solar light. The sol–gel synthetic method covers the cotton fibers with TiO_2 and Au/TiO_2 films, which ensured a great stability for repeatable washing cycles and prolonged photodegradation. These composite cotton fibers show high potential and commercial significance for self cleaning under visible light [46].

4.1.2. Organic destruction

Organic destruction is a common mechanism where organic targets, such as organic dye and volatile organic compounds (VOCs), are adsorbed onto TiO_2 surface via attachment by reactive oxygen species (ROS), or direct oxidation by donating electrons to trapped holes on the TiO_2 surface [26]. Matsubara [12] and Iguchi et al. [28] described the preparation of TiO_2 handsheets and their use to decompose acetaldehyde vapors; and since then many studies have improved the photocatalytic properties of TiO_2 paper in terms of organic destruction. Commercial TiO_2 paper-based products have been extensively used as air filter papers, wallpapers, calendars, writing papers and magazines [28].

Hashimoto et al. [14] designed photocatalytic sheets to sanitize VOCs-polluted soil by using natural sunlight. As shown in Fig. 6, the photocatalytic sheet is made of corrugated paper consisting of TiO_2 attached on activated carbon powders. Polluted soil can be purified by covering it with the sheet, followed by heating via mixing with calcium oxide. This procedure volatilizes the pollutant gases, which then adsorb on the activated carbon of the sheet. TiO_2 subsequently decomposes the pollutants by photocatalytic mechanism.

According to Pelton's review [26], there are a few commercial applications of photocatalytic TiO_2 paper. Ahlstrom has made photocatalytic nonwoven products since 1996 [47]. Nippon Paper (Tokyo, Japan) has developed “Light Catalytic Newsprint” with Yomiuri, one of Japan's largest newspaper publishers [48]. The newsprint contained TiO_2 which cleaned the surrounding air photocatalytically when irradiated by UV and visible light (Fig. 7). Nippon Paper [48] has also produced air-deodorizing tissue box which can purify air for babies, rooms with pets and the interior of vehicles.

4.1.3. Disinfection

TiO_2 paper can detect pathogenic organisms and disinfect, by destroying their cellular structure. Most common disinfection technologies are insufficient to kill microorganisms since some generate exotoxins (heat sensitive proteins) and endotoxins (lipopolysaccharides) that remain after the bacteria is eliminated [26]. However, it was shown that TiO_2 can destroy the endotoxins which are associated with *Escherichia coli* (*E. coli*) photocatalytically. Matsubara et al. [12] reported that *E. coli* on TiO_2 -containing paper was almost completely disinfected by 90 min upon UV light irradiation. Geng et al. [6] studied the feasibility of producing paper with antibacterial properties based on the photocatalytic activity of TiO_2 ; 80% of the bacteria deposited onto the photocatalytic paper were killed by 30 min exposure to 25 W/m^2 UVA [6]. It was discovered that the water content of the paper must be at least 40%, and that the

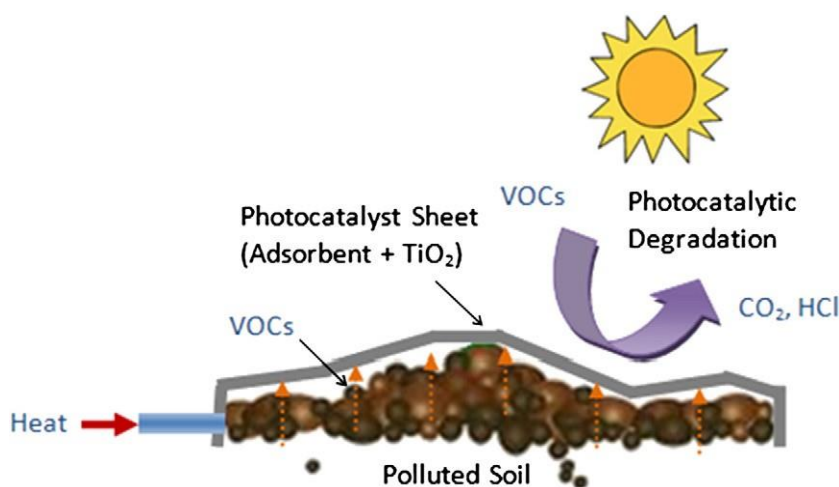


Fig. 6. Purification of polluted soil using solar energy and photocatalytic TiO_2 paper. (redrawn from [45]).

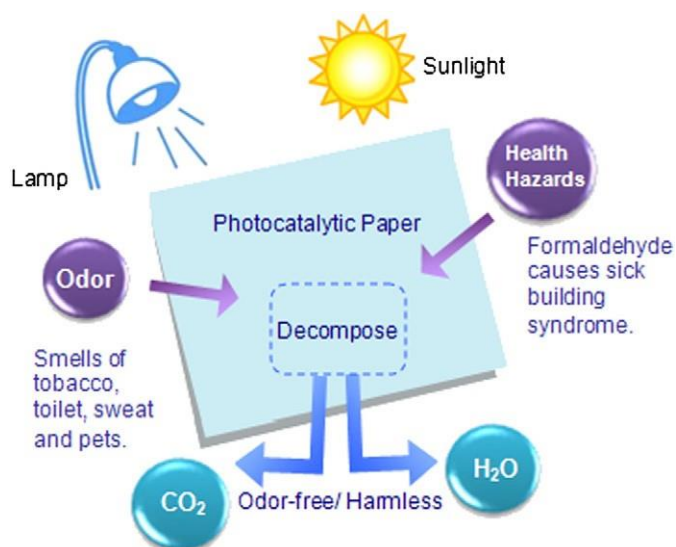


Fig. 7. Organic destruction by photocatalytic paper. (redrawn from [49]).

TiO₂ must be well positioned on the exposed surface to attain this good performance.

The market for antibacterial paper containing TiO₂ is significant. Domtar [50] launched North America's first antimicrobial office paper for protection against bacteria growth, surrounding odours, fungus, mould and mildew in order to reduce the propagation of bacteria in offices. Japan [51] developed the technology to adhere small amounts

of anatase TiO₂ to pulp. They produced an antibacterial wall paper which utilized paper's natural porous surface to absorb bacteria or hazardous substances floating within a hospital room, and paper's filtering function to fully decompose them.

4.2. Gold nanoparticle paper

4.2.1. Colorimetric sensor

Innovative developments in bioactive papers and paper microfluidic system can be found with applications in blood testing [52], biomolecular stability [53–55] and functional printing [56,57]. Martinez et al. [58] demonstrated the prospect of paper as a platform for bioassays where dye molecules were responsible for color changes that were altered by enzymatic reactions. Since then, the potential of AuNPs (which possess a higher extinction coefficient than dye molecules on paper) as a biosensor has been explored. Liu and Lu demonstrated a AuNPs' dipstick assay in their publication [59] and patent [60]. This dipstick assay detects target analytes by immersing a lateral flow device into a testing solution. Blue-colored aggregates of AuNPs were immobilized on the lateral flow device. They were broken into red-colored dispersed AuNPs upon addition of target analytes in the flow buffer (Fig. 8). However, these devices involve rather complicated components such as wicking pads, conjugate pads, polymer membranes, absorbent pads and plastic adhesive backing, which may limit their practical use.

Zhao et al. [10] prepared a paper-supported AuNPs biosensor (gold bioactive paper) which is capable of detecting the presence of DNase I, an endonuclease (Fig. 9), as well as adenosine, a small biomolecule (Fig. 10). This sensitive biosensor can be dried on paper, heated and stored while still maintaining its activity during the detection of target solution. Basically, it functions based on the unique SPR of AuNPs:

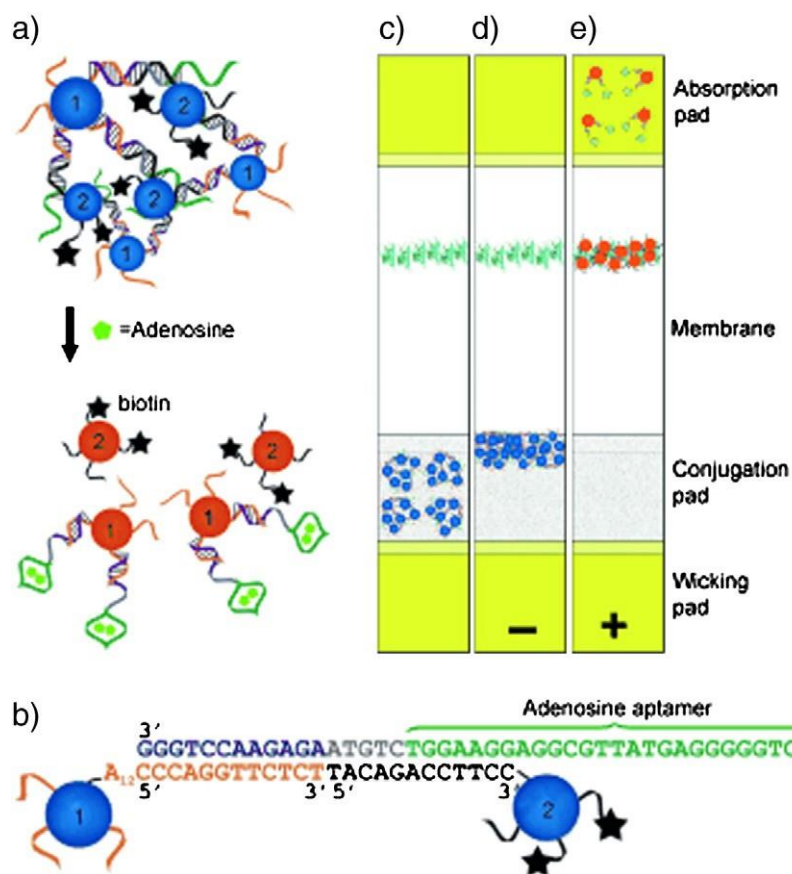


Fig. 8. Aptamer (nucleic acid that specifically binds a target compound or moiety)/nanoparticle-based lateral flow device. (a) Blue color of AuNP aggregates is broken into red colored AuNP dispersion upon the addition of adenosine. (b) DNA sequences and linkages in AuNP aggregates. Lateral flow devices loaded with the aggregates (on the conjugation pad) and streptavidin (on the membrane in cyan color) (c) before use and in (d) negative or (e) positive test. Reprinted with permission from [59]. Copyright 2010 WILEY-VCH.

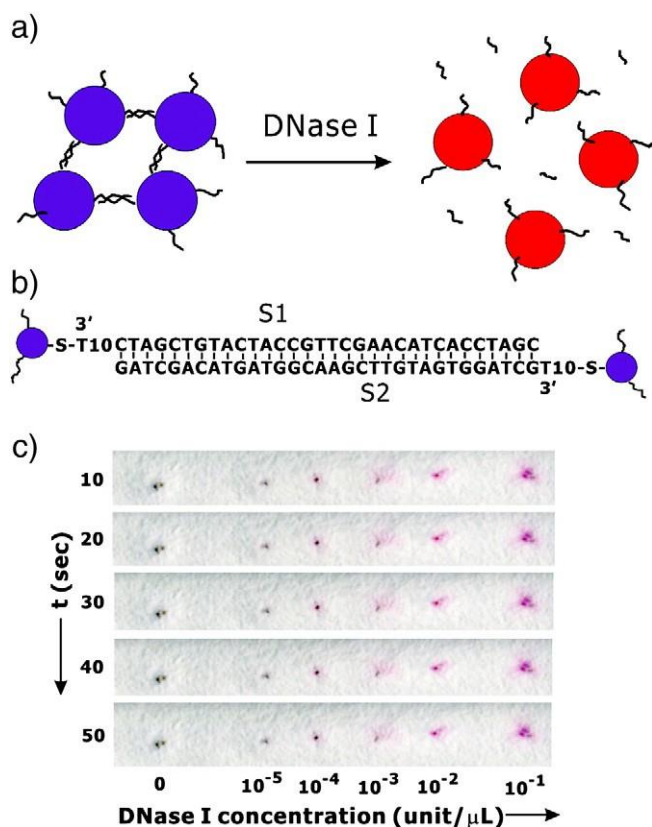


Fig. 9. DNase I-sensing bioactive paper. (a) Color shift from blue to red when redispersion of DNA crosslinked AuNP aggregates is triggered by the addition of DNase I. (b) The sequences of DNA oligonucleotides. (c) Reaction of DNase I assay on PVA-coated hydrophilic paper [10]. Copyright (2008), with permission from American Chemical Society. (For interpretation of the references to color in this figure legend, the reader is referred to the web version of this article.)

well-dispersed AuNPs show a red color; whereas aggregated AuNPs have a blue or purple color. These significant color changes can be detected whenever the aggregation and redispersion of AuNPs are

triggered by a target analyte or a biological process. Since the interparticle plasmon coupling results in a huge absorption band shift (up to 300 nm), the color shift can be observed instantly by naked eye without analytical instrumentation [10].

By controlling the interparticle distance of the AuNPs, their corresponding aggregation and dispersion can give visual detection for a wide range of biological entities. This makes AuNPs a perfect transmitter for paper-based assays. Furthermore, the AuNPs sensor is cost effective, as only small volumes (1 μL in the Zhao's work [10]) of both DNA–AuNPs aggregate probes and target samples are required due to the exceptionally high extinction coefficient of AuNPs.

4.2.2. Rewritable paper

Klajn et al. [61] developed a novel self-erasing material which consists of AuNPs and AgNPs embedded in thin, flexible organogel films. Both “writing” and self-erasure of color images are controlled by dynamic non-equilibrium aggregation of the NPs (Fig. 11). Upon exposure to UV light, the trans-4-(11-mercaptopundecanoxyl)azobenzene (trans-MUA) groups, which coat the NPs, isomerize to cis-azobenzene (cis-MUA), having a large dipole moment [61]. The NPs then aggregate into supra-spherical (SS) assemblies, whose apparent color depends on the duration of UV irradiation.

Since the SS are metastable and fall apart spontaneously in the absence of UV irradiation, the two-color or multicolor images written onto the films gradually self-erase. Erasure times can be controlled by the number of dipoles induced on the NPs, and can also be accelerated upon exposure to visible light or heat [61]. Multiple images can be written into the same film, either concurrently or sequentially after erasure.

These materials are practical for storing temporary information such as self-expiring tickets. However, the organogels used are not environmentally-friendly, hence alternative substrates, such as paper, and technologies, such as coating and printing, should be explored.

4.2.3. SERS

Surface-enhanced Raman scattering (SERS) using AuNPs is an exceptional technique for quantifying the adsorption of target molecules on substrates, and allowing different orientations and interactions of the molecules with the substrates to be determined [9].

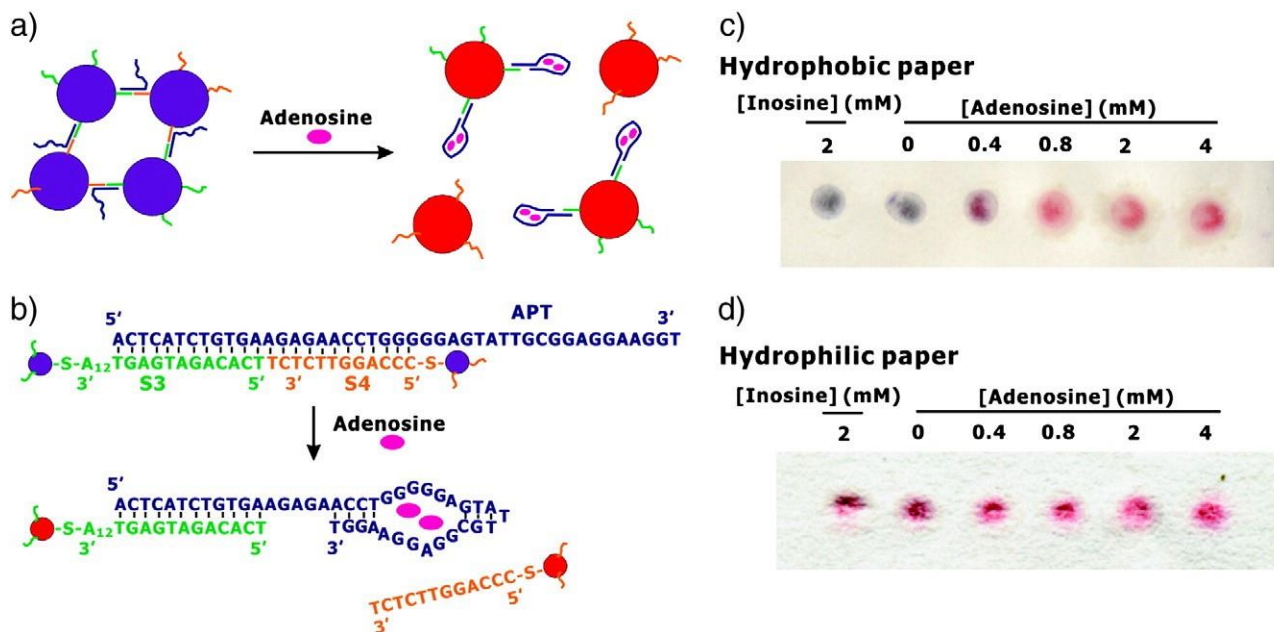


Fig. 10. Adenosine-sensing bioactive paper. (a) Color shift from blue to red when redispersion of DNA crosslinked AuNP aggregates is triggered by the addition of Adenosine. (b) The sequences of the DNA molecules used. (c) and (d) Reaction of Adenosine assays on hydrophobic and hydrophilic paper. Reprinted from [10], Copyright (2008), with permission from American Chemical Society. (For interpretation of the references to color in this figure legend, the reader is referred to the web version of this article.)

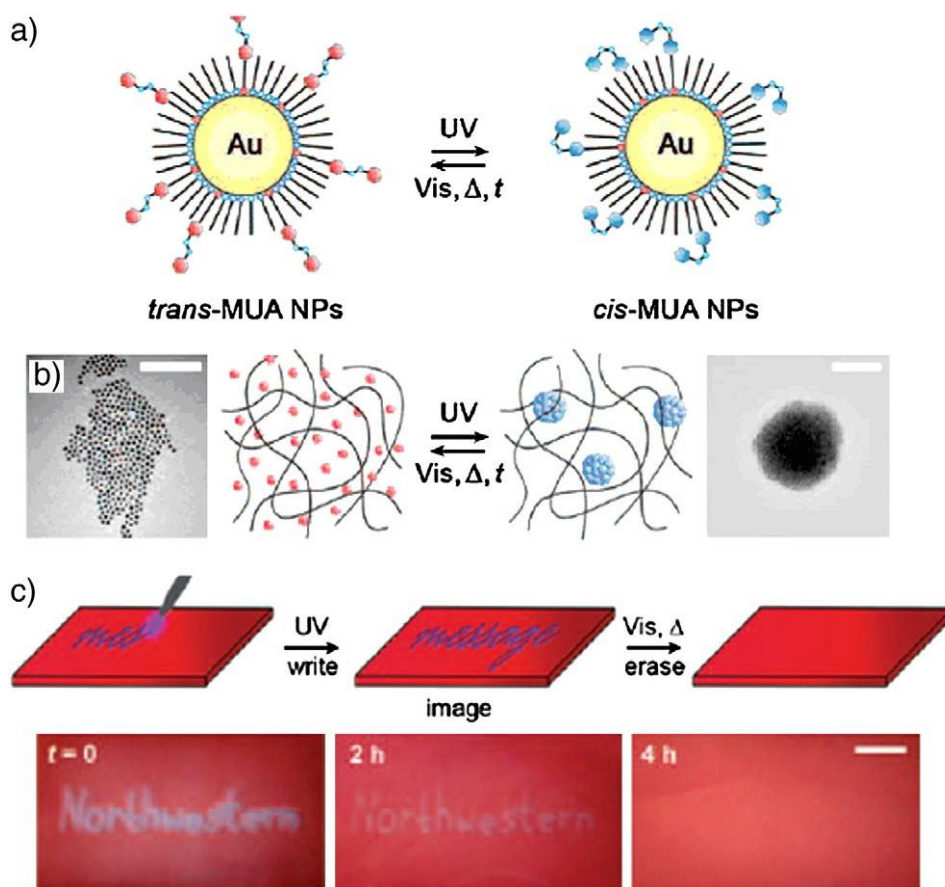


Fig. 11. Self-erasing films for rewritable paper. (a) Upon UV irradiation, *trans*-MUA coated AuNPs isomerize to *cis*-MUA. (b) During UV irradiation, photoactive AuNPs (red) form metastable aggregates (blue) (c) Writing into AuNPs film using a light pen ($I_{UV} = 10 \text{ mWcm}^{-2}$) at 3 mms^{-1} . Reprinted with permission from [61]. Copyright 2009 WILEY-VCH. (For interpretation of the references to color in this figure legend, the reader is referred to the web version of this article.)

Single molecule detection is achievable via SERS and this concept has been used to design protein and nucleic acid biosensors [62].

A highly SERS-active substrate is the most important factor in producing efficient SERS applications. Previously, aqueous metal colloids were employed in most SERS techniques, but this limits the application of SERS since the specimen analyzed must be water-soluble. To overcome this restriction and enhance the SERS techniques, solid and rough SERS-active surfaces such as nanorod arrays on glass [63], metal island films formed through thermal evaporation [62,64] and laser ablated metal plates [65] were explored. However, these methods involve complex preparations of substrates, which limit the applications of SERS. Filter paper coated with AuNPs offers a much simpler method and the compounds examined do not have to be water-soluble.

Luo et al. [66] and Ma et al. [40] demonstrated the use of AuNPs-coated filter paper in a variety of SERS measurements. They studied the SERS of C60/C70 adsorbed on filter paper coated with highly SERS active AuNPs. This AuNPs paper had a greater enhancement factor than AuNPs solution, since it was not influenced by solvents in a C60/C70 solution or water in gold hydrosols [66]. They discovered that the distribution and aggregation of AuNPs strongly influenced the SERS intensity of C60/C70 and that the Raman intensity saturated as the thickness of AuNPs coating was increased. However, the ideal aggregation state of nanoparticles and paper structure were not identified nor explored.

Niu et al. [44] also reported SERS spectra of single-walled carbon nanotubes (SWCNTs) on AuNPs-coated filter paper. Enhancement of common Raman spectrum of SWCNTs, as well as several new bands, were obtained (Fig. 12) [44]. These produced an excellent sensor for analyzing fine molecular structures. Furthermore, this method is promising and highly sensitive for examining feature of SWCNTs, compared to the existing methods.

SERS spectra of *p*-, *m*-, and *o*-nitroaniline (PNA, MNA, and ONA) adsorbed on AuNPs were also studied by Ma et al. [40] on dried AuNPs-coated filter paper. They found that the coverage density of AuNPs affected the SERS spectra of the PNA molecules, but did not affect MNA and ONA. The adsorption performance of molecules is dependent on the substrate's surface and the surface configurations of adsorbate. This demonstrates the potential of AuNPs-coated filter paper as a powerful tool for studying the surface configuration of

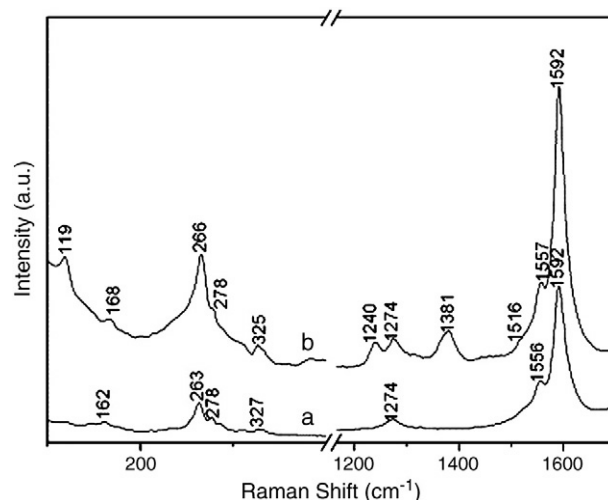


Fig. 12. (a) Raman spectrum of SWCNTs and (b) SERS of SWCNTs on gold coated filter paper. Reprinted from [44]. Copyright (2006), with permission from Elsevier.

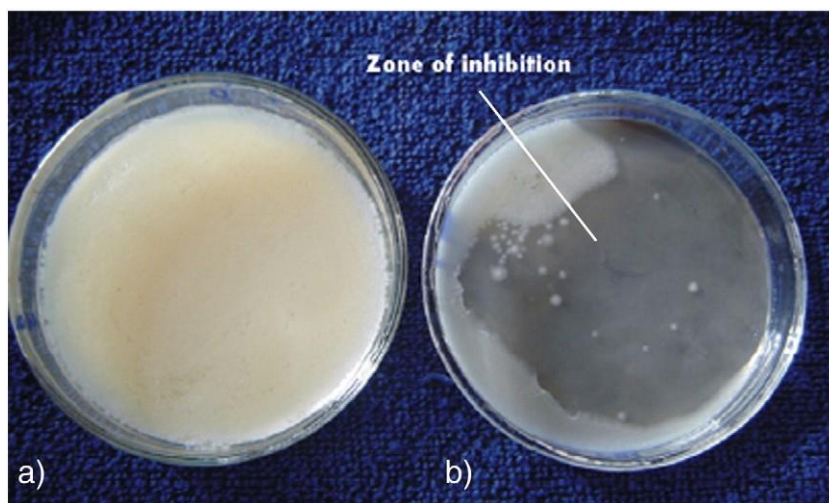


Fig. 13. (a) Growth of bacterial colonies around grafted filter paper (b) zone of inhibition around the AgNPs loaded grafted filter paper. Reprinted from [7], Copyright (2009), with permission from Elsevier.

molecules in SERS applications. However, little information on the AuNPs-paper interaction or their heterogeneity has been provided.

4.3. Silver nanoparticle paper

4.3.1. Antimicrobial

With increasing awareness of disease and infection transmissions from microorganisms, the number of antimicrobial products such as protective clothing for medical and chemical works, antibacterial packaging materials and tissue papers has recently increased. AgNPs are well known for their broad spectrum antimicrobial activity. They deactivate bacteria by interacting with thiol groups of bacterial proteins and enzymes [23].

Fernández et al. [43] studied cellulose substrates as holders of AgNPs to form a cellulose-AgNPs hybrid material in order to preserve aseptic conditions in an absorbent pad. Relationships between both Ag ion release and antimicrobial efficiency against *E. coli* and *Staphylococcus aureus* bacteria were confirmed. Furthermore, the highest concentrations tested were able to decrease microbial content in poultry exudates. Therefore, AgNPs shows high potential to be used in the food industry. In a separate study, Tankhiwale and Bajpai [7] developed AgNP-loaded filter papers with excellent antimicrobial properties against *E. coli* (Fig. 13). The degradable nature of paper makes it an attractive alternative for antibacterial food-packaging material, as a replacement for synthetic polymeric films [7]. However, the effects of distribution and bonding strength of AgNPs on the paper structure were not reported.

4.3.2. SERS

Similar to AuNPs, AgNPs can also be coated on paper to produce a highly SERS-active substrate. Niu et al. [44] obtained a SERS spectrum of Single Wall Carbon Nanotubes (SWCNTs) on AgNPs-coated filter paper which can be used as a highly sensitive probe for analyzing the synthesis quality of SWCNTs (Fig. 14). The AgNPs SERS substrates have a higher Raman signal enhancement than AuNPs. However, since the Ag metal surface tends to oxidize in air, it has a limited durability as a SERS substrate compared to AuNPs [67].

Wu et al. [9] also obtained excellent SERS signals of p-hydroxybenzoic acid (PHBA) on AgNPs-coated filter paper. The adsorption state of PHBA molecules on AgNPs-coated filter paper was unlike the adsorption in the AgNPs colloid. The molecules were located in an upright position on the surfaces of the AgNPs colloids through the carboxyl moiety, but were tilted between the benzene ring and the surfaces of AgNPs on the filter paper [9]. As shown in Fig. 15, AgNPs-

coated filter paper provided higher SERS signal of PHBA than AgNPs colloid.

Laserna et al. [68] [69] [62] reported the assembly, morphology and optical properties of AgNPs-coated filter paper as a promising substrate for SERS. High and reproducible spectra of a range of ionic and molecular adsorbates including p-aminobenzoic acid, acridine, 9-aminoacridine, 2-aminoanthracene, 6-nitroquinoline and 5-a minoquinoline were achieved [70]. These filter-paper substrates could be used when a random dispersion of particle sizes and shapes is required, but were inadequate for theoretical studies requiring monodispersed systems. However, the main advantages of AgNPs-coated filter papers are their ease of use, low production cost and detection speed.

4.3.3. Anti-counterfeiting

Counterfeiting has increased around the world where almost all kinds of documents including banknotes, passports, certificates, bus and train tickets have been virtually forged [8]. More advanced security printing methods are continuously being designed to protect such documents, including security inks and security paper. Fluorescence plays a key function in many of these anti-counterfeiting technologies by identifying source subject from detected optical

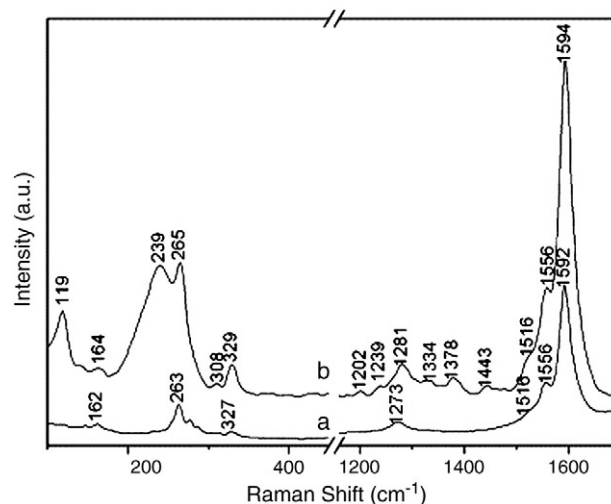


Fig. 14. (a) Raman spectrum of SWCNTs and (b) SERS of SWCNTs on silver coated filter paper. Reprinted from [44], Copyright (2006), with permission from Elsevier.

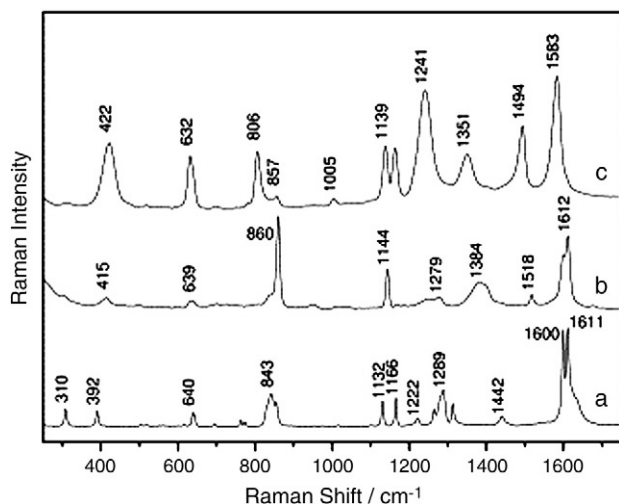


Fig. 15. (a) Raman spectrum of solid PHBA (b) FT-SERS spectra of PHBA in AgNPs solution and (c) on AgNPs-coated filter paper. Reprinted from [9], Copyright (2003), with permission from Elsevier.

signal through irradiation [8]. However, fluorophores typically have low quantum yield and poor photostability, which lead to their photophysical limitation. AgNPs can augment the fluorescence emission intensity of up to 3000-fold upon close contact with the fluorophores and increase their detection limits [8]. Numerous studies have reported fluorescence emission from different AgNP surfaces, such as AgNP colloids, nano-triangles and nano-rods, as well as fractal-like AgNP surfaces.

Zhang et al. [8] first reported metal-enhanced fluorescence (MEF) from AgNPs-coated filter paper. The luminescence intensities of Rose Bengal (RB) and Pt(II) octaethylporphine (PtOEP) were increased by 5- and 9-fold, respectively, on AgNPs-deposited paper substrates (Fig. 16). The background luminescence emission from standard filter paper is rather large, but could be reduced subsequently by MEF. This work shows the great potential of AgNPs-functionalized paper to be used in security paper and anti-counterfeiting applications.

5. Challenges and opportunities

Most studies have relied on paper as an inert support for nanoparticles and very few, if any, have considered the distribution of nanoparticles in the three dimensions (3D) of paper, or the concept of heterogeneity and the effect of manipulating different length scales

possible. Furthermore, little attention has been devoted to engineer the properties of nanoparticles-paper composite. In some instances of photocatalysis, SPR and SERS, nanoparticles on paper have provided better properties than unsupported nanoparticles (in air or in solution). Hence, there clearly remains some substrate-nanoparticles effect that can be optimized. Various nanoparticles-functionalized papers, which are reviewed in this article, differ mostly in terms of type, size, shape, aggregation and content of nanoparticles, as well as their distribution within the 3D paper structure. The vast majority of studies used filter paper which is entirely made of cellulose fibers (cotton, softwood), without any additives such as fillers or dye. The structure, chemical composition and heterogeneity length scale of paper can now be well engineered and controlled with current technology. It is therefore of interest to investigate the optimal structure and chemical composition of paper for each application, whether it relies on SPR, SERS, colorimetric or photocatalytic principles. This section analyses the effect of heterogeneity, interaction between light with nanoparticles-functionalized paper (optical and photocatalytic properties) as well as their analytical techniques.

5.1. Paper chemical and physical heterogeneities

Paper is a heterogeneous substrate involving many length scales of physical and chemical periodicity. Paper can be considered as a non-woven material made of short discontinuous fibers with additives. From a chemical point of view, paper is made of lignocellulosic fibers and functional additives. Commonly used additives are inorganic filler (calcium carbonate, titanium dioxide, kaolin), dyes (UV brightener, colour, anti-yellowing), sizing agents (Alkyl Ketene Dimer (AKD), Alkenyl Succinic Anhydride (ASA), rosin/alum), retention aids (poly-electrolytes: Polyacrylamide (PAM), Polyethyleneimine (PEI); neutral polymers: Polyethylene Oxide (PEO), starch; and microparticles: bentonite, silica), coating (latex, starch, calcium carbonate, styrene maleic anhydride) and strength agents (Polyamide-epichlorohydrin (PAE), Carboxymethyl cellulose (CMC), Poly(diallyldimethylammonium chloride) (polyDADMAC)). As additives are normally added at 0.5 to 5 kg/ton fibers and with processes to maximize the dispersion, they form distinct chemical domains on the fibers at a surface coverage typically ranging from 5 to 50%. The length scales of the chemical domains are in the order of 0.1 nm for the dyes, 10–50 nm for the polymer coils and polymer domains, 100–2000 nm for the fillers.

Paper is mostly made of softwood fibers (length (L) = 2–3 mm, diameter (d) = 20–30 μ m) or hardwood fibers (L = 1–2 mm, d = 10–20 μ m) and fines/small fiber fragments (L = 50 μ m, d = 1 μ m). Fig. 17 presents the comparative length scale of the paper constituents. From

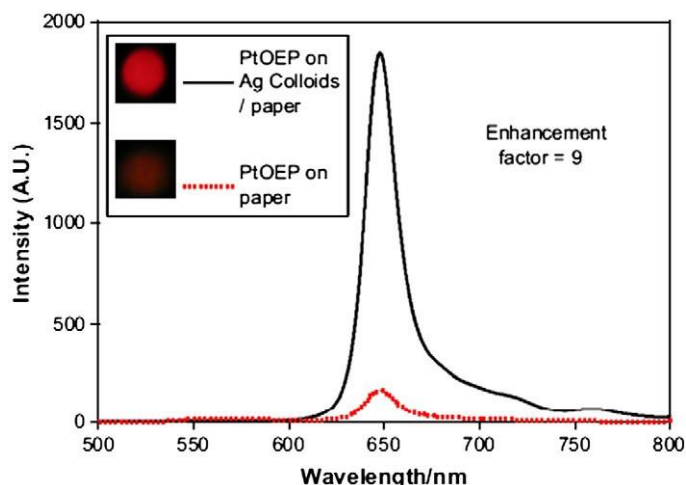
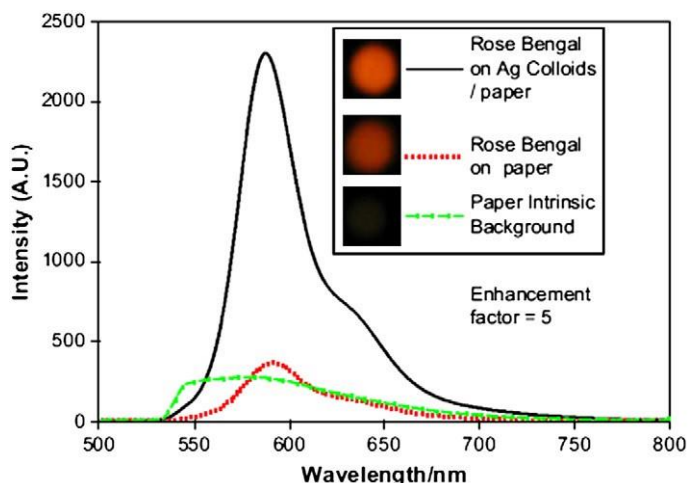


Fig. 16. Fluorescence emission spectra of Rose Bengal on paper and Ag colloid deposited paper (left) and fluorescence emission spectra of PtOEP on paper and Ag colloid-deposited paper (right). Reprinted from [8], Copyright (2008), with permission from Elsevier.

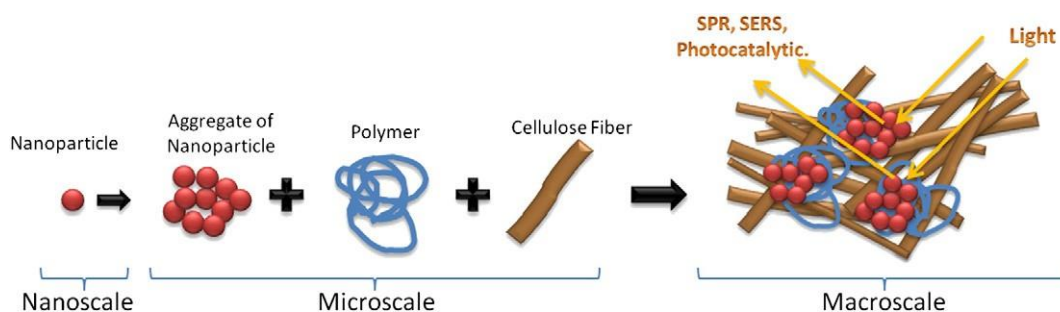


Fig. 17. Different length scales of the constituents of paper.

a physical aspect, paper has complementary length scales ranging over 7 decades, from the nanometer (nanoparticles) to the centimeter (fiber floc). Important physical heterogeneity is found in the 3D structure of paper. In the X–Y plane, there is a distinct fiber floc size distribution (often referred to as formation) and a preferential fiber orientation. Small fibers in a suspension have a tendency to flocculate as they lose some of their rotational and translation freedom due to a crowding effect amplified by the fiber concentration, rigidity and length. Since the fiber flocs are not completely destroyed during the dewatering process on the drainage wire, the paper web is made of periodic zones of high fiber density having diameters ranging from 2 to 12 mm. These flocculated zones have slightly different optical, strength and absorption properties than the bulk of paper.

Paper is made by impinging a suspension of cellulosic fibers onto a continuous wire moving (1000 to 2500 m/min) over a series of drainage elements. Any speed differential between the wire and the furnish solution therefore causes a preferential fiber alignment. In “rushing”, fibers are impinged at a velocity typically 5 to 50 m/min slower than the wire, therefore causing preferential fiber alignment in the machine direction (MD); in “dragging”, the fiber furnish is deposited at a faster speed than the moving wire, causing preferential alignment in the cross-machine direction (CD).

All these processes result in paper having a networked, heterogeneous and highly porous structure. Paper pore diameter ranges over five orders of magnitude, corresponding to interfiber gap (100 μm), cellulose fiber cell wall's pore (bordered pit with torus 1–10 μm) and fibrils' thickness and gap (nm). Hence, there are many capillarities in the pores in which nanoparticles can be attached.

5.2. Optical properties

Amongst all of the unique properties of nanoparticles, their optical properties on novel substrate supports have gained the most research interests in chemical and biosensing. This is due to large electromagnetic fields generated in the vicinity of their surface when excited near plasmon frequency. High localization of this electromagnetic energy renders their optical properties as excellent SPR and SERS probes. Since the optical properties of nanoparticles are responsive to electric permittivity of their surrounding medium, they will also be affected by the presence of their substrates. Effects of substrates on the optical properties of nanoparticles are well addressed by a full numerical solution of Maxwell's equations [71] and other numerical techniques such as finite-difference time-domain [72] and discrete dipole approximation [73]. However, these methods do not account for substrate-nanoparticles interactions for heterogeneous substrates (e.g. paper) in which nanoparticles are absorbed within the cellulose fiber matrix. Consequently, there is still no clear understanding on how paper substrates can influence the optical properties of nanoparticles.

In this review, we proposed three important factors which affect the optical properties and light interactions between nanoparticles and paper substrates: (1) spatial location of nanoparticles, (2) refractive index of paper substrates and (3) aggregation state of nanoparticles within the

cellulose fibers of paper substrates. As shown in Fig. 18, the spatial location of nanoparticles after absorption on paper substrate (Fig. 18b) is different compared to their location on flat substrates such as glass (Fig. 18a). The penetration of nanoparticles through the rough and porous structure of paper will produce a different light interaction compared to a flat and nonporous substrate. To our knowledge, no study has analyzed the effect of refractive index and thickness of nanoparticles-impregnated paper (Fig. 18c) on the optical properties of nanoparticles. We propose that the intertwined structure of cellulose fibers is able to retain the aggregate state of nanoparticles upon drying (Fig. 18d), which is important to control their SPR and SERS properties. However, the reproducibility of the aggregation and adsorption state of nanoparticles are restricted by the roughness and random fibrous morphology of paper substrates. Therefore, more in-depth studies are required to understand the optical properties of nanoparticles paper as functions of location of nanoparticles, refractive index, and aggregation state of nanoparticles within the paper substrates.

5.2.1. SERS and SPR

SERS is optimal when contact points of multiple metal nanoparticles (Au, Ag) enhance the intensity of Raman scattering. This means that aggregates made of very small NPs would provide best use of the noble

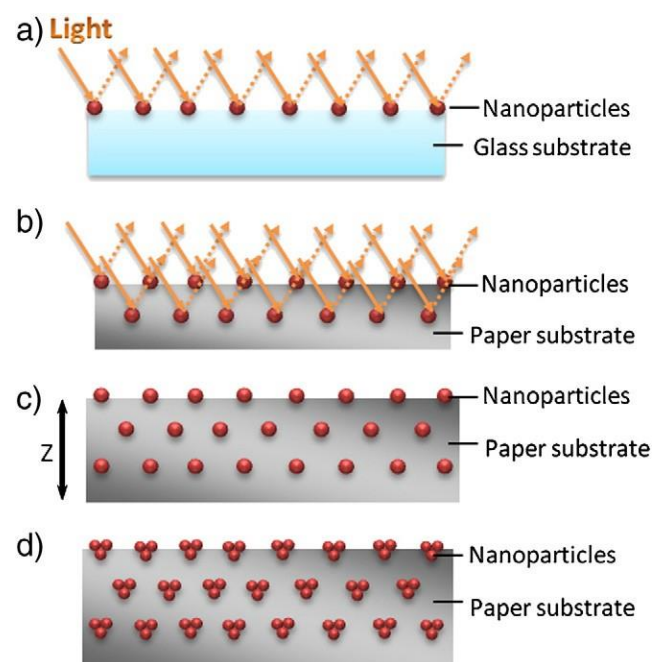


Fig. 18. Schematic cross section illustration of light interaction with (a) nanoparticles on a glass substrate, (b) nanoparticles on a paper substrate, (c) Thickness, z of nanoparticles paper, (d) Ideal control of aggregation state of nanoparticles on paper substrates.

metals. However, at some point as the aggregate size increases, light will not be able to reach the inner most nanoparticles within the paper substrate, and clearly an optimum in the size of nanoparticles' aggregate is expected. Little is known on the effect of aggregate polydispersity, size or distribution within 3D porous media have on SERS performance. Furthermore, there has been no effort to optimize the structure of paper for SERS applications. So far, filter paper has been used as an inert substrate. Preliminary results in our laboratory have shown that SERS intensity of analyte adsorbed on AuNPs can be higher on paper than in aqueous solution. This suggests that there exists a preferential 3D structure for nanoparticles and that the interaction between nanoparticles and paper can be beneficial. The effect of substrate refractive index (air, water, cellulose) and heterogeneity on SERS is therefore of interest.

SPR is controlled by the nanoparticles' diameter, shape, volume fraction and aggregate state, dielectric constant, refractive index and interparticle distance. The challenge for SPR applications of nanoparticles-functionalized paper is to report the event in a simple and convenient way. In most analytical SPR techniques (such as for the BIAcore), adsorbed target molecules are detected by measuring a shift in plasmon angle which indicates a change in refractive index caused by change of mass at the interphase (around 50 nm above of AuNPs). Specificity is assured by immobilizing probe specific molecules such as antigens and enzymes that only bind with the analyte of interest (such as antibody, substrate). For paper tests, this practice is not convenient due to the diffused reflectance characteristic of the paper surface. Direct use of color change upon the shift of surface plasmon would be preferred. However, porosity of paper as well as size of nanoparticles and their aggregates should be optimized to allow easy dispersion and aggregation of nanoparticles within the cellulose structure of paper upon detection of target molecules.

5.3. Photocatalytic properties

TiO₂-functionalized papers suffer a major drawback, low degradation rate. Currently, the time frame of degradation of organic compounds by TiO₂ photocatalytic reaction (hours–days) is often orders of magnitudes longer than the typical period of product use (seconds–minutes). Strategies involving the capture and retention of the component or pathogen are then used to compensate this mismatch. What is the maximum photocatalytic reaction rate of TiO₂? And how can paper best be engineered to operate TiO₂ under its optimum conditions? These are two critical questions. The photocatalytic degradation of a component/pathogen involves two steps: (1) light irradiation of TiO₂ and its substrate,

(2) UV emission from TiO₂; alternative steps include: (3) the retention of contaminant/pathogen within the porous structure and (4) the liberation of degradation products. These last two steps are diffusion-controlled phenomena which are slow. A priori, TiO₂ nanoparticles are best dispersed at the external surface, forming a TiO₂ monolayer on paper. This configuration would maximize steps 1 and 2.

Is there an opportunity to amplify incident light of the emitted UV through design of the paper structure on reflecting additives? Should entrapment of microorganisms and organic compounds within paper be useful? Would semi-permeable external layers of TiO₂ over a porous paper structure maximize photocatalysis and pathogen capture/retention within paper? Development is needed to identify these questions and maximize the critical optical properties of the TiO₂ functionalized paper and cellulosic fibers.

5.4. Analytical techniques

There is a vast literature on understanding the colloid and surface science related to adsorption of nanoparticles from their colloidal suspensions onto a solid substrate and control of their arrangements. However, most research has focused on the adsorption assembly of nanoparticles onto flat substrates, such as glass and silicon. There is a lack of understanding on the underlying mechanisms involved in the self-assembled architectures of nanoparticles on the imperfect, rough and fibrous paper surface. The analytical techniques for nanoparticles-functionalized papers need to be focused on three length scales: nano, micro and macro. This involves quantifying the dispersion and aggregation state of nanoparticles (nanoscale), analyzing the adsorption state and coverage of nanoparticles on the microporous paper surface (microscale) as well as exploring the optical properties of nanoparticles-functionalized paper (macroscale). By merging these three lines of analytical techniques, a novel methodology to enhance the properties of nanoparticles-functionalized paper can be achieved.

Nanoparticles-functionalized paper has promising applications due to their unique photocatalytic, SPR, SERS and antimicrobial properties. Controlling these properties depends particularly on a fundamental understanding of the dispersion and aggregation state of nanoparticles on paper. Quantification techniques such as zeta potential sizing, electronic microscopy analysis (SEM, TEM) coupled with image analysis (Fig. 19) are able to characterize the interaction between paper substrates and nanoparticles as well as the dispersion/aggregation state of the nanoparticles on paper. Characterization techniques such as UV–Vis spectroscopy and Raman analysis can also be employed to quantify the

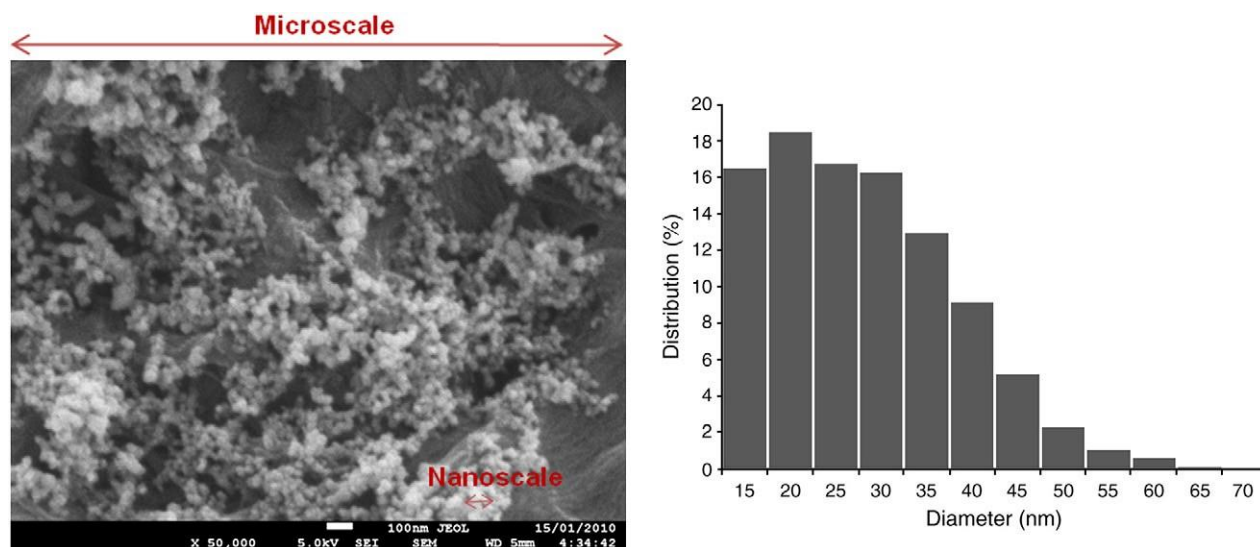


Fig. 19. SEM with image analysis (analysed via Image J) for analyzing the distribution and adsorption state of TiO₂ on filter paper substrate. Unpublished results from [74].

properties of the nanoparticles-functionalized paper. Since nanoparticles-functionalized paper has great potential as photocatalytic, SPR and SERS active substrates, it is critical to develop comprehensive analytical techniques to achieve reproducible nanoparticles-functionalized paper substrates.

6. Conclusion

A critical review of the properties, attachment methods and applications of nanoparticles-functionalized paper has been presented. Three types of nanoparticles were reviewed: titania, AuNPs and AgNPs. Paper is a low cost, cellulosic non-woven and only a very small volume fraction of these nanoparticles is needed to significantly alter its properties, especially the photocatalytic and optical properties. The emerging applications of nanoparticles-functionalized paper mostly involve interaction of light with the nanoparticles. These applications can be divided into three categories: (1) low-cost diagnostics for health and environment, (2) photocatalytic, disinfections and antimicrobial non-woven products, and (3) anti-counterfeiting and security papers.

Most previous research has focused on demonstrating some novel application of nanoparticles-functionalized paper. Filter paper has been universally used as an inert support due to simplicity, and there remains a lack of understanding of paper as a composite. Very few studies have characterized the distribution of nanoparticles within paper, and none has optimized paper as a nanoparticles' substrate. The application of nanoparticles-functionalized paper for SERS and SPR is a new technology in which some synergetic effects of nanoparticles-paper have been observed but not explained. Different adsorption state of nanoparticles would produce different coupling of electromagnetic fields surrounding the nanoparticles. These regions of high electromagnetic field intensity are responsible for large enhancement effects of their optical signals. Therefore, controlling the absorption state of nanoparticles on the paper surface (i.e. singlet, doublet or triplet) is critical in achieving the desired magnitude of the SERS and SPR effects.

There is a need to better understand interaction of light-nanoparticles and how it is affected by the distribution of nanoparticles within the heterogeneous structure of paper substrate. More specifically, for each application, whether it is SPR, SERS or photocatalysis, the question remains as to the best spatial distribution of nanoparticles within the 3D structure of paper. What is their critical aggregation state? How can it best be achieved? A few of the related challenges include the ability to: (1) control the state of particle aggregation or size of nanoparticles on paper, and (2) control the average distance between nanoparticles and the spatial location of nanoparticles within the 3D heterogeneous paper structure. Better and simpler analytical techniques are also desired for quantifying the distribution of nanoparticles, to produce the best conditions for SERS, SPR, photocatalytic and other specific applications.

The properties of paper also need to be optimized. Paper is a heterogeneous, porous composite. Effects of different length scales of its physical and chemical heterogeneity can be reconciled with the distribution of nanoparticles and the properties of the composites. For example, the optical properties of paper (refractive index, opacity) can be engineered using dyes, treating fibers and functionalized micro-particles. Papermaking also offers opportunities to engineer the chemical composition, 3D structure and heterogeneity length scale of paper. Furthermore, coating nanoparticles on paper by printing is an attractive process to enhance nanoparticles-functionalized paper in terms of reproducibility. Nanoparticles-functionalized paper can become a disruptive technology for diagnostics and catalysis, should the critical challenges be overcome, whilst retaining the low cost and product/process flexibility associated with papermaking, surface treatment and printing.

Acknowledgements

Many thanks to Dr. Peter Miller and Dr. Tim Williams from the Monash Centre for Electron Microscopy (MCEM) for discussions and SEM technical suggestions. The financial supports of the ARC Linkage – Project grant (LP0989823), the Australian Pulp and Paper Institute and Monash University are acknowledged.

References

- [1] Farhang B. Nanotechnol lipids Lipid Technol 2007;19:132–5.
- [2] Xu X, Stevens M, Cortie MB. In situ precipitation of gold nanoparticles onto glass for potential architectural applications. Chem Mater 2004;16:2259–66.
- [3] Hutter E, Cha S, Liu JF, Park J, Yi J, Fendler JH, et al. Role of substrate metal in gold nanoparticle enhanced surface plasmon resonance imaging. J Phys Chem B 2000;105:8–12.
- [4] Wang Y, Yang Q, Shan G, Wang C, Du J, Wang S, et al. Preparation of silver nanoparticles dispersed in polyacrylonitrile nanofiber film spun by electrospinning. Mater Lett 2005;59:3046–9.
- [5] Klajn R, Wesson Paul J, Bishop Kyle JM, Grzybowski Bartosz A. Writing self-erasing images using metastable nanoparticle inks. Angew Chem Int Ed 2009;48:7035–9.
- [6] Geng X, Filipe C, Pelton R. Antibacterial paper from photocatalytic TiO₂. Appita J 2008;61:456–60.
- [7] Tankhiwale R, Bajpai SK. Graft copolymerization onto cellulose-based filter paper and its further development as silver nanoparticles loaded antibacterial food-packaging material. Colloids Surf, B 2009;69:164–8.
- [8] Zhang Y, Aslan K, Previte MJR, Geddes CD. Metal-enhanced fluorescence from paper substrates: modified spectral properties of dyes for potential high-throughput surface analysis and assays and as an anti-counterfeiting technology. Dyes Pigm 2008;77:545–9.
- [9] Wu D, Fang Y. The adsorption behavior of p-hydroxybenzoic acid on a silver-coated filter paper by surface enhanced Raman scattering. J Colloid Interface Sci 2003;265:234–8.
- [10] Zhao W, Ali MM, Aguirre SD, Brook MA, Li Y. Paper-based bioassays using gold nanoparticle colorimetric probes. Anal Chem 2008;80:8431–7.
- [11] Fujishima A, Honda K. Electrochemical photolysis of water at a semiconductor electrode. Nature 1972;238:37–8.
- [12] Matsubara H, Takada M, Koyama S, Hashimoto K, Fujishima A. Photoactive TiO₂ containing paper: preparation and its photocatalytic activity under weak UV light illumination. Chem Lett 1995;24:767–8.
- [13] Carp O, Huisman CL, Reller A. Photoinduced reactivity of titanium dioxide. Prog Solid State Chem 2004;32:33–177.
- [14] Hashimoto K, Wasada K, Osaki M, Shono E, Adachi K, Tokai N, et al. Photocatalytic oxidation of nitrogen oxide over titania-zeolite composite catalyst to remove nitrogen oxides in the atmosphere. Appl Catal, B 2001;30:429–36.
- [15] Fujishima A, Rao TN, Tryk DA. Titanium dioxide photocatalysis. J Photochem Photobiol, C 2000;1:1–21.
- [16] DDE Jr, Chumanov G. Synthesis and optical properties of silver nanoparticles and arrays. Chem Phys Chem 2005;6:1221–31.
- [17] Chin C. Fabrication of metallic nanoparticle arrays. Process and Characterization; 2006. [18] Nath N. Gold Nanoparticles: Worth their Weight in Gold! Vol. 20102009
- [19] Fleischmann M, Hendra PJ, McQuillan AJ. Raman spectra of pyridine adsorbed at a silver electrode. Chem Phys Lett 1974;26:163–6.
- [20] Freeman R, Grabar K, Allison K, Bright R, Davis J, Guthrie A, et al. Self-assembled metal colloid monolayers: an approach to SERS substrates. Science 1994;267:1629–32.
- [21] Michaels AM, Jiang J, Brus L. Ag nanocrystal junctions as the site for surface-enhanced Raman scattering of single rhodamine 6 G molecules. J Phys Chem B 2000;104:11965–71.
- [22] Toderas F, Baia M, Baia L, Astilean S. Controlling gold nanoparticle assemblies for efficient surface-enhanced Raman scattering and localized surface plasmon resonance sensors. Nanotechnology 2007;18.
- [23] Morones JR, Elechiguerra JL, Camacho A, Holt K, Kouri JB, Ramirez JT, et al. The bactericidal effect of silver nanoparticles. Nanotechnology 2005;16:2346–53.
- [24] Rai M, Yadav A, Gade A. Silver nanoparticles as a new generation of antimicrobials. Biotechnol Adv 2008;27:76–83.
- [25] Sharma VK, Yngard RA, Lin Y. Silver nanoparticles: green synthesis and their antimicrobial activities. Adv Colloid Interface Sci 2009;145:83–96.
- [26] Pelton R, Geng X, Brook M. Photocatalytic paper from colloidal TiO₂—fact or fantasy. Adv Colloid Interface Sci 2006;127:43–53.
- [27] Fukahori S, Iguchi Y, Ichiura H, Kitaoka T, Tanaka H, Wariishi H. Effect of void structure of photocatalyst paper on VOC decomposition. Chemosphere 2007;66:2136–41.
- [28] Iguchi Y, Ichiura H, Kitaoka T, Tanaka H. Preparation and characteristics of high performance paper containing titanium dioxide photocatalyst supported on inorganic fiber matrix. Chemosphere 2003;53:1193–9.
- [29] Nishibori S. Process For Producing A Photocatalytic Pulp Composition and Molded Photocatalytic Pulp. United States Patent. Vol. US007060160B2. Japan: Ein Kohsan Co., Ltd.; 2006.
- [30] Escaffre P., Girard P., Dussaud J., Bouvier L. Photocatalytic Composition. United States Patent. Vol. US006878191B2: Ahlstrom Research and Services; 2005.
- [31] Kimura N, Abe S, Yoshimoto T, Fukayama S. Photocatalyst-carrying Structure and Photocatalyst Coating Material. United States Patent. Vol. US006228480B1: Nippon Soda Co., Ltd.; 2001.

- [32] Aguedach A, Brosillon S, Morvan J, Lhadi EK. Photocatalytic degradation of azo-dyes reactive black 5 and reactive yellow 145 in water over a newly deposited titanium dioxide. *Appl Catal B* 2005;57:55–62.
- [33] Raillard C, Héquet V, Le Cloirec P, Legrand J. Kinetic study of ketones photocatalytic oxidation in gas phase using TiO₂-containing paper: effect of water vapor. *J Photochem Photobiol, A* 2004;163:425–31.
- [34] Lu Z, Eadula S, Zheng Z, Xu K, Grozdits G, Lvov Y. Layer-by-layer nanoparticle coatings on lignocellulose wood microfibers. *Colloids Surf, A* 2007;292:56–62.
- [35] Varahramyan K, Lvov Y. Nanomanufacturing by layer-by-layer assembly. *Nanoeeng nanosystems* 2006;220:29–37.
- [36] Pinto RJB, Marques PAAP, Martins MA, Neto CP, Trindade T. Electrostatic assembly and growth of gold nanoparticles in cellulosic fibres. *J Colloid Interface Sci* 2007;312:506–12.
- [37] Uddin MJ, Cesano F, Bonino F, Bordiga S, Spoto G, Scarano D, et al. Photoactive TiO₂ films on cellulose fibres: synthesis and characterization. *J Photochem Photobiol, A* 2007;189:286–94.
- [38] Dong H, Hinestroza JP. Metal nanoparticles on natural cellulose fibers: electrostatic assembly and in situ synthesis. *Appl Mater Interfaces* 2009;1:797–803.
- [39] Henglein A, Giersig M. Formation of colloidal silver nanoparticles: capping action of citrate. *J Phys Chem B* 1999;103:9533–9.
- [40] Ma W, Fang Y. Experimental (SERS) and theoretical (DFT) studies on the adsorption of p-, m-, and o-nitroaniline on gold nanoparticles. *J Colloid Interface Sci* 2006;303:1–8.
- [41] Cai J, Kimura S, Wada M, Kuga S. Nanoporous cellulose as metal nanoparticles support. *Biomacromolecules* 2009;10:87–94.
- [42] He J, Kunitake T, Nakao A. Facile in situ synthesis of noble metal nanoparticles in porous cellulose fibers. *Chem Mater* 2003;15:4401–6.
- [43] Fernández A, Soriano E, López-Carballo G, Picouet P, Lloret E, Gavara R, et al. Preservation of aseptic conditions in absorbent pads by using silver nanotechnology. *Food Res Int* 2009;42:1105–12.
- [44] Niu Z, Fang Y. Surface-enhanced Raman scattering of single-walled carbon nanotubes on silver-coated and gold-coated filter paper. *J Colloid Interface Sci* 2006;303:224–8.
- [45] Hashimoto K, Irie H, Fujishima A. TiO₂ photocatalysis: a historical overview and future prospects. *Jpn J Appl Phys* 2005;44:8269–85.
- [46] Uddin MJ, Cesano F, Scarano D, Bonino F, Agostini G, Spoto G, et al. Cotton textile fibres coated by Au/TiO₂ films: synthesis, characterization and self cleaning properties. *J Photochem Photobiol, A* 2008;199:64–72.
- [47] Ahlstrom. Vol. 2009: Photocatalytic Media; 2006.
- [48] Nippon paper industries develops photocatalytic newsprint with air purification effect. Nippon Paper Group; 2006.
- [49] Japan W. Air-purifying paper. In: Inc. JE, (editor). Vol. 20102008 [50] New antibacterial office paper. Vol. 2009. US: Domtar Paper; 2006 [51] Antibacterial pulp. Vol. 2009. Japan: Ein; 2006.
- [52] Khan MS, Thouas G, Shen W, Whyte G, Garnier G. Paper Diagnostic for Instantaneous Blood Typing. *Anal Chem* 2010;82:4158–64.
- [53] Peng P, Garnier G. Effect of cationic polyacrylamide adsorption kinetics and ionic strength on precipitated calcium carbonate flocculation. *Langmuir* 2010;16949–57.
- [54] Khan MS, Haniffa SBM, Slater A, Garnier G. Effect of polymers on the retention and aging of enzyme on bioactive papers. *Colloids Surf, B* 2010;79:88–96.
- [55] Khan MS, Li X, Shen W, Garnier G. Thermal stability of bioactive enzymatic papers. *Colloids Surf, B* 2010;75:239–46.
- [56] Khan MS, Fon D, Li X, Tian J, Forsythe J, Garnier G, et al. Biosurface engineering through ink jet printing. *Colloids Surf, B* 2010;75:441–7.
- [57] Li X, Tian J, Garnier G, Shen W. Fabrication of paper-based microfluidic sensors by printing. *Colloids Surf, B* 2010;76:564–70.
- [58] Martinez Andres W, Phillips Scott T, Butte Manish J, Whitesides George M. Patterned Paper as a Platform for Inexpensive, Low-Volume, Portable Bioassays13. *Angew Chem Int Ed* 2007;46:1318–20.
- [59] Liu J, Lu Y. A simple and sensitive “dipstick” test in serum based on lateral flow separation of aptamer-linked nanostructures. *Angew Chem* 2006;118:8123–7. [60] Debapriya M., Juewen L., Yi L. Lateral Flow Devices. United States Patent. Vol. 20070269821. United States2007.
- [61] Klajn R, Wesson Paul J, Bishop Kyle JM, Grzybowski Bartosz A. Writing self-erasing images using metastable nanoparticle ‘ink’. *Angew Chem Int Ed* 2009;48:7035–9.
- [62] Bizzarri MSPAR, Cannistraro MSPS. SERS detection of thrombin by protein recognition using functionalized gold nanoparticles. *Nanomed Nanotechnol Biol Med* 2007;3:306–10.
- [63] Kincade K. RAMAN SPECTROSCOPY: SERS and silver nanorods quickly reveal viral structures. *Laser Focus World*; 2007.
- [64] Hesse E, Creighton JA. Investigation of cyanide ions adsorbed on platinum and palladium coated silver island films by surface-enhanced Raman spectroscopy. *Chem Phys Lett* 1999;303:101–6.
- [65] Chen Y-H, Yeh C-S. Laser ablation method: use of surfactants to form the dispersed Ag nanoparticles. *Colloids Surf, A* 2002;197:133–9.
- [66] Luo Z, Fang Y. SERS of C60/C70 on gold-coated filter paper or filter film influenced by the gold thickness. *J Colloid Interface Sci* 2005;283:459–63.
- [67] Coluccio ML, Das G, Mecarini F, Gentile F, Pujia A, Bava L, et al. Silver-based surface enhanced Raman scattering (SERS) substrate fabrication using nanolithography and site selective electroless deposition. *Microelectron Eng* 2008;86:1085–8.
- [68] Berthod A, Laserna JJ, Winefordner JD. Analysis by surface enhanced Raman spectroscopy on silver hydrosols and silver coated filter papers. *J Pharm Biomed Anal* 1988;6:599–608.
- [69] Cabalín LM, Laserna JJ. Fast spatially resolved surface-enhanced Raman spectrometry on a silver coated filter paper using charge-coupled device detection. *Anal Chim Acta* 1995;310:337–45.
- [70] Laserna JJ, Campiglia AD, Winefordner JD. Surface-enhanced Raman spectrometry on a silver-coated filter paper substrate. *Anal Chim Acta* 1988;208:21–30.
- [71] Garnett JCM. Colours in metal glasses and in metallic films. *Philos Trans R Soc A* 1904;203:385–420.
- [72] Jason MM, et al. Theory and modeling of light interactions with metallic nanostructures. *J Phys Condens Matter* 2008;20:323201.
- [73] Noguez C. Optical properties of isolated and supported metal nanoparticles. *Opt Mater* 2005;27:1204–11.
- [74] Ngo Y, Li D, Simon GP, Garnier G. Paper surface functionalized by nanoparticles. APPITA Conference. Melbourne; 2010

Gold Nanoparticle–Paper as a Three-Dimensional Surface Enhanced Raman Scattering Substrate

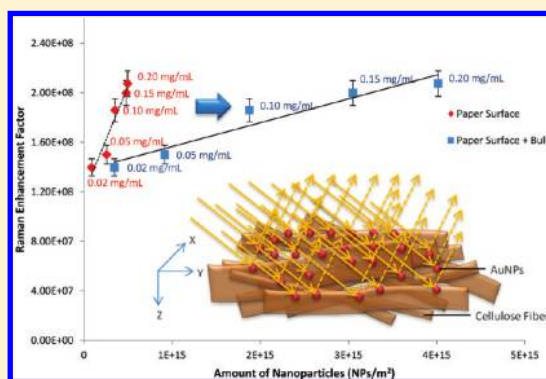
Ying Hui Ngo,[†] Dan Li,[‡] George P. Simon,[‡] and Gil Garnier^{*,†}

[†]BiOPRIA, Australian Pulp and Paper Institute (APPI), Department of Chemical Engineering, Monash University, Clayton, VIC 3800, Australia

[‡]Department of Material Engineering, Monash University, Clayton, VIC 3800, Australia

S Supporting Information

ABSTRACT: This work investigates the effect of gold nanoparticle (AuNP) addition to paper substrate and examines the ability of these composite materials to amplify the surface enhanced Raman scattering (SERS) signal of a dye adsorbed. Paper has a three-dimensional (3D), porous, and heterogeneous morphology. The manner in which paper adsorbs the nanoparticles is crucial to its SERS properties, particularly with regards to aggregation. In this work, we sought to maintain the same degree of aggregation, while changing the concentration of nanoparticles deposited on paper. We achieved this by dipping paper into AuNP solutions of different, known concentration and found that the initial packing density of AuNPs in solutions was retained on paper with the same degree of aggregation. The surface coverage of AuNPs on paper was found to scale linearly to their concentration profile in solutions. The SERS performances of the AuNP-treated papers were evaluated with 4-aminothiophenol (4-ATP) as the Raman molecule, and their SERS intensities increased linearly with the AuNPs' concentration. Compared to AuNP-treated silicon, the Raman enhancement factor (EF) from paper was relatively higher due to a more uniform and greater degree of adsorption of AuNPs. The effect of the spatial distribution of AuNPs in their substrates on SERS activity was also investigated. In this experiment, the number of AuNPs was kept constant (a 1 μ L droplet of AuNPs was deposited on all substrates), and the distribution profile of AuNPs was controlled by the nature of the substrate: paper, silicon, and hydrophobized paper. The AuNP droplet on paper showed the most reproducible and sensitive SERS signal. This highlighted the role of the z-distribution (through film) of AuNPs within the bulk of the paper, producing a 3D multilayer structure to allow inter- and intralayer plasmon coupling, and hence amplifying the SERS signal. The SERS performance of nanoparticle-functionalized paper can thus be optimized by controlling the 3D distribution of the metallic nanoparticles, and such control is critical if these systems are to be implemented as a low-cost and highly sensitive bioassay platform.



INTRODUCTION

Paper has recently been rediscovered as a substrate for low-cost analytical tests in health and environmental applications.^{1–3} Flexible microfluidic systems, reactors, and valves have already been printed on paper to regulate, measure, and control the flow of analytes and reagents.^{3,4} In paper blood typing assays, blood group antigens can be displayed directly by the red blood cells that elude or absorb on paper depending on whether they react with a specific or a nonspecific antibody which was previously adsorbed.⁵ However, the identification of antibodies can be complicated because of their typical low concentration and small dimensions, such as for immunoglobulin G (IgG). While enzyme-linked immunosorbent assay (ELISA) is a standard solution-based technique, its application to paper, while possible, requires multiple reactants and washing steps.^{6,7} A direct approach involving a simple contact between paper substrate and analytes, followed by signal amplification using some instrumentation techniques would be ideal. Surface enhanced Raman scattering (SERS) presents an attractive technique where

analytes such as antibodies can be selectively adsorbed onto antigen-capped metallic nanoparticles on treated paper substrate and detected at very low concentrations.

SERS is a technique that enhances Raman scattering, which measures the small energy changes of the light scattered from a molecule absorbed on a metallic surface, typically a metallic nanoparticle. The enhancement factor (EF) can be as much as 10^{14} – 10^{15} ,⁸ which enables SERS as a single-molecule detection technique to identify analytes at trace levels. The critical requirements of a substrate for SERS application in routine analytical procedures include low cost, sensitivity, robustness, reproducibility, and stability to allow for long-term storage between measurements. The immobilization of metallic nanoparticles onto solid substrates provides an attractive alternative to metal aqueous colloid as SERS substrates because of its higher

Received: April 6, 2012

Revised: May 16, 2012

Published: May 17, 2012



flexibility and easy application to non water-soluble compounds. In particular, there has been significant progress in surface sciences and nanofabrication technology that have allowed the control of size, shape, and aggregation of nanoparticles deposited on conventional SERS substrates such as silicon and glass by electron beam lithography,⁹ focused ion beam patterning,¹⁰ and thermal evaporation.¹¹ However, these techniques are time-consuming, costly, require sophisticated equipment, and the substrates are often fragile and suffer from poor storage stability.

With excellent features such as low cost, flexibility, robustness, long-term stability (1 month to 1 year) and ease of use, paper offers a promising platform as a SERS substrate for bioassays. The soft texture of paper substrates allows conformal contact with the surface of analytes by swabbing.¹² This provides an efficient and practical method to collect traces of analytes from the body and many surfaces, compared to silicon and glass, which are rigid, brittle, and confined to laboratory experiments. Paper is an efficient substrate for routine SERS analysis as highlighted in many articles.^{12–20} However, most of these studies have used paper simply as an inert support and have not explored how the rough, composite, and heterogeneous nature of paper can affect the distribution of nanoparticles and the SERS signal generated.

In this study, the heterogeneity of paper as a SERS substrate was explored by depositing gold nanoparticles (AuNPs) on paper using a dipping method. Our objective was to quantify the effect of AuNPs' concentration and three-dimensional (3D) distribution profile on paper to their SERS performance. Standard filter paper (Whatman #1), which consists of 98% α -cellulose, was selected, as it is a convenient model paper of well-defined structure and it ensures minimal interference from process components (polymers or coatings). The filter papers were dipped into AuNP solutions of different concentration. This simple dipping method was selected to ensure that the size of AuNPs retained on papers is constant, and to minimize aggregation. The distribution profile and particle size of AuNPs adsorbed on papers were characterized by field emission scanning electron microscopy (FESEM)/image analysis. A model Raman dye, 4-aminothiophenol (4-ATP), was adsorbed on the AuNP–paper substrates, and their SERS spectra were measured. To better understand the effect of substrates, AuNPs were also adsorbed onto a silicon wafer and hydrophobized paper, and their SERS spectra were analyzed in terms of signal enhancement and reproducibility. It is the goal of this study to optimize the SERS efficiency of AuNP-coated paper as a platform for emerging bioassay applications.

EXPERIMENTAL SECTION

Materials. Hydrogen tetrachloroaurate trihydrate ($\text{HAuCl}_4 \cdot 3\text{H}_2\text{O}$), sodium citrate tribasic dihydrate ($\text{Na}_3\text{C}_6\text{H}_5\text{O}_7 \cdot 2\text{H}_2\text{O}$), 4-ATP, and alkyl ketene dimer (AKD) were purchased from Sigma-Aldrich and used as received. Whatman filter paper #1 and precut silicon wafers purchased from ProSciTech were selected as substrates. Hydrophobized paper was prepared by treating the Whatman filter paper #1 with AKD. Ultrapure water purified with a Millipore system (18 M Ω ·cm) was used in all aqueous solutions and rinsing procedures.

Synthesis and Deposition of Nanoparticles on Paper. AuNPs were synthesized by using 1 mM $\text{HAuCl}_4 \cdot 3\text{H}_2\text{O}$ and 1% aqueous $\text{Na}_3\text{C}_6\text{H}_5\text{O}_7 \cdot 2\text{H}_2\text{O}$ according to the Turkevich method.²¹ Filter papers were used as received and dipped into Petri dishes that contained 10 mL solution of AuNPs for 24 h. After dipping, the paper substrates were rinsed thoroughly with distilled water to remove loosely bound AuNPs, and the papers were dried and equilibrated at 50% relative humidity and 23 °C before further analysis.

Preparation of Raman Active Substrates. Solutions of 1 mM of 4-ATP were prepared in ethanol. Since 4-ATP is well-known for its strong affinity to the surface of AuNPs (its S–H bond is easily cleaved to form an Au–S bond upon adsorption), the dried AuNP-deposited substrates were dipped into 2 mL of the 4-ATP ethanol solution for a shorter period of time of 5 min to create a 4-ATP monolayer on the substrates. After thorough rinsing with ethanol and drying, the treated papers were subjected to Raman characterization. The Raman EF of 1 mM of 4-ATP on a substrate was calculated according to^{22,23}

$$\text{EF} = \frac{[I_{\text{SERS}}]}{[I_{\text{bulk}}]} \times \frac{[N_{\text{bulk}}]}{[N_{\text{ads}}]} \quad (1)$$

where I_{SERS} is the intensity of a specific band in the SERS spectrum of 4-ATP, and I_{bulk} is the intensity of the same band in the Raman spectrum from the bulk solution sample. For all spectra, the intensity of the band at 1077 cm^{-1} was used to calculate EF values. N_{bulk} is the number of molecules of the bulk 4-ATP in the laser illumination volume, while N_{ads} is the number of molecules adsorbed and sampled on the SERS active substrate within the laser spot.

Instrumentation. FESEM, which produces higher resolution, less sample charging, and less damaged images than conventional FESEM, was performed using a JEOL 7001 field emission gun (FEG) system operating at 5 kV and 180 pA. The ζ potential and dynamic light scattering (DLS) measurements were performed with a Zetasizer Nano ZS (Malvern Instruments) in a folded capillary cell (DTS1060) at 25 °C. UV–vis absorbance was measured using a Varian Cary 300Bio spectrophotometer. All Raman and SERS spectra were obtained in air using a Renishaw Invia Raman microscope equipped with a 300 mW 633 nm laser. The laser beam was positioned through a Leica imaging microscope objective lens (50 \times), while the instrument's wavenumber was calibrated with a silicon standard centered at 520.5 cm^{-1} shift. Due to the smaller spot size of the laser compared with the large surface area of the samples, the spectra were obtained at five different points of the surface. The position of the spectra bands remained the same, but differed only in intensity. The average Raman intensity of five measurements was presented after baseline subtraction from the control sample.

RESULTS AND DISCUSSION

Deposition of AuNPs on Paper. AuNPs are the nanoparticles of choice for analyzing the SERS potential of paper, since they are more stable and less susceptible to oxidation than most other SERS-active nanoparticles, such as silver nanoparticles (AgNPs).²⁴ A stock solution of 0.20 mg/mL of AuNPs was synthesized using the Turkevich method²¹ (method of calculation in the Supporting Information, S1). The resulting red wine-colored AuNPs suspension showed the typical UV–vis absorbance spectra centered at around 530 nm, which was assigned to their surface plasmon resonance (SPR). Particle size measurement by DLS revealed a highly monodispersed AuNPs suspension with an average diameter of 23.2 nm (Supporting Information, S2). During the synthesis of AuNPs, the citrate groups served the dual role of reducing agent and stabilizer.²⁵ The weakly bound citrate ions imparted a negative surface charge onto the AuNPs, which prevented their agglomeration in solution.²⁶ ζ potential analysis revealed a strong negative charge of AuNPs higher than 30 mV, providing colloidal stability.²⁷ AuNPs of different concentrations (0.15 mg/mL, 0.10 mg/mL, 0.05 mg/mL, 0.02 mg/mL) were prepared by diluting the stock solution (0.20 mg/mL). The negative charge of AuNPs decreased upon dilution; this might be due to the decrease in the quantity of citrate-capped AuNPs (Table 1). However, the AuNPs still maintain their stability, even when diluted up to 0.02 mg/mL.

Filter paper samples were dipped into the AuNP solutions for 24 h. This procedure was aimed at keeping the size of AuNPs

Table 1. Effect of Concentration on ζ Potential of AuNPs

	concentration of AuNPs (mg/mL)				
	0.02	0.05	0.10	0.15	0.20
ζ potential (mV)	−36.2	−37.4	−40.9	−43.2	−44.6

retained on the paper constant. The color intensity of the dried AuNP-treated papers was analyzed with ImageJ software (Figure 1). AuNP-treated paper turned from white to red purple, and the color became more intense as the concentration of AuNP solutions was increased.

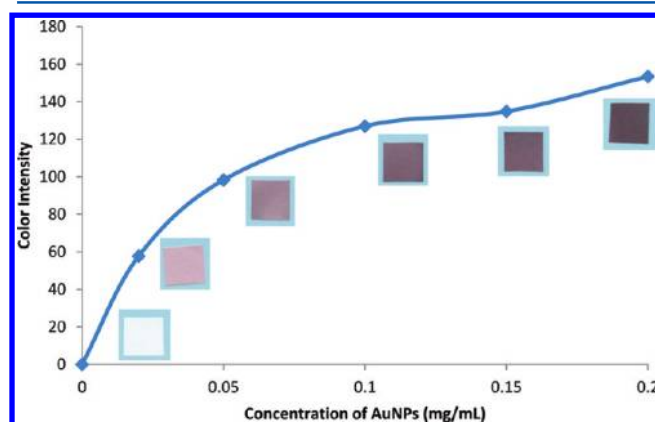


Figure 1. Color intensity of filter papers treated with AuNP solutions of different concentrations.

FESEM images (Figure 2) were analyzed by using ImageJ software to measure the quantity and size distribution of AuNPs adsorbed on paper. The size distribution of AuNPs remained constant for all experiments with an average size of 25 ± 3 nm; this means that most AuNPs are retained on paper as individual particles. The total number of AuNPs was estimated by dividing the total area of AuNPs on paper (in each FESEM image) by the area of an individual AuNP ($d = 23.2$ nm). The concentration of AuNPs on paper increased monotonically with the solution concentration in which the papers were dipped; the particle distribution was denser and more uniform on paper when treated with AuNP solutions of higher concentration. The average distances between the AuNPs on paper decreased from 100 to 200 nm to 10–50 nm (Figure 2). At high concentrations, AuNPs were electrostatically stabilized and closely packed in solution. This high packing density and uniform configuration of AuNPs was retained on the paper. This required the AuNPs to diffuse from solution into the porous structure of paper, adsorb onto a cellulose surface, and resist the capillary forces of drying.

Paper has a weak negative charge caused by the hydroxyl groups of cellulose.²⁸ The AuNPs were well dispersed and adsorbed on paper, even though both materials were negatively charged. Such high adsorption of AuNPs was easily achieved on paper by van der Waals binding without any retention aid. This contrasts earlier works^{12,28} where cationically modified AuNPs/Au nanorods were produced and deemed necessary to achieve effective adsorption on the cellulose fibers.

FESEM cross sectional analysis of 0.20 mg/mL AuNP-treated paper was performed to analyze the distribution of AuNPs through the thickness of the paper substrate (Supporting Information, S3). The AuNPs were relatively uniformly distributed across the thickness of the paper, suggesting intense

electrostatic repulsion among the NPs. AuNPs were present both on the surfaces and within the bulk of paper.

UV–vis analysis was performed on the AuNP solutions before and after paper dipping to quantify the total amount of AuNPs retained on paper from the differences in the intensities of absorbance peaks (Supporting Information, S4). The amount of AuNPs adsorbed on paper increased relatively linearly with the concentration of AuNP solutions into which the paper was immersed. This quantity of adsorbed AuNPs on paper was approximately an order of magnitude higher than that measured from FESEM image analysis (Figure 3). Since the FESEM image analysis (Figure 2) only quantified the number of AuNPs on the paper surface, this suggests that most of the AuNPs were retained within the bulk of paper, as confirmed by the cross-sectional FESEM analysis (Supporting Information, S3). The density of AuNPs in the bulk of paper was estimated by subtracting their density on the paper surface (FESEM) from their total density (UV–vis). There was only 40% of AuNPs adsorbed on both surfaces of paper, while the remaining fraction (60%) appeared to have diffused and adsorbed within the bulk of paper (Figure 3). The attachment of AuNPs on paper is controlled by the 3D network of paper, which consists of a large volume fraction of pores providing strong capillary forces for the diffusion of AuNPs from solution.

4-ATP was selected as the probe molecule in the Raman analysis because of its distinct Raman features, strong affinity for metal surfaces via thiol bonding, and formation of self-assembled monolayers.²⁹ Control paper and AuNP-treated papers were dipped into 1 mM of 4-ATP for 5 min, washed, dried, and analyzed by Raman spectroscopy. The concentration effect of AuNP solutions on the SERS signal from paper substrates was quantified (Figure 4). All spectra exhibited similar peak positions and relative height; only the intensity of the spectra varied. The spectra were dominated by three strong bands: $\delta(\text{C-S})$ at 387 cm^{-1} , $\nu(\text{C-S})$ at 1077 cm^{-1} , and $\nu(\text{C-C})$ at 1584 cm^{-1} , which were the a_1 vibrational modes (in-plane, in-phase modes) of the 4-ATP molecules.³⁰ The significant enhancement of a_1 modes was related to the enhancement of the electromagnetic field between the AuNPs, which was produced by the strong internanoparticle coupling among the close contacted AuNPs. Notably, the b_2 bending modes (in-plane, out-of-phase modes) were $\delta(\text{C-H})$ at 1137 cm^{-1} , $\delta(\text{C-H}) + \nu(\text{C-C})$ at 1386 cm^{-1} , and $\delta(\text{C-H}) + \nu(\text{C-C})$ at 1433 cm^{-1} .³⁰ The significant enhancement of b_2 modes may be attributed to the charge transfer of AuNPs to the adsorbed 4-ATP molecules, which was largely dependent on the energy of the excitation laser.

The SERS potential of AuNP-treated papers was demonstrated by the drastic increase in intensities. Treating paper with 0.02 mg/mL of AuNPs significantly enhanced the Raman signal of 4-ATP (Figure 4a,b). The SERS intensity of AuNP-treated paper was found to increase linearly with the concentration of AuNP solutions applied to paper (Figure 4). As the concentration increased, AuNPs were more closely packed together in the solution; they adsorbed onto the paper substrate and maintained their packing density. As the average distance between the AuNPs decreased from approximately 100–200 nm to 10–50 nm, it is believed that effective “hot spots” appeared, and their interparticle plasmon coupling gave rise to the enhancement of electromagnetic field, which intensified the SERS signals of the 4-ATP.³¹ This significant SERS signal enhancement was particularly observed when paper was treated with 1.0 mg/mL of AuNPs (Figure 4) as the inter-

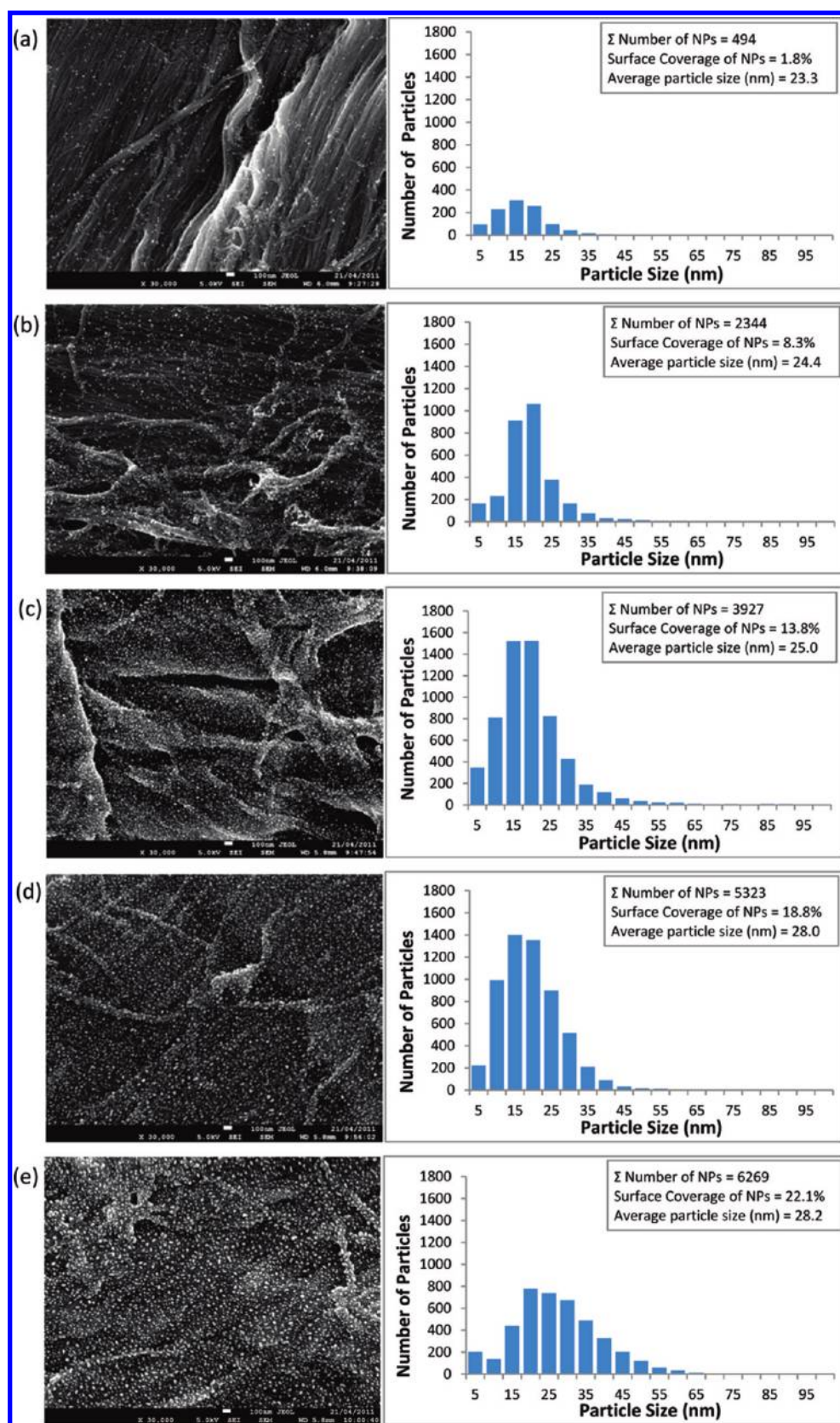


Figure 2. FESEM images and histograms of particle size distribution of filter papers dipped into (a) 0.02 mg/mL, (b) 0.05 mg/mL, (c) 0.10 mg/mL, (d) 0.15 mg/mL, and (e) 0.20 mg/mL of AuNP solutions.

particle distance of the AuNPs became closer to their diameter (25 ± 3 nm).

The SERS sensitivity of AuNP paper was quantified. Paper treated with 0.20 mg/mL of AuNP solutions was exposed to different concentrations of 4-ATP, and their Raman spectra were

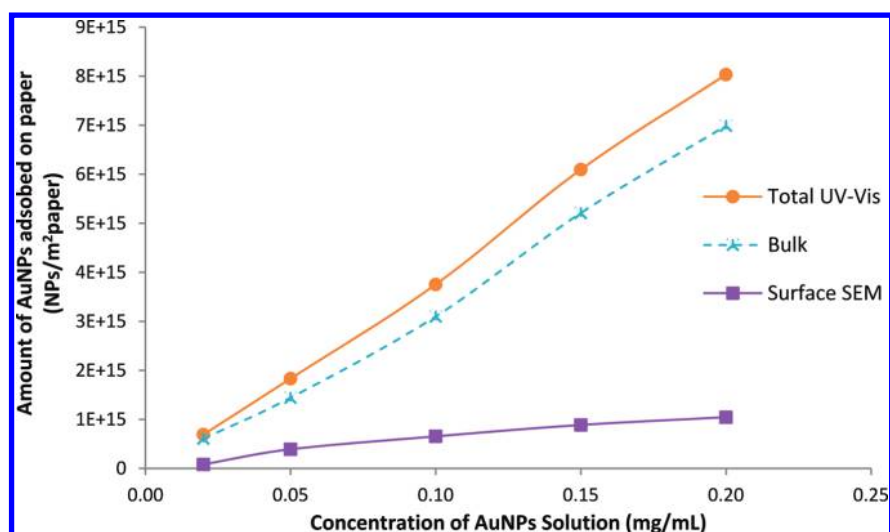


Figure 3. Effect of the concentration of AuNP solutions on the amount of AuNPs retained on the paper surface and bulk after dipping (estimated from UV–vis and FESEM analysis based on the FESEM images in Figure 2).

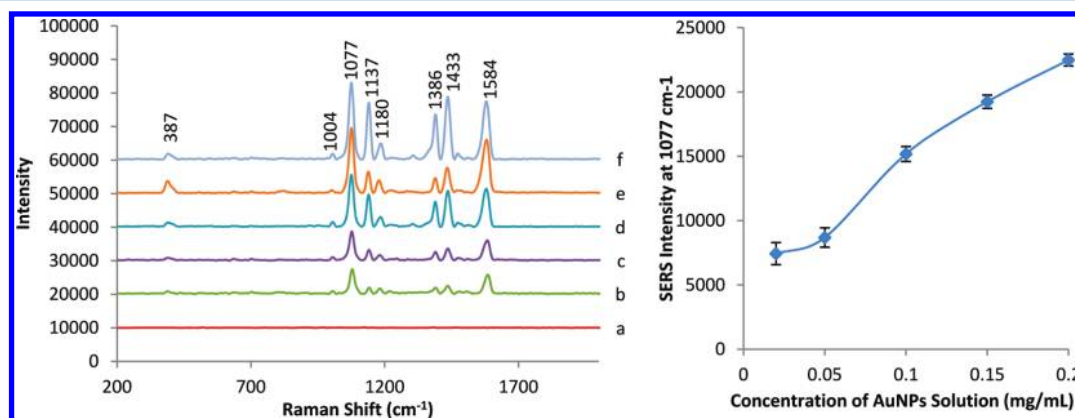


Figure 4. (Left) Raman spectrum of 1 mM of 4-ATP adsorbed on (a) plain filter paper, and SERS spectra of 4-ATP on filter paper dipped in AuNP solutions of (b) 0.02 mg/mL, (c) 0.05 mg/mL, (d) 0.10 mg/mL, (e) 0.15 mg/mL, and (f) 0.20 mg/mL. (Right) SERS intensity of 4-ATP at 1077 cm^{-1} band from paper dipped in different concentrations of AuNP solutions.

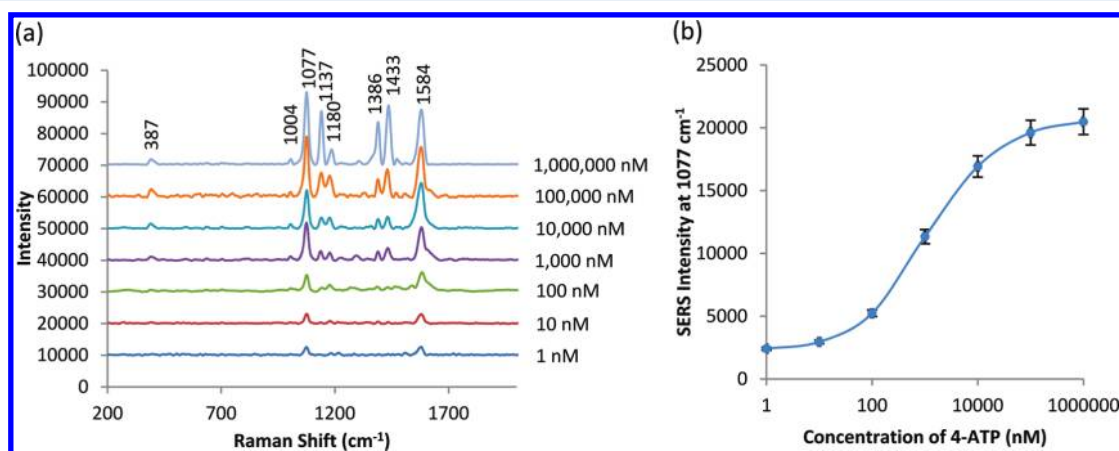


Figure 5. (a) SERS spectra of different concentrations of 4-ATP from AuNP-treated paper (0.20 mg/mL AuNP solutions). (b) SERS intensity of different concentrations of 4-ATP from the AuNP-treated paper at the 1077 cm^{-1} band.

measured (Figure 5a). The concentration of 4-ATP investigated ranged over 6 orders of magnitude, from 1 mM to 1 nM. The detection limit of AuNP paper substrates for 4-ATP is lower than 1 nM, because even the spectrum of the 1 nM sample had a good signal-to-noise ratio, and the main peaks at 1077 cm^{-1} and 1584 cm^{-1}

were still observable. A sigmoidal relationship between the SERS intensity and concentration of 4-ATP was observed. The SERS intensities were mostly linear when the concentration of 4-ATP was low. At high concentration, a nonlinear response emerged, and

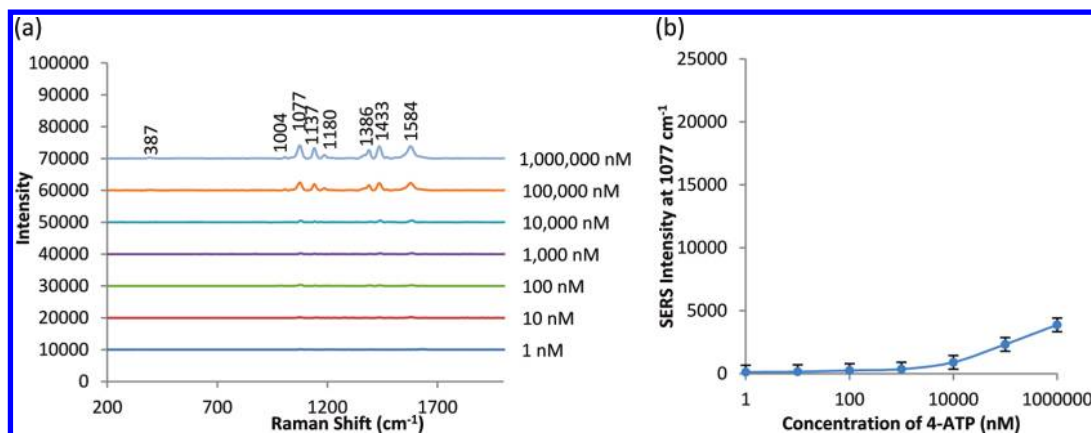


Figure 6. (a) SERS spectra of different concentrations of 4-ATP from AuNP-treated silicon (0.20 mg/mL of AuNP solutions). (b) SERS intensity of different concentrations of 4-ATP from the AuNP-treated silicon at the 1077 cm^{-1} band.

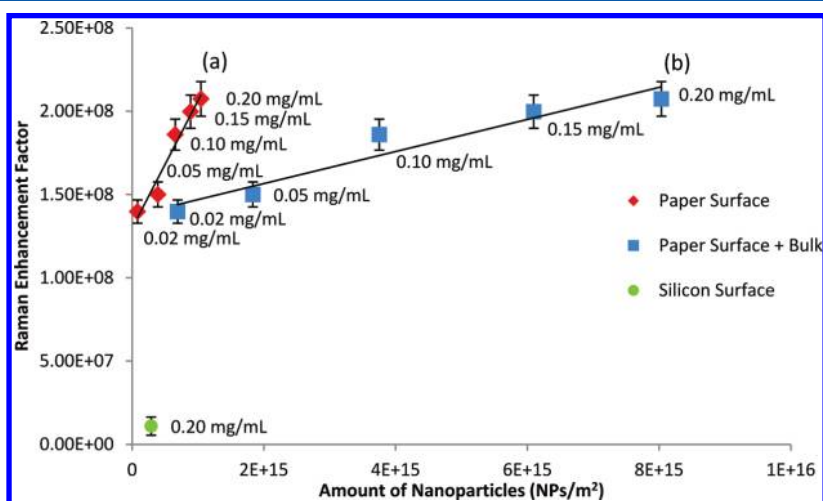


Figure 7. Relationship between the amount of AuNPs and the EF of 4-ATP measured at the 1077 cm^{-1} band for filter paper and silicon. The contributions of the AuNPs adsorbed at (a) the surface of paper and also in (b) the bulk of paper were analyzed.

saturation of SERS signal occurred, indicating that the adsorption of 4-ATP onto the AuNPs became saturated beyond this level.^{32,33}

Deposition of AuNPs on Silicon. To investigate the effect of the substrate on the distribution of AuNPs and their SERS properties, a silicon wafer was dipped into a AuNP suspension of 0.20 mg/mL; the spatial distribution of AuNPs was measured and compared with paper. Silicon is a flat and smooth substrate, while paper is heterogeneous, with a rough, porous, and fibrillar morphology. Silicon has a point of zero charge between pH 2 and 3³⁴ with a negative charge at pH greater than 3. Thus, the silicon surface was negatively charged when dipped in the AuNP solutions (pH 6). The attachment of the negatively charged AuNPs on the silicon wafer was also driven by van der Waals force. The adsorption of AuNPs from solution onto the silicon substrate (Supporting Information, S5) was much lower than that on paper (Figure 2e) due to the absence of a porous and hydrophilic surface, as found in paper, which readily absorbed and retained AuNPs upon dipping or drying. The particle size of AuNPs adsorbed on silicon was constant with an average diameter of 25 ± 3 nm.

The SERS sensitivity of a AuNP-treated silicon wafer (0.20 mg/mL of AuNP solutions) to a concentration range of 4-ATP was evaluated (Figure 6). Compared to paper (Figure 5), the SERS intensity of most Raman peaks from silicon was relatively low. At low concentrations of 4-ATP, the spectra became poorly

resolved. Unlike the SERS signal from paper, the main peaks of 4-ATP at 1077 cm^{-1} and 1584 cm^{-1} were hardly detectable below 100 nM 4-ATP.

The EFs calculated for 4-ATP on paper and silicon substrates were calculated for the corresponding density of AuNPs and are shown in Figure 7. Relatively linear relationships relate the EF of 4-ATP to the density of AuNPs on the substrates (Figure 7), the aggregation state of AuNPs for all materials being constant. The EF of AuNP-treated silicon (0.20 mg/mL of AuNP solutions) was lower by more than an order of magnitude compared to paper, even though its surface concentration of AuNPs was only half that of paper. AuNPs can only be retained on the surface of silicon wafer, while paper has additional AuNPs adsorbed through its cellulose layers. Taking into account the amount of AuNPs within the bulk of paper, the SERS intensity curve of paper in Figure 7 is shifted to the right. This suggests that the significant difference of SERS intensity between paper and silicon wafer can be due to (1) the different amount of AuNPs retained by the substrates and (2) the difference in the spatial location of AuNPs (surface/bulk for paper, and surface only for silicon).

AuNPs Droplet Test. To better understand the role of the substrate and the x - y - z distribution of AuNPs on the SERS efficiency, a 1 μL droplet from 0.20 mg/mL of AuNP solutions was deposited on paper and silicon to provide an identical amount of AuNPs on the different substrates. The AuNP droplet

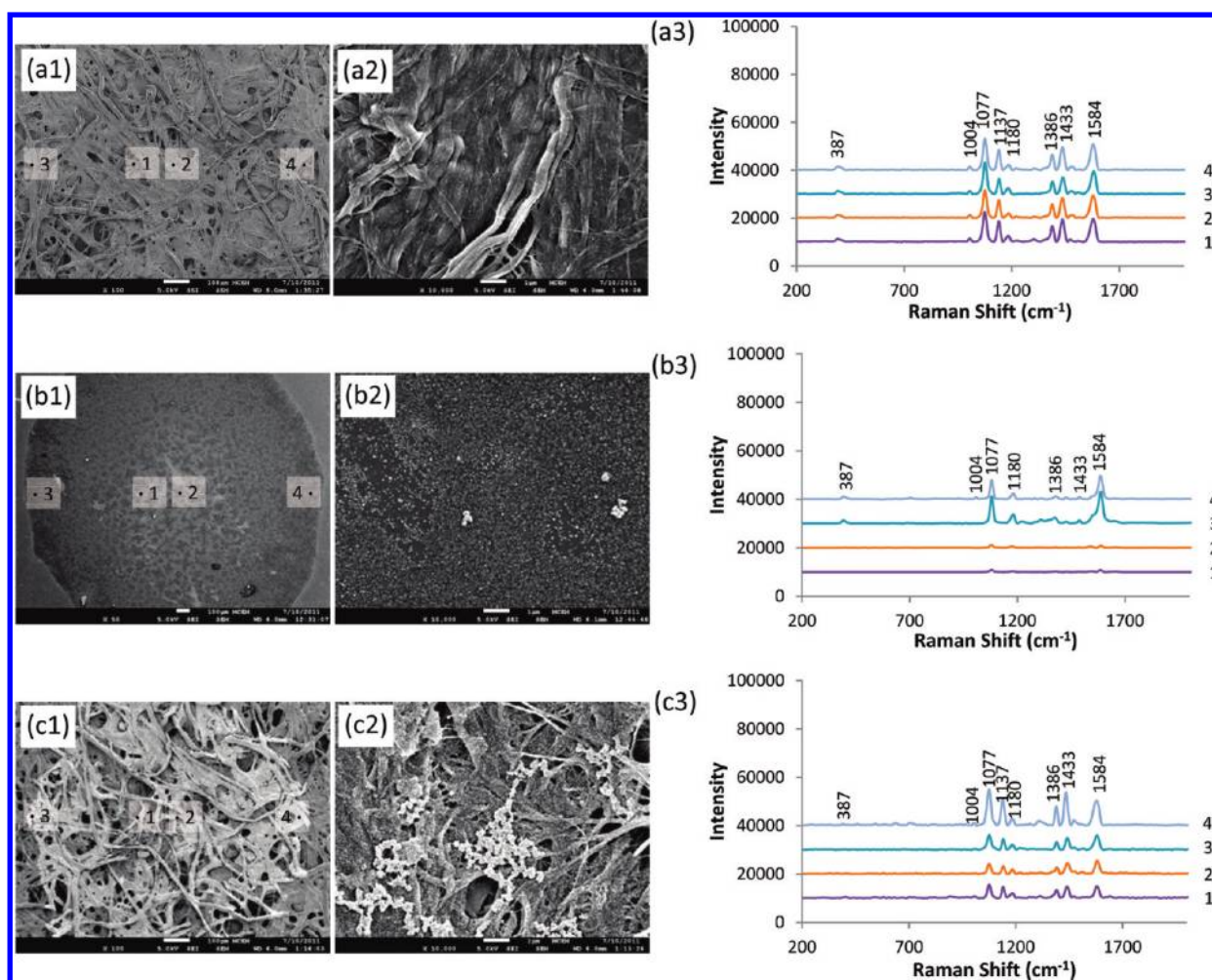


Figure 8. (a) Low- and (b) high-magnification FESEM images of (1) filter paper, (2) silicon wafer, and (3) hydrophobized paper substrates treated with 1 μ L droplet of AuNPs (0.20 mg/mL). (c) SERS spectra of 4-ATP absorbed on the droplets respectively (taken at four different spots: two from the center and two from the edge of the droplet as indicated with numbers in the FESEM images).

on paper diffused and dried instantly, while the droplet on silicon took a longer time to dry. The intertwined structure of cellulose fibers was able to “freeze” the adsorption state of nanoparticles by rapidly drawing away the water upon drying, resulting in a more uniform distribution of AuNPs on paper (Figure 8a1,a2). However, the nonporous and smooth surface of silicon wafer caused the AuNP droplet to form aggregates around its edge, which led to uneven distribution (Figure 8b1,b2). This was due to the slower evaporation of water in the vicinity of the NPs, which promoted the AuNPs suspension to concentrate around the edge of the droplet, forming a “coffee ring” during drying.³⁵ The SERS spectra of 4-ATP was measured at four different locations (two at the center and two at the edge of the AuNPs droplet) on paper (Figure 8a3) and silicon wafer (Figure 8b3). The peak spectra of 4-ATP were constant for both substrates, but the peaks’ intensity from paper was higher compared to silicon. For silicon, the SERS signal was not reproducible: the signal from the edge of the droplet had a higher intensity than at its center due to the presence of AuNPs aggregates, which led to a higher contact point between the NPs for electromagnetic field enhancement. This means that SERS intensity and reproducibility of the same amount of AuNPs is much higher on paper than on silicon wafer.

The difference between the SERS performance of silicon and paper substrates might be due to the presence of AuNPs within

the bulk of paper, which increases the concentration of “hotspots”. To explore the effect of the 3D spatial distribution of AuNPs, a 1 μ L droplet from 0.20 mg/mL of AuNP solution was deposited onto a hydrophobized paper. Similar to silicon, the AuNPs droplet on the hydrophobized paper took a longer time to dry and formed a ring (smaller). FESEM analysis revealed that adsorption and aggregation of AuNPs on the hydrophobized paper was higher compared to that on the normal paper (Figure 8a,c). FESEM cross-sectional analysis showed that the AuNPs were only retained on the surface of cellulose fibers and were absent from the bulk of paper (Supporting Information, S6). The SERS spectra of 4-ATP had a higher intensity at the edge compared to the center of the AuNPs droplet (Figure 8c3). However, the overall SERS signal showed a lower signal-to-noise ratio than the normal paper. The AuNPs absorbed through the bulk of paper played an important role in quenching the background noise, thus producing a more sensitive SERS signal.

The silicon and hydrophobized paper treated with a single droplet of AuNP solutions did not have a significantly higher SERS intensity than that of the normal paper, even though their AuNPs had higher aggregation. The AuNPs on silicon and hydrophobized paper were only adsorbed on the surface but not distributed within the interface/bulk of the substrates. Hence, the interparticle plasmon coupling only occurred in a monolayer on the two-dimensional (2D) surface. By contrast, the adsorption of

AuNPs on the surface and into the bulk of paper presented a 3D multilayer architecture for intralayer and interlayer plasmon coupling. The *z*-distribution of AuNPs throughout the multilayer of cellulose fibers is believed to be responsible for amplifying the SERS signal via interlayer enhancement.

CONCLUSION

The effect of AuNP concentration and 3D distribution profile within paper on the SERS performance of paper was quantified. The objective was to drastically increase the sensitivity and selectivity of a low-cost SERS paper substrate as a biodiagnostic platform. AuNPs were adsorbed from solutions onto paper and a silicon wafer by physisorption using a dipping method, and the particle distribution (size, surface coverage) was quantified by FESEM/image analysis. A surface coverage of AuNPs ranging from 1.8 to 22.1% was achieved on paper; however, the particles on the surfaces represented only 40% of the AuNPs' loading, with the majority uniformly adsorbed within the bulk of paper. The AuNPs were mostly adsorbed as singlets and as very small aggregates. In the absence of any retention aid, the adsorption of AuNPs on paper substrate was still relatively high, even higher by an order of magnitude than on silicon when both substrates were treated similarly. The EF of a model dye (4-ATP) adsorbed onto AuNP-treated paper was higher by more than 1 order of magnitude than AuNP-treated silicon. The high loading and uniform distribution of AuNPs on paper contributed toward the excellent SERS reproducibility and high EF.

The role of AuNPs within the bulk of paper was explored by depositing a 1 μ L droplet of AuNP solutions on paper, silicon wafer, and hydrophobized paper. The paper treated with an AuNPs droplet had a higher SERS efficiency than the silicon and hydrophobized paper similarly treated, regardless of its lower surface aggregation. This highlights the importance of the *z*-distribution of AuNPs within the bulk of paper in quenching the background noise through interlayer plasmon coupling, thus enhancing the SERS signal of the analyte.

The paper substrate effectively "transferred" the high packing density and uniform distribution from the AuNPs in solutions onto the cellulose fibers, and "froze" their adsorption state during the drying process. The SERS intensity scaled linearly with the density of AuNPs on paper. This highlights the great potential of paper as an inert and robust substrate to maintain a controlled adsorption state of AuNPs for carrying out molecular sensing with high sensitivity.

Paper is a cheap, flexible, stable, easy to use and dispose SERS substrate. It emerges as a viable substitute to commercial silicon substrate (Klarite) for routine biodiagnostic applications. All that is needed is to optimize the distribution of NPs on the heterogeneous structure of paper to enhance SERS performance.

ASSOCIATED CONTENT

Supporting Information

Calculation of AuNP concentration, particle size distribution of 0.20 mg/mL of AuNPs in aqueous solution measured by DLS, FESEM cross sectional view of 0.20 mg/mL of AuNP-treated paper, UV-vis absorbance spectra of AuNP solutions before and after dipping of filter papers, FESEM image and particle size distribution of a silicon wafer dipped in 0.20 mg/mL AuNP solutions, and FESEM cross sectional view of a 1 μ L 0.20 mg/mL AuNP droplet on hydrophobic paper. This material is available free of charge via the Internet at <http://pubs.acs.org>.

AUTHOR INFORMATION

Corresponding Author

*E-mail: Gil.Garnier@monash.edu; Tel: +61-3-9905-9180; Fax: +61-3-9905-3413.

Notes

The authors declare no competing financial interest.

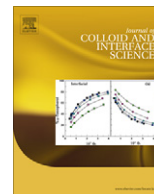
ACKNOWLEDGMENTS

Thanks to Dr. T. Williams, Monash Centre for Electron Microscopy (MCEM), for FESEM technical expertise, F. Shanks from Monash Molecular Spectroscopy and Centre for Biospectroscopy for Raman technical advice, and S. Narayanan and Dr. X. Li for technical expertise. The financial support from the ARC Linkage LP0989823 and Visy, Amcor, SCA, Norske Skog, Australian Paper, the Australian Pulp and Paper Institute, and Monash University are acknowledged.

REFERENCES

- (1) Martinez, A. W.; Phillips, S. T.; Butte, M. J.; Whitesides, G. M. Patterned Paper as a Platform for Inexpensive, Low-Volume, Portable Bioassays. *Angew. Chem., Int. Ed.* **2007**, *46* (8), 1318–1320.
- (2) Martinez, A. W.; Phillips, S. T.; Carrilho, E.; Thomas, S. W.; Sindi, H.; Whitesides, G. M. Simple Telemedicine for Developing Regions: Camera Phones and Paper-Based Microfluidic Devices for Real-Time, Off-Site Diagnosis. *Anal. Chem.* **2008**, *80* (10), 3699–3707.
- (3) Li, X.; Tian, J.; Shen, W. Quantitative Biomarker Assay with Microfluidic Paper-Based Analytical Devices. *Anal. Bioanal. Chem.* **2010**, *396* (1), 495–501.
- (4) Li, X.; Tian, J.; Nguyen, T.; Shen, W. Paper-Based Microfluidic Devices by Plasma Treatment. *Anal. Chem.* **2008**, *80* (23), 9131–9134.
- (5) Khan, M. S.; Thouas, G.; Shen, W.; Whyte, G.; Garnier, G. Paper Diagnostic for Instantaneous Blood Typing. *Anal. Chem.* **2010**, *82* (10), 4158–4164.
- (6) Tian, J.; Li, X.; Shen, W. Printed Two-Dimensional Micro-Zone Plates for Chemical Analysis and ELISA. *Lab Chip* **2011**, *11* (17), 2869–2875.
- (7) Cheng, C.-M.; Martinez, A. W.; Gong, J.; Mace, C. R.; Phillips, S. T.; Carrilho, E.; Mirica, K. A.; Whitesides, G. M. Paper-Based ELISA. *Angew. Chem., Int. Ed.* **2010**, *49* (28), 4771–4774.
- (8) Toderas, F.; Baia, M.; Baia, L.; Astilean, S. Controlling Gold Nanoparticle Assemblies for Efficient Surface-Enhanced Raman Scattering and Localized Surface Plasmon Resonance Sensors. *Nanotechnology* **2007**, *18*, 255702.
- (9) Lee, S. W.; Shin, Y.-B.; Jeon, K. S.; Jin, S. M.; Suh, Y. D.; Kim, S.; Lee, J. J.; Kim, M.-G. Electron Beam Lithography-Assisted Fabrication of Au Nano-dot Array as a Substrate of a Correlated AFM and Confocal Raman Spectroscopy. *Ultramicroscopy* **2008**, *108* (10), 1302–1306.
- (10) Min, Q.; Santos, M. J. L.; Girotto, E. M.; Brolo, A. G.; Gordon, R. Localized Raman Enhancement from a Double-Hole Nanostructure in a Metal Film. *J. Phys. Chem. C* **2008**, *112* (39), 15098–15101.
- (11) Stokes, D. L.; Chi, Z.; Vo-Dinh, T. Surface-Enhanced-Raman-Scattering-Inducing Nanoprobe for Spectrochemical Analysis. *Appl. Spectrosc.* **2004**, *58* (3), 257–354.
- (12) Lee, C. H.; Tian, L.; Singamaneni, S. Paper-Based SERS Swab for Rapid Trace Detection on Real-World Surfaces. *ACS Appl. Mater. Interfaces* **2010**, *2* (12), 3429–3435.
- (13) Luo, Z.; Fang, Y. SERS of C60/C70 on Gold-Coated Filter Paper or Filter Film Influenced by the Gold Thickness. *J. Colloid Interface Sci.* **2005**, *283* (2), 459–463.
- (14) Berthod, A.; Laserna, J. J.; Winefordner, J. D. Analysis by Surface Enhanced Raman Spectroscopy on Silver Hydrosols and Silver Coated Filter Papers. *J. Pharm. Biomed. Anal.* **1988**, *6* (6–8), 599–608.
- (15) Cabalín, L. M.; Laserna, J. J. Fast Spatially Resolved Surface-Enhanced Raman Spectrometry on a Silver Coated Filter Paper Using Charge-Coupled Device Detection. *Anal. Chim. Acta* **1995**, *310* (2), 337–345.

- (16) Ma, W.; Fang, Y. Experimental (SERS) and Theoretical (DFT) Studies on the Adsorption of p-, m-, and o-Nitroaniline on Gold Nanoparticles. *J. Colloid Interface Sci.* **2006**, *303* (1), 1–8.
- (17) Niu, Z.; Fang, Y. Surface-Enhanced Raman Scattering of Single-Walled Carbon Nanotubes on Silver-Coated and Gold-Coated Filter Paper. *J. Colloid Interface Sci.* **2006**, *303* (1), 224–228.
- (18) Wu, D.; Fang, Y. The Adsorption Behavior of p-Hydroxybenzoic Acid on a Silver-Coated Filter Paper by Surface Enhanced Raman Scattering. *J. Colloid Interface Sci.* **2003**, *265* (2), 234–238.
- (19) Lee, C. H.; Hankus, M. E.; Tian, L.; Pellegrino, P. M.; Singamaneni, S. Highly Sensitive Surface Enhanced Raman Scattering Substrates Based on Filter Paper Loaded with Plasmonic Nanostructures. *Anal. Chem.* **2011**, *83* (23), 8953–8958.
- (20) Cheng, M.-L.; Tsai, B.-C.; Yang, J. Silver Nanoparticle-Treated Filter Paper As a Highly Sensitive Surface-Enhanced Raman Scattering (SERS) Substrate for Detection of Tyrosine in Aqueous Solution. *Anal. Chim. Acta* **2011**, *708* (1–2), 89–96.
- (21) Turkevich, J.; Stevenson, P. C.; Hillier, J. A Study of the Nucleation and Growth Processes in the Synthesis of Colloidal Gold. *Discuss. Faraday Soc.* **1951**, *11*, 55–75.
- (22) Camargo, P. H. C.; Au, L.; Rycenga, M.; Li, W.; Xia, Y. Measuring the SERS Enhancement Factors of Dimers with Different Structures Constructed from Silver Nanocubes. *Chem. Phys. Lett.* **2010**, *484* (4–6), 304–308.
- (23) Hu, X.; Wang, T.; Wang, L.; Dong, S. Surface-Enhanced Raman Scattering of 4-Aminothiophenol Self-Assembled Monolayers in Sandwich Structure with Nanoparticle Shape Dependence: Off-Surface Plasmon Resonance Condition. *J. Phys. Chem. C* **2007**, *111* (19), 6962–6969.
- (24) Schwartzberg, A. M.; Grant, C. D.; Wolcott, A.; Talley, C. E.; Huser, T. R.; Bogomolni, R.; Zhang, J. Z. Unique Gold Nanoparticle Aggregates as a Highly Active Surface-Enhanced Raman Scattering Substrate. *J. Phys. Chem. B* **2004**, *108* (50), 19191–19197.
- (25) Dong, H.; Hinestroza, J. P. Metal Nanoparticles on Natural Cellulose Fibers: Electrostatic Assembly and in Situ Synthesis. *ACS Appl. Mater. Interfaces* **2009**, *1* (4), 797–803.
- (26) Henglein, A.; Giersig, M. Formation of Colloidal Silver Nanoparticles: Capping Action of Citrate. *J. Phys. Chem. B* **1999**, *103* (44), 9533–9539.
- (27) Kim, T.; Lee, K.; Gong, M.-s.; Joo, S.-W. Control of Gold Nanoparticle Aggregates by Manipulation of Interparticle Interaction. *Langmuir* **2005**, *21* (21), 9524–9528.
- (28) Pinto, R. J. B.; Marques, P. A. A. P.; Barros-Timmons, A. M.; Trindade, T.; Neto, C. P. Novel SiO₂/Cellulose Nanocomposites Obtained by in Situ Synthesis and via Polyelectrolytes Assembly. *Compos. Sci. Technol.* **2008**, *68* (3–4), 1088–1093.
- (29) Peacock, A. C.; Amezcua-Correa, A.; Yang, J.; Sazio, P. J. A.; Howdle, S. M. Highly Efficient Surface Enhanced Raman Scattering Using Microstructured Optical Fibers with Enhanced Plasmonic Interactions. *Appl. Phys. Lett.* **2008**, *92* (14).
- (30) Hu, X.; Wang, T.; Wang, L.; Dong, S. Surface-Enhanced Raman Scattering of 4-Aminothiophenol Self-Assembled Monolayers in Sandwich Structure with Nanoparticle Shape Dependence: Off-Surface Plasmon Resonance Condition. *J. Phys. Chem. C* **2007**, *111* (19), 6962–6969.
- (31) Oh, M. K.; Yun, S.; Kim, S. K.; Park, S. Effect of Layer Structures of Gold Nanoparticle Films on Surface Enhanced Raman Scattering. *Anal. Chim. Acta* **2009**, *649* (1), 111–116.
- (32) Qiu, C.; Zhang, L.; Wang, H.; Jiang, C. Surface-Enhanced Raman Scattering on Hierarchical Porous Cuprous Oxide Nanostructures in Nanoshell and Thin-Film Geometries. *J. Phys. Chem.* **2012**, *3* (5), 651–657.
- (33) Wang, H. H.; Liu, C. Y.; Wu, S. B.; Liu, N. W.; Peng, C. Y.; Chan, T. H.; Hsu, C. F.; Wang, J. K.; Wang, Y. L. Highly Raman-Enhancing Substrates Based on Silver Nanoparticle Arrays with Tunable Sub-10 nm Gaps. *Adv. Mater.* **2006**, *18* (4), 491–495.
- (34) Wang, Y.; Ferrari, M. Surface Modification of Micromachined Silicon Filters. *J. Mater. Sci.* **2000**, *35* (19), 4923–4930.
- (35) Bankar, A.; Joshi, B.; Ravi Kumar, A.; Zinjarde, S. Banana Peel Extract Mediated Synthesis of Gold Nanoparticles. *Colloids Surf., B* **2010**, *80* (1), 45–50.



Effect of cationic polyacrylamides on the aggregation and SERS performance of gold nanoparticles-treated paper

Ying Hui Ngo^a, Dan Li^b, George P. Simon^b, Gil Garnier^{a,*}

^a BioPRIA, Australian Pulp and Paper Institute (APPI), Department of Chemical Engineering, Monash University, Clayton, VIC 3800, Australia

^b Department of Material Engineering, Monash University, Clayton, VIC 3800, Australia

ARTICLE INFO

Article history:

Received 14 August 2012

Accepted 29 September 2012

Available online 22 October 2012

Keywords:

SERS

Gold nanoparticles (AuNPs)

Aggregates

Paper

Cationic polyacrylamide (CPAM)

Concentration

Charge density

Molecular weight

ABSTRACT

This study examines and quantifies the effect of cationic polyelectrolyte adsorption on paper on the aggregation and retention of gold nanoparticles (AuNPs) to optimize their Surface Enhanced Raman Scattering (SERS) enhancement factor and sensitivity. Aggregation of metallic nanoparticles is known as a key factor for intense SERS enhancement. Paper substrates were treated with aqueous solutions of cationic polyacrylamide (CPAM) varying in concentration, charge density, and molecular weight to control the AuNPs' aggregate size distribution and surface coverage on paper. The Raman Enhancement Factor of AuNPs-CPAM paper was almost an order of magnitude greater than for the untreated AuNPs paper. The high loading and uniform distribution of AuNPs aggregates on CPAM pre-treated paper contributed toward the excellent SERS reproducibility, sensitivity, and high enhancement factor. This configuration of AuNP on paper was favoured by treating the substrate with CPAM solutions of higher concentrations, higher charge density, and greater molecular weight.

Crown Copyright © 2012 Published by Elsevier Inc. All rights reserved.

1. Introduction

Paper is gaining wide interest as a low-cost diagnostic platform for health and environmental applications. Paper is cheap and easy to engineer, biodegradable, biocompatible, and allows full use of functional printing technology [1,2]. Flexible micro-fluidic systems, reactors, and valves have been printed on paper to regulate, measure, and control the flow of analytes and reagents [3–7]. Paper also allows the use of Enzyme-Linked Immunosorbent Assay (ELISA) for the quantification of antibody concentration [2,3]. However, ELISA methods often require the preparation of multiple reactants and tedious washing procedures. A straight-forward and attractive alternative involves direct contact between paper substrate and analytes, followed by rapid molecular signal detection using Surface Enhanced Raman Scattering (SERS) spectroscopy.

SERS involves enhancement of Raman signal to detect small energy changes occurring when light is scattered from a molecule which is absorbed on a metallic surface, typically a metallic nanoparticle. The enhancement factor can be as much as 10^{14} – 10^{15} [8], which makes SERS a sensitive, single-molecule detection technique to identify analytes in trace levels. In the recent years, Raman spectroscopy has been developed from conventional laboratory system

to portable handheld device for rapid on-site detection. The emerging applications of SERS include prompt detection of chemical warfare, biological agents, explosives, and drug compounds.

With all the advantages offered by SERS, many studies have been directed toward fabricating an ideal SERS substrate which is low-cost, sensitive, selective, reproducible, flexible, and stable for long term storage between measurements. Metal aqueous colloids are one of the first commonly used substrate; but unfortunately, their application has been challenged by low reproducibility and stability. This has led to the development of different techniques to immobilize metallic nanoparticles on solid substrates, in particular electron beam lithography [9], focused ion beam patterning [10], and thermal evaporation [11] have all been used to deposit nanoparticles of controlled size, shape, and aggregation on inorganic substrates such as glass and silicon. However, these techniques are time consuming, costly, require sophisticated equipment, and the substrates are often fragile and suffer from poor storage stability.

While many issues are still associated with other SERS substrates, paper has emerged as an efficient substrate for routine SERS analysis in a few studies due to its robustness [12–17]. However, very few studies have controlled the distribution of nanoparticles within paper, and none has optimized the aggregation of nanoparticles on paper as a SERS substrate. In a previous study [18], we reported the fabrication of SERS paper substrates by dipping filter paper into suspensions of gold nanoparticles (AuNPs)

* Corresponding author. Fax: +61 3 9905 3413.

E-mail address: Gil.Garnier@monash.edu (G. Garnier).

of constant particle size with different nanoparticle concentrations. The AuNPs were mostly adsorbed as singlets and as very small aggregates on the paper. We found that different surface coverage and spatial distribution of the AuNPs produced different electromagnetic coupling and thus degree of SERS enhancement. Here, we report a method based on pre-treatment of paper with polyelectrolytes to induce and control the aggregation state of AuNPs in order to optimize the magnitude of their SERS effects.

Aggregation of metallic nanoparticles is known as a key factor for intense SERS enhancement since it was first reported by Brus et al. [19]. As the metal nanoparticles are contacted to form aggregates, their transition dipoles couple to each other and the enhanced fields of each nanoparticle start to coherently interfere at their contact points. When analyte molecules are adsorbed in this contact point (“hot spot”), their Raman signals can be significantly enhanced (10^{14} – 10^{15}) [8]. Hence, aggregates of nanoparticles have more efficient SERS properties than individual nanoparticles, because larger enhancements can be achieved at the particle junctions of aggregates.

This study has two objectives. The first is to quantify the effect of cationic polyelectrolyte's adsorption on paper on the aggregation and retention of AuNPs. The second objective is to relate the aggregation and surface coverage of AuNPs on paper to the optimum SERS enhancement factor and sensitivity. Paper was treated with aqueous solutions of cationic polyacrylamide (CPAM) varying in concentration, charge density, and molecular weight. The aggregate size distribution and surface coverage of AuNPs on paper were quantified and related to their SERS performance. The longer term aim of this study is thus to develop AuNPs treated paper as a multifunctional platform for low-cost bio-diagnostics.

2. Experimental section

2.1. Materials

Hydrogen tetrachloroaurate trihydrate ($\text{HAuCl}_4 \cdot 3\text{H}_2\text{O}$), sodium citrate tribasic dihydrate ($\text{Na}_3\text{C}_6\text{H}_5\text{O}_7 \cdot 2\text{H}_2\text{O}$), and 4-aminothiophenol (4-ATP) were purchased from Sigma–Aldrich and used as received. The cationic trimethylamino-ethyl-methacrylate polyacrylamide (CPAM) polymers were supplied by AQUA + TECH, Switzerland, from their Snowflake Cationics product range and used as received (chemical structure shown in [Supporting information](#)). They were identified as: I1 (5 wt% charge density, molecular weight 13 MDa), H1 (10 wt% charge density, molecular weight 13 MDa), F1 (40 wt% charge density, molecular weight 13 MDa), and F3 (40 wt% charge density, molecular weight 6 MDa). Whatman qualitative filter paper #1, which consists of 98% α -cellulose, was selected as the paper substrate as it is a convenient model paper of well defined structure and to ensure minimal SERS interference from process components (polymers or coatings). Ultrapure water purified with a Millipore system (18 M Ω cm) was used in all aqueous solutions and rinsing procedures.

2.2. Synthesis and deposition of nanoparticles on paper substrates

AuNPs were synthesized by using 1 mM $\text{HAuCl}_4 \cdot 3\text{H}_2\text{O}$ and 1% aqueous $\text{Na}_3\text{C}_6\text{H}_5\text{O}_7 \cdot 2\text{H}_2\text{O}$ according to the Turkevich method [20]. A stock solution of CPAM was prepared on the day of the experiment by diluting dry powder to 0.1 mg/mL with Millipore water and gently mixing the dispersions for 8 h at 23 °C to facilitate the dissolution process. Filter papers (55 mm diameter) were used as received or were pretreated with the cationic polymer. For treatment, the filter papers were dipped into 10 mL polymer solutions for 1 h, rendering the paper cationic. The treated papers were rinsed with distilled water to remove any unbounded poly-

mer. Wet pieces of untreated and polymer-treated paper substrates were then dipped immediately into Petri dishes containing 10 mL solution of AuNPs for 24 h. After dipping, the paper substrates were rinsed thoroughly with distilled water to remove any loosely bound AuNPs, and the papers were air-dried and stored at 50% relative humidity and 23 °C until further analysis.

2.3. Preparation of Raman active substrates

Solutions of 1 mM of 4-ATP were prepared in ethanol. 4-ATP is known for its strong affinity to the surface of AuNPs (its S–H bond is easily cleaved to form Au–S bond upon adsorption). The dried AuNPs-treated substrates were dipped into 2 mL of the 4-ATP ethanol solution 5 min to obtain a monolayer of 4-ATP on the substrates. After thorough rinsing with ethanol and drying, they were subjected to Raman characterization. The Raman Enhancement Factor (EF) of 1 mM of 4-ATP on a substrate was calculated according to [21,22]:

$$\text{EF} = \frac{[I_{\text{SERS}}]}{[I_{\text{bulk}}]} \times \frac{[N_{\text{bulk}}]}{[N_{\text{ads}}]} \quad (1)$$

where I_{SERS} is the intensity of a specific band in the SERS spectrum of 4-ATP and I_{bulk} is the intensity of the same band in the Raman spectrum from the bulk solution sample. For all spectra, the intensity of the band at 1077 cm^{-1} was used to calculate EF values. N_{bulk} is the number of molecules of the bulk 4-ATP in the laser illumination volume while N_{ads} is the number of molecules adsorbed and sampled on the SERS active substrate within the laser spot.

2.4. Instrumentation

Field Emission Scanning Electron Microscopy (FESEM), which produces higher resolution, less sample charging, and less damaged images than conventional SEM, was performed using a JEOL 7001 Field Emission Gun (FEG) system operating at 5 kV and 180 pA. ImageJ analysis software was used to determine the coverage of AuNPs on the cellulose fibers in the FESEM images and estimate particle size distribution. The total number of AuNPs was calculated by dividing the total area of AuNPs on paper (in each FESEM images) by the area of an individual AuNP measured by Dynamic Light Scattering (DLS) method ($d = 23.2$ nm). The Zeta-potential and DLS measurements were performed with a Zetasizer Nano ZS (Malvern Instruments) in a Folded Capillary cell (DTS1060) at 25 °C. For the zeta-potential measurement, laser Doppler electrophoresis measures the net velocity of the nanoparticles in the liquid that results when an electric field is applied. The fundamental quantity measured is the net electrophoretic mobility (μ) of the particles, which is then converted to the zeta potential using Henry's approximation. UV–Vis absorbance was measured using a Varian Cary 300Bio spectrophotometer. All Raman and SERS spectra were obtained in air using a Renishaw InVia Raman microscope equipped with a 300 mW 633 nm laser. The laser beam was positioned through a Leica imaging microscope objective lens (50 \times), while the instrument's wavenumber was calibrated with a silicon standard centered at 520.5 cm^{-1} shift. Due to the smaller spot size of the laser compared with the large surface area of the samples, the spectra were obtained at five different points of the surface. The position of the spectra band from different points on the surface were the same, but differed only in intensity. The average Raman intensity (of five measurements) was presented as the final result after baseline subtraction from the control samples.

3. Results

3.1. Effect of CPAM concentration

Aggregates of nanoparticles are expected to have a higher SERS efficiency than individual nanoparticles because of the greater SERS enhancement at their points of contact [19]. To investigate this hypothesis, filter paper samples were pre-treated with CPAM solutions of different concentrations. A high molecular weight and highly charged CPAM was selected. This was to induce a positive charge on paper (which is originally negatively charged) and to create a polymer layer able to adsorb, retain, and aggregate the negatively charged AuNPs. The CPAM used here had a molecular weight of 13 MDa and 40 wt% of charge density. The positive charge of the CPAM solutions increased with their polymer concentration, as measured by their zeta potential (Table 1). After CPAM pre-treatment, the filter papers were rinsed and directly dipped into a 0.20 mg/mL AuNPs solution for 24 h. The AuNPs had a zeta potential of -44.6 mV, and an average diameter of 23.2 nm, as judged by Field Emission Scanning Electron Microscopy (FESEM).

The color intensity of the dried AuNPs and AuNPs-CPAM-treated papers was analyzed with ImageJ software (Fig. 1). The color of the paper turned from reddish-purple (AuNPs on untreated paper) to dark purple when the paper was pre-treated with CPAM, followed by AuNPs, and the color became darker as the concentration of CPAM was increased.

FESEM analysis was performed to examine the adsorption of AuNPs on the untreated and CPAM pre-treated papers. Pre-treating paper with the dilute 0.01 mg/mL CPAM did not increase AuNP

aggregate size but more than doubled the AuNP paper surface coverage (Fig. 2a and b). A significant increase was observed in the AuNPs' surface coverage on CPAM pre-treated papers compared to untreated paper. As the concentration of CPAM solution was increased, the assembly of AuNPs was drawn together, forming a random distribution of two- and three-dimensional clusters within the paper microstructure (Fig. 2). The surface coverage and size of AuNPs aggregates also increased dramatically to 84.6% and 59.6 nm, respectively, for paper pre-treated with the concentrated CPAM solution (0.10 mg/mL) (Fig. 2d).

4-Aminothiophenol (4-ATP) was selected as the probe molecule in the Raman analysis for its distinct Raman features strong affinity for Au surfaces via thiol bonding and formation of self-assembled monolayers [23]. The concentration effect of CPAM solutions on the SERS signal of 4-ATP from paper substrates was quantified (Fig. 3). The SERS spectra were dominated by three strong characteristic bands: $\delta(\text{C-S})$ at 387 cm^{-1} , $\nu(\text{C-S})$ at 1077 cm^{-1} , and $\nu(\text{C-C})$ at 1584 cm^{-1} , which represent the a_1 vibrational modes (in-plane, in-phase modes) of the 4-ATP molecules [22]. The significant enhancement of a_1 modes was related to the enhancement of the electromagnetic field between the AuNPs, which was produced by the strong inter-nanoparticles coupling among the close contacted AuNPs. Notably, the b_2 bending modes (in-plane, out-of-phase modes) were $\delta(\text{C-H})$ at 1137 cm^{-1} , $\delta(\text{C-H}) + \nu(\text{C-C})$ at 1386 cm^{-1} , and $\delta(\text{C-H}) + \nu(\text{C-C})$ at 1433 cm^{-1} [22]. The significant enhancement of b_2 modes may be attributed to the charge transfer of AuNPs to the absorbed 4-ATP molecules, which was largely dependent on the energy of the excitation laser. Fig. 3 also shows the Raman Enhancement Factor (EF) of 4-ATP doubled when paper was pre-treated with 0.01 mg/mL of CPAM. The Raman Enhancement Factor (EF) increased pseudo-linearly with the concentration of CPAM used for paper pre-treatment.

Table 1

Zeta potential of CPAM solutions with different concentration, charge density, and molecular weight.

	Concentration of CPAM (40 wt% charge density, 13 MDa molecular weight) (mg/mL)			Charge density of CPAM (0.10 mg/mL concentration, 13 MDa Molecular Weight) (wt%)			Molecular weight of CPAM (0.10 mg/mL concentration, 40 wt% charge density) (MDa)	
	0.01	0.05	0.10	5	10	40	6	13
Zeta potential (mV)	12.2	27.2	32.6	18.7	25.3	32.6	5.08	32.6

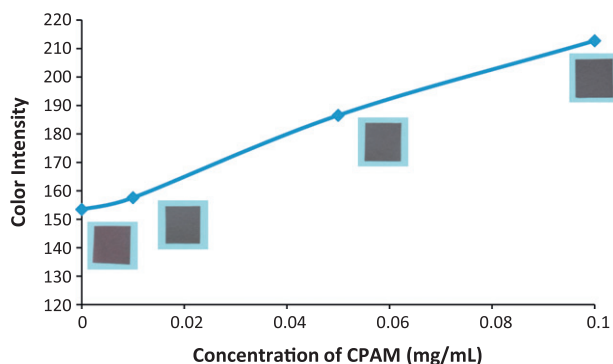


Fig. 1. Color intensity of filter paper dipped in 0.20 mg/mL of AuNP solutions without CPAM pre-treatment and with CPAM pre-treatment of 0.01 mg/mL, 0.05 mg/mL, and 0.10 mg/mL polymer concentration.

3.2. Effect of CPAM charge density

The paper substrates were pre-treated with 0.10 mg/mL CPAM solutions of constant molecular weight (13MDa) but different charge density, after which they were dipped in 0.20 mg/mL of AuNP solution. CPAM with a charge density of 5 wt%, 10 wt% and 40 wt% was tested. The zeta potential of the CPAM solutions is shown in Table 1; the zeta potential increasing with the charge density of polymer. The surface coverage and average aggregate diameters of AuNPs increased from 62.2% to 84.6% and from 34.8 nm to 59.6 nm, respectively, as a function of the CPAM's charge density (Fig. 4). The cluster size distribution also became wider.

The charge density of the CPAM solution strongly affected the SERS enhancement of the AuNPs-CPAM paper (Fig. 5). From an initial Raman EF of 2.1×10^8 , the EF increased by a factor of 4– 8.9×10^8 .

3.3. Effect of CPAM molecular weight

The effect of CPAM's molecular weight on the aggregation and adsorption of AuNPs on paper was investigated. Paper was pre-treated with a lower molecular weight CPAM of 6 MDa (40 wt% charge density and 0.10 mg/mL concentration). CPAM of 6 MDa has a relatively lower zeta potential compared to CPAM of 13 MDa (Table 1).

The molecular weight of the CPAM strongly influenced the surface coverage and aggregation state of AuNPs. By doubling CPAM's molecular weight, the surface coverage and average diameter of AuNP aggregates increased from 49% to 85% and 35–60 nm, respectively (Fig. 6). The Raman EF of AuNPs-CPAM paper was increased almost by a factor 3, from 3.1×10^8 to 8.9×10^8 , when paper was pre-treated with CPAM of higher molecular weight (Fig. 7).

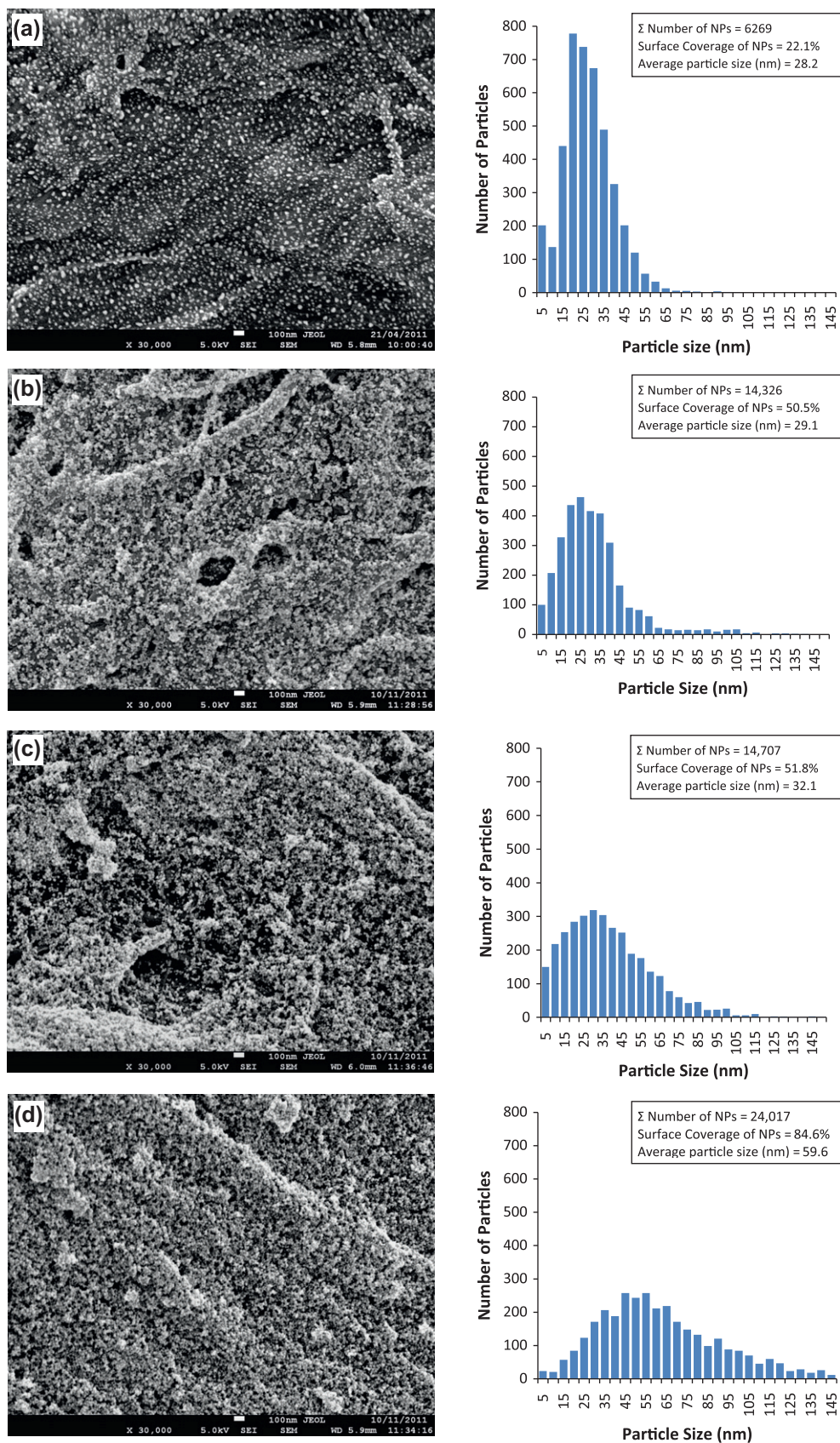


Fig. 2. FESEM images and histograms of AuNPs' particle size distribution of filter paper dipped in 0.20 mg/mL of AuNP solutions: (a) without CPAM pre-treatment and with CPAM pre-treatment of, (b) 0.01 mg/mL, (c) 0.05 mg/mL, and (d) 0.10 mg/mL polymer concentration.

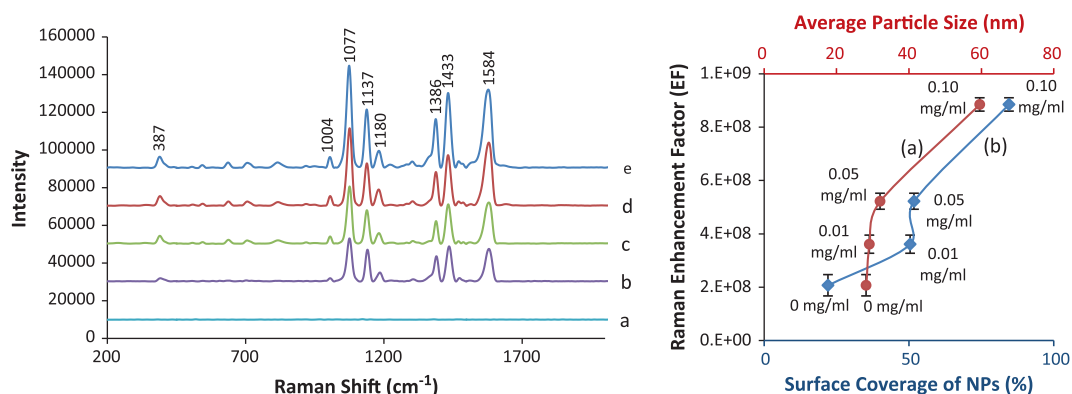


Fig. 3. (Left) Raman spectrum of 4-ATP adsorbed on: (a) plain filter paper, SERS spectra of 4-ATP on AuNPs paper, (b) without CPAM pre-treatment and with CPAM pre-treatment of, (c) 0.01 mg/mL, (d) 0.05 mg/mL, and (e) 0.10 mg/mL polymer's concentration. (Right) Relationship between the: (a) average size and (b) surface coverage of AuNP aggregates and the EF of 4-ATP measured at the 1077 cm^{-1} band (error bars show standard deviation of five measurements from different spots on the substrate).

3.4. Sensitivity of AuNPs-CPAM paper

The SERS sensitivity of AuNPs-CPAM paper was quantified and compared with untreated AuNPs paper. Both untreated paper and paper pre-treated with CPAM (0.10 mg/mL, 13 MDa, and 40 wt% charge density) were dipped into 0.20 mg/mL AuNP solutions, exposed to different concentrations of 4-ATP, and their Raman spectra were measured (Figs. 8 and 9). The concentration of 4-ATP investigated ranged over six orders of magnitude, from 1 mM to 1 nM. While the SERS spectra of 4-ATP for both papers were very similar, the SERS peaks were better defined on CPAM pre-treated paper. The detection limit of AuNPs-CPAM paper substrates was lower than for AuNPs on untreated paper as the spectrum of 1 nM of 4-ATP had good signal-to-noise ratio and the main peaks at 1077 cm^{-1} and 1584 cm^{-1} were more distinct (Fig. 9). The Raman intensity from AuNPs-CPAM-treated paper was doubled than that of the AuNPs on the untreated paper over the entire range of 4-ATP concentration.

3.5. Stability of AuNPs-CPAM paper

The FESEM images of AuNPs-CPAM paper (CPAM of 0.10 mg/mL, 13 MDa and 40 wt% charge density) before and after dipping in the 4-ATP ethanolic solution were analyzed to investigate the possibility of AuNPs desorption (Supporting Information, S1). It was found that 99.7% of the AuNPs were retained on paper after 4-ATP deposition, and the cluster size of the NPs remained constant. This confirms that immersion in 4-ATP ethanolic solution did not affect the AuNPs paper.

The Raman spectra of plain paper and AuNPs-CPAM paper (CPAM of 0.10 mg/mL, 13 MDa and 40 wt% charge density) were measured to ensure that the CPAM pre-treatment of paper did not alter the analyte's Raman spectra (Supporting Information, S2). Both spectra exhibited Raman bands of very weak intensity, and no significant variation of their spectral features was observed.

4. Discussion

4.1. SERS optimization

Filter paper pre-treated by CPAM of high concentration, high charge density, and high molecular weight was found to lead to a more uniform and denser distribution of AuNP aggregates. The increased proportion of aggregated AuNPs and smaller interparticle spacing in CPAM-treated AuNP-deposited paper increased the coupling of Localized Surface Plasmon Resonances (LSPRs), which arise

from the collective oscillation of electrons within metallic NPs [24]. This resulted in the formation of enhanced electromagnetic fields (hot spots), particularly at curved surfaces or gaps in between the AuNPs, thereby improving amplification of SERS signal. Increasing the SERS enhancement factor by decreasing the spacing between the nanostructures has previously been studied; nanostructures with gaps smaller than 10 nm can achieve higher Raman Enhancement Factor (EF) [25–29]. Pre-treating paper with CPAM maximized the spatial density of AuNPs aggregates, forming hot spots with less than 10 nm of interparticle spacing (Figs. 2, 4 and 6). The three-dimensional and porous structure of paper is able to provide a greater surface area to localize the adsorption of analyte molecules in the vicinity of the hot spots, particularly at ultra-low concentrations. Fig. 3 shows that the Raman EF of 1 mM of 4-ATP from the AuNPs-CPAM paper (8.9×10^8) was almost an order of magnitude greater than that of untreated AuNPs paper (2.1×10^8). This Raman EF exceeds 10^7 , which is a typical enhancement factor for many micro/nanofabricated nanoclusters SERS substrates under excitation of Raman red laser [30–32]. Such EF (within the range of 10^7 – 10^8) is sufficient for single-molecule SERS detection [33,34]. Besides the magnitude of EF, reproducibility of a SERS substrate is critical since most of the SERS-based sensing is relying on the intensity of particular spectral bands to determine the analyte concentration. The AuNPs-CPAM paper showed a lower signal deviation ($\pm 12\%$) than the untreated AuNPs paper ($\pm 29\%$) (Fig. 3), therefore improving reproducibility. The AuNPs-CPAM paper also scattered the surface enhanced Raman signal at different points with minimum variation in intensity.

An ideal SERS active substrate needs uniform distribution of nanoparticles at the sub-micrometer scale to achieve high degree of reproducibility [35]. This is a critical issue to develop paper as a SERS substrate, since it is a challenge to achieve uniform distribution of nanoparticles on paper due to heterogeneity at the micron level (fiber and surface roughness), meso level (porosity fibers dimensions), and macro-level (fiber flocculation). This issue was overcome with CPAM pre-treated paper which produced a coating of uniform AuNPs aggregates compared to the plain paper substrate (Fig. 2); this contributed to a more reproducible SERS signal (Fig. 3). Important considerations in the fabrication of AuNPs-CPAM paper substrates are the stability of substrate during application of analyte and SERS signal interference of CPAM to the SERS signal of analyte. It was found that AuNPs were well retained on paper by CPAM, and their desorption was negligible during the analyte detection process (Supporting information, S1). Furthermore, CPAM adsorbed on paper has very weak SERS spectral features (Supporting information S2) and does not interfere with the SERS signal of analyte.

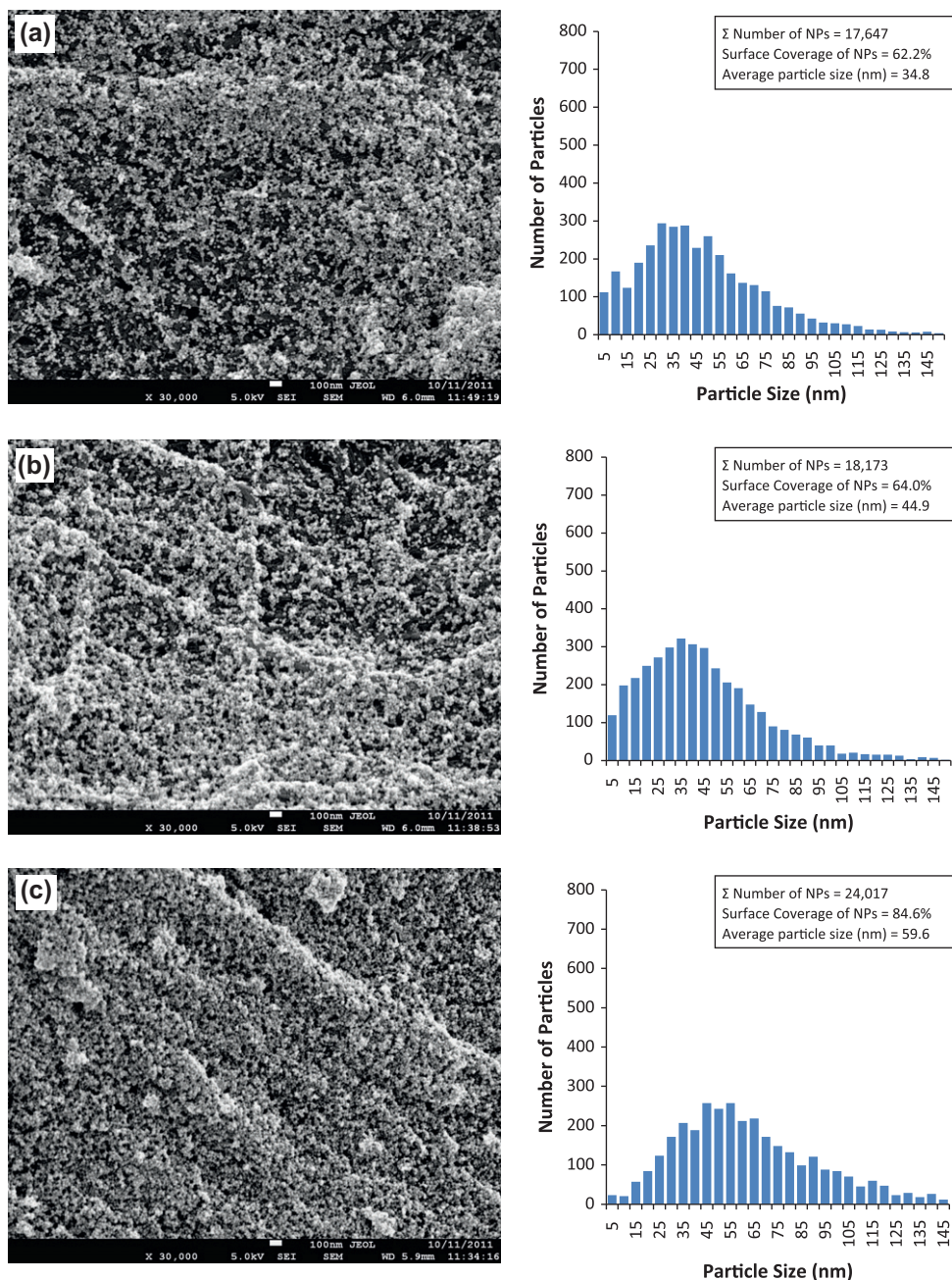


Fig. 4. FESEM images and histograms of particle size distribution of AuNPs-CPAM papers treated with polymer solution charge density of: (a) 5 wt%, (b) 10 wt%, and (c) 40 wt%.

In terms of SERS sensitivity, AuNPs-CPAM paper showed a higher SERS intensity at all concentrations of 4-ATP and lower detection limit than for AuNPs on untreated paper (Figs. 8 and 9). A sigmoidal relationship between the SERS intensity and concentration of 4-ATP was observed for both paper substrates (Fig. 10). At low analyte concentration, the response was linear, while SERS intensity became saturated when the concentration of 4-ATP was high. The intensity plateau for AuNPs-CPAM paper is three times higher than that of the AuNPs paper, probably because of the higher surface coverage and concentration of AuNPs. Overall, the aggregation and higher density of AuNPs induced by CPAM at least doubled the SERS sensitivity of the substrate over the complete 4-ATP concentration range.

4.2. Mechanism

AuNPs were previously adsorbed and retained as individual particles on paper upon dipping in an AuNPs suspension [18]; their surface coverage on paper scaled linearly with the concentration of AuNP solutions, and the Raman Enhancement Factor (EF) increased proportionally with the surface coverage of AuNPs. In this study, paper was pre-treated with cationic polyacrylamides (CPAM) of different concentration, charge densities, and molecular weight to drastically increase the surface coverage of AuNPs on paper, as well as to control and increase their aggregate size. CPAM polymers are generally used as retention aids in the papermaking process, but they have not been investigated for their ability to retain

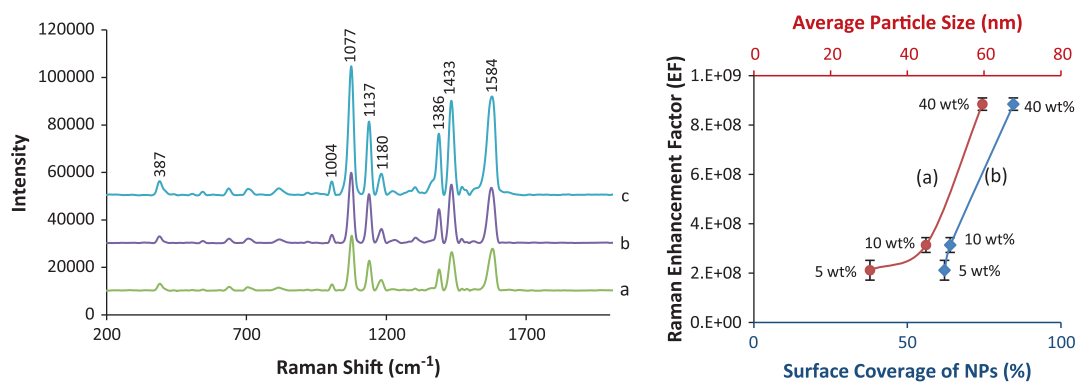


Fig. 5. (Left) SERS spectra of 4-ATP on AuNPs-CPAM papers with polymer's charge density of (a) 5 wt%, (b) 10 wt%, and (c) 40 wt%. (Right) Relationship between the: (a) average size and (b) surface coverage of AuNP aggregates and the EF of 4-ATP measured at the 1077 cm^{-1} band (error bars show standard deviation of five measurements from different spots on the substrate).

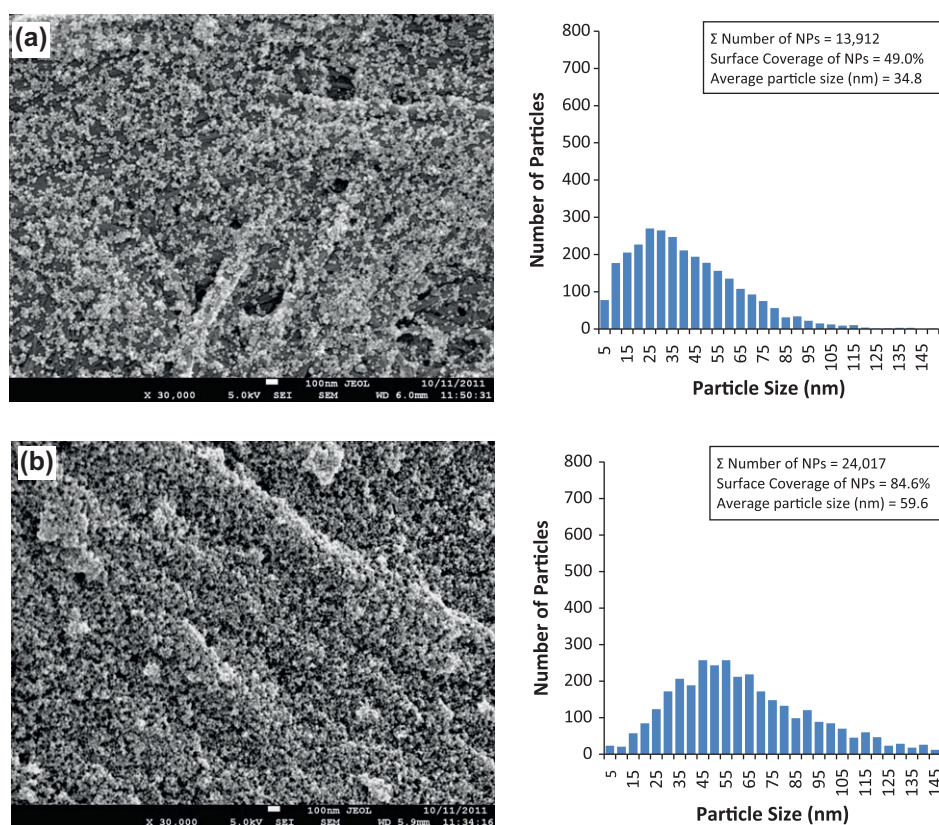


Fig. 6. FESEM images and histograms of particle size distribution of AuNPs-CPAM papers with polymer's molecular weight of: (a) 6 MDa and (b) 13 MDa.

or flocculate NPs onto paper. An objective of this study was to exploit this mechanism to significantly amplify the SERS signal by increasing the concentration of hot spots.

CPAM affected both the AuNPs inter-particle interaction and their adsorption on cellulose fibers. The adsorption of CPAM contributed to an electrostatic attraction (AuNP–AuNP and AuNPs–fiber) and introduced bridging and steric components. The extended and adsorbed conformation of a polyelectrolyte in solution or adsorbed on a surface is affected by pH, ionic strength, concentration, charge density, and molecular weight of the polymer. In this study, ionic strength and pH were kept constant.

The main driving forces for the adsorption of CPAM on cellulose fibers are Van der Waals and electrostatic forces [36,37]. The cationic polyelectrolyte adsorbed onto the negatively charged cellu-

lose fibers forming train, loop, and tail. The tails and loops extended into the solution phase, driven by strong intramolecular electrostatic repulsion and affinity for water, while the train sections adhered to the surface due to electrostatic affinity [38–41]. During the dipping of CPAM pre-treated papers into AuNPs solution, aggregation and retention of AuNPs could be induced by a combination of bridging, charge neutralization, or patch interaction mechanisms [42]. This triple role of CPAM produced a much higher surface coverage and higher aggregation of AuNPs compared to the untreated paper (Fig. 2a and b).

The concentration of the CPAM solution with which paper was pre-treated played a dominant role in the adsorption and aggregation of AuNPs on paper (Fig. 2). Charged patch mechanisms would be most likely for papers pre-treated with CPAM at lower

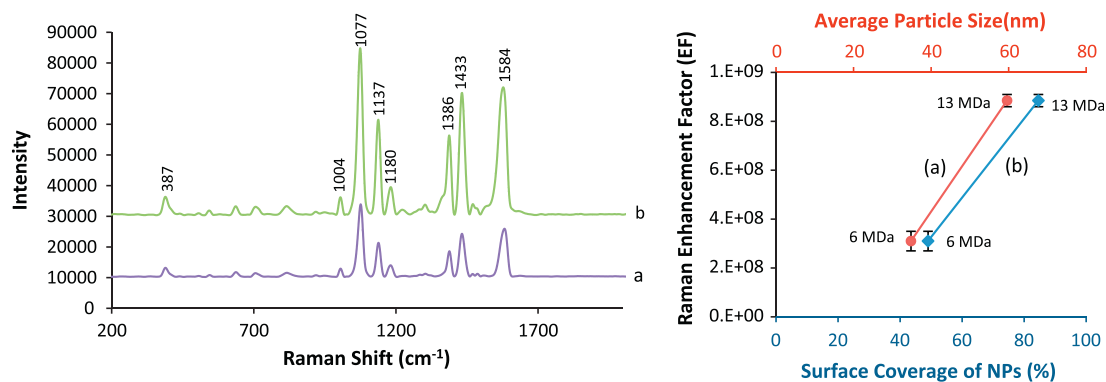


Fig. 7. (Left) SERS spectra of 4-ATP on AuNPs-CPAM papers with polymer's molecular weight of: (a) 6 MDa and (b) 13 MDa. (Right) Relationship between the: (a) average size and (b) surface coverage of AuNP aggregates and the EF of 4-ATP measured at the 1077 cm^{-1} band (error bars show standard deviation of five measurements from different spots on the substrate).

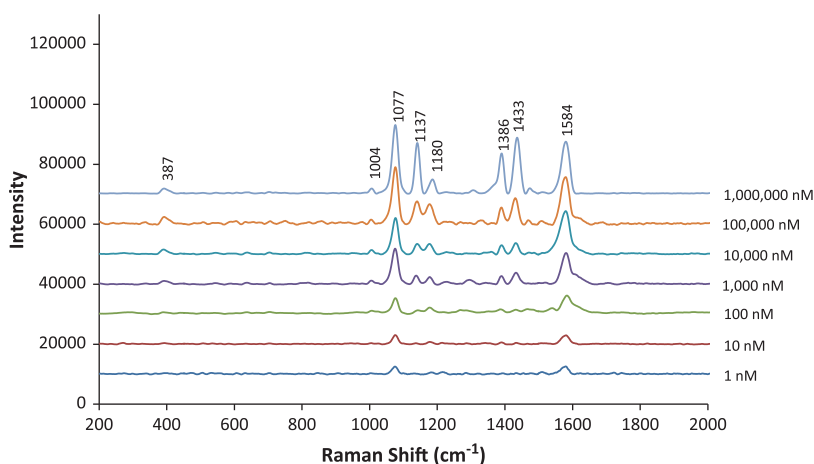


Fig. 8. SERS spectra of different concentration of 4-ATP from untreated AuNPs paper.

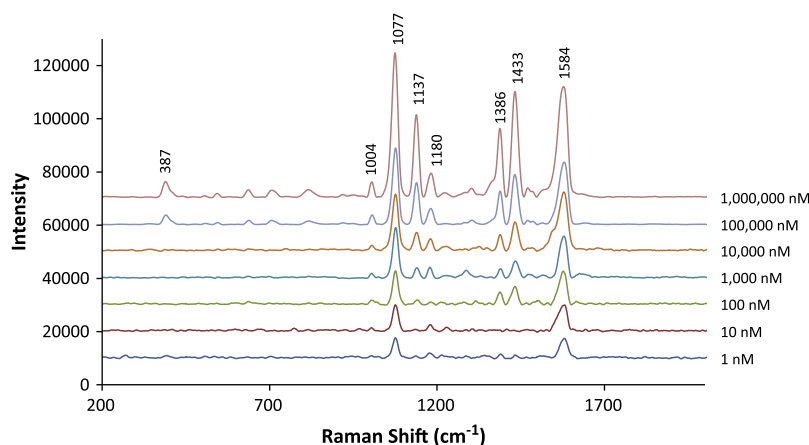


Fig. 9. SERS spectra of different concentration of 4-ATP from AuNPs-CPAM paper.

concentration [41]. At such low CPAM concentrations, a flat polymer chain conformation (Fig. 11a) is expected due to a low density of chains on the surface and their tendency to relax into a flatter configuration [42]. Increasing the polymer concentration in solution leads to increased extended polymer tails and loops having a superior bridging ability [42] and results in a higher adsorption

and aggregation of AuNPs (Fig. 11b). Charge neutralization can also occur, where the average negative charge of cellulose fibers is reduced, neutralized, and reverted to a positive charge upon adsorption of CPAM. The increased positive charge on paper with increased concentration of CPAM produced a greater electrostatic interaction between paper surface and negatively charged AuNPs.

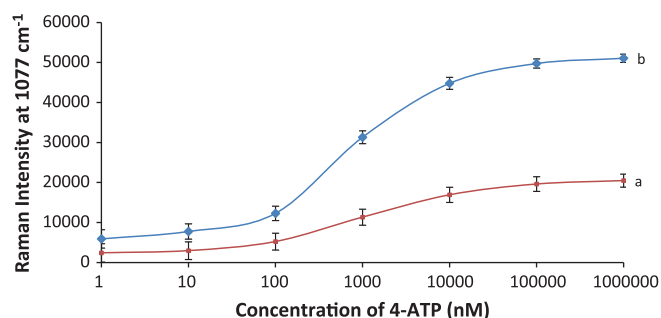


Fig. 10. SERS intensity of different concentration of 4-ATP from: (a) AuNPs paper and (b) AuNPs-CPAM paper at 1077 cm^{-1} band.

The magnitude of the Raman EF of the AuNPs-CPAM paper substrate can be tuned by controlling the concentration of CPAM (Fig. 3). Higher surface coverage and aggregation of AuNPs resulted in the formation of rough metallic surfaces ("hot spots") as paper was pre-treated with higher concentration of CPAM. This gave rise to stronger electromagnetic coupling to enhance the Raman signal of 4-ATP (EF of almost an order of magnitude higher than the untreated AuNPs paper).

Coulombic interactions between polymer segments and surface, as well as between charges in the polymer chains affect polymer adsorption. Flocculation of AuNPs by lower charged CPAM was expected to occur through bridging since polymer with lower charge density tends to form loops and tails upon adsorption [37,39]. Higher surface coverage and aggregation of AuNPs were observed when paper was pre-treated by CPAM of higher charge density (Fig. 4). The high charged CPAM probably adsorbed on cellulose fibers via charge neutralization. This is because polymer with a higher charge density tends to have a flat conformation on the surface [43], and their electrostatic interaction increases with increasing charge density [44,45]. However, bridging could also be involved. Since the highly charged CPAM has a higher charge density than paper, there is a possibility that the excess charge of the polymer could provide an electrostatic force that might repel some polymer segments from those adsorbed on paper, resulting in more loops and tails [46]. We believe that in a combination of charge neutralization and bridging mechanisms, CPAM of higher charge density produced a higher surface coverage and greater aggregation of AuNPs for a higher Raman EF (Fig. 5).

Higher levels of adsorption and greater aggregation of AuNPs were achieved with paper pre-treated with CPAM of higher molecular weight (Fig. 6). This agrees well with several studies [47–49] reporting that the bridging effectiveness of cationic polymer increases with their molecular weight. The increase in the estimated radius of gyration for CPAM with molecular weight of 6 MDa and

13 MDa from 26 nm to 38 nm supported this observation (Supporting information, S3). CPAM of higher molecular weight had a greater bridging effect due to the greater extension of loops and tails, increasing its ability to adsorb more AuNPs (Fig. 11b), which enhanced the SERS performance (Fig. 7).

5. Conclusion

Paper treated with gold nanoparticles (AuNPs) was engineered as substrate for SERS application to develop a robust and low-cost biodiagnostic platform. The objective of this study was to drastically increase the SERS enhancement factor (EF) of AuNPs paper by controlling the aggregation size and surface coverage of AuNPs on paper. This was achieved by pre-treating paper with a cationic polyelectrolyte to control the extent of AuNPs coagulation on paper. A series of cationic polyacrylamides (CPAM) was studied. The effect of CPAM solution concentration, polymer charge density, and molecular weight on AuNPs' adsorption/aggregation behavior and SERS properties was measured. Paper was first dipped into the CPAM solution before a second dipping in the AuNP suspension, and 4-aminothiophenol (4-ATP) was selected as the SERS probe. The aggregate size distribution and surface coverage of AuNPs on paper were quantified by FESEM image analysis.

The Raman Enhancement Factor (EF) increased pseudo-linearly with the surface coverage and the aggregation size of AuNPs on paper. The surface coverage, average particle size, and particle size distribution all increased with the concentration, charge density, and molecular weight of CPAM solution with which paper was pre-treated.

The CPAM pre-treated paper produced a more uniform coating of AuNPs compared to bare paper substrate. A surface coverage of AuNPs on paper up to 80% with average AuNP aggregates up to 60 nm were achieved. The AuNPs were adsorbed as uniformly distributed aggregates on paper despite the inherent heterogeneity of the substrate morphology. These AuNP aggregates formed a rough metallic surface, with increased particles junction for a stronger electromagnetic coupling that tremendously amplified the Raman signal of 4-ATP. The Raman EF of AuNPs-CPAM paper was almost an order of magnitude higher and more reproducible than the untreated AuNPs paper at constant concentration of AuNPs suspension.

We believe the CPAM chains adsorbed on paper in a high loops and tails conformation, which promote efficient bridging of AuNPs to adsorb at higher surface coverage on paper and form larger aggregates. This configuration was favored by CPAM solutions of higher concentration, charge density, and molecular weight.

AuNPs paper is an excellent substrate for SERS applications, especially when the aggregation state and surface coverage of AuNPs are engineered by pre-treating paper with CPAM. This

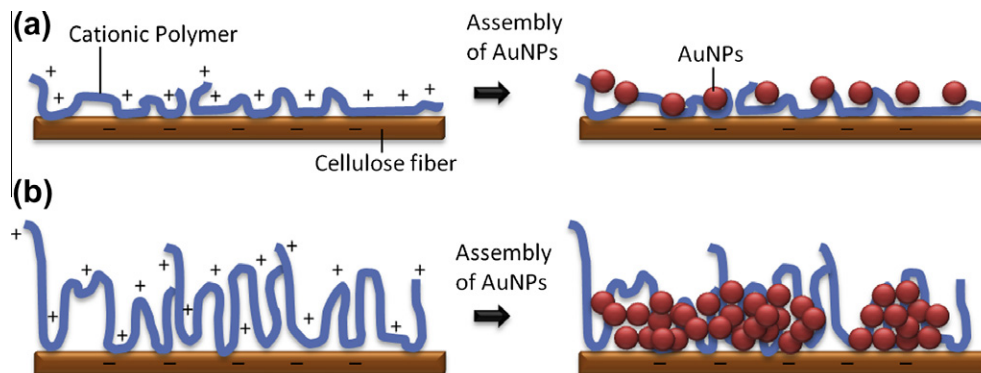


Fig. 11. (a) Polymer attains a flat conformation with many trains at the interface. (b) Polymer attains a conformation with many loops and tails tangling out of the surface.

approach offers a robust bio-diagnostics platform to yield molecular structural information for qualitative analysis.

Acknowledgments

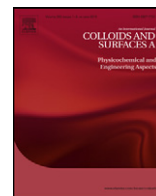
Thanks to Dr. T. Williams, Monash Centre for Electron Microscopy (MCEM), for FESEM technical expertise and F. Shanks from Monash Molecular Spectroscopy and Centre for Biospectroscopy for Raman technical advice. The financial supports from the ARC Linkage LP0989823 and Visy, Amcor, SCA, Norske Skog, Australian Paper, the Australian Pulp and Paper Institute and Monash University are all acknowledged.

Appendix A. Supplementary material

Supplementary data associated with this article can be found, in the online version, at <http://dx.doi.org/10.1016/j.jcis.2012.09.080>.

References

- [1] M. Al-Tamimi, W. Shen, R. Zeineddine, H. Tran, G. Garnier, *Anal. Chem.* 84 (2011) 1661.
- [2] M.S. Khan, G. Thouas, W. Shen, G. Whyte, G. Garnier, *Anal. Chem.* 82 (2010) 4158.
- [3] X. Li, J. Tian, W. Shen, *Anal. Bioanal. Chem.* 396 (2010) 495.
- [4] X. Li, J. Tian, T. Nguyen, W. Shen, *Anal. Chem.* 80 (2008) 9131.
- [5] M.S. Khan, D. Fon, X. Li, J. Tian, J. Forsythe, G. Garnier, W. Shen, *Colloids Surf. B* 75 (2010) 441.
- [6] X. Li, J. Tian, G. Garnier, W. Shen, *Colloids Surf. B* 76 (2010) 564.
- [7] M.S. Khan, J. Tian, L. Xu, W. Shen, G. Garnier, *Advances in Pulp and Paper Research*, St. Anne's College, Oxford, 2009.
- [8] F. Toderas, M. Baia, L. Baia, S. Astilean, *Nanotechnology* 18 (2007).
- [9] S.W. Lee, Y.-B. Shin, K.S. Jeon, S.M. Jin, Y.D. Suh, S. Kim, J.J. Lee, M.-G. Kim, *Ultramicroscopy* 108 (2008) 1302.
- [10] Q. Min, M.J.L. Santos, E.M. Girotto, A.G. Brolo, R. Gordon, *J. Phys. Chem. C* 112 (2008) 15098.
- [11] D.L. Stokes, Z. Chi, T. Vo-Dinh, *Appl. Spectrosc.* 58 (2004) 257.
- [12] Z. Luo, Y. Fang, *J. Colloid Interface Sci.* 283 (2005) 459.
- [13] A. Berthod, J.J. Laserna, J.D. Winefordner, *J. Pharm. Biomed. Anal.* 6 (1988) 599.
- [14] L.M. Cabalín, J.J. Laserna, *Anal. Chim. Acta* 310 (1995) 337.
- [15] W. Ma, Y. Fang, *J. Colloid Interface Sci.* 303 (2006) 1.
- [16] Z. Niu, Y. Fang, *J. Colloid Interface Sci.* 303 (2006) 224.
- [17] D. Wu, Y. Fang, *J. Colloid Interface Sci.* 265 (2003) 234.
- [18] Y.H. Ngo, D. Li, G.P. Simon, G. Garnier, *Langmuir* 28 (2012) 8782.
- [19] A.M. Michaels, J. L. Brus, *J. Phys. Chem. B* 104 (2000) 11965.
- [20] J. Turkevich, P.C. Stevenson, J. Hillier, *Discuss. Faraday Soc.* 11 (1951) 55.
- [21] P.H.C. Camargo, L. Au, M. Rycenga, W. Li, Y. Xia, *Chem. Phys. Lett.* 484 (2010) 304.
- [22] X. Hu, T. Wang, L. Wang, S. Dong, *J. Phys. Chem. C* 111 (2007) 6962.
- [23] A.C. Peacock, A. Amezcua-Correa, J. Yang, P.J.A. Sazio, S.M. Howdle, *Appl. Phys. Lett.* 92 (2008).
- [24] J. He, P. Zhang, J. Gong, Z. Nie, *Chem. Commun.* 48 (2012) 7344.
- [25] A. Dhawan, Y. Zhang, F. Yan, M. Gerhold, T. Vo-Dinh, in: T. Vo-Dinh, J.R. Lakowicz (Eds.), first ed., SPIE, San Jose, CA, USA, 2008, p. 68690G.
- [26] A. Chen, A.E. DePrince, A. Demortière, A. Joshi-Imre, E.V. Shevchenko, S.K. Gray, U. Welp, V.K. Vlasko-Vlasov, *Small* 7 (2011) 2365.
- [27] T. Cuifeng, L. Zhen, J. Jiehong, L. Sergei, H. Cheng, Y. Hongjun, L. Rui, W. Liqun, S. Xiaoping, D. Bingjun, W. Stefan, S. Thomas, F. Jixiang, *Nanotechnology* 23 (2012) 165604.
- [28] H. Chu, J. Wang, L. Ding, D. Yuan, Y. Zhang, J. Liu, Y. Li, *J. Am. Chem. Soc.* 131 (2009) 14310.
- [29] W.J. Cho, Y. Kim, J.K. Kim, *ACS Nano* 6 (2011) 249.
- [30] W.W. Yu, I.M. White, *Anal. Chem.* 82 (2010) 9626.
- [31] M.-L. Cheng, B.-C. Tsai, J. Yang, *Anal. Chim. Acta* 708 (2011) 89.
- [32] C.H. Lee, M.E. Hankus, L. Tian, P.M. Pellegrino, S. Singamaneni, *Anal. Chem.* 83 (2011) 8953.
- [33] P.G. Etchegoin, E.C. Le Ru, *Phys. Chem. Chem. Phys.* 10 (2008) 6079.
- [34] E.C. Le Ru, E. Blackie, M. Meyer, P.G. Etchegoin, *J. Phys. Chem. C* 111 (2007) 13794.
- [35] Y. Ngo, D. Li, G.P. Simon, G. Garnier, APPITA Conference, Melbourne, 2010.
- [36] M. Borkovec, G. Papastavrou, *Interface Sci.* 13 (2008) 429.
- [37] M.A. Hubbe, H. Nanko, M.R. McNeal, *Bioresources* 4 (2009) 850.
- [38] B. Abu-Sharkh, *Langmuir* 22 (2006) 3028.
- [39] G.J. Fleer, M.A.C. Stuart, J.M.H.M. Scheutjens, T. Cosgrove, B. Vincent, *Polymers at Interfaces*, Chapman & Hall, London, 1998.
- [40] L. Wågberg, *Nord. Pulp Pap. Res. J.* 15 (2000) 586.
- [41] W.K.J. Mosse, D.V. Boger, G.P. Simon, G. Garnier, *Langmuir* 28 (2012) 3641.
- [42] T. Sennerfors, *Encyclopedia of Surface and Colloid Science*, second ed., 2006, p. 4874.
- [43] Y. Shin, J.E. Roberts, M.M. Santore, *J. Colloid Interface Sci.* 247 (2002) 220.
- [44] M. Polverari, T.G.M. van de Ven, *J. Phys. Chem.* 100 (1996) 13687.
- [45] T. Lindstrom, C. Soremark, C. Heinegard, S. Martin-Lof, *Tappi J.* 57 (1974) 94.
- [46] P.M. Claesson, M.A.G. Dahlgren, L. Eriksson, *Colloids Surf. A* 93 (1994) 293.
- [47] T. Lindström, C. Söremark, *J. Colloid Interface Sci.* 55 (1976) 305.
- [48] H. Zhang, F. Chen, H. Hu, *China Pulp Paper* 22 (2003) 15.
- [49] R.I.S. Gill, T.M. Herrington, *Colloids Surf.* 25 (1987) 297.



Effect of cationic polyacrylamide dissolution on the adsorption state of gold nanoparticles on paper and their Surface Enhanced Raman Scattering properties

Ying Hui Ngo¹, Dan Li², George P. Simon², Gil Garnier^{1,*}

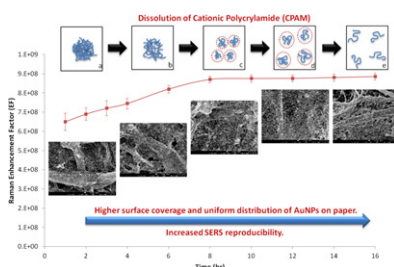
¹ BioPRIA, Australian Pulp and Paper Institute (APPI), Department of Chemical Engineering, Monash University, Clayton, VIC 3800, Australia

² Department of Material Engineering, Monash University, Clayton, VIC 3800, Australia

HIGHLIGHTS

- Dissolution kinetic of CPAM greatly affected AuNPs distribution on paper.
- Higher charge density CPAM dissolves faster and produces uniformly distributed AuNPs for higher SERS reproducibility.
- Understanding CPAM dissolution kinetic is able to optimize SERS performance of AuNPs-paper.

GRAPHICAL ABSTRACT



ARTICLE INFO

Article history:

Received 8 November 2012

Received in revised form

10 December 2012

Accepted 12 December 2012

Available online 20 December 2012

Keywords:

Cationic polyacrylamide (CPAM)

Dissolution

SERS

Gold nanoparticles (AuNPs)

Aggregates

Paper

Charge density

Reproducibility

ABSTRACT

This study examines and quantifies the effect of cationic polyacrylamide (CPAM) dissolution kinetics and charge density on the adsorption and aggregation state of gold nanoparticles (AuNPs) on paper and the resulting Surface Enhanced Raman Scattering (SERS) performance. Dissolution kinetics of CPAM of different charge density was studied by monitoring their viscosity and hydrodynamic diameter over regular intervals of time. It was found that the degree of dissolution of CPAM greatly affected the surface coverage and aggregation of AuNPs on the CPAM pre-adsorbed paper substrate and their SERS reproducibility. CPAM of higher charge density dissolves faster and produced a more uniform aggregation and higher surface coverage of AuNPs on paper for a higher and more reproducible Raman EF. Understanding the CPAM dissolution process enables the optimization of SERS performance of the AuNPs-paper as a bio-diagnostic platform.

Crown Copyright © 2012 Published by Elsevier B.V. All rights reserved.

1. Introduction

Paper has emerged as a substrate of choice in the fabrication of low-cost diagnostic platforms for medical and environmental applications [1–2]. One of these developing applications is bioactive paper diagnostic for blood typing, wherein blood agglutination is triggered by specific antibody–antigen interactions

and indicated by chromatographic separation on paper [1–3]. However, bioactive papers often suffer from four major issues: Specificity, Selectivity, Sensitivity and Simplicity (4S). Among these issues, sensitivity can be a major limiting factor, with a detection range of 10^{-6} M for many colorimetric techniques. For certain applications, such as cancer detection, this can be inadequate and a detection range up to 10^{-9} or 10^{-12} M might be desirable. To address this issue, paper can be treated with metallic nanoparticles to produce a Surface Enhanced Raman Scattering (SERS) active substrate to identify analytes at trace levels [4–10].

* Corresponding author. Tel: +61 3 9905 9180

E-mail address: Gil.Garnier@monash.edu (G. Garnier).

SERS involves the enhancement of Raman signal to detect small energy changes occurring when light is scattered from a molecule which is absorbed on a metallic substrate, typically metallic nanoparticles [11]. The SERS enhancement factor is generally increased with the density of “hotspots” created by close contact points between metallic nanoparticles. In a previous study, filter paper was pre-treated with high molecular weight cationic polyacrylamide (CPAM) to retain gold nanoparticles (AuNPs) on paper and to increase the “hot spot” concentration by controlling the aggregation of AuNPs [12]. The aggregate size, surface coverage of AuNPs on paper and SERS enhancement factor all increased with the concentration, charge density and molecular weight of CPAM adsorbed on paper. Importantly, the preparation of CPAM solution was found to have a strong influence on the aggregation state of AuNPs on paper and the SERS reproducibility. The optimum preparation method was also found to vary depending on the CPAM charge density and molecular weight. CPAM was selected as polyelectrolyte for its wide industrial use as retention aid and flocculant; very high molecular CPAM were chosen for their enhanced ability to coagulate nano-colloids and also to serve as spacer for biomolecules.

Reproducibility of SERS substrate is critical, since SERS-based sensing typically rely on the intensity of particular spectral bands to determine analyte concentration. The reproducibility of SERS intensity from nanoparticles treated paper depends on the packing density and arrangement of the nanoparticles. The formation of uniform surface coverage, aggregation state and distribution of the AuNPs on paper at the nano- and micron-scale is especially important and challenging due to the high heterogeneity inherent of paper. The porosity, surface roughness, fiber size and distribution within a floc all affect paper heterogeneity over three orders of magnitude, from the micrometer (μm) to the centimetre (cm) length scale. It is therefore important to understand and optimize how polymer can retain the AuNPs in a constant and reproducible distribution on paper.

In this study, we first quantify the effect of CPAM dissolution kinetics and charge density on the adsorption and aggregation state of AuNPs on paper. We then link the AuNPs distribution on paper to the resulting SERS performance. We investigate the hypothesis that the preparation of the CPAM solution is a critical variable affecting the final conformation and uniformity of CPAM adsorbed on paper, which then controls the subsequent AuNPs adsorption state on paper and the reproducibility of the SERS signal. It is the objective of this study to quantify and control the effect of polymer dissolution kinetics on its adsorption conformation and the aggregation state of nanoparticle to optimize the SERS efficiency of AuNPs treated paper used as a bio-diagnostic platform.

2. Materials and methods

2.1. Material

Hydrogen tetrachloroaurate trihydrate ($\text{HAuCl}_4 \cdot 3\text{H}_2\text{O}$), sodium citrate tribasic dihydrate ($\text{Na}_3\text{C}_6\text{H}_5\text{O}_7 \cdot 2\text{H}_2\text{O}$) and 4-aminothiophenol (4-ATP) were purchased from Sigma–Aldrich and used as received. The cationic polyacrylamide (CPAM) polymers were kindly supplied by AQUA+TECH Switzerland from their SnowFlake Cationics product range, and used as received. These were copolymers of uncharged acrylamide with cationic dimethylaminoethylacrylate methyl chloride and identified as: I1 (5 wt% charge density, molecular weight 13 MDa), H1 (10 wt% charge density, molecular weight 13 MDa) and F1 (40 wt% charge density, molecular weight 13 MDa). The granulometry (particle size distribution) of all the CPAMs was similar and ranges from 0.125 mm to 1.120 mm, as specified by the supplier. Whatman

qualitative filter paper #1, which consists of 98% α -cellulose, was selected as the paper substrate; it is a convenient model paper of well defined structure and to ensure minimal SERS interference from process components (polymers or coatings). Ultrapure water purified with a Millipore system ($18\text{ M}\Omega\text{ cm}$) was used in all aqueous solutions and rinsing procedures.

2.2. Dissolution rate of CPAM

The dissolution rate of CPAM in solution was studied by dissolving dry powder of CPAM to 0.1 mg/mL with Millipore water in 10 beakers, and gently shaking the dispersions in a shaking incubator (23°C , 150 rpm). Each beaker of CPAM solution was taken out from the incubator every 1–2 h to test its viscosity. The viscosity was determined with a BS/U-tube capillary viscometer of size A (viscosity range from 0.9 to 3 cSt) to measure the time needed for the solution to pass through a certain length of the capillary. The viscosity of CPAM was estimated using the following equation:

$$\eta_2 = \frac{\eta_1 \rho_2 t_2}{\rho_1 t_1} \quad (1)$$

where η_1 , ρ_1 and t_1 are the viscosity, density and average time for water (control) and η_2 , ρ_2 and t_2 are the viscosity, density and average time for CPAM. For this experiment, $\eta_1 = 1\text{ cSt}$, $\rho_1 = 1.00\text{ gm/cm}^3$ and $\rho_2 = 0.97\text{ gm/cm}^3$.

2.3. Synthesis and deposition of nanoparticles on paper substrates

AuNPs were synthesized by using 1 mM $\text{HAuCl}_4 \cdot 3\text{H}_2\text{O}$ and 1% aqueous $\text{Na}_3\text{C}_6\text{H}_5\text{O}_7 \cdot 2\text{H}_2\text{O}$ according to the Turkevich method [13]. Filter papers (55 mm diameter) were used as received, or were pre-treated with the cationic polymer. For polymer treatment, the filter papers were dipped into 10 mL polymer solutions for 1 h, rendering the paper cationic. The treated papers were then rinsed with distilled water. Without drying, pieces of untreated and polymer-treated paper substrates were subsequently dipped directly into Petri dishes which contained 10 mL solution of AuNPs for 24 h. After dipping, the paper substrates were rinsed thoroughly with distilled water to remove any loosely bound AuNPs, and the papers were air-dried and stored at 50% relative humidity and 23°C until further analysis.

2.4. Preparation of Raman active substrates

Solutions of 1 mM of 4-ATP were prepared in ethanol. 4-ATP is known for its strong affinity for the gold surface of AuNPs; its S–H bond is easily cleaved to form Au–S bond upon adsorption. The dried AuNPs-deposited substrates were dipped into 2 mL of the 4-ATP ethanol solution for a shorter period of time of 5 min to obtain a monolayer of 4-ATP on the substrates. After thorough rinsing with ethanol and drying, they were subjected to Raman characterization. The Raman enhancement factor (EF) of 1 mM of 4-ATP on a substrate was calculated according to [14–15]:

$$EF = \frac{[I_{\text{SERS}}]}{[I_{\text{bulk}}]} \times \frac{[N_{\text{bulk}}]}{[N_{\text{SERS}}]} \quad (2)$$

where I_{SERS} is the intensity of a specific band in the SERS spectrum of 4-ATP and I_{bulk} is the intensity of the same band in the Raman spectrum from the bulk solution sample. For all spectra, the intensity of the band at 1077 cm^{-1} was used to calculate EF values. N_{bulk} is the number of molecules of the bulk 4-ATP in the laser illumination volume while N_{ads} is the number of molecules adsorbed and sampled on the SERS active substrate within the laser spot.

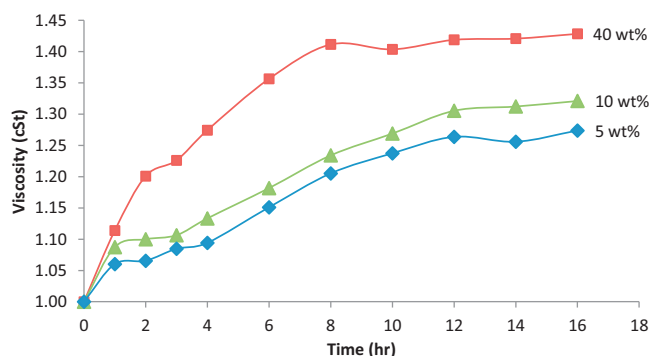


Fig. 1. Effect of dissolution time and CPAM charge density on the viscosity of polymer solutions. CPAM (13 MDa) 0.10 mg/mL at room temperature in water.

2.5. Instrumentation

Field Emission Scanning Electron Microscopy (FESEM), which produces higher resolution, less sample charging and less damaged images than conventional SEM, was performed using a JEOL 7001 Field Emission Gun (FEG) system operating at 5 kV and 180 pA. The Dynamic Light Scattering (DLS) measurements were performed with a Zetasizer Nano ZS (Malvern Instruments) in a Folded Capillary cell (DTS1060) at 25 °C. All Raman and SERS spectra were obtained in air using a Renishaw Invia Raman microscope equipped with 300 mW 633 nm laser (integration time of 1 s). The laser beam was positioned through a Leica imaging microscope objective lens (50×), whilst the instrument's wavenumber was calibrated with a silicon standard centered at 520.5 cm⁻¹. Due to the smaller spot size of the laser compared with the large surface area of the samples, the spectra were obtained at 5 different points of the surface. The position of the spectra band from different points on the surface were the same, but differed only in intensity. The averaged Raman intensity (of 5 measurements) was presented as the final result, after baseline subtraction from the control samples.

3. Results

3.1. Dissolution of CPAM

The different CPAM polymer powders were dissolved in water under constant shear, temperature and concentration, and the viscosity of the polymer solution was measured as a function of time. The viscosity of all CPAM solutions initially increased with mixing time and levelled-off (Fig. 1). The viscosity of the CPAM solutions increased with the polymer charge density at a constant molecular weight. The viscosity of CPAM of 40 wt% charge density increased to reach a plateau after 8 h. For CPAM of 10 wt% and 5 wt% charge density, the solution viscosity became constant only after 12 h of mixing.

The viscosity of a polymer solution is an indication of the concentration, structure, organization and size of the dissolving polymer molecules. Dynamic light scattering (DLS) measurements of the CPAM solutions were performed at the same regular intervals. The relationship between the hydrodynamic diameter of CPAM and their dissolution time (Fig. 2) was similar to the relationship between their viscosity and mixing time (Fig. 1). For polymer solutions made with CPAM 5 wt% charge density, viscosity increased in a similar fashion as with the other CPAMs (although with less intensity), but hydrodynamic diameter remained fairly constant over the dissolution time. The absolute value of the hydrodynamic diameters of CPAM aggregate/coil must be interpreted with care, as the measured values were often outside the usual range of polydispersity ($P \geq 1$), indicated by the instrument

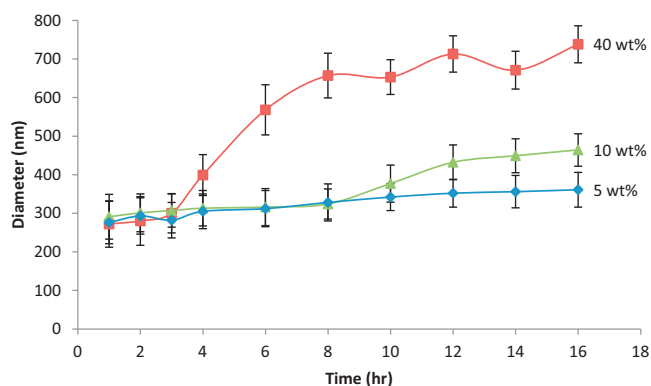


Fig. 2. Effect of dissolution time and CPAM charge density on the average hydrodynamic diameter. CPAM (13 MDa) 0.10 mg/mL at room temperature in water. Error bars indicate the standard deviations from five measurements.

software. The hydrodynamic diameter of dissolved CPAM molecules increased with mixing time to reach a plateau after 8 h and 12 h of mixing for CPAM of 40 wt%, 10 wt% and 5 wt% (less gradual increase) charge density, respectively.

3.2. Properties of AuNPs-CPAM paper

Filter papers were pre-treated with a series of CPAM solutions, which were prepared for different mixing time periods; and followed by dipping in a 0.20 mg/mL of AuNP solution. Particle size measurement of the AuNP solution by DLS revealed highly monodispersed AuNPs with an average diameter of 23.2 nm. FESEM analysis was performed to examine the adsorption of AuNPs on the CPAM pre-treated paper substrates (Fig. 3). The average aggregate diameter and surface coverage of AuNPs were quantified by applying a threshold so that the AuNPs in the FESEM images were changed to black colour and the cellulose fibers to white using ImageJ software from the National Institute of Health (NIH). The surface coverage of AuNPs was the proportional percentage of black coloured area to the total area of the images. The average diameter (Fig. 4) and surface coverage (Fig. 5) of AuNPs on paper increased and levelled off as a function of the CPAM's charge density. The levelling effect of AuNPs surface coverage (Fig. 5) was not attributed to the depletion of the NPs concentration as the amount of AuNPs in suspension was in large excess (Supporting Information). The AuNPs were adsorbed as aggregates of random size and lower surface coverage when papers were pre-treated with CPAM dissolved in a shorter period of time. As the CPAM solution was mixed longer, the distribution of AuNP aggregates on paper was more uniform and denser (Fig. 3).

4-Aminothiophenol (4-ATP) was selected as the probe molecule for the Raman analysis, as in our previous studies [12]. The SERS spectra of 4-ATP were dominated by three strong characteristic peaks: $\delta(\text{C-S})$ at 387 cm⁻¹, $\nu(\text{C-S})$ at 1077 cm⁻¹ and $\nu(\text{C-C})$ at 1584 cm⁻¹, which were the a_1 vibrational modes (in-plane, in-phase modes) of the 4-ATP molecules (Fig. 6). The significant enhancement of a_1 modes was related to the enhancement of the electromagnetic field between the AuNPs, which was produced by strong inter-nanoparticle coupling among the AuNPs in close contact. The SERS spectra showed a higher signal to noise ratio as the dissolution period of CPAM was increased; the characteristic peaks were better defined. The SERS intensity was increased as the charge density of CPAM was increased from 5 wt% to 40 wt% (Fig. 6). Fig. 7 shows the Raman EF of 4-ATP measured at 1077 cm⁻¹ band when paper was pre-treated with CPAM solutions of different charge density which were prepared at different dissolution times. As the charge density of the CPAM solution was increased, the EF of

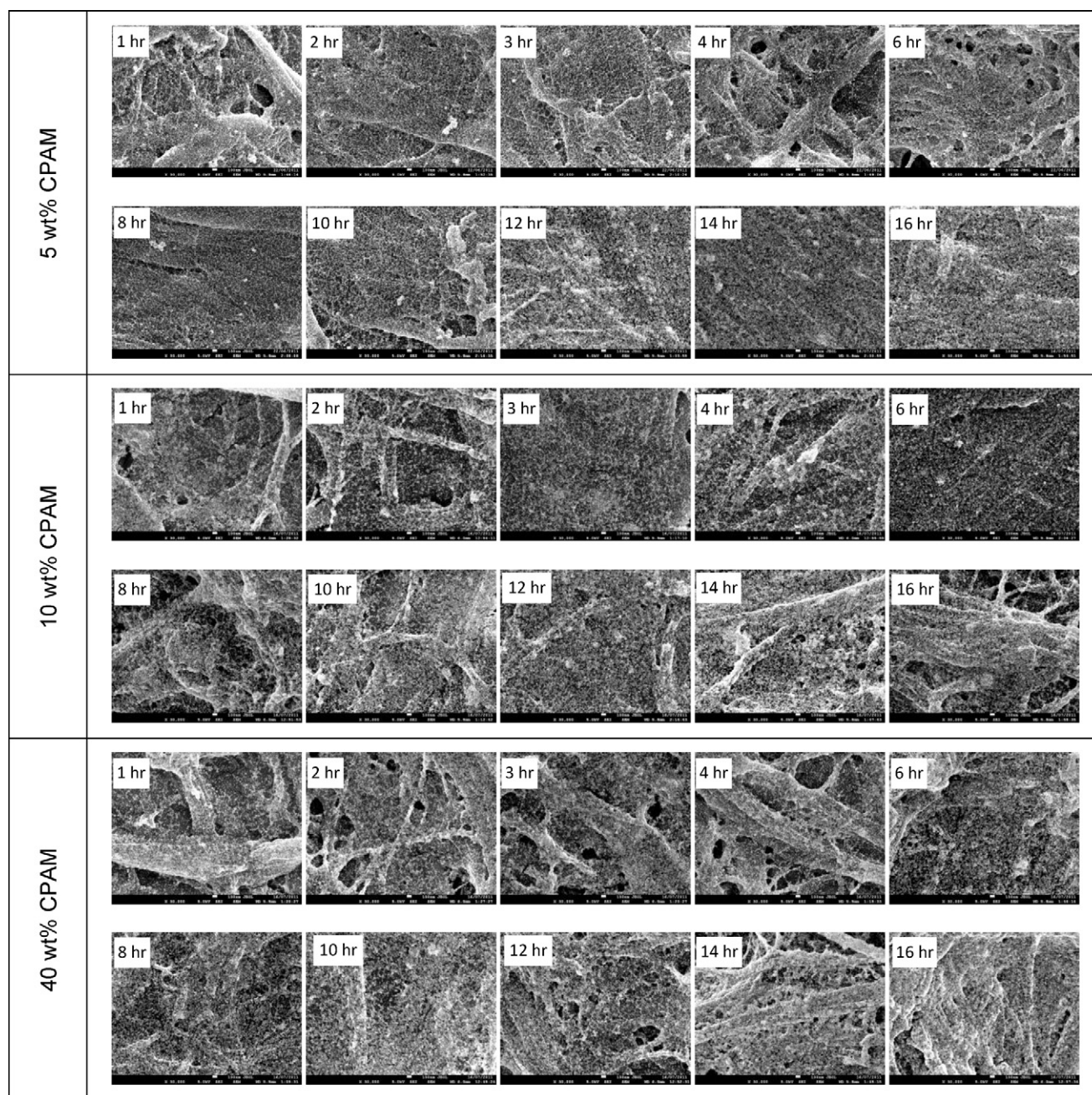


Fig. 3. FESEM of AuNPs on paper substrate pre-treated by CPAM of 5 wt%, 10 wt% and 40 wt% charge density at different dissolution time.

the AuNPs-CPAM paper increased by almost an order of magnitude. The standard deviations of EF were smaller for paper pre-treated with CPAM solutions that were allowed to mix and dissolve for a longer period.

4. Discussion

4.1. Mechanism of CPAM dissolution

The degree of dissolution of CPAMs, which were pre-adsorbed on paper, greatly affected the adsorption state of AuNPs on paper substrates and their SERS reproducibility. The CPAMs studied have a very high molecular weight (13 MDa). Their dissolution process from a powder to a solution at equilibrium is long and complex as many different configurations are achievable by the polymer, giving

rise to high entropy. The long polymer chains are made of numerous flexible segments which tend to entangle with each other. According to the Stokes-Einstein equation, viscosity scales inversely with diffusion coefficient [16]. The rate of a diffusion-controlled dissolution decreases as the viscosity increases, whilst the viscosity of a polymer solution depends on the size of the critical unit of the dissolved polymers [17–18]. The dissolution rate of CPAM in solution was monitored by measuring macroscopic viscosity and hydrodynamic diameter.

The viscosity and hydrodynamic diameter of the polymer solution show a similar trend when the CPAM powder was added to water and mixed up to 16 h (Figs. 1 and 2). DLS measurements of the CPAM solutions had very high polydispersity indexes, indicating preferential size measurement of the larger polymer aggregates instead of reflecting the average hydrodynamic diameter of the polymer units. The radius of gyration calculated for the

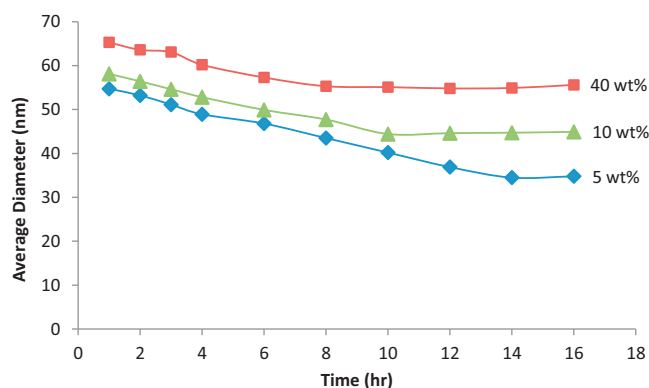


Fig. 4. Average size of AuNP aggregates on paper substrate pre-treated by CPAM of different charge density vs. dissolution time of CPAM.

polymer random coil (3 nm) is almost an order of magnitude smaller than the critical polymer dimension measured by DLS (250 nm). However, since the trend of the DLS measurement (Fig. 2) is consistent with the viscosity results (Fig. 1), it can be interpreted in a relative sense. Both the viscosity and average diameter of CPAM increased and reached a plateau after a critical time. A two stages process is proposed: an induction period followed by the dissolution step [18–19]. During the induction period, water diffuses into the polymer powder (Fig. 8a and b) and a swollen surface layer results (Fig. 8c). Attraction and repulsion forces start acting between the segments of the dissolved polymer as they gain mobility. The polymer-solvent and charge-charge interactions overcome the polymer-polymer attraction forces, causing the chain segment to absorb solvent molecules, increasing the volume of the polymer matrix, and the dimensions of its coils (Fig. 8d). At this stage, the polymer segments are considered as “solvated”. The “solvation-unfolding-swelling” process continues until all segments are solvated [19]. The viscosity and critical unit size of CPAM solution slowly increases during the induction period at 1–3 h of mixing (Figs. 1 and 2). Fig. 8 schematically illustrates the process. It was expected that the polymer size of CPAM at the earlier stages of dissolution (Fig. 8a and b) to be larger than those at the subsequent stages (Fig. 8d and e). However, the hydrodynamic diameter measured by DLS (Fig. 2) shows the opposite. This could be due to limitation of the DLS equipment, which can only detect size ranging from 0.6 nm to 6 μ m; the particle size of the original CPAM polymer particles is between 0.125 mm and 1.120 mm. The CPAM powder could also settle down at the bottom of the capillary cell during DLS measurement.

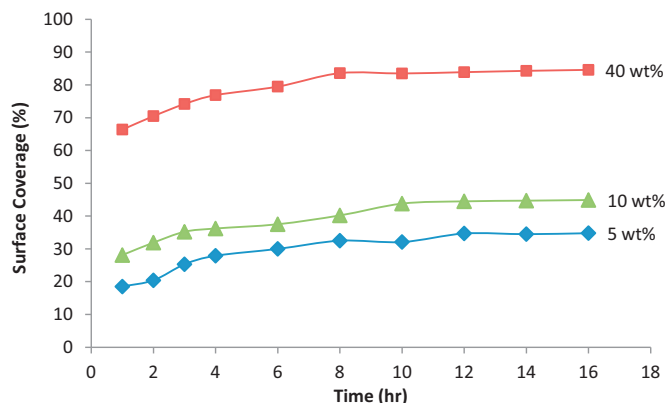


Fig. 5. Surface coverage of AuNP aggregates on paper substrate pre-treated by CPAM of different charge density vs. dissolution time of CPAM.

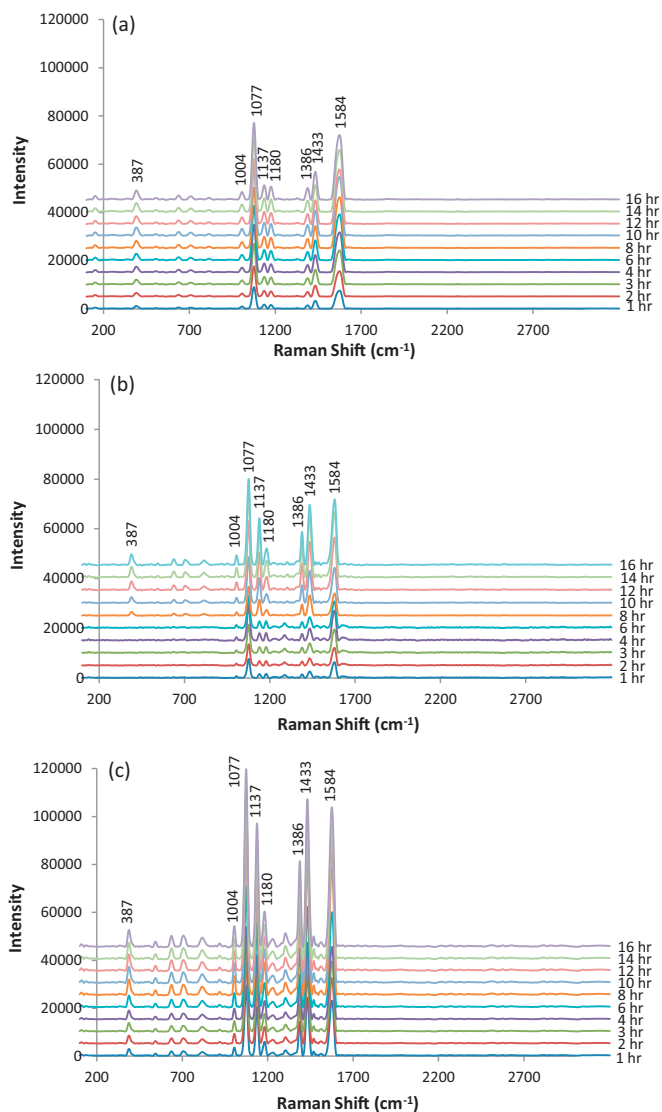


Fig. 6. Average SERS spectra of 4-ATP on AuNPs-CPAM papers with CPAM of (a) 5 wt%, (b) 10 wt% and (c) 40 wt% charge density prepared at different dissolution times.

The viscosity and critical unit size of CPAM increased dramatically after 4 h of mixing (Figs. 1 and 2); this is particularly evident for CPAM of 40 wt% charge density. The dissolution mechanism dominates this stage as the loosened coil can diffuse from the swollen

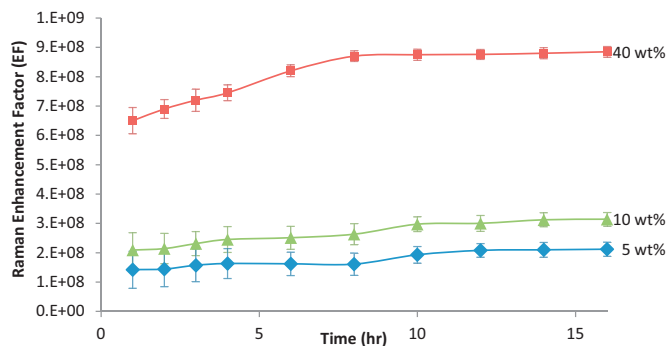


Fig. 7. Raman enhancement factor (EF) of 4-ATP at 1077 cm⁻¹ on AuNPs-CPAM papers treated by CPAM of different charge density as a function of CPAM dissolution time. Error bars are standard deviations from five measurements at different point on the substrates.

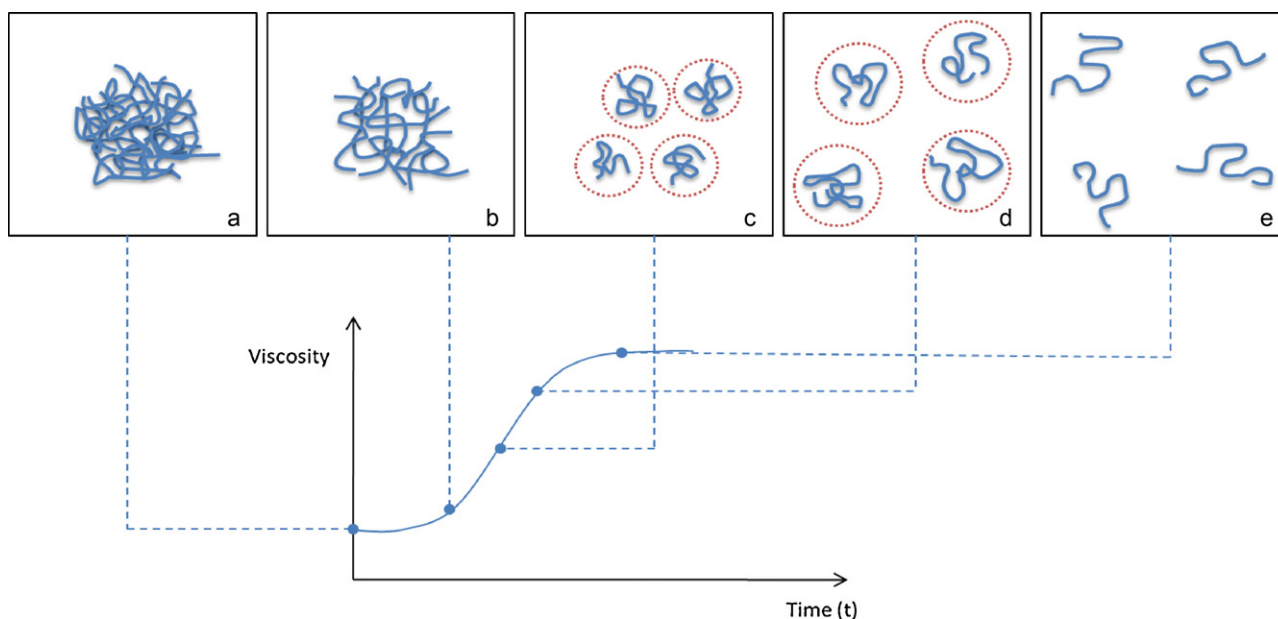


Fig. 8. Schematic representation of the dissolution kinetic of CPAM; the red circles represent the gel aggregates (For interpretation of the references to colour in this figure legend, the reader is referred to the web version of this article).

polymer and become intimately mixed with solvent. The plateaux of Figs. 1 and 2 correspond to the full dissolution and solvation of CPAM. The hydrated polymer coils are expected to adopt a spherical or ellipsoidal shape (Fig. 8e).

The interactions between charged groups on a CPAM molecule have a strong influence on the conformation of the polymer coil in solution. The viscosity and DLS measurements show that the dimensions of the polymer critical unit vary linearly with the charge density of CPAM (Figs. 1 and 2). A highly charged polymer has a more extended conformation in solution due to stronger inter- and intra-molecular repulsion between charged segments [20]. Therefore, CPAM with the highest charge density can dissolve and reach its plateau the fastest (Figs. 1 and 2).

4.2. Properties of AuNPs-CPAM paper

The adsorption and aggregation state of AuNPs were strongly influenced by the extent of CPAM dissolution upon paper dip-coating (Fig. 3). Polymer molecules are known to adsorb on fibrous paper substrates in a conformation where some of its segments maintain contact with the fibre surface (trains), some segments between two adjacent trains extend into solution (loops) and some free ends are dangling into solution (tails) [21]. In this study, the adsorption and aggregation of AuNPs induced by CPAM which was pre-adsorbed onto paper were analysed in terms of the CPAM dissolution behaviour.

AuNPs were adsorbed onto the cellulose fibers of paper as well dispersed individual nanoparticles when plain paper was directly dipped into the AuNP solution without CPAM pre-treatment [10]. When the paper pre-treated with CPAM solutions, which were dissolved only for 1–4 h (prior to the viscosity and coil diameter reaching a plateau), was dipped into the AuNP solution, partial coverage resulted with AuNPs aggregates (Fig. 3). CPAM dissolution is incomplete at this stage and the polymer exists in a mixture of swollen gel aggregates and polymer coils (Fig. 8b–c). The cationic polymer adsorbs onto the negatively-charged cellulose fibers mostly in an entangled conformation [22]. A charged polymer patch mechanism is expected to be predominant; the partial surface coverage of one or more molecules of CPAM

created a positively charged “patch” which interacts with a negatively charged “patch” of AuNPs through electrostatic interaction [23]. These patches of AuNP aggregates produced low SERS enhancement and reproducibility (Fig. 7). This is probably due to the absence of uniformity and the densely distributed AuNP aggregates at the sub-micrometer scale. The length scale of AuNP heterogeneity is higher than the critical dimension of the Raman detection; the diameter of the Raman’s laser beam is approximately 1 μm .

As the dissolution period increases, the CPAM polymer chains loosen and uncoil, adsorbing on cellulose fibers in a more extended train–loop–tail conformation. The tails and loops extend into the solution phase driven by strong intramolecular electrostatic repulsion and affinity for water, while the train sections adhere to the negatively charged cellulose by electrostatic affinity. This state of extended polymer tails and loops produced uniformly distributed AuNP aggregates through polymer bridging and charge neutralization [24] (Fig. 4). At uniform CPAM coverage, the negative charge of cellulose fibers was reduced, neutralized and even reversed. This created an electrostatic interaction between paper and AuNPs (negatively-charged), leading to a higher AuNPs surface coverage (Fig. 5). This higher surface coverage and uniformly distributed AuNP aggregates contributed to SERS spectra having a higher signal to ratio and well defined characteristic peaks (Fig. 6). Raman EF and reproducibility were increased as the lateral dimension of AuNP distribution heterogeneity became smaller than the critical dimension of Raman measurement (1 μm).

The charge density of CPAM polymer chain has a drastic effect on their conformations, which affects the adsorption and aggregation state of NPs (Figs. 4 and 5). At lower charge density, polymer molecules tends to form more loops and tails upon adsorption [21,25]. The flocculation of AuNPs is expected to occur mostly through bridging [21]. When paper was pre-treated with CPAM of higher charge density, higher surface coverage and more uniform distribution of AuNP aggregates resulted. Polymers of higher charge density tend to reorganize in a flatter conformation upon adsorption [26]. Flocculation of AuNPs is probably driven by a charge neutralization mechanism. Bridging could also be involved.

As the highly charged CPAM had a higher charge density than paper, intra-molecular repulsive forces induced by the excess polymer charge could generate an adsorbed polymer configuration with more loops and tails [27]. CPAM with higher charge density produced a uniform aggregation (Fig. 4) and higher surface coverage (Fig. 5) of AuNPs, leading to the formation of rough metallic surfaces ('hot spots') which gave rise to stronger electromagnetic coupling to enhance the Raman signal of 4-ATP (Figs. 6 and 7).

5. Conclusion

The dissolution kinetics of a polyelectrolyte, from a powder to an equilibrium solution, can affect the adsorption and coagulation behaviour of colloids. An example is in the retention and coagulation of gold nanoparticles (AuNPs), which are used as Surface Enhanced Raman Scattering (SERS) signal enhancer in the fabrication of paper bio-diagnostics platform, with cationic polyacrylamide (CPAM) serving as retention aid. This study aimed at improving the sensitivity and reproducibility of AuNPs treated paper used as routine substrate for SERS analysis.

A series of high molecular weight (13 MDa) CPAM powders varying in charge density was dissolved in water. The viscosity and the critical aggregate size of the CPAM solutions were measured as a function of their dissolution time. Filter papers were dipped into a polymer solution, rinsed and dipped again into a standard AuNP solution. The ability of CPAM to adsorb and coagulate AuNPs on paper was quantified. The surface coverage and aggregate size of AuNPs on paper were both measured by FESEM/image analysis. A model dye (4-ATP) was adsorbed onto the AuNP paper substrates, its Raman spectra were measured and the SERS performance was analysed.

The viscosity and critical aggregate/coil size of a high molecular weight, low charge density CPAM solution both slowly increase to reach a plateau after 12 h. Increasing the charge density of the polymer shortened the time required to reach steady state (8 h). The surface coverage of AuNPs on paper increased and their average aggregate size decreased as paper was pre-treated with a CPAM solution which had been mixed for a longer period; increasing CPAM charge density accentuated this tendency. SERS intensity and reproducibility of AuNPs paper both increase with dissolution time of CPAM, as the heterogeneity of AuNP distribution and aggregate size decreases below 1 μm , the critical SERS dimension corresponding to the diameter of the Raman laser beam.

Controlling the dissolution time of a high molecular weight polyelectrolyte from a powder to a solution affects the conformation of its critical unit in water (aggregates to coil), influences its subsequent adsorption on a surface, and determines its ability to coagulate nanoparticles. The heterogeneity of AuNPs distribution on paper is related to variability in the bridging and aggregation of nanoparticles caused by the dissolution kinetic of CPAM. This understanding of polymer dissolution kinetic is critical to optimize the SERS performance of AuNPs paper.

Acknowledgements

Thanks to Dr. T. Williams and F. Shanks, Monash University for technical expertise and AQUA + TECH for supplying the CPAM polymers (Snowflake Cationics). The financial support from the ARC Linkage LP0989823 and Visy, Amcor, SCA, Norske Skog, Australian Paper, the Australian Pulp and Paper Institute and Monash University are acknowledged.

Appendix A. Supplementary data

Supplementary data associated with this article can be found, in the online version, at <http://dx.doi.org/10.1016/j.colsurfa.2012.12.018>.

References

- [1] M. Al-Tamimi, W. Shen, R. Zeineddine, H. Tran, G. Garnier, Validation of paper-based assay for rapid blood typing, *Anal. Chem.* 84 (3) (2011) 1661–1668.
- [2] M.S. Khan, G. Thouas, W. Shen, G. Whyte, G. Garnier, Paper diagnostic for instantaneous blood typing, *Anal. Chem.* 82 (10) (2010) 4158–4164.
- [3] M. Li, J. Tian, M. Al-Tamimi, W. Shen, Paper-based blood typing device that reports patient's blood type "in writing", *Angew. Chem. Int. Ed.* 51 (22) (2012) 5497–5501.
- [4] Z. Luo, Y. Fang, SERS of C60/C70 on gold-coated filter paper or filter film influenced by the gold thickness, *J. Colloid Interface Sci.* 283 (2) (2005) 459–463.
- [5] A. Berthod, J.J. Laserna, J.D. Winefordner, Analysis by surface enhanced Raman spectroscopy on silver hydrosols and silver coated filter papers, *J. Pharm. Biomed. Anal.* 6 (6–8) (1988) 599–608.
- [6] L.M. Cabalín, J.J. Laserna, Fast spatially resolved surface-enhanced Raman spectrometry on a silver coated filter paper using charge-coupled device detection, *Anal. Chim. Acta* 310 (2) (1995) 337–345.
- [7] W. Ma, Y. Fang, Experimental (SERS) and theoretical (DFT) studies on the adsorption of p-, m-, and o-nitroaniline on gold nanoparticles, *J. Colloid Interface Sci.* 303 (1) (2006) 1–8.
- [8] Z. Niu, Y. Fang, Surface-enhanced Raman scattering of single-walled carbon nanotubes on silver-coated and gold-coated filter paper, *J. Colloid Interface Sci.* 303 (1) (2006) 224–228.
- [9] D. Wu, Y. Fang, The adsorption behavior of p-hydroxybenzoic acid on a silver-coated filter paper by surface enhanced Raman scattering, *J. Colloid Interface Sci.* 265 (2) (2003) 234–238.
- [10] Y.H. Ngo, D. Li, G.P. Simon, G. Garnier, Gold nanoparticle? Paper as a three-dimensional surface enhanced Raman scattering substrate, *Langmuir* 28 (23) (2012) 8782–8790.
- [11] F. Toderas, M. Baia, L. Baia, S. Astilean, Controlling gold nanoparticle assemblies for efficient surface-enhanced Raman scattering and localized surface plasmon resonance sensors, *Nanotechnology* (2007) 18.
- [12] Ngo, Y.H., G. Garnier, D. Li, and G. Simon, Effect of Cationic Polyacrylamides on the Aggregation and SERS Performance of Gold Nanoparticles-treated Paper, *J. Colloid Interface Sci.*, <http://dx.doi.org/10.1016/j.jcis.2012.09.080>, in press.
- [13] J. Turkevich, P.C. Stevenson, J. Hillier, A study of the nucleation and growth processes in the synthesis of colloidal gold, *Discuss. Faraday Soc.* 11 (1951) 55–75.
- [14] P.H.C. Camargo, L. Au, M. Rycenga, W. Li, Y. Xia, Measuring the SERS enhancement factors of dimers with different structures constructed from silver nanocubes, *Chem. Phys. Lett.* 484 (4–6) (2010) 304–308.
- [15] X. Hu, T. Wang, L. Wang, S. Dong, Surface-enhanced Raman scattering of 4-Aminothiophenol self-assembled monolayers in sandwich structure with nanoparticle shape dependence: off-surface plasmon resonance condition, *J. Phys. Chem. C* 111 (19) (2007) 6962–6969.
- [16] N. Sarisuta, E.L. Parrott, Relationship of dissolution rate to viscosity of polymeric solutions, *J. Pharm. Sci.* 71 (12) (1982) 1375–1380.
- [17] R.O. Ebewele, in: *Polymer Science, and Technology*, CRC Press, Boca Raton, FL, 2000.
- [18] B.A. Miller-Chou, J.L. Koenig, A review of polymer dissolution, *Prog. Polym. Sci.* 28 (8) (2003) 1223–1270.
- [19] F.W. Billmeyer, in: *Textbook of Polymer Science*, Wiley, New York, 1984.
- [20] A.V. Dobrynin, M. Rubinstein, Theory of polyelectrolytes in solutions and at surfaces, *Prog. Polym. Sci.* 30 (11) (2005) 1049–1118.
- [21] G.J. Fleer, M.A.C. Stuart, J.M.H.M. Scheutjens, T. Cosgrove, B. Vincent, in: *Polymers at Interfaces*, Chapman & Hall, London, 1998.
- [22] L. Wågberg, Polyelectrolyte adsorption on cellulose fibres – a review, *Nord. Pulp Pap. Res. J.* 15 (5) (2000) 586–597.
- [23] W.K.J. Mosse, D.V. Boger, G.P. Simon, G. Garnier, Effect of cationic polyacrylamides on the interactions between cellulose fibers, *Langmuir* 28 (7) (2012) 3641–3649.
- [24] T. Sønnerfors, Polymer-nanoparticle complexes: fundamentals and applications of interfacial behavior, in: *Encyclopedia of Surface and Colloid Science*, second edition, 2006, pp. 4874–4884.
- [25] M.A. Hubbe, H. Nanko, M.R. McNeal, Retention aid polymer interactions with cellulosic surfaces and suspensions: a review, *Bioresources* 4 (2) (2009) 850–906.
- [26] J.E. Roberts, M.M. Santore, Y. Shin, The relationship between polymer/substrate charge density and charge overcompensation by adsorbed polyelectrolyte layers, *J. Colloid Interface Sci.* 247 (1) (2002) 220–230.
- [27] P.M. Claesson, M.A.G. Dahlgren, L. Eriksson, Forces between polyelectrolyte-coated surfaces: relations between surface interaction and floc properties, *Colloids Surface A: Physicochem. Eng. Aspect.* 93 (1994) 293–303.

Appendix II: Related Co-Authored Manuscript Not Included in the Main Body of This Thesis

Gold Nanoparticle-Functionalized Thread as a Substrate for Surface Enhanced Raman Scattering (SERS)

Ying Hui Ngo, David Ballerini, Purim Jarujamrus, Gil Garnier and Wei Shen *

Australian Pulp and Paper Institute (APPI), Department of Chemical Engineering Monash University, Clayton, VIC 3800, Australia.

*Corresponding author. Email: [REDACTED]

Introduction

Surface-enhanced Raman scattering (SERS) using metallic nanoparticles is a prominent technique for quantifying the adsorption of target molecules on substrates, and allowing different orientations and interactions of the molecules with the substrate to be determined. A highly SERS-active substrate is the most important factor in producing efficient SERS analysis. Previously, aqueous metal nanoparticles were employed in most SERS techniques, but this limits the applications of SERS since the specimens analyzed must be water-soluble. To overcome this limitation and enhance the SERS technique, solid and rough SERS-active surfaces such as silicon wafers [1-3] nanorod arrays on glass [4], metal island films formed through thermal evaporation [5-6] and laser ablated metal plates [7] were explored among others. However, these methods involve complex preparation of substrates and sophisticated instrumentation and thus, result in high costs which limit the applications of SERS. Therefore, the development of low-cost, efficient, reliable and reproducible SERS substrates is imperative.

Performing SERS with metallic nanoparticle coated filter paper substrate eliminates the need for the analytes examined to be water soluble, offering a much simpler method. The intertwined structure of cellulose fibers of paper was found to be able to ‘freeze’ the adsorption state of nanoparticles by rapidly drawing away the water upon drying, resulting in a uniform distribution of AuNPs on paper, which is an important criteria for higher SERS reproducibility [8]. Besides that, adsorption of nanoparticles on the 3-dimensional (3D) multilayer cellulose structure of paper allows inter- and intra-layer plasmon coupling which is able to amplify the SERS signal [9].

Having similar cellulose structure as paper, thread can also be used as a highly SERS-active substrate. This work demonstrates the first use of thread as a low cost SERS substrate. Thread is inexpensive and globally ubiquitous. It possesses excellent color display properties, physical strength and wettability. Thread is able to wick liquids through capillary action due to its porous structure formed by spaces between fibres comprising the thread [10]. This study employed cotton thread exclusively, an ancient material used for centuries which is also an attractive substrate for the fabrication of low-cost and low volume devices for SERS [11]. To the best of our knowledge, no work has reported using cotton or other multifilament threads for fabricating simple and low-cost substrates for SERS applications to date.

This study demonstrates the potential of gold nanoparticles (AuNPs) treated cotton thread as a powerful tool for studying the surface configuration of molecules in SERS applications. The natural porous morphology and high oxygen density of the thread structure provides a strong capillary force to absorb AuNP-solution, allowing the deposition of AuNPs over a higher surface area than other flat substrates such as glass or polymer. In addition, cotton thread is inexpensive and only a tiny volume of AuNPs deposited on cotton thread can produce a wide range of diagnostic devices which show excellent Surface Enhanced Raman Scattering (SERS) behavior. Cotton thread has the advantage of being biodegradable, biocompatible, and renewable, and its structural morphology and surface chemistry can be readily engineered. Unlike paper, thread can be used to form fabric, which can be incorporated into apparel, for instance military attire, which can be used for detection of explosive, drugs or biological hazard.

In this work we have explored the optimum condition to produce SERS active of AuNPs treated cotton thread by studying effect of size, concentration and aggregation state of AuNPs on the SERS activity of the thread. The application of AuNP-functionalized thread in analyzing different molecule structures through SERS was demonstrated. This study also investigated the impacts of analyte polarizability and nanoparticle binding on SERS signals, results which are no doubt applicable to other different substrates and not thread alone.

Experimental section

Materials and Instrumentation

Hydrogen tetrachloroaurate trihydrate ($\text{HAuCl}_4 \cdot 3\text{H}_2\text{O}$), sodium tetrachloroaurate dehydrate ($\text{NaAuCl}_4 \cdot 2\text{H}_2\text{O}$), sodium citrate tribasic dihydrate ($\text{Na}_3\text{C}_6\text{H}_5\text{O}_7 \cdot 2\text{H}_2\text{O}$) and 4-

aminothiophenol (4-ATP), 1-Decanethiol (1-DT), L-Methionine (LM) and Phenolphthalein were purchased from Sigma-Aldrich. Ninhydrin reagent was provided by CSIRO, Clayton. Cationic polyacrylamide (CPAM) of high molecular weights (~13 MDa) and charge densities at 40% wt (F1, SnowFlake Cationics) was purchased from AQUA+TECH, Switzerland. Ultrapure water purified with a Millipore system (18 M Ω .cm) and Absolute ethanol were used in all aqueous solutions and rinsing procedures. Precut 5x7 mm silicon wafers were purchased from ProSciTech as a solid support for SERS.

Cotton thread was kindly provided by the school of Fashion and Textiles, RMIT University, Melbourne, Australia. Natural cotton thread is not wettable by aqueous liquids due to the presence of naturally occurring waxes on the surface of fibres and within the fiber wall. As such, natural cotton thread needs to be dewaxed, or surface treated, to allow the wicking of aqueous liquids [13]. In this study, natural cotton thread was rendered hydrophilic by exposure to plasma in a vacuum plasma reactor (K1050X plasma asher (Quorum Emitech, UK)) for 1 min at an intensity of 50 W. The vacuum level for the treatment was 6×10^{-1} mbar.

The morphology of the AuNP functionalized thread was observed via Field Emission Scanning Electron Micrograph (FESEM) using a JEOL 7001 FEG system operating at 5 kV and 180 pA. The Zeta potential measurements were performed with a Zetasizer Nano ZS (Malvern Instruments) in a Folded Capillary cell (DTS1060) at 25 °C. All Raman and SERS spectra were obtained in the air on a Renishaw Invia Raman microscope equipped with 300 mW 633 nm laser. Typically, the laser was set to 10% of maximum power. The laser beam was positioned through a Leica imaging microscope objective lens (50 \times), whilst the instrument's wavenumber was calibrated with a silicon standard centered at 520.5 cm $^{-1}$ shift. Due to the smaller spot size of the laser compared with the large surface area of the samples, spectra were obtained at different points along the thread surfaces, and were the same shape, differing only in intensity. The average intensity (of 5 measurements) was presented as the final result.

Methods

Preparation of Gold Nanoparticles (AuNPs)

AuNPs were synthesized using 1 mM of hydrogen tetrachloroaurate, HAuCl₄.3H₂O and 1% aqueous sodium citrate according to the Turkevich method [12]. To synthesize a stock solution of larger AuNPs (approximately 40 nm in diameter), a modification of the Turkevich

method was performed using 0.65mM $\text{HAuCl}_4 \cdot 3\text{H}_2\text{O}$ and 0.5% aqueous sodium citrate. A 20-mL solution of 1 mM of aqueous hydrogen tetrachloroaurate was heated to 100°C . 2-mL of 1% aqueous sodium citrate was then added to the heated aqueous hydrogen tetrachloroaurate. The mixture was then stirred and heated until its colour transitioned from pale yellow to pale blue and then into a brilliant red upon completion. The AuNPs solution obtained was then allowed to cool to room temperature, and stored at 4°C . To obtain concentrated AuNPs solution, the original AuNPs solutions were concentrated 10x by centrifugation at 6000g for 20 min.

The Adsorption of AuNPs to Cotton-thread Substrate

CPAM is among the most extensively used cationic polyelectrolyte flocculants for liquid/solid separation, retention and drainage aids in papermaking and flotation aids [4, 13]. In order to induce more adsorption and aggregation of AuNPs in an effort to promote SERS signal amplification, thread substrates were treated with CPAM to engineer their surface charge. A stock solution of CPAM was prepared on the day of experiment by diluting dry powder to 0.01% with Ultrapure water purified with a Millipore system (18 $\text{M}\Omega\cdot\text{cm}$) and the dispersions were gently shaken for 1 hour to facilitate the dissolution process. Plasma-treated cotton-thread substrates of 10 mm length were dipped into the CPAM solution for 1 hour, rendering the thread cationic. The treated cotton threads were then rinsed with distilled water and left to air dry. The treated cotton threads were then soaked individually in solutions of AuNPs. After soaking, the AuNP-treated cotton threads were rinsed thoroughly with distilled water to remove loosely bound AuNPs and then air-dried.

Preparation of Raman active cotton-thread substrates and silicon wafers

Solutions of different concentrations of 4-ATP, 1-DT, Ninhydrin reagent and Phenolphthalein were prepared in ethanol while LM was prepared in distilled water. The dried nanoparticle-deposited thread substrates (both untreated and pre-treated with cationic polymers) were dipped into solution of analyte molecules for 5 minutes. After thorough rinsing with MilliQ water and drying, they were subjected to Raman characterization.

Silicon wafers with dimensions of 10mmx10mm were cleaned with ‘piranha’ solution (mixture of sulfuric acid and hydrogen peroxide) and ultrasonicated before use. Silicon wafers were also treated in the vacuum plasma reactor for 1 min at an intensity of 50 W. The vacuum level for the treatment was 6×10^{-1} mbar. 5 μ L of AuNPs was applied to each silicon wafer and dried in air before analysis.

Results and Discussion

Cotton threads were analyzed under SEM to study their structure and morphology. It was found that cotton thread is composed of many cellulose fibers which are similar to those found in filter paper. However, the cellulose fibers of cotton thread (Figure 1a) are arranged in a twisted structure, as opposed to paper (Figure 1b) which has a layered cellulose fiber structure.

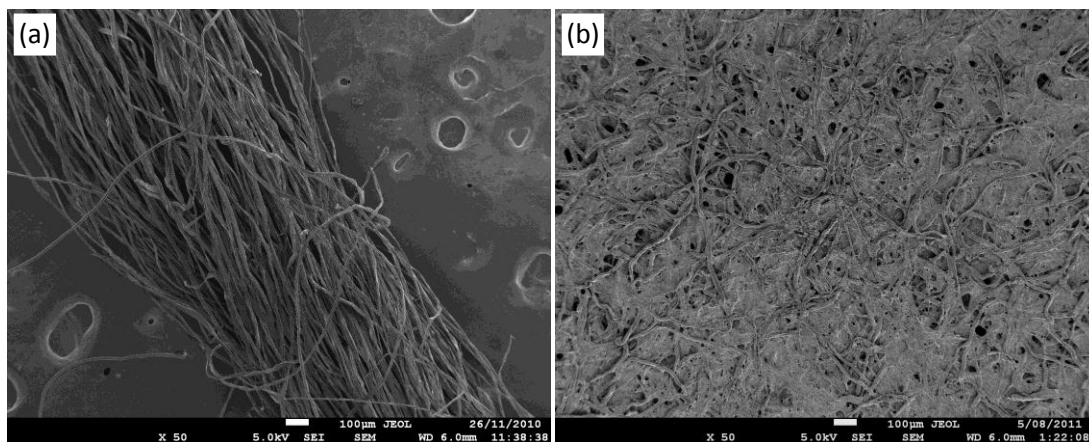


Figure 1: FESEM images of (a) cotton thread and (b) filter paper.

Analyte testing

Proof of concept

In order to assess the SERS potential of these AuNP-CPAM treated threads, the aromatic thiol known as 4-ATP (Figure 2) was chosen as a probe molecule for the Raman analysis due to its distinct Raman features, strong affinity for metal surfaces, and formation of self-assembled monolayers [20]. Figure 3 shows the SERS spectra obtained from AuNPs treated threads which were exposed to different concentration of 4-ATP. Overall, the spectral features of 4-ATP are

clearly shown, as opposed to the Raman spectrum of 4-ATP on untreated, plain thread. These spectra are dominated by six strong bands: $\delta(\text{C-S})$ at 387 cm^{-1} , $\nu(\text{C-S})$ at 1077 cm^{-1} and $\nu(\text{C-C})$ at 1584 cm^{-1} , (in-plane, in-phase modes) and $\delta(\text{C-H})$ at 1137 cm^{-1} , $\delta(\text{C-H}) + \nu(\text{C-C})$ at 1386 cm^{-1} and $\delta(\text{C-H}) + \nu(\text{C-C})$ at 1433 cm^{-1} (in-plane, out-of-phase modes) of the 4-ATP molecules [14]. By increasing the concentration of 4-ATP, the SERS intensity is increased accordingly and their characteristic peaks become more prominent (Figure 3). This result demonstrates the potential of thread to be developed as SERS active substrate like paper for both qualitative and quantitative analysis.

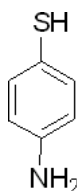


Figure 2: Molecular structure of 4-ATP.

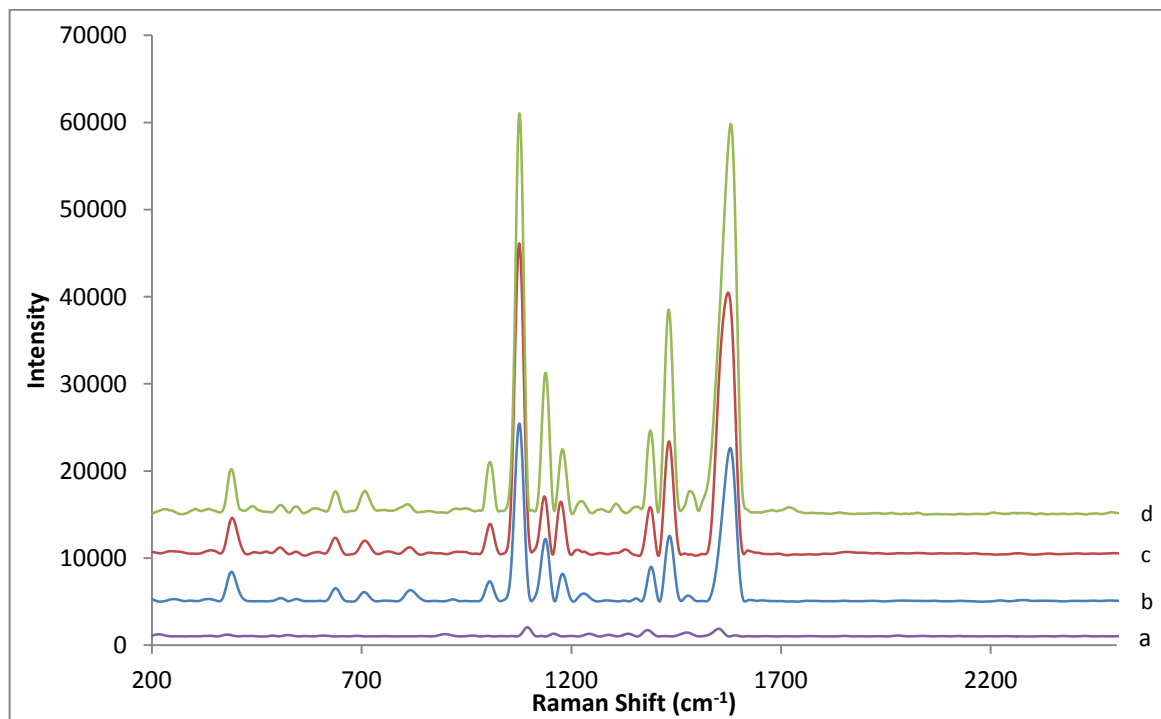


Figure 3: (a) Raman spectrum of 1 mM 4-ATP on plain thread, SERS spectra of (b) 0.1 mM (c) 1 mM and (d) 5 mM of 4-ATP on AuNPs-CPAM treated thread.

Effect of Polarizability on SERS signal

In this study, 1-decanethiol (1-DT) and L-methionine (LM) were also selected to be studied. Threads were treated with 1-DT (Figure 4) and LM (Figure 5) to study their SERS properties. Interestingly, the SERS spectrum of 1-DT in Figure 6 does not show the characteristic peaks expected which are $\delta(\text{C-H}_2)$ at 1450 cm^{-1} , $\tau(\text{CH}_2)$ and $\rho(\text{CH}_2)$ at 1280 cm^{-1} , $\nu(\text{C-C})$ at 1050 cm^{-1} , $\rho(\text{CH}_3)$ at 880 cm^{-1} , $\tau(\text{CH}_2)$ and $\rho(\text{CH}_2)$ at 720 cm^{-1} and $\delta(\text{S-S-C})$ at 370 cm^{-1} [15]. Besides that, the spectra are irreproducible and their intensity are similar to that of the blank AuNP-CPAM treated thread even though the concentration of 1-DT was increased up to 5 mM. The SERS spectrum of LM (Figure 7) also follow the same trend as 1-DT, the characteristic peaks of $\nu(\text{C}^4\text{-S})$ at 680 cm^{-1} , $\nu(\text{C}^2\text{-C}^3)$ at 860 cm^{-1} , $\nu(\text{C}^1\text{-C}^2)$ at 945 cm^{-1} , $\nu(\text{C}^2\text{-N})$ at 1040 cm^{-1} and $\nu_s(\text{COO}^-)$ at 1400 cm^{-1} [16] are not visible and similar to the plain thread. However, for both analytes, the SERS intensity increases as their concentrations are increased. As the citrate ion on the AuNPs surface is a weakly bound capping agent which could be readily displaced by other molecules including thiols [17-18], we believe that the increased SERS intensity was caused by the aggregation of AuNPs induced by the excess thiols (by increasing the concentration of thiols).



Figure 4: Molecular structure of 1-DT.

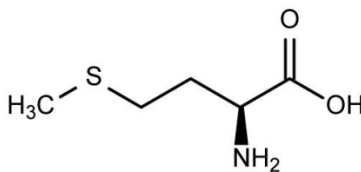


Figure 5: Molecular structure of LM.

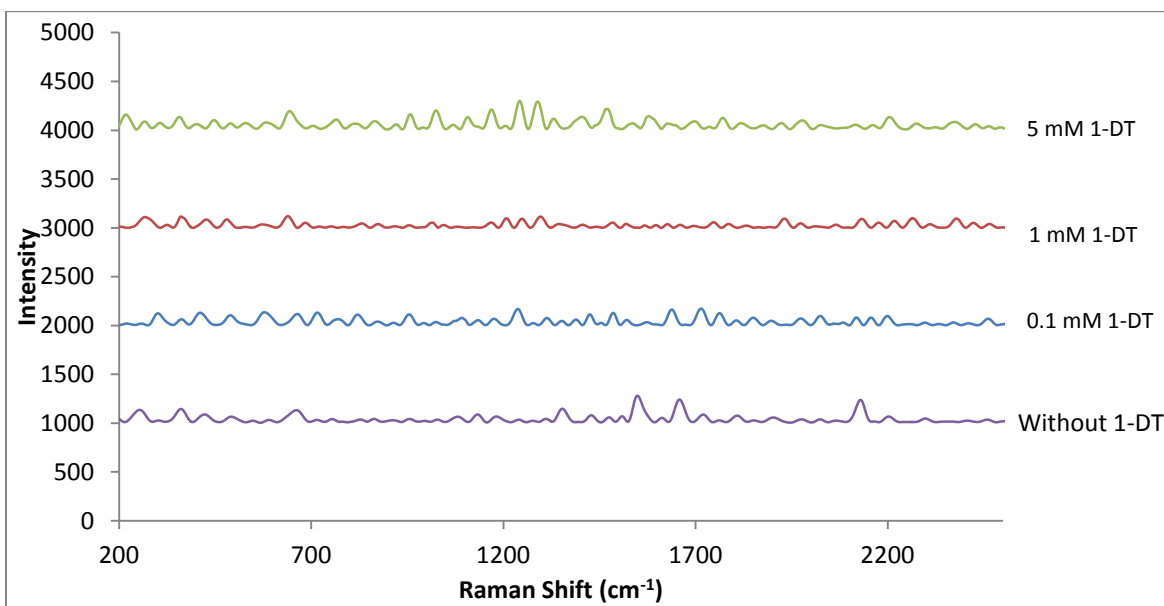


Figure 6: SERS spectra of different concentration of 1-DT on AuNPs-CPAM treated thread.

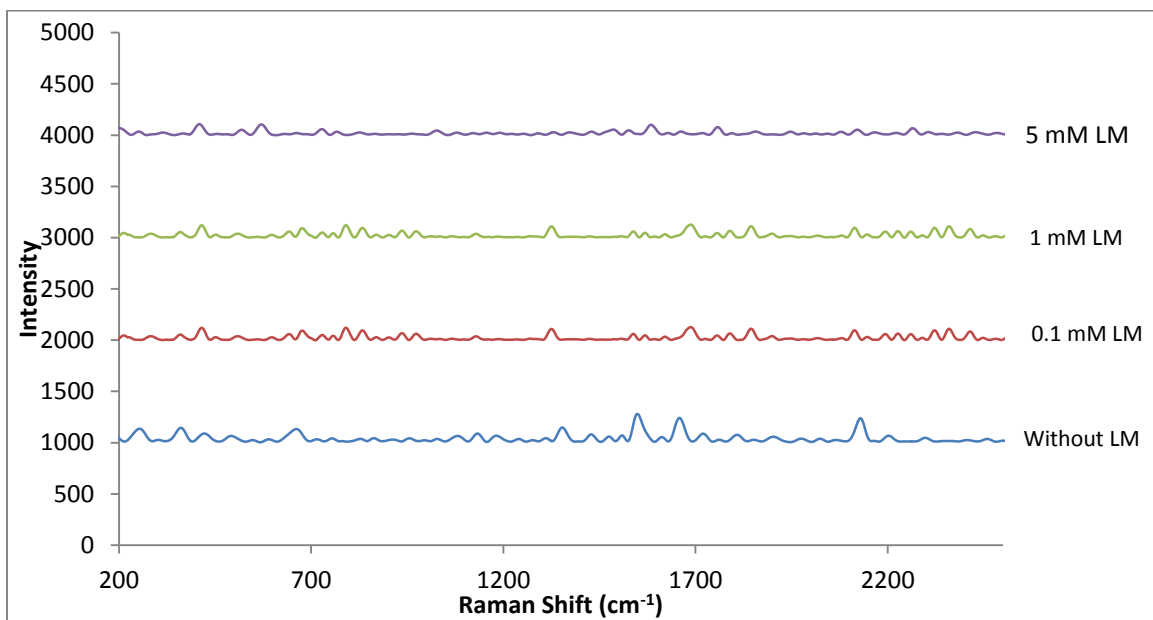


Figure 7: SERS spectra of different concentration of LM on AuNPs-CPAM treated thread.

Since there is no SERS signal coming from both 1-DT and LM on the AuNPs-CPAM treated threads, it is important to make sure these molecules are attached and reacted to AuNPs on the thread substrates. Therefore, 1 mM of 1-DT was mixed with AuNPs and dropped on silicon substrate. As observed on Figure 8, the SERS spectrum of 1-DT clearly show a difference compared to the SERS spectrum of AuNPs treated silicon without 1-DT. The Raman peak for

silicon at 520.5cm^{-1} is absent when 1-DT was deposited on the silicon substrate. This could be due to the background signal from 1-DT which overcomes the signal from the silicon substrate. The spectrum of 1-DT does not show the characteristic peaks and is similar to those that are obtained from the thread substrates (Figure 6). It is well known that thiol molecules can easily form a self-assembled monolayer on AuNPs through the strong S-Au bond [19-22]. There is no doubt that both 1-DT and LM molecules are within the vicinity of the AuNPs, since both molecules possess the strongly gold-binding thiol group, and should therefore be subject to signal enhancement. This result therefore suggests that another factor is at play which prevents the enhancement of the Raman signals for these particular analytes.

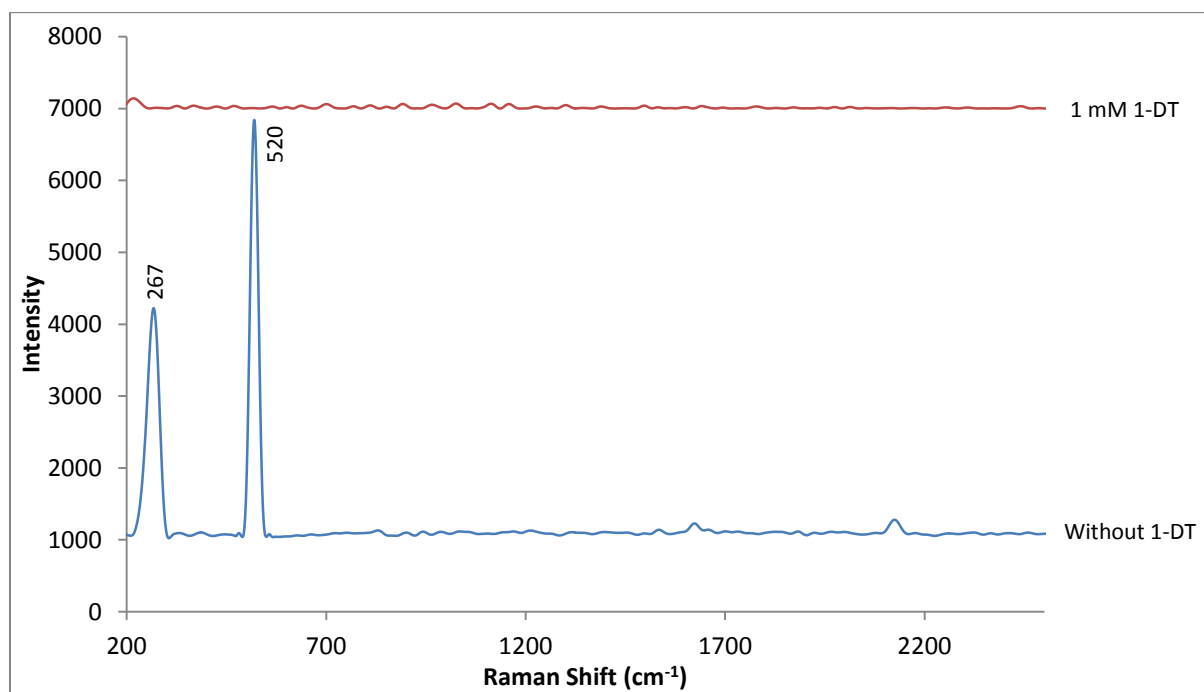


Figure 8: SERS spectra of AuNPs-CPAM treated silicon wafer without 1-DT and with 1 mM of 1-DT.

Raman spectroscopy (and therefore SERS) measures the wavelength and intensity of light scattered from a molecule due to the excitation of the molecule's chemical bonds (molecular vibration). The intensity of Raman scattering I_R is given by:

$$I_R \propto \nu^4 I_0 N \left(\frac{\partial \alpha}{\partial Q} \right)^2$$

where I_0 is the incident laser intensity, N is the number of scattering molecules in a given state, ν is the exciting laser frequency, α is the polarizability of the molecules, and Q is the vibrational amplitude [23]. It therefore follows that only molecular vibrations which cause a change in polarizability are Raman active. Polarizability describes the deformability of the electron cloud about a molecule by an external electric field, and is strongly influenced by how tightly the electrons are bound to the nuclei. Compared to 1-DT and LM which belong to the aliphatic group of molecules, 4-ATP consists of an aromatic benzene ring, its six π electrons are free to move throughout the structure. This π electron is more easily distorted and thus shows a more intense result during SERS. On the other hand 1-DT and LM are alkane thiols that have no benzene ring and thus lower polarizability. Therefore, the absence of their characteristic peaks in the SERS spectra is mostly due to their Raman inactivity. This effect also explains why the presence of CPAM on the threads does not have a significant impact on the Raman spectra generated. CPAM (Figure 9) has a molecular structure which lacks any carbon-carbon double bonds, and hence easily distorted π electrons, and this explains how it can have such a negligible effect on the SERS signal despite being directly adjacent to the AuNPs.

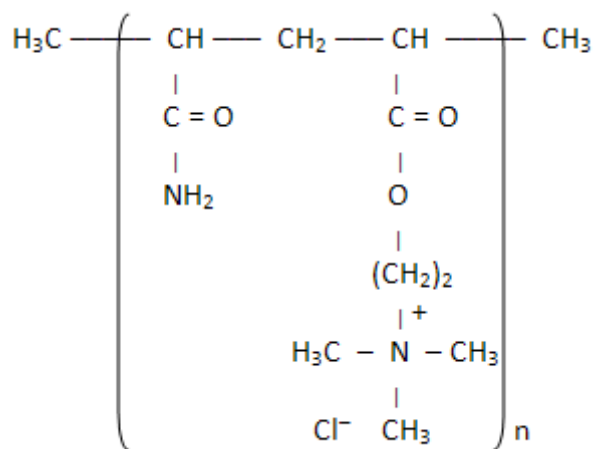


Figure 9: Molecular structure of CPAM.

Unbound Analyte testing

The traditional SERS model suggests that analyte molecules should be chemically bound to nanoparticle surfaces for signal enhancement to be achieved. While it is true that analyte molecules must be located within the enhanced “hotspots” between adjacent nanoparticle clusters to achieve stronger Raman signal enhancement, this study investigated whether or not it

was necessary for them to be strongly chemically bound to the nanoparticle surfaces. The three test molecules used in the proof of concept study, 1-DT, LM and 4-ATP, all possessed the strongly gold binding –SH thiol group. The presence of this functional group ensures that these molecules will be chemically bound to the surface of the gold nanoparticles. In order to evaluate whether this was necessary for achieving enhancement or not, testing of analytes which do not possess the thiol group or any other strongly gold-binding groups was required. Ninhydrin reagent and phenolphthalein (Figures 10 and 11) were selected for this purpose as their structures lack any strongly gold-binding groups but also contain highly polarizable benzene rings which were expected to produce easily visible Raman signals. SERS analysis of the two analytes was performed on both plain, untreated thread and on threads treated with gold nanoparticles. Figure 12 shows the combined spectra from the SERS analysis of ninhydrin ($\nu(\text{CC})$ aromatic ring vibration at 790 cm^{-1} and 906 cm^{-1} , $\delta(\text{CH})_{\text{Ph}}$ 1103 cm^{-1} , $\nu(\text{C=O})$ 1679 cm^{-1} and 1818 cm^{-1}) [23], clearly displaying an enhancement due to the AuNPs on the thread substrate. This result is mirrored in the spectra of phenolphthalein ($\nu(\text{CC})$ aromatic ring vibration at 411 and 468, $\nu(\text{C-O-C})$ at 830 cm^{-1} , $\nu(\text{C-O})$ at 1016 cm^{-1} , $\delta(\text{CH})_{\text{Ph}}$ at 1163 cm^{-1} , $\nu(\text{C=C})$ and $\delta(\text{OH})$ at 1415 cm^{-1} , $\nu(\text{C=O})$ at 1700 cm^{-1}) [23-25] in Figure 13 with a significant increase in the height of the signal peaks due to the presence of the AuNPs. These results strongly suggest that the enhancement effect of SERS is not entirely dependent on whether the analyte molecules are chemically bound to the gold nanoparticles. It is instead likely that weaker forces of attraction are at work and acting to position analyte molecules within the hotspot enhancement regions, such as Van der Waal's forces, for example. These weaker forces result in less analyte molecules being located in the hotspots compared to those which chemically bind, but there are still enough to enable the enhancement effect to be observed.

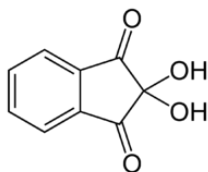


Figure 10: Molecular Structure of Ninhydrin

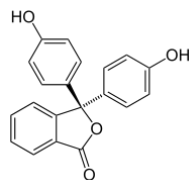


Figure 11: Molecular Structure of Phenolphthalein

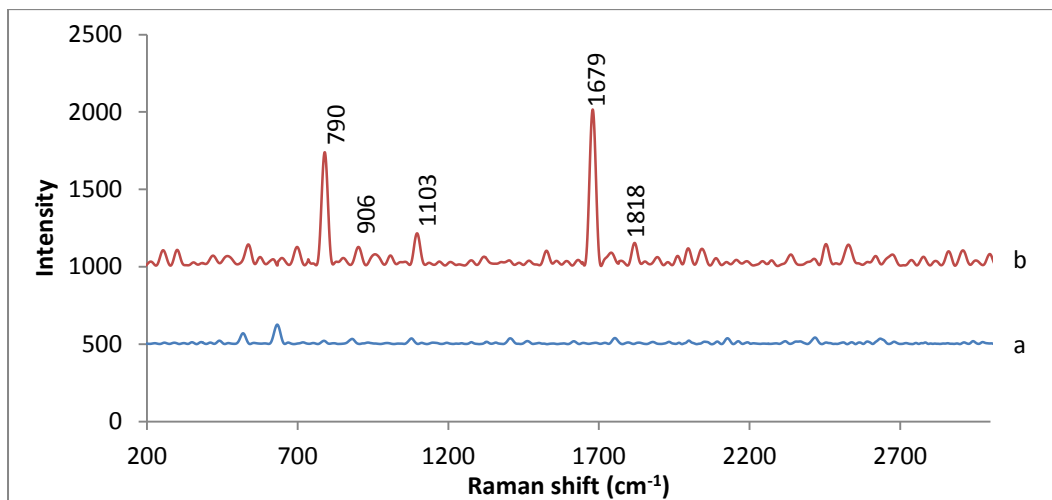


Figure 12: (a) Raman spectra of 1mM of Ninhydrin on plain thread and (b) SERS spectra of 1mM Ninhydrin on of AuNPs-CPAM treated thread.

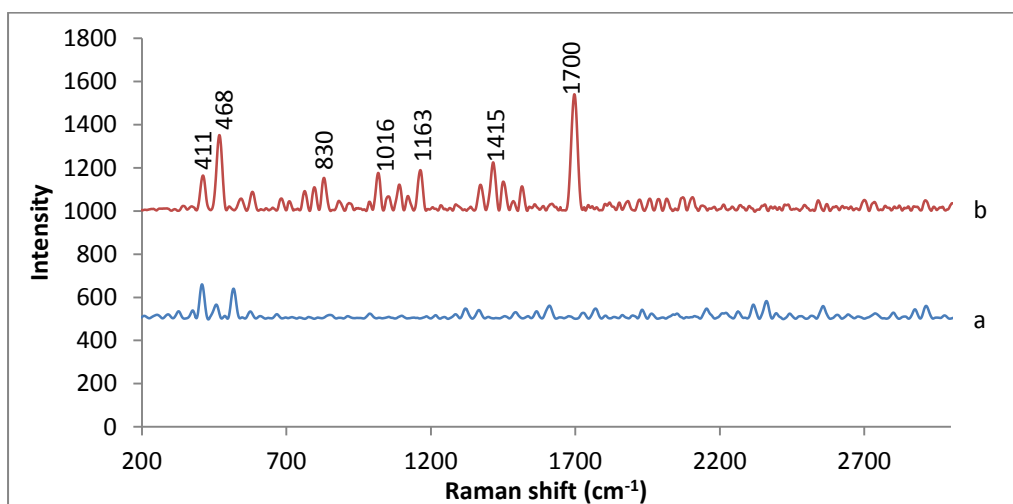


Figure 13: (a) Raman spectra of 1mM of Phenolphthalein on plain thread and (b) SERS spectra of 1mM Phenolphthalein on of AuNPs-CPAM treated thread.

Parameters affecting SERS performance of AuNPs treated thread

Following initial proof of concept studies, experiments were performed to determine if the size or concentration of the NPs played a role in the enhancement achieved during SERS. To determine the effects of NP size, threads were treated with AuNPs of different sizes: 20 nm and 40 nm. After soaking in the AuNP solution for 24 hours, the color of the cotton thread changed from a cream-white to dark purple/red as a result of the plasmon absorption of the AuNPs assembled on the substrates. The FESEM image shows that the adsorption of AuNPs is well dispersed on the surface of thread (Figure 14a and 14b). Figure 15b and 15c shows the SERS spectra obtained from threads which were treated with AuNPs of two different sizes and exposed to 1 mM of 4-ATP. Both SERS spectra clearly show the spectral features of 4-ATP as opposed to the Raman spectrum of 4-ATP on untreated thread (Figure 15a) and are very similar in terms of their intensity.

In order to study the effect of concentration, the 20nm AuNPs were concentrated using an ultra-centrifuge (by 10 times). FESEM analysis (Figure 14c) showed that a higher surface coverage of AuNPs was achieved on the thread surfaces when the thread was treated with the concentrated AuNPs. Additionally, the SERS intensity increased and the characteristic peaks of the 4-ATP became more distinct (Figure 15d). This suggests that the concentration of AuNPs has more impact on the SERS signal enhancement compared to their size.

According to the literature, aggregates of nanoparticles have higher SERS efficiency than individual nanoparticles due to increased enhancement at the junctions between nanoparticles [26-27]. In order to amplify the SERS signal of the concentrated 20 nm AuNP treated thread, the aggregation of AuNPs was induced by pre-treating the thread with 0.01% CPAM. CPAM is a cationic polyelectrolyte which is extensively used as a retention and flocculation aid in the papermaking industry. It is able to produce a positive surface charge on cotton thread substrates and then promote the aggregation of the negatively-charged AuNPs. As shown in Figure 14d, there was a significant increase in the adsorption and aggregation of AuNPs when the thread was pre-treated by CPAM. The assembly of the AuNPs is brought into closer vicinity by forming a random distribution of two- and three-dimensional clusters, compared to the AuNP thread without CPAM (Figure 14c). As AuNPs become in close contact when aggregated, their transition dipoles become coupled to each other and the enhanced fields of each nanoparticle

start to coherently interfere at their contact point. Hence, their SERS signal is significantly enhanced (Figure 15e).

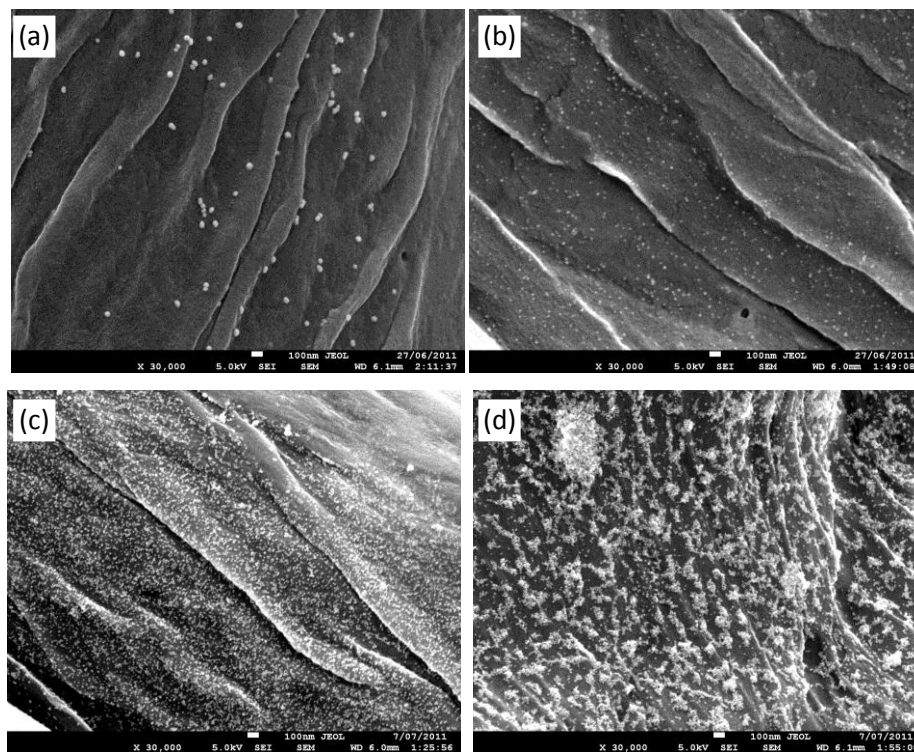


Figure 14: FESEM image of (a) 40 nm, (b) 20 nm, (c) concentrated 20 nm AuNPs on cotton thread and (d) 20 nm concentrated AuNPs on CPAM pre-treated cotton thread.

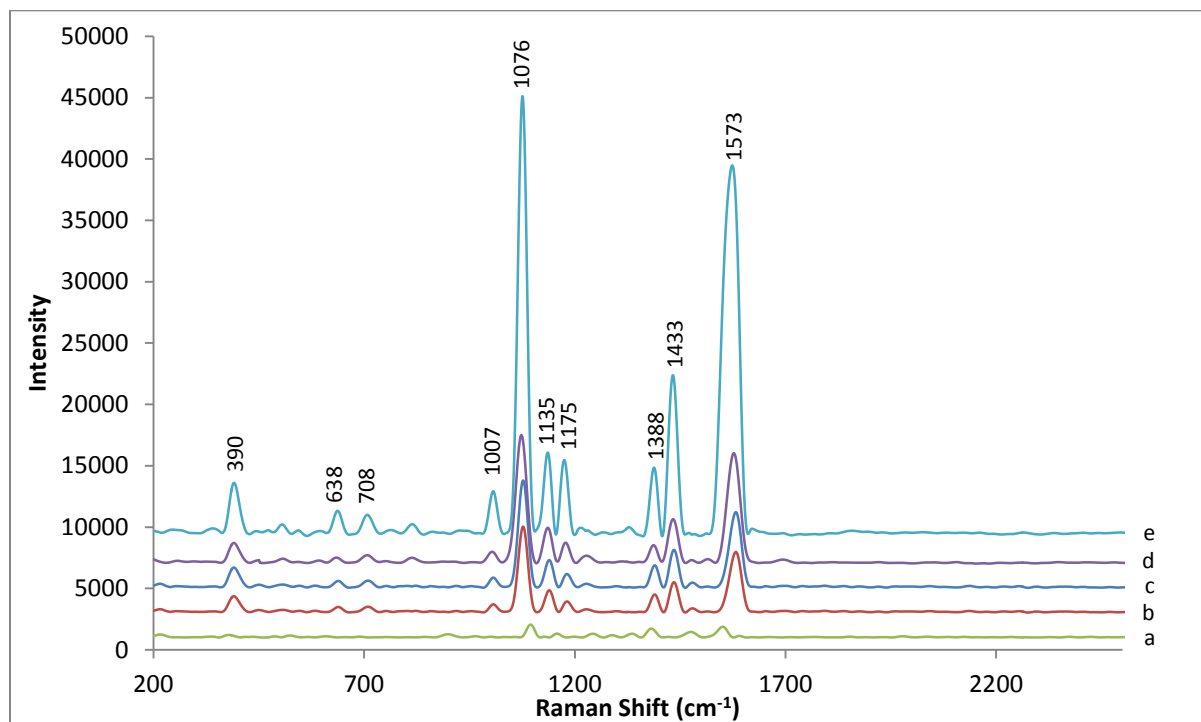


Figure 15: (a) Raman spectrum of 1 mM 4-ATP on untreated cotton thread. SERS spectra of 1 mM 4-ATP on cotton thread treated by (b) 40 nm AuNPs, (c) 20 nm AuNPs, (d) concentrated 20 nm AuNPs and (e) concentrated 20 nm AuNPs and CPAM.

Conclusions

This study presents the first use of cotton thread as an efficient SERS active substrate for probing 4-ATP. By controlling the aggregation state of the AuNPs on thread using cationic polymer, greatly amplified SERS signals were achieved for a range of analytes. Additionally, this study also demonstrated that the polarizability of analyte molecules was an important factor in how much signal enhancement could be achieved, while the presence or absence of chemical bonding between the analyte and the nanoparticle surfaces was not. It was observed that SERS analysis was only effective for detecting certain analyte molecules which possess higher polarizability. Molecules which lack structural elements such as benzene rings or carbon-carbon double bonds (which lead to π - electrons) like 1-DT, LM and CPAM have poor polarizability and thus display little Raman activity. This study illustrated that analytes do not have to be chemically bound to the surface of the Au-NPs in order to generate an enhancement of Raman signal. Analyte molecules which lacked gold-binding functional groups but possessed high polarizability were still subject to signal enhancement. This study shows the viable potential of AuNP-functionalized thread substrates to be used and optimized as low cost, disposable biodiagnostics, for routine SERS spectroscopy. The threads used were inexpensive and required only small volumes of both sample solution and treatment solution to produce strong results. Overall, a novel, low-cost platform for SERS analysis has been developed which possesses several desirable advantages over contemporary alternatives.

References

1. Kaminska, A., et al., *Chemically bound gold nanoparticle arrays on silicon: assembly, properties and SERS study of protein interactions*. Physical Chemistry Chemical Physics, 2008. **10**(28): p. 4172-4180.
2. *Surface-enhanced Raman scattering on tunable plasmonic nanoparticle substrates*. Proceedings of the National Academy of Sciences, 2004. **101**(52): p. 17930.
3. Luo, L.-B., et al., *Surface-Enhanced Raman Scattering from Uniform Gold and Silver Nanoparticle-Coated Substrates*. The Journal of Physical Chemistry C, 2009. **113**(21): p. 9191-9196.

4. Petlicki, J. and T.G.M. van de Ven, *Adsorption of polyethylenimine onto cellulose fibers*. Colloids and Surfaces A: Physicochemical and Engineering Aspects, 1994. **83**(1): p. 9-23.
5. Bizzarri, M.S.P.A.R. and M.S.P.S. Cannistraro, *SERS detection of thrombin by protein recognition using functionalized gold nanoparticles*. Nanomedicine: Nanotechnology, Biology and Medicine, 2007. **3**(4): p. 306-310.
6. Hesse, E. and J.A. Creighton, *Investigation of cyanide ions adsorbed on platinum and palladium coated silver island films by surface-enhanced Raman spectroscopy*. Chemical Physics Letters, 1999. **303**(1-2): p. 101-106.
7. Chen, Y.-H. and C.-S. Yeh, *Laser ablation method: use of surfactants to form the dispersed Ag nanoparticles*. Colloids and Surfaces A: Physicochemical and Engineering Aspects, 2002. **197**(1-3): p. 133-139.
8. Ngo, Y.H., et al., *Gold Nanoparticle–Paper as a Three-Dimensional Surface Enhanced Raman Scattering Substrate*. Langmuir, 2012. **28**(23): p. 8782-8790.
9. Ngo, Y.H., et al., *Paper surfaces functionalized by nanoparticles*. Advances in Colloid and Interface Science, 2011. **163**(1): p. 23-38.
10. Ballerini, D., X. Li, and W. Shen, *An inexpensive thread-based system for simple and rapid blood grouping*. Analytical and Bioanalytical Chemistry, 2011. **399**(5): p. 1869-1875.
11. Li, X., et al., *Fabrication of paper-based microfluidic sensors by printing*. Colloids and Surfaces B: Biointerfaces, 2010. **76**(2): p. 564-570.
12. Turkevich, J., P.C. Stevenson, and J. Hillier, *A study of the nucleation and growth processes in the synthesis of colloidal gold*. Discussions of the Faraday Society 1951. **11**: p. 55-75.
13. Cadotte, M., et al., *Flocculation, Retention and Drainage in Papermaking: A Comparative Study of Polymeric Additives*. The Canadian Journal of Chemical Engineering, 2007. **85**(2): p. 240-248.
14. Hu, X., et al., *Surface-Enhanced Raman Scattering of 4-Aminothiophenol Self-Assembled Monolayers in Sandwich Structure with Nanoparticle Shape Dependence: Off-Surface Plasmon Resonance Condition*. Journal of Physical Chemistry C, 2007. **111**(19): p. 6962-6969.
15. Aponte, M.I., *Effect of alkanethiol self-assembled monolayers on the plastic and elastic deformation of gold(III) films*, in *Materials Science and Engineering*. 2010, The state University of New Jersey: New Jersey. p. 209.
16. Graff, M. and J. Bukowska, *Surface-enhanced Raman scattering (SERS) spectroscopy of enantiomeric and racemic methionine on a silver electrode-evidence for chiral discrimination in interactions between adsorbed molecules*. Chemical Physics Letters, 2011. **509**(1-3): p. 58-61.
17. Wang, F., et al., *Chemical controlled reversible gold nanoparticles dissolution and reconstruction at room-temperature*. Chemical Communications, 2012. **48**(49): p. 6136-6138.
18. Moon, S., S.-i. Tanaka, and T. Sekino, *Crystal Growth of Thiol-Stabilized Gold Nanoparticles by Heat-Induced Coalescence*. Nanoscale Research Letters, 2010. **5**(5): p. 813 - 817.
19. Vericat, C., M.E. Vela, and R.C. Salvarezza, *Self-assembled monolayers of alkanethiols on Au(111): surface structures, defects and dynamics*. Physical Chemistry Chemical Physics, 2005. **7**(18): p. 3258-3268.
20. Bisio, F., et al., *Interaction of Alkanethiols with Nanoporous Cluster-Assembled Au Films*. Langmuir, 2011. **27**(13): p. 8371-8376.
21. Shalom, D., et al., *Synthesis of thiol functionalized gold nanoparticles using a continuous flow microfluidic reactor*. Materials Letters, 2007. **61**(4-5): p. 1146-1150.
22. Jadzinsky, P.D., et al., *Structure of a Thiol Monolayer-Protected Gold Nanoparticle at 1.1 Å Resolution*. Science, 2007. **318**(5849): p. 430-433.
23. Larkin, P., *Infrared and Raman Spectroscopy*. 2011, Elsevier.
24. Kunitomo, K.-K., et al., *Molecular structure and vibrational spectra of phenolphthalein and its dianion*. Spectrochimica Acta Part A: Molecular and Biomolecular Spectroscopy, 2001. **57**(2): p. 265-271.

25. Chattopadhyay, S., et al., *Resonance Raman spectrum of phenolphthalein in alkaline solution and vibrational spectra of the pure compound and its potassium salts*. Journal of Raman Spectroscopy, 1989. **20**(10): p. 651-654.
26. Toderas, F., et al., *Controlling gold nanoparticle assemblies for efficient surface-enhanced Raman scattering and localized surface plasmon resonance sensors*. Nanotechnology, 2007. **18**.
27. Michaels, A.M., Jiang, and L. Brus, *Ag Nanocrystal Junctions as the Site for Surface-Enhanced Raman Scattering of Single Rhodamine 6G Molecules*. The Journal of Physical Chemistry B, 2000. **104**(50): p. 11965-11971.

Appendix III: Patent Generated from This Thesis

METALLIC NANOPARTICLE TREATED CELLULOSIC SUBSTRATE AS A SERS BIODIAGNOSTIC PLATFORM

FIELD OF THE INVENTION

[0001] The invention is generally directed to Surface Enhanced Raman Scattering (SERS) substrates suitable for use as a SERS biondiagnostic platform, and in particular to metallic nanoparticle treated substrates formed of paper or other cellulosic material.

BACKGROUND TO THE INVENTION

[0002] Paper has recently been rediscovered as substrate for low cost analytical tests in health and environmental applications. Flexible micro-fluidic systems, reactors and valves have already been printed on paper to regulate, measure and control the flow of analytes and reagents. In paper blood typing assays, blood group antigens can be displayed directly by the red blood cells that elude or absorb on the paper depending on whether they react with a specific or a non-specific antibody which was previously adsorbed. However, the identification of antibodies can be complicated because of their typical low concentration and small dimensions, such as for example immunoglobulin G (IgG). While Enzyme-Linked Immunosorbent Assay (ELISA) is a standard solution-based technique, its application to paper, while possible, requires multiple reactants and washing steps. A direct approach involving a simple contact between a paper substrate and analytes, followed by signal amplification using some instrumentation techniques would be ideal. Surface Enhanced Raman Scattering (SERS) presents an attractive technique where analytes such as antibodies can be selectively adsorbed onto antigens capped metallic nanoparticles on a treated paper substrate and detected at very low concentrations.

[0003] SERS is a technique that enhances the Raman scattering which measures the small energy changes of the light scattered from a molecule absorbed on a metallic surface, typically a metallic nanoparticle. The enhancement factor can be as much as 10^{14} – 10^{15} , which enables SERS as a single-molecule detection technique to identify analytes at trace levels. The critical requirements of a substrate for SERS application in routine analytical procedures include low cost, sensitivity, robustness, reproducibility and stability to allow for long term storage between measurements. The immobilization of metallic nanoparticles onto solid substrates provides an attractive alternative to metal aqueous colloid as SERS substrates because of its higher flexibility and easy application to non water-soluble compounds. In particular, there has been significant progress in surface sciences and nanofabrication technology that have allowed the control of size, shape and aggregation of nanoparticles deposited on conventional SERS substrates such as silicon and glass by electron beam lithography, focused ion beam patterning and thermal evaporation. However, these techniques are time consuming, costly, require sophisticated equipment, and the substrates are often fragile and suffer from poor storage stability.

[0004] With excellent features such as low cost, flexibility, robustness, long term stability and ease of use, cellulosic materials such as paper offers a promising platform as a SERS substrate for bioassays. The soft texture of paper substrates allows conformal contact with the surface of analytes by swabbing. This provides an efficient and practical method to collect traces of analytes from the body and many surfaces, compared to silicon and glass which are rigid, brittle and confined to laboratory experiments. Paper is an efficient substrate for routine SERS analysis as highlighted in many studies. However, most of these studies have used paper simply as an inert support and have not explored how the rough, composite and heterogeneous nature of paper can affect the distribution of nanoparticles and the SERS signal generated.

[0005] Paper was first reported as a SERS substrate in 1984 by Tran [Tran, C.D., *Subnanogram detection of dyes on filter paper by surface-enhanced Raman scattering spectrometry*. Analytical Chemistry, 1984. 56(4): p. 824-826] which

demonstrated subnanogram detection of dyes on filter paper. Silver colloidal hydrosols were synthesized. Various concentrations of aqueous dye solutions and silver colloidal were applied onto filter paper by microsyringe, either as premixed mixture or separately. The Raman spectra were taken on wet paper.

[0006] Vo-Dinh [Vo-Dinh, T., M. Uziel, and A.L. Morrison, Surface-Enhanced Raman Analysis of Benzo[A]Pyrene-DNA Adducts on Silver-Coated Cellulose Substrates. *Appl. Spectrosc.*, 1987. 41(4): p. 605-610] and Laserna [Berthod, A., J.J. Laserna, and J.D. Winefordner, *Analysis by surface enhanced Raman spectroscopy on silver hydrosols and silver coated filter papers*. *Journal of Pharmaceutical and Biomedical Analysis*, 1988. 6(6-8): p. 599-608] [Cabalin, L.M. and J.J. Laserna, *Fast spatially resolved surface-enhanced Raman spectrometry on a silver coated filter paper using charge-coupled device detection*. *Analytica Chimica Acta*, 1995. 310(2): p. 337-345] [Bizzarri, M.S.P.A.R. and M.S.P.S. Cannistraro, SERS detection of thrombin by protein recognition using functionalized gold nanoparticles. *Nanomedicine: Nanotechnology, Biology and Medicine*, 2007. 3(4): p. 306-310] reported the assembly, morphology and optical properties of AgNPs-coated filter paper as a promising SERS substrate. The AgNPs coated papers were prepared by immersing the filter paper in AgNO₃ solution and the wet filter paper was sprayed with sodium borohydride solution by thermal evaporation in a vacuum chamber. These filter-paper had a random dispersion of particle sizes and shapes.

[0007] Luo [Luo, Z. and Y. Fang, *SERS of C60/C70 on gold-coated filter paper or filter film influenced by the gold thickness*. *Journal of Colloid and Interface Science*, 2005. 283(2): p. 459-463], Niu [Niu, Z. and Y. Fang, *Surface-enhanced Raman scattering of single-walled carbon nanotubes on silver-coated and gold-coated filter paper*. *Journal of Colloid and Interface Science*, 2006. 303(1): p. 224-228], Wu. [Wu, D. and Y. Fang, *The adsorption behavior of p-hydroxybenzoic acid on a silver-coated filter paper by surface enhanced Raman scattering*. *Journal of Colloid and Interface Science*, 2003. 265(2): p. 234-238] and Ma. [Ma, W. and Y. Fang, *Experimental (SERS) and theoretical (DFT) studies on the adsorption of p-, m-, and o-nitroaniline on gold nanoparticles*. *Journal of Colloid*

and Interface Science, 2006. 303(1): p. 1-8.] performed direct synthesis of gold and silver colloids by chemical oxidation-reduction using potassium tetrachloroaurate (KAuCl_4) and silver nitrate (AgNO_3). The resulting colloids were added drop wise onto filter papers for SERS application. Nanoparticles coated paper was shown a highly SERS active substrate. However, the spotting method used did not achieve reproducible and uniform distribution of nanoparticles on paper; aggregation is formed at the edge of the droplets during drying (coffee stain phenomenon).

[0008] International Publication No. WO 2010/073260 describes a SERS active paper substrate comprising in-situ synthesized nanoparticles. The nanoparticles paper was prepared by immersing the paper strip in a metal precursor solution and then immersion in a boiling reducing solution. However, the process used is not practical.

[0009] Yu and White [Yu, W.W. and I.M. White, Inkjet Printed Surface Enhanced Raman Spectroscopy Array on Cellulose Paper. *Analytical Chemistry*, 2010. 82(23): p. 9626-9630] printed silver nanoparticle on hydrophobic paper with an inkjet printer. This method to fabricate SERS paper involved tedious pre-concentration of the silver ink and required multiple printing to produce adequate amount of nanoparticles on paper. This is not practical.

[0010] Cheng [Cheng, M.-L., B.-C. Tsai, and J. Yang, *Silver nanoparticle-treated filter paper as a highly sensitive surface-enhanced Raman scattering (SERS) substrate for detection of tyrosine in aqueous solution*. *Analytica Chimica Acta*, 2011. 708(1–2): p. 89-96] prepared silver nanoparticle doped filter papers with a silver mirror reaction. Gold nanorod loaded filter paper was also demonstrated by Lee. [Lee, C.H., L. Tian, and S. Singamaneni, *Paper-Based SERS Swab for Rapid Trace Detection on Real-World Surfaces*. *ACS Applied Materials & Interfaces*, 2010. 2(12): p. 3429-3435; Lee, C.H., et al., *Highly Sensitive Surface Enhanced Raman Scattering Substrates Based on Filter Paper Loaded with Plasmonic Nanostructures*. *Analytical Chemistry*, 2011. 83(23):

p. 8953-8958] by dipping paper in a gold nanorod suspension synthesized by a seed-mediated approach.

[0011] US Patent Publication No. 2010/0245814 describes an analytical substrate where a film having metal nanoparticles is deposited on a substrate to form a metallic film thereon for amplifying Raman signals.

SUMMARY OF THE INVENTION

[0012] It would be advantageous to have a metal nanoparticle treated cellulosic substrate which provides improved SERS performance over known SERS substrates.

[0013] It would also be preferable that the SERS substrate not lose efficiency following wetting during usage.

[0014] According to one aspect of the present invention there is provided a metal nanoparticle treated cellulosic substrate for use as a surface enhanced Raman scattering (SERS) biondiagnostic platform, the substrate including metal nanoparticles coating the substrate, wherein the nanoparticles are agglomerated on the substrate due to pre-treatment with a coagulant.

[0015] This invention may be used as a solid, flexible and conformable substrate platform for SERS analysis for health, analytical and environment application. The applicants have determined that the aggregation state of the nanoparticles is the main contributing factor to SERS performance. Furthermore, the nanoparticles can be controlled by use of a coagulant to control the distribution of the nanoparticles on the substrate surface.

[0016] The substrate may be formed from paper. The term 'paper' refers to a non-woven composite made from cellulosic fibers. These fibers may include pulp fibers, from mechanical or chemical pulping process, from hardwood or hardwood

sources, wood or non-wood sources (hemp, bagasse, flax), cotton fibers, nanocellulose and micro fibers. The paper non-woven composite may have a basis weight ranging from 15 to 500 g/m², and better 40- 400 g/m². Paper is a non-woven material either made from wet-process or by air-laid process.

[0017] The coagulant used to agglomerate the nanoparticles may preferably be a polymer. These polymers may include high molecular weight (100,000 Dalton to 20,000,000 Dalton), high charge density (5% to 100% based on monomer charged) polymers. The polymer can have a linear, branched, dendritic, alternating or block morphology. The polymers that may be utilised include CPAM, PEI, PEO, PVAm, PAE, polyDADMAC and similar polymers and their copolymers and blends. The polymer can be added to paper either as bulk treatment (during formation of paper by wet end addition, or by dipping paper in a polymer solution) or as a surface treatment (by printing, surface sizing, surface coating, dripping, or spraying). The polymer can also be added to the nanoparticle suspension to preform aggregates to be subsequently adsorbed on paper. The polymer also acts to retain the nanoparticles on the substrate following wetting during usage such that there is little to no loss in efficiency of the substrate.

[0018] It is however also envisaged that the coagulant may be a salt or poly salt having a valency of between 1 to 4.

[0019] The metal nanoparticles may be formed from one or more metals selected from a group consisting of gold, silver, copper or titanium dioxide. The individual said nanoparticles may have an average diameter of between 10 and 100 nm. The nanoparticles may preferably be agglomerated in aggregates having an average diameter of between 1.1 to 10 or preferably 1.1 to 7, or more preferably 1.1 to 5 times the average diameter of the individual nanoparticles. Furthermore, the nanoparticles may coat between 5% to 100%, and preferably 25% to 90% of the substrate surface.

[0020] The metal nanoparticles may be functionalised with an antigen or an antibody. The metal nanoparticles may be functionalised through a self assembling system such as thiol coupling or a bioaffinity system such as streptavidin-biotin type.

[0021] It is envisaged that the substrate may have a Raman enhancement factor (EF) of 1,000, 10,000, 100,000, 1,000,000 or higher.

[0022] According to another aspect of the present invention, there is provided a method of producing a metal nanoparticles treated cellulosic substrate for use as a surface enhanced Raman scattering (SERS) biodiagnostic platform including the steps of:

- a) adsorbing metal nanoparticles on the substrate from a nanoparticles suspension solution; and
- b) treating the nanoparticles with a coagulant so that the nanoparticles agglomerate on the substrate.

[0023] The coagulant may be a polymer that is adsorbed on the substrate from a polymer solution. The polymer may be added as a surface treatment on the substrate. Alternatively, the polymer may be added to the solution containing the metal nanoparticles suspension.

[0024] Paper or other cellulosic substrates treated with agglomerated metal nanoparticles provides a low-cost flexible platform for bioassays using SERS technology to increase the sensitivity (signal intensity) by more than 4 orders of magnitude. This paper can be used for health, environmental (water test), industrial and analytical applications. This generic AuNp can be functionalized with any selective ligand sensitive to the analyte of interest using 2 convenient chemistries. The paper can be used as follows. The metal NP-paper is first functionalized with a captor selective to the analyte of interest. This can be an antigen to detect an antibody, an enzyme to reveal a substrate or a ligand for an

analyte. The functionalized metal NP-paper is then contacted with the liquid sample of interest: bio-fluid (blood, urine, saliva, feces, water) or water- to adsorb the analyte of interest. Selectivity is insured by bio-recognition (enzyme-substrate, antibody-antigen) or specific ligand chemistry. The paper is then used, wet or dry, in a hand held battery operated or with a laboratory Raman scattering Spectrophotometer that will produce an intensity- wavelength spectrum. The peaks frequency is a function of the chemistry on the nanoparticles with analytes, and the intensity function of the concentration. Selectivity is insured in 2 ways: with the ligand only capturing the target molecule of interest and with the Raman spectra specific to each substance.

[0025] The applicants discovered that the SERS intensity signal is directly proportional to gold nanoparticle surface coverage on paper and increases faster than linearly with the average size of nanoparticle aggregate. The heart of the invention lies in pre-treating paper with a polymer or other coagulant to engineer the exact NP surface coverage and average size aggregates. The effect of polymer concentration, charge density and molecular weight was quantified using a CPAM. Best performances were achieved with the high charge, high molecular weight CPAM used at higher concentration. The distribution of the nanoparticles through the thickness of paper also affects SERS and can be engineered. Best results were achieved with nanoparticles distributed over a thin interphase of a few paper fibers thickness.

[0026] The immobilization of biomolecules, such as antibodies and antigens, onto AuNp/metal NP provides a good diagnostic platform in health and medicine. Taking advantage of the high affinity association between the *Streptomyces avidinii*-derived protein, streptavidin, and biotin, the AuNp/metal surface can be functionalized with the desired biomolecule. Streptavidin has four active binding sites, thereby providing a stable and selective host protein for surface immobilization. Firstly, streptavidin is bound to the AuNp/Metal surface using biotinylated-thiol. Subsequently the desired biotinylated-biomolecule is bound to streptavidin, thus creating a biomolecular monolayer on the AuNp surface. The interaction of the biomolecule with a specific analyte can then be detected using

SERS. No blockage is required to prevent competitive adsorption (such as with BSA, casein, milk as for ELISA tests). AuNP can also be functionalized with the molecule of interested end capped with a thiol group; the molecule-thiol self assembles on gold/metal surfaces.

[0027] The invention has advantages over existing known technology for a few reasons. First it relies on simple contact method of the paper or other cellulosic substrate with a suspension of nanoparticle and does not require the electron beam lithography, focused ion beam patterning and thermal evaporation typical of nanofabrication. Second, the metal nanoparticle are adsorbed onto paper or other cellulosic substrate at high surface coverage and as aggregates of controlled size. SERS enhancement factor is known to increase exponentially with the number of nanoparticle-nanoparticle contact. Third, direct assembly of nanoparticles is performed instead of in-situ assembly. This allows a much better control of particle size, distribution in the substrate and reduces possibilities of contamination. Fourth, a polymer may be used to retain nanoparticles on the substrate. As bioactive papers are used WET, it is critical to retain the particles on paper during the test.

[0028] The previously noted prior art does not disclose the control of the size of nanoparticle aggregate or nanoparticle surface coverage on paper or other cellulosic substrate by coagulation of the nanoparticles. Coagulation is significantly cheaper and versatile than the alternative technics of nanofabrication. Coagulation can be engineered either by pre-treating the substrate with a polymer (bulk treatment or surface treatments: printing, spraying, surface sizing, coating) or by controlling the stability of the nanoparticle with salt (mono, bi, tri and 4 valency salt) or polymer.

BRIEF DESCRIPTION OF THE DRAWINGS

[0029] It will be convenient to describe the invention with reference to the following examples and accompanying drawings. The particularity of the examples and drawings are not to be understood as superseding the generality of the preceding description of the invention.

[0030] In the drawings:

[0031] Figure 1 shows FESEM images and histograms of particle size distributions of nanoparticles showing the effect of different AuNP solutions;

[0032] Figure 2 shows a Raman spectrum and SERS intensity showing the effect of different AuNP solutions;

[0033] Figure 3 shows FESEM images and histograms of particle size distributions of nanoparticles showing the effect of different CPAM concentrations;

[0034] Figure 4 respectively shows a Raman spectrum and a graph showing the relationship between the average particle size and surface coverage of the nanoparticles and the Raman Enhancement Factor (EF) of 4-ATP showing the effect of different CPAM concentrations;

[0035] Figure 5 shows FESEM images and histograms of particle size distribution of nanoparticles showing the effect of different polymer charge density;

[0036] Figure 6 respectively shows a Raman spectrum and a graph showing the relationship between the average particle size and the surface coverage of nanoparticles and the Raman Enhancement Factor (EF) of 4-ATP showing the effect of different polymer charge density;

[0037] Figure 7 shows FESEM images and histograms of particle size distribution of nanoparticles showing the effect of different polymer molecular weight; and

[0038] Figure 8 respectively shows a Raman spectrum and a graph showing the relationship between the average particle size and surface coverage of nanoparticles and the Raman Enhancement Factor (EF) of 4-ATP showing the effect of different polymer molecular weight.

DETAILED DESCRIPTION OF THE INVENTION

[0039] The invention will now be described with reference to the following four experimental test examples.

1) Effect of AuNP concentration

[0040] The first experimental example shows that the normal treatment of paper with AuNP solutions results in the adsorption of the AuNP as individual particles. The surface coverage is directly proportional to the concentration of the AuNP suspension with which is treated the paper. A surface coverage of AuNPs ranging from 1.8 to 22.1% was achieved on paper; however, the particles on the surfaces represented only 40% of the AuNPs' loading, with the majority uniformly adsorbed within the bulk of the paper. The SERS enhancement factor (EF) is directly proportional to the density of AUNPs on the paper. The adsorption of AuNPs on the surface and into the bulk of the paper presented a 3D multilayer architecture for intralayer and interlayer plasmon coupling. The z-distribution of AuNPs throughout the multilayer of cellulose fibers is believed to be responsible for amplifying the SERS signal via interlayer enhancement.

METHOD

SYNTHESIS AND DEPOSITION OF NANOPARTICLES ON PAPER

[0041] AuNPs were synthesized by using 1 mM $\text{HAuCl}_4 \cdot 3\text{H}_2\text{O}$ and 1% aqueous $\text{Na}_3\text{C}_6\text{H}_5\text{O}_7 \cdot 2\text{H}_2\text{O}$ according to the Turkevich method [Turkevich, J., P.C. Stevenson, and J. Hillier, A study of the nucleation and growth processes in the synthesis of colloidal gold. Discussions of the Faraday Society 1951. 11: p. 55-75]. Filter papers were used as received and dipped into Petri dishes which contained 10 mL solution of AuNPs for 24 hours. After dipping, the paper substrates were rinsed thoroughly with distilled water to remove loosely bound AuNPs, and the papers were dried and equilibrated at 50% relative humidity and 23°C before further analysis.

PREPARATION OF RAMAN ACTIVE SUBSTRATES

[0042] Solutions of 1 mM of 4-ATP were prepared in ethanol. Since 4-ATP is well known for its strong affinity to the surface of AuNPs (its S-H bond is easily cleaved to form an Au-S bond upon adsorption), the dried AuNPs-deposited substrates were dipped into 2 mL of the 4-ATP ethanol solution for a shorter period of time of 5 minutes to create a 4-ATP monolayer on the substrates. After thorough rinsing with ethanol and drying, the treated papers were subjected to Raman characterization. The Raman enhancement factors (EF) of 1 mM of 4-ATP on a substrate was calculated according to the following equation:

$$EF = \frac{[I_{SERS}]}{[I_{bulk}]} \times \frac{[N_{bulk}]}{[N_{ads}]}$$

where I_{SERS} is the intensity of a specific band in the SERS spectrum of 4-ATP and I_{bulk} is the intensity of the same band in the Raman spectrum from the bulk solution sample. For all spectra, the intensity of the band at 1077 cm^{-1} was used to calculate EF values. N_{bulk} is the number of molecules of the bulk 4-ATP in the

laser illumination volume while N_{ads} is the number of molecules adsorbed and sampled on the SERS active substrate within the laser spot.

INSTRUMENTATION

[0043] Field Emission Scanning Electron Microscopy (FESEM), which produces higher resolution, less sample charging and less damaged images than conventional FESEM, was performed using a JEOL 7001 Field Emission Gun (FEG) system operating at 5 kV and 180 pA. The Zeta potential and Dynamic Light Scattering (DLS) measurements were performed with a Zetasizer Nano ZS (Malvern Instruments) in a Folded Capillary cell (DTS1060) at 25 °C. UV-Vis absorbance was measured using a Varian Cary 300Bio spectrophotometer. All Raman and SERS spectra were obtained in air using a Renishaw Invia Raman microscope equipped with a 300 mW 633 nm laser. The laser beam was positioned through a Leica imaging microscope objective lens (50×), whilst the instrument's wavenumber was calibrated with a silicon standard centered at 520.5 cm^{-1} shift. Due to the smaller spot size of the laser compared with the large surface area of the samples, the spectra were obtained at different points of the surface. The position of the spectra bands remained the same, but differed only in intensity. The average Raman intensity of 5 measurements was presented after baseline subtraction from the control sample.

[0044] Figure 1 shows FESEM images and histograms of particle size distribution of filter papers dipped into (a) 0.02 mg/mL, (b) 0.05 mg/mL, (c) 0.10 mg/mL, (d) 0.15 mg/mL and (e) 0.20 mg/mL of AuNP solutions

[0045] Figure 2 shows (Left) Raman spectrum of 1 mM of 4-ATP adsorb on (a) plain filter paper and SERS spectra of 4-ATP on filter paper dipped in AuNP solutions of (b) 0.02 mg/mL, (c) 0.05 mg/mL, (d) 0.10 mg/mL, (e) 0.15 mg/mL and (f) 0.20 mg/mL. (Right) SERS intensity of 4-ATP at 1077 cm^{-1} band from paper dipped in different concentration of AuNP solutions.

2) EFFECT OF POLYMER SOLUTION CONCENTRATION

[0046] In a second experimental example, paper is treated with polymer solutions of different concentrations. This example shows the drastic effect of controlled coagulation of the AuNP with a polymer. Paper was treated with a CPAM polymer solution (CPAM, 13 MD, 40% charge density); AuNP deposits as aggregates on paper and the average size of the aggregate increases with polymer concentration. SERS enhancement factor increases both with AUNP surface coverage and average particle size.

METHOD

DEPOSITION OF NANOPARTICLES ON PAPER

[0047] The method is similar to the first example except for the additional treatment of the paper with CPAM:

[0048] Hydrogen tetrachloroaurate trihydrate ($\text{HAuCl}_4 \cdot 3\text{H}_2\text{O}$), sodium citrate tribasic dihydrate ($\text{Na}_3\text{C}_6\text{H}_5\text{O}_7 \cdot 2\text{H}_2\text{O}$) and 4-aminothiophenol (4-ATP) were purchased from Sigma-Aldrich and used as received. The cationic polyacrylamide (CPAM) polymers were supplied by AQUA+TECH Switzerland from their SnowFlake Cationics product range, and used as received. These were copolymers of uncharged acrylamide with cationic dimethylaminoethylacrylate methyl chloride and identified as: I1 (5 wt% charge density, molecular weight 13 MDa), H1 (10 wt% charge density, molecular weight 13 MDa), F1 (40 wt% charge density, molecular weight 13 MDa) and F3 (40 wt % charge density, molecular weight 6 MDa). Whatman qualitative filter paper #1, which consists of 98% α -cellulose, was selected as the paper substrate. Ultrapure water purified with a Millipore system (18 M Ω .cm) was used in all aqueous solutions and rinsing procedures.

[0049] Figure 3 shows FESEM images and histograms of particle size distribution of filter paper dipped in 1.65 nM of AuNP solutions (a) without CPAM pre-treatment and with CPAM pre-treatment of (b) 0.01 mg/ml (c) 0.05 mg/ml and (d) 0.10 mg/ml polymer concentration.

[0050] Figure 4 shows (Left) Raman spectrum of 4-ATP adsorb on (a) plain filter paper, SERS spectra of 4-ATP on AuNPs paper (b) without CPAM pre-treatment and with CPAM pre-treatment of (c) 0.01 mg/ml (d) 0.05 mg/ml and (e) 0.10 mg/ml polymer's concentration. (Right) Relationship between the average size, surface coverage of AuNP aggregates and the EF of 4-ATP measured at the 1077 cm⁻¹ band.

3) EFFECT OF POLYMER CHARGE DENSITY

[0051] In a third experimental example, paper is treated with polymer solutions of different charge density (constant molecular weight and polymer concentration). AuNP aggregate size and surface coverage on paper both increases with polymer charge density. SERS enhancement factor increases both with AUNP surface coverage and average particle size.

METHOD

[0052] The method is the same as described in the second example except for the treatment of the paper with polymer of different charge density.

[0053] Figure 5 shows FESEM images and histograms of particle size distribution of AuNPs-CPAM papers with polymer's charge density of (a) 5 wt%, (b) 10 wt% and (c) 40wt%.

[0054] Figure 6 shows (Left) SERS spectra of 4-ATP on AuNPs-CPAM papers with polymer's charge density of (a) 5 wt%, (b) 10 wt% and (c) 40wt%. (Right) Relationship between the average size and surface coverage of AuNP aggregates and the EF of 4-ATP measured at the 1077 cm⁻¹ band.

4) EFFECT OF POLYMER MOLECULAR WEIGHT

[0055] In a fourth experimental example, paper is treated with polymer solutions of different molecular weight (constant charge density and polymer concentration). AuNP aggregate size and surface coverage on paper both increases with polymer molecular weight. SERS enhancement factor increases both with AUNP surface coverage and average particle size.

METHOD

[0056] The method is the same as described in the second example except for the treatment of the paper with polymer of different molecular weight.

[0057] Figure 7 shows FESEM images and histograms of particle size distribution of AuNPs-CPAM papers with polymer's molecular weight of (a) 6 MDa and (b) 13 MDa.

[0058] Figure 8 shows (Left) SERS spectra of 4-ATP on AuNPs-CPAM papers with polymer's molecular weight of (a) 6 MDa and (b) 13 MDa. (Right) Relationship between the average size and surface coverage of AuNP aggregates and the EF of 4-ATP measured at the 1077 cm⁻¹ band.

[0059] Modifications and variations as would be deemed obvious to the person skilled in the art are included within the ambit of the present invention as claimed in the appended claims.

THE CLAIMS DEFINING THE INVENTION ARE AS FOLLOWS:

1. A metal nanoparticle treated cellulosic substrate for use as a surface enhanced Raman scattering (SERS) biodiagnostic platform, the substrate including metal nanoparticles coating the substrate, wherein the nanoparticles are agglomerated on the substrate due to pre-treatment with a coagulant.
2. A metal nanoparticle treated cellulosic substrate according to claim 1, wherein the substrate is formed from paper.
3. A metal nanoparticle treated cellulosic substrate according to claim 2, wherein the paper has a basic weight between 15 to 500 g/m², and preferably 40 to 400 g/m².
4. A metal nanoparticle treated cellulosic substrate according to claims 1 or 2, wherein the coagulant is a polymer.
5. A metal nanoparticle treated cellulosic substrate according to claim 4, wherein the polymer has a molecular weight of between 100,000 Dalton to 20,000,000 Dalton.
6. A metal nanoparticle treated cellulosic substrate according to claim 4, wherein the polymer has a charge density of between 5% to 100% based on monomer charged.
7. A metal nanoparticle treated cellulosic substrate according to claim 4, wherein the polymer has a linear, branched, dendritic, alternating or block morphology.
8. A metal nanoparticle treated cellulosic substrate according to claim 4, wherein the polymer is selected from a group consisting of CPAM, PEI, PEO, PVAM, PAE, polyDADMAC and copolymers and blends thereof.
9. A metal nanoparticle treated cellulosic substrate according to claim 1, wherein the coagulant is a salt or poly salt having a valency of between 1 to 4.
10. A metal nanoparticle treated cellulosic substrate according to any one of the preceding claims, wherein the metal nanoparticles are formed from one or more metals selected from a group consisting of gold, silver, copper or titanium dioxide.

11. A metal nanoparticle treated cellulosic substrate according to any one of the preceding claims, wherein individual said nanoparticles have an average diameter of between 10 and 100 nm.
12. A metal nanoparticle treated cellulosic substrate according to any one of the preceding claims, wherein the nanoparticles are agglomerated in aggregates having an average diameter of between 1.1 to 10 or preferably 1.1 to 7, or more preferably 1.1 to 5 times the average diameter of the individual nanoparticles.
13. A metal nanoparticle treated cellulosic substrate according to any one of the preceding claims, wherein the nanoparticles coat between 5% to 100%, and preferably 25% to 90% of a surface of the substrate.
14. A metal nanoparticle treated cellulosic substrate according to any one of the preceding claims, wherein the metal nanoparticles are functionalised with an antigen or an antibody.
15. A metal nanoparticle treated cellulosic substrate according to any one of claims 1 to 13, wherein the metal nanoparticles are functionalised through a self assembling system such as thiol coupling or a bioaffinity system such as streptavidin-biotin type.
16. A metal nanoparticle treated cellulosic substrate according to any one of the preceding claims, wherein the substrate has a Raman enhancement factor (EF) of 1,000, 10,000, 100,000, 1,000,000 or higher.
17. A method of producing a metal nanoparticles treated cellulosic substrate for use as a surface enhanced Raman scattering (SERS) biondiagnostic platform including the steps of:
 - a) adsorbing metal nanoparticles on the substrate from a nanoparticles suspension; and
 - b) treating the nanoparticles with a coagulant so that the nanoparticles agglomerate on the substrate.

18. A method of producing a metal nanoparticle treated cellulosic substrate according to claim 17, wherein the coagulant is a polymer that is adsorbed on the substrate from a polymer solution.

19. A method of producing a metal nanoparticle treated cellulosic substrate according to claim 17, wherein the coagulant is a polymer that is added as a surface treatment on the substrate.

20. A method of producing a metal nanoparticle treated cellulosic substrate according to claim 17, wherein the coagulant is a polymer that is added to the nanoparticles suspension.

MONASH UNIVERSITY

WATERMARK PATENT AND TRADE MARKS ATTORNEYS

P36131AUP1

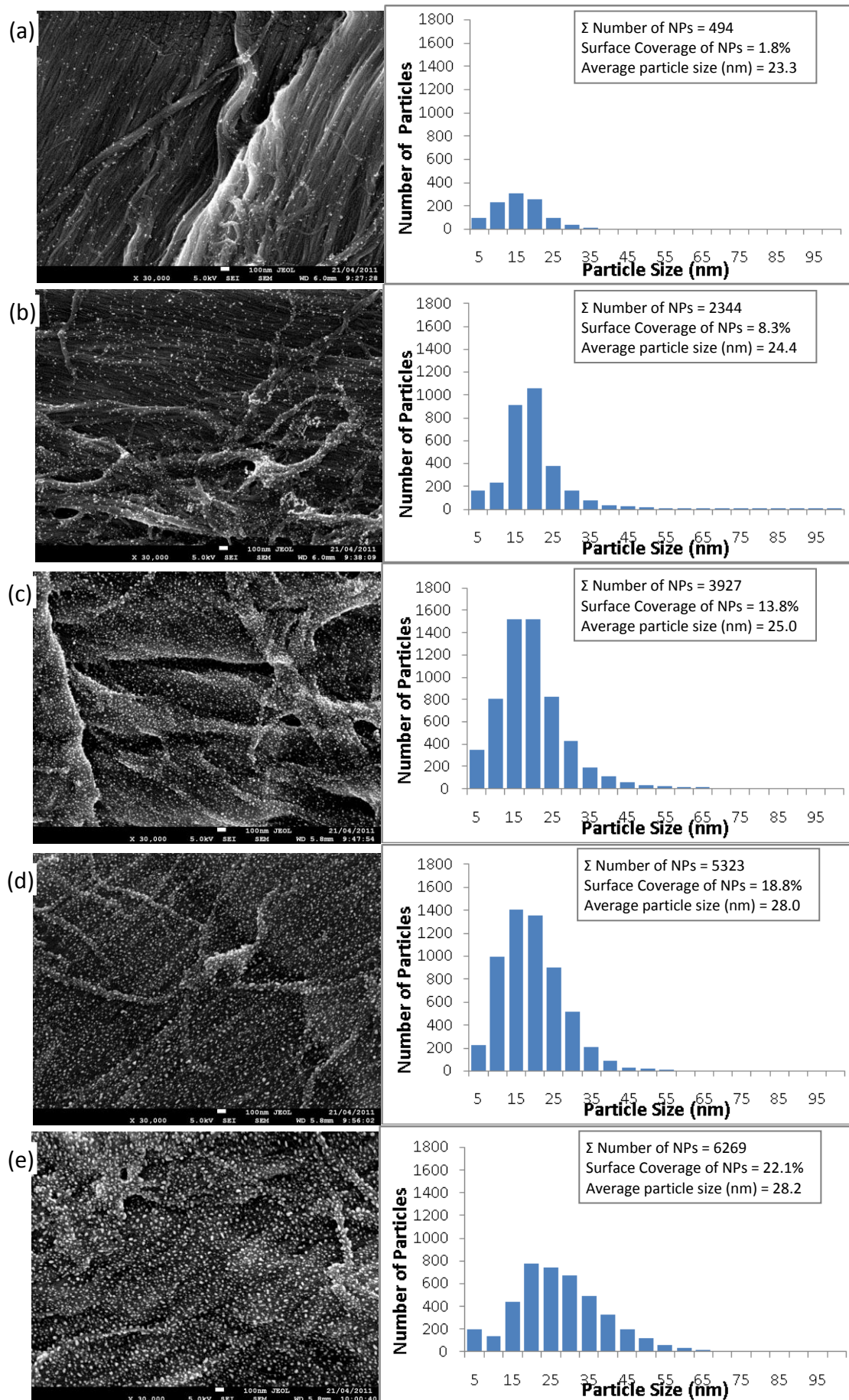


Fig. 1

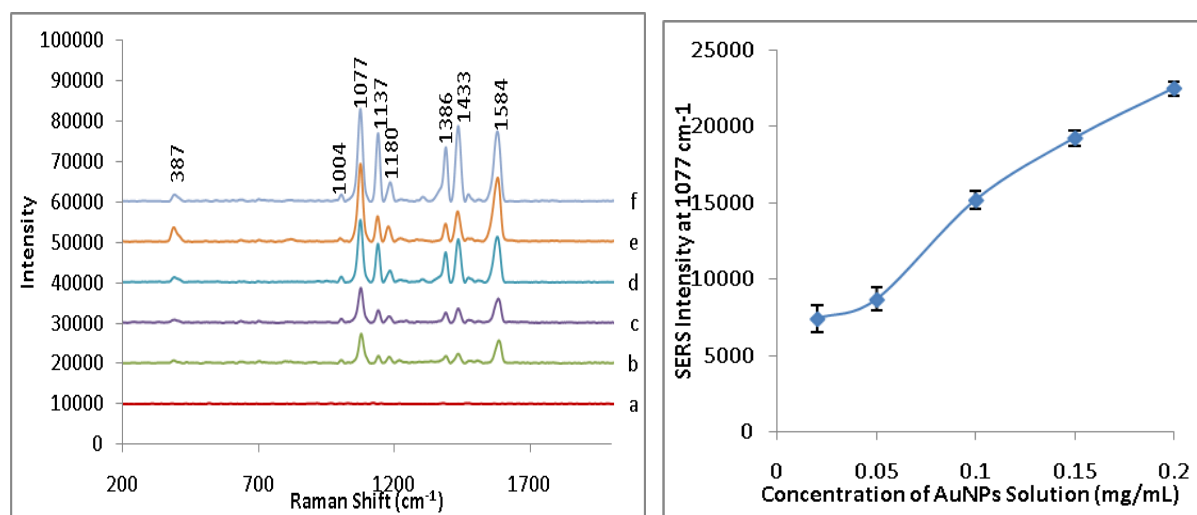


Fig. 2

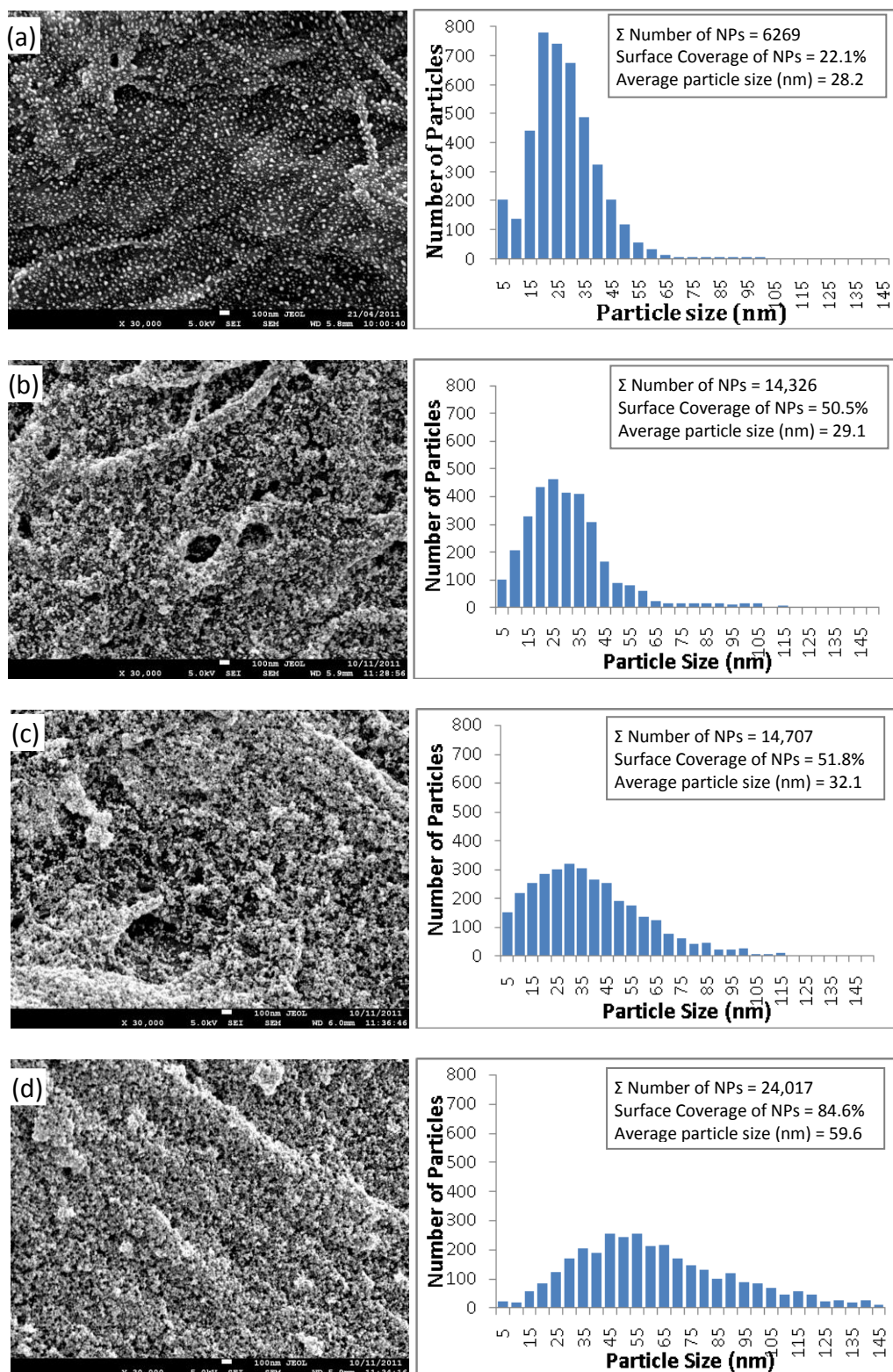


Fig. 3

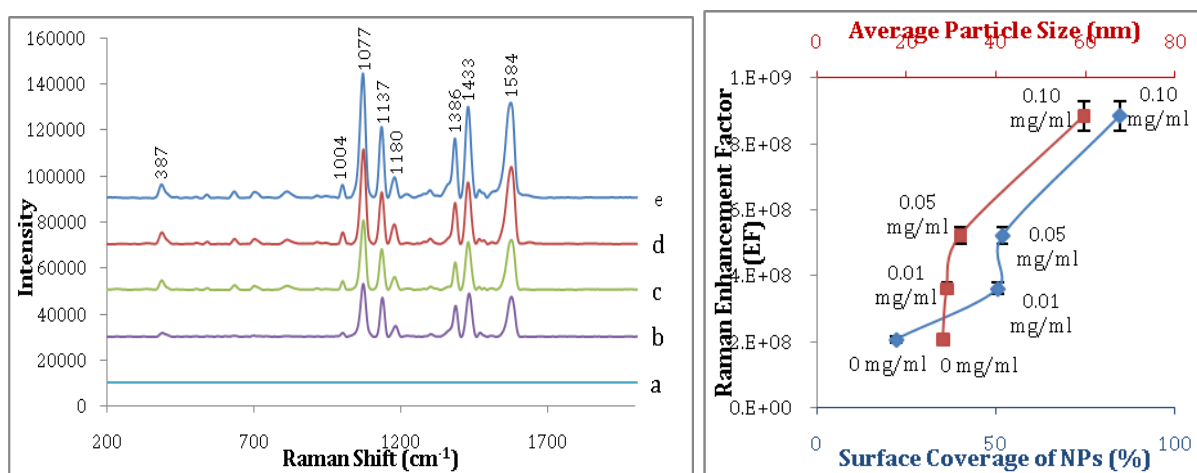


Fig. 4

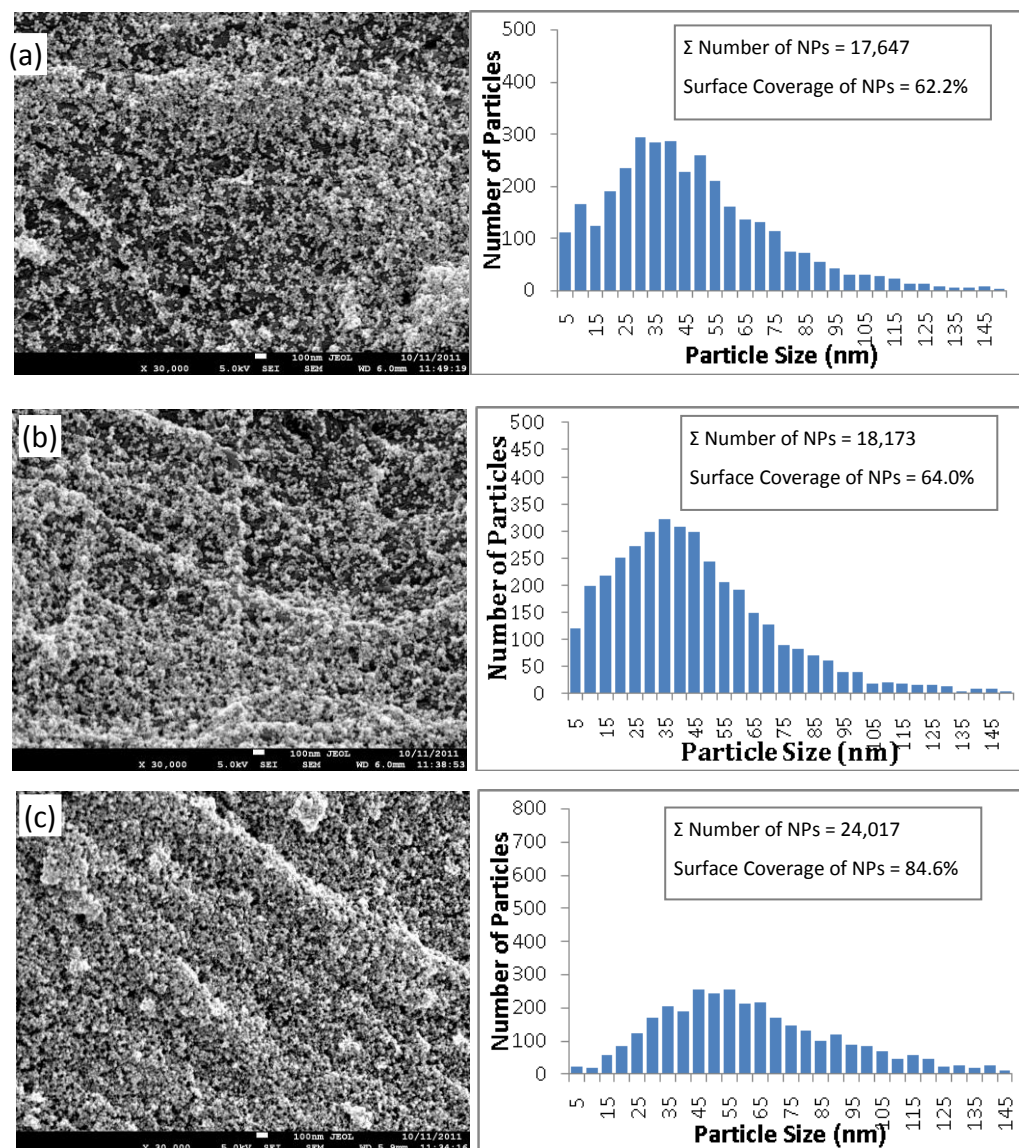


Fig. 5

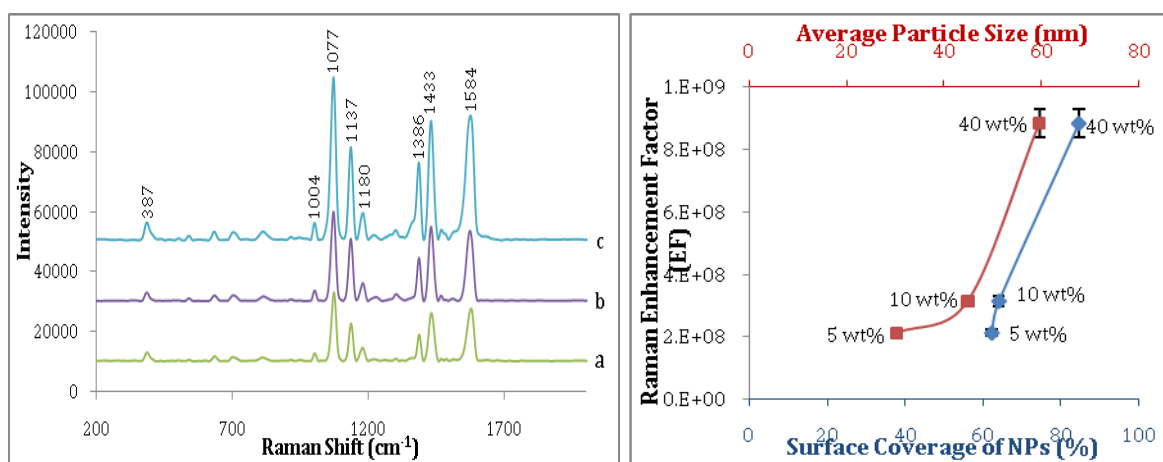


Fig. 6

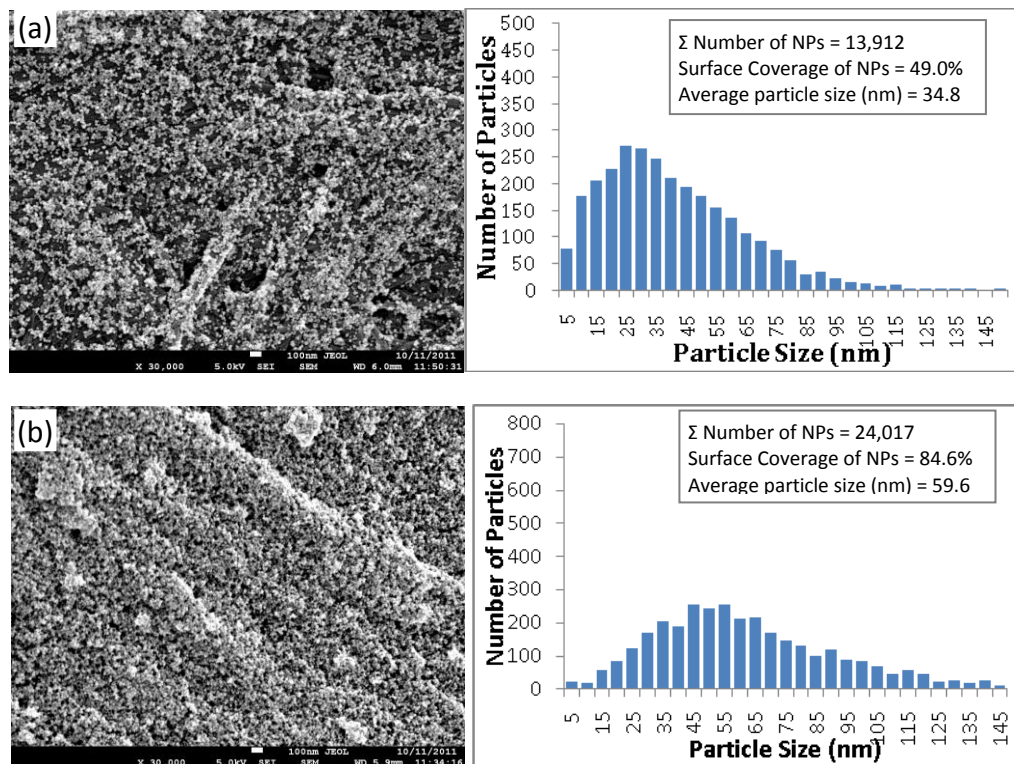


Fig. 7

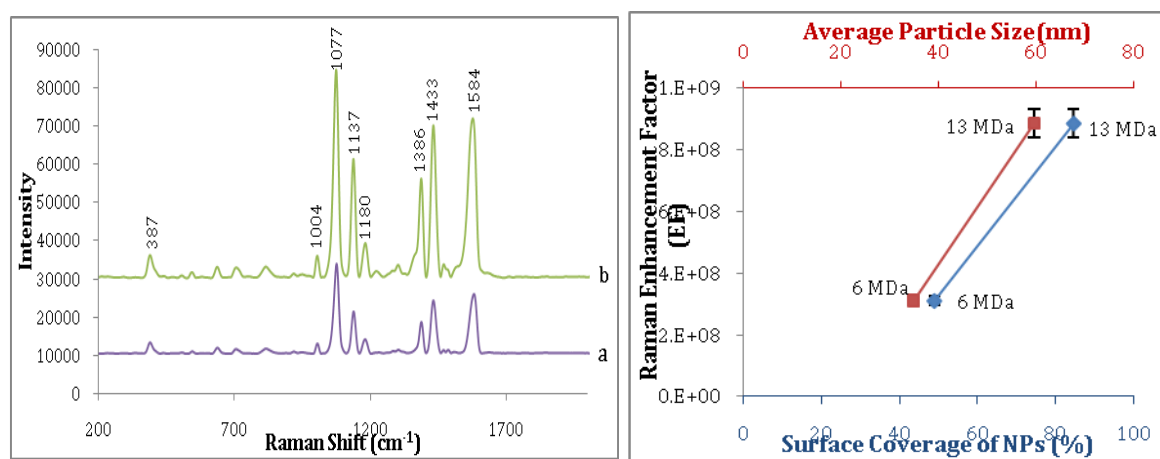


Fig. 8

Appendix IV: Book Chapter Generated from This Thesis

Paper, Printing and the Apple Pie

Gil Garnier, Mohidus Samad Khan*, Ying Ngo, Wade Mosse

BioPRia, Australian Pulp and Paper Institute
Department of Chemical Engineering, Monash University, Clayton, Australia

* Current Address: Department of Chemistry, McGill University, Montreal, Canada.

E-mail: [REDACTED]



ABSTRACT

For 200 years paper has been the main means of communication. Like the apple pie, paper was improved in the early stages by trial and error with a few critical innovations, mostly in process operation. Now the electronic cloud, which constantly transfers information from the internet to portable devices such as electronic pads, phones and light weight computers, challenges the *raison d'être* of newsprint, advertising, office documents and even books. The successful communication era of over 600 years for paper is now challenged. Paper has to evolve as an advanced material with new functions.

Paper combined with printing to develop functional materials can give high value products at a low price. Three examples are given: 1) Bioactive papers: enzymes maintain their selectivity when adsorbed on paper, but the reaction rate decreases with increased stability and aging. To produce a low cost, instantaneous and disposable bioactive paper for blood typing is also possible. 2) Gold nanoparticles (AuNP) on paper significantly increase the sensitivity and specificity of the paper diagnostic which rely on surface enhanced Raman scattering (SERS), and 3) A new family of salt-temperature sensitive poly-zwitterion improves paper strength.

KEYWORDS:

Functional paper, printing, bioactive paper, AuNP paper, nanoparticles, zwitterion enzymatic paper, blood typing paper.

INTRODUCTION

What is the analogy between paper, printing and the apple pie? There are many types of apple pie. The apple strudel is a typical Germanic culinary dessert; the tarte Tatin is a typical French culinary dessert while the typical North-American apple pie is served with ice cream or cheese. The apple pie is regional, and lovingly perfected over centuries through trial and error. It carries with it the traditions, cultures and feelings of a society and is individually loved for taste and with nostalgia. The apple pie remains immune to fashion, economic crises, time and technology. Can we link paper/printing to the concept of the apple pie?

For 200 years paper has been the main way to communicate. Like the apple pie, paper has been improved by trial and error with critical innovations, mostly in process operation. Key technical innovations were the development of the hydrolytic headbox, the twin wire paper machine and the shoe press. The twin wire paper machine increased manufacturing speed, because a web was significantly better maintained by two wires, and to be drained more aggressively without disturbing paper formation. This was achieved with strong jet impingement on the wire, foils and vacuum boxes. The shoe press offers a longer contact time of the wire-web-felt system at a medium pressing intensity giving better drainage without web damage. Over time, paper progressively improved mainly by decreasing the basis weight, increasing printability, and quality control. The major change in paper probably occurred with the neutral/alkaline papermaking process which replaced the acidic paper process which caused poor aging and conservation of paper. The neutral/alkaline process was made possible by new, cheaper and whiter filler, calcium carbonate, which replaced the clay and kaolin. The new filler required a change of sizing system. The increased process efficiency decreased production cost and made paper a commodity. The sustainability of paper making process was improved by paper recycling, and control of air and water emissions. Until the mid-1990's, paper, printing and the apple pie all reflected economic stability, economic growth and personal comfort. Apple pie and paper diverged with the development of the electronics for communication.

The electronic is the emblem of the generations X and Y, marks an irreversible turning point. Companies such as Apple, with its ipod, ipad, iphone, ibook, are dislodging paper as a popular and universal communication means, after a most successful communication era lasting over 600 years. Paper must evolve to become an advanced functional material with properties of use to society.

In the first part of this article, the attributes of paper and printing as functional material and process are defined. In the second section, three examples of functional paper are presented: 1) Bioactive paper, 2) Gold nanoparticle treated paper and 3) salt sensitive paper bonding.

EXPERIMENTAL

Enzymatic Paper:

Materials:

Alkaline phosphatase (ALP) from bovine intestinal mucosa, was purchased from Aldrich and used as received [1]. ALP was physically adsorbed on paper or immobilized using three different water soluble polymers. A cationic polyacrylamide (CPAM) of $M_w = 5 \times 10^6$ and medium charge density (2.1 meq/g), Percol 1550*, was provided by BASF, Ludwigshafen, Germany. Polyacrylic acid (PAA), $M_w = 2,000$ and polyethylene oxide (PEO), $M_w = 4 \times 10^6$, were purchased from Aldrich. All polymers were dissolved to a concentration of 1g/L in deionised water (Millipore, 18M Ω).

ALP was dissolved to a concentration of 0.5 mg/mL in 1 M diethanolamine buffer with 0.50 mM magnesium chloride and drops of 5 M HCl to maintain pH at 9.8. Water (Millipore, 18M Ω) was used for making all dilutions. The 5-bromo-4-chloro-3-indolyl phosphate and 3,3'-(3,3'-dimethoxy-4,4'-biphenylene)-bis-(2-p-nitrophenyl-5-phenyl-2H-tetrazolium chloride) liquid substrate system (BCIP/NBT), purchased from Aldrich, was selected to quantify the enzymatic activity of ALP on paper [2]. The biochemical reaction of ALP with BCIP/NBT under alkaline conditions results in a blue-purple complex; its intense colour can be directly observed, is very stable and does not fade upon exposure to light [2, 3]. The system was selected to optimize colour intensity contrast as blue is the complementary colour of the white/yellowish paper support. Whatman #4 filter paper (basis weight: 96 gsm) was chosen as paper substrate to immobilize enzymes.

Methods:

Polymer on Paper: Paper samples (diameter of 16 cm) were soaked into polymer solutions (25mL; 1g/L) contained in a glass tray for about 1 minute. To remove the un-retained free polymer, the paper samples were then rinsed thoroughly in excess water for 1 minute (Figure 1). This methodology created a consistent polymer layer on paper. The polymer treated samples were immediately soaked into the enzymatic solution.

Enzyme on Paper: Enzyme aqueous solutions were homogeneously applied onto paper following TAPPI (T 205 sp-95) standard. Paper samples ($d = 16\text{cm}$), with and without polymer treatment, were immersed into the ALP enzymatic solution contained in a large Petri-dish (Figure 1). The well soaked paper samples were then blotted using standard blotting papers (Drink Coster Blotting, 280 GSM) to remove any extra solution. A polyethylene sheet (3M, PP2500, $d = 16\text{cm}$) was deposited underneath each blotted sample. Paper and polyethylene sheet were placed into a drying ring assembled so that each sample is uppermost and in contact with the rubber seat of the next ring. The samples were left to dry in a dark chamber at 23°C and 50% relative humidity (RH), for 24hr. The enzymatic paper samples were then used for further deactivation experiment and this time was defined as $t = 0$. Analyses of the surface profiles, histogram distribution of gray values generated by image processing software and Calibration Curve are described elsewhere [3].

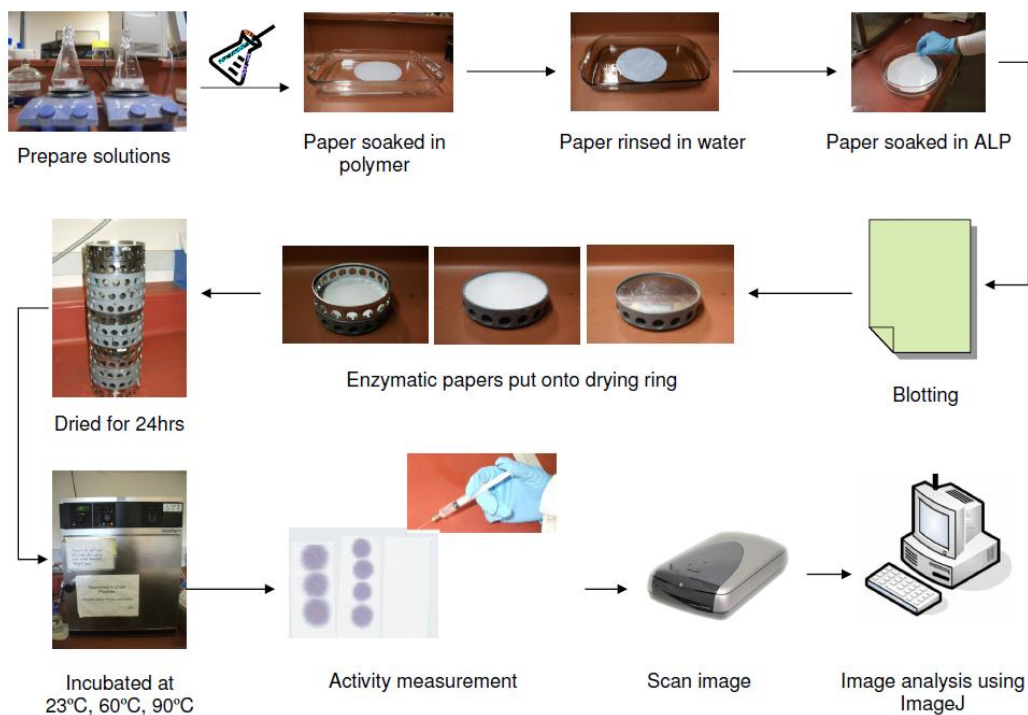


Figure 1: Experimental system to prepare the ALP enzymatic papers.

Thermal treatment of enzymatic papers: The ALP enzymatic papers were cut into small samples (6cm×2cm) and aged at different temperatures (23°C, 60°C or 90°C). For 23°C, the samples were treated in a temperature and humidity controlled lab (23°C and 50% RH). Two ovens (Mettler Universal Oven, Schwabach, Germany) were used to heat samples at 60°C and 90°C. A digital humidity and temperature indicator (VAISALA Humidity and Temperature Indicator, Finland; operating range: −20°C to +60°C) were used to measure the relative humidity (RH) in the ovens. At 60°C, the RH was in range of 6.5–7.0%. For the second oven, the limiting RH reading was 5–5.5% for 65°C, which indicates even dryer conditions at 90°C. After the aging treatment, the liquid substrate (BCIP/NBT) was applied onto the enzymatic papers: small droplets of fresh BCIP/NBT were applied onto the aged enzymatic papers using a 1.0mL syringe equipped with a stainless steel flat tipped needle (0.21mm outer diameter). The enzyme–substrate (E–S) reaction was allowed to proceed in a dark chamber for half an hour at standard condition, 23°C and 50% RH; this insures complete enzymatic reaction [3]. From the colour intensity of the enzyme–substrate reaction, the relative activity of the enzymatic paper was measured. Each measurement reported results from the average of 6–8 full replicates.

Activity measurement: The colour resulting from the E–S reaction on enzymatic papers was measured at 1200dpi using a standard scanner (EPSON PERFECTION 2450 PHOTO) (Figure 1). The scanned images were analysed using ImageJ 1.41o software. For any selected area, the ImageJ software calculates the weighted average gray value within the selection, which can be related to the activity of enzymatic paper [3]. Activity corresponding to the gray value at $t = 0$ hr was considered as 100%. The relative activity at different time intervals was measured and normalized by the activity at $t = 0$ hr, i.e. relative activity, $[E_a]_t/[E_a]_0 = I/I_0$. The log value of

relative activity is defined as the residual activity, $\log(I \times 100 / I_0) = \log([E_a]_t \times 100 / [E_a]_0)$. The colour intensity increase with enzyme concentration on paper is described elsewhere [3, 4].

Leaching of enzymatic papers: The enzymatic paper samples deposited in a glass tray were thoroughly leached in excess water for 1min. The paper samples were then dried and aged under controlled conditions (23°C, 50% RH). For each sample, the enzymatic activity was measured before and after performing leaching test.

Blood typing Paper:

Materials

Antibody solutions of red cell antigens A, B and D (Epiclone™ Anti-A, Anti-B and Anti-D) were purchased from CSL, Australia. Antibodies-A and B come as blue and yellow colour reagents, respectively, and Antibody-D is a clear solution. Anti-D can agglutinate any blood (A, B, O) with the Rhesus factor (D). These antibodies are made of immunoglobulin M (IgM) [5, 6]. Phosphate buffer saline (PBS) (Invitrogen, Australia) was used as diluent for all antibody solutions. 2 mm wide paper strips (Whatman filter paper #4) were used as porous substrate for antibody. To measure the wicking distance, 2 mm units were laser printed with a HP LaserJet 4250n on each paper strip. Standard blotting papers (Drink Coster Blotting, 280 g/m²) were used to remove the excess of antibody solution from the treated paper strips. Reflex paper (80 g/m²) served as semi-hydrophobic surface. For elution test, Whatman filter paper (#4), Drink Coster Blotting Paper and Kleenex towel paper (Kimberly-Clark, Australia) were used. Blood samples (AB+, A+, B+ and O+) were collected from male and female (adult) volunteers. Blood samples were kept in standard plastic vials containing the standard citrate anti-coagulant. All the antibody and blood samples were stored below 4°C. Blood samples were used within 5 days. A calibrated micro-pipette served to dispense standard (20 µL) droplets on the paper strips.

Methods

Blood Chromatographic Separation: Paper strips were soaked into antibody solutions of different concentrations. Excess antibody was removed from the paper strips with blotting papers. The wicking distance was measured from centre to either direction.

Image Capture and Analysis: The wicking kinetics images were captured using a standard video camera (JVC Camcorder Everio GZ-MG530) and a digital SLR camera (SONY-DSLR-A100) with additional close-up lenses. The video clips were transferred to a computer and converted using Prism Video Converter v 1.27 and VirtualDub-1.8.8 software. The still and video images were analyzed using Image-Pro Plus 5.0 software.

Gold Nanoparticle Treated Paper:

Materials

Hydrogen tetrachloroaurate trihydrate (HAuCl₄.3H₂O), sodium citrate tribasic dihydrate (Na₃C₆H₅O₇.2H₂O), 4-aminothiophenol (4-ATP) and alkyl ketene dimer (AKD) were purchased from Sigma-Aldrich and used as received. Whatman filter paper #1 and precut silicon wafers

purchased from ProSciTech were selected as substrates. Hydrophobized paper was prepared by treating the Whatman filter paper #1 with AKD. Ultrapure water purified with a Millipore system (18 MΩ.cm) was used in all aqueous solutions and rinsing procedures.

Methods

Synthesis and Deposition of Nanoparticles on Paper: AuNPs were synthesized by using 1mM HAuCl₄·3H₂O and 1% aqueous Na₃C₆H₅O₇·2H₂O according to the Turkevich method [7]. Filter papers were used as received and dipped into Petri dishes which contained 10mL solution of AuNPs for 24hrs. After dipping, the paper substrates were rinsed thoroughly with distilled water to remove loosely bound AuNPs, and the papers were dried and equilibrated at 50% relative humidity and 23°C before further analysis.

Preparation of Raman Active Substrates: Solutions of 1mM of 4-ATP were prepared in ethanol. Since 4-ATP is well known for its strong affinity to the surface of AuNPs (its S-H bond is easily cleaved to form an Au-S bond upon adsorption), the dried AuNPs-deposited substrates were dipped into 2mL of the 4-ATP ethanol solution for a shorter period of time of 5 minutes to create a 4-ATP monolayer on the substrates. After thorough rinsing with ethanol and drying, the treated papers were subjected to Raman characterization. The Raman enhancement factors (EF) of 1mM of 4-ATP on a substrate was calculated according to Eqn. 1 [8, 9]:

$$EF = \frac{[I_{SERS}]}{[I_{bulk}]} \times \frac{[N_{bulk}]}{[N_{ads}]} \quad (1)$$

where I_{SERS} is the intensity of a specific band in the SERS spectrum of 4-ATP and I_{bulk} is the intensity of the same band in the Raman spectrum from the bulk solution sample. For all spectra, the intensity of the band at 1077cm⁻¹ was used to calculate EF values. N_{bulk} is the number of molecules of the bulk 4-ATP in the laser illumination volume while N_{ads} is the number of molecules adsorbed and sampled on the SERS active substrate within the laser spot.

Instrumentation

Field Emission Scanning Electron Microscopy (FESEM), which produces higher resolution, less sample charging and less damaged images than conventional SEM, was performed using a JEOL 7001 Field Emission Gun (FEG) system operating at 5kV and 180pA. The Zeta potential and Dynamic Light Scattering (DLS) measurements were performed with a Zetasizer Nano ZS (Malvern Instruments) in a Folded Capillary cell (DTS1060) at 25°C. UV-Vis absorbance was measured using a Varian Cary 300Bio spectrophotometer. All Raman and SERS spectra were obtained in air using a Renishaw Invia Raman microscope equipped with a 300mW 633 nm laser. The laser beam was positioned through a Leica imaging microscope objective lens (50×), whilst the instrument's wavenumber was calibrated with a silicon standard cantered at 520.5 cm⁻¹ shift. Due to the smaller spot size of the laser compared with the large surface area of the samples, the spectra were obtained at different points of the surface. The position of the spectra bands remained the same, but differed only in intensity. The average Raman intensity of 5 measurements was presented after baseline subtraction from the control sample.

Salt sensitive Paper binding:

Methods

Poly-zwitterion Synthesis: The poly-zwitterion samples were synthesized by free radical polymerization of the monomer [2-(Methacryloyloxy)ethyl]dimethyl-(3-sulfopropyl) ammonium hydroxide (Sigma-Aldrich) [10, 11]. Approximately 15-20 g of monomer was dissolved in 80mL of water in a round bottomed flask, and stripped of dissolved oxygen by bubbling nitrogen for 10 minutes. Approximately 40mg of ammonium persulfate, dissolved in 20mL of water, was used as an initiator. The mixture was gently stirred and bubbled with nitrogen for a further 30min. Following this, the reaction mixture was heated and maintained at 60°C for 18hr while stirring under nitrogen.

After the mixture was cooled, a viscous polymer mass formed at the bottom of the flask with a water-rich region above. Most of the supernatant was decanted, the remainder of the mixture was reheated to 70°C to reduce the viscosity and allow pipetting. The polymer was precipitated by drop-wise addition to a stirred mixture of 80% v/v acetone with the balance methanol. The precipitated polymer was recovered by filtration, and dried under a vacuum.

Polymer Characterization: The reaction of the monomer was confirmed by 300MHz NMR; two vinyl hydrogen signals seen in the monomer, at around 6ppm, were not present in the polymerized sample.

Gel permeation chromatography was used to determine the molecular weight and polydispersity of the polymer. The polymer was dissolved in 80% vol 0.5M aqueous NaBr, with the balance acetonitrile. The samples were run through columns with a hydrophilic methacrylate matrix, and measured against a set of polyethylene glycol/polyethylene oxide size standards (Fluka, $M_p=200-1200000$).

Polymer Properties: The solubility behaviour of the poly-zwitterion samples was studied as a function of temperature and NaCl concentration. 2mg/mL solutions of each polymer in aqueous solution, with NaCl concentrations of 0, 3, 10, 30, and 100mM, were prepared in glass scintillation vials. The vials were placed in a water bath heated to 95°C and allowed to stand until all solutions were clear with the polymer fully dissolved. The bath temperature was then incrementally lowered, in 1°C increments, and the turbidity of each vial was observed at each temperature. The temperature, at which turbidity was first observed, was recorded as being the cloud point for that particular polymer and salt concentration.

Interactions between Poly-zwitterions and Cellulose: NIST hardwood pulp was used to prepare hand-sheets (60gsm) containing poly-zwitterion additive at 10 mg /g pulp and 100 mg/g pulp. As the polymer requires heat and/or salt for solubility, two methods were used for adding the polymer to the pulp stock. In the first, the polymer stock (5 mg/mL) was dissolved at 95°C, added to pulp slurry heated to 90°C, and the mixture was stirred for 30 seconds before forming a

hand-sheet. In the second method, both pulp and polymer stocks were prepared with 100 mM NaCl and the mixture was stirred for 30 seconds before forming a hand-sheet.

RESULTS AND DISCUSSION

This section examines the material and the processes to develop novel functional papers. Three examples are analyzed: 1) bioactive paper (enzymatic and blood typing), 2) gold nanoparticle paper for diagnostic application and 3) poly-zwitterion for salt-temperature sensitive systems.

Paper:

Paper is a porous and flexible interphase, defined as a region over which properties vary across thickness. Paper is a composite made from cellulosic fibres and functional colloids that can be made into materials tailor made for many different applications.

Paper is a non-woven material, manufactured by a wet laid process, which involves: 1) fibre preparation, 2) forming, 3) bonding and 4) surface treatment. *Fibre preparation* consists of selecting and preparing fibres to optimize the properties of the paper: the selection of the fibres is whether recycled or virgin fibres are used. The fibres can be long softwood or short hardwood fibres. They can also be chemical or mechanical pulp. The fibres are lightly refined to provide the optimal surface area and bonding ability. Additives, such as polymers, micro particles and dye, are then added to control the strength and the optical properties of paper. *Forming* transforms the pulp suspension into paper, a uniform and continuous network of cellulosic fibres and functional colloids. The fibre suspension is deposited onto a moving wire where it is drained and pressed to give fibre orientation, thickness and structure to the paper. *Bonding* links the discontinuous fibres into a continuous non-woven paper network, which is achieved by pressing and drying. The ‘Hydrogen Bond’ (according to traditional valance bond theory) forms a network between the cellulosic surfaces and provides the bonding between fibres. Polymeric strength agents increase the paper wet and dry strength. *Surface treatments* allow paper specific properties. This is achieved by calendering, surface sizing, coating, spraying or other surface treatments. Calendering passes the paper through a series of roll nips of increasing pressure, to decrease paper porosity and increase thickness uniformity and surface smoothness. Surface sizing applies a polymer solution, usually starch with a surface active polymer, onto both surfaces of paper, which creates an interphase when the fluid polymer solution penetrates a finite thickness of the paper surfaces. Coating applies a viscous solution of inorganic (filler) and organic (latex) colloids, which smooth the surfaces of paper and to provide a controlled surface micro-porosity, surface energy and wettability [12].

Many structures and interphase morphologies of paper are achieved using the conventional paper technology (Figure 2). Refining and blending fibres, such as nano-cellulose or micro-fibrillated fibres can increase the internal surface area, bonding and density, while reducing internal pore sizes of paper (Figure 2a). Functional colloids, such as gold nanoparticles (AuNP), can be adsorbed either as individual particles (Figure 2a) or as aggregates (Figure 2b) [13]. By controlling the conditions of the process at the size press and the properties of the solution, polymer layers of different thickness and concentration gradients can be deposited and

pressed into both surfaces of the paper (Figure 2c) [14-16]. The color contrast by SEM (Figure 2c) was achieved using a marker (KI) [15]. The polymer sizing solution can contain a surface active polymer that migrates to the surface to minimize differences in surface energies. The polymer can assemble into polymer domains, as for styrene-maleic anhydride copolymers (Figure 2d) [17, 18].

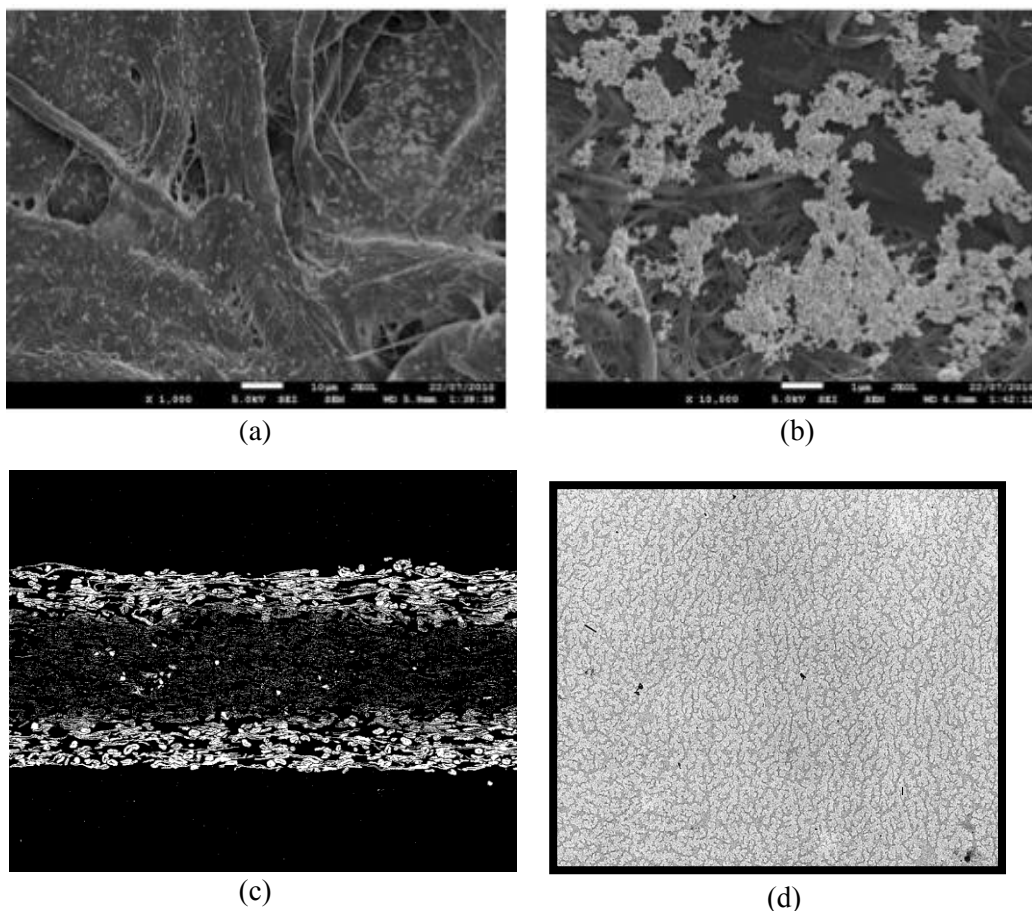


Figure 2: Paper as an advanced material: a) cellulosic fibre bonding and micro-fibrillation, b) retention of aggregated gold nanoparticles on paper, c) creation of an interregion on paper: surface sizing a starch-polymer solution, d) creation of surface active assembled alternating copolymers.

Functional Printing:

Printing is a process which transfers controlled patterns of liquids or dye onto a surface: traditionally this has been ink on a surface. Ink is made of dyes and particles, dispersed in water or an organic solvent, containing additives to control viscosity and surface tension, to give required optical properties. Contact printing, such as flexography, lithography and rotogravure, and non-contact printing like ink jet or laser jet, allow a printing resolution better than 20 μm. If dye/nanoparticles are replaced by a hydrophobic wax, such as AKD, ASA or wax, hydrophobic barriers can be printed to produce microfluidic systems on paper [19]. Biomolecules such as

enzyme, antibody molecules or cells in an aqueous media form a bio-ink which can inkjet in a microfluidic system to give desired paper diagnostics [20].

Bioactive Paper:

A bioactive paper is a paper substrate supporting biomolecules reacting with a biological system. Bioactive paper offers new applications for health, environmental and industrial activities at an economical cost [21-23]. The chemical stability, the ability to be sterilized, the ease of functionalization, the porosity, strength and brightness of paper make it an attractive substrate. Paper allows, through capillarity, the controlled transport of liquids and offers a substrate, which retain biomolecules. Bioactive papers are used wet; therefore, the retention of the biomolecules in use is important. The life time of the bioactive papers is important; bioactive papers must survive the often harsh conditions of shipping.

Enzymatic Papers

Enzymes are good model biomolecules [24-26]. The effect of adsorption on the secondary and tertiary structure of the enzyme, its functionality, stability and selectivity of substrate recognition, is critical for bio-catalysis [27, 28]. Several research groups have investigated polymers as a spacer for solid-region enzyme immobilization [29-31]. However, there is little understanding of the effect of polymer retention aids on the orientation and bio-functionality of biomolecules adsorbed on paper.

Polymer as Binding Agent and Retention Aid: Water soluble polymers adsorbed on paper were efficient at anchoring enzymes but affected enzyme aging [26]. The effect of the retention aid polymers on the kinetics and stability of the enzymes on the paper has been analyzed. Three water soluble polymers were selected: the cationic polyacrylamide (CPAM) is a high molecular weight linear polymer ($M_w = 5 \times 10^6$ D) of medium charge density, which can bridge colloids and weakly interact with the ALP enzyme by electrostatic interactions; the poly-acrylic acid (PAA) is a highly charged anionic oligomer ($M_w = 2000$ D) that can retain colloids by electrostatic interaction and charge neutralization; the non-ionic poly(ethylene oxide) ($M_w = 4 \times 10^6$ D) is efficient at bridging colloids. Anionic and cationic polymers were chosen to modify the enzymatic reaction rate through preferential orientation of the active site on the paper.

Paper was soaked in a large volume of weak polymer solution (1 min) followed by rinsing in excess water to form a full polymer monolayer, which is expected to adsorb in a flat train-loop-tail configuration. The polymers are expected to increase the strength of the adhesion of the enzyme on paper.

The initial enzyme activity of paper treated with a monolayer of CPAM, PAA and PEO was higher by 52%, 56% and 49%, respectively, than that of the untreated paper. Polymers used as retention aids increased the initial enzyme concentration on paper and their retention upon immersion in water. The enzyme retention efficiency of the three polymers was similar.

After 24hr aging, the relative activity of ALP enzymatic paper, without polymer, was 81%. The relative activity reduced to 58% for the leached paper sample aged for 24hr. ALP enzymatic paper without polymer lost 23% of its relative activity by enzyme leaching. Enzyme desorption was also significant for PAA and PEO treated ALP enzymatic papers. Enzyme retention was slightly higher for the leached ALP CPAM paper. The relative activities of 24hr aged ALP CPAM paper reduced from 67% to 60% because of enzyme desorption. However, the absolute amount of retained ALP for the leached polymer papers was higher than that of non-leached non-polymer papers [4].

Stability of Enzymatic Papers: Heat deactivates and denatures enzymes by modifying their conformation due to increased thermal movement and decreased solvent stabilization [32, 33]. The idea that immobilization of an enzyme on paper prevents aggregation and retards the conformation disorder by stabilizing the secondary and tertiary structures of the enzyme is studied.

ALP enzymatic paper samples were aged at different temperatures for different times. After applying the liquid substrate to the aged enzymatic paper and letting the enzyme-substrate reaction proceed to completion, the paper samples were scanned. The relative activities of enzymatic papers were calculated from the weighted mean gray value of the scan images. Pictures of ALP enzymatic papers heated to 60°C and 90°C for periods up to 24hr are shown (Figure 3). Paper yellowing is becoming visible for papers treated at the higher temperature for longer times (≥ 4 hr). The paper yellowing effect is not discussed here.

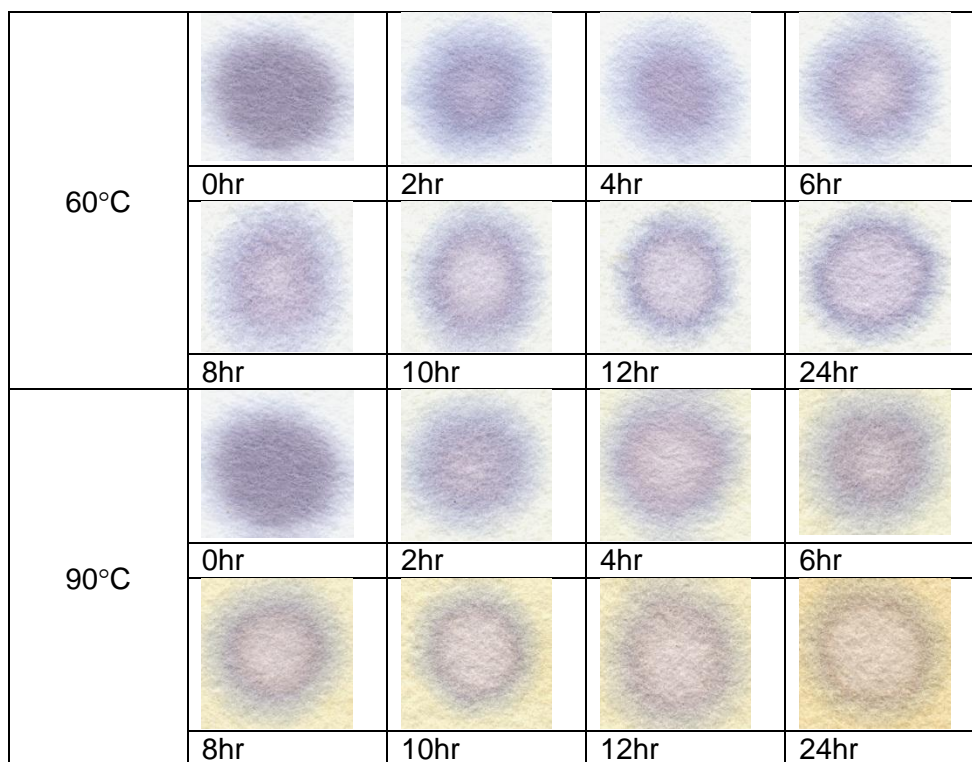


Figure 3: Aging of ALP-enzymatic paper treated to 60°C and 90°C for different times. The blue purple colour reveals the enzyme (ALP) - substrates (BCIP/NBT) reaction.

The effect of aging time and temperature on the relative activity of ALP enzymatic papers, with and without polymer treatment, is illustrated in Figure 4. In Figure 4, the I_0 is the gray value at 0hr for an enzymatic paper and I is the gray value at 't' hr: these values depend upon the enzymatic papers being studied. The enzymatic activity quickly dropped within the initial hours of thermal treatment and then gradually decreased at a slower rate. For any type of enzymatic paper the enzyme deactivation was faster at higher temperatures. ALP enzymatic papers, without polymer, retained their activity at 23°C and exhibit only a moderate loss of activity when exposed to 60°C (Figure 4a). The deactivation rates of ALP enzymatic papers, treated with polymers, were much faster in the early hours of thermal treatment, at 60°C and 90°C, than the untreated paper (Figure 4b-d). At high temperatures the ALP polymer papers lost 50% or more of their activity within the first 4hr. The deactivation rates slowed down after the quick fall. By contrast, at 23°C the deactivation rates of the ALP enzymatic papers with polymers were much slower and they retained their activities for longer periods (Figure 4b – d).

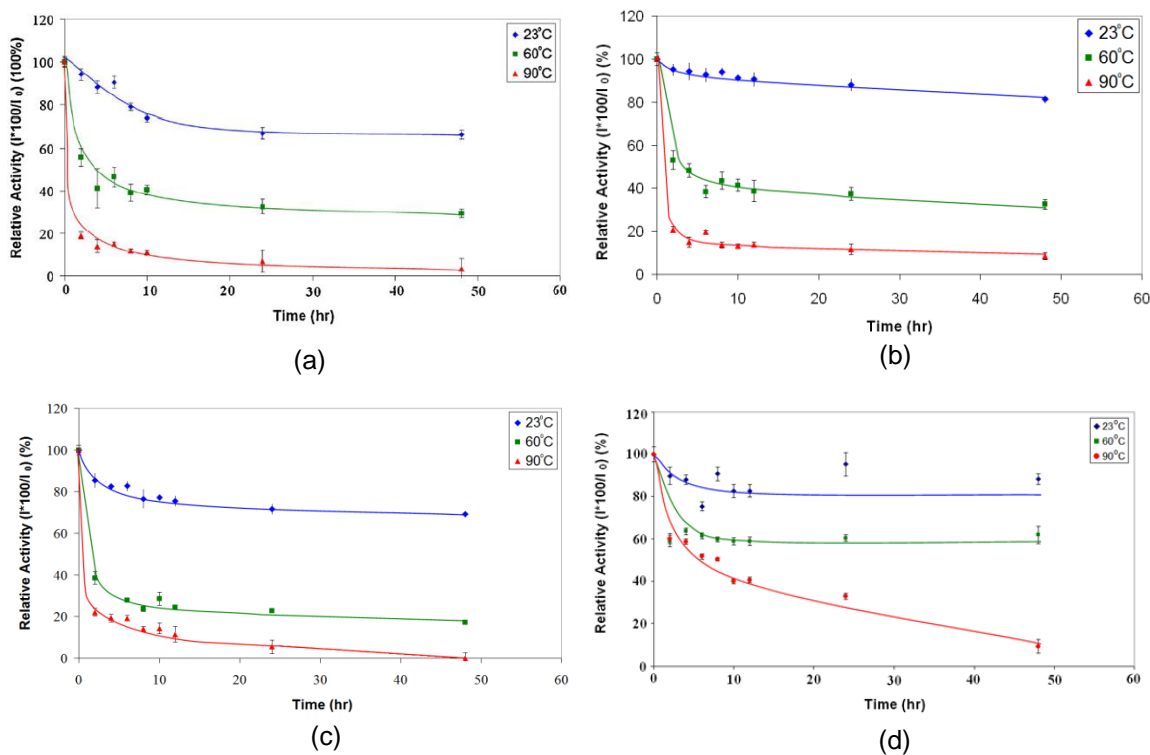


Figure 4: Effect of time and temperature on the relative activity of enzymatic papers. ALP stabilized on paper using: (a) ALP paper without polymer, (b) – (d) ALP CPAM, PAA and PEO papers.

Deactivation Kinetics of Enzymatic Papers: The simplest enzymatic deactivation model consists of an active enzyme (E_a) molecule undergoing an irreversible structural or chemical change to some inactive form (E_i^*) [33].



The enzyme deactivation rate (r_d) can be written as being proportional to the active enzyme concentration:

$$r_d = -\frac{d[E_a]}{dt} = k_d[E_a] \quad (3)$$

where, k_d is the deactivation rate constant. By integrating,

$$\ln \frac{[E_a]_{t=t}}{[E_a]_{t=0}} = -k_d t \quad (4)$$

From which the half-life ($t_{1/2}$) of the enzymatic deactivation can be calculated. At time $t_{1/2}$, the residual enzymatic activity decreases to half of its initial value: $[E_a]_{t=t_{1/2}} = 0.5[E_a]_{t=t_0}$, or:

$$t_{1/2} = \frac{0.693}{k_d} \quad (5)$$

The temperature dependency of rate constant k_d can be correlated using Arrhenius equation [34] :

$$\log k_d = \log A - \frac{E}{2.303R} \left(\frac{1}{T} \right) \quad (6)$$

where, A, E, R and T represent the pre-exponential factor, activation energy of the deactivation process (kJ/mol), gas constant (8.314 J/mol·K) and absolute temperature (K). Reactions with high activation energies are temperature sensitive, whereas, reactions with low activation energies are temperature insensitive [35].

Enzyme deactivation follows first order kinetics with enzyme concentration (Eqn. 4). Enzyme activity plotted on a logarithmic scale will vary linearly with time (Eqn. 6). This is not true for enzymes immobilized on paper, with or without polymer treatment (Figure 5), where two first order kinetic regimes were observed. This phenomenon is reported by Bailey and Ollis 1986 [33] and Machado and Saravia 2005 [36].

Figure 5 presents the evolution of the residual activity on a log scale, as function of time. The enzyme deactivation behaviour is described by two linear regimes: region-1 and region-2. In region-1, the enzyme activity drops steeply over a short aging time. This is followed by a slower deactivation regime which lasted at least 40hr. The slope of the first region represents the reaction constant, which is strongly dependent on temperature. The slope of the second region has a weaker dependence on temperature. From the slopes in Figure 5b-d, it can be seen that the polymer influences the kinetics of enzyme deactivation.

Two first order reactions might indicate a reaction in which different enzyme molecules denature by two reaction pathways over different time periods. Explanations to account for the first order kinetic deactivations are: 1) two different active sites on the ALP molecule could denature by different kinetics. ALP has three types of metal binding sites: A and B involve Zn ions, and C contains Mg ion. 2) The enzyme deactivation could proceed by two different mechanisms, having different time frames. 3) The equilibrium moisture content of the enzymatic papers could be important. The quick fall of the first deactivation region might represent transient moisture content of the enzymatic paper; the slower deactivation rate in the second region might be for paper at equilibrium. This deserves further attention. In region-1, at high temperature (60°C and 90°C) the enzymatic activities of ALP polymer papers dropped to 50% or less within the first few hours. After the drastic initial reduction, the deactivation rate was slower in region-2.

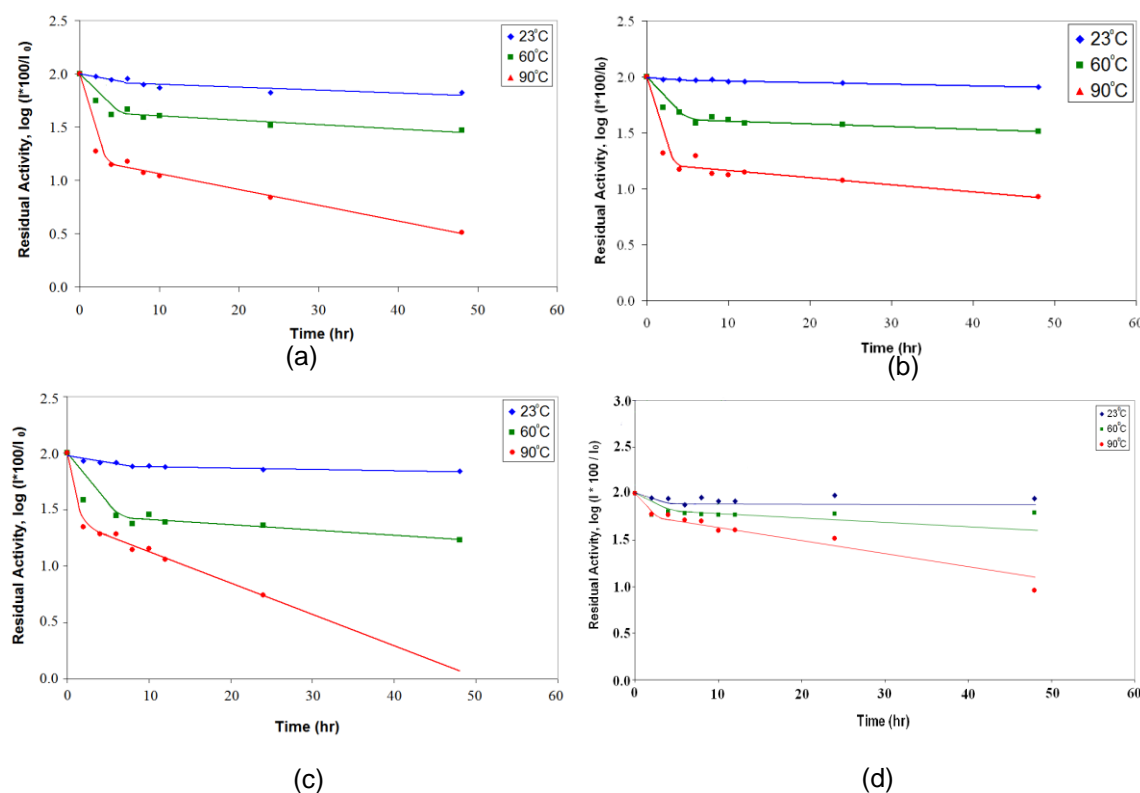


Figure 5: Residual activity of enzyme active papers heated at different temperatures. ALP stabilized on paper using: (a) ALP paper without polymer, (b) – (d) ALP CPAM, PAA and PEO papers.

Let's define t^* as the inflection time defining the transition from region-1 to region-2; t^* to represent the time at which enzymatic degradation slows down to region-2. For different enzymatic papers, t^* varied from 2.5 to 4hr at 90°C, 4 to 6hr at 60°C and 6 to 8hr at 23°C

(Figure 5). The variation of t^* as a function of temperature is in Figure 6. For simplicity consider t^* of ALP enzymatic papers to be a linear function of temperature (Figure 6).

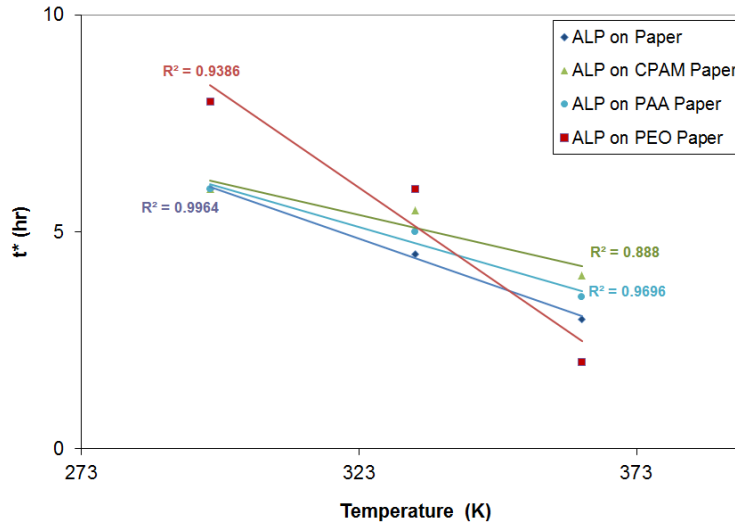


Figure 6: Variation of t^* as a function of temperature.

The rate constants for the two regions of ALP deactivation on paper calculated from Figure 5 are shown in Table I. Subscript 1 refers to the deactivation rate constant of the region-1 and subscript 2 describes region-2. The activation energy of enzymatic deactivation (E) on paper was calculated using the Arrhenius plots (Eqn. 6, Figure 7). The ' E_1 ' values were 2 to 3 times higher for ALP enzymatic papers with polymers than that without (Table II, Figure 7), which indicates a higher temperature sensitivity of ALP polymer paper deactivation.

Table I: Deactivation Rate Constants, k_d for ALP enzymatic papers

Temp	Region-1, k_{d1} (hr^{-1})				Region-2, k_{d2} (hr^{-1})			
	ALP on paper	ALP on CPAM paper	ALP on PAA paper	ALP on PEO paper	ALP on paper	ALP on CPAM paper	ALP on PAA paper	ALP on PEO paper
23°C	62.8×10^{-3}	31.6×10^{-3}	14.3×10^{-3}	28.3×10^{-3}	1.3×10^{-3}	6.45×10^{-3}	3.22×10^{-3}	2.76×10^{-3}
60°C	102.1×10^{-3}	166.7×10^{-3}	177.1×10^{-3}	202.4×10^{-3}	6.05×10^{-3}	9.44×10^{-3}	5.53×10^{-3}	10.6×10^{-3}
90°C	229.5×10^{-3}	560.6×10^{-3}	538.4×10^{-3}	755.2×10^{-3}	32.2×10^{-3}	34.1×10^{-3}	14.5×10^{-3}	67.5×10^{-3}
0°C	32.77×10^{-3}	8.37×10^{-3}	2.91×10^{-3}	6.32×10^{-3}	2.42×10^{-4}	2.66×10^{-3}	1.51×10^{-3}	0.57×10^{-3}

Table II: Activation Energy of Deactivation Process of ALP Enzymatic Papers

Samples	Activation energy of enzyme deactivation, E	
	E_1 (kJ/mol)	E_2 (kJ/mol)
ALP on paper	16.74	42.09
ALP on CPAM paper	38.25	21.09

ALP on PAA paper	49.00	19.41
ALP on PEO paper	43.76	41.57
ALP in Buffer [37]	97.2±7.2	

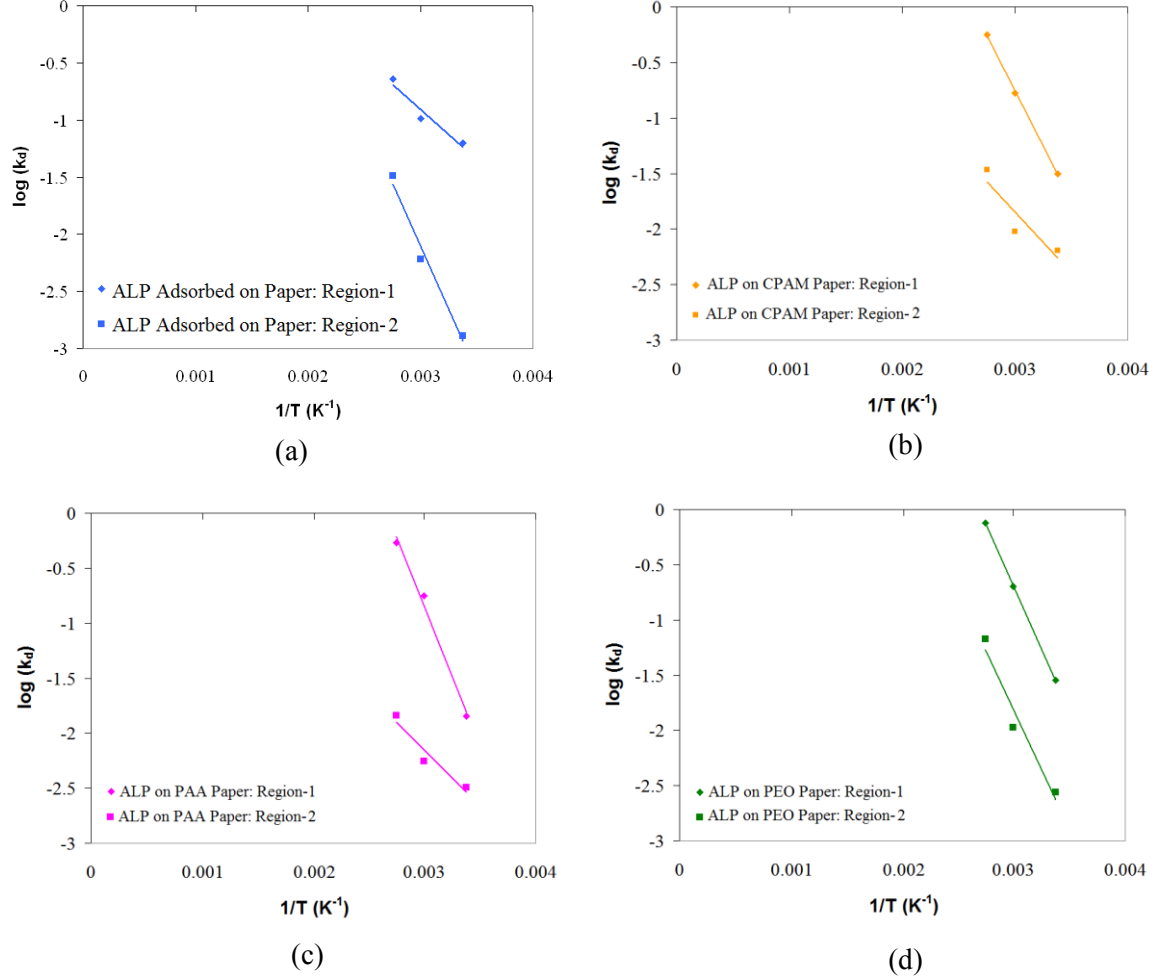


Figure 7: Arrhenius plot for the thermal deactivation of ALP enzymatic papers. (a) ALP paper without polymer, (b) – (d) ALP CPAM, PAA and PEO papers.

In region-2, the deactivation rate constants (k_{d_2}) of ALP enzymatic papers exhibit a different trend than for region-1 (Table I).

Half Life of Enzymatic Papers: To predict the shelf-life of enzymatic paper and to model the effect of temperature on performance. The half-life ($t_{1/2}$) of enzymatic papers can be modelled from the deactivation kinetics (Eqn. 4 – 6). The sharp decrease in enzymatic activity defined by region-1 lasts for a short time (t^*) for the various ALP enzymatic papers studied at different temperatures (Figures 5 and 6). The relative activity corresponding to the transition time t^* can be defined as RA^* , and calculated from Eqn. 3:

$$[RA]_{t=t^*} = RA^* = [RA]_{t=0} e^{-k_{d1} t^*} \quad (7)$$

The two deactivation conditions of enzymatic papers are schematically represented in Figure 8 for (a) $RA^* \leq 50\%$ and (b) $RA^* > 50\%$. The half-life time ($t_{1/2}$) at any temperature can then be modelled with Equations (7) and (8):

$$\text{Condition-1: } RA^* \leq 50\%, \quad t_{1/2} = \frac{0.693}{k_{d1}} \quad (8)$$

$$\text{Condition-2: } RA^* > 50\%, \quad t_{1/2} = t^* + \frac{\ln \frac{[RA]_{t=t^*}}{[RA]_{t=t_{1/2}}}}{k_{d2}} \quad (9)$$

t^* and RA^* are functions of temperature and define the duration of region-1 deactivation. If $RA^* \leq 50\%$, the enzymatic paper half-life is defined by region-1 (Figure 8a); if $RA^* > 50\%$, region-1 and region-2 are both required to model $t_{1/2}$ (Figure 8b). For any specific temperature, the kinetic properties: k_{d1} , k_{d2} , t^* , RA^* and the corresponding $t_{1/2}$ can be calculated from the kinetic model.

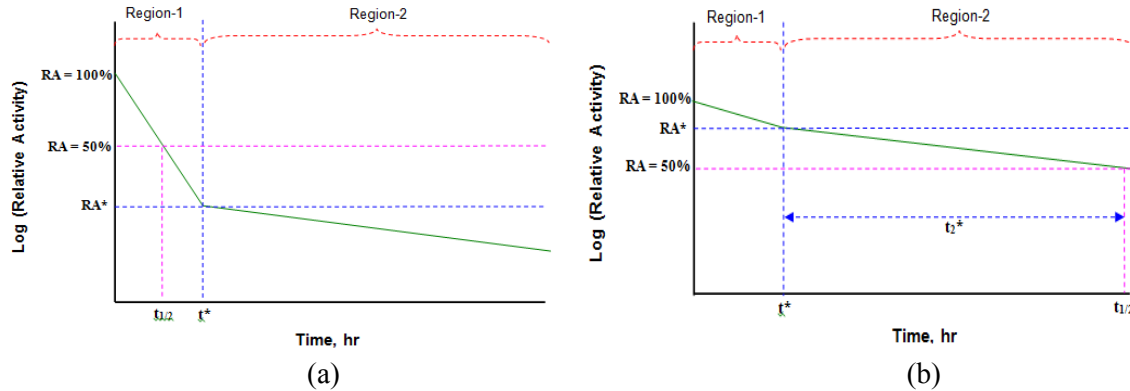


Figure 8: Schematic of half-life model of ALP enzymatic papers. (a) $RA^* < 50\%$, (b) $RA^* > 50\%$.

At 0°C, the half-lives for the different ALP enzymatic papers: without polymer, with CPAM, PAA and PEO are respectively 2932hr, 260hr, 496hr and 1211hr (Figure 9). ALP enzymatic paper without polymer remains bioactive for 4 months when refrigerated which is much longer than for the ALP polymer papers. The polymer treatment required to increase enzyme retention decreases the shelf-life of enzymes immobilized on paper. It is possible that the polymer interferes with the tertiary structure of the enzyme; or, that the enzyme is immobilized on paper in a more rigid conformation which affects its ability to reconfigure.

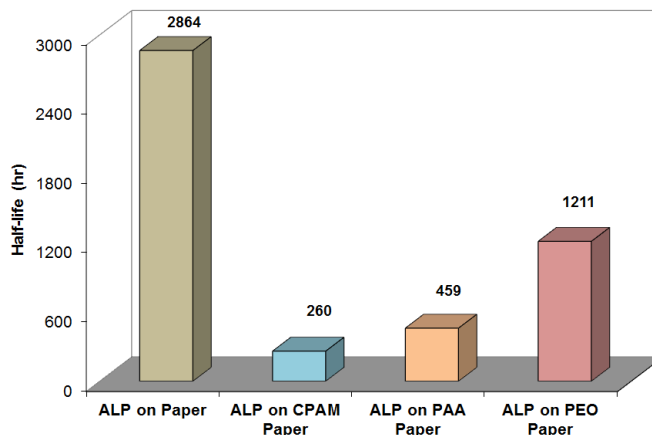


Figure 9: Half-lives of ALP enzymatic paper predicted at 0°C.

Bioactive Paper for Blood Typing

Blood type (ABO) detection is critical for health related problems. Different blood typing techniques are available [38-42]: gel column, TLC-immuno-staining, a fibre optic-microfluidic device and the spin tube method. These techniques often require optical or microfluidic analytical instruments which are not always available [43-47]. Blood transport in paper widely varies depending on whether the red cells are agglutinated or not; this observation allows cheap paper based diagnostics to be engineered.

Blood is a concentrated stable colloidal suspension of red blood cells, white blood cells, and platelets dispersed in an aqueous solution containing biomolecules [48-51]. Some of these biomolecules, such as the glycoproteins and carbohydrates, are responsible for blood type and tissue immunity (antigens). These are directly adsorbed onto the surface of the blood cells [52]. Unfortunately, there are no robust, convenient low cost tests available for “on the spot” analysis of blood type. Blood samples are typically outsourced to an analytical laboratory. Reliable tests to instantaneously provide blood analysis would be invaluable for on the spot health diagnostics.

Transport of Blood-Antibody Solution on Paper: Transport of blood droplets on paper depends on whether blood agglutinates or not. This was investigated to develop blood typing tests [53]. Paper strips were impregnated with solutions containing different concentrations of antibody-A: 20 μ L of blood was deposited in the middle of a wet paper strip, and the blood transport and separation dynamics were measured by image analysis. Two blood types were investigated: AB+ and B+. The interaction of AB+ and B+ blood droplets with antibody-A treated paper is shown in Figure 10. When RBC agglutination occurs by antigen-antibody interaction, two layers form on the paper: RBC and blood serum. The blood serum separated from RBC on the paper to produce a white contrast on the blue paper surface (Figure 10a). Without agglutination, blood wicking on the paper gave a faint gradient at the wicking threshold caused by paper chromatography (Figure 10b). The effect of RBC agglutination through specific antibody-antigen interaction on paper wicking can be quantified. Figure 11 represents the phenomena with ‘ z_1 ’ defining the wicking length of blood, serum with red blood cells, and ‘ z_2 ’ the wicking distance of serum, no red blood cells. The total wicking length is $z = z_1 + z_2$.











Antibody-A concn. on Paper	'AB+' blood on paper-A	'B+' blood on paper-A
0.0 x		
0.2 x		
0.6 x		
0.8 x		
1.0 x		
	(a)	(b)

Figure 10: Blood wicking on Antibody-A treated paper: 10mins after blood is put on the paper: (a) AB+ and (b) B+ blood drops were put on papers treated with different concentrations of Antibody-A. 'x' represents the dilution.

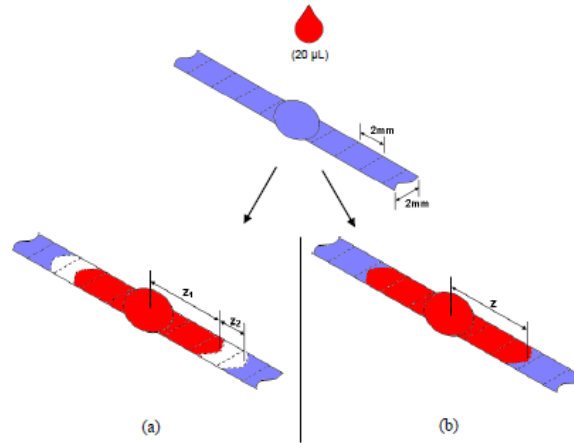


Figure 11: Schematic representation of the wicking of blood on paper treated with antibody-A. (a) AB+ blood interacts with antibody-A to create separate layers of RBC and serum, (b) B+ blood does not interact with antibody-A and does not separate.

The extent of blood wicking as a function of antibody concentration is in Figure 12. Two types of blood, AB+ and B+, were compared. Figure 12a quantifies the RBC/blood serum separation for AB+ blood on paper strips after 4 min. Six replicates were used and the average and standard deviations are reported. Blood serum, with the red blood cells agglutinated and separated by specific antibody-antigen interaction, gave longer wicking lengths (z_2); this was further accentuated by increasing the antibody concentration (Figure 12a). Figure 12b quantifies the effect of antibody-A concentration on blood, B+, wicking after 4 minutes for a non-specific system. There was no separation of the red blood cells from the serum ($z = z_1$, $z_2 \approx 0$). The separated layer of blood (z_1) at the wicking threshold was much smaller than that of the specific system, AB+ blood. The total wicking distance (z) for the non-specific system, B+ blood, was shorter than for AB+ blood. The wicking distance decreased with increased concentration of the non-specific antibody on paper; caused either by non-specific interactions, or by the blocking or collapsing of some pores of the paper caused by the antibody adsorption.

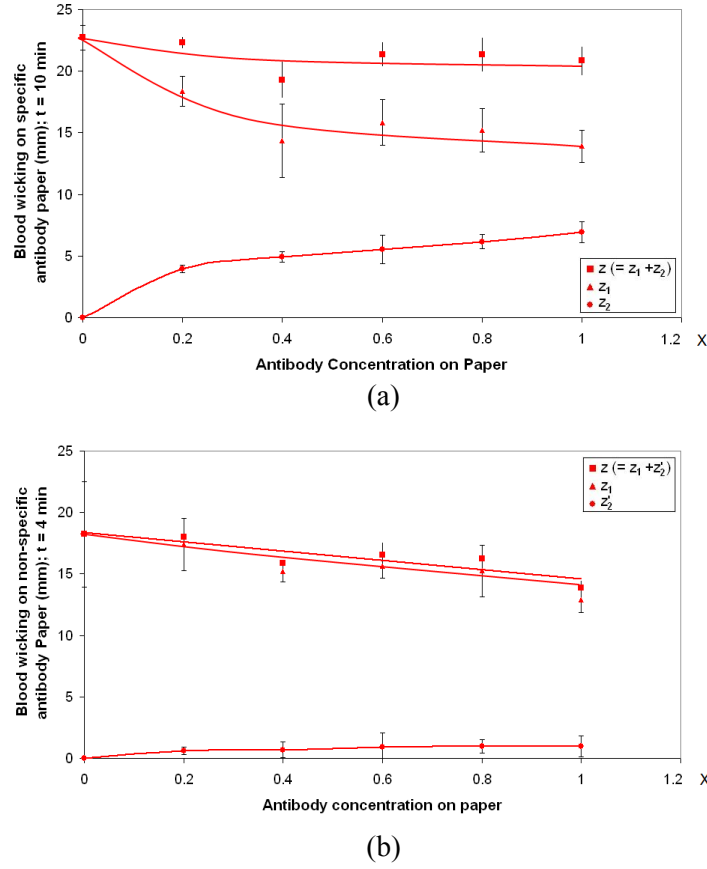


Figure 12: Blood wicking on paper treated with different concentrations of antibody-A. (a) AB+ blood wicking after 4min, (b) B+ blood wicking after 4 min; n = 6. 'x' represents the dilution factor.

Mechanism of Blood Transport on Paper: The transport of agglutinated blood on paper varies from non-agglutinated blood. When a droplet of stable blood is deposited on paper, it wicks as a uniform region with the red cells well dispersed in the serum. When blood is agglutinated on paper, the red blood cells separate from the serum and chromatographic separation occurs. Wicking of the serum fraction proceeds at a faster rate than that of the original blood sample. Blood transports in paper mostly by wicking through the inter-fibre spaces. The capillary driving force is caused by the difference in surface energy between the fluid and solid. The resistances are friction and viscous dissipation. Wicking can be described by the liquid flow in a capillary. The Lucas-Washburn equation states that a liquid of viscosity η and surface tension γ will flow in a capillary of radius r and length l at a velocity V by [51]:

$$V = \frac{\gamma r \cos \theta_E}{\eta l} \quad (10)$$

where θ_E is the equilibrium contact angle formed by the fluid in the capillary.

Red blood cell agglutination has two effects: 1) A drastic increase in local red cell blood viscosity (η) and reduction of paper capillary (r); both effects decrease the wicking of the red blood cells (Eqn. 10); and 2) The separation of the serum from the blood; this reduces the viscosity of the liquid region, which increases wicking velocity. Agglutination can affect the surface tension of blood solutions; agglutination of tension active molecules, such as lipids, would increase the surface tension of the solution.

Fixation of Agglutinated Blood on Paper Substrates: Blood was spotted on antibody treated papers and chromatographically eluted with 0.9% NaCl buffer for 10 min. Agglutinated blood resists elution and remains fixed. Non-agglutinated blood can be easily eluted by NaCl buffer which forms a faint blood spot (Figure 13).

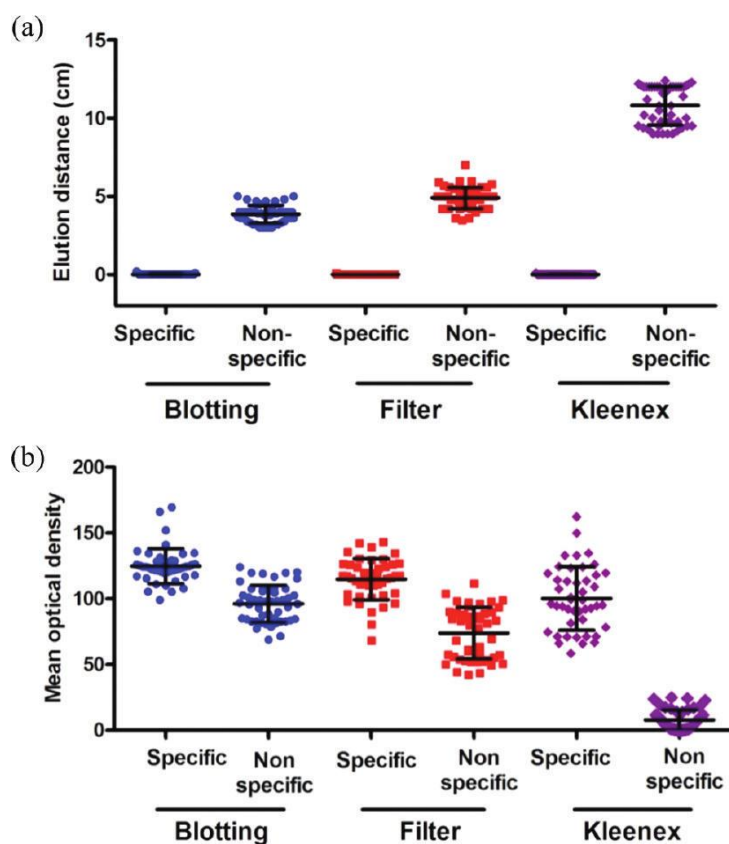


Figure 13: Quantitative agglutinated blood fixation of blood spotted on blotting, filter, and Kleenex papers treated with specific and nonspecific antibodies and chromatographically eluted with 0.9% NaCl for 10 min: (a) the elution distance, and (b) the mean optical density. It shows an expected relationship between the two techniques. When the elution occurs the optical density of the spot decreases through spread.

Blood collected from 31 donors having different blood groups (A, B, AB, O, Rh+, and Rh-) was spotted on Antibodies-A, B, and D absorbed on blotting, filter, and Kleenex paper and treated as mentioned. Blood samples spotted on specific antibody treated papers resisted elution with minimal variability, while blood samples on nonspecific antibodies eluted easily. There was no detectable overlap in the elution distance with the blood samples on specific antibodies on all paper substrates (Figure 13a). The elution distance was significantly higher with non-agglutinated blood compared to agglutinated blood. Agglutinated blood samples on Kleenex have optical density above a cut-off point (50 as mean optical density) and non-agglutinated blood samples have optical density below the cut-off point (Figure 13b). Clear cut-off points were not achieved with blotting and filter paper with optical density.

Paper Diagnostic for Blood Typing: Instantaneous paper based blood diagnostics can be made from the difference in wicking between a stable and an agglutinated blood sample. An antibody treated paper diagnostic was designed for blood typing [53]. Figure 14 illustrates blood group detection from RBC-serum separation on the antibody treated paper. Figure 14a illustrates 'B+' blood detection using wicking of agglutinated colloids from specific antigen-antibody interaction on paper strips. In Figure 14b, blood wicking occurred in three fluidic channels, each fluidic channel was treated with a different antibody solution (A, B, D) [53].

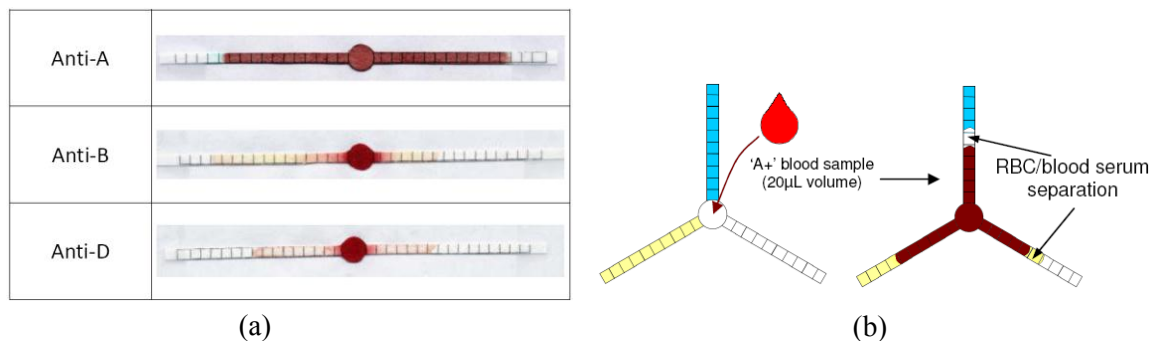


Figure 14: Blood group detection using RBC-blood serum separation on antibody active paper fluidic device; (a) 'B+' blood detection using wicking of agglutinated colloids from specific antigen-antibody interaction on paper strips, (b) schematic colour indication of blood typing relying on RBC-blood plasma separation on antibody treated paper.

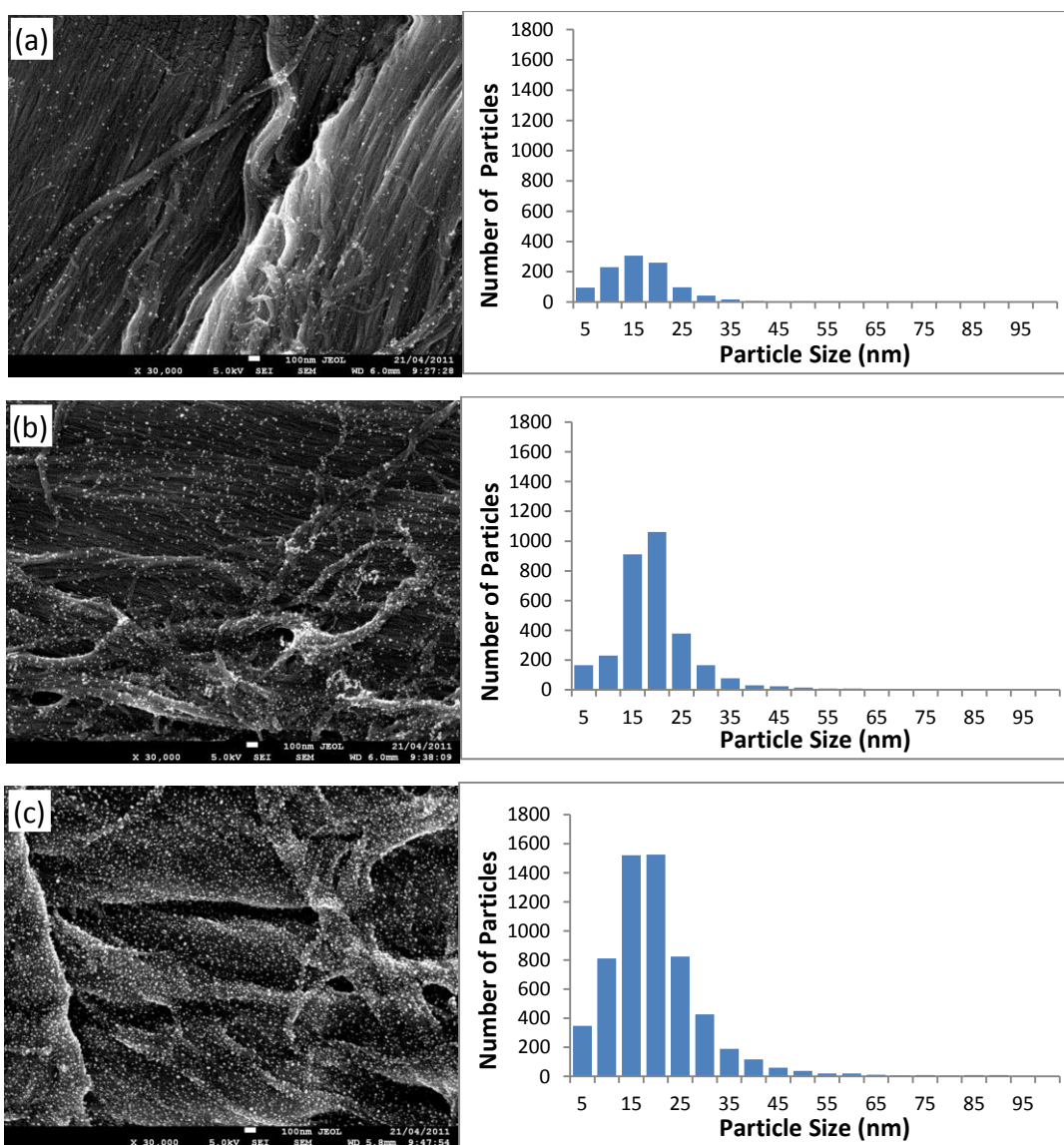
Gold nanoparticle Paper:

Most Bioactive papers rely on colour to give analytical results: the accuracy of these techniques is often limited to 10^{-6} M. For particular applications, such as detection of cancer, detection ranging from 10^{-9} to 10^{-12} M is needed.

Surface Enhanced Raman Scattering (SERS) presents an attractive technique to solve the molality issues. Paper substrates are treated with metallic nanoparticles followed by adsorption of the analyte molecules of interest. In Raman spectroscopy, small energy changes of the

scattered light from the molecules is enhanced and measured, producing a molecular fingerprint of the analyte. The enhancement can be 10^{14} – 10^{15} [54], which enables SERS as a single-molecule detection technique to identify analytes at trace levels.

Paper is good for a controlled adsorption of gold nano-particles (AuNPs) to carry out molecular sensing with high sensitivity. The paper effectively ‘transfers’ the high packing density and uniform distribution from the AuNPs in solutions onto the cellulose fibres, and ‘freezes’ their adsorption during the drying process. The concentration of AuNPs increases monotonically with the solution concentration in which the papers are dipped; the particle distribution is denser and more uniform on paper treated with AuNP solutions of higher concentration (Figure 15). This is illustrated by the Field Emission Scanning Electron Microscopic (FESEM) images and histograms which show particle size distribution on filter papers dipped into different concentration of AuNP solutions.



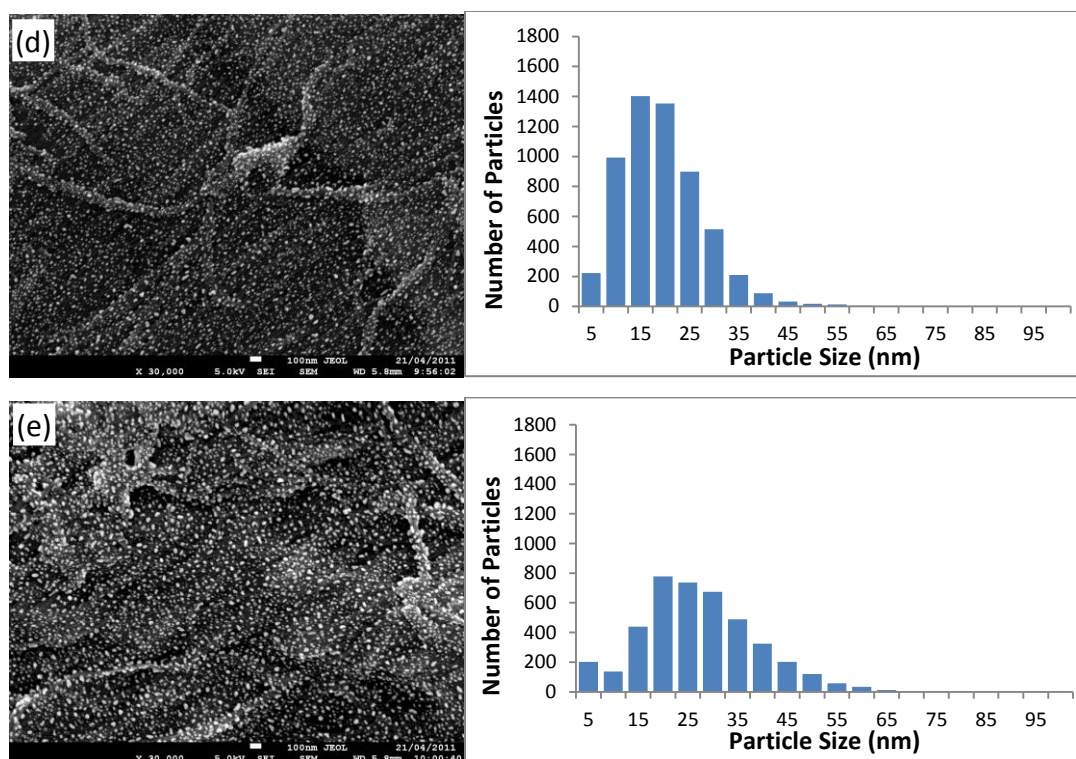


Figure 15: Field Emission Scanning Electron Microscopic (FESEM) images and histograms of particle size distribution on filter papers dipped into (a) 0.02mg/mL, (b) 0.05mg/mL, (c) 0.10mg/mL, (d) 0.15mg/mL and (e) 0.20mg/mL of AuNP solutions.

The SERS potential of AuNP treated papers was shown by the increase in intensities (Figure 16). Treating paper with 0.02mg/mL of AuNPs significantly enhanced the Raman signal of 4-ATP (Figure 16). The SERS intensity of AuNPs treated paper increased linearly with the concentration of AuNP solutions. With increasing concentration the AuNPs were packed closer together in solution; they were adsorbed onto paper maintaining their packing density. As the average distance between the AuNPs decreased from 100-200nm to 10-50 nm, it is believed that effective ‘hot spots’ appeared and their inter-particle Plasmon coupling gave rise to the enhancement of electromagnetic field which intensified the SERS signals of the 4-ATP [55]. This SERS signal enhancement was observed when paper was treated with 1.0mg/mL of AuNPs (Figure 16) as the inter-particle distance of the AuNPs became closer to the diameter of AuNPs (25 ± 3 nm).

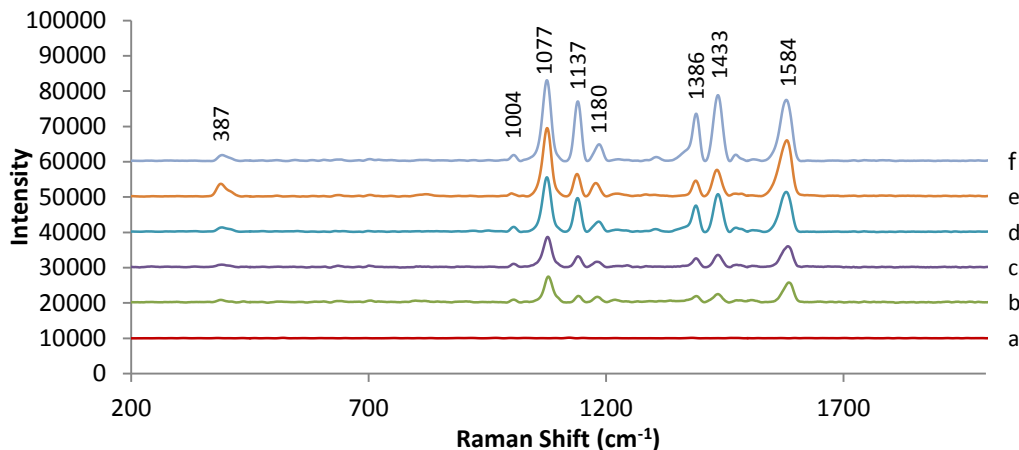


Figure 16: Surface Enhanced Raman spectrum of 1 mM of 4-ATP adsorbed on (a) plain filter paper and SERS spectra of 4-ATP on filter paper dipped in AuNP solutions of (b) 0.02mg/mL, (c) 0.05mg/mL, (d) 0.10mg/mL, (e) 0.15mg/mL and (f) 0.20mg/mL.

Without retention aid, the adsorption of AuNPs on paper was relatively high: by an order of magnitude higher than on similarly treated silicon [56]. The enhancement factor (EF) of 4-ATP adsorbed onto AuNP treated paper was higher by more than one order of magnitude than AuNP treated silicon (Figure 17). The high loading and uniform distribution of AuNPs on paper contributed towards the excellent SERS signal and higher EF.

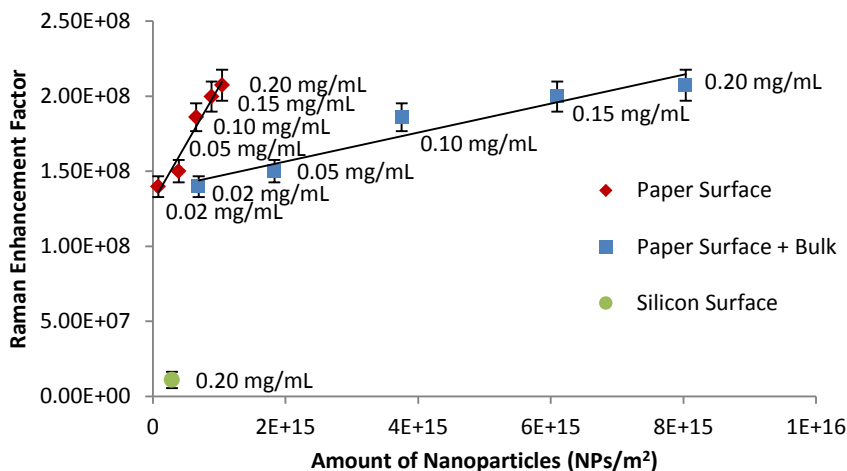


Figure 17: Relationship between the amount of AuNPs and the Enhancement Factor (EF) of 4-ATP measured at 1077cm^{-1} for filter paper and silicon. The contributions of the AuNPs adsorbed at (a) the surface of paper (♦) and (b) the bulk of paper (■) were analysed.

The SERS sensitivity of AuNPs paper was quantified. Paper treated with a 0.20mg/mL of AuNP solutions was exposed to different concentrations of 4-ATP (Figure 18). The

concentration of 4-ATP investigated ranged over 6 orders of magnitude, from 1 mM to 1 nM. The detection limit of AuNPs paper for 4-ATP is lower than 1 nM; the spectrum of the 1 nM sample had good signal-to-noise ratio and the main peaks at 1077cm^{-1} and 1584cm^{-1} were still observable. A sigmoidal relationship between the SERS intensity and concentration of 4-ATP was observed. The SERS intensities were mostly linear when the concentration of 4-ATP was low; at high concentration, a nonlinear response emerged and saturation of SERS signal occurred, because the adsorption of 4-ATP onto the AuNPs became saturated [57, 58].

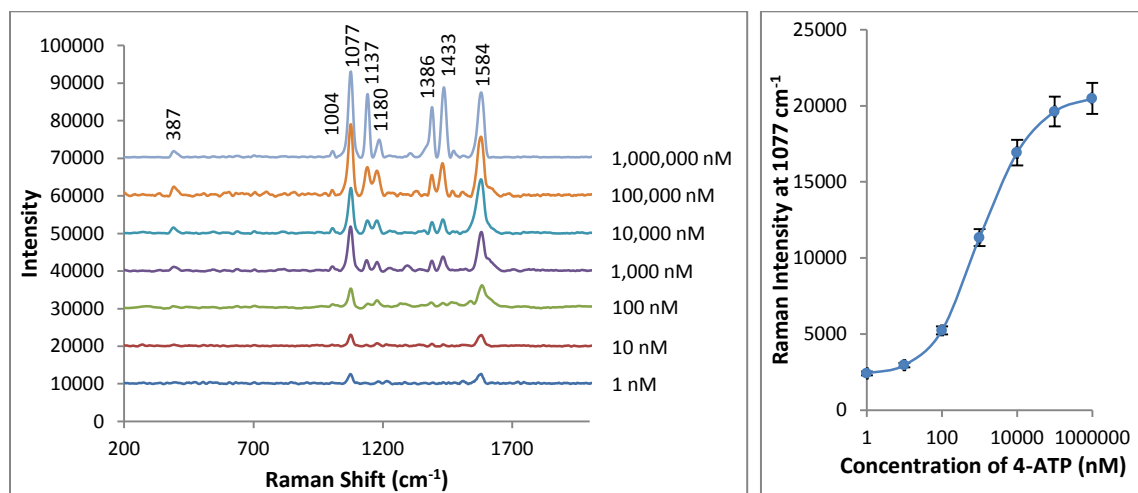


Figure 18: (a) SERS spectra of different concentration of 4-ATP from AuNPs treated paper (0.20 mg/mL AuNP solutions). (b) SERS intensity of different concentration of 4-ATP from the AuNPs treated paper at 1077 cm^{-1} band.

Salt-Temperature Sensitive Polymers:

In an open configuration, papermaking is a very water intensive process requiring up to 100 tons of water per ton of paper produced. Water is also extensively used in the process to wash pulp and to generate heat for the dryer section. In the last decade, the consumption of water has radically been reduced through recycling in the process. A modern close mill, such as Visy Tumut, Australia, can use as little as 3 m^3 water/ton pulp and even less. Water recycling has two main consequences on the process water quality: a drastic increase in the ionic strength and dissolved solids concentration, and an increase in temperature (from 40°C up to 65°C). The increase in salt and solids concentration is particularly detrimental on the paper machine during papermaking. The first issue is the increase in deposits. And the second issue is the increase in corrosion catalyzed by higher salt concentration and temperature. The drop in efficiency of the water soluble polymers used as retention and process aids is rather disturbing. These polymers are typically high molecular weight cationic polyelectrolytes used as retention aid to bridge colloids (fines, small fillers) onto fibres, or a strength agent adsorbing at the fibre-fibre bond and developing covalent bonds. Ionic strength disrupts the electrostatic attractive force driving the process. The level of system closure or extent of water recycling is often dictated by the limitation of the polymer system. Considerable effort has been directed toward the development

of retention aid polymers and strength agents less affected by salt. These include non-ionic polymers (PEO/cofactor), micro-particulate polymer complex systems and even polymers of higher charge density. An alternative approach is to rely on the increase in salt concentration and temperature in the process.

In this study a family of poly-zwitterion is investigated as salt-temperature sensitive retention aid strength agent. The concept is to rely on the high salt and temperature of the process water to trigger polymer phase separation which then adsorbs onto the cellulosic fibres and fillers, causing binding and strengthening. For recycling, a lower temperature and a lower salt concentration will trigger the polymer to dissolve, liberating fibres from the paper web. The feasibility of the concept was tested with a high molecular weight poly-zwitterion.

Poly-zwitterion in Papermaking

High molecular weight poly-zwitterions of 1 and 2MD were synthesized and characterized by Gas Phase Chromatography (GPC) (Table III).

Table III. Molecular weight and poly-dispersity of poly-zwitterion samples

Mass of Monomer (g)	Mass of Initiator (mg)	Weighted Average Molecular Weight, M_w (Da)	Poly-dispersity (M_w/M_n)
15.0	40	1.9×10^6	1.47
20.0	42	1.1×10^6	2.29

The solubility of the poly-zwitterions was affected by salt and temperature (Figure 20). This is commonly referred to as the anti-polyelectrolyte effect. At high salt concentrations: 100mM NaCl, both samples become soluble at room temperature. However, with little salt the polymer must be heated to become soluble.

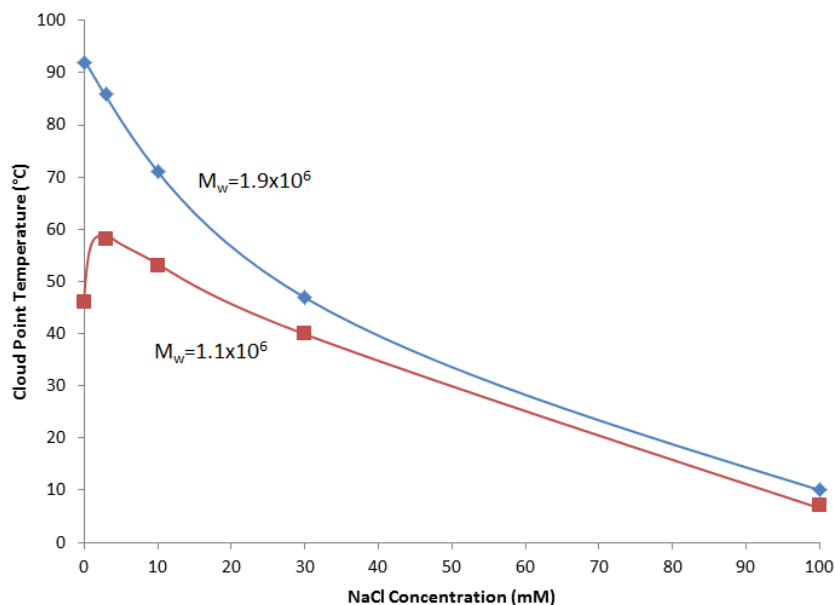


Figure 20. Effect of temperature and salt (NaCl) concentration on poly-zwitterion solubility. Samples are insoluble in water at room temperature, and require addition of salt or increased temperature to dissolve.

The heaviest poly-zwitterion sample (1.9×10^6 Da) was tested to see if it could bridge between cellulose fibres, and strengthen the paper. Hardwood hand-sheets were prepared at 60gsm, with poly-zwitterion added during formation. The tensile strength of 10mm strips cut from these sheets is in Tables IV and V. These data suggest a possible small increase in both wet and dry tensile strength, when the poly-zwitterion is added with salt.

Table IV. Tensile strength of paper strips with and without poly-zwitterion addition: heated to dissolve polymer

Sample	Dry Tensile Strength (N)	Change from Blank	Wet Tensile Strength (N)	Change from Blank
Blank	12.5±0.6	NA	0.95±0.06	NA
10 mg/g poly-zwitterion, heated	11.5±0.9	-8%	0.93±0.07	-2%
100 mg/g poly-zwitterion, heated	10.7±1.3	-14%	0.88±0.15	-7%

Table V. Tensile strength of paper strips with and without poly-zwitterion addition: 100mM NaCl added to dissolve polymer

Sample	Dry Tensile Strength (N)	Change from Blank (%)	Wet Tensile Strength (N)	Change from Blank (%)
Blank, no NaCl	17.6±1.6	NA	1.21±0.32	NA
10mg/g polyzwitterion, 100mM NaCl	20.7±1.8	+18%	1.45±0.37	+20%
100mg/g polyzwitterion, 100mM NaCl	20.1±2.7	+14%	1.50±0.28	+24%

The paper strength change, with changes in temperature and NaCl concentration, when the poly-zwitterion was added, was not as important as expected. A similar poly-zwitterion (PolySBMA) was shown to adsorbed onto silica and affect rheology; silica flocculation and viscosity were affected by temperature and salt concentration [10].

CONCLUSION

After 600 years of dominance, the era of paper as preferred media of communication is under threat, which is led by technological development with devices and systems, such as computers, ‘smart phones’, and electronic pads linked to the internet. Apple and similar computer-electronic communication companies have taken over the tradition linking paper to the apple pie as both being time immune and consumer preferred. Many attributes of paper, its porosity, wettability, ease of engineering and very low cost still offer fantastic new opportunities.

To embrace these opportunities it is necessary to destroy the preconception that paper is a high volume, low value commodity product.

Combining paper with printing to develop functional materials can produce many high value new products at low prices. In this paper three examples were examined. 1) Bioactive papers were analysed: enzymes maintain their selectivity once adsorbed on paper, enzyme stability improved on paper; using polymers improved enzyme retention on paper. Paper is also a very effective substrate to develop low cost instantaneous and disposable paper diagnostic for blood typing analysis. 2) Gold nanoparticles (AuNP) on paper significantly increased the sensitivity and specificity of paper diagnostic (6-8 orders of magnitude) as shown by Surface Enhanced Raman Scattering (SERS); the homogeneous but porous paper gave significantly better signal than the usual silicon surface. 3) A new concept converting a major papermaking process issue into an advantage and innovation was investigated. A salt-temperature sensitive poly-zwitterion was chosen as a novel strength agent for paper. It was tested that high salt and temperature could trigger polymer phase separation which then adsorbs onto the fibre to increase the bond strength. Re-pulping paper in low salt and colder water would dissolve the polymer and release fibres, therefore facilitating recycling. This research opens a new way of thinking and requires further study.

Paper, available in large volume, emerges as a new functional material for special value-added applications. This article aimed at opening new horizons and perspectives by presenting paper as an advanced engineered material for health and novel applications.

ACKNOWLEDGEMENTS

Many thanks to Professors George Simons, Dan Li, Kei Sato and Wei Shen for stimulating discussion. Special thanks to Professor Tony Whitehead for helping with editing.

REFERENCES

- [1] Product Information (P7640): Enzymatic Assay of PHOSPHATASE, ALKALINE, in: SIGMA (Ed.), Sigma Quality Control Test Procedure, Sigma-Aldrich, 1995.
- [2] BCIP/NBT Liquid Substrate System (B 1911), Product Information, Sigma Aldrich (web: www.sigmaaldrich.com), 2009.
- [3] M.S. Khan, X. Li, W. Shen, G. Garnier, Thermal Stability of Bioactive Enzymatic Papers, *Colloids and Surfaces B: Biointerfaces* 75 (2010) 239-246.
- [4] M.S. Khan, S.B.M. Haniffa, A. Slater, G. Garnier, Effect of Polymers on the Retention and Aging of Enzymatic Bioactive Papers, *Colloids and Surfaces B: Biointerfaces* 79 (2010) 88-96.
- [5] CSL, Epiclone™ Anti-A, Anti-B and Anti-A/B, Murine Monoclonal IgM Blood Grouping Reagents, CSL Limited (www.csl.com.au), Melbourne, 2007.
- [6] CSL, Epiclone™ - 2 Anti-D (IgM), Murine Monoclonal IgM Blood Grouping Reagents, CSL Limited (www.csl.com.au), Melbourne, 2007.
- [7] J. Turkevich, P.C. Stevenson, J. Hillier, A study of the nucleation and growth processes in the synthesis of colloidal gold, *Discussions of the Faraday Society* 11 (1951) 55-75.
- [8] P.H.C. Camargo, L. Au, M. Rycenga, W. Li, Y. Xia, Measuring the SERS enhancement factors of dimers with different structures constructed from silver nanocubes, *Chem. Phys. Lett.* 484 (2010) 304-308.
- [9] X. Hu, T. Wang, L. Wang, S. Dong, Surface-Enhanced Raman Scattering of 4-Aminothiophenol Self-Assembled Monolayers in Sandwich Structure with Nanoparticle Shape Dependence: Off-Surface Plasmon Resonance Condition, *J. Phys. Chem. C* 111 (2007) 6962-6969.
- [10] P. Starck, W.K.J. Mosse, N.J. Nicholas, M. Spiniello, J. Tyrrell, A. Nelson, G.G. Qiao, W.A. Ducker, Surface Chemistry and Rheology of Polysulfobetaine-Coated Silica, *Langmuir* 23 (2007) 7587-7593.
- [11] A.B. Lowe, C.L. McCormick, Synthesis and Solution Properties of Zwitterionic Polymers, *Chemical Reviews* 102 (2002) 4177-4189.
- [12] F. Kendel, P.D. Morton, C. Kugge, N. Vanderhoek, G. Garnier, Effects of Pre-Coat and Substrate Porosity on Conventional Barrier Coating Performance, *APPITA* 63 (2010) 214-217.
- [13] Y.H. Ngo, G.P. Simon, G. Garnier, Paper Surfaces Functionalized by Nanoparticles, *Advances in Colloid and Interfaces Science* 163 (2011) 23-38.
- [14] B.-U. Cho, G. Garnier, Effect of the Paper Structure and Composition on the Surface Sizing Pick-Up, *TAPPI* 83 (2000) 60-.
- [15] M. Shirazi, T.G.M. Van de Ven, G. Garnier, Adsorption of Modified Starches on Pulp Fibers, *Langmuir* 19 (2003) 10835-10842.
- [16] M. Shirazi, N. Esmail, G. Garnier, T.G.M. Van de Ven, Starch Penetration into Paper in a Size Press, *Journal of Dispersion Science and Technology* 25 (2005) 457-468.
- [17] G. Garnier, M. Duskova-Smrckova, R. Vyhnalkova, T.G.M. Van de Ven, J.-F. Revol, Association in Solution and Adsorption at an Air-Water Interface of Alternating Copolymers of Maleic Anhydride and Styrene, *Langmuir* 16 (2000) 3757-3763.

- [18] M. Duskova-Smrckova, R. Vyhnanekova, G. Garnier, Association of Alternating Poly(Styrene-Maleic Acid) in Aqueous solution And Adsorption At An Air-Liquid Interface, *Polymeric Materials Science and Engineering* 80 (1999) 337-338.
- [19] M.S. Khan, D. Fon, X. Li, J. Tian, J. Forsythe, G. Garnier, W. Shen, Biosurface Engineering Through Ink Jet Printing, *Colloids and Surfaces B: Biointerfaces* 75 (2010) 441-447.
- [20] X. Li, J. Tian, G. Garnier, W. Shen, Fabrication of Paper-Based Microfluidic Sensors by Printing, *Colloids and Surfaces B: Biointerfaces* 76 (2010) 564-570.
- [21] A.W. Martinez, S.T. Phillips, M.J. Butte, G.M. Whitesides, Patterned paper as a platform for inexpensive, low-volume, portable bioassays, *Angewandte Chemie International Edition* 46 (2007) 1318-1320.
- [22] A.W. Martinez, S.T. Phillips, E. Carrihe, S.W. Thomas III, H. Sindi, G.M. Whitesides, Simple Telemedicine for Developing Regions: Camera Phones and Paper-Based Microfluidic Devices for Real-Time, Off-Site Diagnosis, *Analytical Chemistry* 80 (2008) 3699-3707.
- [23] S. Aikio, S. Grönqvist, L. Hakola, E. Hurme, S. Jussila, O.-V. Kaukonen, H. Kopola, M. Käsäkoski, M. Leinonen, S. Lippo, R. Mahlberg, S. Peltonen, P. Qvintus-Leino, T. Rajamäki, A.-C. Ritschkoff, M. Smolander, J. Vartiainen, L. Viikari, M. Vilkmann, Bioactive Paper and Fibre Products: Patent and Literature Survey, *VTT Working Papers* 51, 2006, pp. 1-84.
- [24] K.M. Holtz, E.R. Kantrowitz, The Mechanism of the Alkaline Phosphatase Reaction: Insights from NMR, Crystallography and Site-Specific Mutagenesis, *FEBS Letters* 462 (1999) 7-11.
- [25] D.B. Craig, E.A. Arriaga, J.C.Y. Wong, H. Lu, N.J. Dovichi, Studies on Single Alkaline Phosphatase Molecules: Reaction Rate and Activation Energy of a Reaction Catalyzed by a Single Molecule and the Effect of Thermal Denaturation The Death of an Enzyme, *Journal of The American Chemical Society* 118 (1996) 5245-5253.
- [26] J.E. Coleman, Structure and Mechanism of Alkaline Phosphatase, *Annual Review of Biophysics and Biomolecular Structure* 21 (1992) 441-483.
- [27] G. Masao, Preparation of Enzyme-Immobilized Filter Paper for Determination of Freshness of Fish Meat, *Jpn Kokai Tokkyo Koho*, Japan, 1989.
- [28] Y. Akahori, H. Yamazaki, G. Nishio, H. Matsunaga, K. Mitsubayashi, An alcohol gas - sensor using an enzyme immobilized paper, *Chemical Sensors* 20 (2004) 468-469.
- [29] K.M.d. Lathouder, D.T.J.v. Benthema, S.A. Wallin, C. Mateo, R.F. Lafuente, J.M. Guisan, F. Kapteijn, J.A. Moulijn, Polyethyleneimine (PEI) Functionalized Ceramic Monoliths as Enzyme Carriers: Preparation and Performance, *Journal of Molecular Catalysis B: Enzymatic* 50 (2008) 20-27.
- [30] C. Manta, N. Ferraz, L. Betancor, G. Antunes, F. Batista-Viera, J. Carlsson, K. Caldwell, Polyethylene Glycol as a Spacer for Solid-Phase Enzyme Immobilization, *Enzyme and Microbial Technology* 33 (2003) 890-898.
- [31] I.M. Klotz, G.P. Royer, I.S. Scarpa, Synthetic Derivatives of Polyethyleneimine with Enzyme-Like Catalytic Activity (Synzymes), *Proceedings of the National Academy of Sciences of the United States of America* 68 (1970) 263-264.

- [32] R.D. Schmid, Stabilized Soluble Enzymes, in: T.K. Ghose, A. Fiechter, N. Blakebrough (Eds.), *Advances in Biochemical Engineering*, Springer-Verlag, Berlin Heidelberg, 1979, pp. 41-118.
- [33] J.E. Bailey, D.F. Ollis, *Biochemical Engineering Fundamentals*, 2nd ed., McGraw-Hill, New York, 1986.
- [34] H.S. Fogler, *Elements of Chemical Reaction Engineering*, Prentice-Hall, Englewood Cliffs, New Jersey, 1986.
- [35] O. Levenspiel, *Chemical Reaction Engineering*, 3rd ed., John Wiley & Sons, New York, USA, 1999.
- [36] M.F. Machado, J.M. Saraiva, Thermal Stability and Activity Regain of Horseradish Peroxidase in Aqueous Mixtures of Imidazolium-Based Ionic Liquids *Biotechnology Letters* 27 (2005) 1233-1239.
- [37] S. Fadiloglu, O. Erkmén, G. Sekeroglu, Thermal Inactivation Kinetics of Alkaline Phosphatase in Buffer and Milk, *Journal of Food Processing and Preservation* 30 (2006) 258-268.
- [38] D. Proverbio, E. Spada, L. Baggiani, R. Perego, Assessment of a Gel Column Technique for Feline Blood Typing, *Veterinary Research Communications* 33 (2009) S201-S203.
- [39] D. Swarup, B.P.S. Dhot, J. Kotwal, A.K. Verma, Comparative Study of Blood Cross Matching Using Conventional Tube and Gel Method, *Medical Journal Armed Forces India* 64 (2008) 129-130.
- [40] I.M. Bromilow, Gel Techniques in Blood Group Serology, *Medical Laboratory Science* 49 (1992) 129-132.
- [41] M. Ota, H. Fukushima, I. Yonemura, H. Hasekura, Detection of ABO Blood Group-active Glycolipids Extracted from Red Cell Membrane and Heat Hematoma Using TLC-Immunostaining, *Zeitschrift für Rechtsmedizin* 100 (1988) 215-221.
- [42] M.K. Ramasubramanian, S.P. Alexander, An Integrated Fiberoptic-Microfluidic Device for Agglutination Detection and Blood Typing, *Biomedical Microdevices* 11 (2009) 217-229.
- [43] F. Masaki, A. Yoshinori, A. Toshihiro, N. Takeshi, N. Masataka, M. Toshiki, H. Kenichi, H. Kiyohiro, M. Koji, Blood Test Device, in: E.P. Application (Ed.), EP1997432 (A1), Panasonic Corp (JP), Japan, 2009.
- [44] B.E. Clawson, Occult Blood Testing Device, in: U.S.P. Office (Ed.), Newport Beach, CA, United State, 2009, p. 11.
- [45] B. Bilgicer, S.W. Thomas, B.F. Shaw, G.K. Kaufman, V.M. Krishnamurthy, L.A. Estroff, J. Yang, G.M. Whitesides, A Non-Chromatographic Method for the Purification of a Bivalently Active Monoclonal IgG Antibody from Biological Fluids, *Journal of American Chemical Society* 131 (2009) 9361-9367.
- [46] J. Maule, N. Wainwright, A. Steele, Lab-on-a-Chip: From Astrobiology to the Space Station, *NASA Astrobiology Conference*, Santa Clara, CA, 2008.
- [47] T.A. Bland, Blood Collection and Testing Device, in: U.S. Patent (Ed.), United States, 1995.
- [48] B.F. Rodak, G.A. Fritsma, K. Doig, *Hematology : clinical principles and applications*, 3rd ed., Elsevier Saunders, Philadelphia, Pa., 2007.
- [49] J.G. Webster, *Encyclopedia of Medical Devices and Instrumentation*, John Wiley & Sons, 2006.

- [50] P. Ganguly, Studies on Platelet Proteins. IV. Some Physical and Chemical Properties of Thrombosthenin, *Blood* 34 (1969) 511-520.
- [51] R.L. Cecil, T.E. Andreoli, Cecil Essentials of Medicine, Saunders, Philadelphia, 1993.
- [52] M.E. Reid, C. Lomas-Francis, The Blood Group Antigen FactsBook, 2nd ed., Academic Press, London ; San Diego, Calif. , 2004.
- [53] M.S. Khan, G. Thouas, W. Shen, G. Whyte, G. Garnier, Paper Diagnostic for Instantaneous Blood Typing, *Analytical Chemistry* 82 (2010) 4158-4164.
- [54] F. Toderas, M. Baia, L. Baia, S. Astilean, Controlling gold nanoparticle assemblies for efficient surface-enhanced Raman scattering and localized surface plasmon resonance sensors, *Nanotechnol.* 18 (2007).
- [55] M.K. Oh, S. Yun, S.K. Kim, S. Park, Effect of layer structures of gold nanoparticle films on surface enhanced Raman scattering, *Anal. Chim. Acta* 649 (2009) 111-116.
- [56] Y.H. Ngo, D. Li, G. Simon, G. Garnier, Gold nanoparticles-paper as a 3-dimensional SERS substrate, *Langmuir* (2012, In Press).
- [57] C. Qiu, L. Zhang, H. Wang, C. Jiang, Surface-Enhanced Raman Scattering on Hierarchical Porous Cuprous Oxide Nanostructures in Nanoshell and Thin-Film Geometries, *J. Phys. Chem.* 3 (2012) 651-657.
- [58] H.H. Wang, C.Y. Liu, S.B. Wu, N.W. Liu, C.Y. Peng, T.H. Chan, C.F. Hsu, J.K. Wang, Y.L. Wang, Highly Raman-Enhancing Substrates Based on Silver Nanoparticle Arrays with Tunable Sub-10 nm Gaps, *Adv. Mater.* 18 (2006) 491-495.